

André Berger
Fedor Mesinger
Djordje Šijački
Editors

Climate Change

Inferences from Paleoclimate
and Regional Aspects

Climate Change

André Berger • Fedor Mesinger •
Djordje Šijački
Editors

Climate Change

Inferences from Paleoclimate
and Regional Aspects

 Springer

Editors

André Berger
Université Catholique de Louvain
Louvain-la-Neuve
Belgium

Fedor Mesinger
Serbian Academy of Sciences and Arts
Belgrade
Serbia

Djordje Šijački
Institute of Physics
University of Belgrade
Belgrade
Serbia

ISBN 978-3-7091-0972-4 ISBN 978-3-7091-0973-1 (eBook)
DOI 10.1007/978-3-7091-0973-1
Springer Wien Heidelberg New York Dordrecht London

Library of Congress Control Number: 2012937046

© Springer-Verlag Wien 2012

This work is subject to copyright. All rights are reserved by the Publisher, whether the whole or part of the material is concerned, specifically the rights of translation, reprinting, reuse of illustrations, recitation, broadcasting, reproduction on microfilms or in any other physical way, and transmission or information storage and retrieval, electronic adaptation, computer software, or by similar or dissimilar methodology now known or hereafter developed. Exempted from this legal reservation are brief excerpts in connection with reviews or scholarly analysis or material supplied specifically for the purpose of being entered and executed on a computer system, for exclusive use by the purchaser of the work. Duplication of this publication or parts thereof is permitted only under the provisions of the Copyright Law of the Publisher's location, in its current version, and permission for use must always be obtained from Springer. Permissions for use may be obtained through RightsLink at the Copyright Clearance Center. Violations are liable to prosecution under the respective Copyright Law.

The use of general descriptive names, registered names, trademarks, service marks, etc. in this publication does not imply, even in the absence of a specific statement, that such names are exempt from the relevant protective laws and regulations and therefore free for general use.

While the advice and information in this book are believed to be true and accurate at the date of publication, neither the authors nor the editors nor the publisher can accept any legal responsibility for any errors or omissions that may be made. The publisher makes no warranty, express or implied, with respect to the material contained herein.

Printed on acid-free paper

Springer is part of Springer Science+Business Media (www.springer.com)

Logos of the Major Financial Contributors to the Milankovitch Anniversary Symposium, 2009, Belgrade, Serbia



*This book is dedicated to the memory of Stevan Koički,
former Vice-President of the Serbian Academy of Sciences and Arts,
the original proposer to UNESCO of the Milankovitch Anniversary
Symposium held 2009 in Belgrade*



Milutin Milankovitch
a photograph from the year 1926
(Photo Library of the Serbian Academy of Sciences and Arts, Belgrade)

Preface

Once again, for the third time, in 2009, the Serbian Academy of Sciences and Arts organized an international symposium on the occasion of the birth anniversary of Milutin Milankovitch. As in 2004, the 2009 symposium was held under the patronage of the United Nations Educational, Scientific and Cultural Organization (UNESCO). What were the motives, supported by UNESCO, that led the Academy to organize another Milankovitch symposium 5 years after the second one? Several considerations were behind this move.

Paleoclimate, with its records of numerous drastic climatic changes, is a rich reservoir of real-world information on the patterns of change in the earth's climate system. While in 2004 there were some people skeptical about global warming and also of it being a phenomenon caused by man's activities, in 2009 there were not many left of either kind. Thus, understanding paleoclimate, following in the footsteps of Milankovitch, not only adds to our basic knowledge of the history of the world we live in, but it also adds to our abilities to anticipate future climate changes as the emission of greenhouse gasses by the increasing world population continues with little abatement in sight.

This last point was brought into focus recently by the work of James Hansen and collaborators who pointed out that the information on which way the earth's climate is going should best rely on three sources: observations, results of numerical models, and paleoclimate data. This is because the former two sources have limitations: observations are obtained from the earth's climate system which is now not in equilibrium, and numerical models include processes that are insufficiently understood and thus contain errors, and in their most advanced forms cannot be run for as long as one would wish. Paleoclimate data, on the other hand, are obtained from the time when the earth's climate system was close to equilibrium, such as the time of the maximum extent of the last ice age, and the time when there was no ice cover on the earth, some 40 million years ago.

With this new awareness of the significance of paleoclimate in the context of the climate change in progress, it seemed appropriate to open the 2009 symposium with a brief review of the present climate change situation, especially in view of the post 2007 Intergovernmental Panel on Climate Change (IPCC) Fourth Assessment Report (AR4). Given that the proceedings are being printed about 2 years after the symposium was held, the review paper by Richard Somerville included here has been updated so as to contain information on global climate during the 2 years following the symposium: 2009 and 2010.

The review of the present climatic condition is followed by invited presentations reporting the progress made in the field of paleoclimate science. The session on paleoclimate started on Tuesday, 22 September and ended on Thursday, 24

September, and included 12 papers. The session was subdivided into two main parts. The first one was on glacial–interglacial cycles and the second on modeling the Last Glacial Maximum and the Holocene. Then, additional papers discuss Milankovitch’s contribution to the understanding of climate evolution (Aleksandar Petrović), the feedbacks in the climate system (Ray Bates), and the snowball Earth (David Spiegel). Brief remarks on the contributions of Milankovitch made by André Berger in his presentation have been expanded into a full-length paper on the history of the astronomical theory of climate change.

In the first part, Peter Ditlevsen indicates the dynamic origin of the Mid-Pleistocene transition from the 41-ka world to the 100-ka one, and the role of the internal stochastic noise in the period prior to the last five glacial cycles. Andrey Ganopolski and Reinhard Calov apply the model Climber-2 to simulate the last eight glacial–interglacial cycles forced by variations in the astronomical parameters and in the concentration of the major greenhouse gases. André Berger and Qiuzhen Yin discuss the climate associated with the peaks of the interglacials of the last one million years, stressing the difference between the interglacials before and after the Mid-Brunhes Event. Slobodan Marković explains the role of loess sediments in reconstructing the climatic variations in Serbia. Qiuzhen Yin discusses the origin of the strong East Asian summer monsoon seen in the loess of China during MIS-13.

Four papers in the second part demonstrate the power of models in simulating past climates. Bette Otto-Bliesner stresses the role of the astronomical parameters in shaping the last interglacial using experiments with the NCAR Community climate system model. Didier Roche shows the importance of the different forcings in simulating the last deglaciation, whereas André Paul proposes ways to reduce the uncertainty pertaining to the Atlantic meridional overturning circulation of the Last Glacial Maximum by employing paleo-data assimilation techniques.

Several papers address the impact of climate change on hydrologic ecosystems and on regional watershed issues. Possible effects of climate change on the aquatic vegetation in river and floodplain habitats are described by Georg Janauer. He also discusses sensible solutions to problems envisaged, so as to include ecohydrology principles and mediating between diverging stakeholder interests. The analysis presented in the paper by Musić and coauthors addresses the challenging task of evaluating the uncertainties associated with the projection of climate change impact on hydrological regimes at the watershed scale. Dejan Dimkić and Jovan Despotović analyze the expected changes in stream flows in Serbia by looking at flows of previous years of under and above average temperature and precipitation in available records, and trends projected by the IPCC AR4 report.

Given that an overview of climate change was the symposium’s main topic and that it is not only a scientific but also a societal need to understand regional changes that could be expected, regional climate modeling was looked into at some length by a number of invited and contributed papers. Basic issues such as what can be done by running regional climate models (RCMs) and other not fully understood problems are extensively reviewed by René Laprise and collaborators, in a paper presented by Dragana Kornić. The paper by Fedor Mesinger and coauthors discusses the issues of the domain size and lateral boundary conditions in view of the possible desirability of attempting to improve the RCMs on a large scale. They include a summary of the very recent results obtained by Katarina Veljovic, as well as the earlier results of Michael Fennessy and Eric Altshuler, arguing that if a small improvement on a large

scale were to be achieved, a still greater improvement on a small scale should be expected. How well a specific polar region problem, that of open water, can be dealt with is looked into by Sandra Morelli and Flavio Parmiggiani. Finally, of the papers included here, one that focuses on the climate changes to be expected in the region of Southern Europe and the Mediterranean, thus including the symposium venue, is that of Aleksandra Kržič and collaborators.

The 17 papers published in this volume were, of course, typically submitted some months and, in some cases, even up to more than a year after the symposium itself, and all have gone through a customary peer-review process. Thus, it is expected that they contain “added value” compared to the actual presentations at the symposium. The editors hope that having the collection in one volume will be appreciated by the readers.

As to the symposium itself, at the opening session, the participants were addressed by the Serbian Vice Premier and Minister for Science and Technology, Božidar Đelić; by the President of the Academy, academician Nikola Hajdin; by Dr. Patricio Bernal, Assistant Director-General of UNESCO for the Intergovernmental Oceanographic Commission, on behalf of the UNESCO, that extended its patronage to the symposium; and finally by Professor André Berger, Chairman of the International Scientific Committee. The following evening participants enjoyed a very nice reception at the City Hall, hosted by Dragan Đilas; on the penultimate day, they were received by Their Royal Highnesses Crown Prince Alexander and Crown Princess Katherine, at the White Palace, located on the outskirts of Belgrade on a plateau offering a view of the city; all three of these events were accompanied either by fine music performed by acclaimed Belgrade musicians, or, at the White Palace reception, by a colorful traditional Serbian folk dance group. The symposium dinner, on the last evening, organized on a ship cruising the rivers Sava and Danube, offering a night view of downtown Belgrade, its Kalimegdan Park and Fortress, with its walls and towers reflecting off the waters of the two rivers, provided a fitting conclusion for the Belgrade part of the program.

On the last day of the program, Saturday, 26 September, the participants visited the Milankovitch family home in Dalj, Croatia, which is an impressively refurbished building made into a Milankovitch Science Center. An afternoon session was held, with several talks and a concluding discussion. At the final coffee break with refreshments served in the renovated garden of the Milankovitch family home, on the bank of Danube, the participants enjoyed the colorful view of the Danube with a wide vista of the plains to its north, and many places mentioned in Milankovitch’s entertaining and inspiring autobiographical writings.

The symposium was possible because of the financial contribution made by UNESCO. Generous contributions toward organizing the symposium were also made by several Serbian sponsors: the Electric Power Industry of Serbia, the Ministry for Environment and Spatial Planning of Serbia, Hydrometeorological Institute of Serbia, the Agency for the Protection of the Environment of Serbia, and last but not least, by the Dalj hosts, County of Erdut, Croatia, and the Milankovitch Science Center, Dalj.

April 2012

*André Berger
Fedor Mesinger
Djordje Šijački*



Participants who gave presentation or addressed the Milankovitch Anniversary Symposium:

- (1) Richard C. J. Somerville
- (2) Fedor Mesinger
- (3) Vladimir Janković
- (4) Silvio Gualdi
- (5) Didier M. Roche
- (6) Sandra Morelli
- (7) J. Ray Bates
- (8) Sylvie Jousaume
- (9) André Berger
- (10) Nikola Hajdin
- (11) Zoran Knežević
- (12) Patricio Bernal
- (13) Aleksandar Petrović
- (14) Peter Ditlevsen
- (15) Bette Otto-Blisner
- (16) Qiuzhen Yin
- (17) Slobodan Marković
- (18) Dragana Kornić
- (19) Biljana Radojević
- (20) Antonio Navarra
- (21) Andrey Ganopolski
- (22) André Paul
- (23) Dave Spiegel
- (24) Georg A. Janauer
- (25) Emanuela Bruno
- (26) Krešo Pandžić
- (27) Milka Radojević
- (28) Dejan Dimkić
- (29) Stefan Rahmstorf
- (30) Claudine P. Dereczynski
- (31) Biljana Musić
- (32) Sin Chan Chou
- (33) Aleksandra Kržič
- (34) Carlos Nobre.

Collage design by Duško Čosić.

Contents

List of Contributors	xv
Part I Climate Change at Present	
Science, Politics, and Public Perceptions of Climate Change	3
Richard C. J. Somerville	
Part II Paleoclimate	
Paleoclimate Implications for Human-Made Climate Change	21
James E. Hansen and Makiko Sato	
Simulation of Glacial Cycles with an Earth System Model	49
Andrey Ganopolski and Reinhard Calov	
Modeling the Interglacials of the Last 1 Million Years	57
André Berger and Qiuzhen Yin	
Relating the Astronomical Timescale to the Loess–Paleosol Sequences in Vojvodina, Northern Serbia	65
Slobodan B. Marković, Ulrich Hambach, Thomas Stevens, Biljana Basarin, Ken O’Hara-Dhand, Momčilo M. Gavrilov, Milivoj B. Gavrilov, Ian Smalley, and Nenad Teofanov	
A Spatial View on Temperature Change and Variability During the Last Deglaciation: A Model Analysis	79
Didier M. Roche, Hans Renssen, and Didier Paillard	
Perspectives of Parameter and State Estimation in Paleoclimatology	93
André Paul and Martin Losch	
A Brief History of the Astronomical Theories of Paleoclimates	107
André Berger	
Canon of Eccentricity: How Milanković Built a General Mathematical Theory of Insolation	131
Aleksandar Petrović	

Exaggerated Milankovitch-Like Eccentricity Cycles and Extreme Exoplanet Climate Variation	141
David S. Spiegel, Sean N. Raymond, Courtney D. Dressing, Caleb A. Scharf, and Jonathan L. Mitchell	
Part III Ecohydrology, Water Resources and Climate Change	
Aquatic Vegetation in River Floodplains: Climate Change Effects, River Restoration and Ecohydrology Aspects	149
Georg A. Janauer	
Canadian Regional Climate Model as a Tool for Assessing Hydrological Impacts of Climate Change at the Watershed Scale	157
Biljana Music, Daniel Caya, Anne Frigon, André Musy, René Roy, and David Rodenhuis	
Analysis of the Changes of the Streamflows in Serbia Due to Climate Changes	167
Dejan Dimkić and Jovan Despotović	
Part IV Regional Climate Modeling	
Considerations of Domain Size and Large-Scale Driving for Nested Regional Climate Models: Impact on Internal Variability and Ability at Developing Small-Scale Details	181
René Laprise, Dragana Kornic, Maja Rapačić, Leo Šeparović, Martin Leduc, Oumarou Nikiema, Alejandro Di Luca, Emilia Diaconescu, Adelina Alexandru, Philippe Lucas-Picher, Ramón de Elía, Daniel Caya, and Sébastien Biner	
Value Added in Regional Climate Modeling: Should One Aim to Improve on the Large Scales as Well?	201
Fedor Mesinger, Katarina Veljovic, Michael J. Fennessy, and Eric L. Altshuler	
Eta Model Simulations and AMSR Images to Study an Event of Polynya at Terra Nova Bay, Antarctica	215
Sandra Morelli and Flavio Parmiggiani	
Some Indicators of the Present and Future Climate of Serbia According to the SRES-A1B Scenario	227
Aleksandra Kržič, Ivana Tošić, Borivoj Rajković, and Vladimir Djurdjević	
Index	241

List of Contributors

Adelina Alexandru Centre pour l'Étude et la Simulation du Climat à l'Échelle Régionale (ESCER), UQAM, Montréal, QC, Canada; Canadian Network for Regional Climate Modelling and Diagnostics (CRCMD), Montréal, QC, Canada; Université du Québec à Montréal (UQAM), Montréal, QC, Canada

Eric L. Altshuler Center for Ocean-Land-Atmosphere Studies, Calverton, MD, USA

Biljana Basarin Department of Physical Geography, Faculty of Sciences, University of Novi Sad, Novi Sad, Serbia

André Berger Institute of Astronomy and Geophysics G. Lemaître, Université catholique de Louvain, Louvain-La-Neuve, Belgium

Sébastien Biner Consortium Ouranos, Montréal, QC, Canada

Reinhard Calov Potsdam Institute for Climate Impact Research, Potsdam, Germany

Daniel Caya Ouranos, Consortium sur la climatologie régionale et l'adaptation aux changements climatiques, Montréal, QC, Canada; Centre pour l'Étude et la Simulation du Climat à l'Échelle Régionale (ESCER), Université du Québec à Montréal, Montréal, QC, Canada UQAM, Montréal, QC, Canada; Canadian Network for Regional Climate Modelling and Diagnostics (CRCMD), Montréal, QC, Canada; Consortium Ouranos, Montréal, QC, Canada

Ramón de Elía Centre pour l'Étude et la Simulation du Climat à l'Échelle Régionale (ESCER), UQAM, Montréal, QC, Canada; Canadian Network for Regional Climate Modelling and Diagnostics (CRCMD), Montréal, QC, Canada; Consortium Ouranos, Montréal, QC, Canada

Jovan Despotović Faculty of Civil Engineering, University of Belgrade, Belgrade, Serbia

Alejandro Di Luca Centre pour l'Étude et la Simulation du Climat à l'Échelle Régionale (ESCER), UQAM, Montréal, QC, Canada; Canadian Network for Regional Climate Modelling and Diagnostics (CRCMD), Montréal, QC, Canada; Université du Québec à Montréal (UQAM), Montréal, QC, Canada

Emilia Diaconescu Centre pour l'Étude et la Simulation du Climat à l'Échelle Régionale (ESCER), UQAM, Montréal, QC, Canada; Canadian Network for Regional Climate Modelling and Diagnostics (CRCMD), Montréal, QC, Canada; Université du Québec à Montréal (UQAM), Montréal, QC, Canada

Dejan Dimkić Institute for Water Resources "Jaroslav Černi", Pinosava, Belgrade, Serbia

Vladimir Djurdjević Institute for Meteorology, Faculty of Physics, University of Belgrade, Belgrade, Serbia

Courtney D. Dressing Astronomy, Harvard University, Cambridge, MA, USA

Michael J. Fennessy Center for Ocean-Land-Atmosphere Studies, Calverton, MD, USA

Anne Frigon Ouranos, Consortium sur la climatologie régionale et l'adaptation aux changements climatiques, Montréal, QC, Canada

Andrey Ganopolski Potsdam Institute for Climate Impact Research, Potsdam, Germany

Milivoj B. Gavrilov Department of Physical Geography, Faculty of Sciences, University of Novi Sad, Novi Sad, Serbia

Momčilo M. Gavrilov Faculty of Physics, University of Belgrade, Belgrade, Serbia

Ulrich Hambach Department of Geomorphology, University of Bayreuth, Bayreuth, Germany

James E. Hansen NASA Goddard Institute for Space Studies and Columbia University Earth Institute, New York, NY, USA

Georg A. Janauer Department of Limnology and Hydrobotany, University of Vienna, Vienna, Austria

Dragana Kornic Centre pour l'Étude et la Simulation du Climat à l'Échelle Régionale (ESCER), UQAM, Montréal, QC, Canada; Canadian Network for Regional Climate Modelling and Diagnostics (CRCMD), Montréal, QC, Canada; Université du Québec à Montréal (UQAM), Montréal, QC, Canada

Aleksandra Kržič Southeast European Virtual Climate Change Center, RHSS, Belgrade, Serbia

René Laprise Centre pour l'Étude et la Simulation du Climat à l'Échelle Régionale (ESCER), UQAM, Montréal, QC, Canada; Canadian Network for Regional Climate Modelling and Diagnostics (CRCMD), Montréal, QC, Canada; Université du Québec à Montréal (UQAM), Montréal, QC, Canada

Martin Leduc Centre pour l'Étude et la Simulation du Climat à l'Échelle Régionale (ESCER), UQAM, Montréal, QC, Canada; Canadian Network for Regional Climate Modelling and Diagnostics (CRCMD), Montréal, QC, Canada; Université du Québec à Montréal (UQAM), Montréal, QC, Canada

Martin Losch Alfred Wegener Institute for Polar and Marine Research, Bremerhaven, Germany

Philippe Lucas-Picher Danish Meteorological Institute (DMI), Copenhagen, Denmark

Slobodan B. Marković Department of Physical Geography, Faculty of Sciences, University of Novi Sad, Novi Sad, Serbia

Fedor Mesinger Department of Mathematics, Physics and Geo-Sciences, Serbian Academy of Sciences and Arts, Kneza Mihaila 35, Belgrade, Serbia

Jonathan L. Mitchell Earth and Space Sciences, UCLA, 595 Charles Young Drive East, Los Angeles, CA, USA

Sandra Morelli Department of Physics, University of Modena and Reggio E, Modena, Italy

Biljana Music Ouranos, Consortium sur la climatologie régionale et l'adaptation aux changements climatiques, Montréal, QC, Canada; Centre ESCER, Université du Québec à Montréal, Montréal, QC, Canada

André Musy Ouranos, Consortium sur la climatologie régionale et l'adaptation aux changements climatiques, Montréal, QC, Canada

Oumarou Nikiema Centre pour l'Étude et la Simulation du Climat à l'Échelle Régionale (ESCER), UQAM, Montréal, QC, Canada; Canadian Network for Regional Climate Modelling and Diagnostics (CRCMD), Montréal, QC, Canada; Université du Québec à Montréal (UQAM), Montréal, QC, Canada

Ken O'Hara-Dhand Giotto Loess Research Group, Arkwright Materials Project, Nottingham Trent University, Nottingham, UK

Didier Paillard Laboratoire des Sciences du Climat et de l'Environnement (LSCE), UMR 8212 CEA/INSU-CNRS/UVSQ, Centre d'Etudes de Saclay, Gif-sur-Yvette Cedex, France

Flavio Parmiggiani ISAC-CNR, Bologna, Italy

André Paul MARUM – Center for Marine Environmental Sciences and Department of Geosciences, University of Bremen, Bremen, Germany

Aleksandar Petrović University of Kragujevac, Kragujevac, Serbia

Borivoj Rajković Institute for Meteorology, Faculty of Physics, University of Belgrade, Belgrade, Serbia

Maja Rapaic Centre pour l'Étude et la Simulation du Climat à l'Échelle Régionale (ESCER), UQAM, Montréal, QC, Canada; Canadian Network for Regional Climate Modelling and Diagnostics (CRCMD), Montréal, QC, Canada; Université du Québec à Montréal (UQAM), Montréal, QC, Canada

Sean N. Raymond Observatoire Aquitain des Sciences de l'Univers, Université de Bordeaux, 2 rue de l'Observatoire, BP 89, Floirac Cedex, France

Hans Renssen Section Climate Change and Landscape Dynamics, Department of Earth Sciences, Faculty of Earth and Life Sciences, Vrije Universiteit Amsterdam, Amsterdam, The Netherlands

Didier M. Roche Section Climate Change and Landscape Dynamics, Department of Earth Sciences, Faculty of Earth and Life Sciences, Vrije Universiteit Amsterdam, Amsterdam, The Netherlands; Laboratoire des Sciences du Climat et de l'Environnement (LSCE), UMR 8212 CEA/INSU-CNRS/UVSQ, Centre d'Etudes de Saclay, Gif-sur-Yvette Cedex, France

David Rodenhuis Pacific Climate Impact Consortium, University of Victoria, Victoria, BC, Canada

René Roy Hydro-Québec (IREQ), Varennes, QC, Canada

Makiko Sato NASA Goddard Institute for Space Studies and Columbia University Earth Institute, New York, NY, USA

Caleb A. Scharf Columbia Astrobiology Center, Columbia University, 550 W120 St., New York, NY, USA

Leo Šeparović Centre pour l'Étude et la Simulation du Climat à l'Échelle Régionale (ESCER), UQAM, Montréal, QC, Canada; Canadian Network for Regional Climate Modelling and Diagnostics (CRCMD), Montréal, QC, Canada; Université du Québec à Montréal (UQAM), Montréal, QC, Canada

Ian Smalley Giotto Loess Research Group, Arkwright Materials Project, Nottingham Trent University, Nottingham, UK

Richard C. J. Somerville Scripps Institution of Oceanography, University of California, San Diego, La Jolla, CA, USA

David S. Spiegel Institute for Advanced Study, School of Natural Sciences, Einstein Dr., Princeton, NJ, USA

Thomas Stevens Department of Geography, Royal Holloway, University of London, Egham, Surrey, UK

Nenad Teofanov Department of Mathematics and Informatics, Faculty of Sciences, University of Novi Sad, Novi Sad, Serbia

Ivana Tošić Institute for Meteorology, Faculty of Physics, University of Belgrade, Belgrade, Serbia

Katarina Veljovic Institute of Meteorology, Faculty of Physics, University of Belgrade, Belgrade, Serbia

Qiuzhen Yin Institute of Astronomy and Geophysics G. Lemaître, Université catholique de Louvain, Louvain-la-Neuve, Belgium

Part I

Climate Change at Present

Science, Politics, and Public Perceptions of Climate Change

Richard C. J. Somerville

Abstract

Recent research has demonstrated that climate change continues to occur, and in several aspects, the magnitude and rapidity of observed changes frequently exceed the estimates of earlier projections, such as those published in 2007 by the Intergovernmental Panel on Climate Change in its Fourth Assessment Report. Measurements show that the Greenland and Antarctic ice sheets are losing mass and contributing to sea-level rise. Arctic sea ice has melted more rapidly than climate models had predicted. Global sea-level rise may exceed 1 m by 2100, with a rise of up to 2 m considered possible. Global carbon dioxide emissions from fossil fuels are increasing rather than decreasing. This chapter summarizes recent research findings and notes that many countries have agreed on the aspirational goal of limiting global warming to 2°C above nineteenth-century “preindustrial” temperatures, in order to have a reasonable chance for avoiding dangerous human-caused climate change. Setting such a goal is a political decision. However, science shows that achieving this goal requires that global greenhouse gas emissions must peak within the next decade and then decline rapidly. Although the expert scientific community is in wide agreement on the basic results of climate change science, much confusion persists among the general public and politicians in many countries. To date, little progress has been made toward reducing global emissions.

Introduction

The comprehensive Intergovernmental Panel on Climate Change (IPCC) Fourth Assessment Report (AR4), published in 2007, authoritatively evaluates climate change science published in the peer-reviewed research

literature up to about mid-2006. Viewed from the perspective of what is known in late 2010, the report is thus inevitably somewhat out of date.

In 2007, at the time of the publication of AR4, climate scientists already understood from the most recent research that “observational data underscore the concerns about global climate change. Previous projections, as summarized by IPCC, have not exaggerated but may in some respects even have underestimated the change” (Rahmstorf et al. 2007).

Now, in 2011, more recent research has demonstrated that climate change continues to occur, and in several

R.C.J. Somerville (✉)
Scripps Institution of Oceanography, University of California,
San Diego, La Jolla, CA 92093–0224, USA
e-mail: rsomerville@ucsd.edu

aspects, the magnitude and rapidity of observed changes frequently exceed the estimates of earlier projections, including those of AR4. In addition, the case for attributing much observed recent climate change to human activities is even stronger now than at the time of AR4.

Several recent examples, drawn from many aspects of climate science, but especially emphasizing atmospheric phenomena, support this conclusion. These include temperature, atmospheric moisture content, precipitation, and other aspects of the hydrological cycle.

Motivated by the rapid progress in research, a recent scientific synthesis, *The Copenhagen Diagnosis* (Allison et al. 2009), has assessed recent climate research findings, including:

- Measurements show that the Greenland and Antarctic ice sheets are losing mass and contributing to sea-level rise.
- Arctic sea ice has melted far beyond the expectations of climate models.
- Global sea-level rise may attain or exceed 1 m by 2100, with a rise of up to 2 m considered possible.
- In 2008, global carbon dioxide emissions from fossil fuels were about 40% higher than those in 1990.
- At today's emissions rates, after just 20 more years, the world will no longer have a reasonable chance of limiting warming to less than 2°C.

The Copenhagen Diagnosis also cites research supporting the position that, in order to avoid dangerous climate disruption, global emissions must peak and then start to decline rapidly within the next 5–10 years, reaching near-zero well within this century.

The Copenhagen Diagnosis is available at <http://www.copenhagendiagnosis.org>. A somewhat updated version has been formally published recently (Allison et al. 2011).

This chapter summarizes the rapid recent progress in climate change research and relates it to recent developments in the politics and public perceptions of climate change.

The Intergovernmental Panel on Climate Change and Its 2007 Report

We can begin by looking back at the last IPCC report and asking some key questions:

1. What is the Intergovernmental Panel on Climate Change and how does it work?
2. Were the main conclusions in the IPCC Fourth Assessment Report (AR4), published in 2007, correct?
3. How has climate science changed since the scientific papers that were assessed in AR4?

IPCC was founded in 1988. The history of IPCC has been documented by Bolin (2007). To date, IPCC has produced four major Assessment Reports (ARs). The average interval between reports is about 6 years: 1990: First AR (FAR) 1995: Second AR (SAR) 2001: Third AR (TAR) 2007: Fourth AR (AR4)

In 2013, the Fifth AR (AR5) is expected. During the 20 years since the publication of the First Assessment Report, great progress has been made in climate change science. As an example, much more observational data have become available, and computer simulations of the climate system have made great advances in physical comprehensiveness and realism and also in computational resolution.

The Working Group I (physical science) part of AR4 was written by 152 scientists called "Lead Authors." Twenty-two of the 152 are called "Coordinating Lead Authors." These are the scientists who led the writing teams for each of the 11 chapters. I was a Coordinating Lead Author for AR4. In this discussion, however, I am speaking as an individual scientist, not on behalf of IPCC or any other organization. In this chapter, I shall refer to the Working Group I (WGI) portion of the IPCC report only, and I shall not consider the reports of IPCC Working Groups II and III, which deal with adaptation, impacts, mitigation, and other issues.

There were several diversity criteria in choosing the 152 Lead Authors in WGI of AR4:

The Lead Authors included younger as well as older scientists. At the time of their appointment, 25% of the Lead Authors had earned a Ph.D. within the last 10 years.

The Lead Authors were not a clique composed of authors of earlier IPCC reports. In fact, 75% of them had not been previous IPCC authors.

The Lead Authors were not overwhelmingly representatives of a few developed countries. Fully 35% of them were from developing countries and countries with economies in transition.

The 152 Lead Authors were chosen by IPCC from about 700 nominations by governments.

The WGI portion of the 2007 IPCC report (AR4) is about 1,000 pages long and took 3 years to write. During the writing, more than 30,000 review comments, from both governments and individuals, were received on three separate drafts. The authors' written responses to every review comment are in the public record. The open and transparent nature of the IPCC process, the multiple stages of peer review, and the credentials of the authors all contribute to the stature of the report.

We can start with the iconic figure depicting the atmospheric CO₂ concentration as a function of time, as measured since 1958 (Fig. 1). This is the famous "Keeling curve." This graph shows that the relentless upward trend in the amount of CO₂ in the atmosphere continues. In fact, the concentration now is increasing more rapidly than before. Charles David Keeling, who

began these observations in 1958, died in 2005. However, the meticulous measurements that he undertook, initially made with an instrument that he invented, are now being continued by others at several stations in an international network.

The International Scientific Congress in Copenhagen in March, 2009

There were two noteworthy climate meetings in Copenhagen in 2009. The more famous one, the United Nations Framework Convention on Climate Change (UNFCCC) meeting, was held in Copenhagen in December 2009. This was the 15th Conference of the Parties (COP15). The UNFCCC was the document to which the countries that had ratified it were parties. The primary scientific input to the COP15 negotiations was, of course, AR4, the Fourth Assessment Report of

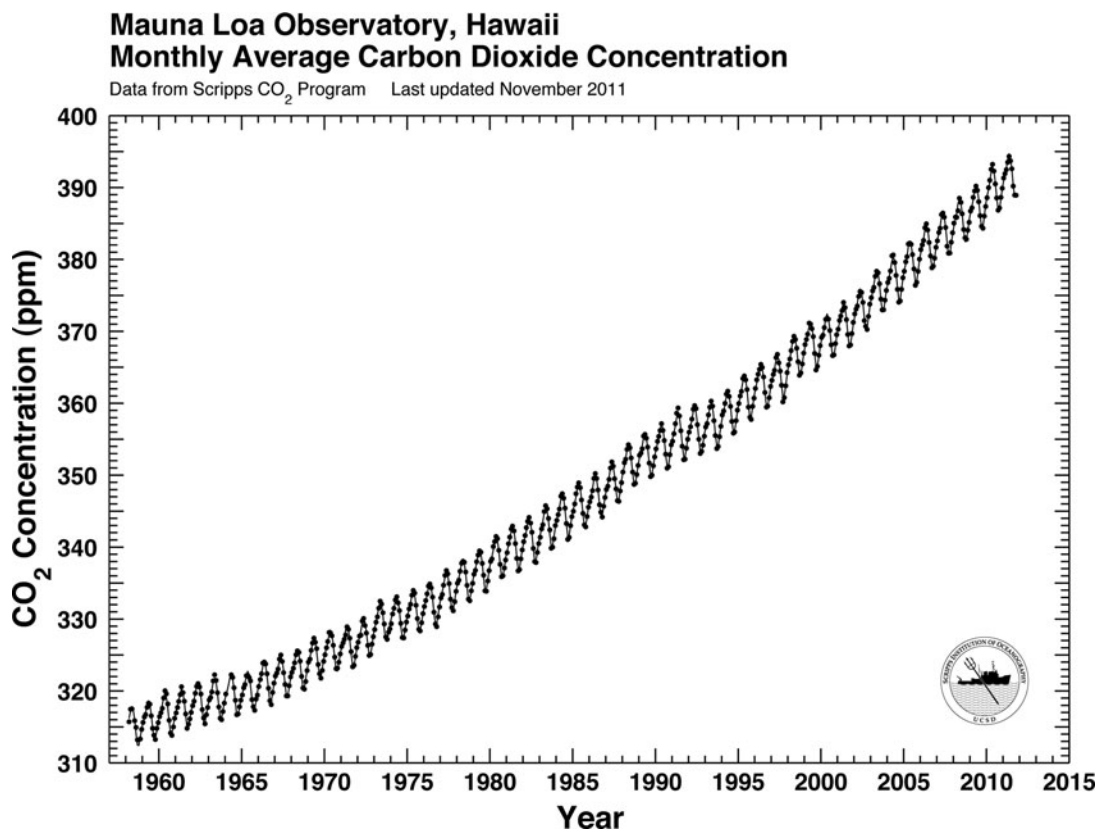


Fig. 1 The Keeling curve, showing atmospheric carbon dioxide amounts as a function of time since 1958 (credit: Scripps Institution of Oceanography CO₂ Program)

the Intergovernmental Panel on Climate Change (IPCC), published in 2007. This report and many other recent IPCC documents are available at <http://www.ipcc.ch> and are also published by Cambridge University Press.

However, new scientific developments occur continually. Since the publication of the AR4 IPCC report, new knowledge has emerged that furthers our understanding of climate change, including the impacts of human influence on the climate. To bring this new knowledge together, about 9 months before COP15, an international scientific congress, called Climate Change: Global Risks, Challenges and Decisions, was held, also in Copenhagen, from 10 to 12 March 2009. One must keep in mind that the AR4 IPCC report was published in 2007 and the most recent papers that it assesses were published in 2006.

The Copenhagen congress in March 2009 covered more recent research results, but the conclusions of this meeting did not go through any procedure resembling the long IPCC process of multiple drafts and extensive review. Nor did the March 2009 Copenhagen meeting report have the full participation of many expert authors, as did the IPCC. This fact illustrates the inevitable trade-off between the slow and painstaking IPCC process and faster but less thorough summaries and assessments of recent science.

We now consider some of the key results presented at the March 2009 Copenhagen meeting. Temperature is the single most important climate variable. Let us first consider recent temperature trends. IPCC in 2007 concluded, “warming of the climate system is unequivocal, as is now evident from observations of increases in global average air and ocean temperatures, widespread melting of snow and ice, and rising global average sea level.”

The 2007 IPCC Fourth Assessment Report (AR4) described “an unambiguous picture of the ongoing warming of the climate system.” This trend is continuing. Small year-to-year differences in global average temperatures are unimportant in evaluating long-term trends. During a warming trend, a given year is not always warmer than all the previous years, because the ongoing warming is sometimes temporarily masked by internal climate variability, a normal and natural phenomenon. For example, 2008 was slightly cooler globally than 2007, in part, because a La Niña occurred in 2008 (NASA Goddard Institute for Space Studies 2009). Such natural events can lead to

slight temporary cooling. Solar output was also at its lowest level of the satellite era, another temporary cooling influence.

Quantitatively, the global average temperature in 2008 was only about 0.1°C less than in the years immediately preceding it. Such a small difference over such a short time is not statistically significant in evaluating trends. It is noteworthy that 2008, while at the time it may have been the coolest year since 2000, remains one of the ten warmest years since instrumental records began in mid-nineteenth century and the most recent 10-year period is still warmer than the previous 10-year period. The long-term trend is clearly still a warming trend (NASA Goddard Institute for Space Studies 2009).

Our knowledge of the causes of this trend has also improved. IPCC said in 2007, “Most of the observed increase in globally averaged temperatures since the mid-twentieth century is ‘very likely’ due to the observed increase in anthropogenic greenhouse gas concentrations.” Science never provides absolute certainty. Here, “very likely” is calibrated language used by IPCC to express the degree of scientific uncertainty or the possible range of given scientific findings. In this terminology, used consistently in AR4, “very likely” means at least 90% probable.

Thanks to recent research, we have learned that by far the greatest part of the observed century-scale warming is due to human rather than natural factors (Lean and Rind 2008). These scientists analyzed the role of natural factors (e.g., solar variability and volcanoes) vs. human influences (e.g., added man-made greenhouse gases and aerosols) on temperatures since 1889. They found, for example, that the sun contributed only about 10% of surface warming in the last century and a negligible amount in the last quarter century, thus contributing far less than had been estimated in earlier assessments.

Recent research has also clarified our understanding of a warming trend in the atmosphere above the lowest layers near the Earth’s surface. By reducing errors in temperature measurements, a warming in the tropical upper troposphere, 10–15 km above the surface, is now apparent in observations, thus reconciling different measurement data and model simulations (Thorne 2008). A new method based on wind observations (Allen and Sherwood 2008) shows a similar warming trend in the upper troposphere, consistent with model results.

The climatic roles of clouds, and of small liquid or solid particles (“aerosols”) in the atmosphere, are among the subjects where intensive research is occurring and progress is being made, but only the results of future research can settle several interesting and important scientific questions. AR4 affirmed this conclusion, and it is still true.

In the 2007 IPCC Fourth Assessment Report (AR4), projections were made that future climates would generally have more precipitation at high latitudes and less in the subtropics, where many major deserts exist. However, at that time, no observational studies could be cited defining precipitation trends on a 50-year time scale. Now, such trends have been identified in measurements. For example, Zhang et al. (2007) found that precipitation has been reduced in the subtropics but has increased in middle latitudes, consistent with model projections of human-caused global warming.

Recent research and new observations have decisively settled the question of whether a warming climate will lead to an atmosphere containing more water vapor and, if so, whether the additional water vapor will add to the greenhouse effect, augmenting the warming. The answers to both these questions are yes. Water vapor does become more plentiful in a warmer atmosphere (Dessler et al. 2008). Satellite data show that atmospheric moisture content over the oceans has increased since 1998, with human causes being responsible (Santer et al. 2007).

Recent research has also found that precipitation tends to increase as atmospheric water-vapor content increases (Wentz et al. 2007; Allan and Soden 2008). These conclusions strengthen those of earlier studies.

In the remainder of this section, I briefly summarize several important findings from recent research. Further details, and citations of many of the original papers in the peer-reviewed literature, on which these summary statements are based, may be found in *The Copenhagen Diagnosis* (Allison et al. 2009, 2011).

Only a small fraction of the heat gained by the planet in recent decades is stored in the atmosphere. By far, the largest portion of heat stored is to be found in the ocean. Recently developed observational advances, such as the deployment of a widespread fleet of thousands of autonomous instrumented floats, have greatly improved our knowledge of ocean heat content. Current estimates indicate that ocean warming is about 50% greater than had been previously reported by the IPCC.

Increased melting of the large polar ice sheets contributes to the observed increase in sea level. Observations of the area of the Greenland ice sheet that has been at the melting point temperature for at least 1 day during the summer period shows a 50% increase during the period 1979–2008. The Greenland region experienced an extremely warm summer in 2007. The whole area of south Greenland reached the melting temperatures during that summer, and the melt season began 10–20 days earlier and lasted up to 60 days longer in south Greenland.

In addition to melting, the large polar ice sheets lose mass by ice discharge, which also depends on regional temperature changes. Satellite measurements of very small changes in gravity have revolutionized the ability to estimate loss of mass from these processes. The Greenland ice sheet has been losing mass at a rate of about 179 Gt/year since 2003.

One of the most dramatic developments since the last IPCC report is the rapid reduction in the area of Arctic sea ice in summer. A new minimum in Arctic sea ice was observed only a few months after the publication of AR4. In summer 2007, the minimum area covered by sea ice in the Arctic decreased by about 2 million square kilometers as compared to previous years. In 2008, the decrease was almost as dramatic, as it is at the time of the final submission of this manuscript in September of 2011. This decreasing ice coverage is important for climate on a larger scale for several reasons, including that an ice-free ocean is far less reflective and so absorbs more heat than an ice-covered ocean. Thus, the loss of Arctic sea ice triggers a strong feedback that amplifies the warming.

The global carbon cycle is in strong disequilibrium because of the input of CO₂ into the atmosphere from fossil fuel combustion and land-use change. Fossil fuels presently account for about 85% of total emissions, and land-use change, for about 15%. Total emissions have grown at about 2% per year since 1800. However, fossil fuel emissions have accelerated since 2000 to grow at about 3.4% per year, an observed growth rate that is at or even somewhat beyond the upper edge of the range of growth rates in IPCC scenarios. Total CO₂ emissions are responsible for two-thirds of the growth of all greenhouse gas radiative forcing.

The IPCC in the TAR (2001) attempted to assess scientific evidence available at the time in terms of “reasons for concern.” The resulting visual representation of that synthesis, the so-called burning embers

diagram, shows the increasing risk of various types of climate impacts with an increase in global average temperature. Using the same methodology, the same diagram of reasons for concern has been updated by several authors (Smith et al. 2009). Although there inevitably is some subjectivity in any such exercise, the results are provocative and disquieting.

Several conclusions follow from the updated “burning embers diagram” and associated recent findings. First, the risks of climate change impacts now tend to appear at lower global average temperature increases. Second, a 2°C limit of warming relative to preindustrial temperatures, which was widely thought in 2001 to be sufficient to avoid serious risks, now appears to be less adequate. Third, the risks of large-scale discontinuities are now considered to be greater than previously thought.

In summary, although a 2°C rise in temperature above preindustrial remains the most commonly quoted limit for avoiding dangerous climate change, there is now a serious case to be made that this level of warming nevertheless carries significant risks of harmful impacts for society and for the environment.

According to the IPCC analysis in AR4, atmospheric CO₂ concentration should not exceed 400 ppm CO₂ if the global temperature rise is to be kept within 2.0–2.4°C. Today, the mean CO₂ concentration is above 385 ppm and is rising by 2 ppm/year. The 2007 concentration of all greenhouse gases, both CO₂ and non-CO₂ gases, was about 463 ppm CO₂ equivalents. Adjusting this concentration for the cooling effects of aerosols yields a CO₂-equivalent concentration of 396 ppm. A recent study estimates that a concentration of 450 ppm CO₂ equivalents (including the cooling effect of aerosols) would give only a 50–50 chance of limiting the temperature rise to 2°C or less.

Thus, atmospheric CO₂ concentrations are already at levels predicted to lead to global warming of between 2.0 and 2.4°C. The conclusion from both the IPCC and subsequent analyses is blunt and stark—immediate and dramatic emission reductions of all greenhouse gases are urgently needed if the 2°C limit is to be respected.

Humanity is now committing future generations to a strongly altered climate. Even beyond the current century, there are major implications for longer-term climate change. Higher temperatures and changes in precipitation caused by CO₂ emissions from human activity are largely irreversible on human time scales.

Atmospheric temperatures are not expected to decrease for many centuries to millennia, even after human-induced greenhouse gas emissions stop completely (Matthews and Caldeira 2008; Solomon et al. 2009; Eby et al. 2009).

An analysis of several decades of data in the western United States suggests that as much as 60% of the hydrological changes in this region are due to human activities. This trend, if sustained, has profound consequences for the future water supply of this already water-stressed part of the world (Barnett et al. 2008).

One complex climate model that had been modified to include recent advances in understanding of the carbon cycle, natural climate factors, and other elements then produced twice as large a global average temperature increase at the end of the twenty-first century as it had before the model was modified: 5.2°C in the new model run compared to 2.4°C for the older version of the model (Sokolov et al. 2009).

Many recent aspects of observed climate change reveal a more rapid pace than had been foreseen by recent model projections. Thus, recent revisions of projected climate change exceed earlier estimates, and it is increasingly clear that the projections reported in the IPCC Fourth Assessment Report in 2007 may well have underestimated the pace of current climate change. This conclusion of Rahmstorf et al. (2007), which appeared after AR4 was published, could stand as a conclusion for this entire survey of the results of climate change science:

Overall, these observational data underscore the concerns about global climate change. Previous projections, as summarized by IPCC, have not exaggerated but may in some respects even have underestimated the change, in particular for sea level.

How *The Copenhagen Diagnosis* Came to Be Written

The Copenhagen Diagnosis (Allison et al. 2009) is a report published online in November 2009. It is available for download at <http://www.copenhagendiagnosis.com> and <http://www.copenhagendiagnosis.org>. A group of 26 climate scientists wrote *The Copenhagen Diagnosis*. All are active researchers. They come from eight countries and include three women and several younger scientists. I am one of the 26 scientists who wrote this

report. Our group is private, independent, and unaffiliated with any organization. We speak only for ourselves, not for the Intergovernmental Panel on Climate Change (IPCC) or anyone else. We are self-selected and self-organized. We have no official leader or formal structure. About half of us are IPCC authors, so we know firsthand what preparing such an assessment entails and what scientific standards it should meet. Our report is firmly based on the more than 200 peer-reviewed papers we cite.

Our aim was to write a readable, short, authoritative report summarizing relevant peer-reviewed climate change research appearing since the cutoff publication date (about mid-2006) for papers assessed in the most recent (2007) IPCC assessment. Like IPCC, we insisted on being policy relevant but policy neutral. We thought that such an update was needed to inform the UN climate negotiations in Copenhagen in December 2009, because there has been so much important recent research. It seemed obvious to us that somebody ought to prepare such an update, so we simply decided to accept this responsibility ourselves. The veracity and value of this report thus rests entirely on the scientific credibility of its authors as well as that of the peer-reviewed publications we cite. Any errors or shortcomings in our report are also the sole responsibility of the 26 named authors.

We worked on this document for about a year. Many of us met in Copenhagen in March 2009, at the time of the congress described above, to organize the work and to agree on deadlines, topics, chapter lengths, etc. In deciding who would be in the group of authors, our primary criterion was scientific expertise on one or more of the various topics that we thought needed to be covered. We sought scientists with excellent research reputations, willing and able to work to deadlines, fluent in English, and able to function as part of a writing team. Typically, one author would draft a given chapter, then several others of the group would review and revise it, and finally, the entire group would consider the revised draft and reach consensus.

The Climate Change Research Centre at the University of New South Wales in Sydney, Australia, contributed some staff support, for example, for developing the web site. A grant paid essential costs such as printing and travel to our meeting in Copenhagen. Nobody had any influence whatever on the contents of the report other than the 26 authors. We, the authors of *The Copenhagen Diagnosis*, all freely contributed

our time and expertise. None of us were paid anything from any source to write this report.

In *The Copenhagen Diagnosis*, the reader is hearing directly from the 26 scientists who wrote it. We made all our own editorial decisions, such as to include “boxes” dealing with common misconceptions. We also decided what each of our chapters would be about and how long they would be. In short, we authors enjoyed complete autonomy to design and write our report as we wished.

The Copenhagen Diagnosis is emphatically not an attack on IPCC or a repudiation of the IPCC process or the 2007 IPCC assessment report. We simply considered that the significance of very recent research, and of many climate observations made after the AR4 IPCC assessment was written, together with novel and important improvements in several areas of scientific tools and technology, all deserved to be brought to the attention of the Copenhagen negotiators, the media, governments, corporations, and the global public. Our goal has been to make our report accessible to all.

The Copenhagen Diagnosis is about climate change science, not policy. For example, we summarize recent research underpinning the scientific rationale for large and rapid reductions in global greenhouse gas emissions, in order to reduce the likelihood of dangerous man-made climate change. However, we have no political or policy agenda, and we do not speak to the issue of formulating policies to achieve such reductions in emissions. As scientists, when climate change research is relevant to public policy, we consider it important to bring that research to the attention of the wider world. We are convinced that sound science can and should inform wise policy. This conviction led us to write *The Copenhagen Diagnosis*.

Main Findings of *The Copenhagen Diagnosis*

According to *The Copenhagen Diagnosis* (Allison et al. 2009), the most significant recent climate change findings are:

Surging greenhouse gas emissions: Global carbon dioxide emissions from fossil fuels in 2008 were nearly 40% higher than those in 1990 (Fig. 2). Even if global emission rates are stabilized at present-day

Fig. 2 Global fossil fuel CO₂ emissions as a function of time (credit: Allison et al. 2009, *The Copenhagen Diagnosis*)

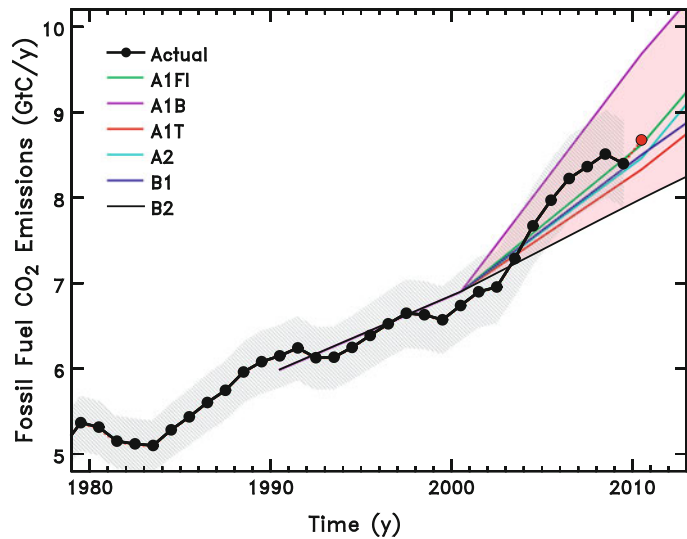
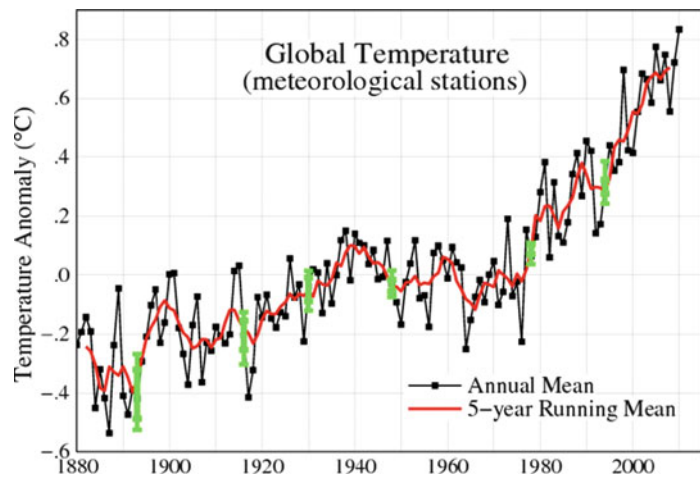


Fig. 3 Global annual-mean surface air temperature change since 1880, with the base period 1951–1980, derived from the meteorological station network [an update of Fig. 6b in Hansen et al. (2001)]. Uncertainty bars (95% confidence limits), shown for both the annual and 5-year means, account only for incomplete spatial sampling of data (credit: NASA, GISS, available online at <http://data.giss.nasa.gov/gistemp/graphs/>)



levels, just 20 more years of emissions would give a 25% probability that warming exceeds 2°C, even with zero emissions after 2030. Every year of delayed action increases the chances of exceeding 2°C warming.

Recent global temperatures demonstrate human-induced warming: Over the past 25 years, temperatures have increased at a rate of 0.19°C per decade, in very good agreement with predictions based on greenhouse gas increases (Fig. 3). Even over the past 10 years, despite a decrease in solar forcing, the trend continues to be one of warming. Natural, short-term fluctuations are occurring as usual, but there have been no significant changes in the underlying warming trend.

Acceleration of melting of ice sheets, glaciers, and ice caps: A wide array of satellite and ice measurements

now demonstrate beyond doubt that both the Greenland and Antarctic ice sheets are losing mass at an increasing rate. Melting of glaciers and ice caps in other parts of the world has also accelerated since 1990.

Rapid Arctic sea-ice decline: Summer melting of Arctic sea ice (Fig. 4) has accelerated far beyond the expectations of climate models (Fig. 5). The area of sea-ice melt during 2007–2010 (Fig. 5) was about 40% greater than the average prediction from IPCC AR4 climate models. The minimum for 2011, about to be attained at the time of the final submission of this manuscript, seems on track to be about the same as the lowest minimum on record so far, for 2007 (see http://nsidc.org/data/seaice_index/images/daily_images/N_stddev_timeseries.png).



Fig. 4 Minimum Arctic sea-ice extent from 1979 to 2007 (credit: Allison et al. 2009, *The Copenhagen Diagnosis*)

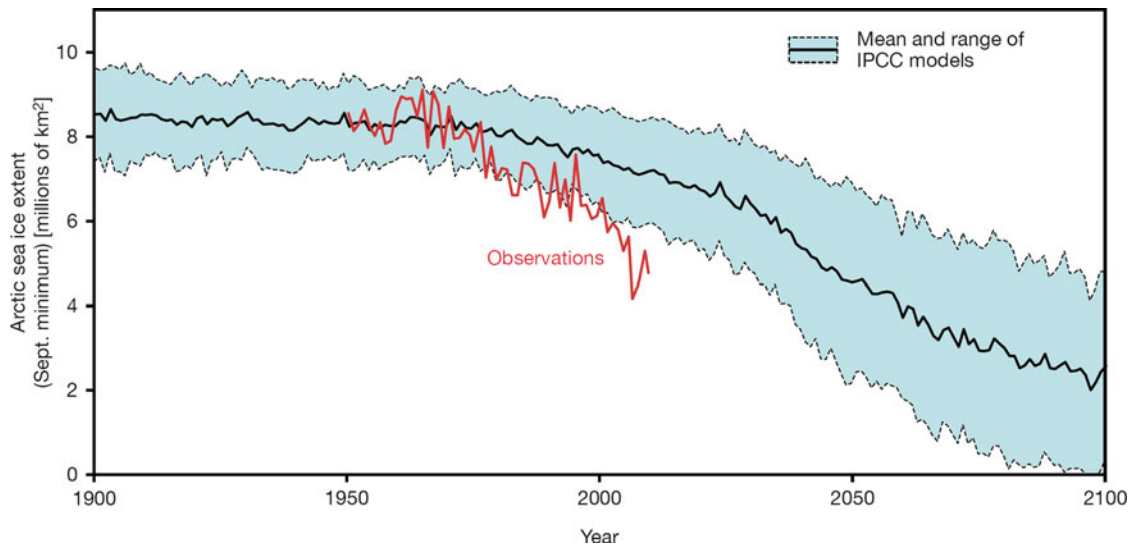


Fig. 5 Observed and modeled Arctic sea-ice extent (credit: Allison et al. 2011, *The Copenhagen Diagnosis*)

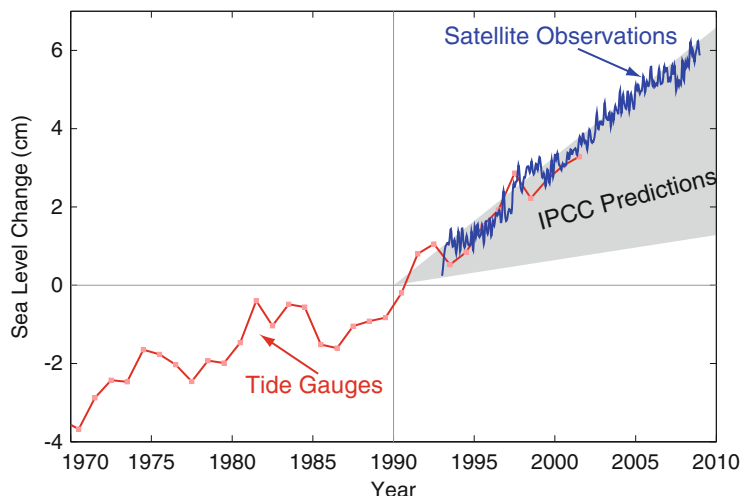
Current sea-level rise underestimated: Satellites show recent global average sea-level rise (3.4 mm/year over the past 15 years) to be ~80% above past IPCC predictions (Fig. 6). This acceleration in sea-level rise is consistent with a doubling in contribution from melting of glaciers, ice caps, and the Greenland and west Antarctic ice sheets.

Sea-level predictions revised: By 2100, global sea level is likely to rise at least twice as much as projected by Working Group I of the IPCC AR4; for

unmitigated emissions, it may well exceed 1 m. The upper limit has been estimated as ~2-m sea-level rise by 2100. Sea level will continue to rise for centuries after global temperatures have been stabilized, and several meters of sea-level rise must be expected over the next few centuries.

Delay in action risks irreversible damage: Several vulnerable elements in the climate system (e.g., continental ice sheets, Amazon rainforest, West African monsoon, and others) could be pushed toward abrupt

Fig. 6 Sea-level change from 1970 to 2010 (credit: Allison et al. 2009, *The Copenhagen Diagnosis*)



or irreversible change if warming continues in a business-as-usual way throughout this century. The risk of transgressing critical thresholds (“tipping points”) increases strongly with ongoing climate change. Thus, waiting for higher levels of scientific certainty could mean that some tipping points will be crossed before they are recognized.

The turning point must come soon: If global warming is to be limited to a maximum of 2°C above preindustrial values, global emissions need to peak between 2015 and 2020 and then decline rapidly. To stabilize climate, a decarbonized global society—with near-zero emissions of CO₂ and other long-lived greenhouse gases—needs to be reached well within this century (Fig. 7). More specifically, the average annual per-capita emissions will have to shrink to well below 1-metric ton CO₂ by 2050. This is 80–95% below the per-capita emissions in developed nations in 2000.

In this chapter, we give only the above brief summary of *The Copenhagen Diagnosis*. Figures 2, 4, 5, and 6 in this chapter are from *The Copenhagen Diagnosis* and are used with permission. The full report is available at <http://www.copenhagendiagnosis.com> and in updated form as Allison et al. (2011).

COP15 in Copenhagen, December 2009

At the beginning of December 2009, one might have naively anticipated that the increasingly somber and compelling results of climate change science would have led the governments of the world to produce an

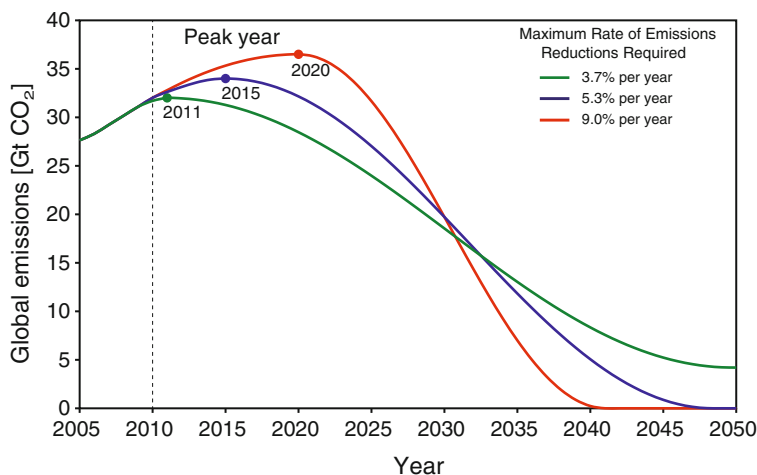
agreement to rapidly reduce global emissions of greenhouse gases. Indeed, such an agreement at COP15 in Copenhagen in 2009 had been widely expected after COP13 in Bali 2 years earlier. Many observers had predicted that a binding treaty, with clear and firm targets and timetables and enforcement mechanisms, was achievable. Furthermore, as we have seen, the passage of time had seen a strengthening of the scientific rationale for such an agreement. This is apparent in the conclusions of AR4 as strengthened by subsequent research summarized in *The Copenhagen Diagnosis*.

However, the outcome of the COP15 climate negotiations in Copenhagen in December 2009 disappointed almost everybody. The final “agreement” among a few countries, known as the Copenhagen Accord (http://en.wikipedia.org/wiki/Copenhagen_Accord), was brokered by the USA and China at the last minute. This document has no legally binding status and is simply an aspirational statement. It is better than nothing, and one must hope for further progress in the future. However, there is no sign, in this minimal diplomatic result, of the clear need for urgency based on solid climate change science.

Yet, many countries have already agreed on the firm aspirational goal of limiting global warming to 2°C above nineteenth-century “preindustrial” temperatures, in order to have a reasonable chance for avoiding dangerous human-caused climate change.

Setting such a goal is a political decision. Now that the goal is set, however, science can say with confidence that meeting the goal requires that *global*

Fig. 7 Emissions pathways to give 67% chance of limiting global warming to 2°C (credit: Allison et al. 2009, *The Copenhagen Diagnosis*)



greenhouse gas emissions must peak within the next decade and then decline rapidly. We say that emphatically in the 2009 report *The Copenhagen Diagnosis*, where we also cite the peer-reviewed research on which this statement is firmly based, such as Meinshausen et al. (2009).

We scientists have been aware of this urgency for more than 30 years. The authoritative IPCC report in 2007 emphasized it. My book *The Forgiving Air: Understanding Environmental Change* (Somerville 2008) cited, “the need to act soon if sensible targets are to be met, the fact that the needed reductions in greenhouse gas emissions will be large, and the fact that both developed and developing countries must be involved.”

These results are sensitive to assumptions, of course. Meinshausen et al. (2009) conclude that “the probability of exceeding 2°C rises to 75% if 2020 emissions are not lower than 50 Gt CO₂ equiv. (25% above 2000).”

We relied on this chapter and others in reaching our conclusion in *The Copenhagen Diagnosis* that “the required decline in emissions coupled with a growing population will mean that by 2050, annual per capita CO₂ emissions very likely will need to be below 1 ton.” Obviously, that is very tough to achieve. See our Fig. 7 in this chapter, which is Fig. 22 on page 51 in *The Copenhagen Diagnosis*.

When I say that we scientists have known about the urgency for more than 30 years, there, I have one particular paper in mind, among others. That paper is Siegenthaler and Oeschger (1978). Here is the conclusion taken from its summary (page 389):

For a prescribed maximum increase of 50 percent above the preindustrial carbon dioxide level, the production

could grow by about 50 percent until the beginning of the next century, but should then decrease rapidly.

So “production” (meaning emissions) has to peak and then quickly decline early in the current century. This 1978 result came from simple models and the limited data available in the 1970s. We know much more today about the numbers and the caveats and other details. However, the essential scientific foundation was already clear more than 30 years ago, at least to two insightful Swiss scientists. That is the message of Fig. 7 in the present paper: the urgency is scientific, not political.

Mother Nature herself thus imposes a timescale on when emissions need to peak and then begin to decline rapidly. This urgency is therefore not ideological, but rather is due to the physics and biogeochemistry of the climate system itself. Diplomats are powerless to alter laws of nature and must face scientific facts.

Thus, it is profoundly regrettable that the dithering and procrastination at COP15 in Copenhagen continued a year later in December 2010 at COP16 in Cancun, Mexico. The Cancun negotiations are just concluding as these lines are being written. The enduring failure to achieve meaningful science-based international agreements will inevitably have serious consequences for the degree of climate disruption that the Earth will undergo.

Public Perceptions and the Politics of Climate Change

In late November 2009, at about the same time that *The Copenhagen Diagnosis* was released, a crime was committed in which thousands of e-mails of prominent climate scientists were illegally obtained from a server at the University of East Anglia in the United

Kingdom. These e-mails, which appear to be authentic, were published online and extensively discussed in the press and the blogosphere.

Extremely serious questions were immediately raised. Is the science of global warming valid, or has it been proven wrong by this episode of e-mails stolen from a climate research center in England? The short answer is that the hacked e-mails do not undermine the science in any way.

There is no doubt that the e-mails have embarrassed several scientists. Writing what they thought were private messages to their close colleagues, they expressed themselves in intemperate language. Angered by what they regarded as intolerable harassment by repeated and unreasonable demands, they lashed out in frustration in e-mails to one another.

Edited excerpts from the e-mails do read poorly, especially out of context, and they might lead some people to conclude that climate research must involve biased, power hungry, and unprincipled scientists. Following the release of the e-mails, many in the blogosphere and media immediately appointed themselves prosecutor, judge, and jury. There was little chance to mount a defense in this rush to judgment.

During the year following the release of the e-mails, several independent investigations were carried out and the outcome of all of them has been to exonerate the scientists from accusations of fraud, incompetence, and dishonesty. Many of the specific charges made against the scientists have been shown to be false. Cherry-picked words like “trick” turn out to be innocent jargon. In science, a “trick” is not an underhanded tactic to conceal the truth. It is just a clever way to solve a technical problem, like finding solutions to certain equations. “Trick” means one thing to scientists, something else to bridge players, and something altogether different to dog trainers. Context matters.

Much has also been made of unsuccessful demands for temperature data to be released from the center at East Anglia. In fact, the scientists did resist such demands. Not all the legal issues have yet been completely resolved. They involve freedom of information laws as well as the proprietary restrictions attached to some data by the organizations that originally supplied the data. Nearly all the data in question, however, is freely available from several sources. Several other centers worldwide independently monitor and analyze global temperatures, and their findings

closely confirm the ones from the English center. The notion that the central scientific results of modern climate change research might be upset by the release of additional data is not credible.

In my opinion, the most serious charge by far against the e-mailing group of scientists is that they blocked publication by other scientists with whom they disagreed and that they prevented the IPCC, the Intergovernmental Panel on Climate Change, from considering the findings of those scientists in its 2007 assessment report, AR4. Work by Soon and Baliunas and by McIntyre and McKittrick was alleged to be in that category.

The facts, however, are that in these cases, scientific practice worked exactly as it should. The papers by these authors were indeed published. Other scientists considered them and did further research and published it too. The IPCC cited and discussed all this in its landmark Fourth Assessment Report, published in 2007. This is the relevant passage from page 466 of that report:

The ‘hockey stick’ reconstruction of Mann et al. (1998) has been the subject of several critical studies. Soon and Baliunas (2003) challenged the conclusion that the 20th century was the warmest at a hemispheric average scale. They surveyed regionally diverse proxy climate data, noting evidence for relatively warm (or cold), or alternatively dry (or wet) conditions occurring at any time within pre-defined periods assumed to bracket the so-called ‘Medieval Warm Period’ (and ‘Little Ice Age’). Their qualitative approach precluded any quantitative summary of the evidence at precise times, limiting the value of their review as a basis for comparison of the relative magnitude of mean hemispheric 20th-century warmth (Mann and Jones, 2003; Osborn and Briffa, 2006). Box 6.4 provides more information on the ‘Medieval Warm Period’.

McIntyre and McKittrick (2003) reported that they were unable to replicate the results of Mann et al. (1998). Wahl and Ammann (2007) showed that this was a consequence of differences in the way McIntyre and McKittrick (2003) had implemented the method of Mann et al. (1998) and that the original reconstruction could be closely duplicated using the original proxy data. McIntyre and McKittrick (2005a,b) raised further concerns about the details of the Mann et al. (1998) method, principally relating to the independent verification of the reconstruction against 19th-century instrumental temperature data and to the extraction of the dominant modes of variability present in a network of western North American tree ring chronologies, using Principal Components Analysis. The latter may have some theoretical foundation, but Wahl and Amman (2006) also show that the impact on the amplitude of the final reconstruction is very small ($\sim 0.05^\circ\text{C}$; for further discussion of these issues see also Huybers, 2005; McIntyre and McKittrick, 2005c, d; von Storch and Zorita, 2005).

It is a standard tactic of many climate skeptics or contrarians to try to frame the issue in terms of the whole edifice of modern climate science hanging from some slender thread. Thus, if a given scientist uses intemperate language, or a particular measurement is missing from an archive, or a published paper has a minor mistake in it, the whole structure comes tumbling down, or so the skeptics would have people believe.

In fact, climate change science is not fragile or vulnerable, and there are multiple lines of evidence in support of all its main conclusions. That is what the 2007 IPCC report says. It remains definitive.

Historians of science tell us that the overwhelming degree of scientific agreement on climate change is rare for such a complex issue. A Galileo does come along every few hundred years to reveal fundamental errors in the prevailing understanding and thus to revolutionize a branch of science. However, almost all the people who think they are a Galileo are simply wrong. Facts matter.

Minor errors have been found in the IPCC reports, though not in the WGI (physical science) portion of AR4, and IPCC has acknowledged these errors and taken steps to reduce the likelihood of such errors in future reports. It is noteworthy, however, that since the WGI AR4 report was published in 2007, no reputable scientist has yet been able to point to a major conclusion of this IPCC report and then point to a persuasive body of peer-reviewed published research that proves that conclusion wrong. *The Copenhagen Diagnosis* has similarly not been challenged successfully. Science can never provide absolute certainty, and any scientific finding is always subject to review and revision on the basis of further research. However, it is highly unlikely that the bedrock conclusions of modern climate science will be proven wrong. Indeed, the most recent research further supports and underscores the fundamental scientific result that man-made climate change is real and serious.

A Scientific Response to Climate Skeptics

Although the expert community is in wide agreement on the basic results of climate change science, as assessed in AR4 and *The Copenhagen Diagnosis*, much confusion exists among the general public and

politicians in many countries, as polling data convincingly shows.

In my opinion, many people need to learn more about the nature of junk or fake science, so they will be better equipped to recognize and reject it. There are a number of warning signs that can help identify suspicious claims. One is failure to rely on and cite published research results from peer-reviewed journals. Trustworthy science is not something that appears first on television or the Internet. Reputable scientists first announce the results of their research by peer-reviewed publication in well-regarded scientific journals. Peer review is not a guarantee of excellent science, but the lack of it is a red flag. Peer review is a necessary rather than a sufficient criterion.

Another warning sign is a lack of relevant credentials on the part of the person making assertions, especially education and research experience in the specialized field in question. For example, it is not essential to have earned a Ph.D. degree or to hold a university professorship. It is important, however, that the person be qualified, not in some general broad scientific area, such as physics or chemistry, but in the relevant specialty. Accomplishments and even great distinction in one area of science do not qualify anybody to speak authoritatively in a very different area. We would not ask even an expert cardiologist for advice on dentistry. One should inquire whether the person claiming expertise in climate science has done first-person research on the topic under consideration and published it in reputable peer-reviewed journals. Is the person actively participating in the research area under question, or simply criticizing it from the vantage point of an outsider? One should be suspicious of a lack of detailed familiarity with the specific scientific topic and its research literature. Good science takes account of what is already known and acknowledges and builds on earlier research by others.

Other warning signs include a blatant failure to be objective and to consider all relevant research results, both pro and con a given position. Scientific honesty and integrity require wide-ranging and thorough consideration of all the evidence that might bear on a particular question. Choosing to make selective choices among competing evidence so as to emphasize those results that support a given position, while ignoring or dismissing any findings that do not support it, is a hallmark of pseudoscience.

Mixing science with ideology or policy or personalities is never justified in research. Scientific validity has nothing to do with political viewpoints. Whether a given politician agrees or disagrees with a research finding is absolutely unimportant scientifically. Science can usefully inform the making of policy, but only if policy considerations have not infected the science. Similarly, one should always be alert to the risk of bias due to political viewpoints, ideological preferences, or connections with interested parties. All sources of funding, financial interests, and other potential reasons for bias should be openly disclosed.

Finally, we must always be alert for any hint of delusions of grandeur on the part of those who would insist that they themselves are correct, while nearly everyone else in the entire field of climate science is badly mistaken. Scientific progress is nearly always incremental, with very few exceptions. Occasionally, an unknown lone genius in a humble position, such as the young Einstein doing theoretical physics while working as a clerk in a patent office, does indeed revolutionize a scientific field, dramatically overthrowing conventional wisdom. However, such events are exceedingly rare, and claims to be such a lone genius deserve the most severe scrutiny. For every authentic Einstein, there must be thousands of outright charlatans, as well as many more ordinary mortals who are simply very badly mistaken.

I have attempted to summarize a number of key points and scientific results in a recently published essay in *Climatic Change* (Somerville 2010), which I paraphrase here:

1. The essential findings of mainstream climate change science are firm. The world is warming. There are many kinds of evidence: air temperatures, ocean temperatures, melting ice, rising sea levels, and much more. Human activities are the main cause. The warming is not natural. It is not due to the sun, for example. We know this because we can measure the effect on the Earth's energy balance of man-made carbon dioxide, and it is much stronger than that of changes in the sun, which we also measure.
2. The greenhouse effect is well understood. It is as real as gravity. The foundations of the science are more than 150 years old. Carbon dioxide in the atmosphere traps heat. We know carbon dioxide is increasing because we measure it. We know the increase is due to human activities like burning fossil fuels because we can analyze the chemical evidence for that.
3. Our climate predictions are coming true. Many observed climate changes, like rising sea level, are occurring at the high end of the predicted changes. Some changes, like melting sea ice, are happening faster than the anticipated worst case. Unless mankind takes strong steps to halt and reverse the rapid global increase of fossil fuel use and the other activities that cause climate change, and does so in a very few years, severe climate change is inevitable. Urgent action is needed if global warming is to be limited to moderate levels.
4. The standard skeptical arguments have been refuted many times over in technical papers published in the peer-reviewed scientific research literature. The refutations are now summarized on many web sites and in many books. For example, natural climate change like ice ages is irrelevant to the current warming. We know why ice ages come and go. That is due to changes in the Earth's orbit around the sun, changes that take thousands of years. The warming that is occurring now, over just a few decades, cannot possibly be caused by such slow-acting processes. But it can be caused by man-made changes in the greenhouse effect.
5. Science has its own high standards. It does not work by unqualified people making claims on television or the Internet. It works by scientists doing research and publishing it in carefully reviewed research journals. Other scientists examine the research and repeat it and extend it. Valid results are confirmed, and wrong ones are exposed and abandoned. Science is self-correcting. People who are not experts, who are not trained and experienced in this field, and who do not do research and publish it following standard scientific practice are not doing science. When they claim that they are the real experts, they are just plain wrong.
6. The leading scientific organizations of the world, like national academies of science and professional scientific societies, have carefully examined the results of climate science and endorsed these results. It is silly to imagine that thousands of climate scientists worldwide are engaged in a massive conspiracy to fool everybody. The first thing that the world needs to do if it is going to confront the challenge of climate change wisely is to learn about what science has discovered and accept it.

References

- Allan RP, Soden BJ (2008) Atmospheric warming and the amplification of precipitation extremes. *Science* 321:1481–1484
- Allen RJ, Sherwood SC (2008) Warming maximum in the tropical upper troposphere deduced from thermal winds. *Nat Geosci* 1:399–403
- Allison I, Bindoff NL, Bindschadler RA, Cox PM, de Noblet N, England MH, Francis JE, Gruber N, Haywood AM, Karoly DJ, Kaser G, Le Quéré C, Lenton TM, Mann ME, McNeil BI, Pitman AJ, Rahmstorf S, Rignot E, Schellnhuber HJ, Schneider SH, Sherwood SC, Somerville RCJ, Steffen K, Steig EJ, Visbeck M, Weaver AJ (2009) The Copenhagen Diagnosis: updating the world on the latest climate science. The University of New South Wales Climate Change Research Centre, Sydney, 60 pp [available online at <http://www.copenhagediagnosis.com>]
- Allison I, Bindoff NL, Bindschadler RA, Cox PM, de Noblet N, England MH, Francis JE, Gruber N, Haywood AM, Karoly DJ, Kaser G, Le Quéré C, Lenton TM, Mann ME, McNeil BI, Pitman AJ, Rahmstorf S, Rignot E, Schellnhuber HJ, Schneider SH, Sherwood SC, Somerville RCJ, Steffen K, Steig EJ, Visbeck M, Weaver AJ (2011) The Copenhagen Diagnosis. Updating the world on the latest climate science. Elsevier, Burlington, 114 pp. ISBN 978-0-12-386999-9
- Barnett TP, Pierce DW, Hidalgo HG, Bonfils C, Santer BD, Das T, Bala G, Wood AW, Nozawa T, Mirin AA (2008) Human induced changes in the hydrology of the western United States. *Science* 319:1080
- Bolin B (2007) A history of the science and politics of climate change: the role of the Intergovernmental Panel on Climate Change. Cambridge University Press, Cambridge
- Dessler AE, Zhang Z, Yang P (2008) Water-vapor climate feedback inferred from climate fluctuations, 2003–2008. *Geophys Res Lett* 35:L20704. doi:10.1029/2008GL035333
- Eby M, Zickfeld K, Montenegro A, Archer D, Meissner KJ, Weaver AJ (2009) Lifetime of anthropogenic climate change: millennial time scales of potential CO₂ and surface temperature perturbations. *J Clim* 22:2501–2511
- Hansen J, Ruedy R, Sato M, Imhoff M, Lawrence W, Easterling D, Peterson T, Karl T (2001) A closer look at United States and global surface temperature change. *J Geophys Res* 106:23947–23963. doi:10.1029/2001JD000354
- Lean JL, Rind DH (2008) How natural and anthropogenic influences alter global and regional surface temperatures: 1889 to 2006. *Geophys Res Lett* 35:L18701. doi:10.1029/2008GL034864
- Matthews HD, Caldeira K (2008) Stabilizing climate requires near zero emissions. *Geophys Res Lett* 35:L04705
- Meinshausen M, Meinshausen N, Hare W, Raper SCB, Frieler K, Knutti R, Frame DJ, Allen MR (2009) Greenhouse-gas emission targets for limiting global warming to 2 deg C. *Nature* 458:1158–1163
- NASA Goddard Institute for Space Studies (2009) GISS Surface Temperature Analysis. Global Temperature Trends: 2008 Annual Summation. <http://data.giss.nasa.gov/gistemp/2008/>. Accessed 17 Aug 2009
- Rahmstorf S, Cazenave A, Church JA, Hansen JE, Keeling RF, Parker DE, Somerville RCJ (2007) Recent climate observations compared to projections. *Science* 316:709
- Santer BD, Mears C, Wentz FJ, Taylor KE, Gleckler PJ, Wigley TML, Barnett TP, Boyle JS, Brüggemann W, Gillett NP (2007) Identification of human-induced changes in atmospheric moisture content. *Proc Natl Acad Sci USA* 104:15248
- Siegenthaler U, Oeschger H (1978) Predicting future atmospheric carbon dioxide levels. *Science* 199:388–395
- Smith JB, Schneider SH, Oppenheimer M, Yohe GW, Hare W, Mastrandrea MD, Patwardhan A, Burton I, Corfee-Merlot J, Magadza CHD, Fussler H-M, Pittock AB, Rahman A, Suarez A, van Ypersele J-P (2009) Assessing dangerous climate change through an update of the Intergovernmental Panel on Climate Change (IPCC) “reasons for concern”. *Proc Natl Acad Sci USA* 106:4133–4137
- Sokolov AP, Stone PH, Forest CE, Prinn R, Sarofim MC, Webster M, Paltsev S, Schlosser CA, Kicklighter D, Dutkiewicz S, Reilly J, Wang C, Felzer B, Jacoby HD (2009) Probabilistic forecast for 21st century climate based on uncertainties in emissions (without policy) and climate parameters. *J Clim*. doi:10.1175/2009JCLI2863.1
- Solomon S, Plattner GK, Knutti R, Friedlingstein P (2009) Irreversible climate change due to carbon dioxide emissions. *Proc Natl Acad Sci USA* 106:1704–1709
- Somerville RCJ (2008) The forgiving air: understanding environmental change, 2nd edn. American Meteorological Society, Boston, MA, 224 pp
- Somerville RCJ (2010) How much should the public know about climate science? *Clim Change*. doi:10.1007/s10584-010-9938-y
- Thorne PW (2008) The answer is blowing in the wind. *Nat Geosci* 1:347–348
- Wentz FJ et al (2007) How much more rain will global warming bring? *Science* 317:233–235
- Zhang X, Zwiers FW, Hegerl GC, Lambert FH, Gillett NP, Solomon S, Stott PA, Nozawa T (2007) Detection of human influence on twentieth-century precipitation trends. *Nature* 448:461

Part II

Paleoclimate

Paleoclimate Implications for Human-Made Climate Change

James E. Hansen and Makiko Sato

Abstract

Paleoclimate data help us assess climate sensitivity and potential human-made climate effects. We conclude that Earth in the warmest interglacial periods of the past million years was less than 1°C warmer than in the Holocene. Polar warmth in these interglacials and in the Pliocene does not imply that a substantial cushion remains between today's climate and dangerous warming, but rather that Earth is poised to experience strong amplifying polar feedbacks in response to moderate global warming. Thus, goals to limit human-made warming to 2°C are not sufficient—they are prescriptions for disaster. Ice sheet disintegration is nonlinear, spurred by amplifying feedbacks. We suggest that ice sheet mass loss, if warming continues unabated, will be characterized better by a doubling time for mass loss rate than by a linear trend. Satellite gravity data, though too brief to be conclusive, are consistent with a doubling time of 10 years or less, implying the possibility of multimeter sea level rise this century. Observed accelerating ice sheet mass loss supports our conclusion that Earth's temperature now exceeds the mean Holocene value. Rapid reduction of fossil fuel emissions is required for humanity to succeed in preserving a planet resembling the one on which civilization developed.

Introduction

Climate change is likely to be the predominant scientific, economic, political, and moral issue of the twenty-first century. The fate of humanity and nature may depend upon early recognition and understanding of human-made effects on Earth's climate (Hansen 2009).

J.E. Hansen (✉)
NASA Goddard Institute for Space Studies and Columbia
University Earth Institute, New York, NY, USA
e-mail: jhansen@giss.nasa.gov

Tools for assessing the expected climate effects of alternative levels of human-made changes of atmospheric composition include (1) Earth's paleoclimate history, showing how climate responded to past changes of boundary conditions including atmospheric composition, (2) modern observations of climate change, especially global satellite observations, coincident with rapidly changing human-made and natural climate forcings, and (3) climate models and theory, which aid interpretation of observations on all time scales and are useful for projecting future climate under alternative climate forcing scenarios.

This chapter emphasizes use of paleoclimate data to help assess the dangerous level of human

interference with the atmosphere and climate. We focus on long-term climate trends of the Cenozoic Era and on Milankovitch (1941) glacial–interglacial climate oscillations. The Cenozoic encompasses a wide range of climates, including a planet without large ice sheets, and it allows study of greenhouse gases (GHGs) as both a climate forcing and feedback. Glacial–interglacial climate swings, because they are slow enough for Earth to be in near energy balance, allow us to determine accurately the “fast feedback” climate sensitivity to changing boundary conditions.

We first discuss Cenozoic climate change, which places Milankovitch and human-made climate change in perspective. We then use Milankovitch climate oscillations in a framework that accurately defines climate sensitivity to a natural or human-made climate forcing. We summarize how temperature is extracted from ocean cores to clarify the physical significance of this data record because, we will argue, ocean core temperature data have profound implications about the dangerous level of human-made interference with global climate. Finally, we discuss the temporal response of the climate system to the human-made climate forcing.

Cenozoic Climate Change

The Cenozoic Era, the time since extinction of dinosaurs at the end of the Cretaceous Era, illustrates the huge magnitude of natural climate change. The early Cenozoic was very warm—indeed, polar regions had tropical-like conditions with alligators in Alaska (Markwick 1998). There were no large ice sheets on the planet, so sea level was about 70 m higher than today.

Figure 1 shows estimated global deep ocean temperature in the Cenozoic, the past 65.5 million years. Deep ocean temperature is inferred from a global compilation of oxygen isotopic abundances in ocean sediment cores (Zachos et al. 2001), with temperature extracted from oxygen isotopes via the approximation of Hansen et al. (2008) as discussed below (section “What Is the Dangerous Level of Global Warming?”). (The data for the entire Cenozoic is available at <http://www.columbia.edu/~mhs119/TargetCO2>). Deep ocean temperature change is similar to global surface temperature change during the Cenozoic, we will argue,

until the deep ocean temperature approaches the freezing point of ocean water. Late Pleistocene glacial–interglacial deep ocean temperature changes (Fig. 1c) are only about two-thirds as large as global mean surface temperature changes (section “What Is the Dangerous Level of Global Warming?”).

Earth has been in a long-term cooling trend for the past 50 million years (Fig. 1a). By approximately 34 million years ago (Mya), the planet had become cool enough for a large ice sheet to form on Antarctica. Ice and snow increased the albedo (literally, the “whiteness”) of that continent, an amplifying feedback that contributed to the sharp drop of global temperature at that time. Moderate warming between 30 and 15 Mya was not sufficient to melt all Antarctic ice. The cooling trend resumed about 15 Mya and accelerated as the climate became cold enough for ice sheets to form in the Northern Hemisphere and provide their amplifying feedback.

The Cenozoic climate changes summarized in Fig. 1 contain insights and quantitative information relevant to assessment of human-made climate effects. Carbon dioxide (CO₂) plays a central role in both the long-term climate trends and the Milankovitch oscillations (Fig. 1b) that were magnified as the planet became colder and the ice sheets larger. Cenozoic climate change is discussed by Zachos et al. (2001), IPCC (2007), Hansen et al. (2008), and many others. We focus here on implications about the role of CO₂ in climate change and climate sensitivity.

CO₂ is the principal forcing that caused the slow Cenozoic climate trends. The total amount of CO₂ in surface carbon reservoirs (atmosphere, ocean, soil, and biosphere) changes over millions of years due to imbalance of the volcanic source and weathering sink and changes of the amount of carbon buried in organic matter. CO₂ is also a principal factor in the short-term climate oscillations that are so apparent in parts (b) and (c) of Fig. 1. However, in these glacial–interglacial oscillations, atmospheric CO₂ operates as a feedback: total CO₂ in the surface reservoirs changes little on these shorter time scales, but the distribution of CO₂ among the surface reservoirs changes as climate changes. As the ocean warms, for example, it releases CO₂ to the atmosphere, providing an amplifying climate feedback that causes further warming.

The fact that CO₂ is the dominant cause of long-term Cenozoic climate trends is obvious from Earth’s

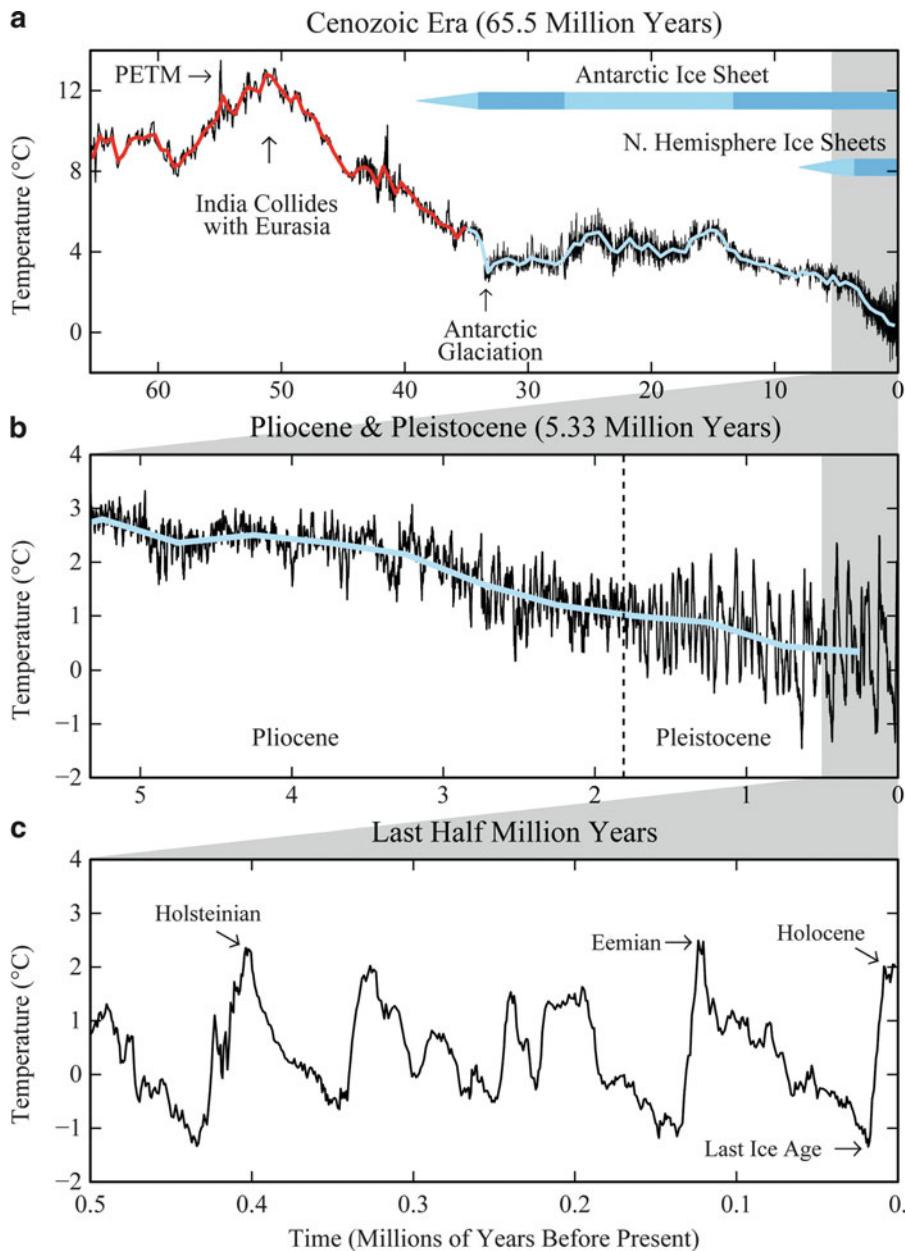


Fig. 1 Estimated Cenozoic global deep ocean temperature (a). Pliocene/Pleistocene is expanded in (b) and the last half million years in (c). High-frequency variations (*black*) are 5-point running means of original data (Zachos et al. 2001); *red* and *blue* curves have 500-kilo year resolution. PETM is the

Paleocene–Eocene Thermal Maximum. *Blue bars* indicate ice sheet presence, with *dark blue* for ice sheets near full size. Holsteinian and Eemian are known in paleoclimate literature as Marine Isotope Stages 11 and 5e

energy budget. Redistribution of energy in the climate system via changes of atmosphere or ocean dynamics cannot cause such huge climate change. Instead, a substantial global climate forcing is required. The climate forcing must be due to a change of energy coming into the planet or changes within the

atmosphere or on the surface that alter the planet’s energy budget.

Solar luminosity is increasing on long time scales, as our sun is at an early stage of solar evolution, “burning” hydrogen, forming helium by nuclear fusion, slowly getting brighter. The sun’s brightness

increased steadily through the Cenozoic, by about 0.4% according to solar physics models (Sackmann et al. 1993). Because Earth absorbs about 240 W/m^2 of solar energy, the 0.4% increase is a forcing of about 1 W/m^2 . This small linear increase of forcing, by itself, would have caused a modest global warming through the Cenozoic Era.

Continent locations affect Earth's energy balance, as ocean and continent albedos differ. However, most continents were near their present latitudes by the early Cenozoic (Blakey 2008; Fig. S9 of Hansen et al. 2008). Cloud and atmosphere shielding limit the effect of surface albedo change (Hansen et al. 2005), so this surface climate forcing did not exceed about 1 W/m^2 .

In contrast, atmospheric CO_2 during the Cenozoic changed from about 1,000 ppm in the early Cenozoic (Beerling and Royer 2011) to as small as 170 ppm during recent ice ages (Luthi et al. 2008). The resulting climate forcing, which can be computed accurately for this CO_2 range using formulae in Table 1 of Hansen et al. (2000), exceeds 10 W/m^2 . CO_2 was clearly the dominant climate forcing in the Cenozoic.

Global temperature change in the first half of the Cenozoic is consistent with expected effects of plate tectonics (continental drift) on atmospheric CO_2 . Subduction of ocean crust by an overriding tectonic plate causes crustal melt and metamorphism of the subducted plate and sediments, with release of volatiles including CO_2 . Carbon amount in surface reservoirs depends on the balance between this outgassing (via volcanoes and seltzer springs) from Earth's crust and burial in the crust, including change in the amount of buried organic matter (Bernier 2004). CO_2 outgassing occurs during subduction of oceanic crust and weathering (oxidation) of previously buried organic matter. Burial is via chemical weathering of rocks with deposition of carbonates on the ocean floor and burial of organic matter, some of which eventually may form fossil fuels.

Rates of outgassing and burial of CO_2 are each typically 10^{12} – 10^{13} mol C/year (Staudigel et al. 1989; Edmond and Huh 2003; Bernier 2004). Imbalance between outgassing and burial is limited by negative feedbacks in the geochemical carbon cycle (Bernier and Caldeira 1997), but a net natural imbalance of the order of 10^{12} mol C/year can be maintained on long time scales, as continental drift affects the rate of outgassing. Such an imbalance, after distribution

among surface reservoirs, is only ~ 0.0001 ppm/year of atmospheric CO_2 . That rate is negligible compared to the present human-made atmospheric CO_2 increase of ~ 2 ppm/year, yet in a million years such a consistent crustal imbalance can alter atmospheric CO_2 by ~ 100 ppm.

India was the only land area located far from its current location at the beginning of the Cenozoic. The Indian plate was still south of the equator, but moving northward at a rate of about 20 cm/year (Kumar et al. 2007), a rapid continental drift rate. The Indian plate moved through the Tethys Ocean, now the Indian Ocean, which had long been the depocenter for carbonate and organic sediments from major world rivers.

The strong global warming trend between 60 and 50 Mya was presumably a consequence of increasing atmospheric CO_2 , as the Indian plate subducted carbonate-rich ocean crust while traversing the Tethys Ocean (Kent and Muttoni 2008). The magnitude of the CO_2 source continued to increase until India crashed into Asia and began pushing up the Himalaya Mountains and Tibetan Plateau. Emissions from this tectonic source continue even today, but the magnitude of emissions began decreasing after the Indo-Asian collision and as a consequence the planet cooled. The climate variations between 30 and 15 Mya, when the size of the Antarctic ice sheet fluctuated, may have been due to temporal variations of plate tectonics and outgassing rates (Patriat et al. 2008). Although many mechanisms probably contributed to climate change through the Cenozoic Era, it is clear that CO_2 change was the dominant cause of the early warming and the subsequent long-term cooling trend.

Plate tectonics today is producing relatively little subduction of carbonate-rich ocean crust (Edmond and Huh 2003; Gerlach 2011), consistent with low Pleistocene levels of CO_2 (170–300 ppm) and the cool state of the planet, with ice sheets in the polar regions of both hemispheres. Whether Earth would have cooled further in the absence of humans,¹ on time scales of millions of years, is uncertain. But that is an academic

¹Paleoanthropological evidence of *Homo sapiens* in Africa dates to about 200,000 years ago, i.e., over two glacial cycles. Earlier human-like populations, such as Neanderthals and *Homo erectus*, date back at least 2,000,000 years, but, as is clear from Fig. 1a, even the human-like species were present only during the recent time of ice ages.

question. The rate of human-made change of atmospheric CO₂ amount is now much larger than slow geological changes. Humans now determine atmospheric composition, for better or worse, and they are likely to continue to do so, as long as the species survives.

The Cenozoic Era helps us determine the dangerous level of human-made climate change. However, implications of Cenozoic climate change become clearer if we first discuss empirical data on climate sensitivity provided by recent Milankovitch climate oscillations.

Climate Sensitivity

A climate forcing is an imposed perturbation of Earth's energy balance. Natural forcings include changes of solar irradiance and volcanic aerosols that scatter and absorb solar and terrestrial radiation. Human-made forcings include GHGs and tropospheric aerosols, i.e., aerosols in Earth's lower atmosphere, mostly in the lowest few kilometers.

A forcing, F , is measured in watts per square meter (W/m^2) averaged over the planet. For example, if the sun's brightness increases 1%, the forcing is $F \sim 2.4 \text{ W/m}^2$ because Earth absorbs about 240 W/m^2 of solar energy averaged over the planet's surface. If the CO₂ amount in the air is doubled,² the forcing is $F \sim 4 \text{ W/m}^2$. This CO₂ forcing is obtained by calculating its effect on the planetary energy balance with all other atmospheric and surface properties fixed. The CO₂ opacity as a function of wavelength is known from basic quantum physics and verified by laboratory measurements to an accuracy of a few percent. No climate model is needed to calculate the forcing. It requires only summing over the planet the change of heat radiation to space, which depends on known atmospheric and surface properties.

Climate sensitivity (S) is the equilibrium global surface temperature change (ΔT_{eq}) in response to a specified unit forcing after the planet has come back to energy balance,

$$S = \frac{\Delta T_{\text{eq}}}{F}, \quad (1)$$

i.e., climate sensitivity is the eventual (equilibrium) global temperature change per unit forcing.

Climate sensitivity depends upon climate feedbacks, the many physical processes that come into play as climate changes in response to a forcing. Positive (amplifying) feedbacks increase the climate response, while negative (diminishing) feedbacks reduce the response.

Climate feedbacks are the core of the climate problem. Climate feedbacks can be confusing because in climate analyses, what is sometimes a climate forcing is other times a climate feedback. As a preface to quantitative evaluation of climate feedbacks and climate sensitivity, we first make a remark about climate models and then briefly summarize Earth's recent climate history to provide specificity to the concept of climate feedbacks.

Climate models, based on physical laws that describe the structure and dynamics of the atmosphere and ocean, as well as processes on land, have been developed to simulate climate. Models help us understand climate sensitivity because we can change processes in the model one by one and study their interactions. But if models were our only tool, climate sensitivity would always have large uncertainty. Models are imperfect, and we will never be sure that they include all important processes. Fortunately, Earth's history provides a remarkably rich record of how our planet responded to climate forcings in the past. Paleoclimate records yield, by far, our most accurate assessment of climate sensitivity and climate feedbacks.

Now let us turn to a more general discussion of climate feedbacks, which determine climate sensitivity. Feedbacks do not come into play coincident with a forcing. Instead, they occur in response to climate change. It is assumed that, to a useful approximation, feedbacks affecting the global mean response are a function of global temperature change.

"Fast feedbacks" appear almost immediately in response to global temperature change. For example, as Earth becomes warmer, the atmosphere holds more water vapor. Water vapor is an amplifying fast feedback because water vapor is a powerful greenhouse gas. Other fast feedbacks include clouds, natural aerosols, snow cover, and sea ice.

² CO₂ climate forcing is approximately logarithmic because its absorption bands saturate as CO₂ amount increases. An equation for climate forcing as a function of CO₂ amount is given in Table 1 of Hansen et al. (2000).

“Slow feedbacks” may lag global temperature change by decades, centuries, millennia, or longer time scales. Principal slow feedbacks are surface albedo and long-lived GHGs. It thus turns out that slow feedbacks on millennial time scales are predominantly amplifying feedbacks. As a result, the feedbacks cause huge climate oscillations in response to minor perturbations of Earth’s orbit that alter the geographical and seasonal distribution of sunlight on Earth.

Surface albedo refers to continental reflectivity. Changes of ice sheet area, continental area, or vegetation cover affect surface albedo and temperature. Hydrologic effects associated with vegetation change also can affect global temperature. Numerical experiments (Hansen et al. 1984) indicate that ice sheet area is the dominant surface feedback in glacial to interglacial climate change, so ice sheet area is a useful proxy for the entire slow surface feedback in Pleistocene climate variations. Surface albedo is an amplifying feedback because the amount of solar energy absorbed by Earth increases when ice and snow area decreases.

GHGs are also an amplifying feedback on millennial time scales, as warming ocean and soils drive more CO₂, CH₄, and N₂O into the air. This GHG feedback exists because the atmosphere exchanges carbon and nitrogen with other surface reservoirs (ocean, soil, and biosphere).

Negative carbon cycle feedbacks occur, especially on long time scales, via exchange of carbon with the solid earth (Berner 2004; Archer 2005). Chemical weathering of rocks, with deposition of carbonates on the ocean floor, slowly removes from surface reservoirs CO₂ that is in excess of the amount in equilibrium with natural tectonic (volcanic) CO₂ sources. Weathering is thus a diminishing feedback. Unfortunately, the weathering feedback is substantial only on millennial and longer time scales, so it does not alter much the human-made perturbation of atmospheric CO₂ on time scales that are of most interest to humanity.

Milankovitch Climate Oscillations

The glacial–interglacial climate oscillations manifest in Fig. 1b, c, which grow in amplitude through the Pliocene and Pleistocene, are often referred to as

Milankovitch climate oscillations. Milankovitch (1941) suggested that these climate swings occur in association with periodic perturbations of Earth’s orbit by other planets (Berger 1978) that alter the geographical and seasonal distribution of insolation over Earth’s surface.

The varying orbital parameters are (1) tilt of Earth’s spin axis relative to the orbital plane, (2) eccentricity of Earth’s orbit, and (3) day of year when Earth is closest to the sun, also describable as precession of the equinoxes (Berger 1978). These three orbital parameters vary slowly, the dominant time scales being close to 40,000; 100,000; and 20,000 years, respectively.

Hays et al. (1976) confirmed that climate oscillations occur at the frequencies of the periodic orbital perturbations. Wunsch (2003) showed that the dominant orbital frequencies account for only a fraction of total long-term climate variability. That result is not surprising given the small magnitude of the orbital forcing. The orbital forcing, computed as the global-mean annual-mean perturbation of absorbed solar radiation with fixed climate, is less than ± 0.25 W/m² (Fig. S3 of Hansen et al. 2008). Climate variability at other frequencies in the observational data is expected because orbital changes are more complex than three discrete time scales and because the dating of observed climate variations is imprecise. But it is clear that a large global climate response to the weak orbital forcing does exist (Roe 2006), demonstrating that climate is very sensitive on millennial time scales and implying that large amplifying feedbacks exist on such time scales. Thus, large climate change should also be expected in response to other weak forcings and climate noise (chaos).

A satisfactory quantitative interpretation of how each orbital parameter alters climate has not yet been achieved. Milankovitch argued that the magnitude of summer insolation at high latitudes in the Northern Hemisphere was the key factor determining when glaciation and deglaciation occurred. Huybers (2006) points out that insolation integrated over the summer is affected only by axial tilt. Hansen et al. (2007a) argue that late spring (mid-May) insolation is the key because early “flip” of ice sheet albedo to a dark wet condition produces a long summer melt season; they buttress this argument with data for the timing of the last two deglaciations (termination I 13,000–14,000 years ago and termination II about 130,000 years ago).

Fortunately, it is not necessary to have a detailed quantitative theory of the ice ages in order to extract vitally important information. In the following section, we show that Milankovitch climate oscillations provide our most accurate assessment of climate sensitivity.

Fast-Feedback Climate Sensitivity

Fast-feedback climate sensitivity can be determined precisely from paleoclimate data for recent glacial–interglacial climate oscillations. This is possible because we can readily find times when Earth was in quasi-equilibrium with its “boundary forcings.” Boundary forcings are factors that affect the planet’s energy balance, such as solar irradiance, continental locations, ice sheet distribution, and atmospheric amount of long-lived GHGs (CO_2 , CH_4 , and N_2O).

Quasi-equilibrium means Earth is in radiation balance with space within a small fraction of 1 W/m^2 . For example, the mean planetary energy imbalance was small averaged over several millennia of the Last Glacial Maximum (LGM, which peaked about 20,000 years ago) or averaged over the Holocene (prior to the time of large human-made changes). This assertion is proven by considering the contrary: a sustained imbalance of 1 W/m^2 would have melted all ice on Earth or changed ocean temperature a large amount, neither of which occurred.

The altered boundary conditions that maintained the climate change between these two periods had to be changes on Earth’s surface and changes of long-lived atmospheric constituents, because the incoming solar energy does not change much in 20,000 years. Changes of long-lived GHGs are known accurately for the past 800,000 years from Antarctic ice core data (Luthi et al. 2008; Loulergue et al. 2008). Climate forcings due to GHG and surface albedo changes between the LGM and Holocene were approximately 3 and 3.5 W/m^2 , respectively, with largest uncertainty ($\pm 1 \text{ W/m}^2$) in the surface change (ice sheet area, vegetation distribution, shoreline movement) due to uncertainty in ice sheet sizes (Hansen et al. 1984; Hewitt and Mitchell 1997).

Global mean temperature change between the LGM and Holocene has been estimated from paleotemperature data and from climate models constrained by paleodata. Shakun and Carlson (2010)

obtain a data-based estimate of 4.9°C for the difference between the Altithermal (peak Holocene warmth, prior to the past century) and peak LGM conditions. They suggest that this estimate may be on the low side mainly because they lack data in some regions where large temperature change is likely, but their record is affected by LGM cooling of 17°C on Greenland. A comprehensive multimodel study of Schneider von Deimling et al. (2006) finds a temperature difference of $5.8 \pm 1.4^\circ\text{C}$ between LGM and the Holocene, with this result including the effect of a prescribed LGM aerosol forcing of -1.2 W/m^2 . The appropriate temperature difference for our purpose is between average Holocene conditions and LGM conditions averaged over several millennia. We take $5 \pm 1^\circ\text{C}$ as our best estimate. Although the estimated uncertainty is necessarily partly subjective, we believe it is a generously (large) estimate for 1σ uncertainty.

The empirical fast-feedback climate sensitivity that we infer from the LGM–Holocene comparison is thus $5^\circ\text{C}/6.5 \text{ W/m}^2 \sim \pm 1/4^\circ\text{C}$ per W/m^2 or $3 \pm 1^\circ\text{C}$ for doubled CO_2 . The fact that ice sheet and GHG boundary conditions are actually slow climate feedbacks is irrelevant for the purpose of evaluating the fast-feedback climate sensitivity.

This empirical climate sensitivity incorporates all fast-response feedbacks in the real-world climate system, including changes of water vapor, clouds, aerosols, aerosol effects on clouds, and sea ice. In contrast to climate models, which can only approximate the physical processes and may exclude important processes, the empirical result includes all processes that exist in the real world—and the physics is exact.

If Earth were a blackbody without climate feedbacks, the equilibrium response to 4 W/m^2 forcing would be about 1.2°C (Hansen et al. 1981, 1984; Lacis et al. 2010), implying that the net effect of all fast feedbacks is to amplify the equilibrium climate response by a factor 2.5. GISS climate models suggest that water vapor and sea ice feedbacks together amplify the sensitivity from 1.2°C to $2\text{--}2.5^\circ\text{C}$. The further amplification to 3°C is the net effect of all other processes, with the most important ones probably being aerosols, clouds, and their interactions.

The empirical sensitivity $3 \pm 1^\circ\text{C}$ for doubled CO_2 is consistent with the Charney et al. (1979) estimates of $3 \pm 1.5^\circ\text{C}$ for doubled CO_2 and with the range of model results, $2.1\text{--}4.4^\circ\text{C}$, in the most recent IPCC

report (Randall and Wood 2007). However, the empirical result is more precise, and we can be sure that it includes all real-world processes. Moreover, by examining observed climate change over several Milankovitch oscillations, we can further improve the accuracy of the fast-feedback climate sensitivity.

Figure 2 shows atmospheric CO₂ and CH₄ and sea level for the past 800,000 years and resulting calculated climate forcings. Sea level implies the total size of the major ice sheets, which thus defines the surface albedo forcing as described by Hansen et al. (2008). Note that calculation of climate forcings due to GHG and ice sheet changes is a radiative calculation; it does not require use of a global climate model. Clouds and other fast-feedback variables are fixed with modern distributions. We do not need to know paleoclouds and aerosols, because the changes of those quantities at earlier climates are in the fast feedback being evaluated.

Multiplying the sum of greenhouse gas and surface albedo forcings by climate sensitivity °C per W/m² yields the predicted global temperature change (blue curves in Fig. 2d, e). Observed temperature change in Fig. 2d is from Dome C in Antarctica (Jouzel et al. 2007). The global deep ocean temperature record in Fig. 2e is from data of Zachos et al. (2001), with temperature extracted from oxygen isotope data as described below and by Hansen et al. (2008).

Observed Antarctic and deep ocean temperature changes have been multiplied by factors (0.5 and 1.5, respectively) to yield observed LGM–Holocene global temperature change of 5°C. Climate sensitivity °C per W/m² provides a good fit to the entire 800,000 years. An exception is Dome C during the warmest interglacial periods, when warming was greater than calculated. We show in section “What Is the Dangerous Level of Global Warming?” that peak interglacial warming was probably confined to the ice sheets, so deep ocean temperature change provides a better indication of global temperature change.

The close fit of observed and calculated temperatures for 800,000 years includes multiple tests and thus reduces uncertainty of the implied climate sensitivity. The greatest uncertainty is in the actual global temperature changes. Including our partly subjective estimate of uncertainty, our inferred climate sensitivity is $3 \pm 0.5^\circ\text{C}$ for doubled CO₂ ($3/4 \pm 1/8^\circ\text{C}$ per W/m²).

Regardless of the exact error bar, this empirically derived fast-feedback sensitivity has a vitally important characteristic: it incorporates all real-world fast-feedback processes. No climate model can make such a claim.

Charney Climate Sensitivity and Aerosols

The high precision of the empirical fast-feedback climate sensitivity seems to be at odds with many other climate sensitivity estimates in the scientific literature. Explanation requires background information and clarification of terminology.

Charney et al. (1979), in an early study of climate sensitivity, focused on climate change on the century time scale. Ice sheets were assumed to be fixed, and changes of long-lived GHGs were taken as specified climate forcings. In reality, long-lived GHGs are altered by climate change, i.e., there is a GHG feedback effect, but Charney assumed that the feedback change of GHGs would be calculated or estimated separately. This approach, treating ice sheets and long-lived GHGs as fixed boundary conditions or forcings, is an invaluable gedanken experiment and analysis approach, as we have discussed in this chapter—even though we know that ice sheets and GHGs will begin to change in response to climate change well before a new fast-feedback climate equilibrium can be achieved.

Charney et al. (1979) used climate models to estimate climate sensitivity. The models included fast feedbacks due to changes of water vapor, clouds, and sea ice, but not other fast feedbacks such as changes of aerosols and tropospheric ozone. This landmark study has provided guidance for further studies for decades. But unfortunately, the terminology “Charney sensitivity” has come to be used for multiple definitions of climate sensitivity. Does Charney sensitivity include all fast feedbacks, as we have above, or does it include only the fast feedbacks in the models employed in the Charney study?

Specifically, are glacial–interglacial aerosol changes considered to be a boundary forcing or a fast feedback? In models, it is possible, and useful, to turn individual feedbacks on or off—but it is necessary to make clear which feedbacks are included. Similarly, when climate sensitivity is inferred empirically from records of past

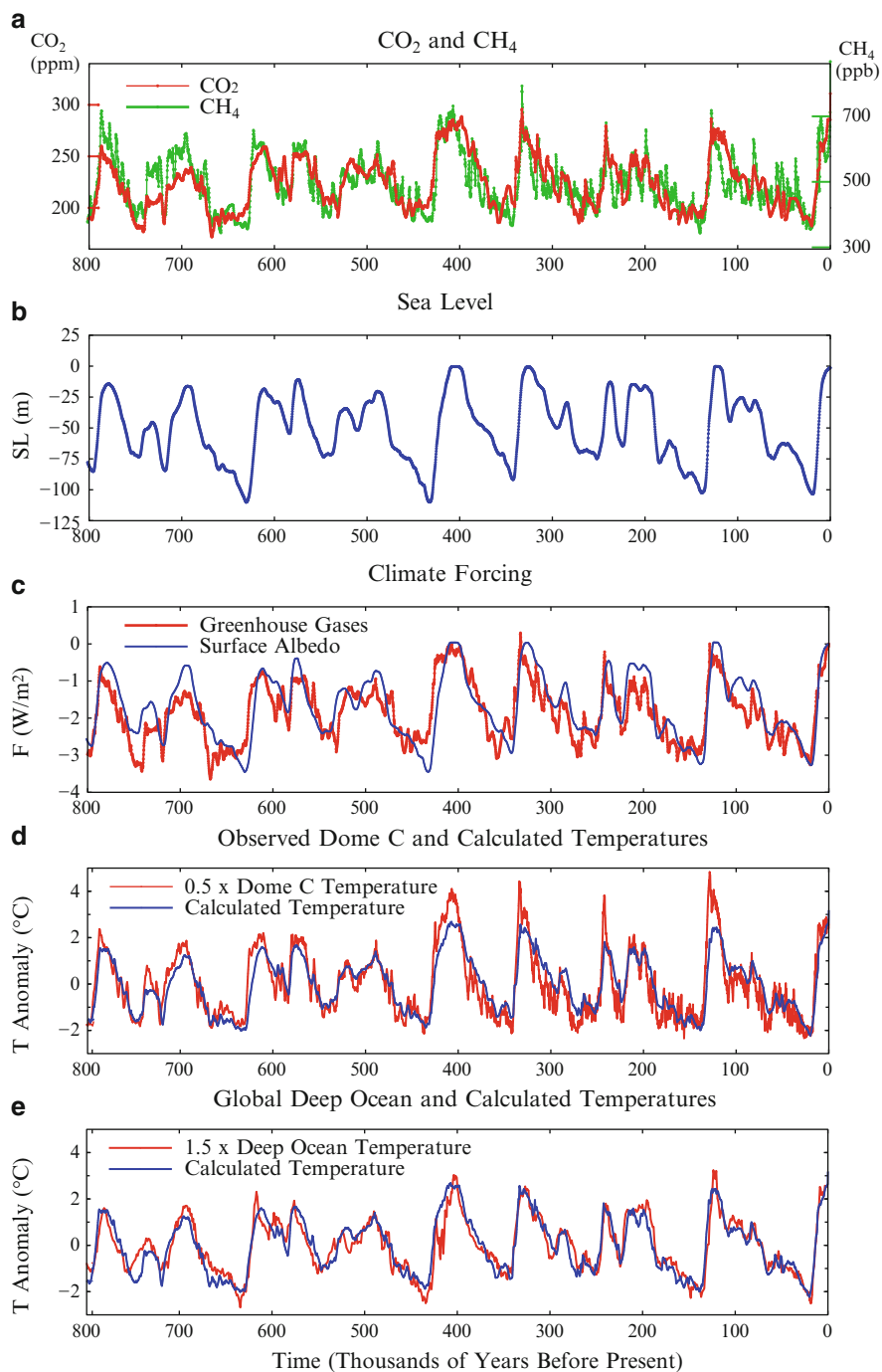


Fig. 2 (a) CO₂ (Luthi et al. 2008) and CH₄ (Loulergue et al. 2008) for past 800,000 years, (b) sea level (Bintanja et al. 2005), (c) resulting climate forcings, (d, e) calculated global temperature anomalies compared with 0.5 × Antarctic Dome C and

1.5 × deep ocean temperatures. Calculations are the product of the forcing and sensitivity °C per W/m². Anomalies are relative to the 800,000-year mean

climate change, it is essential to define which boundary conditions have been defined as climate forcings.

Moreover, the *all* fast-feedback climate sensitivity has special importance. First, observed climate change necessarily includes all fast feedbacks. Second, it is only the all fast-feedback climate sensitivity that can be derived precisely from paleoclimate records.

Unfortunately, Hansen et al. (1984) chose to estimate climate sensitivity from paleoclimate data by treating the aerosol change between glacial and interglacial conditions as a forcing. There is nothing inherently wrong with asking the question: what is the sensitivity of the remaining processes in the system if we consider ice sheets, GHGs, and aerosols to be specified forcings, even though the ice sheets and GHGs are slow feedbacks and aerosol changes are a fast feedback. The problem is that it is impossible to get an accurate answer to that question. The aerosol forcing depends sensitively on aerosol absorption (the aerosol single scatter albedo) and on the altitude distribution of the aerosols, but worse, it depends on how the aerosols modify cloud properties. The large uncertainty in the value of the aerosol forcing causes the resulting empirical climate sensitivity to have a large error bar.

Chylek and Lohmann (2008), for example, estimate the aerosol forcing between the Last Glacial Maximum and the Holocene to be 3.3 W/m^2 , and they thus infer that climate sensitivity for doubled CO_2 is $1.8 \pm 0.5^\circ\text{C}$ for doubled CO_2 . With the same approach, but assuming a dust forcing of 1.9 W/m^2 , Kohler et al. (2010) conclude that climate sensitivity is in the range $1.4\text{--}5.2^\circ\text{C}$ for doubled CO_2 . Both of these studies consider only dust aerosols, so other aerosols are implicitly treated as a climate feedback. Neither study includes aerosols such as black soot, organic particles, and dimethyl sulfide (Charlson et al. 1987), whose changes are potentially significant on paleoclimate time scales. Furthermore, neither study includes aerosol indirect forcings, i.e., the effect of aerosols on cloud albedo and cloud cover. IPCC (2007) estimates that the aerosol indirect forcings exceed the direct aerosol forcing, but with a very large uncertainty.

Thus, interpretation of an empirical climate sensitivity that treats natural aerosol changes as a forcing is complex, and the error bar on the derived sensitivity is necessarily large.

Also an empirical climate sensitivity that mixes fast and slow processes is less useful for climate analyses. Ice sheet change and natural CO_2 change are necessarily slow, while aerosol amount and composition adjust rapidly to climate change. Of course, there are aerosol changes on long time scales; for example, some periods are dustier than others. But these aerosol changes are analogous to the cloud changes that occur between climates with or without an ice sheet. Changed surface conditions (e.g., ice sheet area, vegetation cover, land area, and continental shelf exposure) cause clouds and aerosols to exhibit changes over long time scales, but the adjustment time of clouds and aerosols to surface conditions is fast.

Clearly, aerosol changes should be included as part of the fast-feedback processes in most climate analyses. It makes sense to pull aerosols out of the fast feedbacks only when one is attempting to evaluate the specific contribution of aerosols to the net all-fast-feedback sensitivity. But with such a separation, it must be recognized that the error bars will be huge.

Henceforth, by fast-feedback climate sensitivity, S_{ff} , we refer to the all fast-feedback sensitivity. S_{ff} is thus the fast-feedback sensitivity that we estimated from empirical data to be

$$S_{\text{ff}} = 0.75 \pm 0.125^\circ\text{C per W/m}^2, \quad (2)$$

which is equivalent to $3 \pm 0.5^\circ\text{C}$ for doubled CO_2 . High precision is possible for fast-feedback climate sensitivity because GHG amount is known accurately, sea level is known within 20 m, and conversion of sea level change to surface albedo forcing between glacial and interglacial states is not very sensitive to sea level uncertainties (Hansen et al. 2008).

Climate sensitivity studies that include aerosols as a boundary forcing should use specific appropriate nomenclature. For example, $S_{\text{ff} - \text{a}}$ can be used to indicate that aerosols are not included in the fast feedbacks. However, it is also necessary to define which aerosols are included as boundary forcings and whether indirect aerosol forcings are included as part of the boundary forcing. Studies evaluating $S_{\text{ff} - \text{a}}$ can also readily report the implied value for the fast-feedback climate sensitivity, S_{ff} . It would be helpful if the information were included for the sake of clarity and comparison with other studies.

If the terminology “Charney sensitivity” is to be retained, we suggest that it be reserved for the fast-feedback sensitivity, S_{ff} . This all fast-feedback sensitivity is the logical building block for climate sensitivity on longer time scales as successive slow processes are added.

Slow Climate Feedbacks

Figure 2 shows that glacial-to-interglacial global temperature change is accounted for by changing GHGs and surface albedo. Changes of these boundary forcings affect Earth’s temperature by altering the amount of sunlight absorbed by the planet and the amount of heat radiated to space. However, the millennial climate swings were not initiated by GHG and surface albedo changes. Changes of these two boundary forcings were slow climate feedbacks that magnified the climate change. This role is confirmed by the fact that temperature turning points precede the GHG and surface albedo maxima and minima (Mudelsee 2001). This sequencing is as expected. For example, as the climate warms, it is expected that the area of ice and snow will decline, and it is expected that the ocean and continents will release GHGs.

Figure 3 examines the relation of GHG and surface albedo boundary forcings with global temperature during the past 800,000 years. Each dot is a 1,000-year mean temperature anomaly (relative to the most recent 1,000 years) plotted against total (GHG + surface albedo) forcing in the upper row, against GHG forcing in the middle row, and against surface albedo forcing in the bottom row. (Surface albedo forcing was computed using the nonlinear two-ice-sheet model shown in Fig. S4 of Hansen et al. 2008, but results were indistinguishable for the linear model in that figure.) Temperatures in the left column are from the Dome C Antarctic ice core (Jouzel et al. 2007). Temperatures in the right column are from ocean sediment cores (see section “What Is the Dangerous Level of Global Warming?”).

Dome C temperatures are multiplied by 0.5 and deep ocean temperatures by 1.5 in Fig. 3 so that resulting temperatures approximate global mean temperature. These scale factors were chosen based on the LGM–Holocene global temperature change, as discussed above.

Figure 3 reveals that the GHG and surface albedo feedbacks increase approximately linearly as a function of global temperature. Moderate nonlinearity of the Dome C temperature, i.e., the more rapid increase of temperature as it approaches the modern value, confirms our contention that deep ocean temperature is a better measure of global temperature change than Antarctic temperature. That conclusion is based on the fact that the temperature changes in Fig. 3 are a result of the fast-feedback climate change that is maintained by the changing boundary forcings (GHG amount and ice sheet area). Fast-feedback climate sensitivity is nearly linear until Earth approaches either the snowball Earth or runaway greenhouse climate states (Fig. S2 of Hansen et al. 2008). The upturn of Dome C temperatures as a function of boundary forcing is not an indication that Earth is approaching a runaway greenhouse effect. Instead, it shows that the Dome C temperature does not continue to be proportional to global mean temperature by a constant factor when Earth is near present day and higher temperatures.

The conclusion that Dome C temperature change cannot be taken today as simply proportional to global temperature change has practical implications. One implication, discussed in section “Discussion,” is that a target of 2°C for limiting human-made climate change is too high. We must check the sea level record (Fig. 2b) used to obtain surface albedo forcing because that sea level curve is based in part on an ice sheet model (Bintanja et al. 2005). The ice sheet model helps separate contributions of ice volume and deep ocean temperature, which both affect the oxygen isotope record in ocean sediment cores. Our reason for caution is that ice sheet models may be too lethargic, responding more slowly to climate change than real-world ice sheets (Hansen 2005, 2007; Hansen et al. 2007a). We use the Bintanja et al. (2005) sea level data set because it is reasonably consistent with several other sea level data records for the past 400,000 years that do not depend on an ice sheet model (Fig. 2a of Hansen et al. 2007a), and it provides a data set that covers the entire 800,000 years of the Dome C Antarctica record. However, there is one feature in the surface albedo vs. temperature scatter plots (Fig. 3e, f) that seems unrealistic: the tail at the warmest temperatures, where warming of 1°C produces no change of sea level or surface albedo.

Our check consists of using an independent sea level record based on water residence times in the

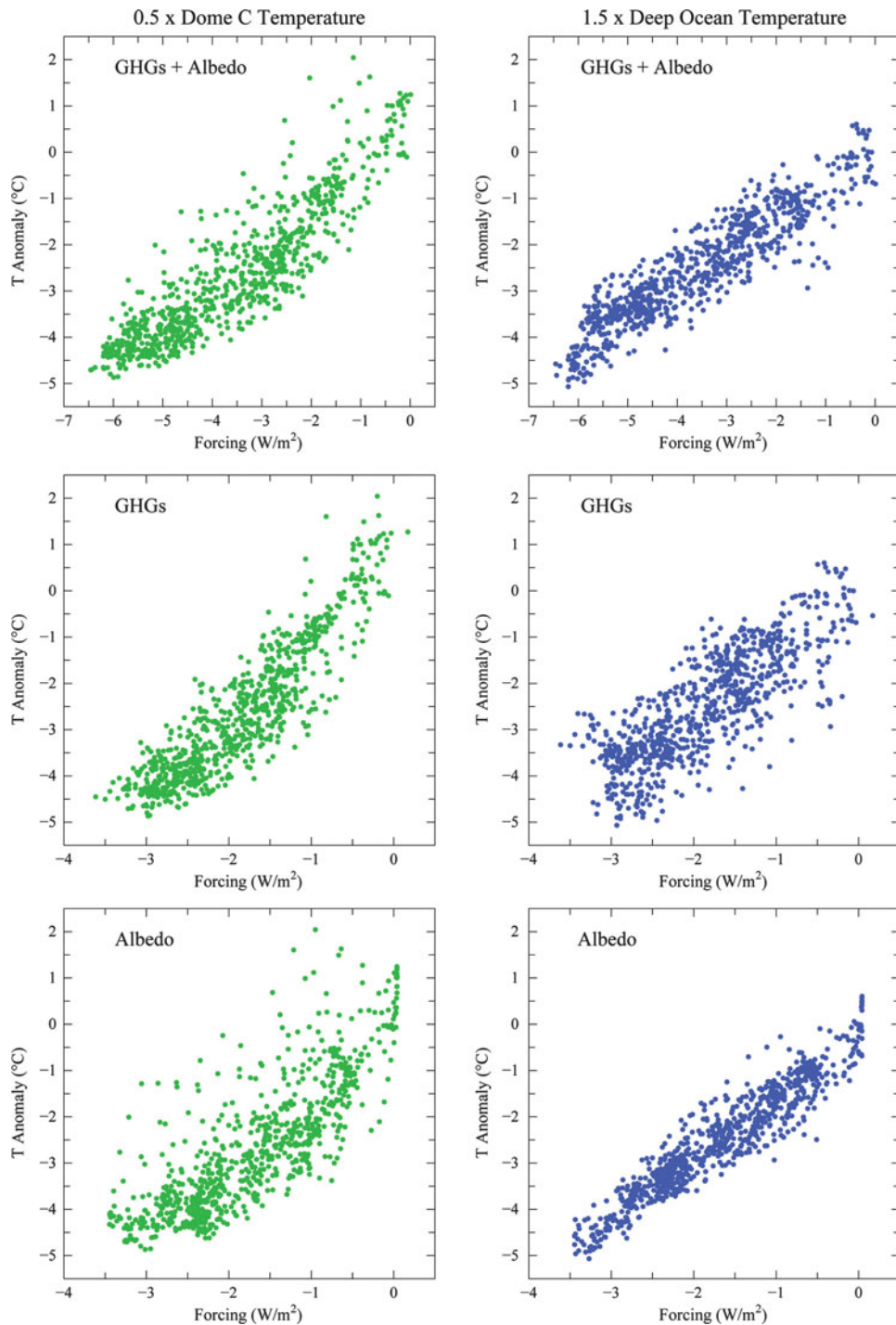


Fig. 3 Dome C and deep ocean temperature plotted vs. GHG and surface albedo forcings for nominally the same time. Each point is a 1,000-year mean from the past 800,000 years (see text)

Red Sea (Siddall et al. 2003). The Siddall et al. data are compared with other sea level records in Fig. 2 of Hansen et al. (2007a) and with GHG and temperature

records in Fig. 1 of Hansen et al. (2008). The Siddall et al. (2003) data necessarily cause the scatter plot (surface albedo vs. deep ocean temperature) to become

noisier because of inherent imprecision in matching the different time scales of deep ocean temperature and sea level from Red Sea data, but that increased scatter does not obviate the check that we seek.

Figure 4 confirms the principal characteristic of the Bintanja et al. 2005 sea level data set, a nearly linear relation between deep ocean temperature and sea level. Figure 4 also confirms our suspicion that the absence of significant sea level response to temperature increase at current temperatures is an artifact, suggesting that the ice sheet model is excessively lethargic. The data not affected by an ice sheet model (Fig. 4b) give no indication of a change in the linear relation of about 20 m equilibrium sea level rise for each 1°C increase of global mean temperature.

Climate Sensitivity Including Slow Feedbacks

Climate sensitivity including slow feedbacks is now frequently described as “Earth system sensitivity” (Lunt et al. 2010; Pagani et al. 2010; Park and Royer 2011; Royer et al. 2011), but not always with the same definition. There are merits in alternative choices for which feedbacks are included, but the choice needs to be precisely defined. Otherwise, values inferred for Earth system sensitivity may be ambiguous and yield a greater range than dictated by the physics.

We suggest that it is useful to define additional climate sensitivities that build on the fast-feedback sensitivity, S_{ff} , via sequential addition of slow feedback processes. We focus first on climate sensitivity combining fast feedbacks and slow surface change, S_{ff+sur} .

S_{ff+sur} can be evaluated empirically from documented climate changes. Sensitivity S_{ff+sur} is useful for cases in which atmospheric GHG changes are known. We note two specific cases.

One case in which S_{ff+sur} is useful is the era of human-made climate change. Past GHG amounts are known from ice core data and in situ measurements, and future GHG changes can be estimated from GHG emission scenarios and carbon cycle calculations. A portion of the GHG change is due to slow climate feedbacks, but by specifying observed GHG amounts, the GHG effect is included precisely. This approach improves the prospect of assessing other contributions to climate sensitivity, including the surface climate feedback.

A second case in which S_{ff+sur} is useful is CO₂ change over millions of years due to plate tectonics. Such long-term CO₂ changes, which can be estimated from proxy CO₂ measures (Beerling and Royer 2011) or carbon cycle models (Berner 2004), are a climate forcing, an imposed perturbation of the planet’s energy balance.

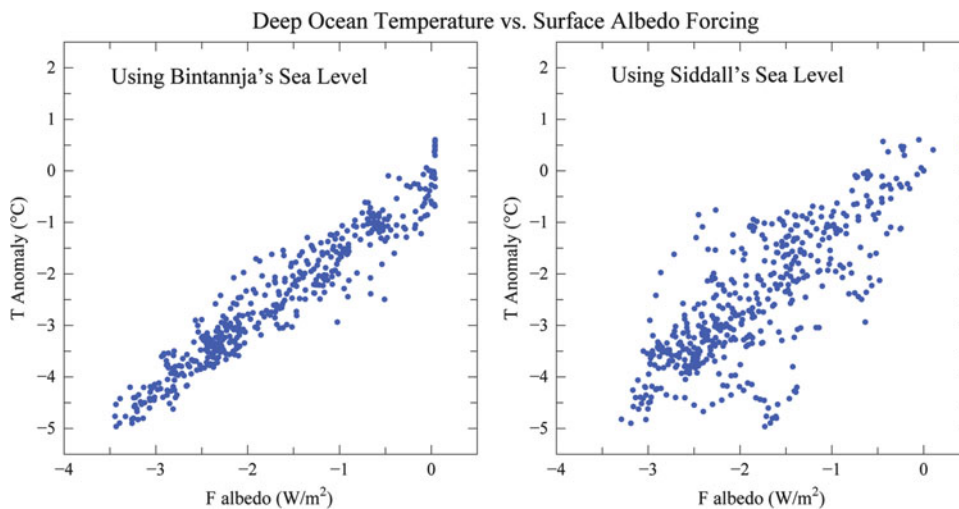


Fig. 4 Deep ocean temperature anomalies for the past 470,000 years relative to the past millennium. Each point is the average anomaly over 1,000 years plotted against the surface albedo

climate forcing calculated from sea level records of Bintanja et al. (2005) for the same 1,000 years. Deep ocean anomalies are multiplied by 1.5 to approximate global temperature anomalies

Specifically, let us consider CO₂ changes during the Cenozoic Era. Earth was so warm in the early Cenozoic (Fig. 1) that there were no large ice sheets. But long-term cooling began about 50 Mya, and by about 34 Mya, a large ice sheet formed on Antarctica. After further global cooling, ice sheets formed in the Northern Hemisphere during the past several million years. An increasing amplitude of temperature oscillations accompanied increasingly large ice sheets in the Pliocene and Pleistocene (Fig. 1b).

Ice sheet changes in the Cenozoic make it clear that climate sensitivity including slow feedbacks is a strong function of the climate state. The growing amplitude of glacial–interglacial oscillations in the Pliocene–Pleistocene is due to an increasing surface albedo feedback. But surface albedo feedback vanishes as the ice sheets disappear. It follows that climate sensitivity $S_{\text{ff} + \text{sur}}$ is a function of climate state and the sign (positive or negative) of the climate forcing.

$S_{\text{ff} + \text{sur}}$ is $\sim 1.5^\circ\text{C}$ per W/m^2 (6°C for doubled CO₂) during the Pleistocene (Hansen et al. 2008). That conclusion is obvious from Fig. 3, which shows that the GHG and surface albedo, as boundary forcings, contribute equally to global temperature change. With both of them considered as boundary forcings, the fast-feedback sensitivity is 3°C for doubled CO₂. But with GHGs considered to be a forcing, the sensitivity becomes 6°C for doubled CO₂.

Sensitivity $S_{\text{ff} + \text{sur}} \sim 1.5^\circ\text{C}$ per W/m^2 does not necessarily apply to positive forcings today, because present climate is near the warm extreme of the Pleistocene range. The decreasing amplitude of glacial–interglacial temperature oscillations between the late Pleistocene and Pliocene (Fig. 1b) suggests a substantially smaller $S_{\text{ff} + \text{sur}}$ for the Holocene–Pliocene climate change than for the Holocene–LGM climate change. Hansen et al. (2008) show that the mean $S_{\text{ff} + \text{sur}}$ for the entire range from the Holocene to a climate just warm enough to lose the Antarctic ice sheet is almost 1.5°C per W/m^2 . But most of the surface albedo feedback in that range of climate is associated with loss of the Antarctic ice sheet. Thus, the estimate of Lunt et al. (2010) that S_{ff} is increased by a factor of 1.3–1.5 by slow surface feedbacks (reduced ice and increased vegetation cover) for the climate range from the Holocene to the middle Pliocene is consistent with the Hansen et al. (2008) estimate for the mean $S_{\text{ff} + \text{sur}}$ between 34 Mya and today.

Another definition of Earth system sensitivity with merit is the sensitivity to CO₂ change, with accompanying natural changes of non-CO₂ GHG changes counted as feedbacks. We could call this the $\text{ff} + \text{sur} + \text{ghg}$ sensitivity ($\text{ghg} = \text{GHG} - \text{CO}_2$), but for brevity, we suggest S_{CO_2} . This sensitivity has the merit that CO₂ is the principal GHG forcing and perhaps the only one with good prospects for quantification of its long-term changes. It is likely that non-CO₂ trace gases increase as global temperature increases, as found in chemical modeling studies (Beerling et al. 2009, 2011). Non-CO₂ GHGs contributed $0.75 \text{ W}/\text{m}^2$ of the LGM–Holocene forcing, thus amplifying CO₂ forcing ($2.25 \text{ W}/\text{m}^2$) by one-third (Sect. S1 of Hansen et al. 2008). GHG and surface boundary forcings covaried 1-to-1 in the late Pleistocene as a function of temperature (Fig. 5). Thus, if non-CO₂ trace gases are counted as a fast feedback, the fast-feedback sensitivity becomes 4°C for doubled CO₂, and S_{CO_2} becomes 1°C per W/m^2 , for the planet without ice sheets (no slow surface albedo feedback). S_{CO_2} from the Holocene as initial state is thus 8°C for doubled CO₂ and 2°C per W/m^2 for negative forcings; S_{CO_2} is smaller for a positive forcing, but it is nearly that large for a positive forcing just large enough to melt the Antarctic ice sheet. S_{CO_2} is the definition of Earth system sensitivity used by Royer et al. (2011), which substantially accounts for the high sensitivities that they estimate.

When climate sensitivity is inferred empirically from long-term climate change and GHG changes, it is necessary to include the effect of other changing boundary forcings, such as solar irradiance and continental locations, if the changes are substantial. However, such changes are negligible for a rapid change of GHGs as in the Paleocene-Eocene Thermal Maximum.

The ultimate Earth system sensitivity is $S_{\text{ff} + \text{sf}}$, the sensitivity including all fast and slow feedbacks, i.e., surface feedbacks and all GHG feedbacks including CO₂. $S_{\text{ff} + \text{sf}}$ is relevant to changing solar irradiance, for example. Apparently, $S_{\text{ff} + \text{sf}}$ is remarkably large in the late Pleistocene. However, the extreme sensitivity implied by late Pleistocene climate oscillations was associated with a cooling climate that caused the surface (ice sheet) albedo feedback to be the largest it has been since perhaps the early Permian, about 300 Mya (Royer 2006). Given human-made GHGs, including movement of fossil carbon into surface reservoirs, the

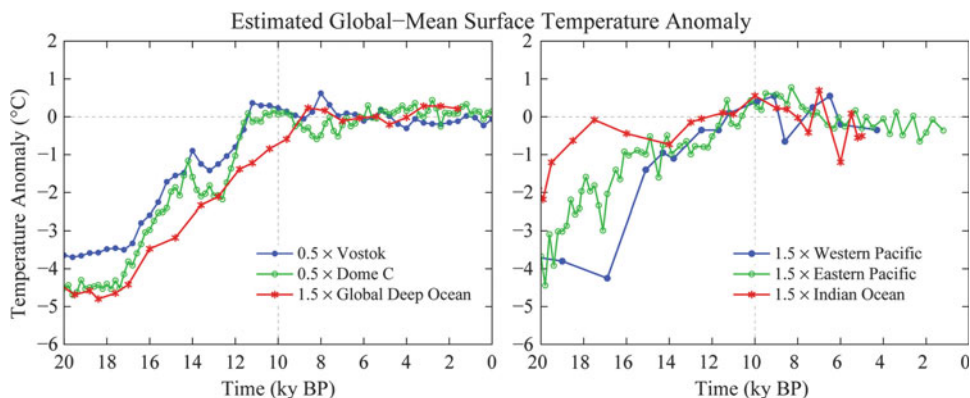


Fig. 5 Estimates of global temperature change inferred from Antarctic ice cores (Vimeux et al. 2002; Jouzel et al. 2007) and ocean sediment cores (Medina-Elizade and Lea 2005; Lea et al.

2000, 2006; Saraswat et al. 2005). Zero-point temperature is the mean for the past 10-kilo years

extreme $S_{ff + sf}$ of the late Pleistocene will not be relevant as long as humans exist.

In principle, $S_{ff + sf}$ is relevant for interpretation of past climate change due to Earth orbital forcing. However, Earth orbital forcing is subtle and complex. Useful applications will require definition of an appropriate effective forcing, i.e., a forcing that incorporates the efficacy (Hansen et al. 2005) of the orbital forcing as a function of latitude and season.

In conclusion, which sensitivity, if any, deserves the moniker “Earth system sensitivity”? From an academic perspective, $S_{ff + sf}$ is probably the best choice. From a practical perspective, S_{ff} and $S_{ff + sur}$ are both needed for analysis of human-made climate change. From a paleoclimate perspective, S_{CO_2} is very useful. So there is more than one useful choice. The important point is to make clear exactly what is meant. And remember to specify the reference climate state. Table 1 summarizes alternative climate sensitivities.

What Is the Dangerous Level of Global Warming?

Paleoclimate data yield remarkably rich and precise information on climate sensitivity. We suggest that paleoclimate data on climate change and climate sensitivity can be pushed further to yield an accurate evaluation of the dangerous level of global warming.

Broad-based assessments, represented by a “burning embers” diagram in IPCC (2001, 2007), suggested that major problems begin with global warming of 2–3°C relative to global temperature in year 2000. Sophisticated probabilistic analyses (Schneider and Mastrandrea 2005) found a median “dangerous” threshold of 2.85°C above global temperature in 2000, with the 90% confidence range being 1.45–4.65°C.

The IPCC analyses contributed to a European Union (2008) decision to support policies aimed at keeping global warming less than 2°C relative to preindustrial times (1.3°C relative to the 11-year running mean global temperature in 2000). Subsequent documents of the European Union (2010) and a group of Nobel laureates (Stockholm Memo 2011) reaffirm this 2°C target.

We will suggest, however, that paleoclimate data imply that 2°C global warming would be a disaster scenario for much of humanity and many other species on the planet.

Prior interglacial periods that were warmer than the Holocene can play a key role in assessing the dangerous level of global warming. As shown in Fig. 2d, e, the interglacials peaking near 125 and 400 kilo years ago (Eemian and Holsteinian, known in paleoclimate literature as Marine Isotope Stages 5e and 11, respectively) were warmer than the Holocene. However, the ice cores and ocean cores do not seem to agree on how warm those prior interglacials were. So we must first consider the differences between these two paleoclimate records.

Table 1 Climate sensitivities, which are equilibrium responses to a specified forcing

Name, explanation	Estimated value	Comments
S_{ff} , all fast feedbacks including aerosols	0.75°C per W/m ² , 3°C for $2 \times \text{CO}_2$	Valid for positive and negative forcings from current climate
$S_{ff + sur}$, fast feedbacks plus surface feedbacks	1.5°C per W/m ² , 6°C for $2 \times \text{CO}_2$	Valid for negative forcing from Holocene climate state; value is less for positive forcing (see text)
S_{CO_2} , specified CO ₂ amount as forcing	2°C per W/m ² , 8°C for $2 \times \text{CO}_2$	Valid for negative forcing from Holocene climate state; value is less for positive forcing (see text)
$S_{ff + sf}$, fast feedbacks plus surface and GHG feedbacks	Remarkably large, especially for negative forcings	For CO ₂ forcing, the long climate response time for high sensitivity implies that negative (diminishing) feedbacks will be important

Ice Cores vs. Ocean Cores

The Antarctic Dome C ice core, with the approximation that global temperature change on millennial time scales is half as large as polar temperature change, indicates that the Eemian and Holsteinian may have been 1–2°C warmer than the Holocene (Fig. 2d). However, the ocean core record (Fig. 2e) suggests that these interglacial periods were only a fraction of a degree warmer than the Holocene. Assessment of dangerous global warming requires that we understand the main reasons for these different pictures, and achieving that objective requires discussion of the nature of these two different records.

Ice Cores

H₂O isotope amounts in the polar ice cores depend upon the air temperature where and when the snowflakes formed above the ice sheets. Several adjustments³ to the ice core temperature record have been suggested with the aim of producing a more homogeneous record,

³One adjustment accounts for estimated glacial–interglacial change of the source region for the water vapor that forms the snowflakes (Vimeux et al. 2002). The source location depends on sea ice extent. This correction reduces interglacial warmth and thus reduces the discrepancy with the calculated interglacial temperatures in Fig. 4a.

Another adjustment accounts for change of ice sheet thickness (Masson-Delmotte et al. 2010). This adjustment increases the fixed-altitude temperature in the warmest interglacials. The correction is based on ice sheet models, which yield a greater altitude for the central part of the ice sheet, even though sea level was higher in these interglacials and thus ice sheet volume was smaller. This counterintuitive result is conceivable because snowfall is greater during warmer interglacials, which could make the central altitude greater despite the smaller ice sheet volume. But note that the correction is based on ice sheet models that may be “stiffer” than real-world ice sheets.

i.e., a result that more precisely defines the surface air temperature change at a fixed location and fixed altitude. However, these adjustments are too small to remove the discrepancy that exists when global temperature inferred from ice cores is compared with either ocean core temperature change (Fig. 2e) or with our calculations based on greenhouse gas and albedo climate forcings (Fig. 2d).

The principal issue about temperature change on top of the ice sheet during the warmest interglacials is whether the simple (factor of two) relationship with global mean temperature change is accurate during the warmest interglacials. That simple prescription works well for the Holocene and for all the glacial–interglacial cycles during the early part of the 800,000-year record, when the interglacials were no warmer than the Holocene.

We suggest that interglacial periods warmer than the Holocene, such as the Eemian, had moved into a regime in which there was less summer sea ice around Antarctica and Greenland, there was summer melting on the lowest elevations of the ice sheets, and there was summer melting on the ice shelves, which thus largely disappeared. In such a regime, even small global warming above the level of the Holocene could generate disproportionate warming on the Antarctic and Greenland ice sheets, more than double the global mean warming.

Summer melting on lower reaches of the ice sheets and on ice shelves introduces the “albedo flip” mechanism (Hansen et al. 2007a). This phase change of water causes a powerful local feedback, which, together with moderate global warming, can increase the length of the melt season. Increased warm season melting increases the ice sheet temperature and affects sea level on a time scale that is being debated, as discussed below. Increased surface melting, loss of

ice shelves, and reduced summer sea ice around Antarctica and Greenland would have a year-round effect on temperature over the ice sheets. Indeed, more open water increases heat flow from ocean to atmosphere with the largest impact on surface air temperature in the cool seasons.

We interpret the stability of Holocene sea level as a consequence of the fact that global temperature was just below the level required to initiate the “albedo flip” mechanism on the fringes of West Antarctica and on most of Greenland. An important implication of this interpretation is that the world today is on the verge of, or has already reached, a level of global warming for which the equilibrium surface air temperature response on the ice sheets will exceed global warming by much more than a factor of two. Below, we cite empirical evidence in support of this interpretation. First, however, we must discuss limitations of ocean core data.

Ocean Cores

Extraction of surface temperature from ocean cores has its own problems. Although obtained from many sites, the deep ocean data depend mainly on surface temperature at high latitude regions of deep water formation that may move as climate changes. As climate becomes colder, for example, sea ice expands, and the location of deep water formation may move equatorward. Fortunately, the climates of most interest range from the Holocene toward warmer climates. Because of geographical constraints, it seems unlikely that the present sites of deep water formation would move much in response to moderate global warming.

A second problem with ocean cores is that deep ocean temperature change is limited as ocean water nears its freezing point. That is why deep ocean temperature change between the LGM and the Holocene was only two-thirds as large as global average surface temperature change. However, by using a constant adjustment factor (1.5) in Fig. 2, based on the LGM to Holocene climate change, we overstate this magnification at interglacial temperatures and understate the magnification at the coldest climates, thus maximizing the possibility for the deep ocean temperature to reveal (and exaggerate) interglacial warmth. Yet no interglacial warm spikes appear in the ocean core temperature record (Fig. 2e).

A third issue concerns the temporal resolution of ocean cores. Bioturbation, i.e., mixing of ocean

sediments by worms, smoothes the ocean core record, especially at locations where ocean sediments accumulate slowly. However, the interglacial periods of primary concern, the Eemian and Holsteinian, were longer than the resolution limit of most ocean cores.

We conclude that ocean cores provide a better measure of global temperature change than ice cores during those interglacial periods that were warmer than the preindustrial Holocene.

Holocene vs. Prior Interglacial Periods and the Pliocene

How warm is the world today relative to peak Holocene temperature? Peak Holocene warmth is commonly placed about 8,000 years ago, but it varies from one place to another (Mayewski et al. 2004). Our interest is global mean temperature, not regional variations.

Figure 5 compares several temperature records for the sake of examining Holocene temperature change. Zero temperature is defined as the mean for the past 10,000 years. The records are made to approximate global temperature by dividing polar temperatures by two and multiplying deep ocean and tropical ocean mixed layer⁴ temperature by a factor 1.5. Figure 5 indicates that global temperature has been relatively stable during the Holocene.

So how warm is it today relative to peak Holocene warmth? Figure 5, especially the global deep ocean temperature, shows that the world did not cool much in the Holocene. Consistent with our earlier study (Hansen et al. 2006), we conclude that, with the global surface warming of 0.7°C between 1880 and 2000 (Hansen et al. 2010), global temperature in year 2000 has reached at least the Holocene maximum.

How does peak Holocene temperature compare with prior warmer interglacial periods, specifically the Eemian and Holsteinian interglacial periods, and with the Pliocene?

⁴Indian and Pacific Ocean temperatures in Fig. 5 are derived from forams that lived in the upper ocean, as opposed to benthic forams used to obtain global deep ocean temperature. The eastern Pacific temperature in Fig. 5b is the average for two locations, north and south of the equator, which are shown individually by Hansen et al. (2006).

Figure 6 shifts the temperature scale so that it is zero at peak Holocene warmth. The temperature curve is based on the ocean core record of Fig. 1 but scaled by the factor 1.5, which is the scale factor relevant to the total LGM–Holocene climate change. Thus, for climates warmer than the Holocene, Fig. 6 may *exaggerate* actual temperature change.

One conclusion deserving emphasis is that global mean temperatures in the Eemian and Holsteinian were less than 1°C warmer than peak Holocene global temperature. Therefore, these interglacial periods were also less than 1°C warmer than global temperature in year 2000.

Figure 6 also suggests that global temperature in the early Pliocene, when sea level was about 25 m higher than today (Dowsett et al. 1994), was only about 1°C warmer than peak Holocene temperature, thus 1–2°C warmer than recent (preindustrial) Holocene. That conclusion requires a caveat about possible change of location of deepwater formation, stronger than the same caveat in comparing recent interglacial periods. Substantial change in the location of deep water formation is more plausible in the Pliocene because of larger Arctic warming at that time (Dowsett et al. 1999); also ocean circulation may have been altered in the early Pliocene by closure of the Panama Seaway, although the timing of that closure is controversial (Haug and Tiedemann 1998).

Is such small Pliocene warming inconsistent with PRISM (Pliocene Research, Interpretation and Synoptic Mapping Project) reconstructions of mid-Pliocene (3–3.3 Mya) climate (Dowsett et al. 1996, 2009 and references therein)? Global mean surface temperatures in climate models forced by PRISM boundary conditions yield global warming of about 3°C (Lunt et al. 2010) relative to preindustrial climate. However, it must be borne in mind that “PRISM’s goal is a reconstruction of a ‘super interglacial,’ not mean conditions” (Dowsett et al. 2009), which led to (intentional, as documented) choices of the warmest conditions in a variety of data sets that were not necessarily well correlated in time.

Perhaps, the most striking characteristic of Pliocene climate reconstructions is that low-latitude ocean temperatures were similar to those today, except that the east–west temperature gradient was reduced in the tropical Pacific Ocean, possibly resembling permanent El Niño conditions (Wara et al. 2005). High latitudes were warmer than today, the ice sheets smaller, and sea level about 25 m higher (Dowsett et al. 2009; Rohling et al. 2009). Atmospheric CO₂ amount was larger in the Pliocene, recent estimates being 390 ± 25 ppm (Pagani et al. 2010) and 365 ± 35 ppm (Seki et al. 2010). It is likely that both elevated CO₂ and increased poleward heat transports by the ocean and atmosphere contributed to large high-latitude

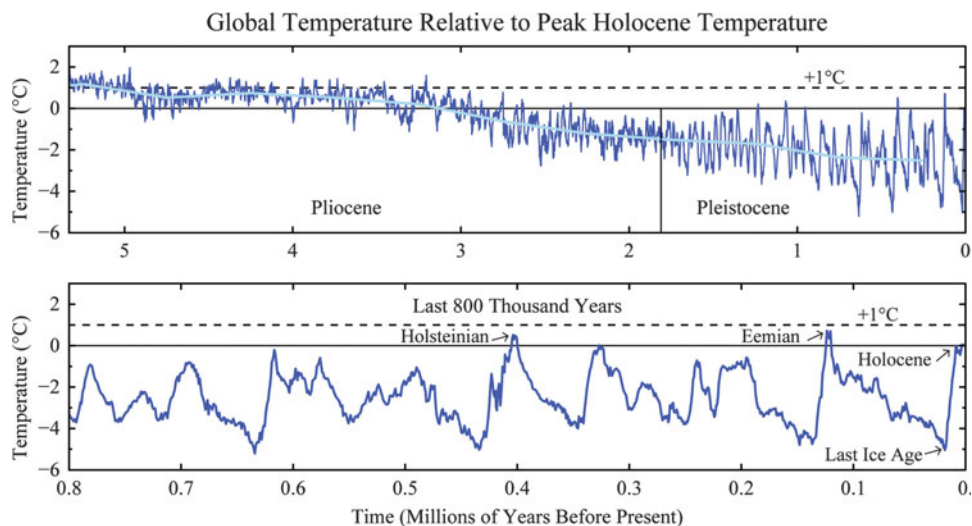


Fig. 6 Global temperature relative to peak Holocene temperature, based on ocean core records in Fig. 1. Deep ocean temperature change is amplified by factor 1.5 to obtain this estimate of surface change

warming, but Pliocene climate has not been well simulated from first principles by climate models. Indeed, today's climate models generally are less sensitive to forcings than the real world (Valdes 2011), suggesting that models do not capture well some amplifying climate feedbacks and thus making empirical assessment via Earth's history of paramount importance.

We conclude that Pliocene temperatures probably were no more than 1–2°C higher on global average than peak Holocene temperature. Regardless of precise Pliocene temperatures, the extreme polar warmth and diminished ice sheets in the Pliocene are consistent with the picture we painted above: Earth today, with global temperature having returned to at least the Holocene maximum, is poised to experience strong amplifying polar feedbacks in response to even modest additional global mean warming.

Sea Level

Sea level rise potentially sets a low limit on the dangerous level of global warming. Civilization developed during a time of unusual climate stability and sea level stability. Much of the world's population and infrastructure are located along coastlines.

Sea level rise, despite its potential importance, is one of the least well-understood impacts of human-made climate change. The difficulty stems from the fact that ice sheet disintegration is a complex nonlinear phenomenon that is inherently difficult to simulate, as well as from the absence of a good paleoclimate analogue for the rapidly increasing human-made climate forcing. Here, we try to glean information from several different sources.

Paleoclimate Data

Figure 4 shows that the equilibrium (eventual) sea level change in response to global temperature change is about 20 m for each degree Celsius global warming. (The variable in Fig. 4 is the albedo forcing due to change of ice sheet size, but albedo forcing and sea level change are proportional; cf. Fig. S4 of Hansen et al. 2008.)

This relationship, an equilibrium sea level rise of 20 m per degree Celsius, continues to be valid for warmer climates. Figure 6 shows that average temperature in the early Pliocene, when sea level was of the

order of 20 m higher than today, was about 1°C above peak Holocene temperature. Figure 1 shows that just prior to Antarctic glaciation, 34 Mya, global temperature was at most about 3°C above peak Holocene temperature, and sea level must have been at least 60 m higher because there were no large ice sheets on the planet.

We conclude that eventual sea level rise of several tens of meters must be anticipated in response to the global warming of several degrees Celsius that is expected under business-as-usual (BAU) climate scenarios (IPCC 2001, 2007).

Paleoclimate data are less helpful for estimating the expected *rate* of sea level rise. Besides the lack of a good paleoanalogue to the rapid human-made forcing, the dating of paleoclimate changes is imprecise. Hansen et al. (2007a) conclude that there is no discernable lag between climate forcing (Northern Hemisphere late spring insolation maximum) and the maximum rate of sea level rise for the two deglaciations that are most accurately dated. Thus, they argue that it does not require millennia for substantial ice sheet response to a forcing, but the weak, slowly changing paleoclimate forcing prevents a more quantitative conclusion.

Sea Level Change Estimates for Twenty-First Century

IPCC (2007) projected sea level rise by the end of this century of about 29 cm (midrange 20–43 cm, full range 18–59 cm). These projections did not include contributions from ice sheet dynamics, on the grounds that ice sheet physics is not understood well enough.

Rahmstorf (2007) made an important contribution to the sea level discussion by pointing out that even a linear relation between global temperature and the rate of sea level rise, calibrated with twentieth century data, implies a twenty-first sea level rise of about a meter, given expected global warming for BAU greenhouse gas emissions. Vermeer and Rahmstorf (2009) extended Rahmstorf's semiempirical approach by adding a rapid response term, projecting sea level rise by 2100 of 0.75–1.9 m for the full range of IPCC climate scenarios. Grinsted et al. (2010) fit a 4-parameter linear response equation to temperature and sea level data for the past 2,000 years, projecting a sea level rise of 0.9–1.3 m by 2100 for a middle IPCC scenario (A1B). These projections are typically a factor of 3–4 larger than the IPCC (2007) estimates, and

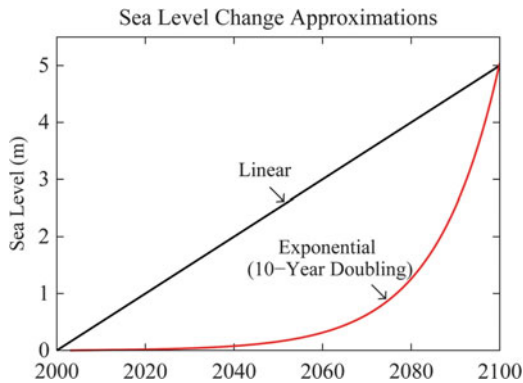


Fig. 7 Five-meter sea level change in twenty-first century under assumption of linear change and exponential change (Hansen 2007), the latter with a 10-year doubling time

thus, they altered perceptions about the potential magnitude of human-caused sea level change (Fig. 7).

Alley (2010) reviewed projections of sea level rise by 2100, showing several clustered around 1 m and one outlier at 5 m, all of these approximated as linear in his graph. The 5-m estimate is what Hansen (2007) suggested was possible under IPCC's BAU climate forcing. Such a graph is comforting—not only does the 5-m sea level rise disagree with all other projections, but its half-meter sea level rise this decade is clearly preposterous.

However, the fundamental issue is linearity vs. non-linearity. Hansen (2005, 2007) argues that amplifying feedbacks make ice sheet disintegration necessarily highly nonlinear and that IPCC's BAU forcing is so huge that it is difficult to see how ice shelves would survive. As warming increases, the number of ice streams contributing to mass loss will increase, contributing to a nonlinear response that should be approximated better by an exponential than by a linear fit. Hansen (2007) suggested that a 10-year doubling time was plausible and pointed out that such a doubling time, from a 1-mm/year ice sheet contribution to sea level in the decade 2005–2015, would lead to a cumulative 5-m sea level rise by 2095.

Nonlinear ice sheet disintegration can be slowed by negative feedbacks. Pfeffer et al. (2008) argue that kinematic constraints make sea level rise of more than 2 m this century physically untenable, and they contend that such a magnitude could occur only if all variables quickly accelerate to extremely high limits. They conclude that more plausible but still

accelerated conditions could lead to sea level rise of 80 cm by 2100.

The kinematic constraint may have relevance to the Greenland ice sheet, although the assumptions of Pfeffer et al. (2008) are questionable even for Greenland. They assume that ice streams this century will discharge ice no faster than the fastest rate observed in recent decades. That assumption is dubious, given the huge climate change that will occur under BAU scenarios, which have a positive (warming) climate forcing that is increasing at a rate dwarfing any known natural forcing. BAU scenarios lead to CO₂ levels higher than any since 32 Mya, when Antarctica glaciated. By midcentury, most of Greenland would be experiencing summer melting in a longer melt season. Also some Greenland ice stream outlets are in valleys with bedrock below sea level. As the terminus of an ice stream retreats inland, glacier sidewalls can collapse, creating a wider pathway for discharging ice.

The main flaw with the kinematic constraint concept is the geology of Antarctica, where large portions of the ice sheet are buttressed by ice shelves that are unlikely to survive BAU climate scenarios. West Antarctica's Pine Island Glacier (PIG) illustrates non-linear processes already coming into play. The floating ice shelf at PIG's terminus has been thinning in the past two decades as the ocean around Antarctica warms (Shepherd et al. 2004; Jenkins et al. 2010). Thus, the grounding line of the glacier has moved inland by 30 km into deeper water, allowing potentially unstable ice sheet retreat. PIG's rate of mass loss has accelerated almost continuously for the past decade (Wingham et al. 2009) and may account for about half of the mass loss of the West Antarctic ice sheet, which is of the order of 100 km³/year (Sasgen et al. 2010).

PIG and neighboring glaciers in the Amundsen Sea sector of West Antarctica, which are also accelerating, contain enough ice to contribute 1–2 m to sea level. Most of the West Antarctic ice sheet, with at least 5 m of sea level, and about a third of the East Antarctic ice sheet, with another 15–20 m of sea level, are grounded below sea level. This more vulnerable ice may have been the source of the 25 ± 10 m sea level rise of the Pliocene (Dowsett and Cronin 1990; Dowsett et al. 1994). If human-made global warming reaches Pliocene levels this century, as expected under BAU scenarios, these greater volumes of ice will surely begin to contribute to sea level change. Indeed,

satellite gravity and radar interferometry data reveal that the Totten Glacier of East Antarctica, which fronts a large ice mass grounded below sea level, is already beginning to lose mass (Rignot et al. 2008).

The eventual sea level rise due to expected global warming under BAU GHG scenarios is several tens of meters, as discussed at the beginning of this section. From the present discussion, it seems that there is sufficient readily available ice to cause multimeter sea level rise this century if dynamic discharge of ice increases exponentially. Thus, current observations of ice sheet mass loss are of special interest.

Ice Sheet Mass Loss

The best indication and quantification of possible nonlinear behavior will be precise measurements of ice sheet mass change. Mass loss by the Greenland and Antarctic ice sheets can be deduced from satellite measurements of Earth's gravity field. Figure 8 shows the changing mass of both ice sheets as reported by Velicogna (2009).

These data records suggest that the rate of mass loss is increasing, indeed nearly doubling over the period of record, but the record is too short to provide a meaningful evaluation of a doubling time. Also there is substantial variation among alternative analyses of the gravity field data (Sorensen and Forsberg 2010), although all analyses have the rate of mass loss increasing over the period of record.

We conclude that available data for the ice sheet mass change are consistent with our expectation of a nonlinear response, but the data record is too short and

uncertain to allow quantitative assessment. A 10-year doubling time, or even shorter, is consistent with the gravity field data, but because of the brevity of the record, even a linear mass loss cannot be ruled out. Assessments will rapidly become more meaningful in the future if high-precision gravity measurements are continued.

Iceberg Cooling Effect

Exponential change cannot continue indefinitely. The negative feedback terminating exponential growth of ice loss is probably regional cooling due to the thermal and freshwater effects of melting icebergs. Temporary cooling occurs as icebergs and cold fresh glacial meltwater are added to the Southern Ocean and the North Atlantic Ocean.

As a concrete example, Fig. 9 shows the global temperature change in simulations with GISS modelE (Schmidt et al. 2006; Hansen et al. 2007c) with and without the melting iceberg effect. GHGs follow the A1B scenario, an intermediate business-as-usual scenario (IPCC 2001, 2007; see also Figs. 2 and 3 of Hansen et al. 2007b). Ice melt rate is such that it contributes 1 mm/year to sea level in 2010, increasing with a 10-year doubling time; this melt rate constitutes 0.034 Sv (1 Sverdrup = 1 million m³/s) in 2065 and 0.1 Sv in 2080. Half of this meltwater is added in the North Atlantic and half in the Southern Ocean.

By 2065, when the sea level rise (from ice melt) is 60 cm relative to 2010, the cold freshwater reduces global mean warming (relative to 1880) from 1.86°C to 1.47°C. By 2080, when sea level rise is 1.4 m,

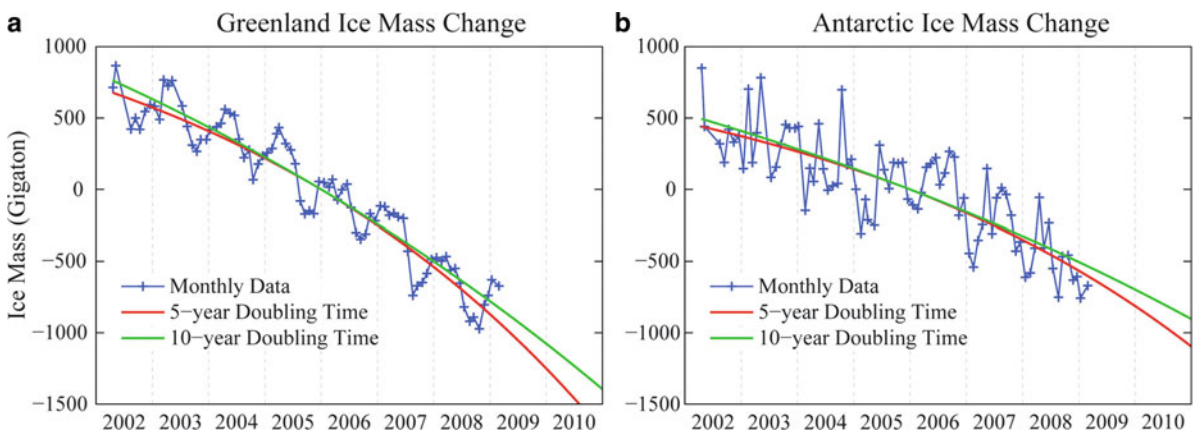


Fig. 8 Greenland (a) and Antarctic (b) mass change deduced from gravitational field measurements by Velicogna (2009) and best fits with 5- and 10-year mass loss doubling times

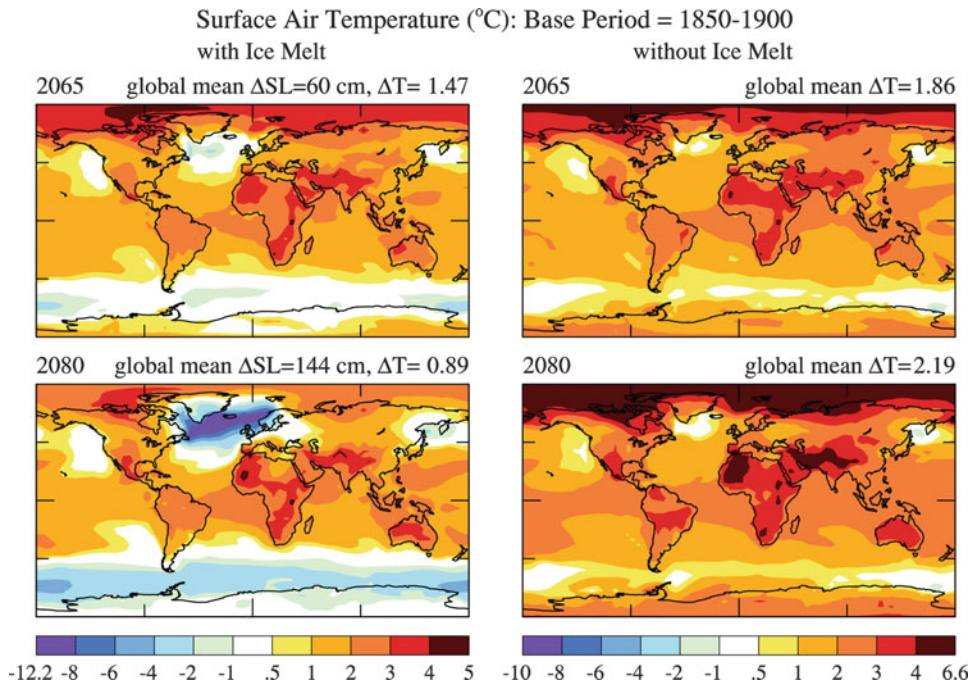


Fig. 9 Surface air temperature change in 2065 (*above*) and 2080 (*below*) relative to 1850–1900 in simulations with GISS climate model using IPCC A1B scenario. Maps on *left* include

ice melt, which is put half into the North Atlantic and half into the Southern Ocean, with ice melt doubling every 10 years

global warming is reduced from 2.19°C to 0.89°C . These experiments are described in a paper in preparation, which includes other GHG scenarios, cases with ice melt in one hemisphere but not the other, and investigation of the individual effects of freshening and cooling by icebergs (the freshening is more responsible for the reduction of global warming). Note that the magnitude of the regional cooling is comparable to that in “Heinrich” events in the paleoclimate record (Bond et al. 1992), these events involving massive iceberg discharge at a rate comparable to that in our simulations. Given that the possibility of sea level rise of the order of a meter is now widely accepted, it is important that simulations of climate for the twenty-first century and beyond include the iceberg cooling effect.

Detailed consideration of the climate effects of freshwater from ice sheet disintegration, which has a rich history (Broecker et al. 1990; Rahmstorf 1996; Manabe and Stouffer 1997), is beyond the scope of our present chapter. However, we note that the temporary reduction of global warming provided by icebergs is not likely to be a blessing. Stronger storms driven by increased latitudinal temperature gradients, combined with sea level rise, likely will produce global havoc.

It was the prospect of increased ferocity of continental-scale frontal storms, with hurricane-strength winds powered by the contrast between air masses cooled by ice melt and tropical air that is warmer and moister than today, which gave rise to the book title “Storms of My Grandchildren” (Hansen 2009).

Discussion

Earth’s paleoclimate history is remarkably rich in information on how sensitive climate is to forcings, both natural forcings and human-made forcings. Huge glacial-to-interglacial climate swings have been driven by very weak climate forcings, as the climate response is amplified by both fast feedbacks, such as water vapor and aerosols, and slow feedbacks, especially CO_2 and surface albedo. The paleoclimate record allows us to deduce that the fast-feedback climate sensitivity is about 3°C global warming for doubled CO_2 . Climate sensitivity including slow feedbacks depends upon the initial climate state, but it is generally much greater than the fast-feedback climate sensitivity.

Carbon dioxide functions as an amplifying slow climate feedback because the division of CO₂ among its surface reservoirs (atmosphere, ocean, soil, and biosphere) shifts toward more CO₂ in the atmosphere as the planet becomes warmer. However, CO₂ is also a climate forcing when it is extracted from the solid earth and injected into the surface reservoirs either by enhanced volcanic activity or by humans burning fossil fuels. The CO₂ so extracted from the deep Earth remains in the surface reservoirs for millennia, until the weathering process eventually results in deposition of carbonates on the ocean floor. Thus, the slow CO₂ and albedo feedbacks, as well as the fast feedbacks, will eventually have time to respond to human-made fossil fuel CO₂ emissions.

The paleoclimate record is also a good source of information on the level of global warming that will eventually yield a markedly different planet than the one on which civilization developed. Paleoclimate data help us assess climate sensitivity and potential human-made climate effects. We conclude that Earth in the warmest interglacial periods of the past million years was less than 1°C warmer than in the Holocene. Polar warmth in those interglacials and in the Pliocene does not imply that a substantial cushion remains between today's climate and dangerous warming, but rather that Earth is poised to experience strong amplifying polar feedbacks in response to moderate additional global warming.

How Warm Were Recent Interglacial Periods and the Pliocene?

There are numerous statements and presumptions in the scientific literature that prior interglacial periods such as the Eemian were as much as a few degrees warmer than the Holocene (e.g., Rohling et al. 2008; Church et al. 2010), and this perception has probably influenced estimates of what constitutes a dangerous level of global warming. These perceptions about interglacial global temperature must derive at least in part from the fact that Greenland and Antarctica did achieve such higher temperatures during the Eemian.

However, we interpret these temperatures on the ice sheets as being local and unrepresentative of global mean temperature anomalies. The polar ice sheet temperature anomalies were likely magnified by the fact that these warmer interglacial periods had little

summer sea ice or ice shelves around the Greenland and Antarctic continents.

We argue that global deep ocean temperatures provide a better measure of global mean temperature anomalies than polar ice cores during the interglacial periods. Ocean cores have a systematic difficulty as a measure of temperature change when the deep ocean temperature approaches the freezing point, as quantified by Waelbroeck et al. (2002). However, in using the known surface temperature change between the Last Glacial Maximum and the Holocene as an empirical calibration, we maximize (i.e., we tend to exaggerate) the ocean core estimate of global surface warming during warmer interglacials relative to the Holocene.

Ocean core data are also affected by the location of deep water formation, which may change. However, the location of deep water formation around Antarctica, which affects deep Pacific Ocean temperature, is limited by the Antarctic geography and is unlikely to be shifted substantially in interglacial periods warmer than the Holocene.

Figure 2 provides unambiguous discrimination between ice and ocean core measures of global temperature change. Climate forcings for the past 800,000 years are known accurately. Climate sensitivity cannot vary much from one interglacial period to another. Ocean core temperatures give a consistent climate sensitivity for the entire 800,000 years. In contrast, ice core temperature (Fig. 2d) leads to the illogical result that climate sensitivity depends on time.

We conclude that ocean core data are correct in indicating that global surface temperature was only slightly higher in the Eemian and Holsteinian interglacial periods than in the Holocene, at most by about 1°C, but probably by only several tenths of a degree Celsius. By extension (see Fig. 6), the Pliocene was at most 1–2°C warmer than the Holocene on global mean.

How Slow Are Slow Feedbacks?

Observed time scales of GHG and surface albedo variability (Fig. 2) are the time scales of orbital variations, thus not necessarily an internal time scale of the feedback processes. Indeed, we do not expect slow feedbacks to be inherently *that* slow. We have argued (Hansen 2005; Hansen et al. 2007a) that the ice sheet response to a strong rapid forcing is much faster

than the time scale of orbital changes, with substantial response likely within a century.

Debating what sea level will be on a specific date such as 2100, however, misses an important point concerning response times. The carbon cycle response time, i.e., the time required for CO₂ from fossil fuel burning to be removed from the surface carbon reservoirs, is many millennia (Berner 2004; Archer 2005). The ice sheet response time is clearly shorter than this carbon cycle response time, in view of the absence of a discernable lag between paleoclimate forcings and the maximum rate of ice sheet disintegration (Hansen et al. 2007a) and in view of the fact that ice sheet disintegration proceeds at rates up to several meters of sea level rise per century (Fairbanks 1989) even in response to weak paleoclimate forcings.

Thus, burning all or most fossil fuels guarantees tens of meters of sea level rise, as we have shown that the eventual sea level response is about 20 m of sea level for each degree Celsius of global warming. We suggest that ice sheet disintegration will be a nonlinear process, spurred by an increasing forcing and by amplifying feedbacks, which is better characterized by a doubling time for the rate of mass disintegration, rather than a linear rate of mass change. If the doubling time is as short as a decade, multimeter sea level rise could occur this century. Observations of mass loss from Greenland and Antarctica are too brief for significant conclusions, but they are not inconsistent with a doubling time of a decade or less. The picture will become clearer as the measurement record lengthens.

There are physical constraints and negative feedbacks that may limit nonlinear ice sheet mass loss. An ice sheet sitting primarily on land above sea level, such as most of Greenland, may be limited by the speed at which it can deliver ice to the ocean via outlet glaciers. But much of the West Antarctic ice sheet, resting on bedrock below sea level, is not so constrained.

We recognize the negative feedback that comes into play as iceberg discharge reaches a rate that cools the regional ocean surface. But that negative feedback would be cold comfort. High-latitude cooling and low-latitude warming would drive more powerful mid-latitude cyclonic storms, including more frequent cases of hurricane force winds. Such storms, in combination with rising sea level, would be

disastrous for many of the world's great cities, and they would be devastating for the world's economic well-being and cultural heritage.

How Much Warming Is Too Much?

The most substantial political effort to place a limit on global warming has been the European Union's target to keep global temperature from exceeding the preindustrial level by more than 2°C (European Union 2008). This goal was later reaffirmed (European Union 2010), and it was endorsed by a group of Nobel Laureates in the Stockholm Memo (2011).

However, based on evidence presented in this chapter, a target of 2°C is not safe or appropriate. Global warming of 2°C would make Earth much warmer than in the Eemian, when sea level was 4–6 m higher than today. Indeed, with global warming of 2°C, Earth would be headed back toward Pliocene-like conditions.

Conceivably, a 2°C target is based partly on a perception of what is politically realistic, rather than a statement of pure science. In any event, our science analysis suggests that such a target is not only unwise but likely a disaster scenario.

Detailed consideration of targets is beyond the scope of this chapter, but we note that our present study is consistent with the “target CO₂” analysis of Hansen et al. (2008). Those authors argued that atmospheric CO₂ should be rolled back from its present ~390 ppm at least to the level of approximately 350 ppm. With other climate forcings held fixed, CO₂ at 350 ppm would restore the planet's energy balance and keep human-made global warming less than 1°C, as we and several colleagues discuss in two papers (“Earth's Energy Imbalance” and “The Case for Young People and Nature”) in preparation.

Acknowledgments We thank referee (Dana Royer) for helpful suggestions, Gerry Lenfest (Lenfest Foundation), Lee Wasserman (Rockefeller Family Foundation), Stephen Toben (Flora Family Foundation) and NASA program managers Jack Kaye and David Considine for research support, and Gavin Schmidt, Pushker Kharecha, Richard Alley, Christopher Barnett, Peter Barrett, Phil Blackwood, John Breithaupt, Tim Dean, Bruce Edwards, J. Gathright, Michael Le Page, Robert Maginnis, Jon Parker, Tom Parrett, Les Porter, Warwick Rowell, Ken Schatten, Colin Summerhayes, and Bart Verheggen for comments on a draft version of this chapter.

References

- Alley RB (2010) Ice in the hot box – what adaptation challenges might we face? In: 2010 AGU Fall Meeting, San Francisco, December 17, U52A-02
- Archer D (2005) Fate of fossil fuel CO₂ in geologic time. *J Geophys Res* 110:C09505. doi:10.1029/2004JC002625
- Berling DJ, Royer DL (2011) Earth's atmospheric CO₂ history by proxy. *Nat Geosci* 4:1–2
- Berling D, Berner RA, Mackenzie FT, Harfoot MB, Pyle JA (2009) Methane and the CH₄-related greenhouse effect over the past 400 million years. *Am J Sci* 309:97–113
- Berling DJ, Fox A, Stevenson DS, Valdes PJ (2011) Enhanced chemistry-climate feedbacks in past greenhouse worlds. *Proc Natl Acad Sci USA* 108:9770–9775
- Berger AL (1978) Long term variations of daily insolation and quaternary climate changes. *J Atmos Sci* 35:2362–2367
- Berner RA (2004) *The Phanerozoic carbon cycle: CO₂ and O₂*. Oxford University Press, Oxford, 150 pp
- Berner RA, Caldeira K (1997) The need for mass balance and feedback in the geochemical carbon cycle. *Geology* 25:955–956
- Bintanja R, van de Wal RSW, Oerlemans J (2005) Modelled atmospheric temperatures and global sea levels over the past million years. *Nature* 437:125–128
- Blakey R (2008) Global paleogeographic views of Earth history – Late Precambrian to Recent. <http://jan.ucc.nau.edu/~rcb7/globaltext2.html>
- Bond G, Heinrich H, Broecker W, Labeyrie L, McManus J, Andrews J, Huon S, Jantschik R, Clasen S, Simet C, Tedesco K, Klas M, Bonani G, Ivy S (1992) Evidence for massive discharges of icebergs into the North Atlantic ocean during the last glacial period. *Nature* 360:245–249
- Broecker WS, Bond G, Klas M, Bonani G, Wolfi W (1990) A salt oscillator in the glacial North Atlantic? *Paleoceanography* 5:469–477
- Charlson RJ, Lovelock JE, Andreae MO, Warren SG (1987) Oceanic phytoplankton, atmospheric sulphur, cloud albedo and climate. *Nature* 326:655–661
- Charney JG, Arakawa A, Baker D, Bolin B, Dickenson R, Goody R, Leith C, Stommel HM, Wunsch CI (1979) *Carbon dioxide and climate: a scientific assessment*. National Academy of Sciences Press, Washington, DC, 33 pp
- Church JA et al (2010) Sea-level rise and variability: synthesis and outlook for the future. In: Church JA, Woodworth PL, Aarup T, Wilson WS (eds) *Understanding sea-level rise and variability*. Blackwell, Oxford
- Chylek P, Lohmann U (2008) Aerosol radiative forcing and climate sensitivity deduced from the Last Glacial Maximum to Holocene transition. *Geophys Res Lett* 35:L04804. doi:10.1029/2007GL032759
- Dowsett HJ, Cronin T (1990) High eustatic sea level during the middle Pliocene: evidence from the southeastern U.S. Atlantic coastal plain. *Geology* 18:435–438
- Dowsett H, Thompson R, Barron J, Cronin T, Fleming F, Ishman S, Poore R, Willard D, Holtz T Jr (1994) Joint investigations of the Middle Pliocene climate I: PRISM paleo-environmental reconstructions. *Global Planet Change* 9:169–195
- Dowsett H, Barron J, Poore R (1996) Middle Pliocene sea surface temperatures: a global reconstruction. *Mar Micropaleontol* 27:13–26
- Dowsett HJ, Barron JA, Poore RZ, Thompson RS, Cronin TM, Ishman SE, Willard DA (1999) Middle Pliocene paleoenvironmental reconstruction: PRISM2, U.S. Geol. Surv. Open File Rep., 99-535. <http://pubs.usgs.gov/openfile/of99-535>
- Dowsett HJ, Robinson MM, Foley KM (2009) Pliocene three-dimensional global ocean temperature reconstruction. *Clim Past* 5:769–783
- Edmond JM, Huh Y (2003) Non-steady state carbonate recycling and implications for the evolution of atmospheric P_{CO₂}. *Earth Planet Sci Lett* 216:125–139
- European Union (2008) *The 2°C target*. Information Reference Document. http://ec.europa.eu/clima/policies/international_docs/brochure_2c.pdf
- European Union (2010) *Scientific Perspectives After Copenhagen*. Information Reference Document. http://www.eutrio.be/files/bveu/media/documents/Scientific_Perspectives_After_Copenhagen.pdf
- Fairbanks RG (1989) A 17,000-year glacio-eustatic sea level record – influence of glacial melting rates on the Younger Dryas event and deep sea circulation. *Nature* 433:637–642
- Gerlach T (2011) Volcanic versus anthropogenic carbon dioxide. *Eos Trans Am Geophys Union* 92:201–202
- Gristed A, Moore JC, Jevrejeva S (2010) Reconstructing sea level from paleo and projected temperatures 200 to 2100 AD. *Clim Dyn* 34:461–472
- Hansen JE (2005) A slippery slope: how much global warming constitutes “dangerous anthropogenic interference”? An editorial essay. *Climatic Change* 68:269–279
- Hansen JE (2007) Scientific reticence and sea level rise. *Environ Res Lett* 2:024002, 6 pp
- Hansen J (2009) *Storms of my grandchildren: the truth about the coming climate catastrophe and our last chance to save humanity*. Bloomsbury, New York, 304 pp
- Hansen J, Johnson D, Lacis A, Lebedeff S, Lee P, Rind D, Russell G (1981) Climate impact of increasing atmospheric carbon dioxide. *Science* 213:957–966
- Hansen J, Lacis A, Rind D, Russell G, Stone P, Ruedy R, Lerner J (1984) Climate sensitivity: analysis of feedback mechanisms. In: Hansen JE, Takahashi T (eds) *Climate processes and climate sensitivity*, vol 5, Geophysical Monograph 29, Maurice Ewing. American Geophysical Union, Washington, DC, pp 130–163
- Hansen J, Sato M, Ruedy R, Lacis A, Oinas V (2000) Global warming in the twenty-first century: an alternative scenario. *Proc Natl Acad Sci USA* 97:9875–9880
- Hansen J, Sato M, Ruedy R et al (2005) Efficacy of climate forcings. *J Geophys Res* 110:D18104. doi:10.1029/2005JD005776
- Hansen J, Sato M, Ruedy R, Lo K, Lea DW, Medina-Elizade M (2006) Global temperature change. *Proc Natl Acad Sci USA* 103:14288–14293
- Hansen J, Sato M, Kharecha P, Russell G, Lea DW, Siddall M (2007a) Climate change and trace gases. *Philos Trans R Soc A* 365:1925–1954
- Hansen J, Sato M, Ruedy R et al (2007b) Dangerous human-made interference with climate: a GISS modelE study. *Atmos Chem Phys* 7:2287–2312

- Hansen J, Sato M, Ruedy R et al (2007c) Climate simulations for 1880-2003 with GISS modelE. *Clim Dyn* 29:661–696. doi:[10.1007/s00382-007-0255-8](https://doi.org/10.1007/s00382-007-0255-8)
- Hansen J, Sato M, Kharecha P, Beerling D, Berner R, Masson-Delmotte V, Pagani M, Raymo M, Royer DL, Zachos JC (2008) Target atmospheric CO₂: where should humanity aim? *Open Atmos Sci J* 2:217–231
- Hansen J, Ruedy R, Sato M, Lo K (2010) Global surface temperature change. *Rev Geophys* 48:RG4004, 29 pp
- Haug GH, Tiedemann R (1998) Effect of the formation of the Isthmus of Panama on Atlantic Ocean thermohaline circulation. *Nature* 393:673–676
- Hays JD, Imbrie J, Shackleton NJ (1976) Variations in the Earth's orbit: pacemaker of the ice ages. *Science* 194:1121–1132
- Hewitt CD, Mitchell JFB (1997) Radiative forcing and response of a GCM to ice age boundary conditions: cloud feedback and climate sensitivity. *Clim Dyn* 13:821–834
- Huybers P (2006) Early Pleistocene glacial cycles and the integrated summer insolation forcing. *Science* 313:508–511
- Intergovernmental Panel on Climate Change (IPCC) (2001) In: Houghton JT, Ding Y, Griggs DJ et al (eds) *Climate change 2001: the scientific basis*. Cambridge University Press, Cambridge, 881 pp
- Intergovernmental Panel on Climate Change (IPCC) (2007) In: Solomon S, Dahe Q, Manning M et al (eds) *Climate Change 2007: the physical science basis*. Cambridge University Press, Cambridge, 996 pp
- Jenkins A, Dutrieux P, Jacobs SS, McPhail SD, Perrett JR, Webb AT, White D (2010) Observations beneath Pine Island Glacier in West Antarctica and implications for its retreat. *Nat Geosci* 3:468–472
- Jouzel J, Masson-Delmotte V, Cattani O et al (2007) Orbital and millennial Antarctic climate variability over the past 800,000 years. *Science* 317:793–796
- Kent DV, Muttoni G (2008) Equatorial convergence of India and early Cenozoic climate trends. *Proc Natl Acad Sci USA* 105:16065–16070
- Kohler P, Bintanja R, Fischer H, Joos F, Knutti R, Lohmann G, Masson-Delmotte V (2010) What caused Earth's temperature variations during the last 800,000 years? Data-based evidence on radiative forcing and constraints on climate sensitivity. *Quat Sci Rev* 29:129–145
- Kumar P, Yuan X, Kumar MR, Kind R, Li X, Chadha RK (2007) The rapid drift of the Indian tectonic plate. *Nature* 449:894–897
- Lacis AA, Schmidt GA, Rind D, Ruedy RA (2010) Atmospheric CO₂: principal control knob governing Earth's temperature. *Science* 330:356–359. doi:[10.1126/science.1190653](https://doi.org/10.1126/science.1190653)
- Lea DW, Pak DK, Spero HJ (2000) Climate impact of late Quaternary equatorial Pacific sea surface temperature variations. *Science* 289:1719–1723
- Lea DW, Pak DK, Belanger CL, Spero HJ, Hall MA, Shackleton NJ (2006) Paleoclimate history of Galapagos surface waters over the last 135,000 years. *Quat Sci Rev* 25:1152–1167
- Loulergue L, Schilt A, Spahni R, Masson-Delmotte V, Blunier T, Lemieux B, Barnola J-M, Raynaud D, Stocker TF, Chappellaz J (2008) Orbital and millennial-scale features of atmospheric CH₄ over the past 800,000 years. *Nature* 453:383–386
- Lunt DJ, Haywood AM, Schmidt GA, Salzmann U, Valdes PJ, Dowsett HJ (2010) Earth system sensitivity inferred from Pliocene modeling and data. *Nat Geosci* 3:60–64
- Luthi D, Le Floch M, Bereiter B et al (2008) High-resolution carbon dioxide concentration record 650,000-800,000 years before present. *Nature* 453:379–382
- Manabe S, Stouffer R (1997) Coupled ocean-atmosphere model response to freshwater input: comparison to Younger Dryas event. *Paleoceanography* 12:307–320
- Markwick PJ (1998) Fossil crocodylians as indicators of Late Cretaceous and Cenozoic climates: implications for using paleontological data in reconstructing palaeoclimate. *Palaeogeogr Palaeoclimatol Palaeoecol* 137:205–271. doi:[10.1016/S0031-0182\(97\)00108-9](https://doi.org/10.1016/S0031-0182(97)00108-9)
- Masson-Delmotte V, Stenni B, Pol K et al (2010) EPICA Dome C record of glacial and interglacial intensities. *Quat Sci Rev* 29:113–128
- Mayewski PA, Rohling EE, Stager JC, Karlen W, Maasch KA, Meeker LD, Meyerson EA, Gasse F, van Kreveld S, Holmgren K, Lee-Thorp J, Rosqvist G, Rack F, Staubwasser M, Schneider RR, Steig EJ (2004) Holocene climate variability. *Quat Res* 62:243–255
- Medina-Elizade M, Lea DW (2005) The mid-Pleistocene transition in the tropical Pacific. *Science* 310:1009–1012
- Milankovitch M (1941) *Kanon der Erdbestrahlung und seine Anwendung auf das Eiszeiten-problem*. Royal Serbian Academy, Belgrade
- Mudelsee M (2001) The phase relations among atmospheric CO₂ content, temperature and global ice volume over the past 420 ka. *Quat Sci Rev* 20:583–589
- Pagani M, Liu Z, LaRiviere J, Ravelo AC (2010) High Earth-system climate sensitivity determined from Pliocene carbon dioxide concentrations. *Nat Geosci* 3:27–30
- Park J, Royer DL (2011) Geologic constraints on the glacial amplification of Phanerozoic climate sensitivity. *Am J Sci* 311:1–26
- Patriat P, Sloan H, Saunter D (2008) From slow to ultraslow: A previously undetected event at the Southwest Indian Ridge at ca. 24 Ma. *Geology* 36:207–210
- Pfeffer WT, Harper JT, O'Neel S (2008) Kinematic constraints on glacier contributions to 21st century sea level rise. *Science* 321:1340–1343
- Rahmstorf S (1996) On the freshwater forcing and transport of the Atlantic thermohaline circulation. *Clim Dyn* 12:799–811
- Rahmstorf S (2007) A semi-empirical approach to projecting future sea-level rise. *Science* 315:368–370
- Randall DA, Wood RA (2007) Climate models and their evaluation. In: Solomon S, Dahe Q, Manning M et al (eds) *IPCC Climate Change 2007: the physical science basis*. Cambridge University Press, Cambridge, 996 pp
- Rignot E, Bamber JL, van den Broeke MR, Davis C, Li Y, van de Berg WJ, van Meijgaard E (2008) Recent Antarctic ice mass loss from radar interferometry and regional climate modeling. *Nat Geosci* 1:106–110
- Roe G (2006) In defense of Milankovitch. *Geophys Res Lett* 33: L24703. doi:[10.1029/2006GL027817](https://doi.org/10.1029/2006GL027817)
- Rohling EJ, Grant K, Hemleben Ch, Siddall M, Hoogakker BAA, Bolshaw M, Kucera M (2008) High rates of sea-level rise during the last interglacial period. *Nat Geosci* 1:38–42
- Rohling EJ, Grant K, Bolshaw M, Roberts AP, Siddall M, Hemleben Ch, Kucera M (2009) Antarctic temperature and global sea level closely coupled over the past five glacial cycles. *Nat Geosci* 2:500–5004
- Royer DL (2006) CO₂-forced climate thresholds during the Phanerozoic. *Geochim Cosmochim Acta* 70:5665–5675

- Royer DL, Pagani M, Beerling DJ (2011) Geologic constraints on earth system sensitivity to CO₂ during the Cretaceous and early Paleogene. *Earth Syst Dyn Discuss* 2:211–240
- Sackmann I-J, Boothroyd AI, Kraemer KE (1993) Our sun III. Present and future. *Astrophys J* 418:457–468
- Saraswat R, Nigam R, Weldeab S, Mackensen A, Naidu PD (2005) A first look at past sea surface temperatures in the equatorial Indian Ocean from Mg/Ca in foraminifera. *Geophys Res Lett* 32:L24605, 4 pp
- Sasgen I, Martinec Z, Bamber J (2010) Combined GRACE and InSAR estimate of West Antarctic ice mass loss. *J Geophys Res* 115:F04010. doi:10.1029/2009JF001525
- Schmidt GA, Ruedy R, Hansen JE et al (2006) Present day atmospheric simulations using GISS ModelE: Comparison to in-situ, satellite and reanalysis data. *J Clim* 19:153–192. doi:10.1175/JCLI3612.1
- Schneider von Deimling T, Held H, Ganopolski A, Rahmstorf S (2006) Climate sensitivity estimated from ensemble simulations of glacial climate. *Clim Dyn* 27:149–163
- Schneider SH, Mastrandrea MD (2005) Probabilistic assessment of “dangerous” climate change and emissions pathways. *Proc Natl Acad Sci USA* 102:15728–15735
- Seki O, Foster GL, Schmidt DN, Mackensen A, Kawamura K, Pancost RD (2010) Alkenone and boron-based Pliocene pCO₂ records. *Earth Planet Sci Lett* 292:201–211
- Shakun JD, Carlson AE (2010) A global perspective on Last Glacial Maximum to Holocene climate change. *Quat Sci Rev* 29:1801–1816
- Shepherd A, Wingham D, Rignot E (2004) Warm ocean is eroding West Antarctic ice sheet. *Geophys Res Lett* 31:L23402, 4 pp
- Siddall M, Rohling EJ, Almogi-Labin A, Hemleben Ch, Meischner D, Schmelzer I, Smeed D (2003) Sea-level fluctuations during the last glacial cycle. *Nature* 423:853–858
- Sorensen LS, Forsberg R (2010) Greenland ice sheet mass loss from GRACE monthly models. In: Gravity, geoid and earth observations, vol 135, International Association of Geodesy Symposia. Springer, Berlin, doi:10.1007/978-3-642-10634-7_70
- Staudigel H, Hart SR, Schmincke H-U, Smith BM (1989) Cretaceous ocean crust at DSDP Sites 417 and 418: Carbon uptake from weathering versus loss by magmatic outgassing. *Geochim Cosmochim Acta* 53:3091–3094
- Stockholm Memo (2011) Tipping the scales towards sustainability. In: 3rd Nobel Laureate symposium on global sustainability, Stockholm, 16–19 May 2011. <http://globalsymposium2011.org/wp-content/uploads/2011/05/The-Stockholm-Memorandum.pdf>
- Valdes P (2011) Built for stability. *Nat Geosci* 4:414–416
- Velicogna I (2009) Increasing rates of ice mass loss from the Greenland and Antarctic ice sheets revealed by GRACE. *Geophys Res Lett* 36:L19503. doi:10.1029/2009GL040222
- Vermeer M, Rahmstorf S (2009) Global sea level linked to global temperature. *Proc Natl Acad Sci USA* 106:21527–21532
- Vimeux F, Coffey KM, Jouzel J (2002) New insights into Southern Hemisphere temperature changes from Vostok ice cores using deuterium excess correction. *Earth Planet Sci Lett* 203:829–843
- Waelbroeck C, Labeyrie L, Michel E, Duplessy JC, McManus JF, Lambeck K, Balbon E, Labracherie M (2002) Sea-level and deep water temperature changes derived from benthic foraminifera isotopic records. *Quat Sci Rev* 21:295–305
- Wara MW, Ravelo A, Delaney ML (2005) Permanent El Niño-like conditions during the Pliocene warm period. *Science* 309:758–761
- Wingham DJ, Wallis DW, Shepherd A (2009) The spatial and temporal evolution of Pine Island Glacier thinning, 1995–2006. *Geophys Res Lett* 36:L17501
- Wunsch C (2003) The spectral description of climate change including the 100 ky energy. *Clim Dyn* 20:353–363
- Zachos J, Pagani M, Sloan L, Thomas E, Billups K (2001) Trends, rhythms, and aberrations in global climate 65 Ma to present. *Science* 292:686–693

Simulation of Glacial Cycles with an Earth System Model

Andrey Ganopolski and Reinhard Calov

Abstract

It is generally accepted that, as postulated by the Milankovitch theory, variations of the Earth's orbital parameters play a fundamental role in driving glacial cycles. However, many aspects of glacial climate variability, such as strongly nonlinear response of the ice sheets to orbital forcing and the role of carbon-dioxide climate ice-sheet feedback, still remain poorly understood. In recent years, it became increasingly clear that solving of the glacial cycle problem requires application of comprehensive Earth system models. Here we use the Earth system model of intermediate complexity CLIMBER-2 to simulate the last eight glacial cycles. The model was forced by variations of the Earth's orbital parameters and atmospheric concentration of the major greenhouse gases. Simulated temporal dynamics of ice volume and other climate characteristics agree favorably with the paleoclimate reconstructions. Additional experiments performed with fixed concentrations of the greenhouse gases demonstrate that the 100-kiloyear cyclicity appears even in model simulations with constant greenhouse forcing as a direct and strongly nonlinear response to orbital variations. However, the simulated 100-kiloyear cyclicity is much weaker with constant CO₂, which suggests that the carbon-dioxide climate ice-sheet feedback strongly amplifies the 100-kiloyear cycles. Our experiments also reveal the important role of eolian dust in shaping of glacial cycles and, especially, glacial terminations. Simulations with fully interactive carbon and dust cycle models are required for a better understanding of Quaternary climate dynamics.

Introduction

Study of past climates plays an increasing role in gaining a better understanding of climate dynamics and testing climate models applied for predictions of future climate change. Pronounced climate variability at orbital timescales during past several million years, which is well documented in numerous paleoclimate archives, provides a wealth of information to advance our understanding of the Earth system. It is generally

A. Ganopolski (✉)
Potsdam Institute for Climate Impact Research,
PO Box 601203, 14412 Potsdam, Germany
e-mail: andrey@pik-potsdam.de

accepted that, as postulated by the Milankovitch theory (Milankovitch 1941), the Earth's orbital variations play a fundamental role in driving glacial cycles. However, many aspects of glacial cycles, such as the strongly nonlinear response of the ice sheets to orbital forcing and the role of carbon-dioxide climate ice-sheet feedback, still remain poorly understood. One of the major problems of the classical Milankovitch theory is the prevailing 100-kiloyear cyclicality seen in the reconstructed global ice volume and other climate characteristics over the past million years. This periodicity is practically absent in the principal "Milankovitch forcing"—variations of summer insolation at high latitudes of the Northern Hemisphere (NH). The eccentricity of the Earth's orbit does contain a periodicity close to 100 kiloyears, but the direct effect of the eccentricity changes on the global Earth's energy budget does not exceed 0.1% and, therefore, is unlikely to play any role in driving glacial cycles. Alternatively, the 100-kiloyear signal can result from a nonlinear response of the climate–cryosphere system to variations of the magnitude of precessional component of the orbital forcing, which is modulated by eccentricity. In this case, the eccentricity signal might appear in the climate system response to the orbital forcing as the result of amplitude demodulation. However, in this case, it is unclear why only one of several dominant eccentricity frequencies is picked up by such demodulation. In a view of this problem, some workers proposed that 100-kiloyear cyclicality does not originate directly from the orbital forcing but rather represents internal oscillations in the climate–cryosphere or climate–cryosphere–carbonosphere system (Saltzman and Maasch 1988). Alternatively, it was proposed that 100-kiloyear cycle appears from the terminations of the ice sheets buildup by each second or third obliquity cycle (Huybers and Wunsch 2005) or each fourth or fifth precessional cycle (Ridgwell et al. 1999). Several decades, which passed since the discovery of the dominant 100-kiloyear cyclicality, clearly demonstrated that data analysis or development of conceptual models alone is insufficient to solve the glacial cycle problem, and using of comprehensive Earth system models is required.

First simulations of glacial cycles were performed with rather simple climate–cryosphere models such as zonally averaged or two-dimensional energy-balance climate models coupled to simplified ice-sheet models (Pollard 1982; Deblonde et al. 1992; Gallée et al.

1991). These experiments demonstrated that, when forced by variations of the Earth's orbital parameters, simulated ice sheets experience large variations at all major orbital frequencies (precessional, obliquity, and eccentricity) with clearly asymmetric temporal dynamics consistent with paleoclimate data. It was shown by Berger et al. (1999) that the 100-kiloyear cyclicality appears only when CO₂ concentration is below a certain threshold and, although CO₂ alone is insufficient to drive the glacial cycles (Loutre and Berger 2000), it is an important amplifier of the 100-kiloyear cycle.

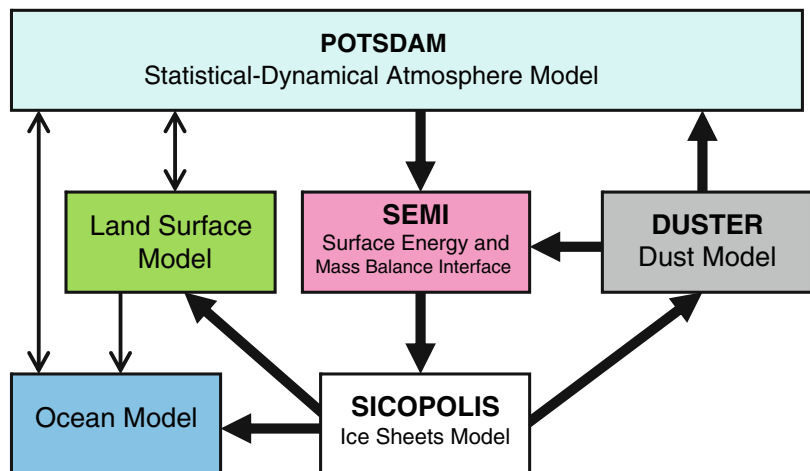
In recent years, a new class of models, the so-called Earth system model of intermediate complexity (EMICs), became available for the study of glacial cycles. These models are far less computationally demanding than coupled GCMs but incorporate substantially more physical processes than simple models. In particular, EMICs were used to simulate the last glacial inception (Wang and Mysak 2002; Calov et al. 2005) and the entire last glacial cycle (Bonelli et al. 2009; Ganopolski et al. 2010).

The decisive testing of the Milankovitch theory would require simulations of Quaternary climate dynamics on the million years timescale with comprehensive Earth system models which include all major components of the Earth system and use variations of the Earth's orbital parameters as the only prescribed forcing. The current work represents a step in this direction. Further development, which includes incorporation of fully interactive carbon cycle, dust cycle, and sediment models, is under way.

Model and Experimental Setup

The model used in this study is the newest version of CLIMBER-2. The CLIMBER-2 model includes six components of the Earth system: atmosphere, ocean, sea ice, land surface, terrestrial vegetation, and ice sheets (see Fig. 1 for illustration). The first five components are represented by coarse-resolution modules of intermediate complexity and were described in detail by Petoukhov et al. (2000). The ice-sheet component is represented by the three-dimensional polythermal ice-sheet model SICOPOLIS (Greve 1997) with latitudinal resolution of 0.75° and longitudinal resolution of 1.5°. The ice-sheet model is only applied to the NH. The effect of Antarctic ice sheet

Fig. 1 Flow diagram of the model version used in this study. *Thick arrows* represent new flows of information compared to the “standard” version of CLIMBER-2 described in Petoukhov et al. (2000)



was crudely accounted for by enhancement of simulated sea level variations by 20%. Similarly to our previous works, we used three different sliding laws for areas covered by marine and terrestrial sediments, and land area without sediment cover. The distribution of the sediment was prescribed from the data for the sediment thickness by Laske and Masters (1997). All oceanic grid points were treated as covered by marine sediments.

The coupling between climate and ice-sheet components is provided via the high-resolution physically based surface energy and mass-balance interface (SEMI) described in Calov et al. (2005). Surface ice-sheet mass balance and temperature are computed on a daily time step using the fields of atmospheric temperature, precipitation, and long- and short-wave radiation, which are computed by the climate component of CLIMBER-2 and interpolated to the ice-sheet model grid. The model explicitly accounts for the direct radiative forcing of the atmospheric dust and the effect of dust deposition on snow albedo. The latter, as shown in Calov et al. (2005) and Ganopolski et al. (2010), plays an important role in controlling the spatial extent of the ice sheets and the rate of deglaciation. The dust deposition is computed as the sum of the background dust deposition, taken from GCM simulations, and the deposition of glaciogenic dust, which is interactively computed in the CLIMBER-2 model (Ganopolski et al. 2010). The cryosphere component influences the climate via changes in surface albedo, elevation, land area, and the freshwater flux into the ocean originating from ice sheet melting and iceberg calving.

The model and modeling setup are the same as used in Ganopolski et al. (2010) for the simulation of the last glacial cycle. Here we use this approach to simulate last 800 kiloyears—the period of time which was dominated by 100-kiloyear cyclicity and for which concentration of GHGs is available from the Antarctic ice cores. Since most components of the Earth system are represented in the model, the experimental setup is rather straightforward. Apart from variations in the Earth’s orbital parameters computed according to Berger (1978), the only climate forcing prescribed in the model is the radiative forcing of GHGs. The combined effect of the CO_2 , CH_4 , and N_2O was represented through the prescribing of the so-called equivalent CO_2 concentration, which is computed in such a way to produce a radiative forcing equal to the sum of the radiative forcings of individual greenhouse gases.

All experiments were started at 860 kiloyears BP (before present) corresponding to the MIS 21 interglacial. Initial conditions were taken from the preindustrial equilibrium climate state, and the model was run for 860 kiloyears. The first 60 kiloyears were considered as the model spin-up, and here we present results for the last 800 kiloyears.

Results

Temporal Dynamics

Figure 2 shows the prescribed external (orbital) and internal (GHGs) forcings and modeled Earth system response. The orbital forcing is represented in the

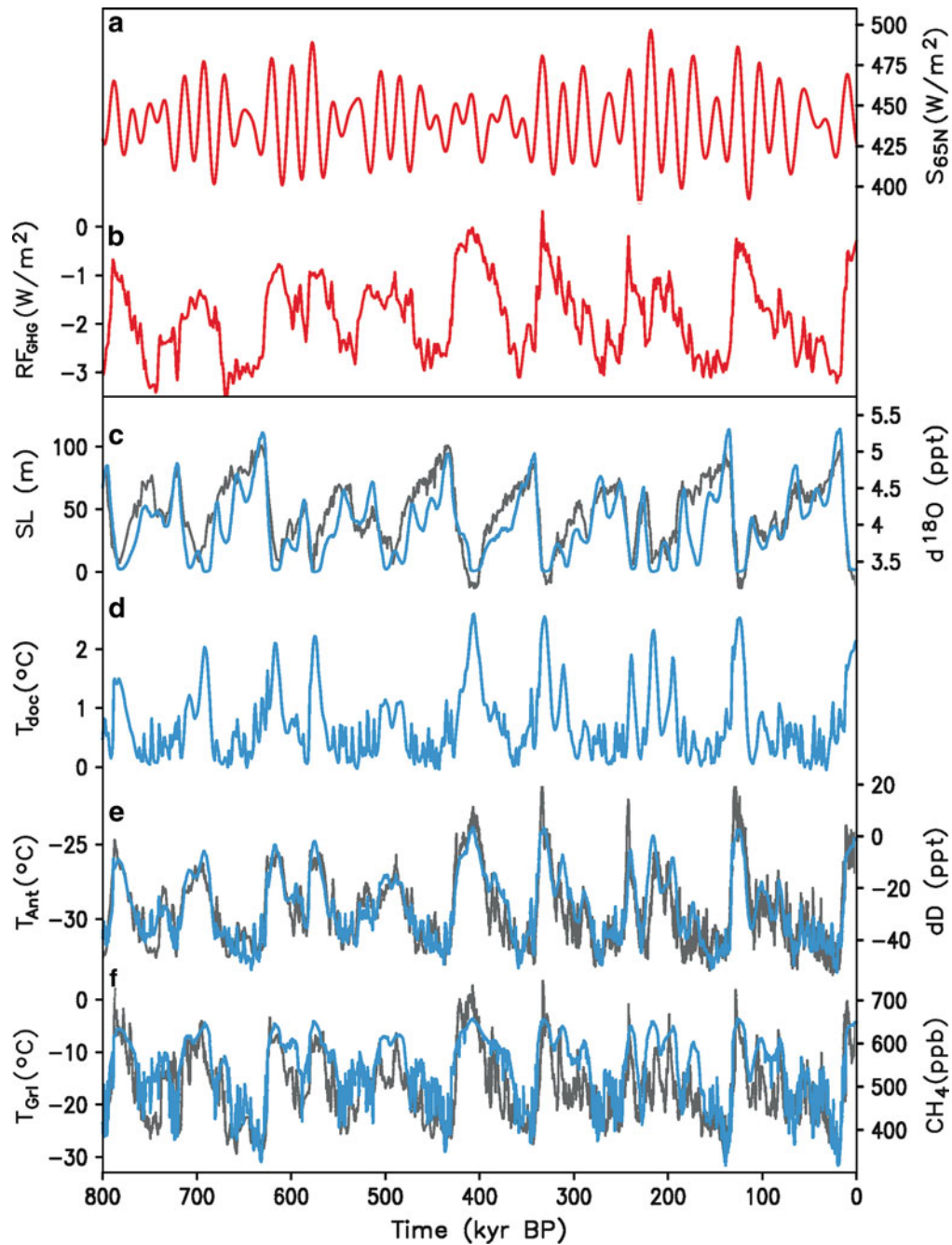


Fig. 2 Temporal variations of prescribed forcings (a, b) and simulated climate–cryosphere characteristics (c–f). (a) orbital forcing illustrated by the maximum summer insolation at 65°N, (b) total radiative forcing of three major greenhouse gases, (c) simulated ice volume (blue line) vs. arbitrarily scaled Lisiecki and Raymo (2005) $\delta^{18}\text{O}_c$ stack (gray line), (d) globally

averaged simulated deep (4 km) ocean temperature, (e) simulated East Antarctic temperature (blue line) vs. EPICA deuterium record (gray line), and (f) simulated Greenland temperature (blue line) vs. arbitrary scaled atmospheric CH_4 concentration (gray line), which is taken as a proxy for the NH temperature

figure by the maximum summer insolation at 65°N. Figure 2c shows the simulated NH ice volume over the past 800 kiloyears. Since reconstructions of global ice volume are available only for the recent glacial cycles, here we compare results of simulations with the benthic oxygen isotope stack LR04 by Lisiecki and Raymo (2005). Although the latter is widely used as a proxy for the global ice volume, it is known that $\delta^{18}\text{O}$ in calcite is also strongly affected by deep ocean temperature and changes in the hydrological cycle. Moreover, our model simulates only the NH ice sheets, and the Southern Hemisphere contributed additionally 10–20% to the global ice volume variations during glacial cycles. Therefore, the comparison of the simulated ice volume with the oxygen isotope stack should be made with caution. Nonetheless, the overall agreement between simulated ice volume and its paleoclimate proxy is reasonably good. Simulated glacial cycles are dominated by the 100-kiloyear cyclicality (see also Fig. 3) and have a pronounced sawtooth shape with a long phase of ice growth and rapid glacial terminations occurring within ten thousand years. The timing of all major glacial terminations agrees with paleoclimate reconstructions within their dating errors. The maximum volume achieved at the end of each glacial cycle is about 100 m in sea level equivalent. At the same time, the simulated ice volume is characterized by a more pronounced variability at precessional timescale compared to the oxygen isotope stack.

This is also clearly demonstrated by the spectral analysis (Fig. 3).

Simulated deep ocean temperature variations, shown in Fig. 2d, have a rather different pattern from that of ice volume, which is consistent with the paleoclimate reconstructions for recent glacial cycles (e.g., Waelbroeck et al. 2002). The magnitude of simulated glacial–interglacial variations of the deep ocean temperature is about 2°C, which also agrees with the paleoclimate reconstructions. Compared to the ice volume, “glacial” parts of the deep ocean temperature record are much flatter, which is explained by the rectification effect of the freezing temperature of sea water on the temperature evolution. Since the deep ocean temperature variations contribute at least one-third to the glacial–interglacial variations in $\delta^{18}\text{O}_c$, comparison of Fig. 2c, d provides additional support to the notion that the benthic oxygen isotope stack should be regarded with great caution if used as proxy of global ice volume.

Simulated Antarctic temperature is in good agreement with paleoclimate reconstructions based on deuterium isotope record (Fig. 2e). This is not surprising since the Antarctic temperature is highly correlated with the prescribed CO_2 concentration, which explains the largest portion of glacial–interglacial Antarctic temperature variations (e.g., Ganopolski and Roche 2009). Modeled Antarctic temperature, similarly to the real one, also contains a pronounced millennial scale variability, which is related to simulated

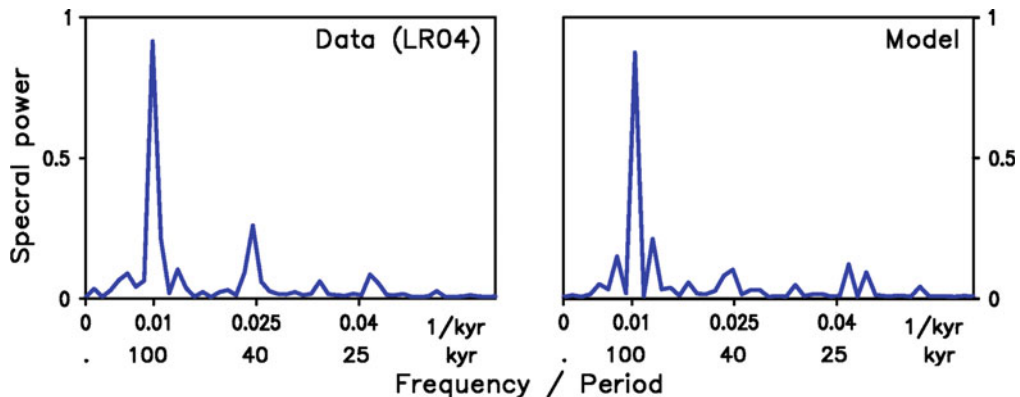


Fig. 3 Power spectra of the Lisiecki and Raymo (2005) $\delta^{18}\text{O}$ stack (*left*) and simulated Northern Hemisphere ice volume (*right*) in arbitrary units

variability of the Atlantic thermohaline circulation through the mechanism of “bipolar thermal seesaw.” For the last glacial cycle, as shown in Ganopolski et al. (2010), agreement between simulated Greenland temperature and the ice core data is rather good. Since there is no reliable Greenland ice core data spanning beyond the Eemian interglacial, we use EPICA methane concentration record as proxy for the Greenland temperature (Fig. 2f). This is justified by the fact that there is a striking similarity between methane concentration and Greenland temperature during the last glacial cycle. Similarly to the Antarctic temperature, simulated Greenland temperature resembles CO₂ concentration but has a more pronounced variability at the precessional and millennial timescales. The latter is related to the simulated Dansgaard–Oeschger events.

The Role of Individual Forcings and Feedbacks

In a separate set of modeling experiments (not shown here), we found that:

1. Switching off the effect of the dust deposition on snow albedo leads to a rapid development of unrealistically large ice sheets, which cannot be melted even during periods of high CO₂ concentration and summer insolation. This confirms our earlier speculation (Calov et al. 2005) about the importance of eolian dust in restriction of growth of the ice sheets and their rapid terminations.
2. Fixing of equivalent CO₂ concentration during the whole model run does not prevent simulation of sufficient realistic glacial cycles; but the 100-kiloyear cyclicity only appears under relative low CO₂ concentrations (below ca. 240 ppm), and the magnitude of the 100-kiloyear component of the ice volume variability remains relatively weak compared to the experiment with prescribed time-dependent CO₂ concentration. This result is in line with the earlier finding by Berger et al. (1999).
3. When equivalent CO₂ concentration varies in time following the EPICA record and the orbital parameters are kept constant and prescribed either for “cold” or “warm” orbital configuration, similarly to Loutre and Berger (2000), no significant variations in the NH ice volume were simulated. For “cold orbit” case, unrealistically large ice

sheets are simulated, and they only modestly respond to the variation of CO₂. For “warm orbit” configuration, ice sheets do not appear even during periods of low CO₂ concentration.

Discussion and Conclusions

Experiments with the Earth system model of intermediate complexity CLIMBER-2, where climate and cryosphere components are coupled bidirectionally and fully interactively through the physically based interface, were presented. They show that, when driven by orbital variations and GHG concentrations, the model simulates rather realistically temporal dynamics of the ice volume and other climate characteristics over the last 800 kiloyears. Both ice volume and temperature variability are dominated by 100-kiloyear cyclicity.

A set of additional experiments demonstrates the role of atmospheric dust in restricting of ice sheet growth and fast glacial terminations. Relatively realistic glacial cycles can be also simulated with orbital forcing alone if the prescribed constant CO₂ concentration is sufficiently low. At the same time, variations of equivalent CO₂ concentration alone cannot drive realistic glacial cycles. These results clearly point on the orbital forcing as the primary driver of the glacial cycles, while CO₂ represents an important internal feedback, which amplifies glacial cycle and, especially, their 100-kiloyear cyclicity. Eolian dust serves as another important climate feedback, negative during initial growth of the ice sheets and positive during glacial terminations. Therefore, the next step in testing the Milankovitch theory should include simulations of glacial cycles with interactive CO₂ and eolian dust models. This work is now under way.

References

- Berger A (1978) Long-term variations of daily insolation and Quaternary climatic change. *J Atmos Sci* 35:2362–2367
- Berger A, Li X, Loutre M-F (1999) Modelling northern hemisphere ice volume over the last 3 Ma. *Quat Sci Rev* 18:1–11
- Bonelli S, Charbit S, Kageyama M, Woillez M-N, Ramstein G, Dumas C, Quiquet A (2009) Investigating the evolution of major Northern Hemisphere ice sheets during the last glacial-interglacial cycle. *Clim Past* 5:329–345

- Calov R, Ganopolski A, Claussen M, Petoukhov V, Greve R (2005) Transient simulation of the last glacial inception with an atmosphere-ocean-vegetation-ice sheet. Part I: glacial inception as a bifurcation of the climate system. *Clim Dyn* 24:545–561
- Deblonde G, Peltier WR, Hyde WT (1992) Simulations of continental ice sheet growth over the last glacial-interglacial cycle: experiments with a one level seasonal energy balance model including seasonal ice albedo feedback. *Glob Planet Change* 6:37–55
- Gallée H, van Ypersele JP, Fichefet T, Tricot C, Berger A (1991) Simulation of the last glacial cycle by a coupled, sectorially averaged climate-ice sheet model. 1. The climate model. *J Geophys Res* 96:13139–13161
- Ganopolski A, Roche D (2009) On the nature of leads and lags during glacial-interglacial transitions. *Quat Sci Rev* 3738:3361–3378. doi:[10.1016/j.quascirev.2009.09.019](https://doi.org/10.1016/j.quascirev.2009.09.019)
- Ganopolski A, Calov R, Claussen M (2010) Simulation of the last glacial cycle with a coupled climate-ice sheet model of intermediate complexity. *Clim Past* 7:1415–1425
- Greve R (1997) A continuum-mechanical formulation for shallow polythermal ice sheets. *Philos Trans R Soc Lond A* 355:921–974
- Huybers P, Wunsch C (2005) Obliquity pacing of the late Pleistocene glacial terminations. *Nature* 434:491–494
- Laske G, Masters GA (1997) Global digital map of sediment thickness. *EOS Trans AGU* 78:F483
- Lisiecki LE, Raymo ME (2005) A Pliocene-Pleistocene stock of 57 globally distributed benthic $\delta^{18}\text{O}$ records. *Paleoceanography* 20:PA1003. doi:[10.1029/2004PA001071](https://doi.org/10.1029/2004PA001071)
- Loutre MF, Berger A (2000) No glacial-interglacial cycle in the ice volume simulated under a constant astronomical forcing and a variable CO_2 . *Geophys Res Lett* 27:783–786
- Milankovitch MM (1941) *Kanon der Erdbestrahlung und seine Anwendung auf das Eiszeitenproblem*. Royal Serbian Sciences, Spec pub 132, Section of Mathematical and Natural Sciences, vol 33. Belgrade, p 633
- Petoukhov V, Ganopolski A, Brovkin V, Claussen M, Eliseev A, Kubatzki C, Rahmstorf S (2000) CLIMBER-2: a climate system model of intermediate complexity. Part I: model description and performance for present climate. *Clim Dyn* 16:1–17
- Pollard D (1982) A simple ice-sheet model yields realistic 100 kyr glacial cycles. *Nature* 296:334–338
- Ridgwell A, Watson A, Raymo M (1999) Is the spectral signature of the 100 kyr glacial cycle consistent with a Milankovitch origin. *Paleoceanography* 14:437–440
- Saltzman B, Maasch KA (1988) Carbon cycle instability as a cause of the late Pleistocene ice age oscillations: modeling the asymmetric response. *Global Biogeochem Cycles* 2:177–185
- Waelbroeck C, Labeyrie L, Michel E, Duplessy JC, McManus JF, Lambeck K, Balbon E, Labracherie M (2002) Sea-level and deep water temperature changes derived from benthic foraminifera isotopic records. *Quat Sci Rev* 21:295–305
- Wang Z, Mysak LA (2002) Simulation of the last glacial inception and rapid ice sheet growth in the McGill Paleoclimate Model. *Geophys Res Lett* 29:2102. doi:[10.1029/2002GL015120](https://doi.org/10.1029/2002GL015120)

Modeling the Interglacials of the Last 1 Million Years

André Berger and Qiuzhen Yin

Abstract

The climate response associated with the interglacial peaks of the last 1 million years is investigated with an Earth model of intermediate complexity, LOVECLIM, to the variations of the astronomically induced insolation and of the greenhouse gas concentrations. The dates selected are those where the Northern Hemisphere summer occurs at perihelion. The simulated global annual mean air temperature shows that, on average, the interglacials after the Mid-Brunhes Event are warmer than those before, as expected from the larger average CO₂ concentration. However, the seasonal response came more as a surprise with the warming being mainly during the winter season in response to the astronomical forcing. The latitudinal and seasonal distribution of insolation is indeed characterized by less energy available, in average, over the Earth during Northern Hemisphere summer but more during Northern Hemisphere winter for the interglacials after Mid-Brunhes Event than before. The relationship to the long-term variations of precession and obliquity is discussed.

Introduction

The succession of glacial–interglacial cycles is a prominent feature of the last 3 million years. From 3 to 1 Ma BP, climate variation was characterized by a 41-ka quasi-cyclicity (Ruddiman et al. 1986). After the mid-Pleistocene transition, at about 900 ka BP, this cyclicity became progressively 100 ka, a transition clearly simulated by Berger et al. (1999). In addition, during the last 1 million years, marine and ice core

records show a clear fracture around 430,000 years ago. Just after MIS-13, at the Mid-Brunhes Event (MBE), the amplitude of the glacial–interglacial cycles has indeed significantly increased in the global ice volume (Lambeck et al. 2002; Bintanja et al. 2005; Lisiecki and Raymo 2005), in the temperature of Antarctica (EPICA 2004; Jouzel et al. 2007), and in the greenhouse gas (GHG) concentrations (Louergue et al. 2008; Luthi et al. 2008). The pre-MBE interglacials appear therefore cooler—at least in Antarctica—and probably more glaciated than the post-MBE interglacials.

To understand such a feature, a series of snapshot simulations were performed to intercompare the interglacials of the last 800 ka, a complementary approach to the transient simulation done by Ganopolski and Calov (2012). The Earth system model of intermediate complexity, LOVECLIM, has been forced with the

A. Berger (✉)
Georges Lemaître Center for Earth and Climate Research
(formerly Institute of Astronomy and Geophysics G. Lemaître),
Université catholique de Louvain, Chemin du Cyclotron 2, 1348
Louvain-la-Neuve, Belgium
e-mail: andre.berger@uclouvain.be

insolation and greenhouse gas concentrations. In this chapter, the atmosphere (Opsteegh et al. 1998), the ocean and sea ice (Goosse and Fichefet 1999), and the vegetation (Brovkin et al. 1997) components are interactively coupled. The selection of the interglacial peaks and their astronomical forcing is the same as in Yin and Berger (2010). The peaks of the Lisiecki-Raymo benthic $\delta^{18}\text{O}$ record have been selected. The peaks of other $\delta^{18}\text{O}$ curves are different in amplitude and in time but fortunately not that much. The selection of the peaks even within a given record is, however, not necessarily straightforward. For some interglacials, like MIS-7, MIS-13, and MIS-15, more than one peak is existing. This was solved in our case by using an astronomical criterion. For our modeling experiments, we selected indeed the dates when Northern Hemisphere (NH) summer occurred at perihelion (it means with the longitude of the perihelion equals to 270° as compared to 102° presently, NH summer occurring now close to aphelion). A detailed analysis shows that these dates correspond quite well to the peaks of the $\delta^{18}\text{O}$ -curve if we accept that the response time of the climate system to the astronomically induced insolation is about 5,000 years. Moreover, such a selection provides a more homogeneous ensemble of experiments to do than if we would have selected the dates of the $\delta^{18}\text{O}$ peaks; our work has indeed to be considered as a sensitivity analysis to the astronomical forcing under the hypothesis that NH summer at perihelion drives the interglacial climate. The astronomical parameters calculated by Berger (1978) are used. For the greenhouse gas concentrations, we use an average over a few thousands of years around the peaks of CO_2 , CH_4 , and N_2O just preceding the $\delta^{18}\text{O}$ peaks to have a maximum response of the model. This is slightly different from the strategy used in Yin and Berger (2010) where the three GHG concentrations are selected at the dates of the CO_2 peaks. This can be considered as a sensitivity experiment to the GHG concentrations (a problem discussed in the supplementary material of Yin and Berger 2010), the results showing that it does not affect our conclusions.

Precession and Obliquity During the Interglacials

The occurrence of glacials has been associated to NH summer at aphelion, a large eccentricity, and a low obliquity by Milankovitch (1941). For the interglacials,

Kukla et al. (1981) have tentatively associated them to NH summer at perihelion, a large eccentricity, and a large obliquity. This kind of simultaneous occurrence guarantees indeed to maximize the energy received by the NH during its summer. A large eccentricity minimizes the Earth–Sun distance at perihelion, and a large obliquity increases the energy received in high northern latitudes during their summer. Figure 1 shows the phase relationship between precession and obliquity at all interglacials:

1. For the peaks of MIS-1, MIS-5.5, MIS-9.3, MIS-15.1, MIS-19, and MIS-21.3, precession minima and obliquity maxima are more or less in phase and lead the $\delta^{18}\text{O}$ minima by about 5 ka (for MIS-1, obliquity maximum lags behind precession minimum by 3 ka, for MIS-5.5 and MIS-21.3, it precedes precession minimum by 3 ka, and for the other three, they are in phase). Three of these interglacials occur before MBE and three after, making a criterion based only on the phasing relationship between precession and obliquity difficult to be used to distinguish between “warmer” (after MBE) and “cooler” (before MBE) interglacials.
2. At the peaks of MIS-7.5, MIS-11.3, and MIS-17, obliquity maxima precede precession minima by about 9 ka, making them almost in opposite phase. However, MIS-17 is much more insolated than MIS-7.5 and 11.3.
3. Finally, MIS-13.1 is the most puzzling. At MIS-13.11, obliquity and precession maxima are almost in phase and lead the $\delta^{18}\text{O}$ minima by about 5 ka, a situation which challenges the relationship between precession and climate, the interglacial being here associated with NH summer at aphelion (or SH summer at perihelion). For MIS-13.13, the precession minimum (at 506 ka BP) occurs 9 ka before the obliquity maximum, a situation similar to MIS-1 but with a larger phase shift. Although MIS-13.13 is not an interglacial peak in Lisiecki and Raymo (2005)—it is in SPECMAP (Imbrie et al. 1984) and in Bassinot et al. (1994)—we selected this date because the astronomical forcing fits better our hypothesis and sensitivity analysis.

This analysis of the precession–obliquity phase relationship leads to about all possible combinations, and no easy conclusion can be drawn. Although it is difficult to see any difference in the astronomical elements of the interglacials before and after the MBE, it happens however that over the five post-MBE interglacials, the

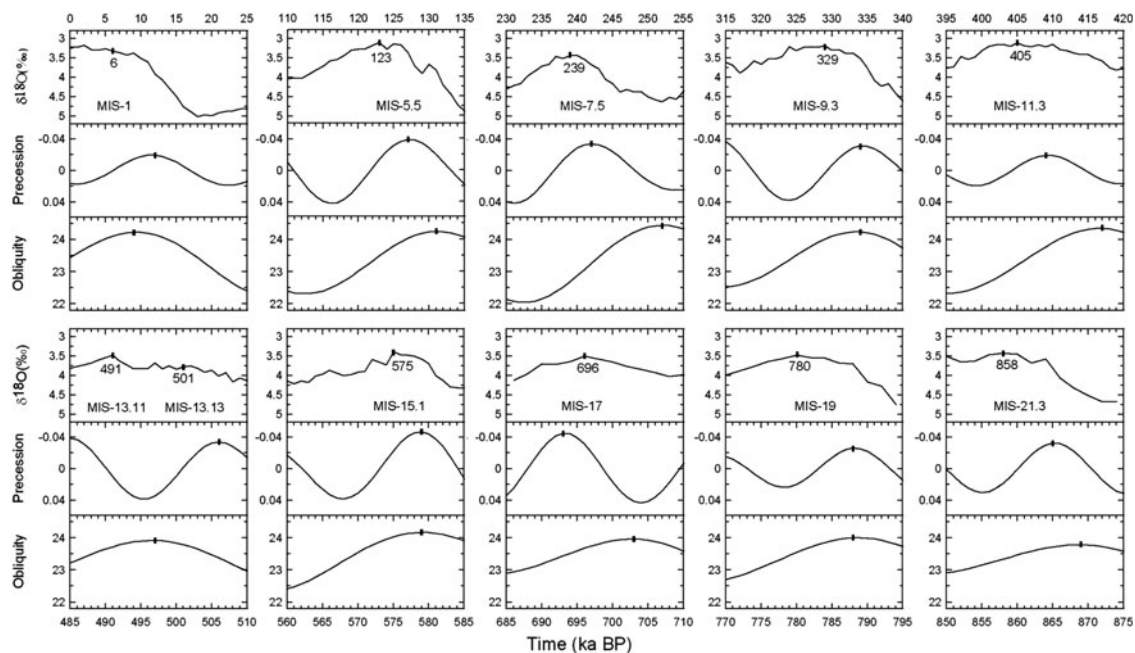


Fig. 1 Marine $\delta^{18}\text{O}$ (Lisiecki and Raymo 2005), precession, and obliquity (Berger 1978) around the last ten interglacial peaks. The *small black bars* localize the $\delta^{18}\text{O}$ minima, precession minima, and obliquity maxima. The selected dates of the

$\delta^{18}\text{O}$ minima and their corresponding marine isotope stages are indicated. For MIS-13, MIS-13.13 (Imbrie et al. 1984) instead of MIS-13.11 is chosen. The astronomical parameters used in our simulations are those at the dates of precession minima

average values of eccentricity (0.028776) and of obliquity (23.90) are significantly different from those calculated over the five pre-MBE interglacials (0.037000 and 23.74, respectively). This is related to the 400-ka cycle of eccentricity which is much stronger after the MBE than before and to the 1.3 million years cycle in the amplitude modulation of obliquity (Berger et al. 1998).

Latitudinal and Seasonal Distribution of Insolation

As the climate system is actually driven by the latitudinal and seasonal distribution of insolation (Berger et al. 1993), the comparison of the insolation distributions between the interglacials is worth to be discussed.

First, as expected, there is a strong coherency between the patterns of all the selected dates. This is coming from the fact that the “mid-month” values of insolation are used; it means that the seasonal cycle is described in terms of the true longitude of the perihelion (Berger 1978). It is also a direct consequence of the selected dates which all correspond to NH summer

at perihelion. This influence can be shown by comparing the insolation patterns over the Holocene at 9, 6, and 3 ka BP to that at 12 ka BP where NH summer occurs at perihelion. At 12 ka BP, the Earth receives more energy than today all over the Earth during NH summer and less during NH winter (SH summer). On the contrary, at 6 ka BP, both NH and SH receive more energy equally during their local summers. At 9 ka BP, both NH summer and SH summer receive also more energy than today, but there is definitely more energy available in NH summer than in SH summer, a remainder left from the 12 ka BP situation with NH summer at perihelion. Such periods of time during which both local summers receive more energy (from 9 to 3 ka BP here) deserve more attention, but at the present, we focus only on situations when NH summer receives more insolation than today and SH summer less.

Second, MIS-5.5, MIS-9.3, and MIS-15.1 are definitely the most insolated. This could have been expected from the analysis of the astronomical elements themselves where MIS-1, 5.5, 9.3, 15.1, 19, and 21.3 show a good correlation between precession minimum and obliquity maximum. But the insolation is not strong at MIS-1, 19, and 21.3 because of a low

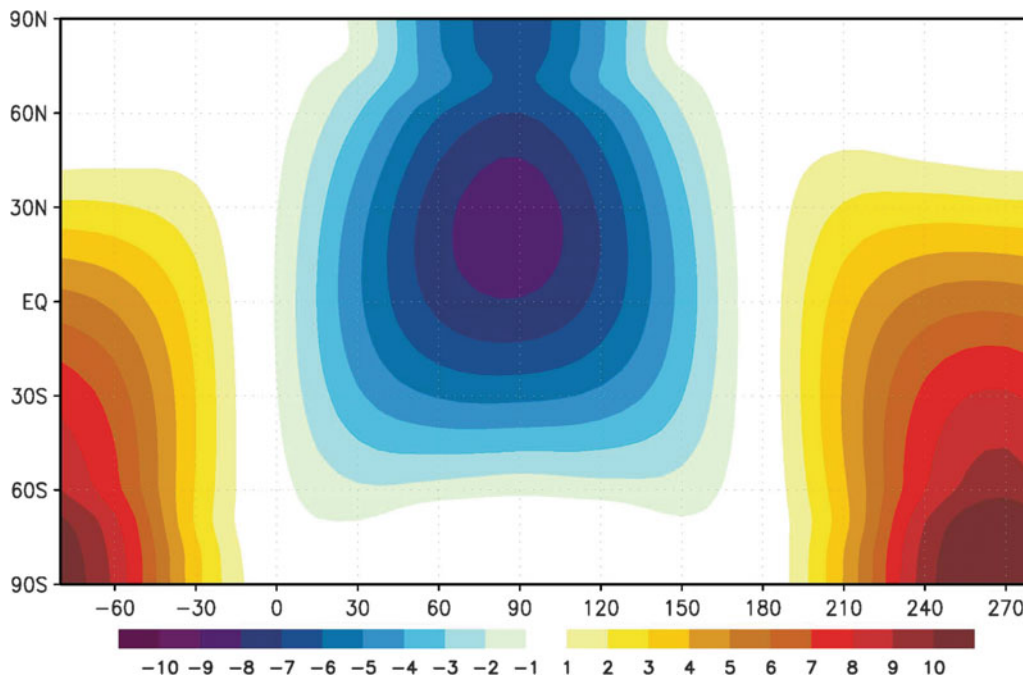


Fig. 2 Difference in the latitudinal and seasonal distribution of insolation (W m^{-2}) between the average of the post-MBE interglacials and the average of the pre-MBE ones. Labels on the X-axis indicate the true longitude of the Sun from the

beginning to the end of the year (0° and 180° are for the spring and fall equinoxes; 90° and 270° are for the summer and winter solstices). Insolation is calculated from the long-term variations of eccentricity, precession, and obliquity (Berger 1978)

eccentricity, which is also the case for MIS-11.3. This low value is associated to the 400-ka cycle of eccentricity, which is at the basis of taking MIS-11 as a potentially good analogue for MIS-1 and at the origin of the prediction of an exceptionally long interglacial MIS-1 (Berger and Loutre 2002).

Despite all these differences between the interglacials, the insolation patterns before and after MBE appear to be clearly different when their averages are considered. This difference was quite unexpected (Fig. 2): NH summer is significantly underinsolated (at 30°N , by 8.6 W m^{-2}) and SH summer overinsolated (at 90°S by 11.7 W m^{-2}). This is mainly due to precession, but as the longitude of the perihelion is fixed, the difference in precession results strictly from a difference in eccentricity. A smaller post-MBE eccentricity value leads to a larger distance at perihelion and therefore to a lower insolation during the NH summer all over the Earth. But at the same time, the influence of a greater obliquity is felt because the high polar latitudes are less underinsolated than expected from a smaller eccentricity.

Modeling the Response to Astronomical and GHG Forcings

The concentration in CO_2 equivalent characterizing the pre-MBE interglacials varies between 229 and 247 ppmv; for the post-MBE, it varies between 260 and 300 ppmv. There is, in average, a difference of 38 ppmv between the post- and the pre-MBE interglacials. The largest value appears during MIS-9, followed by MIS-5 and MIS-11. The lowest values occur for MIS-17 and MIS-13. Let us note that the value for MIS-1 is the lowest among the post-MBE interglacials.

Figure 3a shows the simulated annual mean temperature on the globe for each of the last ten interglacials compared to their average which is 16.3°C . The average temperature of the post-MBE interglacials (MIS-1 to MIS-11) is higher than that of the pre-MBE ones (MIS-13 to MIS-21) by 0.43°C . The post-MBE interglacials, except MIS-7, are all above their average value, with MIS-9 being the warmest followed by MIS-5, MIS-11, MIS-1, and

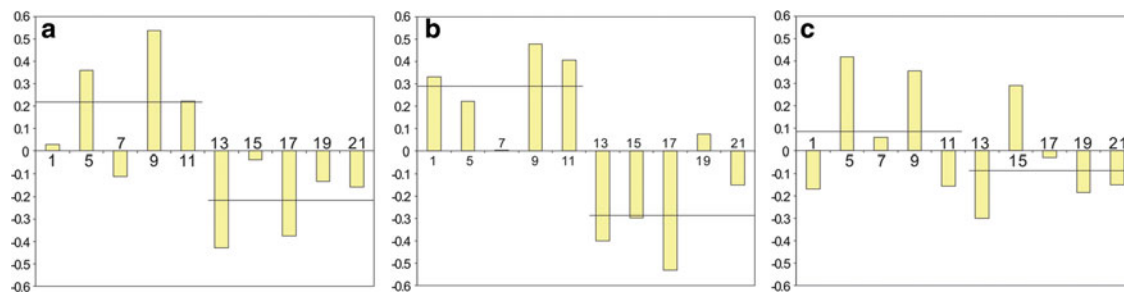


Fig. 3 Deviations of the simulated global average temperature ($^{\circ}\text{C}$) of the ten interglacials from their averages. (a) Annual mean (16.3), (b) January (13.5), and (c) July (19.6). The horizontal lines indicate the averages of the post-MBE and of the pre-MBE interglacials

MIS-7, the coolest. This ranking follows quite well the CO_2 and insolation values, with MIS-9 CO_2 being the largest followed by MIS-5, although MIS-5 is slightly more insolated during NH summer than MIS-9. MIS-11 receives the lowest NH summer insolation but more CO_2 than MIS-1. MIS-7 is coming definitely the last because of both low CO_2 and pretty low insolation.

The five pre-MBE temperatures are all below the average, with MIS-15 being the warmest followed by MIS-19, MIS-21, MIS-17, and MIS-13, the coolest. Here also the insolation pattern and CO_2 concentration are well imprinted in the climate of the interglacials. MIS-15 receives definitely the largest NH summer insolation. At MIS-17, a low CO_2 (the lowest of the last ten interglacials) is compensated by a rather large insolation. The coolest MIS-13 reflects both a low CO_2 and a low insolation. Therefore, for the last ten interglacials, MIS-9 is definitely the warmest followed by MIS-5, and MIS-13 is the coolest. The insolation pattern of the coolest interglacials in each group (MIS-7 and MIS-13) is rather similar, but MIS-7 CO_2 is about 35 ppmv larger than MIS-13. If we compare the global annual mean temperature to the GHG concentrations, we see that the CO_2 equivalent of MIS-7 is 11 ppmv larger than MIS-1 but is cooler. Also MIS-15, MIS-19, and MIS-21 have been forced with a similar CO_2 , but MIS-15 is definitely warmer than the other two. Clearly, both CO_2 and insolation seem to play a role. This requests to analyze the seasonal response to the astronomical and GHG forcings as done below and in section “Causes for the Difference Between the Post-MBE and the Pre-MBE Interglacials.” Although the model is only forced by insolation and GHG, the amplitude of the annual mean temperature of these ten interglacials is in reasonable agreement with the amplitude of the

marine $\delta^{18}\text{O}$ records. If we assume that the $\delta^{18}\text{O}$ of the benthic foraminifera is primarily a function of the global ice volume, the deep-sea records show indeed that there is much less ice over the Earth after 430 ka BP than before and that the (13.5) pre-MBE interglacials are in average more glaciated and therefore most probably cooler than the post-MBE ones. The $\delta^{18}\text{O}$ records show also that MIS-7 is the coolest interglacial over the last 430 ka, and MIS-13 is the coolest one over the whole last 1 million years, which validates our modeling results.

In order to understand which season is responsible for such behavior, Fig. 3b, c shows, for each of the last ten interglacials, the surface mean temperature for the whole globe in January and July compared to their averages (13.5 and 19.6 respectively). Globally, the post-MBE interglacials are in average 0.55°C warmer than the pre-MBE ones in January but only 0.18°C in July. Moreover, in January, all the five post-MBE interglacials except MIS-7 are well above the average, and all the pre-MBE ones, except MIS-19, are well below the average. Definitely, the warming in annual average is mainly due to the warming in January, which fits very well with the insolation pattern of Fig. 2. For the post-MBE interglacials, MIS-9 and MIS-11 are the warmest followed by MIS-1 which is affected by its low CO_2 . In July, the difference between the last five and the previous five interglacials is much smaller, and only MIS-5, 9, and 15 are above the respective averages. Analyzing now the differences between the hemispheres during the same local seasons, Fig. 4 shows that the post-MBE interglacials are on average significantly warmer than the pre-MBE ones in the winter hemispheres (0.53°C for NH in January and 0.33°C for SH in July). For the summer hemispheres, the situation is more complex. The SH

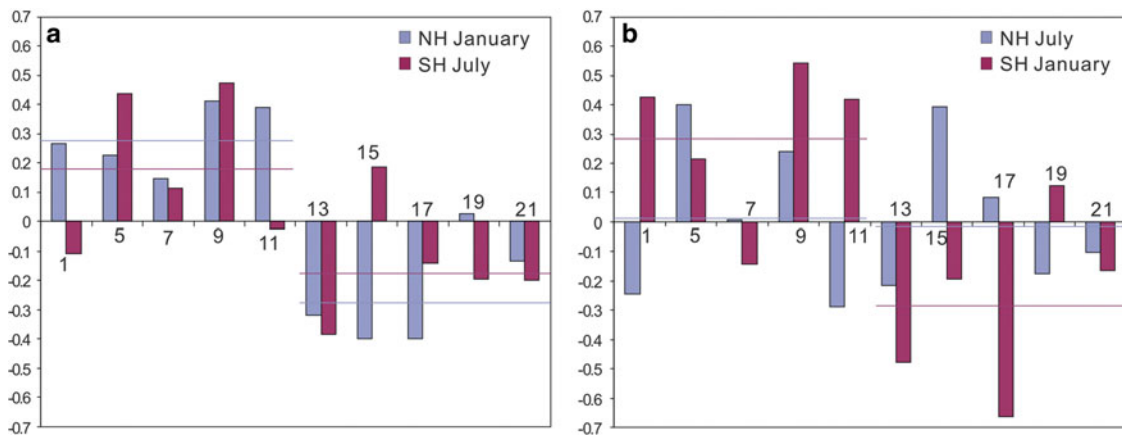


Fig. 4 Deviations of the simulated surface temperature for the winter hemispheres (9.1 for NH and 13.3 for SH) (a) and for the summer hemispheres (25.9 for NH and 18.0 for SH) (b) from their respective averages. The horizontal lines indicate the averages of the post-MBE and of the pre-MBE interglacials

summer (January) is 0.57°C warmer during the post-MBE interglacials, but there is no evident difference between the post-MBE and the pre-MBE interglacials for the NH summer (July). In summary, the response to the astronomical and greenhouse gas forcings is in general more coherent in January. The climate of January, globally and in the Southern Hemisphere particularly, is definitely warmer during the post-MBE interglacials than during the pre-MBE ones, as a direct response to the astronomical forcing (see Fig. 2 and more discussions in next section).

At the regional scale, the post-MBE interglacials are annually warmer than the pre-MBE ones over almost the whole Earth, with the largest warming reaching 4°C over the high latitudes in both hemispheres. There is a slight cooling of less than 1°C over a small area north of East Asia and over Western Australia. Seasonally, the post-MBE interglacials are on average warmer than the pre-MBE ones over the whole Earth in boreal winter, spring, and fall and cooler mostly over the continents but warmer over the Southern Oceans in boreal summer.

In summary, our simulations for the last ten interglacials under the astronomical and GHG forcings only show that (1) in agreement with the marine $\delta^{18}\text{O}$ records, the post-MBE interglacials are in average warmer than the pre-MBE ones; (2) this warming is mainly due to CO_2 , but insolation plays an important role at the seasonal scale; (3) the warming is mainly during boreal winter and covers the whole Earth; (4) the coolest season is definitely boreal summer; and (5) the warming over the southern high latitudes last through the whole year and is maximal during the boreal summer.

Causes for the Difference Between the Post-MBE and the Pre-MBE Interglacials

Let us now try to understand the relative role of insolation and GHG in generating an average climate warmer over the post-MBE interglacials than over the pre-MBE ones. As discussed in previous sections, although there is no apparent major difference in the latitudinal and seasonal distributions of insolation for the individual interglacials, the difference in the insolation pattern between the averages over the post-MBE interglacials and over the pre-MBE ones was quite unexpected with an underinsolated Earth from March to September and an overinsolated one the rest of the year. For the GHG, there is a significant difference in the average between the post-MBE and the pre-MBE interglacials. For the dates that we selected, the average concentrations of CO_2 equivalent are respectively for the post-MBE and the pre-MBE interglacials of the order of 280 and 240 ppmv.

To understand the respective roles played by the insolation and the GHG, we use the factor separation method (Stein and Alpert 1993). Four more experiments were therefore carried out, where the forcings are respectively: (1) the average insolation and GHG of the post-MBE interglacials, (2) the average insolation and GHG of the pre-MBE interglacials, (3) the average insolation of the post-MBE but the average GHG of the pre-MBE ones, and (4) the average insolation of the pre-MBE ones but the average GHG of the post-MBE ones. The results show that the higher global annual mean temperature of the

post-MBE interglacials is almost entirely due to its higher average GHG concentration (as might have been expected). However, this is not the case at the seasonal and hemispheric scales, where the insolation signature becomes highly significant in the response to the differential impact shown in Fig. 2. Compared to the pre-MBE interglacials, insolation is responsible for the global Earth being warmer over the post-MBE ones during boreal winter, reinforcing the warming expected from the higher GHG concentrations. During boreal summer, the insolation deficit cools the Earth, counteracting the global GHG warming.

If we look now the NH, insolation plays a very minor role in winter, but negative insolation anomalies largely cool the Earth in summer, leading to a slight annual cooling. It is different for the SH. Insolation warms the SH significantly during its summer but cools SH during its winter, leading to a slight warming over SH annually. The insolation change is therefore responsible for an increase in the difference between the NH and SH summers in agreement with the pattern of Fig. 2.

Conclusion

As the climate predicted to occur over the next centuries is unprecedented over the last one thousand years, the interglacials of the last 1 million years must be investigated to better understand climates as warm or warmer than today. A series of modeling experiments have been performed to simulate the climates which prevailed at or close to the minima of the marine $\delta^{18}\text{O}$ record. The dates for the astronomical forcing were selected to correspond to minima of the precessional index.

In average, the interglacials after MBE are warmer than before as it was expected from the average larger GHG concentration. On annual average, MIS-9 is the warmest with its largest $\text{CO}_{2\text{eq}}$ concentration, and MIS-13 and MIS-17 are the coolest with their lowest CO_2 . However, CO_2 is not the only forcing, and the insolation plays also a significant role. For example, although the maximum CO_2 concentration is larger at MIS-13 than at MIS-17, their $\delta^{18}\text{O}$ values are almost the same and the simulations lead even to a MIS-13 cooler than MIS-17.

The seasonal response which is related to the insolation forcing comes however as a surprise. In average, compared to the pre-MBE interglacials, the Earth

during the post-MBE interglacials receives less energy during boreal summer and more during boreal winter. The most significant result is that the warming of the post-MBE interglacials is particularly significant during boreal winter in direct agreement with the average insolation pattern, and the southern oceans play an important role.

All the results presented here are very similar to those obtained by Yin and Berger (2010); the scenarios used for the GHG concentrations in the two papers differ only by a few ppmv. This leads to a difference in the average global annual mean temperature between the post- and the pre-MBE interglacials being here 0.1°C more than in Yin and Berger (2010), which does not affect at all our conclusions.

Acknowledgments This work is supported by the European Research Council Advanced Grant EMIS (N°227348 of the Programme “Ideas”). Yin Q.Z. is a Postdoctoral Researcher of the National Fund for Scientific Research (F.R.S.-FNRS). Computer facilities were made easier through a sponsorship from S. A. Electrabel, Belgium.

References

- Bassinot FC, Labeyrie LD, Vincent E, Quidelleur X, Shackleton NJ, Lancelot Y (1994) The astronomical theory of climate and the age of the Brunhes-Matuyama magnetic reversal. *Earth and Planetary Science Letters*, 126 (1–3), 91–108
- Berger A (1978) Long-term variations of daily insolation and Quaternary Climatic Changes. *J Atmos Sci* 35(12): 2362–2367
- Berger A, Loutre MF (2002) An exceptionally long interglacial ahead? *Science* 297:1287–1288
- Berger A, Loutre MF, Tricot Ch (1993) Insolation and Earth's orbital periods. *J Geophys Res* 98(D6):10341–10362
- Berger A, Loutre MF, Mélice JL (1998) Instability of the astronomical periods over the last and next millions of years. *Paleoclim Data Model* 2(4):239–280
- Berger A, Li XS, Loutre MF (1999) Modelling Northern Hemisphere ice volume over the last 3 Ma. *Quat Sci Rev* 18(1): 1–11
- Bintanja R, van de Wal RSW, Oerlemans J (2005) Modelled atmospheric temperatures and global sea level over the past million years. *Nature* 437:125–128
- Brovkin V, Ganapolski A, Svirezhev Y (1997) A continuous climate-vegetation classification for use in climate-biosphere studies. *Ecol Model* 101:251–261
- EPICA Community Members (2004) Eight glacial cycles from an Antarctic ice core. *Nature* 429:623–628
- Ganapolski A, Calov R (2012) Simulation of glacial cycles with an Earth system model. In: Berger A, Mesinger F, Sijacki D (eds) *Climate change: inferences from paleoclimate and*

- regional aspects. Proceedings of Milankovitch 130th anniversary symposium, Belgrade, 2009. Springer-Verlag/Wien
- Goosse H, Fichefet T (1999) Importance of ice-ocean interactions for the global ocean circulation: a model study. *J Geophys Res* 104(C10):23337–23355
- Imbrie J, Hays JD, Martinson DG, McIntyre A, Mix AC, Morley JJ, Pisias NG, Prell WL, Shackleton NJ (1984) The orbital theory of Pleistocene climate: support from a revised chronology of the marine $\delta^{18}\text{O}$ record. In: Berger AL, Imbrie J, Hays J et al (eds) Milankovitch and climate, part 1. D. Reidel, Dordrecht, pp 269–305
- Jouzel J et al (2007) Orbital and millennial Antarctic climate variability over the past 800,000 years. *Science* 317: 793–796
- Kukla G, Berger A, Lotti R, Brown J (1981) Orbital signature of interglacials. *Nature* 290:295–300
- Lambeck K, Esat TM, Potter EK (2002) Links between climate and sea levels for the past three million years. *Nature* 419: 199–206
- Lisiecki LE, Raymo ME (2005) A Pliocene-Pleistocene stack of 57 globally distributed benthic $\delta^{18}\text{O}$ records. *Paleoceanography* 20(1):PA1003. doi:[10.1029/2004PA001071](https://doi.org/10.1029/2004PA001071)
- Loulergue L, Schilt A, Spahni R, Masson-Delmotte V, Blunier T, Lemieux B, Barnola JM, Raynaud D, Stocker TF, Chappellaz J (2008) Orbital and millennial-scale features of atmospheric CH_4 over the past 800,000 years. *Nature* 453: 383–386
- Luthi D, Le Floch M, Bereiter B, Blunier T, Barnola JM, Siegenthaler U, Raynaud D, Jouzel J, Fischer H, Kawamura K, Stocker TF (2008) High-resolution carbon dioxide concentration record 650,000–800,000 years before present. *Nature* 453:379–382
- Milankovitch MM (1941) *Kanon der Erdbestrahlung und seine Anwendung auf des Eizeitenproblem*. Koeniglich Serbische Akademie, Belgrade, R. Serbian Acad. Spec. Publ. vol 132, Sect. Math. Nat. Sci., 633 pp (Canon of Insolation and the ice-age problem, English translation by Israel Program for Scientific Translation, Jerusalem, 1969)
- Opsteegh JD, Haarsma RJ, Selten FM, Kattenberg A (1998) ECBILT: A dynamic alternative to mixed boundary conditions in ocean models. *Tellus* 50A:348–367
- Ruddiman WF, Raymo M, McYntyre A (1986) Matuyama 41,000-year cycles: North Atlantic Ocean and Northern Hemisphere ice sheets. *Earth Planet Sci Lett* 80:117–129
- Stein U, Alpert P (1993) Factor separation in numerical simulations. *J Atmos Sci* 50(14):2107–2115
- Yin QZ, Berger A (2010) Insolation and CO_2 contribution to the interglacial climate before and after the Mid-Brunhes Event. *Nat Geosci* 3(4):243–246

Relating the Astronomical Timescale to the Loess–Paleosol Sequences in Vojvodina, Northern Serbia

Slobodan B. Marković, Ulrich Hambach, Thomas Stevens, Biljana Basarin, Ken O'Hara-Dhand, Momčilo M. Gavrilov, Milivoj B. Gavrilov, Ian Smalley, and Nenad Teofanov

Abstract

In this study the first astronomical time scale for loess–paleosol sequences of Vojvodina region, northern Serbia is presented astronomical timescale for the loess–paleosol sequences of the Vojvodina region, northern Serbia. The sequence is the longest and most detailed orbitally tuned European loess record, comparable to Asian sequences to the east. Magnetic susceptibility (MS) records from two continuous loess–paleosol sequences in Vojvodina have been used to construct the timescale, with the aim of investigating climatic and environmental evolution and variability over the last million years. The 47.3-m-thick Mošorin (MO) section covers the time interval between marine isotope stages (MIS) 1 and 15, while the lower part of the Stari Slankamen (SS) section covers the time frame prior to MIS 16. The MS records were tuned to June 65°N insolation over the period between 0 and approximately 1 million years. The new timescale suggests older than expected ages for a number of the magnetic polarity boundaries, consistent with lock-in depth offsets reported for other loess sequences. Spectral analyses of the stacked MS variations indicate that climatic dynamics are dominated mainly by the changes in orbital eccentricity and subdominantly by obliquity and precession bands, over the past 1 million years.

Introduction

The celebrated Serbian scientist Milutin Milanković (Milankovitch) made a fundamental impact on modern paleoclimate research with his theory of the ice ages and the relationship between variations in the Earth's orbit and long-term climate change (e.g., Berger 1977, 1988; Petrović and Marković 2010). In spite of this

and despite their potential significance, Serbian paleoclimatic and paleoenvironmental archives are still relatively poorly known. However, over the last several years, the loess–paleosol sequences in the Vojvodina region in northern Serbia have been established as some of the oldest, thickest, and most complete climatic archives in Europe (e.g., Marković et al. 2005a, b, 2006, 2007a, b, 2008, 2009a, 2011; Buggle et al. 2008a, b, 2009; Fuchs et al. 2008; Antoine et al. 2009; Bokhorst et al. 2009; Bokhorst and Vandenberghe 2009; Schmidt et al. 2010).

Vojvodina (northern Serbia) is a region, located in the southeastern part of the Carpathian (Pannonian) Basin, encompassing the confluence area of the

S.B. Marković (✉)
Chair of Physical Geography, Faculty of Sciences, University of
Novi Sad, Trg D. Obradovića 3, 21000 Novi Sad, Serbia,
e-mail: slobodan.markovic@dgt.uns.ac.rs

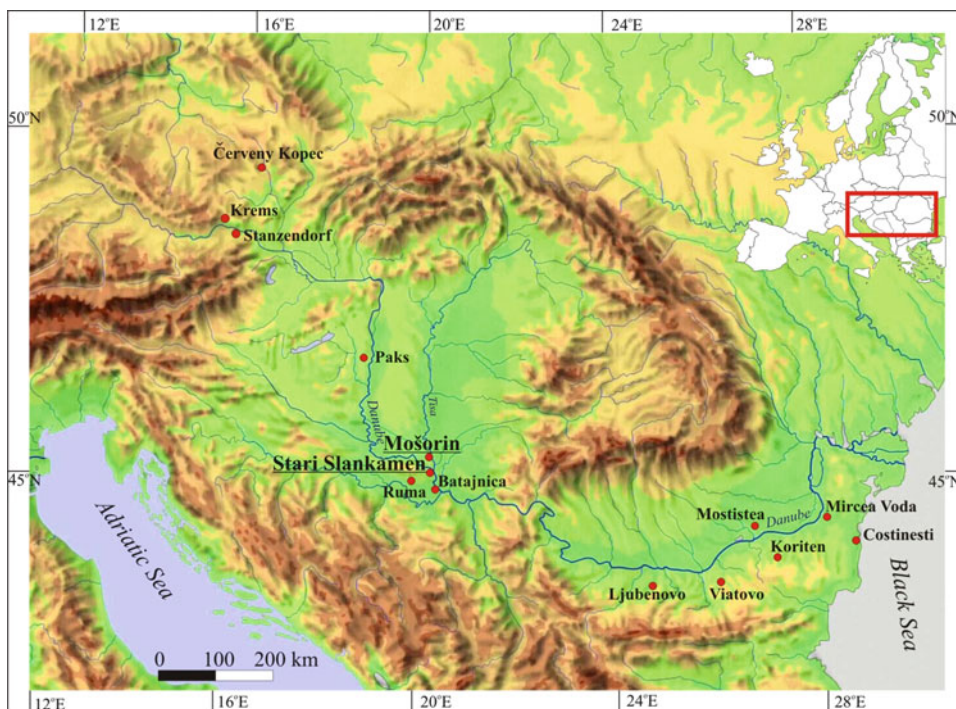


Fig. 1 Topographic map showing the geographical position of the main Middle Pleistocene loess sites in the Danube Basin: Červeny Kopec, Krems, Stranzendorf, Paks, Stari Slankamen, Mošorin, Batajnica, Ruma, Ljubenovo, Viatovo, Koriten, Mostište, Mircea Voda, and Costinesti

Danube, Sava, and Tisa rivers (Fig. 1). More than 60% of this lowland area is covered with loess and loess-like sediments. Aeolian silt accumulation in Vojvodina began as early as the late Early Pleistocene (Marković et al. 2003, 2008, 2011) making Serbian loess deposits among the oldest and most complete loess–paleosol sequences in Europe (Marković et al. 2003, 2007a, 2009a, 2011). This completeness and longtime coverage is unusual in Europe. As such, the sequences in Vojvodina could form the basis of a continental scale stratigraphic scheme that would alleviate much of the current chronostratigraphic uncertainty in European loess sequences and enable more broad-scale climatic reconstructions. As a record of pedogenic alteration that is frequently applied to loess deposits, magnetic susceptibility (MS) of loess provides a means of correlating the sequences in Serbia with key loess sites in Central and Southeastern Europe, Central Asia, and China (e.g., Heller and Evans 1995; Sartori et al. 1999; Jordanova et al. 2007, 2008; Ding et al. 2002; Machalett et al. 2008; Kukla 1987; Kukla and An 1989; Liu and Ding 1998; Bronger 2003; Sun et al. 2006), as well as with key

climate archives such as the marine oxygen isotope (e.g., Shackleton et al. 1990; Bassinot et al. 1994; Lisiecki and Raymo 2005), lake sediment (e.g., Prokopenko et al. 2006; Tzedakis et al. 2006), speleothem (Winograd et al. 1992; Wang et al. 2001), and Antarctic ice core (EPICA Members 2004) records on multimillennial timescales. Hence, in this study, we present the first European orbitally tuned loess record of the last million years from Serbia, with a view to this forming the basis of a multimillennial scale chronostratigraphic tool for the region.

Study Sections and Methods

In the present study, two loess sections were selected to provide proxy climate reference data for orbital tuning. The Mošorin (MO) loess section is situated in the northern part of the Titel loess plateau (45°17–18′N and 20°12–15′E; top of the section is 120 m above mean sea level) (Fig. 2). The modern soil and the last three glacial loess units V-L1, V-L2, and

V-L3 and paleopedocomplexes V-S1, V-S2, and V-S3 are represented in profile MO1, located in the Veliki Surduk deep loess gully. Profile MO2 in the Feudvar loess gully exposes the loess units V-L3 and V-L4, and pedocomplexes V-S3 and V-S4, and is situated 3 km west of the MO1 profile. Finally, profile MO3 is exposed in steep loess cliffs near the Tisa river bank at the locality of Dukatar and includes the lowermost loess–paleosol sequences loess V-L5 and pedocomplex V-S5 at the bottom of the section (Fig. 2). The composite MO section was built up on the basis of interprofile correlation, based on pedo- and MS stratigraphy. The total thickness of MO is 47.3 m. Due to unusually high accumulation rates, it is one of the most detailed European loess records covering the last five glacial–interglacial cycles (Marković et al. 2005b; Hambach et al. in preparation).

The Stari Slankamen (SS) section ($45^{\circ}07'58''\text{N}$ and $20^{\circ}18'44''\text{E}$; top of the section is 130 m above mean sea level) is located 20 km south of the MO site (Fig. 2). The sedimentary sequence is composed of approximately 40 m of loess–paleosol strata. In this study, we focus on the lowermost 14.3 m of the section, where probably the oldest loess deposits found so far in the region crop out. Initial paleomagnetic research indicates the potential for paleoclimatic reconstruction going back at least 1 million years.

Completeness of the last five glacial/interglacial cycles at the MO section was tested by comparison with Batajnica (BA) loess–paleosol sequence. Distance between these two sites is approximately 45 km. The Batajnica loess section is situated about 15 km northwest of Belgrade ($44^{\circ}55'29''\text{N}$; $20^{\circ}19'11''\text{E}$; top of the section is 111 m above mean sea level). Similar to MO

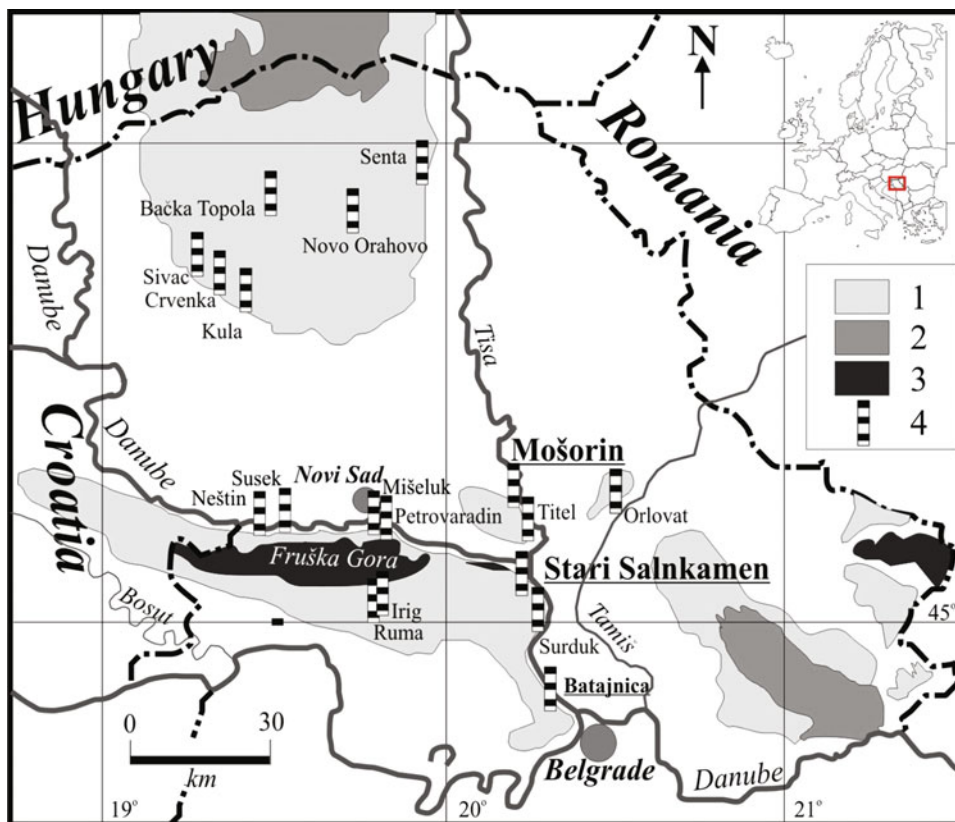


Fig. 2 Map of loess distribution in Vojvodina and adjacent regions, showing geographical position of the investigated sections and other main loess sites (modified from Marković et al. 2004). (1) Loess plateau, (2) sandy area, (3) mountain, (4) investigated exposures

section, the composite BA section was built up on the basis of interprofile correlation, based on pedo- and MS stratigraphy. The total thickness of BA composite profile is 40.5 m, and depth of the paleosol V-S5 is 33.45 m (Marković et al. 2009a).

Investigation of the loess section at MO began in 2005. Samples for initial low-field MS (measurements were taken at 5-cm intervals along 47.35-m profile) resulted in 1,122 individual specimens (including overlapping samples between profiles). The high-resolution MS measurements were obtained in the laboratory for paleo- and enviromagnetism at the Chair of Geomorphology, University of Bayreuth, using the KLY-3-Spinner-Kappa-Bridge (AGICO, Brno, Czech Republic), operating with an AC-field of 300 A/m at 920 Hz. These measurements are indicative of soil formation in loess and can be used as a stratigraphic characterization tool (Maher and Thompson 1992; Marković et al. 2005a).

In 2005, high-resolution sampling was undertaken in the lower part of the SS profile. A total 434 samples were collected from two parallel columns using oriented tubes in steps of 5 cm. Measurements of paleo- and rock-magnetic parameters were performed after thermal and AF demagnetization in the Geophysical laboratory of the Chair of Geomorphology, University of Bayreuth. In this study, only an outline of the results of these measurements is presented, with more detailed interpretations to be presented in a subsequent submission. Additionally, in 2009, further samples were collected from loess unit V-L6 for rock-magnetic measurements.

The procedure for orbital tuning was similar to the one proposed by Heslop et al. (2000). Our loess astronomical timescale was formulated by correlation of the unfiltered MS record to the insolation curve for June 65°N (Berger and Loutre 1991) and the ODP 677 $\delta^{18}\text{O}$ curve (Shackleton et al. 1990). A number of correlation criteria were imposed in order to maintain a consistent relationship between MS variations and the chosen target curves throughout the tuning procedure. Interglacial paleosols were correlated to regional maxima in insolation, maxima in eccentricity, and odd-numbered marine isotope stages (MIS), with the exception of MIS3. The loess units were consequently assigned to insolation minima and even-numbered MIS. Our time model assumes a zero time lag between insolation forcing and response of the climate system, following the concept of Shackleton et al. (1990) and Heslop et al. (2000). Identified paleomagnetic

events were considered to be an important factor in construction of our chronological model which were considered to be an important factor in construction of our chronological model.

The Cooley–Tukey Fast Fourier transform (FFT) was used for spectral analysis of MS time series (e.g., Cooley and Tukey 1965; Gavrilov and Janjić 1989). The sampling interval for FFT is set to approximately 1 kilo years. Relative MS spectral peak amplitudes are plotted as a function of frequencies and periods. The tephra spikes were removed manually as they gave rise to errors. Synthetic data created to fill the gaps in the data left by their removal. No attempt was made to identify the source of these tephra layers. However, this will be attempted later. Highly bioturbated part of MS record between V-S8 and V-S9 was smoothed using polynomial fitting.

Results and Discussion

Chronostratigraphic Interpretation

The existing stratigraphic model is based on the stratigraphic positions of the boundary between the Matuyama and Brunhes paleomagnetic boundary and the position of the Jaramillo normal polarity episode (Hambach et al. 2009; Marković et al. 2011), the relative intensity of principal MS peaks, pedostratigraphic features, amino acid geochronology, and luminescence dating (Marković et al. 2003, 2005a, b, 2006, 2007a, b, 2009a, 2011; Schmidt et al. 2010). We assign the Vojvodinian L (loess) and S (paleosol) stratigraphic units to a numerical system, placed in order of increasing age, similar to that used in Chinese loess stratigraphy (e.g., Kukla 1987; Kukla and An 1989). However, to avoid confusion in our loess and paleosol labeling system, we now use the prefix “V” to refer to the standard Pleistocene loess–paleosol stratigraphy in Vojvodina (Marković et al. 2008). Loess accumulation in the Vojvodina region is represented by plateau-like depositional conditions, similar to the ones observed at central Chinese loess plateau (e.g., Kukla 1987; Liu and Ding 1998). These plateau-like depositional conditions and the resultant low intensity of postdepositional erosion, controlled by mostly dry paleoclimatic conditions, means the loess–paleosol sequences in the Vojvodina region are relatively complete and well preserved. Figure 3 shows significant parallels between the

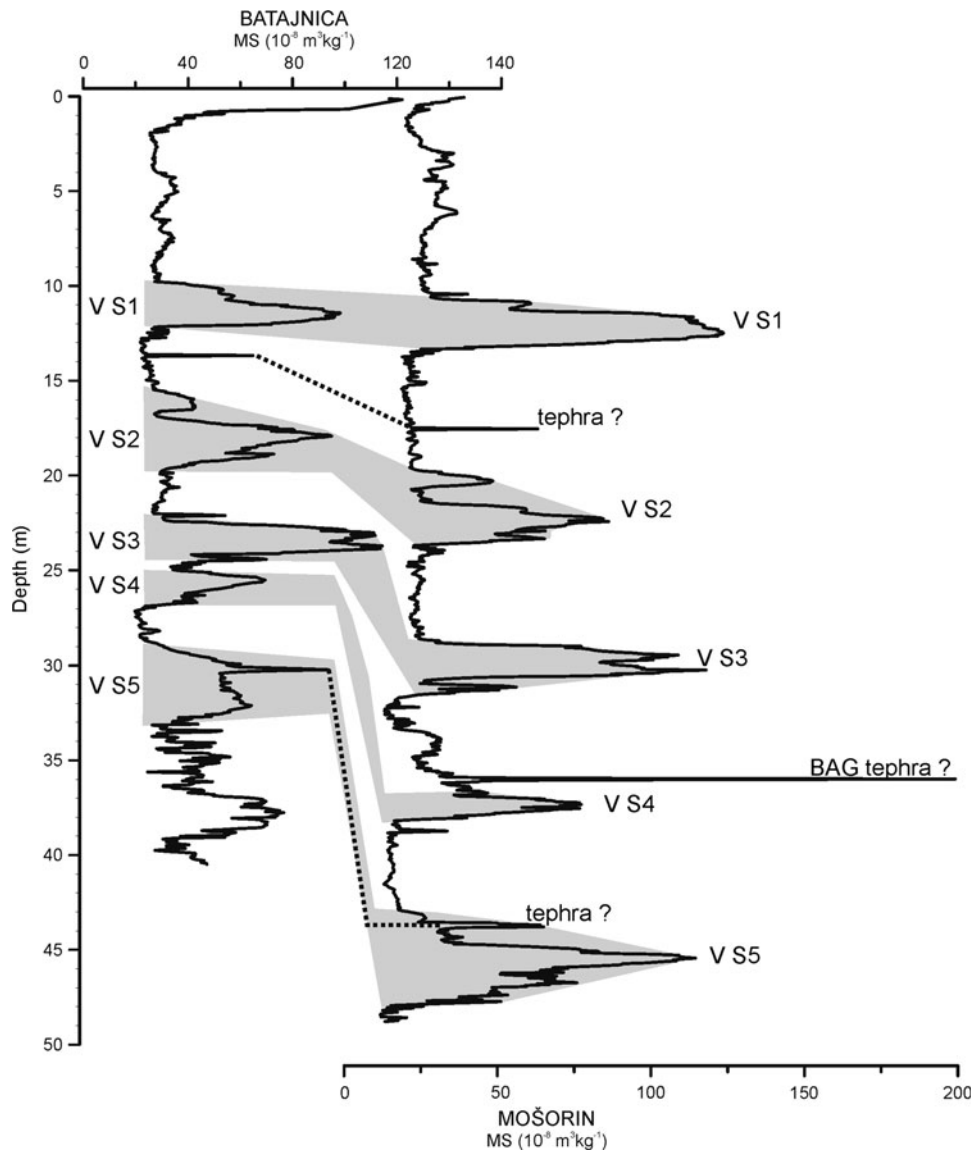


Fig. 3 Comparison between MS records of Batajnica (Marković et al. 2009a) and Mošorin sections

MS records of the MO and BA sections, despite the fact that these sections are located on two different loess plateaus and lie approximately 45 km from each other (Fig. 2). Detailed description of the MO pedostratigraphy was given in Bronger (1976, 2003) and Marković et al. (2009b). According to the revised chronostratigraphy of Marković et al. (2009b), the MO section represents a relatively continuous (on multimillennial timescales) record from MIS 1 to MIS 15.

An important stratigraphic marker at the MO site is denoted by an abrupt increase of MS in the V-L4 loess unit (Figs. 2 and 3). It is probably equivalent of the BAG

tephra identified in southern Slovakia and Hungary (e. g., Pouchlet et al. 1999; Horvath 2001; Bradák 2009). Pouchlet et al. (1999), based on geochemical composition, suggested the Vulsini and Alban Hills (middle Italian volcanic area) are thought to be possible sources of the volcanic ash, and it was correlated with Villa Senni Tuff, dated to around 350 kilo years. This age assignment fits very well with the apparent age of the abrupt V-L4 MS peak under our proposed timescale. This abrupt MS peak is not identified at BA section. Probably between MO and BA sections was the southern limit of the BAG tephra deposition.

A possible tephra layer is also observed in the loess horizon V-L2, as well as at the top of paleosol V-S5, marked by a less pronounced sudden MS peaks, and also identified at the BA section in same stratigraphic units (Marković et al. 2009a).

The pedostratigraphy of the SS loess–paleosol sequence in this region was discussed by Bronger (1976, 2003). This model has subsequently been revised by Marković et al. (2003) and Schmidt et al. (2010). For the purposes of this study, we focus on the lowermost 14.35 m of the section. Detailed paleomagnetic analyses including thermal and AF demagnetization on parallel samples indicate that the position of the Matuyama–Brunhes reversal boundary (MBB) is located in the loess unit V-L9 (time equivalent of MIS 22), see Fig. 5.

The composite MS record of the MO and SS sections was constructed on the basis of interprofile correlation of the MS records. The complete MS

record of the composite sequence and its relationship with general pedostratigraphic interpretations is presented on Fig. 4. Variations in the low-field MS reflect changes in the pedostratigraphy well. MS values observed in the pedocomplexes related to interglacial periods ($\sim 75\text{--}120 \times 10^{-8} \text{ m}^3 \text{ kg}^{-1}$) are higher than those in the interstadial soils ($\sim 30\text{--}50 \times 10^{-8} \text{ m}^3 \text{ kg}^{-1}$) and loess units ($\sim 12\text{--}24 \times 10^{-8} \text{ m}^3 \text{ kg}^{-1}$) (Fig. 4). This type of MS pattern reflects magnetic susceptibility enhancement via pedogenesis and is similar to that exhibited in Chinese and Central Asian loess deposits (e.g., Maher and Thompson 1992).

The proposed new stratigraphic model is also in agreement with recent results of amino acid racemization (AAR) geochronology of different loess sections in the Vojvodina region (Marković et al. 2005a, 2006, 2007b, 2008, 2009a, 2011). These results provide stratigraphic correlations between loess–paleosol

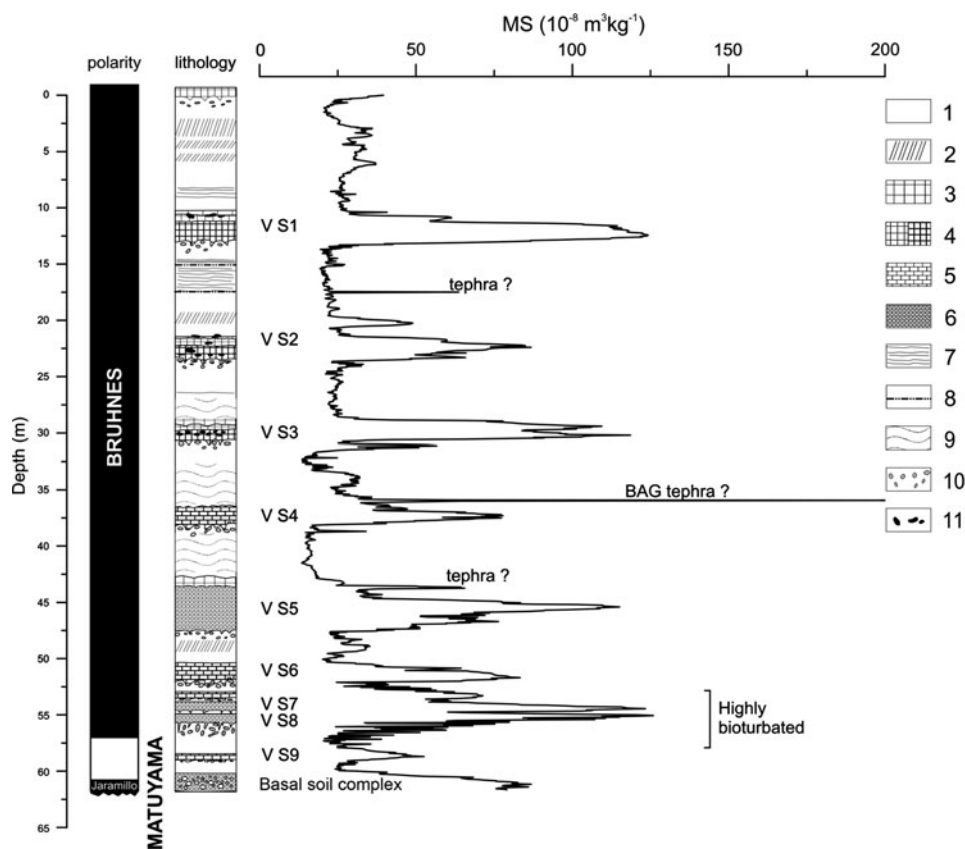


Fig. 4 Comparison between the MS record and paleopedology of the MO and SS composite loess–paleosol sequence. (1) Loess, (2) embryonic pedogenic layer, (3) a horizon, (4) Ah horizon, (5) B horizon, (6) Bwt rubified horizon, (7) sand beds, (8) possible tephra layers, (9) hydromorphic features, (10) carbonate concretions, (11) krotovinas

units V-L1-S1, V-L2-S2, V-L3-S3, and V-L4-S4 in the Vojvodina region with loess of Glacial cycles B, C, D, and E (Kukla 1975), respectively, at other European loess localities (Zöller et al. 1994; Oches and McCoy, 1995a, b, 2001).

The chronostratigraphic interpretation presented here supports the previous suggestion that the strongly developed paleosol V-S5 was formed during MIS 13–15 (Bronger and Heinkele 1989; Bronger et al. 1998; Bronger 2003). Bronger et al. (1998) demonstrated that this paleosol (F6 by their nomenclature) formed over a period several times longer than the Holocene. The pedocomplex shows a much greater degree of pedochemical weathering and clay mineral formation than in modern soils of this region. This strongly developed pedocomplex thus appears to be a characteristic feature of the middle part of all Brunhes loess–paleosol sediments in Eurasia (Bronger 2003) and matches well the poorly developed MIS 14 cold stage in marine records (Bassinot et al. 1994).

Orbital Timescale

Figure 5 shows the orbitally tuned timescale. Following the proposal that the past climate of the loess plateaus in the Vojvodina region was primarily driven by mechanisms responding to the fluctuations in northern hemisphere ice volume (e.g., Marković et al. 2008), we used 65°N summer insolation curve (Berger and Loutre 1991) to tune the record. Two distinct parts of the composite sequence can be identified using the composite MS record: (1) a high-resolution part between the Holocene soil (V-S0) and the base of loess unit V-L5 and (2) a lower part of the sequence where temporal resolution is reduced, especially in the pedocomplexes of V-S5 and the base. The lowermost c. 4.5 m contains evidence of magnetic polarity shifts and proved the most complicated part of the section for orbital tuning. However, several time control marker horizons, such as the probable equivalent of the Bag tephra, or the position of the Jaramillo

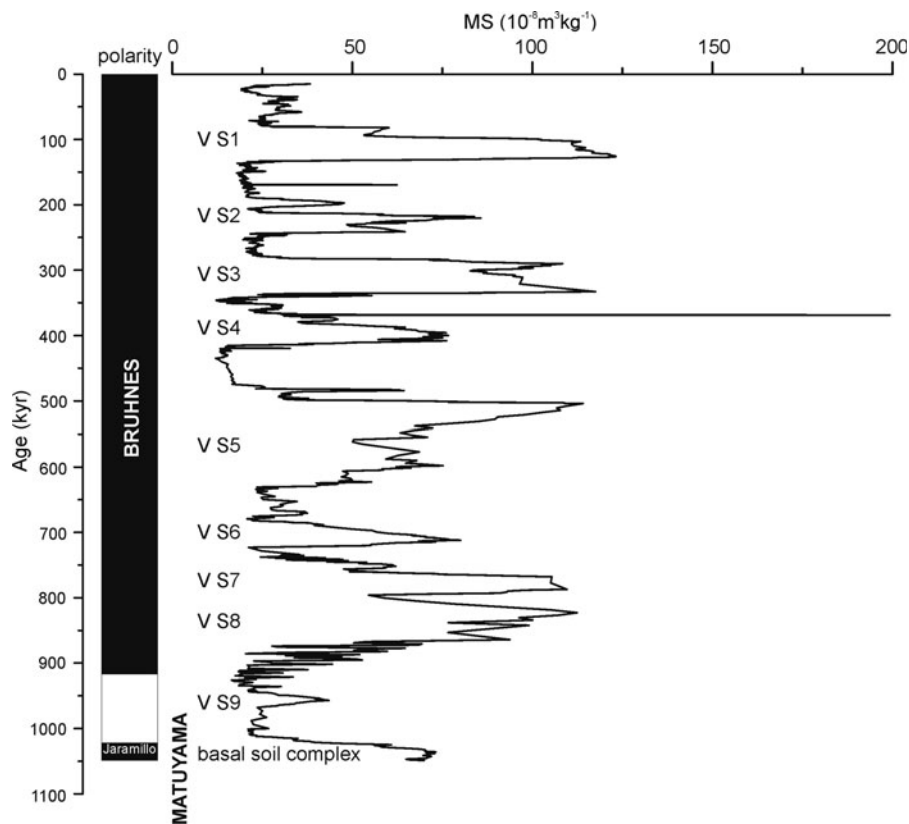


Fig. 5 Comparison of the paleomagnetic boundary position in the SS section to the orbitally tuned MS record of the MO and SS composite loess–paleosol section. Note the offset between the Matuyama–Brunhes Boundary (MBB) and the true age of the reversal (780 ka; Cande and Kent 1995)

paleomagnetic episode (JPE), fit well with our proposed chronology. Finally, the proposed chronological scheme considers the relative structures of the paleoclimatic and paleomagnetic records to produce an accurate timescale that is consistent with current understanding of loess–paleosol depositional and post-depositional processes.

Discrepancies between the loess–paleosol paleomagnetic boundary positions using the orbitally tuned age model and the accepted reversal ages can provide important information concerning the magnitude of any offset in the recording of the polarity signature observed in the SS section. Comparison of orbital ages of the position of Matuyama–Brunhes Boundary (MBB) in the tuned SS section (c. 0.89 million years; Table 1) to the MBB age of 0.778 ± 0.0017 million years (Tauxe et al. 1996) indicates that the acquisition of a stable paleomagnetic signal did indeed occur at a depth below the surface in the Serbian loess record. The MBB is recorded at the V-L9, calculated under our astronomical model as being deposited around 890 kilo years (Table 1), equivalent to MIS 22. Thus, there is an apparent overestimate of the MBB age by approximately 110 kilo years at SS, and the corresponding depth offset

between the true age of the reversal and its appearance in the SS section is about 3 m. Comparison of these results with those from Chinese loess records (e.g., Zhou and Shackleton 1999; Heslop et al. 2000) suggests a significantly larger overestimate at SS. The offset of the MBB position between marine and Chinese loess records was explained evoking the so-called lock-in effect (e.g., Zhou and Shackleton 1999; Spassov et al. 2003), whereby acquisition of the magnetic signal occurs at some depth, not at the surface. In this case, displacement of the MBB downward is likely a consequence of slow accumulation rates at the site and intense pedogenesis and bioturbation of paleosols V-S7 and V-S8 (Fig. 4). This may also be the case for the complex of soils at the base of the sequence, which, although exhibiting normal polarity, most likely associated with the JPE, are probably formed in material deposited prior to this under reversed polarity. This complex may be an amalgamated equivalent of paleosols S10 and S11 in China, which span the JPE (e.g., Sun et al. 2006), or if the lock-in depth offset is more significant, may be the equivalent of earlier stages.

The position of the MBB and JPE at the SS section is in good agreement with the recent results of

Table 1 Comparison between the orbitally tuned ages of the stratigraphic units of Vojvodina and the Chinese loess plateau

Vojvodina			China (Heslop et al. 2000)		
Stratigraphic marker	Depth (cm)	Age (kilo year)	Depth (cm)	Age (kilo year)	Stratigraphic marker
Top of V-S1	10.05	80	6.7	79	Top of S1
Base of V-S1	13.3	133	8.7	129	Base of S1
Top of V-S2	19.35	185	17.7	196	Top of S2
Base of V-S2	24.25	249	20.8	250	Base of S2
Top of V-S3	28.45	278	24.6	290	Top of S3
Base of V-S3	31.6	342	27.4	342	Base of S3
Top of V-S4	34.94	362	31.8	386	Top of S4
Base of V-S4	38.8	421	33.7	417	Base of S4
Top of V-S5	43.1	479	38.5	503	Top of S5
Base of V-S5	47.7	640	42.6	625	Base of S5
Top of V-S6	50.35	686	49.1	693	Top of S6
Base of V-S6	52.85	721	49.7	713	Base of S6
Top of V-S7	52.75	746	53.8	765	Top of S7
Base of V-S7	54.5	794	54.9	778	Base of S7
Top of V-S8	54.7	809	57.2	807	Top of S8
Base of V-S8	55.75	882	59.4	865	Base of S8
Top of V-S9	58	949	66.6	952	Top of S9
Base of V-S9	58.95	973	69.5	984	Base of S9
Top of basal soil complex	59.85	1,014	70.8	1,112	Top of S10

Jordanova et al. (2008) for the Bulgarian loess section Viatovo. At Viatovo, the MBB is identified in the upper part of the loess unit L7, exposed below welded pedocomplex S6, which is the probable equivalent of the paleosols V-S6, V-L7S1, V-S7, and V-S8, respectively (Fig. 4). The younger of two normal magnetozones found in the basal soil/red clay complex at Viatovo probably corresponds to the Jaramillo subchronozone of the Matuyama chron, as at the SS section.

In spite of the fact that the new chronological framework demonstrates significant downward displacement of the MBB, representing a longer age offset and corresponding lock-in depth than that observed in Chinese loess, there is still sufficient accordance between these two loess paleoclimatic records to establish a parallel chronostratigraphy. The loess chronostratigraphies in the Vojvodina region and the central Chinese loess plateau, from V-S0 to V-L10, and S0 to L10, respectively,

absolutely temporally correspond with each other. The basal paleosol complex is an equivalent of several welded loess–paleosol units in China, probably from S10 to S11. Table 1 presents a comparison between the astronomical ages of corresponding stratigraphic units of Vojvodina and Chinese loess plateau (Heslop et al. 2000). Up to paleosol V-S4/S4, the concordance between these loess chronologies is significant. The discrepancies between two timescales recorded below V-S4/S4 are related to the reduced resolution of the loess record of Vojvodina, particularly for the units V-S4, V-S5, V-S7, V-S8, V-S9, and the basal soil complex (Fig. 8).

As some abrupt changes in MS variation, such as tephra layers caused by deposition of volcanic ash or the irregular pattern observed in units from V-S7 to V-L9, which are highly bioturbated, were not consequences of long-term climatic cycles, the lower part of the MS record was smoothed before we performed spectral analyses (Fig. 6).

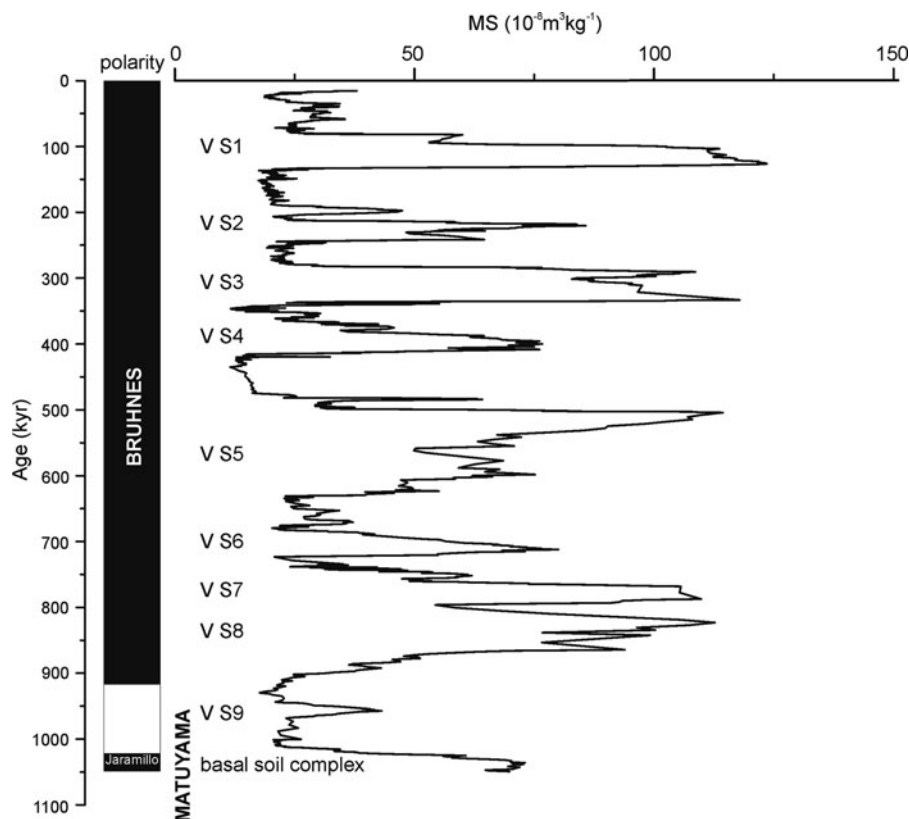
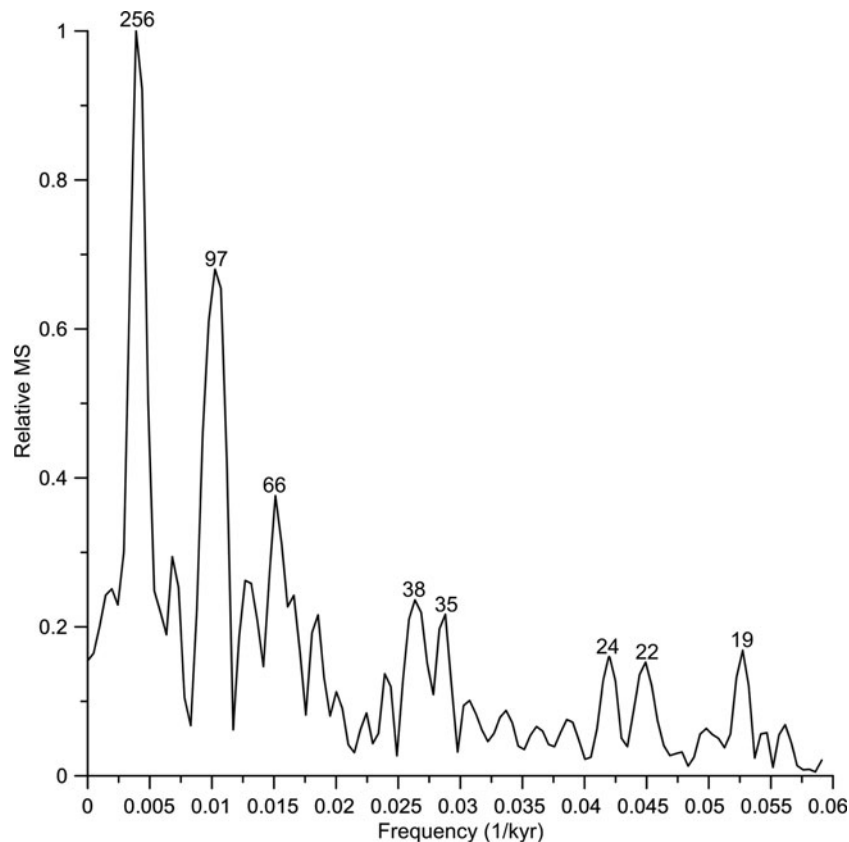


Fig. 6 Smoothed MS record of the MO and SS composite loess–paleosol sequence after removing abrupt non-long-term (multimillennial) climatic signals

Fig. 7 Spectral analysis results using the tuned MS time series record of the MO and SS composite loess–paleosol sequence for the past 1,000 kilo years. The relative amplitudes of MS are shown as a function of period. The numbers above peaks represent dominant cycles in kyr units



Spectral Analysis

Spectral analysis was conducted using the FFT (Cooley and Tukey 1965) on the smoothed MS time series of the Vojvodina composite record (Fig. 7). The relative amplitudes of MS spectral peaks are shown as a function of period. These results suggest that climate dynamics in Vojvodina is dominated mainly by eccentricity represented by the prominent peaks of 256 and 97 kilo years. In addition, a number of significant nonprimary spectral peaks also exist. Obliquity forcing is not represented over the studied interval by a spectral peak of 41 kilo years, but the peaks of 38 and 35 kilo years are observed. Orbital forcing at the 24, 22, and 19 kilo years are consistent with precession parameters. We have no explanation for the prominent peak of 66 kilo years, although a weak 66 kilo year peak is also seen in Chinese loess sequences (Lu et al. 2004). Subsequent investigations would give better insight.

These results underline importance of the long-term cycles related to eccentricity and obliquity as

key mechanisms controlling aeolian dust deposition and alternating pedogenesis during the last million years in southeastern part of Carpathian Basin. This is similar to results obtained from Chinese loess (e.g., Heslop et al. 2000; Guo et al. 2005; Sun et al. 2006).

Comparison with Other Global Paleoclimatic Records

In 2005, Kukla raised the issue of identification and understanding of glacial and interglacial periods in two contrasting geologic domains: the terrestrial and marine. As with terrestrial records globally, most terrestrial European Pleistocene records are discontinuous in time (e.g., river terraces, glacial moraines, and deposits associated with glacial). However, deep sea records are perceived as sensitive recorders of global ice volume, sea temperature, and other climate parameters, where the records remain relatively complete and undisturbed. Most European loess deposits are also somewhat discontinuous and are restricted in time to the Late Pleistocene.

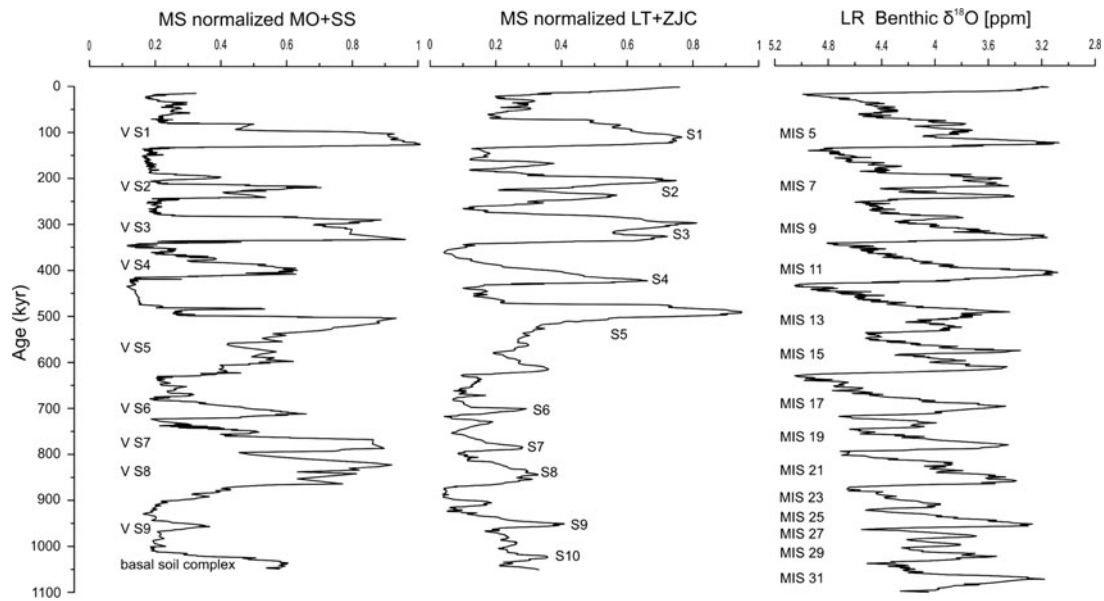


Fig. 8 Comparison between the orbitally tuned marine oxygen isotope (Lisiecki and Raymo 2005), Vojvodina, and Chinese (Sun et al. 2006) normalized loess records

With the exception of some isolated spots in the western and central Europe, older loess deposits in these regions are less highly resolved than those in Eastern Europe, the Danube Basin and the Black Sea coast (e.g., Frechen et al. 2003). A consequence is that orbitally tuned loess records are thus far available only from Romanian loess (Necula and Panaiotu 2008; Timar et al. 2010).

As shown in Fig. 5, although the question over whether sedimentation occurs during interglacial periods is unresolved at present, the Vojvodina composite sequence is relatively complete, with no major gaps on multimillennial timescales. Thus, the Vojvodina loess sequences (and some sections in the lower Danube Basin) are of considerable importance in understanding long-term climatic change in continental Europe. The relative completeness of the loess deposits in the middle and lower Danube Basin is partly related to the relatively dry continental climatic conditions in the region, especially during glacial periods when the Danube yielded a ready supply of sediments. This leads to enhanced accumulation and a reduction in postdepositional erosion during more humid episodes. This completeness and the close correlation with Chinese records suggest that northern Serbian loess can be regarded as a link between midlatitude Pleistocene environments of Europe and Asia, providing potential for temporal and spatial reconstruction of climate dynamics across the

Eurasian continent over the last million years (e.g., Marković et al. 2009a, b, 2011).

Comparison between marine $\delta^{18}\text{O}$ (Lisiecki and Raymo 2005), Chinese (Sun et al. 2006), and Serbian loess MS records plotted on age scale is shown on Fig. 8. Generally, the MS records of Vojvodina and Chinese loess show many similarities, for example, strongly developed pedocomplexes V-S5 and S5 developed during the relatively protracted period of cool interglacials MIS 13 and 15 (600–450 kilo years), separated by a weak glacial (Guo et al. 2009; Yin et al. 2009; Marković et al. 2009a, b). In spite of the many general similarities between these two loess records, there are also several important differences related to specific regional environment (Marković et al. 2009a).

The potential for examining long-term regional and continental scale atmospheric dynamics with no major hiatuses makes our orbitally tuned loess record a rare and important piece in the Quaternary continental environmental mosaic, alongside lake, ice core, and ocean core evidence. As a rare terrestrial archive of the mid-Brunhes event (Jansen et al. 1986), the sequences are contributing to recent increased interest in understanding the mechanism controlling interglacial climate transitions after and before this period (e.g., EPICA 2004; Tzedakis et al. 2009; Guo et al. 2009; Yin et al. 2009; Masson-Delmotte et al. 2010; Yin and Berger 2010).

Conclusions

We have formulated the first Vojvodina loess chronology for the last 1 million years using a composite MS record tuned to target changes in both direct solar forcing and global ice volume. The resulting orbitally tuned timescale provides a detailed age model for Serbian loess–paleosol sequences and enables their precise correlation to other terrestrial loess, marine, or ice core records.

The proposed chronology indicates older than expected ages for the MBB magnetic polarity boundaries, consistent with an enhanced lock-in depth offset. Spectral analyses of the stacked MS variations indicate that climatic dynamics are dominated mainly by the changes in the eccentricity and obliquity bands over the past 1 million years. Comparison with other long-term paleoclimatic records globally reinforces the utility of the composite sequence in understanding the dynamics of climate over continental scales and for linking terrestrial deposits over a continental scale. The new records from Vojvodina hold great potential in examining the terrestrial expression of global climatic reorganization events such as the mid-Brunhes event.

Acknowledgments The Scientific Committee and the Serbian Academy of Sciences and Arts organized a Milanković Anniversary Symposium 2009 dedicated to the scientific challenges in the diverse field of climatic dynamics research during which the results delivered here were presented. Special thanks are due to André Berger for fundamental support. We thank Mladjen Jovanović, Tivadar Gaudenyi, Nebojša Milojković, and Tin Lukić for their help during field work, sample preparation, and laboratory measurements. This research was supported by Project 146019 (176020) of the Serbian Ministry of Science.

References

- Antoine P, Rousseau DD, Fuchs M, Hatté C, Gauthier C, Marković SB, Jovanović M, Gaudenyi T, Moine O, Rossignol J (2009) High-resolution record of the last climatic cycle in the southern Carpathian Basin (Surduk, Vojvodina, Serbia). *Quat Int* 198:19–36
- Bassinot FV, Labryie LD, Vincent E, Quidelleur X, Shackleton NJ, Lancelot Y (1994) The astronomical theory of climate and the age of Brunhes-Matuyama magnetic reversal. *Earth Planet Sci Lett* 126:91–108
- Berger A (1977) Support for the astronomical theory of climatic change. *Nature* 268:44–45
- Berger A (1988) Milankovitch theory and climate. *Rev Geophys* 26:624–657
- Berger A, Loutre MF (1991) Insolation values for the climate of the last 10 million years. *Quat Sci Rev* 10:297–317
- Bokhorst MP, Vandenberghe J (2009) Validation of wiggle matching using a multi-proxy approach and its palaeoclimatic significance. *J Quat Sci* 24:937–947
- Bokhorst M, Beets CJ, Marković SB, Gerasimenko NP, Matviishina ZN, Frechen M (2009) Podo-chemical climate proxies in Late Pleistocene Serbian–Ukrainian loess sequences. *Quat Int* 198:113–123
- Bradák B (2009) Application of anisotropy of magnetic susceptibility (AMS) for the determination of paleo-wind directions and paleo-environment during the accumulation period of Bag Tephra, Hungary. *Quat Int* 198:77–84
- Bronger A (1976) Zur quartären Klima – und Landschaftsentwicklung des Karpatenbeckens auf (paläo-) pedologischer und bodengeographischer Grundlage. *Kieler geographische Schiften Band 45*. Im Selbstverlag des geographischen Instituts der Universität, Kiel
- Bronger A, Heinkele T (1989) Micromorphology and genesis of paleosols in then Luochuan loess section, China: pedostratigraphical and environmental implications. *Geoderma* 45 (2):123–143
- Bronger A, Winter R, Sedov S (1998) Weathering and clay mineral formation in two Holocene soils and in buried paleosols in Tadjikistan towards a Quaternary paleoclimatic record in Central Asia. *Catena* 34(1–2):19–34
- Bronger A (2003) Correlation of loess-paleosol sequences in East and Central Asia with SE Central Europe – towards a continental Quaternary pedostratigraphy and paleoclimatic history. *Quat Int* 106–107:11–31
- Buggle B, Glaser B, Zöller L, Hambach U, Marković SB, Glaser I, Gerasimenko N (2008a) Geochemical characterization and origin of Southeastern and Eastern European loesses (Serbia, Romania, Ukraine). *Quat Sci Rev* 27:1058–1075
- Buggle B, Hambach U, Glaser B, Marković SB, Glaser I, Zöller L (2008b) Long-term paleoclimate records in SE-Europe-the loess paleosol sequences Batajnica/Stari Slankamen (Serbia) and Mircea Voda (Romania). International meeting DEUQUA, Wien, 31 Aug–6 Sept 2008, Geologische Bundesanstalt Abhandlungen, vol 62, pp 15–19
- Buggle B, Hambach U, Glaser B, Gerasimenko N, Marković S, Glaser I, Zöller L (2009) Magnetic susceptibility stratigraphy and spatial and temporal paleoclimatic trends in East European loess paleosol sequences. *Quat Int* 196:86–106
- Cande SC, Kent DV (1995) Revised calibration of the geomagnetic polarity time scale for the Late Cretaceous and Cenozoic. *J Geophys Res* 100:6093–6095
- Cooley JW, Tukey JW (1965) An algorithm for the machine calculation of complex Fourier series. *Math Comput* 19:297–301
- Ding ZL, Ranov V, Yang SL, Finaev A, Han JM, Wang GA (2002) The loess record in southern Tajikistan and correlation with Chinese loess. *Earth Planet Sci Lett* 200:387–400
- EPICA community members (2004) Eight glacial cycles from an Antarctic ice core. *Nature* 429:623–628
- Frechen M, Oches EA, Kohfeld KE (2003) Loess in Europe – mass accumulation rates during the Last Glacial Period. *Quat Sci Rev* 22:1835–1857

- Fuchs M, Rousseau DD, Antoine P, Hatte C, Gautier C, Marković SB, Zöller L (2008) High resolution chronology of the upper Pleistocene loess/paleosol sequence at Surduk, Vojvodina, Serbia. *Boreas* 37:66–73
- Gavrilov MB, Janjić ZI (1989) Computed rotational energy spectra of two energy and enstrophy conserving schemes on semi-staggered grids. *Meteorol Atmos Phys* 41:1–4
- Guo ZT, Hao Q, Wei J, An Z (2005) Astronomical signals in different climate proxies from the Quaternary loess-soil sequences in China. In: Berger A, Ercegovac M, Mesinger F (eds) Milutin Milankovitch Anniversary Symposium “paleoclimate and the earth climate system”, Serbian Academy of Sciences and Arts, Belgrade, 30 Aug–2 Sept 2004, pp 101–111
- Guo ZT, Berger A, Yin QZ, Qin L (2009) Strong asymmetry of hemispheric climates during MIS-13 inferred from correlating China loess and Antarctica ice records. *Clim Past* 5:21–31
- Hambach U, Jovanović M, Marković SB, Rolf C (2009) The Matuyama-Brunhes geomagnetic reversal in the Stari Slankamen loess section (Vojvodina, Serbia): its detailed record and its stratigraphic position. *Geophys Res Abstr* 11 (EGU2009-0)
- Hambach U, Marković SB, Stevens T, Jovanović M, Rolf C (in preparation) The high resolution magnetic record of the last 5 glacial-interglacial cycles recorded at the loess-paleosol sequences of the Titel loess plateau
- Heller F, Evans ME (1995) Loess magnetism. *Rev Geophys* 33:211–240
- Heslop D, Langereis CG, Dekkers MJ (2000) A new astronomical timescale for the loess deposits of Northern China. *Earth Planet Sci Lett* 184:125–139
- Horvath E (2001) Marker horizons in the loesses of the Carpathian Basin. *Quat Int* 76(77):157–163
- Jansen JHF, Kuijpers A, Troelstra SR (1986) A Mid-Brunhes climatic event: long-term changes in global atmospheric and ocean circulation. *Science* 232:619–622
- Jordanova D, Hus J, Geeraerts R (2007) Palaeoclimatic implications of the magnetic record from loess/paleosol sequence Viatovo (NE Bulgaria). *Geophys J Int* 171:1036–1047
- Jordanova D, Hus J, Evlogiev J, Geeraerts R (2008) Palaeomagnetism of the loess/paleosol sequence in Viatovo (NE Bulgaria) in the Danube basin. *Phys Earth Planet Inter* 167:71–83
- Kukla GJ (1975) Loess Stratigraphy of Central Europe. In: Butzer KW, Isaac LI (eds) *After Australopithecines*. Mouton, The Hague, pp 99–187
- Kukla GJ (1987) Loess Stratigraphy in Central China. *Quat Sci Rev* 6:191–219
- Kukla GJ (2005) Saalian supercycle, Mindel/Riss interglacial and Milankovitch’s dating. *Quat Sci Rev* 24:1573–1586
- Kukla GJ, An Z (1989) Loess Stratigraphy in Central China. *Palaeogeogr Palaeoclimatol Palaeoecol* 72:203–225
- Lisiecki LE, Raymo ME (2005) A Pliocene–Pleistocene stack of 57 globally distributed benthic $\delta^{18}\text{O}$ records. *Paleoceanography* 20:PA1003
- Liu TS, Ding Z (1998) Chinese loess and paleomonsoon. *Annu Rev Earth Planet Sci* 26:111–145
- Lu H, Zhang FQ, Liu X, Duce AR (2004) Periodicities of palaeoclimatic variations recorded by loess-paleosol sequences in China. *Quat Sci Rev* 23:1891–1900
- Machalett B, Oches EA, Frechen M, Zöller L, Hambach U, Mavlyanova NG, Marković SB, Endlicher W (2008) Aeolian dust dynamics in Central Asia during the Pleistocene – driven by the long-term migration, seasonality and permanency of the Asiatic polar front. *Geophys Geochem Geosyst* 9:Q08Q09. doi:10.1029/2007GC001938
- Maher BA, Thompson R (1992) Paleoclimatic significance of the mineral magnetic record of the Chinese loess and paleosols. *Quat Res* 37:155–170
- Marković SB, Heller F, Kukla G, Gaudenyi T, Jovanović M, Miljković L (2003) Magnetostratigrafija lesnog profila Čot u Starom Slankamenu. *Zbornik radova Instituta za geografiju* 32:20–28 (In Serbian with English summary)
- Marković SB, Kostić NS, Oches EA (2004) Paleosols in the Ruma loess section (Vojvodina, Serbia). *Revista Mexicana de Ciencias Geológicas* 21(1):79–87
- Marković SB, McCoy WD, Oches EA, Savić S, Gaudenyi T, Jovanović M, Stevens T, Walther R, Ivanišević P, Galić Z (2005a) Paleoclimate record in the Late Pleistocene loess-paleosol sequence at Petrovaradin Brickyard (Vojvodina, Serbia). *Geologica Carpathica* 56:483–491
- Marković SB, Jovanović M, Mijović D, Bokhorst M, Vandenberghe J, Oches E, Hambach U, Zöller L, Gaudenyi T, Kovačev N, Boganović Ž, Savić S, Bojanić D, Milojković N (2005b) Titel loess plateau – geopark. In: Nature Conservation Institute, Proceedings of 2nd conference on the geo-heritage of Serbia, Belgrade, 22–23 June 2004, pp 177–184
- Marković SB, Oches EA, Sümegi P, Jovanović M, Gaudenyi T (2006) An introduction to the Upper and Middle Pleistocene loess-paleosol sequences in Ruma section (Vojvodina, Yugoslavia). *Quat Int* 149:80–86
- Marković SB, Hambach U, Oches EA, McCoy WD, Zoeler L, Jovanović M (2007a) 850 Millennia of paleoclimatic history recorded in the loess sequences of Vojvodina region, Serbia. *Quat Int* 167/168:269
- Marković SB, Oches EA, McCoy WD, Gaudenyi T, Frechen M (2007b) Malacological and sedimentological evidence for “warm” glacial climate from the Irig loess sequence (Vojvodina, Serbia). *Geophys Geochem Geosyst* 8: Q09008. doi:10.1029/2006GC001565
- Marković SB, Bokhorst M, Vandenberghe J, Oches EA, Zöller L, McCoy WD, Gaudenyi T, Jovanović M, Hambach U, Machalett B (2008) Late Pleistocene loess-paleosol sequences in the Vojvodina region, North Serbia. *J Quat Sci* 23:73–84
- Marković SB, Hambach U, Catto N, Jovanović M, Buggle B, Machalett B, Zöller L, Glaser B, Frechen M (2009a) The middle and late Pleistocene loess-paleosol sequences at Batajanica, Vojvodina, Serbia. *Quat Int* 198:255–266
- Marković SB, Hambach U, Machalett B, Jovanović M, Basarin B, Lukić T (2009b) Titel loess plateau – high resolution witness of environmental changes during the last five glacial cycles. In: Loessfest09 conference, Novi Sad, 31 Aug–3 Sept 2009. Fieldguide book, pp 1–21
- Marković SB, Hambach U, Stevens T, Kukla GJ, Heller F, William D, McCoy WD, Machalett B, Oches EA, Buggle B, Zöller L (2011) The last million years recorded at the Stari Slankamen loess-paleosol sequence: revised chronostratigraphy and long-term environmental trends. *Quat Sci Rev* 30(9–10):1142–1154
- Masson-Delmotte V, Stenni B, Pol K, Braconnot P, Cattani O, Falourd S, Kageyama M, Jouzel J, Landais A, Minster B, Barnola JM, Chappellaz J, Krinner G, Johnsen S,

- Röthlisberger R, Hansen J, Mikolajewicz U, Otto-Bliesner B (2010) EPICA Dome C record of glacial and interglacial intensities. *Quat Sci Rev* 29:113–128
- Necula C, Panaiotu C (2008) Application of dynamic programming to the dating of a loess-paleosol sequence. *Rom Rep Phys* 60:157–171
- Oches EA, McCoy WD (1995a) Amino acid geochronology applied to the correlation and dating of Central European loess deposits. *Quat Sci Rev* 14(7–8):767–782
- Oches EA, McCoy WD (1995b) Aminostratigraphic evaluation of conflicting age estimates for the “Young Loess” of Hungary. *Quat Res* 44(2):767–782
- Petrović A, Marković SB (2010) Annus mirabilis and the end of the geocentric causality: why celebrate the 130th anniversary of Milutin Milanković? *Quat Int* 214:114–118
- Pouchlet A, Horvath E, Gabris G, Juvigne E (1999) The Bag Tephra, a widespread tephrochronological marker in Middle Europe: chemical and mineralogical investigations. *Bull Volcanol* 60:265–272
- Prokopenko AA, Hinnov LA, Williams DF, Kuzmin MI (2006) Orbital forcing of continental climate during the Pleistocene: a complete astronomically tuned climatic record from Lake Baikal, SE Siberia. *Quat Sci Rev* 25:3431–3457
- Sartori M, Heller F, Forster T, Borkovec M, Hammann J, Vincent E (1999) Magnetic properties of loess grain size fractions from section Paks (Hungary). *Phys Earth Planet Inter* 116:53–64
- Schmidt E, Machalet B, Marković SB, Tsukamoto S, Frechen M (2010) Luminescence chronology of the upper part of the Stari Slankamen loess sequence (Vojvodina, Serbia). *Quat Geochronol* 5:137–142
- Shackleton NJ, Berger A, Peltier WR (1990) An alternative astronomical calibration of the Lower Pleistocene timescale based on ODP Site 677. *Trans R Soc Edinb Earth Sci* 81:251–261
- Spassov S, Heller F, Evans ME, Yue LP, von Dobeneck T (2003) A lock-in model for the complex Matuyama–Brunhes boundary record of the loess/paleosol sequence at Lingtai (Central Chinese Loess Plateau). *Geophys J Int* 155:350–366
- Sun Y, Clemens SC, An Z, Yu Z (2006) Astronomical timescale and palaeoclimatic implication of stacked 3.6-Myr monsoon records from the Chinese Loess Plateau. *Quat Sci Rev* 25:33–48
- Tauxe L, Herbert T, Shackleton NJ, Kok YS (1996) Astronomical calibration of the Matuyama–Brunhes boundary: consequences for magnetic remanence acquisition in marine carbonates and the Asian loess sequences. *Earth Planet Sci Lett* 140:133–146
- Timar A, Vandenberghe D, Panaiotu EC, Panaiotu CG, Necula C, Cosma C, van den Haute P (2010) Optical dating of Romanian loess using fine-grained quartz. *Quat Geochronol* 5(2–3):143–148
- Tzedakis PC, Hooghiemstra H, Pälike H (2006) The last 1.35 million years at Tenaghi Philippon: revised chronostratigraphy and long term vegetation trends. *Quat Sci Rev* 25:3416–3430
- Tzedakis PC, Raynaud D, McManus JF, Berger A, Brovkin V, Kiefer T (2009) Interglacial diversity. *Nat Geosci* 2:751–755
- Wang YJ, Cheng H, Edwards RL, An ZS, Wu JY, Shen C-C, Dorale JA (2001) A high-resolution absolute dated Late Pleistocene Monsoon record from Hulu Cave, China. *Science* 294:2345–2348
- Winograd IJ, Coplen TB, Landwehr JM, Riggs A, Ludwig KR, Szabo BJ, Kolesar PT, Revesz KM (1992) Continuous 500,000 year climate record from Vein Calcite in Devils Hole, Nevada. *Science* 258:255–260
- Yin QZ, Berger A (2010) Insolation and CO₂ contribution to the interglacials before and after Mid-Brunhes Event. *Nat Geosci* 3:243–246
- Yin QZ, Berger A, Crucifix M (2009) Individual and combined effects of ice sheets and precession on MIS-13 climate. *Clim Past* 5:229–243
- Zhou LP, Shackleton N (1999) Misleading positions of geomagnetic reversal boundaries in Eurasian loess and implications for correlation between continental and marine sedimentary sequences. *Earth Planet Sci Lett* 168:117–130
- Zöller L, Oches EA, McCoy WD (1994) Towards a revised chronostratigraphy of loess in Austria with respect to key sections in the Czech Republic and in Hungary. *Quat Sci Rev* 13(5–7):465–472

A Spatial View on Temperature Change and Variability During the Last Deglaciation: A Model Analysis

Didier M. Roche, Hans Renssen, and Didier Paillard

Abstract

Understanding the sequence of events occurring during the last major glacial to interglacial transition (21 ka BP to 9 ka BP) is a challenging task that has the potential to unveil the mechanisms behind large scale climate changes. Though many studies have focused at a complex understanding of the sequence of rapid climatic change that accompanied or interrupted the deglaciation, few have analysed it in a more theoretical framework with simple forcings. In the following, we address when and where the first significant temperature anomalies appear when using slow varying forcing of the last deglaciation. We use here coupled transient simulations of the last deglaciation, including ocean, atmosphere and vegetation components to analyse the spatial timing of the deglaciation. To keep the analysis in a simple framework, we do not include rapid freshwater forcings that have led to rapid climate shifts during that time period. We aim to disentangle the direct and subsequent response of the climate system to slow forcing and moreover the location where those changes are more clearly expressed. In a data-modelling comparison perspective, this could help understanding the physically plausible phasing between known forcings and recorded climatic changes. Our analysis of climate variability could also help to distinguish deglacial warming signals from internal climate variability. We thus are able to better pinpoint the onset of local deglaciation, as defined by the first significant local warming, and further show that there is a large regional variability associated with it, even with the set of slow forcings used here.

D.M. Roche (✉)

Section Climate Change and Landscape Dynamics, Department of Earth Sciences, Faculty of Earth and Life Sciences, Vrije Universiteit Amsterdam, De Boelelaan 1085, 1081 HV Amsterdam, The Netherlands

Laboratoire des Sciences du Climat et de l'Environnement (LSCE), UMR 8212 CEA/INSU-CNRS/UVSQ, Centre d'Etudes de Saclay, CEA-Orme des Merisiers, bat. 701, 91191 Gif-sur-Yvette Cedex, France
e-mail: Didier.Roche@falw.vu.nl

Introduction

The last deglaciation—21 to 9 kiloyears Before Present (BP)—is Earth's most recent transition from a glacial-like climate to an interglacial-like climate, a type of transition that occurred repeatedly with a periodicity of 100 kiloyears over the late Quaternary. Milutin Milankovitch was one of the first to propose that this low-frequency variability of the climate system is linked to the variations of the orbit of the Earth

around the Sun, thereby modifying the energy received at the top of the atmosphere. He proposed that summer insolation at high northern latitudes could be considered as the main driver of the ice-age cycles as it constrained the capacity of winter snow to survive the summer and hence contribute to the build-up of glacial ice sheets. During peak glacial periods as the Last Glacial Maximum (LGM), they covered most of North America with a 4-km-thick ice sheet (Dyke et al. 2002; Peltier 2004) and a good part of northern Europe and western Siberia (Svendsen et al. 2004). The orbitally forced changes in the insolation received by the Earth are the only long-term forcing truly external to the Earth's climatic system, whereas ice-sheet waxing and waning and greenhouse gases that strongly affect the climate over similar time periods are only internal feedbacks to that one forcing. The analysis of the impact of the long-term insolation forcing is the subject of two studies in this proceeding: Berger and Quizhen (2010) analyses the effect in previous warm interglacials while Ganopolski and Calov (2010) studies the internal feedbacks amplifying the orbital forcing at glacial-to-interglacial timescales.

Over the years, compelling evidence of how drastic climate changes have been through the last deglaciation has arisen from proxy data retrieved from geological records throughout the world (MARGO Project Members 2009; North Greenland Ice Core Project members 2004; EPICA community members 2004). Although there is no doubt that this last transition affected the Earth as a whole, there is still some debate on how changes at different geographical locations on the Earth relate to each other and hence on the relative timing of the transition spatially. Though such debate could in principle be lifted by absolute dating of proxy records and perfect understanding of what is recorded in those proxies, the current science is not there yet.

We therefore propose to help understanding the sequence of climatic changes of the last deglaciation by performing a model study to assess, within the physical hypotheses contained in our climate model, when, why and where the climate started to warm in an experiment forced by low-frequency variability arising from greenhouse gases, orbital and ice-sheet distribution changes. We also define a time period in years needed to distinguish between a large local climate change (such as the deglaciation) and local inter-annual or centennial variability.

Experimental Setup

Model Description

In the present study, we use the LOVECLIM earth system model of intermediate complexity in its version 1.0. It includes an atmosphere (ECBilt), an ocean (CLIO) and a vegetation (VECODE) component. It is a follow-up of the ECBilt–CLIO–VECODE coupled model that has been successful in simulating a wide range of different climate from the Last Glacial Maximum (Roche et al. 2007) to the future (Driesschaert et al. 2007) through the Holocene (Renssen et al. 2005, 2009) and the last millennium (Goosse et al. 2005). The atmospheric component (ECBilt) is a quasi-geostrophic model at T21 spectral resolution (5.6 in latitude/longitude) with additional parametrizations for the non-geostrophic terms (Opsteegh et al. 1998). ECBilt has three vertical layers in which only the first contains humidity as a prognostic variable. Precipitation is computed from the precipitable water of the first layer and falls in form of snow if temperature is below 0°C. The time step of integration of ECBilt is 4 h. The oceanic component (CLIO) is a 3-D Oceanic General Circulation Model (Goosse and Fichefet 1999) run on a B-grid at approximately 3×3 (latitude–longitude) resolution. It has a free surface that allows the use of real freshwater fluxes, a parametrization of downsloping currents and a realistic bathymetry. CLIO also includes a dynamical–thermodynamical sea-ice component (Fichefet and Morales Maqueda 1997, 1999) on the same grid. The interactive vegetation component used is VECODE (Brovkin et al. 1997), a simple dynamical model that computes two Plant Functional Types (PFT: trees and grass) and a dummy type (bare soil). The vegetation model is resolved on the atmospheric grid (hence at T21 resolution) and allows fractional allocation of PFTs in the same grid cell to account for the small scale needed by vegetation. An iceberg trajectory module is also present (Jongma et al. 2009), but is not activated in the present study. The different modules exchange heat, stress and water. It should be noted that there is a precipitation correction needed to avoid the large overestimation of precipitation over the Arctic and the north Atlantic that is present in ECBilt. This surplus fresh water is removed from the latter regions and is added homogeneously to the north Pacific surface.

Deglacial Forcings

Our purpose is to perform a transient simulation of the last deglaciation, from the Last Glacial Maximum (LGM, around 21 kiloyear BP) to the early phase of the Holocene period (around 9 kiloyear BP). It shall be noted that there is still some ice present in North America over the Quebec region at this last date; the northern hemisphere ice sheets reaching a near present-day extent around 7 kiloyears BP (cf. Renssen et al. (2009, 2010) for an analysis of the impact of the remnants of the Laurentide ice sheet on the climate evolution of the Holocene). We start our integration at the LGM, from the climatic state described in Roche et al. (2007). From 21 kiloyears BP onwards, we force the model with insolation changes arising from the long-term changes in orbital parameters (the so-called “Milankovitch forcing”), greenhouse gases changes and ice-sheet distribution, since our model version does not include an interactive ice-sheet component. The orbital parameters are taken from Berger (1978). For greenhouse gases, we prescribe changes in carbon

dioxide, methane and nitrous oxide as recorded in air bubbles from ice cores (cf. Fig. 1). Ice-sheet evolution is taken from the ICE-5gV1.2 reconstruction (Peltier 2004) for both northern and southern hemisphere ice sheets and interpolated on the T21 grid of the atmospheric component of our coupled climate model. We both prescribe the orography and an ice mask so as to ensure their joint evolution during the deglaciation run whereas the land-sea mask is kept fixed at LGM. Indeed, it is not obvious how changes in the land-sea mask should be taken into account from the oceanic perspective in order to properly conserve mass, momentum and salinity. Using this approach means that not only the Barents and Kara seas but also the Hudson Bay remain land throughout and that the Bering strait is kept closed at all times. This is known to have important implication on the sensitivity of the oceanic circulation to freshwater fluxes (Shaffer and Bendtsen 1994; Weijer et al. 2001; Hasumi 2002; Keigwin and Cook 2007; Hu et al. 2008). As we focus here on the long-term changes of climate forced by insolation, orography and greenhouse gases in the

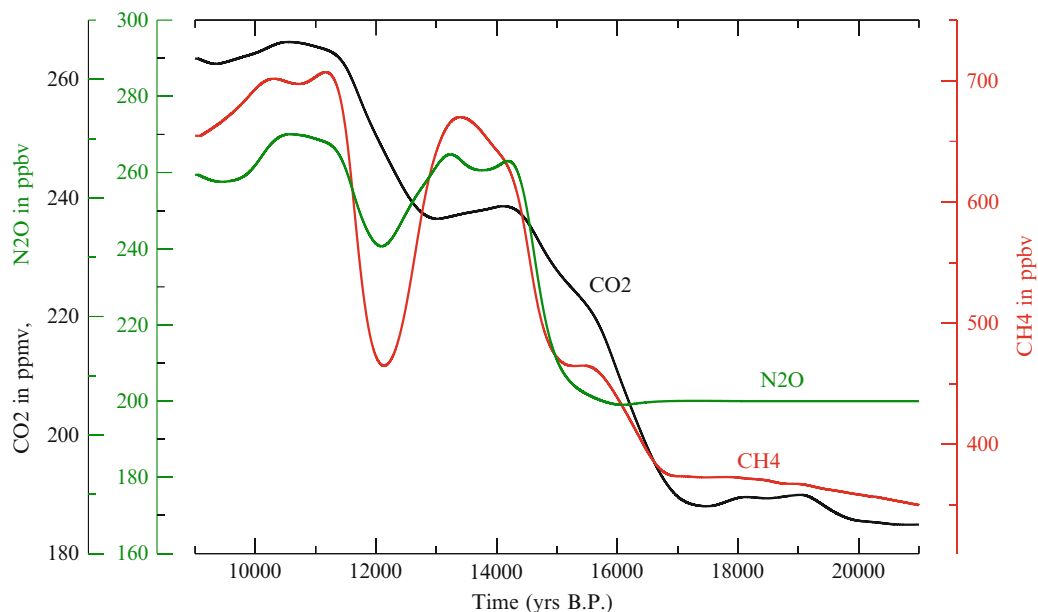


Fig. 1 Greenhouse gas evolution throughout the last deglaciation from air measurements on ice core from both Greenland and Antarctica. CO₂ is taken from Neftel et al. (1988), Staffelbach et al. (1991), Indermühle et al. (1999), Petit et al. (1999), Monnin et al. (2004), CH₄ from Blunier and Brook (2001), Dällenbach et al. (2000), Blunier et al. (1995), Chappellaz

et al. (1993), Brook et al. (2000), Blunier et al. (1998), Spahni et al. (2005) and N₂O from Flueckiger et al. (1999), Spahni et al. (2005). All series are on the EPICA EDC3 timescales and have been smoothed and interpolated on a yearly basis using a cubic spline interpolation scheme for easier use with the model

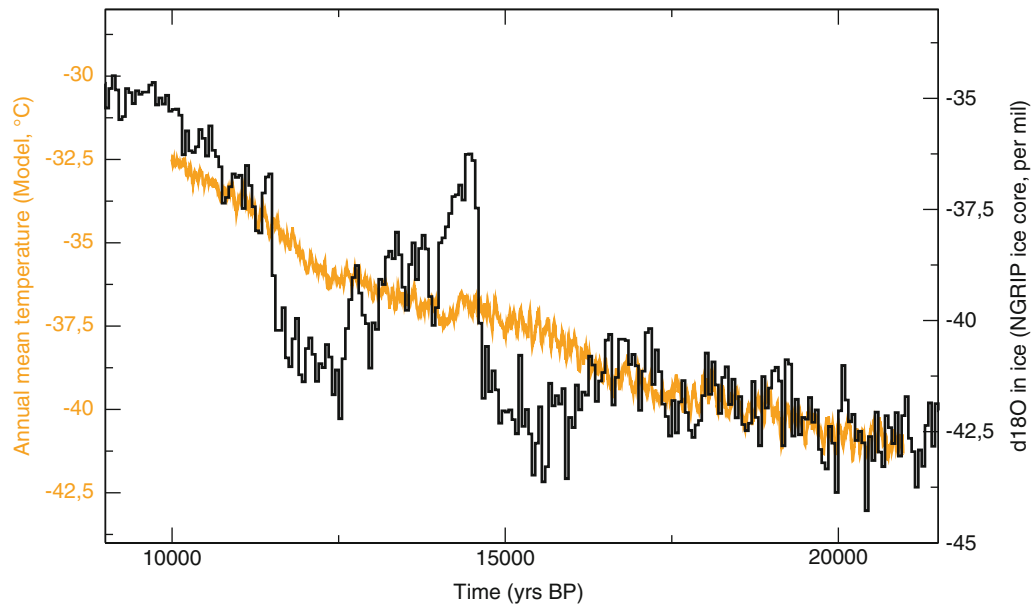


Fig. 2 General outline of the deglaciation simulation: comparison of the modelled annual temperature (*yellow*) at North Grip (North Greenland Ice Core Project members 2004) to the North Grip ^{18}O record (*black*). The ^{18}O of the ice is scaled so as to have a 10°C warming during the Bølling period

following, we should nevertheless capture the first-order changes, though detailed regional features might prove more difficult to interpret.

Finally, in contrast to previous modelling studies of the last deglaciation (Lunt et al. 2006, for example), we do not make use of any acceleration techniques but run the model in real time from 21 kiloyears BP to 9 kiloyears BP, that is we perform a single run of 12 kiloyears duration. This is required in order to properly analyse the phasing of climate change between different locations. Indeed, it has been shown that using accelerated techniques tend to bias temperature evolution in regions where the ocean is playing a major role, especially in the Southern Ocean and in the Nordic Seas (Lunt et al. 2006; Timm and Timmermann 2007). Furthermore, as we analyse the relationships between the mean climate change and the interannual-to-centennial variability, we need to use a transient simulation to ensure consistency of timescales in the forcing and response in the climate system.

We would like to stress that while our external forcings are realistic in general, we do not include here freshwater addition to the oceans caused by melting ice sheets. We do not therefore have the forcing needed to reproduce any abrupt climate change during the deglaciation. Figure 2 shows a comparison of our

modelled temperature at the NorthGRIP ice core site. We reproduce faithfully the temperature trend at NorthGRIP until around 16 ka BP when a sudden cooling in Greenland interrupts the warming trend. This cooling has been associated to the north Atlantic Heinrich Event 1 (cf. Hemming (2004) for a review) that modified the sea surface conditions by addition of excess freshwater to that area. The subsequent sequence of events is likely responding or forced in the same manner. As we do not include the appropriate forcing for such events, we will focus in the following on the long-term trend in climate in a theoretical framework. While our results are general enough to be interpreted likewise should freshwater forcings be included, we will nevertheless not attempt a detailed data—model comparison. Such a comparison will be the focus of further studies.

Analysis Method

Analysing climate change throughout the last deglaciation is complex and could be based on different variables (temperature, precipitations, etc.). The most obvious change that comes to mind when thinking of the deglaciation is warming. We thus chose to

concentrate on the phasing of climate evolution throughout the last deglaciation, with a focus on the first significant warming occurring after the LGM at every location. In the following, we will define the first significant warming using a statistical test. It requires the knowledge of the “internal” (modelled) variance of the LGM climate, computed here from the last 500 years of an equilibrium run under constant LGM boundary conditions. Our 12,000 years deglaciation run is first divided in 120 samples of 100 years that we test independently with respect to the control LGM climate. We also perform the analysis with samples of 25, 200 and 300 years to assess the robustness of the method. In the following, we make use of a t-test with two unequal variances defined as Welsch’s test:

$$\text{test}_{\text{value}} = \frac{\chi_{\text{ref}} - \chi_{\text{sample}}}{\sqrt{\frac{\sigma_{\text{ref}}}{N_{\text{ref}}} + \frac{\sigma_{\text{sample}}}{N_{\text{sample}}}}},$$

where denote the mean of the climatic variable over the considered period, N the size (in time steps) of the period and the variance of the climatic variable, ref denotes the reference period while sample denotes the sample tested against the specified period. In the following, we consider anomalies that are significant at a 95% level, that is when t value > 1.960 for a sample of 100-year or more. We will consider significant temperature anomalies at a given time or the timing of the first significant anomaly as a marker of the local start

of the deglaciation period as modelled with the imposed slow forcings.

Results for Surface Air Temperature Evolution

Annual Mean

In the following, we concentrate on a 100-year sample for discussion. Figure 3 introduces the spatial distribution of the timing of first significant warming from 21 ka BP onwards.

The first regions to respond (between 19 and 18 ka BP) are the Labrador Sea, the northern North Atlantic and the southern part of the Nordic Seas. These are regions mainly affected by the presence of sea ice. During that given period of time, the only forcing is the orbital forcing, greenhouse gases and ice-sheet forcing being quasi-constant (only CO₂ concentration changes by ~5 ppm). Sea ice is sensitive to the total amount of energy received throughout the year. Increasing the energy received in any season will limit (or even reduce) the sea-ice extent, and the buffering effect of the underlying ocean will extend (in time) the anomaly to a year-round effect. The early response seen in the northern north Atlantic and adjacent regions is therefore an effect of the obliquity increase during the early part of the deglaciation that

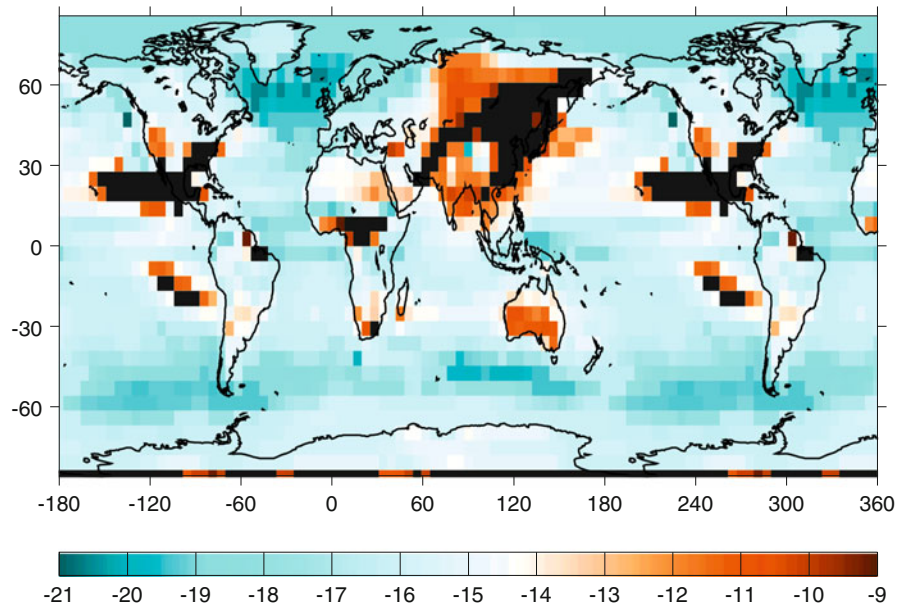


Fig. 3 Timing of first significant warming during the deglaciation from a 100-year sample at 95% significance. Color scale is the date in kiloyears BP. Black denotes regions without significant warming over the deglaciation

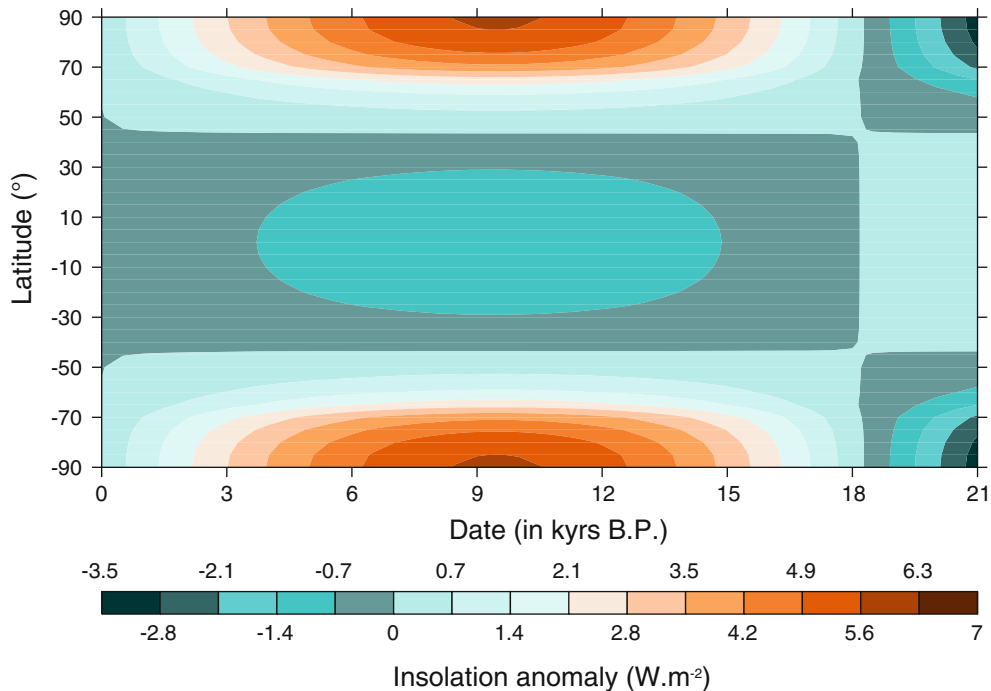


Fig. 4 Insolation anomaly to the mean (30 to 0 kiloyear BP) for the last deglaciation computed from Berger (1978) for the annual mean

increases the total amount of energy received by the Earth at high latitude, as depicted in Fig. 4.

The first response is followed by changes in the Southern Hemisphere in a more or less zonal band 40–60°S with a delay of 300–500 years. Again, this is due to a reduction in the sea-ice extent around Antarctica, a result found in other simulations of the last deglaciation (Timmermann et al. 2009). The delay compared to the northern Hemisphere is short and not significant given the climatic variability within the model. The sea-ice change in the South therefore responds primarily to the local orbital (obliquity) forcing and not to a delayed response to the North Atlantic warming through upwelled waters (Renssen et al. 2010; Duplessy et al. 2007). By increasing the total energy received from the sun at high latitudes, the obliquity signal forces an in phase response of both hemispheres in sea-ice covered regions (cf. Fig. 4).

A later response (17 to 15 ka BP) is then observed around the equator. Given the simplified representation of the physical equations for motion in the atmospheric part of our model, caution is needed in interpreting this pattern. We observe some changes in the precipitation pattern at the same time (not shown) that may be linked

to ITCZ changes in response to the changing Equator-to-pole gradient as well as change in ice-sheet topography. However, a precise assessment of what is occurring in the tropics would require a model with more complex atmospheric physics. The time period around 16 ka BP is also a period when the global greenhouse gas forcing starts to become significant (CO_2 at around 220 ppm, cf. Fig. 1) enough to counterbalance the obliquity induced cooling of the 175 tropics (cf. Fig. 4).

Two different types of regions are lagging the response of the rest of the planet. First are the tropical areas between 20° and 30° north and south. The lag is due to rather small absolute temperature changes in those areas (cf. Fig. 5) as a whole. It is therefore difficult to discriminate between a small temperature change and year-to-year variability within the model in such areas. The other area is over Eastern Siberia, China from the Pacific ocean to India along the Indian ocean, but also Australia. These are areas where the year-to-year variability—as characterized by the sample variance—is higher during the deglaciation and the local temperature change over the deglaciation is not that large. Thus, the deglacial warming becomes

Fig. 5 Annual mean temperature difference (in °C) between 9 ka BP w.r.t. 21 ka BP for a 100-year sample. Colorscale is in °C

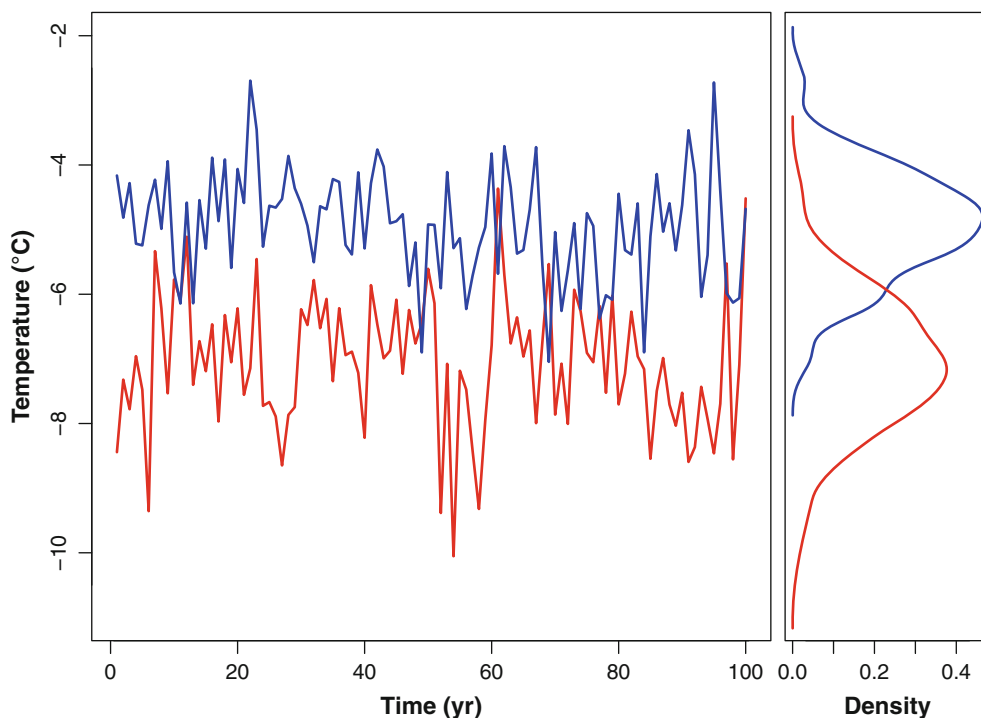
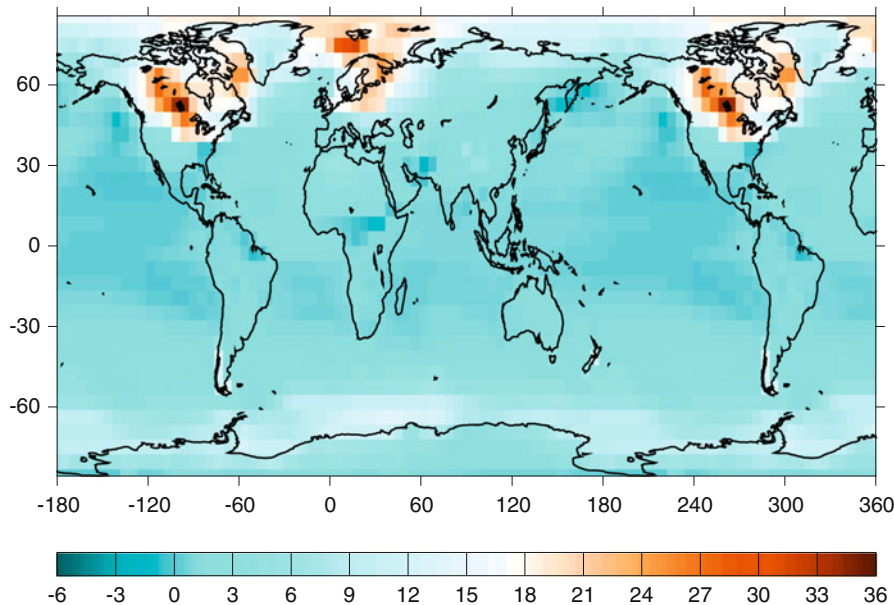


Fig. 6 Comparison of two temperature samples from the deglaciation in Eastern Siberia (55°N, 125°E). The left panel shows the temperature evolution over a 100-year sample taken from the reference LGM run (in blue) and from the deglaciation (at 12 ka BP, in red). The right panel shows the density function associated to that sample on the same temperature axis

significant only late in the deglaciation. Figure 6 shows it for one location in Siberia (55°N, 125°E). The two density distributions are relatively well

separated, but not to a 95% significance level. The deglacial sample has a larger variance (variability) than the glacial one, as characterized by the width of

the density peak. Within the sample, some years cannot be statistically distinguished from one another as, for example a series of 20 years between years 60 and 80. Thus, one can argue that the climate depicted by those to samples is not very different at a 95% confidence level, i.e. a relatively high confidence level.

There are a few areas where the deglacial warming from 21 ka to 9 ka is never significant (shown by black shading on Fig. 3). A few are in the northern tropics and a larger one is in eastern Asia. The reason for this is similar to the late warming previously described, i.e. the local variability is too high for the local warming to become statistically significant. It may be interpreted as regions where a 100-year mean is more representative of interannual to centennial variability than of climate. The time length of the sample needed for the warming to become significant during the transition is discussed in section “Impact of Interannual Variability”.

Seasonal Means

To confirm our first analysis based on annual means, Fig. 7 presents results for December–January–February (DJF, northern winter) and June–July–August (JJA, northern summer).

DJF shows largest areas of non-significant warming over the deglaciation. For a relatively large area centred on the Bering Strait as well as for the Gulf of Mexico, there is no significant warming in DJF at 9 ka BP relative to the LGM as the two regions are significantly cooling in our model. Other large areas of non-significant warming (part of the eastern Pacific, continental tropical regions and eastern Eurasia) are characterized by small temperature anomalies as a whole (below 1°C in DJF), a change that is hardly significant with respect to the model interannual variability in the same regions. We nonetheless note the early response of sea-ice regions, first in the northern North Atlantic (19.5 ka BP) and of the Southern Ocean sea-ice north of 60°S, as was already seen in the yearly mean. Conversely, JJA shows the smallest non-significant warming from 21 k to 9 k. A striking feature is that most regions have a significant warming early in the deglaciation mostly before 15 ka BP. Three large areas are standing out as being earlier than that: the northern north Atlantic, the Southern Ocean around 60°S and the northern Equatorial regions. The

first is due to sea-ice changes and circulation changes as was noted before, followed by the neighbouring Arctic. Accordingly, the Southern Ocean region is linked to sea-ice shrinking winter extent.

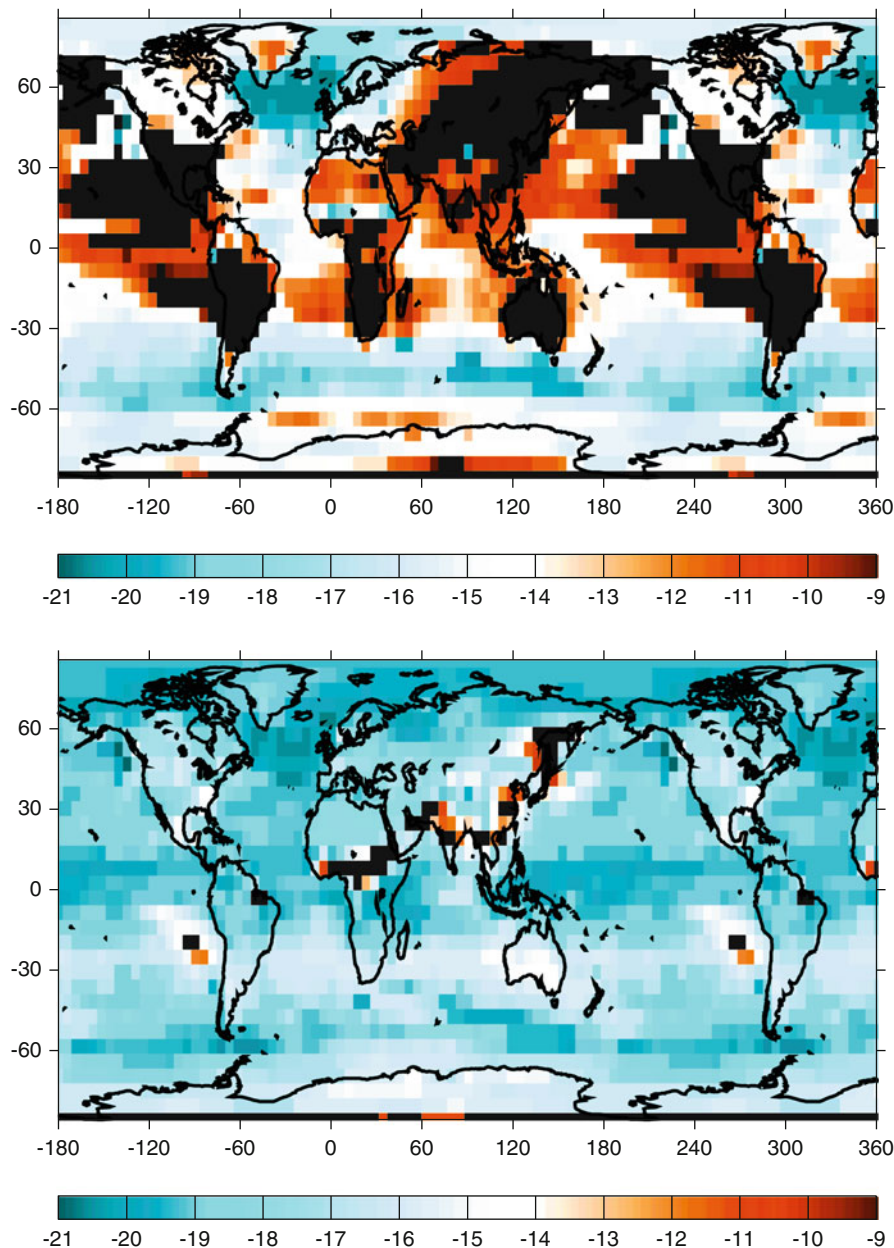
Impact of Interannual Variability

As noted before, our results are sensitive to the sample size used in the study. Indeed, increasing the sample size comparatively reduces the effect of noise (variability) in the model on the definition of the mean temperature of the sample. A large sample is thus less affected by a series of higher temperature than a smaller sample. Using a small sample size (e.g. 25 years), our results therefore emphasize the potential for interannual variability anomalies to be significant at a long-term scale (deglaciation scale). Using different sample sizes (25, 100, 200 and 300 years in the following), we may truly assess what is the timing of climate change in the model and decipher regions where the interannual variability is too large to allow significant climatic anomalies on those longer timescales. Figure 8 compares the timing of first significant warming for four different samples of increasing size.

An evident feature arising from Fig. 8 is that not only a shorter sample yields larger areas where no significant temperature warming occurs during the last deglaciation but also more regions that have a late significant warming (after 13 ka BP). This results from the fact that the value of the Welsch’s test depends strongly on the sample size to determine the significance of the anomaly: if the sample is relatively small and the variability within the sample is large or larger than the reference period, then a larger temperature anomaly is needed to stand out of the local variability. Increasing the sample size thus decreases the importance of the internal variability over the signal and enables a more accurate determination of the first significant, externally forced, warming. In simpler terms, this can be interpreted as looking at climate or looking at internal high-frequency variability: with a small sample having a large variability, one needs a very different sample mean to be significantly different from the reference.

Most interestingly, the size of the sample needed to discuss the climate anomaly vs. the reference climate is variable spatially. Indeed, both the absolute temperature anomaly and local temperature variability vary

Fig. 7 Timing of first significant warming during the deglaciation from a 100-year sample at 95% significance. DJF (*top*) and JJA (*bottom*). Colorscale is the date in kiloyears BP. *Black* denotes regions without significant warming over the deglaciation



in space. Two examples can be taken from Fig. 8 to highlight this feature.

1. In the northern tropical regions over the Pacific and south-western North America, the total temperature anomalies from 21 ka BP to 9 ka BP (cf. Fig. 5) are relatively small in our model, below 2°C . Distinguishing those small anomalies from a larger interannual variability (that is in a sample with a large variance) is therefore difficult and requires a

larger sample. One can note that even with a 300-year sample, not every location in those areas is significantly warmer at 9 ka BP than at LGM.

2. Most regions of continental Asia are not significantly warmer at 9 ka than at LGM using a 25-year sample. In this case, this is not solely the effect of a small LGM to 9 ka BP temperature difference (some areas have a temperature anomaly of about 10°C) but because of very large variance within the

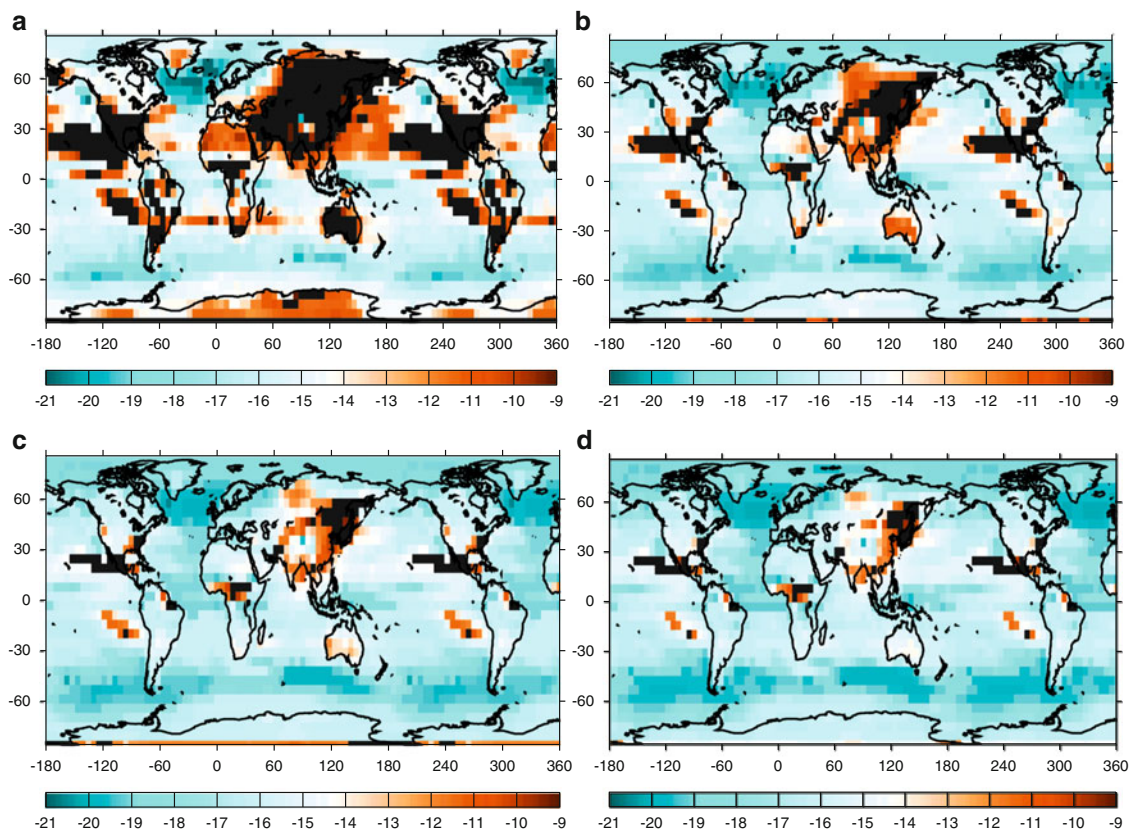


Fig. 8 Impact on sample size on the timing of the first significant temperature warming during the deglaciation. From top left to bottom right sample size are: 25 (a), 100 (b), 200 (c) and 300 (d) years. Colorscale is the date in kiloyears BP. *Black* denotes regions without significant warming over the deglaciation

sample, related to high interannual to centennial variability. In fact, the variance of the samples during the deglaciation are systematically higher than those of the reference run, making it harder to decipher a climate change from internal high-frequency variability (noise). It shall be noted also that the sample size strongly affects in this area the date of first significant anomaly: Eastern Siberia is not significant in the 25-year sample, is significant between 11 and 14 ka BP in the 100-year sample and around 17 ka BP in the 300-year sample. However, part of the area is very robust in showing no significant temperature changes as even with a 300-year sample, not all areas are significant.

The analysis of Fig. 8 confirms our previous inferences that there are three main areas with leading temperature changes: the northern North Atlantic, a north Equatorial band and the Southern Ocean between 45 and 60°S.

Discussion

Our study so far focusses on a single 12,000 years run with slow forcings included. Going one step further would require the use of higher frequency forcings, such as freshwater fluxes from melting ice sheets or understanding how the response to slow forcings can act to produce abrupt events through the nonlinearities of the climate system as is recorded in many different proxies (North Greenland Ice Core Project members 2004; Shackleton et al. 2000; Wang et al. 2001; von Grafenstein et al. 1999, for example). How could we proceed to better determine the response of our climate model to the (imposed) slow forcings? One often used method (Goosse et al. 2005, for example) is to perform ensemble simulations with identical forcings, varying only the initial conditions. The different expression of the internal variability of

the model in the different ensembles would then cancel out in the mean, leading to a more robust response of the forced response. However, such a method is difficult to use on the full deglaciation period due to computational constraints. We are thus limited to a single run for the time being.

Natural (observed) climate on the other hand is only one trajectory, as we never find in past times the exact repetition of two deglaciations with identical boundary conditions. Analysing a single simulation is therefore close to what is recorded by proxy data, albeit that we have a perfect recording of our simulated climate as opposed to the imperfect recording or the Earth's climate in proxy data. We have shown that even with perfect recording of the simulated climate, there are regions where distinguishing between the deglaciation warming and local variability is problematic. Depending on the resolution of the signal recorded in the proxy, a similar issue may arise. Indeed, while the ice cores do record continuously surface conditions and may be analysed to a high resolution (though subjected to seasonal changes in precipitation rates), some other proxies are limited by essence. For example, recording ^{18}O in oceanic sediment cores has the maximal practical resolution of about 10 years (analysis every centimetre of the core). Furthermore, averaging the values of five specimens does not guarantee the consistence of five subsequent and equal periods of time. Thus, analysing an oceanic sediment core at 100 years resolution is not equivalent to obtaining the 100-year mean of the signal. The relationship between the mean of the recorded proxy and the local variability is thus complex. Our results are indicative of regions where the relationship between average climate change and variability is likely to be complicated by the amplitude of the latter.

Finally, the reader should not forget that the results presented are obtained with one climate model and are only indicative of what is physically plausible within the framework of the given model. There is a need to repeat such approaches with different models to identify regions where it is likely that the high local variability will hamper our capability to record the mean climate changes and how such local climate variability is evolving through time. The regions highlighted (like the Pacific coast of Siberia) here are indicative with respect to the mechanisms occurring but are limited to the climate model used. Extension to the real climate system should be done with extreme caution.

Conclusions

A number of conclusions arise from our analysis.

First, the first regions that are showing a significant temperature evolution during the deglaciation are sea-ice covered regions in both northern and southern hemisphere. This points to a crucial importance of sea ice in setting the timing for deglaciation, as well as in constraining feedback mechanisms that will lead to further warming and deglaciation. The understanding of sea-ice evolution is probably crucial in that sense, though probably more via the annual production of sea ice (Paillard and Parrenin 2004; Bouttes et al. 2010) than through the absolute sea-ice cover (Stephens and Keeling 2000; Archer et al. 2003).

Second, regions that are more “passively” responding to the deglaciation forcings and are remote to the ice-sheet locations are likely to respond with a time delay of 3,000 years, that is when a significant global forcing such as greenhouse gases will set in. This delay is to be understood within slowly varying forcing framework as including abrupt climate changes within the deglaciation will complicate the matter, while not suppressing this time delay. Moreover, there is a large spatial variability in the first significant change during the last deglaciation even without abrupt climate changes. Therefore, caution is needed when trying to infer leads/lags and physical interpretation to existing deglaciation records or model results.

Third, regions displaying little glacial to interglacial changes in the considered climatic variable (temperature here) and remote from the “centres of action” of the coupled climate system will not easily record a precise timing for the first change in the deglaciation. The interannual variability whether in the climate model or in reality will tend to cloud the true signal as in any noisy record. We have detailed this mechanism here for regions in eastern Eurasia. There is, therefore, a high dependence of first warming timing to local variability. In that respect, using long averages of about 200 years to describe climate change is a requirement in analysing model results if one wants to avoid biases due to (modelled) variability at shorter timescales. This brings us to the question of what is to be understood as “climate change”: we infer from our simulations that it has

to be a time long enough to be detected against background noise, but how much will vary spatially and in time, making it harder to decipher long time climate changes from different climate model simulations—and/or—data proxies. Ultimately, it will vary both with the resolution of the proxy used to record the climate change and with the time window considered.

Acknowledgements This work is a contribution to the NWO-NERC RAPID project ORMEN. D. M. R. is funded by the NWO under project number 854.00.024 and by INSU-CNRS. The authors wish to thank M. Vrac for useful discussions on the statistical approach and A. Berger for comments on an earlier version of the manuscript.

References

- Archer DE, Martin PA, Milovich J, Brovkin V, Plattner G-K, Ashendel C (2003) Model sensitivity in the effect of Antarctic sea ice and stratification on atmospheric pCO₂. *Paleoceanography* 18:1012. doi:10.1029/2002PA000760
- Berger AL (1978) Long-term variations of caloric insolation resulting from earths orbital elements. *Quat Res* 9:139–167
- Berger A, Quizhen Y (2010) Modelling the interglacials of the last one million years. In: Berger A, Mesinger F (eds) Milutin Milankovitch 130th anniversary symposium: climate change at the eve of the second decade of the century inferences from paleoclimate, and regional aspects. Serbian Academy of Sciences and Arts
- Blunier T, Brook EJ (2001) Timing of millennial-scale climate change in Antarctica and Greenland during the last glacial period. *Science* 291:109–112
- Blunier T, Chappellaz J, Schwander J, Stauffer B, Raynaud D (1995) Variations in atmospheric methane concentration during the Holocene epoch. *Nature* 374:46–49
- Blunier T, Chappellaz J, Schwander J, Dällenbach A, Stauffer B, Stocker TF, Raynaud D, Jouzel J, Clausen HB, Hammer CU (1998) Asynchrony of Antarctic and Greenland climate change during the last glacial period. *Nature* 394:739–743
- Bouttes N, Paillard D, Roche DM (2010) Impact of brine-induced stratification on the glacial carbon cycle. *Clim Past Discuss* 6:681–710. <http://www.clim-past-discuss.net/6/681/2010/cpd-6-681-2010.pdf>
- Brook EJ, Harder S, Severinghaus J, Sterig EJ, Sucher M (2000) On the origin and timing of rapid changes in atmospheric methane during the last glacial period. *Global Biogeochem Cycles* 14:559–572
- Brovkin V, Ganopolski A, Svirezhev Y (1997) A continuous climate-vegetation classification for use in climate-biosphere studies. *Ecol Model* 101:251–261
- Chappellaz J, Blunier T, Raynaud D, Barnola JM, Schwander J, Stauffer B (1993) Synchronous changes in atmospheric CH₄ and Greenland climate between 40 and 8 kyr BP. *Nature* 366:443–445
- Dällenbach A, Blunier T, Flückiger J, Stauffer B, Chappellaz J, Raynaud D (2000) Changes in the atmospheric CH₄ gradient between Greenland and Antarctica during the Last Glacial and the transition to the Holocene. *Geophys Res Lett* 27:1005–1008
- Drisschaert E, Fichet T, Goosse H, Huybrechts P, Janssens I, Mouchet A, Munhoven G, Brovkin V, Weber SL (2007) Modelling the influence of the Greenland ice sheet melting on the Atlantic meridional overturning circulation during the next millennia. *Geophys Res Lett* 34:L10707. doi:10.1029/2007GL029516
- Duplessy J-C, Roche DM, Kageyama M (2007) The deep ocean during the last interglacial period. *Science* 316:89–91. doi:10.1126/science.1138582
- Dyke AS, Andrews JT, Clark PU, England JH, Miller GH, Shaw J, Veillette JJ (2002) The Laurentide and Innuitian ice sheets during the Last Glacial Maximum. *Quat Sci Rev* 21:9–31. doi:10.1016/S0277-3791(01)00095-6
- EPICA community members (2004) Eight glacial cycles from an Antarctic ice core. *Nature* 429:623–628. doi:10.1038/nature02599
- Fichet T, Morales Maqueda MA (1997) Sensitivity of a global sea ice model to the treatment of ice thermodynamics and dynamics. *J Geophys Res* 102:12609–12646
- Fichet T, Morales Maqueda MA (1999) Modelling the influence of snow accumulation and snow-ice formation on the seasonal cycle of the Antarctic sea-ice cover. *Clim Dyn* 15:251–268
- Flückiger J, Dällenbach A, Blunier T, Stauffer B, Stocker TF, Raynaud D, Barnola J-M (1999) Variations in atmospheric N₂O concentration during abrupt climatic changes. *Science* 285:227–230. doi:10.1126/science.285.5425.227
- Ganopolski A, Calov R (2010) Simulation of glacial cycles with an Earth system model. In: Berger A, Mesinger F (eds) Milutin Milankovitch 130th anniversary symposium: climate change at the eve of the second decade of the century inferences from paleoclimate, and regional aspects. Serbian Academy of Sciences and Arts
- Goosse H, Fichet T (1999) Importance of ice-ocean interactions for the global ocean circulation: a model study. *J Geophys Res* 104:23337–23355. doi:10.1029/1999JC900215
- Goosse H, Renssen H, Timmermann A, Bradley RS (2005) Internal and forced climate variability during the last millennium: a model-data comparison using ensemble simulations. *Quat Sci Rev* 24:1345–1360
- Hasumi H (2002) Sensitivity of the global thermohaline circulation to interbasin freshwater transport by the atmosphere and the Bering Strait throughflow. *J Clim* 15:2516–2526
- Hemming SR (2004) Heinrich events: massive late Pleistocene detritus layers of the North Atlantic and their global climate imprint. *Rev Geophys* 42:RG1005
- Hu AX, Otto-Bliesner BL, Meehl GA, Han WQ, Morrill C, Brady EC, Briegleb B (2008) Response of thermohaline circulation to freshwater forcing under present-day and LGM conditions. *J Clim* 21:2239–2258. doi:10.1175/2007JCLI1985.1
- Indermühle A, Monnin E, Stauffer B, Stocker TF, Wahlen M (1999) Atmospheric CO₂ concentration from 60 to 20 kyr BP from the Taylor Dome ice core. *Geophys Res Lett* 27:735–738

- Jongma JJ, Driesschaert E, Fichet T, Goosse H, Renssen H (2009) The effect of dynamic-thermodynamic icebergs on the Southern Ocean climate in a three-dimensional model. *Ocean Model* 26:104–113
- Keigwin LD, Cook MS (2007) A role for North Pacific salinity in stabilizing North Atlantic climate. *Paleoceanography* 22: PA3102. doi:10.1029/2007PA001420
- Lunt DJ, Williamson MS, Valdes PJ, Lenton TM, Marsh R (2006) Comparing transient, accelerated, and equilibrium simulations of the last 30 000 years with the GENIE-1 model. *Clim Past* 2:221–235. doi:10.5194/cp-2-221-2006
- MARGO Project Members (2009) Constraints on the magnitude and patterns of ocean cooling at the Last Glacial Maximum. *Nat Geosci* 2:127–132. doi:10.1038/ngeo411
- Monnin E, Steig E, Siegenthaler U, Kawamura K, Schwander J, Stauffer B, Stocker TF, Morse DL, Barnola J-M, Bellier B, Raynaud D, Fischer H (2004) Evidence for substantial accumulation rate variability in Antarctica during the Holocene, through synchronization of CO₂ in the Taylor Dome, Dome C and DML ice cores. *Earth Planet Sci Lett* 224:45–54. doi:10.1016/j.epsl.2004.05.007
- Nefel A, Oeschger H, Staffelbach T, Stauffer B (1988) CO₂ record in the Byrd ice core 50000–5000 years BP. *Nature* 331:609–611
- North Greenland Ice Core Project members (2004) High-resolution record of Northern Hemisphere climate extending into the last interglacial period. *Nature* 431:147–151. doi:10.1038/nature02805
- Opsteegh J, Haarsma R, Selten F, Kattenberg A (1998) ECBILT: a dynamic alternative to mixed boundary conditions in ocean models. *Tellus* 50:348–367, <http://www.knmi.nl/selten/tellus97.ps.Z>
- Paillard D, Parrenin F (2004) The Antarctic ice sheet and the triggering of deglaciations. *Earth Planet Sci Lett* 227:263–271. doi:10.1016/j.epsl.2004.08.023
- Peltier W (2004) Global glacial isostasy and the surface of the ice-age earth: the ICE-5G (VM2) model and GRACE. *Annu Rev Earth Planet Sci* 32:111–149. doi:10.1146/annurev.earth.32.420.082503.144359
- Petit JR, Jouzel J, Raynaud D, Barkov NI, Barnola JM, Basile I, Bender M, Chappellaz J, Davis J, Delaygue G, Delmotte M, Kotlyakov VM, Legrand M, Lipenkov V, Lorius C, Pépin L, Ritz C, Saltzman E, Stievenard M (1999) Climate and atmospheric history of the past 420,000 years from the Vostok Ice Core. *Nature* 399:429–436
- Renssen H, Goosse H, Fichet T, Brovkin V, Driesschaert E, Wolk F (2005) Simulating the Holocene climate evolution at northern high latitudes using a coupled atmosphere-sea ice-ocean-vegetation model. *Clim Dyn* 24:23–43. doi:10.1007/s00382-004-0485-y
- Renssen H, Seppä H, Heiri O, Roche DM, Goosse H, Fichet T (2009) The spatial and temporal complexity of the Holocene thermal maximum. *Nat Geosci* 2:411–414. doi:10.1038/ngeo513
- Renssen H, Goosse H, Crosta X, Roche DM (2010) Early Holocene Laurentide Ice-sheet deglaciation causes cooling in the high-latitude Southern Hemisphere through oceanic teleconnection. *Paleoceanography* 25:PA3204. doi:10.1029/2009PA001854
- Roche DM, Dokken TM, Goosse H, Renssen H, Weber SL (2007) Climate of the Last Glacial Maximum: sensitivity studies and model-data comparison with the LOVECLIM coupled model. *Clim Past* 3:205–244
- Shackleton NJ, Hall MA, Vincent E (2000) Phase relationships between millennial-scale events 64,000–24,000 years ago. *Paleoceanography* 15:565–569. doi:10.1029/2000PA000513
- Shaffer G, Bendtsen J (1994) Role of the Bering Strait in controlling North Atlantic ocean circulation and climate. *Nature* 367:354–357. doi:10.1038/367354a0
- Spahni R, Chappellaz J, Stocker TF, Loulergue L, Hausamann G, Kawamura K, Flückiger J, Schwander J, Raynaud D, Masson-Delmotte V, Jouzel J (2005) Atmospheric methane and nitrous oxide of the late Pleistocene from Antarctic ice cores. *Science* 310:1317–1321
- Staffelbach T, Stauffer B, Sigg A, Oeschger H (1991) CO₂ measurements from polar ice cores: more data from different sites. *Tellus* 43B:91–96
- Stephens BB, Keeling RF (2000) The influence of Antarctic sea ice on glacial-interglacial CO₂ variations. *Nature* 404:171–174. doi:10.1038/35004556
- Svensden J, Alexanderson H, Astakhov V, Demidov I, Dowdeswell J, Funder S, Gataullin V, Henriksen M, Hjort C, Houmark-Nielsen M, Hubberten H, Ingólfsson O, Jakobsson M, Kjaer K, Larsen E, Lokrantz H, Lunkka J, Lysa A, Mangerud J, Matiouchkov A, Murray A, Møller P, Niessen F, Nikolskaya O, Polyak L, Saarnisto M, Siebert C, Siebert M, Spielhagen R, Stein R (2004) Late Quaternary ice sheet history of northern Eurasia. *Quat Sci Rev* 23:1229–1271. doi:10.1016/j.quascirev.2003.12.008
- Timm O, Timmermann A (2007) Simulation of the last 21 000 years using accelerated transient boundary conditions. *J Clim* 20:4377–4401. doi:10.1175/JCLI4237.1
- Timmermann A, Timm O, Stoll L, Menviel L (2009) The roles of CO₂ and orbital forcing in driving southern hemispheric temperature variations during the last 21 000 yr. *J Clim* 22:1626–1640. doi:10.1175/2008JCLI2161.1
- von Grafenstein U, Erlenkeuser H, Brauer A, Jouzel J, Johnsen SJ (1999) A mid-European decadal isotope-climate record from 15,500 to 5000 years B.P. *Science* 284:1654–1657. doi:10.1126/science.460.284.5420.1654
- Wang YJ, Cheng H, Edwards RL, An ZS, Wu JY, Shen C-C, Dorale JA (2001) A high-resolution absolute-dated late Pleistocene monsoon record from Hulu Cave, China. *Science* 294:2345–2348. doi:10.1126/science.1064618
- Weijer W, De Ruijter WPM, Dijkstra HA (2001) Stability of the Atlantic overturning circulation: competition between Bering Strait freshwater flux and Agulhas heat and salt sources. *J Phys Oceanogr* 31:2385–2402

Perspectives of Parameter and State Estimation in Paleoclimatology

André Paul and Martin Losch

Abstract

Past climates provide a means for evaluating the response of the climate system to large perturbations. Our ultimate goal is to constrain climate models rigorously by paleoclimate data. For illustration, we used a conceptual climate model (a classical energy balance model) and applied the so-called “adjoint method” to minimize the misfit between our model and sea-surface temperature data for the Last Glacial Maximum (LGM, between 19,000 and 23,000 years before present). The “adjoint model” (derivative code) was generated by an “adjoint compiler.” We optimized parameters controlling the thermal diffusion and the sensitivity of the outgoing longwave radiation to changes in the zonal-mean surface temperature and the atmospheric CO₂ concentration. As a result, we estimated that an equilibrium climate sensitivity between 2.2 °C and 2.5 °C was consistent with the reconstructed glacial cooling, and we were able to infer structural deficits of the simple model where the fit to current observations and paleo data was not successful.

Introduction

Milankovitch is mainly renowned for his computation of the incoming solar radiation (insolation) at the top of the atmosphere over the past 600,000 years for different latitudes and seasons (Milankovitch 1920, 1930, 1941). Yet he also formulated one of the early “climate models”: He used the energy balance as implied by the planetary albedo and the outgoing longwave radiation according to the Stefan–Boltzmann law to infer the solar temperatures on the Earth’s surface if it were covered uniformly by land and the atmosphere

and ocean were at rest (Milankovitch 1920, p. 200); he compared these solar temperatures to then-current observations by Hann (1915). Furthermore, he computed the fluctuations in the extent of the polar ice caps in response to the fluctuations in insolation, even taking into account the feedback of the increasing albedo and surface height of a growing ice cap on temperature (Milankovitch 1941). Finally, he related the predictions of his climate model to geological data published by Penck and Brückner (1909). Thus, he could associate four minima of his famous radiation curves, expressed in terms of equivalent latitudes, with the European ice ages as they were known at the time (for more detailed accounts of Milankovitch’s achievements, see Berger 1988; Petrović 2002; Loutre 2003; Grubić 2006).

Formulating a climate model, then solving it either analytically or numerically, calibrating it against

A. Paul (✉)
MARUM – Center for Marine Environmental Sciences and
Department of Geosciences, University of Bremen, PO Box
33 04 40, D-28334 Bremen, Germany
e-mail: apaul@marum.de

current observations, applying it to past conditions, and relating its predictions to geological data—this is the traditional or “forward” method of paleoclimate modeling that Milankovitch pioneered in the first half of the last century. So-called “state-of-the-art” climate models are much more complex than their early predecessors and require long computing times, so that often only a few simulations are carried out. If at all feasible, models are “tuned” by adjusting individual parameters (or a parameterization) and repeating simulations in an *ad hoc* iteration (cf. Fig. 1a).

Today’s comprehensive climate models and wealth of available observations, however, warrant to overcome such a crude tuning procedure and use the data to systematically fit models to data—that is, to (1) optimize model parameter values by “parameter estimation” or “calibration,” (2) test the model for consistency with independent datasets, if available, and (3) use the calibrated model for predictions.

The proper calibration of a climate model, as opposed to simply tuning it, implies the formulation of a statistical model that links evaluations of the climate model, the model parameters, and observations on climate (Rougier 2008). The focus is either on time evolution or the steady state of the climate system. While the “Bayesian” approach deals with probability density functions, the “maximum likelihood” approach aims for a point estimate of the model parameters.

Typically, the departure of the model from the data (the model-data misfit) is measured by an objective or cost function. In formulating this function, the uncertainties of both the model and the data can be considered. The cost function is usually a quadratic function of model-data differences weighted by their prior error estimates, but it can also include constraints that represent other prior knowledge of the climate.

An explicit cost function may be combined with the forward method to quantify the purpose of the numerical model (Wunsch 1996). Then the parameter estimation may be carried out simultaneously with a “state estimation” and yield an estimate of, e.g., the state of the ocean or atmosphere. One of the first examples of combined parameter and state estimation in the context of sparse paleoclimate data is given by Paul and Schäfer-Neth (2005).

It is desirable to automate the manual search for the optimum fit by using an algorithmic process. Available methods include statistical methods (e.g., Monte Carlo and Greene’s function methods, ensemble Kalman and particle filter methods—Fig. 1b) as well as variational techniques and sequential filtering (e.g., the adjoint method or a Kalman filter/smoothen—Fig. 2). The variational methods and the Kalman filter and smoother are especially suited to take into account the uncertainties associated with both model and data (e.g., Kasibhatla et al. 2000).

In the following, we use the adjoint method (e.g., Le Dimet and Talagrand 1986; Errico 1997) to estimate the model parameters based on observations of the steady-state seasonal cycle. For a more probabilistic (Bayesian) approach, we refer to Edwards et al. (2007), Annan and Hargreaves (2007), and Holden et al. (2010).

The adjoint method requires an adjoint or dual model of a given forward model. Often this adjoint model is obtained through the application of an “adjoint compiler,” a software tool that takes the computer source code of the forward model as input, applies the rules of automatic differentiation, and yields the source code of the “adjoint model” (derivative code) as output (Giering 2000; Rayner et al. 2000; Griewank and Walther 2008).

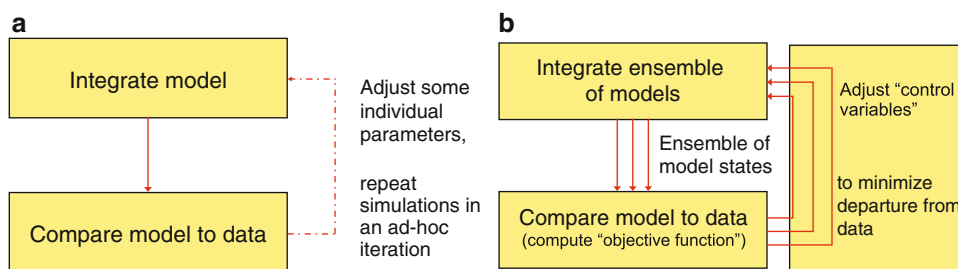


Fig. 1 Schematic diagrams for (a) the traditional forward method and (b) statistical inverse methods

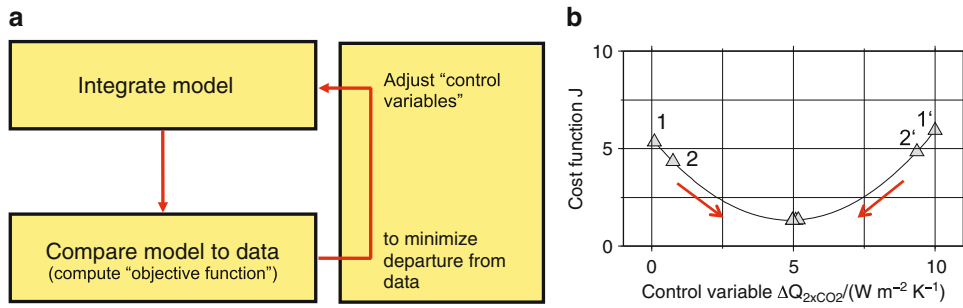


Fig. 2 Schematic diagrams for (a) the assimilation of paleoclimate data by the adjoint method and (b) the approach of the minimum of the cost function in Experiment LGM1

The minimum of the cost function is searched for by varying control variables such as initial conditions, boundary conditions, or internal parameters. The adjoint model computes the gradient of the cost function with respect to these control variables and provides the information required by a gradient descent algorithm. The gradients themselves contain valuable information on the sensitivity of the system to perturbations in the control variables.

We present a simple “textbook example” to illustrate the calibration of a climate model with the adjoint method (i.e., computing exact derivatives using automatic differentiation) in a paleoclimate context. To this end, we implemented a classical one-dimensional energy balance–climate model with seasonal insolation forcing. The corresponding adjoint model was generated by the “Tangent linear and Adjoint Model Compiler” (TAMC, <http://autodiff.com/tamc/>). We defined a seasonal cost function that allowed us to use paleo-sea surface temperature data to constrain the model.¹

Material and Methods

Energy Balance–Climate Model

Our energy balance model is a conceptual climate model based on the difference between absorbed solar radiation Q_{abs} and outgoing longwave radiation F_{∞}^{\uparrow} at the top of the atmosphere (TOA) on the one hand and the divergence of the horizontal heat

transport ΔF_{ao} on the other hand (see Hartmann 1994, p. 237). In its one-dimensional version, the only coordinate variables are latitude ϕ and time t . Climate is expressed in terms of just one model variable, the zonally averaged surface temperature T_s :

$$\bar{C}_{\text{ao}} \frac{\partial}{\partial t} T_s(x, t) = R_{\text{TOA}}(x, t, T_s) - \Delta F_{\text{ao}}(x, t, T_s), \quad (1)$$

where $x = \sin \phi$, $\bar{C}_{\text{ao}} = c_w \rho_w H_o$ is the effective heat capacity of the atmosphere–ocean system (with c_w and ρ_w being the specific heat and density of water and H_o the ocean mixed-layer depth), and R_{TOA} the net incoming radiation at the top of the atmosphere, which is expressed as the difference between absorbed solar radiation $Q_{\text{abs}}(x, t, T_s)$ and outgoing longwave radiation $F_{\infty}^{\uparrow}(x, T_s)$:

$$R_{\text{TOA}}(x, t, T_s) = Q_{\text{abs}}(x, t, T_s) - F_{\infty}^{\uparrow}(x, T_s). \quad (2)$$

The absorbed solar radiation is the product of one-fourth of the solar constant, $S_0/4$, a function that describes the distribution of insolation with latitude and time of year, $s(x, t)$ —cf. Berger (1978), and the absorptivity for solar radiation, $a_p(x, T_s)$:

$$Q_{\text{abs}}(x, t, T_s) = \frac{S_0}{4} s(x, t) a_p(x, T_s). \quad (3)$$

The absorptivity is related to the planetary albedo $\alpha_p(x, T_s)$ through the relationship $a_p(x, T_s) = 1 - \alpha_p(x, T_s)$. In our case, the absorptivity is given by:

$$a_p(x, x_i) = \begin{cases} a_0 + a_2 P_2(x), & T_s > -10^\circ\text{C}, |x| < |x_{\text{ice}}|, \\ b_0, & T_s < -10^\circ\text{C}, |x| > |x_{\text{ice}}|, \end{cases} \quad (4)$$

¹The code of the one-dimensional energy balance–climate model and its adjoint Ebm1D is available upon request from apaul@marum.de.

where a_0 , a_2 , and b_0 are constant coefficients, P_2 refers to the Legendre polynomial of second order in x ,

$$P_2(x) = \frac{1}{2}(3x^2 - 1), \quad (5)$$

and x_{ice} is the position of the point where the temperature equals -10°C . This point is called the iceline.

The outgoing longwave radiation is parameterized as a linear function of the surface temperature and the logarithm of the ratio of the actual value of the atmospheric CO_2 concentration $[\text{CO}_2]$ to a reference value $[\text{CO}_2]_{\text{ref}}$:

$$F_{\infty}^{\uparrow}(x, T_s) = A + BT_s - \Delta Q_{2 \times \text{CO}_2} \log([\text{CO}_2]/[\text{CO}_2]_{\text{ref}}) / \log 2, \quad (6)$$

where A , B , and $\Delta Q_{2 \times \text{CO}_2}$ are constant coefficients; in particular, B describes the efficiency of longwave radiative cooling and $\Delta Q_{2 \times \text{CO}_2}$ is the radiative forcing equivalent to a doubling of the atmospheric CO_2 concentration (cf. Myhre et al. 1998). The outgoing longwave radiation increases only linearly with temperature, rather than as the fourth power of temperature as indicated by the Stefan–Boltzmann law. This is a simple way to account for the effect of the water vapor feedback when the relative humidity is assumed to be constant (Hartmann 1994, p. 233).

Meridional (north–south) heat transport is treated as a diffusive process, driven by latitudinal temperature gradients, an approach considered to be valid at horizontal scales of about 1,500 km and larger and timescales of 6 months and longer (Lorenz 1979):

$$\Delta F_{\text{ao}} = \frac{1}{a} \frac{\partial}{\partial x} \left(\sqrt{1-x^2} F_{\text{ao}} \right) \quad (7)$$

and

$$F_{\text{ao}} = -\bar{C}_{\text{ao}} K_{\text{ao}}(x) \frac{\sqrt{1-x^2}}{a} \frac{\partial T_s}{\partial x}, \quad (8)$$

where a is the mean radius of Earth and the thermal diffusion coefficient K_{ao} is given by:

$$K_{\text{ao}}(x) = K_0(1 + K_2 x^2 + K_4 x^4), \quad (9)$$

where K_0 , K_2 , and K_4 are constant coefficients.

The values of all model parameters are listed in Table 1. The model equations are discretized using centered differences in space and forward differences in time. The meridional grid is staggered. The thermal diffusion coefficient is defined at U grid points that are halfway between the temperature or T grid points.

Data

The target for our present-day simulation (Experiment PD1) is the surface air temperature from the NCEP/NCAR reanalysis data [Kalnay et al. (1996)—see Fig. 3].

As an example target for our paleo-simulations (Experiments LGM1 and LGM2), we chose the sea-surface temperature anomaly between the Last Glacial Maximum (LGM—19,000–23,000 years before present) and present day as reconstructed by the GLAMAP 2000 project (Sarnthein et al. 2003). In the context of a one-dimensional energy balance model, we prefer it over the more recent MARGO reconstruction (Kucera et al. 2005; MARGO Project Members 2009), because the objective mapping by Schäfer-Neth and Paul (2004) of the sparse proxy data at the ocean sediment core locations allows for consistent zonal averaging. The annual mean and February and August monthly means of the reconstructed SST anomaly are shown—along with the model results—in Figs. 5 and 6.

Cost Function

The cost function (also called the objective or mismatch function) used for our present-day experiments is defined by:

$$J = \sum \frac{(T_s^{\text{Feb,mod}} - T_s^{\text{Feb,obs}})^2}{\sigma_{T_s}^2} + \sum \frac{(T_s^{\text{Aug,mod}} - T_s^{\text{Aug,obs}})^2}{\sigma_{T_s}^2}. \quad (10)$$

Here “obs” and “mod” refer to observed and modeled, and $\sigma_{T_s} = 1^\circ\text{C}$ in the denominator refers to the error in surface temperature. The sums extend over all latitude zones of the one-dimensional energy balance–climate model that contain data and are weighted by the respective surface area.

Table 1 First-guess values of model parameters. In case of the selected control variables, they were subject to change during the optimization process. For the value of the solar constant, we followed the protocol of the Paleoclimate Modeling Intercomparison Project (PMIP) 1, see Joussaume and Taylor (1995)

Symbol	Value	Units	Description	References
a	6.371×10^6	m	Mean radius of Earth	
ρ_w	1,000	kg m^{-3}	Density of pure water at 0°C	
c_w	4,218	$\text{J kg}^{-1} \text{K}^{-1}$	Specific heat of liquid water at 0°C	
H_o	70	m	Ocean mixed-layer depth	Hartmann (1994, p. 84)
S_0	1,365	W m^{-2}	Present-day solar constant	Joussaume and Taylor (1995)
<i>Linearized longwave radiation</i>				
A	205.0	W m^{-2}	Constant term	Hartmann and Short (1979, set 2)
B	2.23	$\text{W m}^{-2} \text{K}^{-1}$	Efficiency of longwave radiative cooling	Hartmann and Short (1979, set 2)
$\Delta Q_{2 \times \text{CO}_2}$	4.0	W m^{-2}	$2 \times \text{CO}_2$ radiative forcing	Hartmann (1994, p. 232)
$[\text{CO}_2]_{\text{ref}}$	345	ppmv	Reference atmospheric CO_2 concentration	Joussaume and Taylor (1995)
$[\text{CO}_2]$	345 or 200	ppmv	Actual atmospheric CO_2 concentration	Joussaume and Taylor (1995)
<i>Albedo coefficients</i>				
b_0	0.38		Ice-covered absorptivity	Hartmann and Short (1979, set 2)
a_0	0.697		Coefficient in ice-free absorptivity	Hartmann and Short (1979, set 2)
a_2	-0.175		Coefficient in ice-free absorptivity	Hartmann and Short (1979, set 2)
T_{ice}	-10	°C	Critical temperature for ice formation	Hartmann (1994, p. 238)
<i>Diffusion coefficients</i>				
K_0	1.5×10^5	$\text{m}^2 \text{s}^{-1}$	Constant factor	
K_2	-1.33		Second-order coefficient	North et al. (1983)
K_4	0.67		Fourth-order coefficient	North et al. (1983)

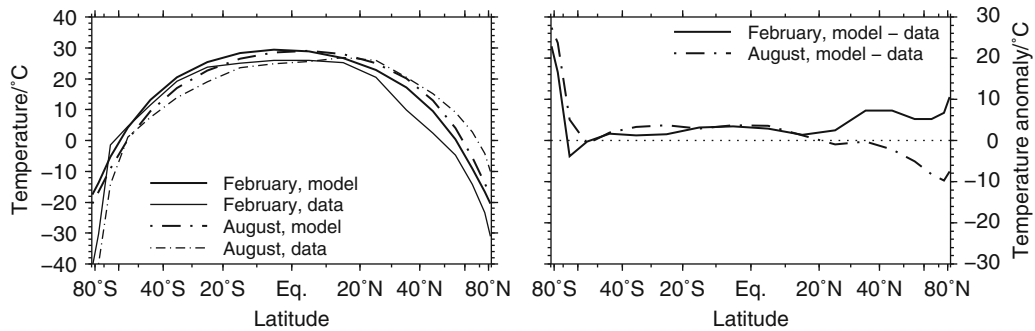


Fig. 3 First guess of present-day climate in Experiment PD0. *Left*: Simulated and observed surface air temperature for February and August. *Right*: Differences between model and data for February and August. Note that in all plots the ordinate is scaled by the sine of latitude to reflect the relative surface area at each latitude

Correspondingly, the cost function used for our LGM experiments is defined by:

$$J = \sum \frac{(\Delta T_s^{\text{Feb,mod}} - \Delta T_s^{\text{Feb,rec}})^2}{\sigma_{\Delta T_s}^2} + \sum \frac{(\Delta T_s^{\text{Aug,mod}} - \Delta T_s^{\text{Aug,rec}})^2}{\sigma_{\Delta T_s}^2}, \quad (11)$$

where “rec” refers to reconstructed and $\sigma_{\Delta T_s} = 1^\circ\text{C}$.

In computing the cost function, we use the angular definition of seasons proposed by Joussaume and Braconnot (1997) (see Table 2).

Optimization Algorithm

For minimization of the cost function, we used a variable memory quasi-Newton algorithm as implemented in M1QN3 by Gilbert and Lemaréchal (1989).

Table 2 Angular definition of seasons. The vernal equinox is taken as a reference. Correspondingly, perihelion occurs at day number 2.85 (1950 AD orbit) and 15.51 (21,000 years before present - or 21 ka BP - orbit), respectively (Berger 1978)

Date	True longitude	Day number	
		1950 AD orbit	21 ka BP orbit
Vernal equinox, 21 March, 12:00	0°	80.0	80.0
1 February, 0:00	-48.78°	31.50	31.91
28 February, 24:00	-20.48°	59.50	59.68
1 August, 0:00	127.97°	212.50	212.27
31 August, 24:00	157.80°	243.50	243.52

Table 3 Experimental setup. The number control variables is denoted by n . The values of the control variables after optimization are given in italics. The number of iterations is given by $N_{\text{iterations}}$, while the total number of simulations performed by the optimization algorithm is referred to as $N_{\text{simulations}}$

Parameter	Units	Experiment						
		PD0	PD1	LGM1	LGM2	2×CO2_1	2×CO2_2	2×CO2_3
n		–	5	1	4	–	–	–
[CO ₂]	ppmv	345	345	200	200	690	690	690
H_o	m	70	27.4	27.4	27.4	27.4	27.4	27.4
A	W m ⁻²	205.0	209.6	209.6	209.6	209.6	209.6	209.6
B	W m ⁻² K ⁻¹	2.23	2.23	2.23	2.23	2.23	2.23	2.23
K_0	10 ⁵ m ² s ⁻¹	1.5	3.8	3.8	3.3	3.8	3.8	3.8
K_2		-1.33	-0.64	-0.64	-0.53	-0.64	-0.64	-0.64
K_4		0.67	-0.32	-0.32	-0.36	-0.32	-0.32	-0.32
$\Delta Q_{2\times\text{CO}_2}$	W m ⁻²	–	–	4.97	4.39	4.0	4.97	4.39
J		28.42	13.27	1.34	0.76	–	–	–
$N_{\text{iterations}}$		–	190	3	39	–	–	–
$N_{\text{simulations}}$		–	236	4	47	–	–	–

This algorithm computes a local approximation of the inverse Hessian matrix based on the gradient of the cost function and generally converges faster than conventional conjugate gradient methods (see also <http://www-rocq.inria.fr/~gilbert/modulopt/optimization-routines/m1qn3/m1qn3.html>).

As a stopping criterion, we required a relative precision on the norm of the gradient of the cost function of 10^{-4} .

Experimental Setup

The meridional resolution was set to 10° . All experiments were integrated for 100 years using a time step of 1 day. The last 10 years of each experiment were used for calculating the cost function and analyzing the model results.

Table 3 lists the seven base experiments that were carried out with the one-dimensional energy balance–climate model. In the case of Experiment PD0,

we used the first-guess values for all model parameters without any optimization, while in Experiment PD1 (the “control simulation” for the present-day climate), we used the parameters H_o for the ocean mixed-layer depth, K_0 , K_2 , and K_4 of the heat diffusion coefficient, and A of the outgoing longwave radiation as control variables that were adjusted using the adjoint method.

In Experiment LGM1, the optimized parameter values of Experiment PD1 were held fixed. The only control variable was the parameter $\Delta Q_{2\times\text{CO}_2}$ affecting the radiative forcing associated with the change of the atmospheric CO₂ concentration from 345 to 200 ppmv. In Experiment LGM2, we added the parameters K_0 , K_2 , and K_4 of the heat diffusion coefficient to the control variables.

For Experiments LGM1 and LGM2, we followed the PMIP1 protocol (see <http://pmip.lsce.ipsl.fr/newsletters/newsletter02.html>) and used 200 ppmv as atmospheric CO₂ concentration.

In Experiments 2×CO2_1, 2×CO2_2, and 2×CO2_3, we studied the effect of doubling the

atmospheric CO₂ concentration from 345 to 690 ppmv on the equilibrium conditions in our one-dimensional energy balance–climate model. Again, we used the optimized parameter values of Experiment PD1. The parameter $\Delta Q_{2\times\text{CO}_2}$ was set to the first-guess value, the value obtained from Experiment LGM1 and the value obtained from Experiment LGM2, respectively (Table 3).

Table 4 lists eight additional experiments that were designed to study the sensitivity of the optimal solution for Experiment LGM2 to the initial values of the control variables. In Experiments LGM2_1 and LGM2_2, the initial value of $\Delta Q_{2\times\text{CO}_2}$ was varied. In Experiments LGM2_3 and LGM2_4, the initial value of K_0 was varied. Experiments LGM2_5 to LGM2_8 allowed for combinations of changes in $\Delta Q_{2\times\text{CO}_2}$ and K_0 .

Results

Table 5 summarizes the results of the four experiments in terms of the planetary albedo, the global mean temperature, and the latitude of the ice boundary. There is almost no change in the annually and globally averaged planetary albedo $\bar{\alpha}_p^{\text{ann}}$ between the different experiments. With all model parameters set to their first-guess values in Experiment PD0, the global mean temperature \bar{T}_s is above 16 °C during all seasons. Optimizing the model parameters in Experiment PD1

led to the reduction of the cost function (10) by one-half and required 190 iterations (Table 3). The ocean mixed-layer depth H_o was reduced to 27.4 m. At the same time, \bar{T}_s^{ann} decreased by 2.4 °C and the icelines $\bar{\phi}_{\text{ice}}^{\text{S,N,ann}}$ moved equatorward by 2°–3° in latitude. Applying the adjoint method to the LGM climate conditions in Experiment LGM1 led to a global mean glacial cooling of 2 °C and a growth of the polar ice caps by about 2 °C in latitude. Adding the parameters in the heat diffusion coefficient to the control variables in Experiment LGM2 hardly affected the global mean temperature, but caused the icelines to shift further equatorward by nearly 1° in latitude. The radiative forcing parameter $\Delta Q_{2\times\text{CO}_2}$ [see (6)] was increased by 24% in Experiment LGM1 and 10% in Experiment LGM2, compared to the first-guess value of 4 W m^{−2} (Table 1). We speculate that this increase partly compensated for other positive feedbacks that are missing from the model, such as the full water-vapor feedback.

Figure 3 shows that in Experiment PD0, the largest differences in the simulated and the observed temperature occurred near the South Pole and in the high northern latitudes. In the south, the model temperatures were generally higher than the observations. In the north, by contrast, the model climate was warmer than observed during winter and colder during summer. Figure 4 indicates for Experiment PD1 a generally closer fit to the observations than for Experiment PD0, except near the poles.

Table 4 Additional experiments on the sensitivity of the optimal solution. *Top*: Initial values of the control variables. Values of the control variables that are different from their first-guess values are given in italics. Experiment LGM2 is the original simulation using the first-guess values for all $n = 4$ control variables. *Bottom*: Values of the control variables and the cost function after optimization

Parameter	Units	Experiment								
		LGM2	LGM2_1	LGM2_2	LGM2_3	LGM2_4	LGM2_5	LGM2_6	LGM2_7	LGM2_8
<i>Initial values of control variables</i>										
K_0	$10^5 \text{ m}^2 \text{ s}^{-1}$	3.7646	3.7646	3.7646	<i>0.3900</i>	<i>8.9000</i>	<i>1.4000</i>	<i>8.9000</i>	<i>0.8400</i>	<i>8.9000</i>
K_2		−0.6408	−0.6408	−0.6408	−0.6408	−0.6408	−0.6408	−0.6408	−0.6408	−0.6408
K_4		−0.3239	−0.3239	−0.3239	−0.3239	−0.3239	−0.3239	−0.3239	−0.3239	−0.3239
$\Delta Q_{2\times\text{CO}_2}$	W m^{-2}	4.0000	<i>1.1000</i>	<i>4.7000</i>	4.0000	4.0000	<i>1.1000</i>	<i>1.1000</i>	<i>4.7000</i>	<i>4.7000</i>
<i>Optimized values of control variables</i>										
K_0	$10^5 \text{ m}^2 \text{ s}^{-1}$	3.2894	3.2933	3.2918	3.3543	3.333	3.3210	3.2840	3.2037	3.3358
K_2		−0.5347	−0.5386	−0.5371	−0.5971	−0.5788	−0.5672	−0.5287	−0.4446	−0.5820
K_4		−0.3578	−0.3536	−0.3552	−0.2913	−0.3102	−0.3225	−0.3643	−0.4548	−0.3066
$\Delta Q_{2\times\text{CO}_2}$	W m^{-2}	4.3858	4.3839	4.3844	4.3483	4.3663	4.3719	4.391	4.4275	4.3626
J		0.7620	0.7620	0.7620	0.7636	0.7627	0.7624	0.7621	0.7655	0.7629

Table 5 Selected experimental results: Annual and global average of the planetary albedo $\bar{\alpha}_p^{\text{ann}}$; annual, February, and August averages of the global mean temperature \bar{T}_s^{ann} , \bar{T}_s^{Feb} , and \bar{T}_s^{Aug} ; and annual-mean latitude of the ice boundary in the Southern and Northern Hemispheres $\phi_{\text{ice}}^{\text{S-ann}}$ and $\phi_{\text{ice}}^{\text{N-ann}}$

Variable	Units	Experiment						
		PD0	PD1	LGM1	LGM2	2×CO2_1	2×CO2_2	2×CO2_3
$\bar{\alpha}_p^{\text{ann}}$		0.31	0.32	0.32	0.32	0.32	0.32	0.32
\bar{T}_s^{ann}	°C	16.21	13.81	11.81	11.88	15.84	16.33	16.04
\bar{T}_s^{Feb}	°C	16.29	14.03	12.00	12.07	16.06	16.55	16.26
\bar{T}_s^{Aug}	°C	16.10	13.51	11.55	11.62	15.55	16.03	15.74
$\phi_{\text{ice}}^{\text{S-ann}}$		−68.69°	−65.42°	−63.31°	−62.56°	−67.37°	−67.83°	−67.56°
$\phi_{\text{ice}}^{\text{N-ann}}$		67.84°	65.49°	63.39°	62.64°	67.44°	67.90°	67.62°

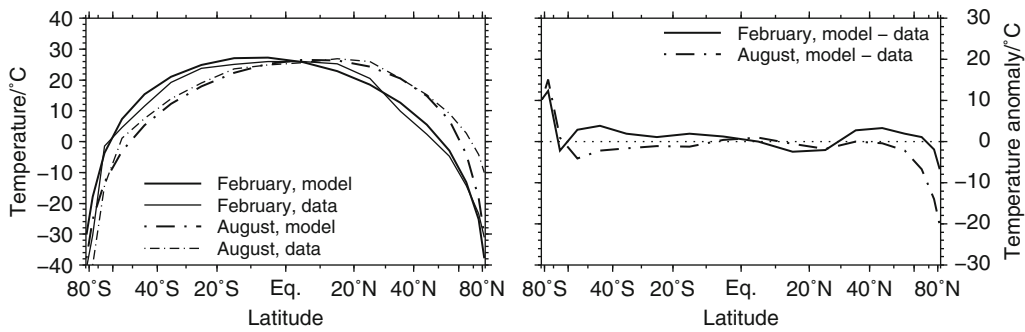


Fig. 4 Fit to present-day climate in Experiment PD1 (control variables: diffusion and outgoing longwave radiation parameters). *Left*: Simulated and observed surface air temperature for February and August. *Right*: Differences between model and data for February and August

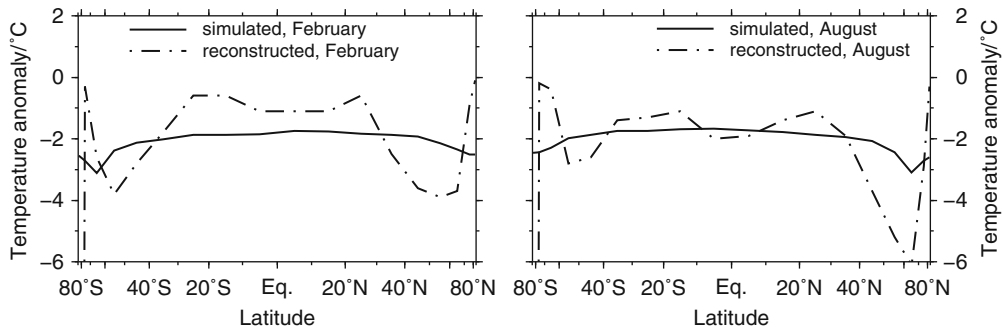


Fig. 5 Fit to LGM anomaly in Experiment LGM1 (control variable: CO₂ sensitivity). Simulated and reconstructed SST anomaly for (*left*) February and (*right*) August

With $\Delta Q_{2\times\text{CO}_2}$ as the only control variable in Experiment LGM1, the glacial cooling as a function of latitude was nearly flat, with only a small polar amplification, as can be seen from Fig. 5. Allowing for changes in the thermal diffusion coefficient in Experiment LGM2, the polar amplification became more prominent (Figs. 6 and 7).

Comparing Experiments PD1 (Fig. 4) and LGM2 (Fig. 6), the meridional heat transport generally decreased during Northern Hemisphere winter (February) and increased during Northern Hemisphere summer (August), except for the high latitudes (Fig. 8). In the high latitudes, the meridional heat transport decreased in the south and increased in the north during the entire year.

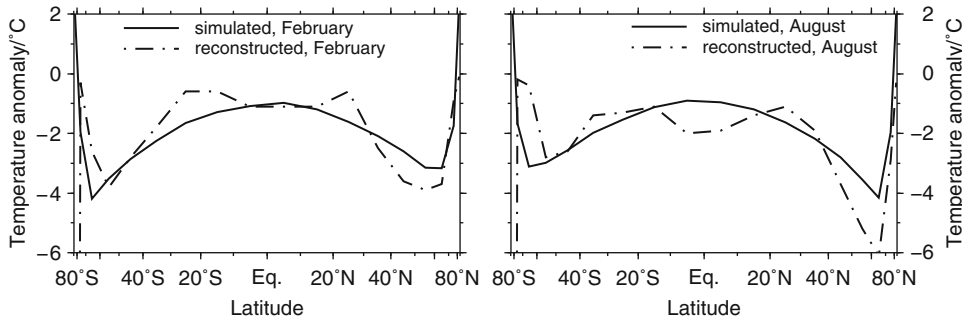


Fig. 6 Fit to LGM anomaly in Experiment LGM2 (control variables: diffusion parameters and CO_2 sensitivity). Simulated and reconstructed SST anomaly for (*left*) February and (*right*) August

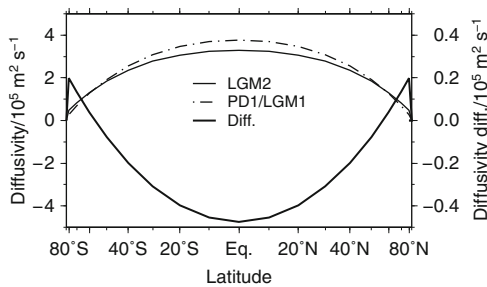


Fig. 7 Diffusivity in Experiments PD1/LGM1 and LGM2

With respect to Experiment PD1, Experiments $2\times\text{CO}_2_1$, $2\times\text{CO}_2_2$, and $2\times\text{CO}_2_3$ led to an increase of the global mean temperature by 2.0 °C, 2.5 °C, and 2.2 °C, respectively (Table 5). At the same time, the icelines in both hemisphere moved poleward by 1.95°, 2.4°, and 2.13° in latitude, respectively.

Regarding the sensitivity of the optimal solution for Experiment LGM2 to the initial values of the control variables, the optimization converged for a wide range of initial values of $\Delta Q_{2\times\text{CO}_2}$ to the same minimum of the cost function with similar values of the optimized control variables (cf. Experiments LGM2_1 and LGM2_2, Table 4). It also converged outside of this range, but not to the required relative precision on the norm of the gradient of the cost function of 10^{-4} . Similarly, the optimization converged for a wide range of initial values of K_0 to nearly the same minimum of the cost function (cf. Experiments LGM2_3 and LGM2_4). Outside of this range, however, it did not converge. Finally, the results of Experiments LGM2_5 to LGM2_8 indicate the common ranges of these two control variables for which convergence was still possible.

Discussion

We illustrated how the so-called adjoint method could be used to adjust the parameters of a simple climate model so that the model predictions were consistent with either modern surface temperature observations (Fig. 4) or reconstructed LGM sea-surface temperature anomalies (Fig. 5). The model-data fit improved further (Fig. 6) by additionally adjusting the thermal diffusion coefficient (Fig. 7), although at the cost of implausibly large positive temperature anomalies very near the poles.

The remaining model discrepancy points to a structural error of our simple climate model. As opposed to a parametric error, this error cannot be removed by adjusting the parameter values; it is rather an error in the functional form of the model equations or their numerical implementation (that is, in their discretization in space and time).

Correspondingly, even after optimizing the parameter values, our energy balance–climate model does not simulate a realistic present-day climate. For example, the simulated latitude of the ice boundary in the Northern Hemisphere in Experiments PD0 ($\approx 67.8^\circ\text{N}$) and PD1 ($\approx 66.5^\circ\text{N}$) is considerably lower than the approximate current position of the ice edge ($\approx 71.8^\circ\text{N}$, e.g., Jentsch 1987). This is likely due to an overly simplistic representation of the ice-albedo feedback. In this respect, the value of the critical temperature for the formation of ice $T_{\text{ice}} = -10^\circ\text{C}$ is derived from the observed annual-mean temperature at which surface ice cover persists throughout the year (Hartmann 1994, p. 238). A higher value (around 0°C) may be more appropriate

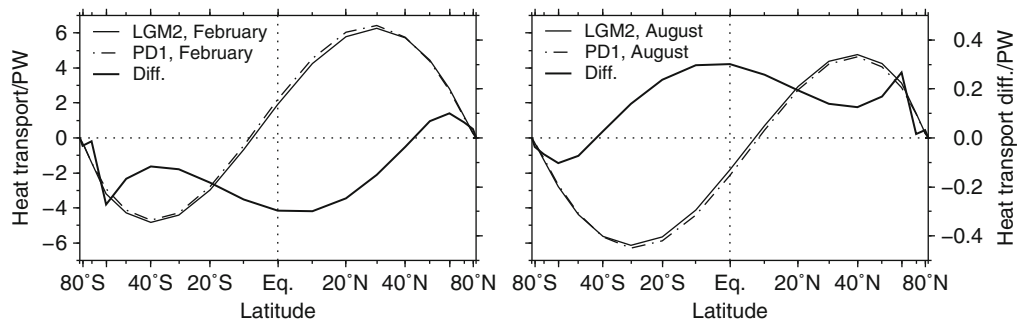


Fig. 8 Meridional heat transport in Experiments PD1 and LGM2 for (left) February and (right) August

to parameterize the seasonal formation of snow and ice but by itself lead to an even lower latitude of the ice boundary.

The optimized value of the ocean mixed-layer depth of 27.4 m is smaller than the value of 50–70 m that is often taken as the depth of the top layer of the ocean that interacts with the atmosphere on a time-scale of a year (Hartmann 1994, p. 84), probably because we ignored the land cover with a much smaller thermal capacity. A slightly more realistic climate model would include a variable land fraction as a function of latitude.

Other contributions to the structural error include the lack of: zonal (east-west) and vertical resolution, a diurnal cycle, clouds, a realistic representation of the greenhouse effect, light scattering within the atmosphere and a separate treatment of the atmosphere, ocean, and land surface components of the climate system and their interactions.

Furthermore, our simulations of the LGM climate were possibly biased toward a low value of the radiative forcing parameter $\Delta Q_{2 \times \text{CO}_2}$, because the GLAMAP 2000 project (Sarnthein et al. 2003) may slightly underestimate the glacial cooling as compared to more recent reconstructions (e.g., MARGO Project Members 2009). Consequently, the optimal values of $\Delta Q_{2 \times \text{CO}_2}$ (5.0 W m^{-2} in Experiment LGM1 and 4.4 W m^{-2} in Experiment LGM2, Table 3) correspond to an equilibrium climate sensitivity (an equilibrium change in global mean temperature for a sustained doubling of the atmospheric CO_2 concentration) between 2.2°C and 2.5°C (Table 5), which is toward the lower end of the range between 1.2°C and 4.3°C estimated from an ensemble of simulations of the LGM climate (Schneider von Deimling et al. 2006) and the range between 2.0°C

and 4.5°C in the current IPCC assessment (Meehl et al. 2007).

The question of how to take into account the structural error (possibly by expert judgment or multi-model ensembles, cf. Rougier 2008) is crucial to the problem of model calibration. In a maximum-likelihood approach as taken by the adjoint method, and assuming a Gaussian probability density distribution, the covariance matrix of the model discrepancy and the covariance matrix of the observational error (σ_{T_s} in (10) and (11)) would both determine the cost and hence the results. However, the two covariance matrices could be very different from each other. What is more, it may even be questioned that the structural error can be properly described by a Gaussian probability density distribution.

We note that our definitions of the present-day and LGM cost functions in (10) and (11) do not contain a term related to the structural error—nor do they include a so-called “background term,” which in our case would penalize deviations between the optimal and the first-guess values of the control variables. Such a term is necessary whenever the system of model equations is underdetermined (i.e., if the information contained in the observations is insufficient to guarantee a unique optimal solution). In our case, however, we used observations in every latitude zone of the model; thus the system was likely to be “well observed.” Indeed, by performing additional experiments using different initial values for the optimization, we confirmed that our optimal solution for the LGM was unique for a broad range of the control variables K_0 and $\Delta Q_{2 \times \text{CO}_2}$, because the optimized values of the control variables were not significantly different from each other (Table 4). Significant differences would have indicated a sensitive dependence on the first-guess

values of the control variables and thus a nonuniqueness of the optimized solution.

Since a sensitive dependence on initial conditions is a characteristic of a nonlinear system, failure of convergence or convergence to a different local minimum of the cost function is to be expected outside of a given range of the optimal values of the control variables. This ambiguity may be removed by including the background term into the cost function, i.e., by adding prior knowledge on the likely values of the control variables (see, e.g., Losch and Wunsch 2003).

We point out that in our application of the adjoint method, the control variables only consisted of internal parameters in the underlying equations of the energy balance–climate model. An application that also includes initial conditions or boundary conditions is referred to as “data assimilation” rather than “parameter estimation” (e.g., Giering 2000).

For many purposes, estimates of the errors of the optimal control variables are highly desirable. The adjoint method allows to estimate these errors, because for a Gaussian error distribution and in a linear approximation, the error covariance matrix of the control variables is the inverse Hessian matrix of the cost function J at its minimum (Thacker 1989; Giering 2000). Indeed, the adjoint compiler TAMC provides a means for computing the uncertainties of a reasonably low number of control variables.

In comparison to the adjoint method, the Bayesian approach is designed from the outset to produce an entire multivariate distribution of parameter values. It may help to select a suitable model by revealing two common symptoms of the structural error (Larson et al. 2008): underfitting (that is, when the structure of a model is not rich enough to capture the full variability in a dataset) and overfitting (when too many parameters are used to fit a limited dataset).

For example, it may happen that in the case of our energy balance–climate model, no single set of parameter values (which are distinct within error bars) yields a good fit for all cases (pre-industrial and LGM), even though optimal parameter values can be obtained for each case separately. This may indicate underfitting in the sense that thermal diffusion is too simple to capture the full glacial–interglacial climate variability.

Regarding previous examples of state estimation in paleoclimatology, we point to the work of LeGrand and Wunsch (1995) and Winguth et al. (2000),

who attempted to infer the ocean circulation during the LGM from reconstructed paleonutrient distributions.

Conclusions

Systematically fitting a “textbook example”-type climate model to paleoclimate data gave useful results: In a one-dimensional energy balance model, the glacial cooling reconstructed by the GLAMAP 2000 project (Samthein et al. 2003) was consistent with an equilibrium climate sensitivity for a doubling of the atmospheric CO₂ concentration between 2.2 °C and 2.5 °C. Besides calibrating our simple model to current observations and paleo data, we were able to infer contributions to its structural error where the fit was not successful.

While the adjoint method proved to be very efficient in optimizing the model parameter values, a Bayesian approach may in addition provide a natural framework to assess their uncertainty and help to avoid underfitting or overfitting the data.

These findings open up a wide field of applications to more complex climate models with many more parameters that can serve as control variables. Estimating model parameters and states and identifying model problems for further model improvement are general goals of paleoclimate research.

We note that in spite of the simplicity of our model, we employed automatic differentiation (through the adjoint compiler TAMC). With complex models one will hardly succeed without such tools, and their development will be as important for this field as the evolution of numerical models.

Acknowledgments AP expresses his sincere gratitude to the organizers of the “Milutin Milankovitch 130th Anniversary Symposium” (Belgrade, 22–25 September 2009), who made this conference a very memorable and inspiring experience. We acknowledge the helpful discussions with Takasumi Kurahashi-Nakamura, as well as the instructive comments by Michel Crucifix and an anonymous reviewer. All graphs were drawn with the Generic Mapping Tools (Wessel and Smith 1998). This research was funded by the DFG-Research Center/Center of Excellence MARUM—“The Ocean in the Earth System.”

References

- Annan JD, Hargreaves JC (2007) Efficient estimation and ensemble generation in climate modelling. *Philos Trans R Soc A* 365(1857):2077–2088

- Berger AL (1978) Long term variations of daily insolation and Quaternary climatic changes. *J Atmos Sci* 35 (12):2362–2367
- Berger A (1988) Milankovitch theory and climate. *Rev Geophys* 26:624–657
- Edwards TL, Crucifix M, Harrison SP (2007) Using the past to constrain the future: how the palaeorecord can improve estimates of global warming. *Prog Phys Geogr* 31:481–500. doi:10.1177/0309133307083295
- Errico RM (1997) What is an adjoint model? *Bull Am Meteorol Soc* 78(11):2577–2591
- Giering R (2000) Tangent linear and adjoint biogeochemical models. In: Kasibhatla P, Heimann M, Rayner P, Mahowald N, Prinn RG, Hartley DE (eds) *Inverse Methods in Global Biogeochemical Cycles*, vol 114, Geophysical Monograph Series. AGU, Washington, DC, pp 33–48
- Gilbert JC, Lemaréchal C (1989) Some numerical experiments with variable storage quasi-Newton algorithms. *Math Program* 45:407–435
- Griewank A, Walther A (2008) *Evaluating derivatives. Principles and techniques of algorithmic differentiation*, vol 19, 2nd edn, *Frontiers in Applied Mathematics*. SIAM, Philadelphia
- Grubić A (2006) The astronomical theory of climatic changes of Milutin Milankovich. *Episodes* 29(3):197–203
- Hann JV (1915) *Lehrbuch der Meteorologie*, 3rd edn. C.H. Tauchnitz, Leipzig
- Hartmann DL (1994) *Global physical climatology*. Academic, San Diego
- Hartmann DL, Short DA (1979) On the role of zonal asymmetries in climate change. *J Atmos Sci* 36:519–528
- Holden PB, Edwards NR, Oliver KIC, Lenton TM, Wilkinson RD (2010) A probabilistic calibration of climate sensitivity and terrestrial carbon change in GENIE-1. *Clim Dyn* 35:785–806. doi:10.1007/s00382-009-0630-8
- Jentsch V (1987) Cloud-ice-vapor feedbacks in a global climate model. In: Nicolis C, Nicolis G (eds) *Irreversible Phenomena and Dynamical Systems Analysis in Geosciences*. D. Reidel, Boston, pp 417–437
- Joussaume S, Braconnot P (1997) Sensitivity of paleoclimate simulation results to season definitions. *J Geophys Res* 102 (D2):1943–1956
- Joussaume S, Taylor K (1995) Status of the Paleoclimate Modeling Intercomparison Project. In: *Proceedings of the first international AMIP scientific conference, WCRP-92, Monterey, CA, 15–19 May 1995*, 532 pp (pp 425–430). Geneva, Switzerland: WMO/TD-No. 732
- Kalnay E, Kanamitsu M, Kistler R, Collins W, Deaven D, Gandin L, Iredell N, Saha S, White G, Woolen J, Zhu Y, Chelliah M, Ebisuzaki W, Higgins W, Janowiak J, Mo KC, Ropelewski C, Leetmaa A, Reynolds R, Jenne R (1996) The NCEP/NCAR reanalysis project. *Bull Am Meteorol Soc* 77:437–471
- Kasibhatla P, Heimann M, Rayner P, Mahowald N, Prinn RG, Hartley DE (2000) *Inverse Methods in Global Biogeochemical Cycles*, vol 114, Geophysical monograph series. AGU, Washington, DC
- Kucera M, Rosell-Melé A, Schneider R, Waelbroeck C, Weinelt M (2005) Multiproxy approach for the reconstruction of the glacial ocean surface (MARGO). *Quat Sci Rev* 24:813–819
- Larson VE, Golaz JC, Hansen J, Schanen DP, Griffitt BM (2008) Diagnosing structural errors in climate model parameterizations. In: *Extended Abstracts, 20th Conference on Climate Variability and Change, 88th Annual Meeting of the American Meteorological Society, New Orleans, LA*
- Le Dimet F-X, Talagrand O (1986) Variational algorithms for analysis and assimilation of meteorological observations: Theoretical aspects. *Tellus* 38A(2):97–110
- LeGrand P, Wunsch C (1995) Constraints from paleotracer data on the North Atlantic circulation during the last glacial maximum. *Paleoceanography* 6:1011–1045
- Lorenz EN (1979) Forced and free variations of weather and climate. *J Atmos Sci* 36(8):1367–1376
- Losch M, Wunsch C (2003) Bottom topography as a control parameter in an ocean circulation model. *J Atmos Ocean Technol* 20(11):1685–1696
- Loure MF (2003) Ice ages (Milankovitch theory). In: Holton JR, Curry JA, Pyle JA (eds) *Encyclopedia of Atmospheric Sciences*. Elsevier Ltd., pp 995–1003
- MARGO Project Members (2009) Constraints on the magnitude and patterns of ocean cooling at the Last Glacial Maximum. *Nat Geosci* 2:127–132. doi:10.1039/NGEO411
- Meehl GA, Stocker TF, Collins WD, Friedlingstein P, Gaye AT, Gregory JM, Kitoh A, Knutti R, Murphy JM, Noda A, Raper SCB, Watterson IG, Weaver AJ, Zhao Z-C (2007) Global climate projections. In: Solomon S, Qin D, Manning M, Chen M, Marquis Z, Averyt K, Tignor M, Miller H (eds) *Climate Change 2007: The Physical Science Basis. Contribution of Working Group I to the Fourth Assessment Report of the Intergovernmental Panel on Climate Change*. Cambridge University Press, Cambridge, pp 747–845
- Milankovitch M (1920) *Théorie Mathématique des Phénomène Thermique Produits par la Radiation Solaire*. Gauthier Villars, Paris
- Milankovitch M (1930) *Mathematische Klimalehre und Astronomische Theorie der Klimaschwankungen*. Volume I, part A of *Handbuch der Klimatologie*. Verlag von Gebrüder Borntraeger, Berlin, pp A1–A176
- Milankovitch M (1941) *Kanon der Erdbestrahlung und seine Anwendung auf das Eiszeitenproblem*. Académie Royal Serbe, Belgrade
- Myhre G, Highwood EJ, Shine KP, Stordal F (1998) New estimates of radiative forcing due to well mixed greenhouse gases. *Geophys Res Lett* 25(14):2715–2718
- North GR, Mengel JG, Short DA (1983) Simple energy balance model resolving the seasons and the continents: Application to the astronomical theory of the ice ages. *J Geophys Res* 88 (C11):6576–6586
- Paul A, Schäfer-Neth C (2005) How to combine sparse proxy data and coupled climate models. *Quat Sci Rev* 23:1095–1107. doi:10.1016/j.quascirev.2004.05.010
- Penck A, Brückner E (1901–1909) *Die Alpen im Eiszeitalter*. C. H. Tauchnitz, Leipzig
- Petrović A (2002) *Insolation and climate. Milutin Milanković and the mathematical theory of climate changes*. Technical report, Ministry for Protection of Natural Resources and Environment of the Republic of Serbia in collaboration with Serbian Society of History of Science
- Rayner PJ, Giering R, Kaminski T, Ménard R, Todling R, Trudinger CM (2000) *Exercises*. In: Kasibhatla P, Heimann M, Rayner P, Mahowald N, Prinn RG, Hartley DE (eds) *Inverse Methods in Global Biogeochemical Cycles*, vol 114, Geophysical Monograph Series. AGU, Washington, DC, pp 81–106

- Rougier J (2008) Comment on article by Sansó et al. *Bayesian Anal* 3(1):45–56
- Sarnthein M, Gersonde R, Niebler S, Pflaumann U, Spielhagen R, Thiede J, Wefer G, Weinelt M (2003) Overview of Glacial Atlantic Ocean Mapping (GLAMAP 2000). *Paleoceanography* 18. doi:[10.1029/2002PA00769](https://doi.org/10.1029/2002PA00769)
- Schäfer-Neth C, Paul A (2004) The Atlantic Ocean at the Last Glacial Maximum: 1. Objective mapping of the GLAMAP sea-surface conditions. In: Wefer G, Mulitza S, Ratmeyer V (eds) *The South Atlantic in the Late Quaternary: Reconstruction of Material Budgets and Current Systems*. Springer, Berlin, pp 531–548
- Schneider von Deimling T, Held H, Ganopolski A, Rahmstorf S (2006) Climate sensitivity estimated from ensemble simulations of glacial climate. *Clim Dyn* 27:149–163. doi:[10.1007/s00382-006-0126-8](https://doi.org/10.1007/s00382-006-0126-8)
- Thacker W (1989) The role of the Hessian matrix in fitting models to measurements. *J Geophys Res* 94:6177–6196
- Wessel P, Smith WHF (1998) New, improved version of Generic Mapping Tools released. *EOS Trans Am Geophys Union* 79:579
- Winguth AME, Archer D, Maier-Reimer E, Mikolajewicz U (2000) Paleonutrient data analysis of the glacial Atlantic using an adjoint ocean general circulation model. In: Kasibhatla P, Heimann M, Rayner P, Mahowald N, Prinn RG, Hartley DE (eds) *Inverse Methods in Global Biogeochemical Cycles*, vol 114, *Geophysical Monograph Series*. AGU, Washington, DC, pp 171–183
- Wunsch C (1996) *The Ocean Circulation Inverse Problem*. Cambridge University Press, New York

A Brief History of the Astronomical Theories of Paleoclimates

André Berger

Abstract

Paleoclimatic reconstructions help us to discover the natural variability of the climate system over time scales ranging from years to hundreds of thousands of years. They are fundamental in climate research, especially now, because they provide a unique set of data to validate models over climatic regimes largely different from those of the last 150 years. The climatic variations of the last century are indeed available in great detail, but with a very poor diversity. Among the different modes of climatic variations, the glacial–interglacial cycles have the advantage that they provide examples of extreme climates with known astronomical forcing.

The Astronomical Theory of paleoclimates aims to explain climatic variations occurring with quasi-periodicities situated between tens to hundreds of thousands of years. Such variations are recorded in deep-sea sediments, ice sheets, and continental sediments. The origin of these quasi-cycles lies in the astronomically driven changes of the latitudinal and seasonal distribution of the energy that the Earth receives from the Sun. Milutin Milankovitch extensively published about this theory between 1912 and 1950, but the relationship between the astronomical parameters, insolation, and climate, had already been suggested at the beginning of the nineteenth century. The evolution of ideas from these early times to the present day is briefly reviewed, but this introductory chapter does not claim to be a full historical survey of what has contributed to structure the astronomical

theory of paleoclimates over the last two centuries. It might rather be viewed as a pedagogical tool for teaching some of the basic concepts in a historical context. Written to be concise, it provides references to authors who have contributed to what is now named (often improperly) the Milankovitch astronomical theory. It also attempts to correct distortions of credit and intellectual contributions.

As this astronomical theory aims to explain the glacial–interglacial cycles, the discovery of their existence is first summarized from the existing literature (e.g., Hann 1903; Bard 2004; Krüger 2008). For the astronomical theory, a brief history of its early elaboration and of its gradual refinement up to the 1980s is provided. The last 20–30 years are characterized by an extremely large number of researches. They use the astronomical theory in an attempt to explain the physical mechanisms through which the long-term variations of the energy received from the Sun is affecting the Earth's climate. For partial reviews of this literature, the reader is referred to Berger (1988, 1995) and/or to proceedings of symposia discussing

A. Berger (✉)
Université catholique de Louvain, Louvain-La-Neuve, Belgium
e-mail: andre.berger@uclouvain.be

more recent applications (e.g., Berger et al. 1984, 2005b; Schellnhuber et al. 2004; Sirocko et al. 2007).

The narrative style used in this chapter cannot mask the fact that, in the early nineteenth century, authors lived in a dramatically different intellectual environment than Milankovitch and not to speak of more recent scientists. The “pool of ideas” on which they could draw their conclusions as well as their motivation for thinking about the ice ages were radically different in many respects. The ideas were not part of a unified theory of paleoclimates, and these early naturalists were not necessarily drawing on each other’s work. It is however amazing to see, when reading their scientific papers, how much they were aware of their respective views, exchanging ideas and critics through scientific communications, papers and letters (for example, those between Tyndall, Lyell, and Herschel, see Fleming 1998, pp. 68, 73, 74).

Introduction to the Astronomical Theory

The seasonal and latitudinal distribution of the solar energy the Earth receives has long-term variations which are related to the orbit of the Earth around the Sun and to the inclination of its axis of rotation. These involve three well-identified astronomical parameters: the eccentricity, e (a measure of the shape of the Earth’s orbit around the Sun), the obliquity, ε (the tilt of the equator with respect to the plane of the Earth’s orbit), and the climatic precession, $e \sin \tilde{\omega}$, a measure of the Earth–Sun distance at the summer solstice ($\tilde{\omega}$, the longitude of the perihelion, is a measure of the angular distance between the perihelion and the vernal point that are both in motion). The present-day value of e is 0.016. As a consequence, although the Earth’s orbit is very close to a circle, the Earth–Sun distance, and consequently the insolation, varies by as much as 3.2 and 6.4% respectively over the course of 1 year. The obliquity, which defines our tropical latitudes and polar circles, is presently $23^{\circ}27'$. The longitude of the perihelion, $\tilde{\omega}$, is 102° , which means that the Northern Hemisphere winter occurs when the Earth is closest to the Sun. The average periods of variations of these eccentricity, obliquity, and precession are respectively 95,800 years (but with others, in particular one of 400,000 years), 41,000 years (very stable), and 21,740 years (with a large dispersion around this value) (Berger 1976).

Early Theories of Quaternary Glaciations

Earth’s history has been characterized by periods, called Ice Ages (with capital letters), when the climate was markedly colder than at other times. The most well known are the Pre-Cambrian Ice Ages, the late-Ordovician Ice Age, the Permo-Carboniferous Ice Age, and the present Ice Age. Our Ice Age, which the Earth entered 2–3 Ma ago, is called the Quaternary Ice Age. This Ice Age is characterized by multiple switches of the global climate between cold periods (named glacials and sometimes ice ages with lower cases) when extensive ice sheets were present, and warm periods (named interglacials) when there was less ice over the Earth (or at least not much more) or when the climate was more or less similar or warmer than today (Tzedakis et al. 2009; Yin and Berger 2010). The need to offer an explanation for the origin and recurrence of these glaciations has progressively led to suggest and finally demonstrate that they are related to celestial mechanics, that is, to the characteristics of the Earth’s orbit around the Sun and the tilt of its axis of rotation.

Early in the eighteenth century, the presence of erratic blocks and of moraines in the Alpine Valleys drew the attention of travelers and naturalists (for a more detailed history of early scientific research on glaciations, see Bard (2004) and Krüger (2008) where references are available.) In 1744, perhaps for the first time, a geographer living in Geneva, Pierre Martel (1706–1767) reported that the inhabitants of the Valley of Chamonix in the Alps of Savoy attributed the dispersion of erratic boulders to glaciers that in the previous times extended further into the lowlands. Similar explanation was given in 1815 by the hunter Jean-Pierre Perraudin (1767–1858), based on his observations in the Val de Bagnes in the Swiss canton of Valais. Horace-Benedict de Saussure (1740–1799), a naturalist with a passion for high mountains and the Mont Blanc in particular, noticed that such erratic blocks were located along the axes of the valleys and that they must have been transported from the peaks of the Alps over long distances, possibly by catastrophic floods (“currents of incredible violence and magnitude”). This explanation was also suggested by the paleontologist Georges Cuvier (1763–1832), who assigned the extinction of species to environmental catastrophes. In 1795, the Scottish naturalist James

Hutton (1726–1797) explained that the presence of erratic boulders in the Alps was due to the action of the glaciers, whereas the Scottish geologist Charles Lyell (1797–1875) proposed the theory that transport of rock blocs can be accounted by the action of ice rafts, ice breaking off the poles, floating across submerged continents, and carrying debris with it (Lyell 1830, vol. 3, 1833).

In Scandinavian countries, the Swedish mining expert Daniel Tilas (1712–1772) suggested, in 1742, that the drifting sea ice could be the reason for the presence of the erratic boulders in Scandinavian and Baltic regions. In 1818, the Swedish botanist Göran Wahlenberg (1780–1851) published his theory of a glaciation of the Scandinavian peninsula that he regarded as a regional phenomena (from Krüger 2008, p. 118). A few years later, the Danish-Norwegian geologist Jens Esmark (1763–1839), for whom the transport of rocks by ice seemed evident, offered a sequence of worldwide ice ages. In 1824, he proposed that the changes in climate were the cause of these glaciations and tried to show, perhaps for the first time, that they originated from changes in the Earth's orbit (Esmark 1824, 1827). We may consider Esmark's ideas as the first distinctly modern formulation of the astronomical theory of long-term climatic change. His chronology differed from the one accepted today because it was based on the contemporary theories that assumed that the Earth developed from an old comet with the ice ages corresponding to the periods when the terrestrial comet was at the aphelion (i.e., at the greatest distance from the Sun).

In 1829, the Swiss engineer Ignaz Venetz (1788–1859) explained the dispersal of erratic boulders in the Alps, the Jura Mountains, and the North German Plain as being due to huge glaciers which variations in the location of the fronts would have been a consequence of climatic changes but not related to astronomical cause. This idea was adopted by the German Professor of forestry Albrecht Reinhard Benhardi (1797–1849) who, in a paper published in 1832, speculated about former polar ice caps reaching as far as the temperate zones of the globe. At about the same time, Jean de Charpentier (1786–1855), using Venetz's explanation but restricted to the Alps, introduced the hypothesis of diluvian glaciers (de Charpentier 1836), the ice equivalent of the de Chaussure-Cuvier floods, to explain the erratic boulders. He presented his paper in

1834 before the Schweizerische Naturforschende Gesellschaft, referring to astronomical causes but only in very general terms “such as for example a change in the ecliptic, the precession of the equinoxes, the progression of the planetary system in space, the asteroids...” (de Charpentier 1841). In the mean time, following several excursions into the Bavarian Alps, the German botanist Karl Friedrich Schimper (1803–1867) came to the conclusion that ice was most likely the explanation for the movement of local boulders. In 1837, he introduced the term “ice age (Eiszeit)” (Schimper 1837a) and assumed that the Earth's history had been characterized by periods of cold climate and frozen water. This idea was similar to Esmark's suggestion of worldwide ice caps. At this time he convinced his former university friend, the Swiss geologist Louis Agassiz (1801–1873), that reality of such periods must be granted on the grounds of empirical findings (Schimper 1837b). In the same year, de Charpentier gave Agassiz a course of field work on glaciers. Subsequently, Agassiz and Schimper developed a theory of a sequence of glaciations based most probably on Esmark whose theory Agassiz knew through Benhardi's paper and upon the work of Johan Wolfgang von Goethe (1749–1832) (although Schimper stated that he did not know Goethe's ice age theory in 1837), of Venetz, of de Charpentier and on their own field work. In the mind of Agassiz, the concept of the ice ages was a Cuvierian catastrophe, in which the catastrophic floods were being replaced by a gigantic glacier which he even called the “God's great plough.” It is with such theory that Agassiz convinced Charles Lyell and that in 1837, at the opening of the Helvetic natural History Society at Neuchatel, he shocked his audience by delivering his address entitled “Upon Glaciers, Moraines and Erratic Blocks” (Agassiz 1838). Because of the high similarity of Agassiz's hypothesis with Schimper's idea, Evans (1887) claimed that “Agassiz actually ‘borrowed’ his conception of glacial theory, usually attributed to him, from K. Schimper” and that, “aware of his indebtedness, he also most carefully concealed it.” A similar complaint came from de Charpentier. Excluded from Agassiz's book (1840), he felt indeed that Agassiz should have given him credit as he had introduced him to in-depth glacial research (Table 1).

Table 1 Pioneers of glaciation theory

Glaciations		
1706–1767	Martel	Erratic boulders due to glaciers
1767–1858	Perraudin	Erratic boulders due to glaciers
1740–1799	de Saussure	Floods to transport erratic blocs
1763–1832	Cuvier	Environmental catastrophes
1797–1875	Lyell	Ice rafts to transport erratic blocs
1712–1772	Tillas	Drifting sea ice to transport
1780–1851	Walhenberg	Glaciations
1763–1839	Esmark	1824 Astronomical theory of glaciations
1788–1829	Venez	Huge glaciers front to transport
1797–1849	Benhardi	Polar ice cap
1786–1855	de Charpentier	Diluvian glaciers
1803–1867	Schimper	1837 Eiszeit
1801–1873	Agassiz	Sequence of glaciations
1749–1832	Goethe	Discover ice ages
1786–1830	Fourier	Greenhouse effect
1820–1893	Tyndall	Greenhouse and glaciers
1858–1945	Penck	Glaciations in the Alps
1862–1927	Brückner	Glaciations in the Alps
1843–1928	Chamberlain	Glaciations in America

Pioneers of the Astronomical Theory

In parallel, research on the scientific concept of the greenhouse effect was going on with the French Physicist Joseph Fourier (1786–1830) and the Frenchman Jacques Joseph Ebelmen (1814–1852) who was probably the first to suggest that past changes in the carbon cycle could have changed the climate of the Earth through changes in the atmospheric concentration of “carbonic acid” (Ebelmen 1845, cited by Bard 2004, p. 626). Some years later, the Irish chemist John Tyndall (1820–1893) came with the same idea (Tyndall 1861) that changes in the atmospheric concentration of greenhouse gases, like carbon dioxide and water vapor, could produce “all the changes revealed by the geologists.” Tyndall was also greatly interested by the high mountains in the Alps and the movement of glaciers (Tyndall and Huxley 1857). Along with these studies on the Alpine glaciers, investigations of the polar ice caps were going to contribute to the debates. The first descriptions of the Antarctic ice cap remained however largely uncertain. For example, the French mathematician Joseph Alphonse Adhémar (1797–1862) evaluated its average

thickness at more than 100 km! Realizing that such an ice cap is difficult to accept and following his brilliant intuition that the glaciations must have been periodic, he turned toward astronomy not only to test his calculations about Antarctica but also to determine the cause of the ice ages and of their recurrence (Table 2). In 1842, Adhémar published his book explaining Agassiz’s hypothesis on the existence of ice ages on the basis of the known precession of the equinoxes, thereby implying that there had likely been more than one. Convinced that the Southern Hemisphere was currently under an ice age (because his estimate of the thickness of Antarctica) and influenced by the current explanation of the mechanisms of seasons and tides at that time, Adhémar invoked the different durations of the seasons between the two hemispheres as a possible cause of the ice ages. By combining the astronomical precession (calculated from the value of 50.1” per year of the French astronomer Jean-Baptiste Joseph Delambre 1749–1822) and the rotation of the terrestrial orbit (calculated from the value of 11.83” per year of the French mathematician Louis Benjamin Francoeur 1773–1849), he further concluded “that a period of 21,000 years must exist between the present time and the moment when the seasons will correspond to the same point of the orbit.” From his calculations, he concluded (1) that the astronomical winter in the Southern Hemisphere is 7 days longer than the summer, (2) that consequently there must presently be an ice age in the Southern Hemisphere, and (3) that 11,000 years from now that there will be an ice age in the Northern Hemisphere. According to Adhémar’s theory, the great accumulation of ice around the pole having a long winter displaced the Earth’s center of gravity resulting in a partial displacement of the ocean waters, and a flooding which further increased the cooling. Similarly, to attempt explaining the deglaciation, he introduced large scale oceanic currents to link the two hemispheres. His meridian circulation of the ocean at the surface and at depth (Adhémar 1842, Figs. 2 and 6 and page 304) is actually a simplified representation of what is called nowadays the thermohaline circulation (a conveyor belt transporting heat from the south to the north in the Atlantic Ocean, with the Gulf Stream being part of it). He was certainly not aware that this concept of oceanic current would play, one century later, a fundamental role in the explanation of the energy transport from the Southern to the

Northern Hemisphere. His prediction about the climatic effect of the Gulf Stream is also remarkable (his page 366): “One might at the maximum conclude that our hemisphere would cool more rapidly if the Gulf Stream would not exist; what is not that certain because it would not be impossible that the vapor produced by the warm water currents would contribute itself to increase the polar ice.” In 1979, Ruddiman and McIntyre invoked the same mechanism to explain the last Glacial Maximum: “The juxtaposition of an ‘interglacial’ stream alongside a ‘glacial’ land mass is regarded as an optimal configuration for delivering moisture to the growing ice sheets.” Many criticisms were raised against Adhémar ideas, like his glaciations affecting the two hemispheres in opposite ways and, more importantly, his hypothesis about the difference in the length of the seasons between the two hemispheres. As underlined by Charles Lyell and the German Alexander von Humboldt (1769–1859) more important than the length of the seasons is indeed the total energy received during a season or the year. The computation of such total irradiation was actually possible based on calculations already made by the French Jean Le Rond d’Alembert (1717–1783) for precession and the English Sir John Frederick William Herschel (1792–1871) for insolation. John Herschel (1832) claimed (page 298): “it is demonstrable that, whatever be the ellipticity of the Earth’s orbit, the two hemispheres must receive equal absolute quantities of light and heat per annum, the proximity of the Sun at perigee exactly compensating its swifter motion.” This is a consequence of the second law by the German astronomer Johannes Kepler (1571–1630), a law that Herschel reformulated as: “The amount of heat received by the Earth, while describing any part of its orbit is proportional to the angle described round the Sun’s center.” Actually the irradiation received at a latitude of the Northern Hemisphere during a given Northern Hemisphere season is equal to the irradiation received by the same latitude of the Southern Hemisphere during the same local Southern Hemisphere season (Berger et al. 2010). Being given the role played by John Herschel in the astronomical theory, let us stress three of his fundamental statements (Herschell 1832). The first one concerns: “the total quantity of heat received by the Earth from the Sun in one revolution is inversely proportional to the minor axis of the orbit (*and consequently depends upon eccentricity*).” The second one is a direct

consequence: “since the major axis is invariable and therefore the absolute length of the year (*through the third law of Kepler*), it follows that the mean annual average of solar radiation is dependent on the eccentricity of the orbit.” These statements implicitly lead to the conclusion that the so-called solar constant (defined as the energy received at the mean distance of the Earth from the Sun) is actually dependent on the eccentricity (see Berger and Loutre 1994, pp. 118–119). In Milankovitch however no difference is made between the semi-major axis and the mean distance. At the bottom of page 212 (of the 1969 English translation of the 1941 Milankovitch’s book), one finds: “the uniform flow of energy across the sphere whose radius represents the mean distance of the Earth to the Sun *or* the semi-major axis of the Earth’s orbit is called the solar constant J_0 .” The third one concerns the application to the Earth’s climate, first noting a present-day agreement between astronomy and geological observations: “The eccentricity of the Earth’s orbit is actually diminishing. . . the annual average of solar radiation is actually on the decrease. So far, this is in accordance with the testimony of geological evidence. . .,” then turning to: “the extreme effects which a variation in the eccentricity may be expected to produce in the summer and winter climates in particular regions of its surface. . . It will appear that a (*large*) amount of variation may operate during great periods of time to mitigate or to exaggerate the difference of winter and summer temperatures . . . but the actual diminution of the eccentricity is so slow that the transition from a state of the orbit to the present nearly circular figure would occupy upwards of 600,000 years (*we know now that the average period of eccentricity is much smaller*)” and referring to Lyell: “adopting the very ingenious idea of Mr Lyell, would suffice, by reason of the combined effect of the precession of the equinox and the motion of the apsides of the orbit itself, to transfer the perigee from the summer to the winter solstice, and thus to produce a transition from the one to the other species of climate, in a period sufficiently great to give room for a material change in the botanical character of a country. . .”.

Herschel finally concludes in confirming his reluctance to accept the astronomical theory: “But if on executing the calculations, it should appear that the limits of the eccentricity are really narrow, it should appear that the mean as well as the extreme temperature of our climates would not be materially

Table 2 Pioneers of astronomical theory

Pioneers of astronomical theory			Astronomers		
1797–1862	Adhémar	Periodic glaciations, southern hemisphere	1749–1822	Delambre	Astr precession
		Precession, length of the seasons	1773–1849	Francoeur	Perihelion
1769–1859	von Humboldt	Season irradiation	1717–1783	Le rond d'Alembert	Precession
1821–1890	Croll	1864 Precession, NH Winter at aphelion	1792–1871	Herschel	Insolation, total energy
		1867 Climatic precession, Le Verrier	1811–1877	Le Verrier	Eccentricity and obliquity
		1867 Obliquity	1855	Meech	Insolation, total energy
1809–1882	Darwin	Supported Croll	1752–1833	Legendre	Elliptic integrals
1835–1924	Geikie A		1749–1827	Laplace	Obliquity max
1839–1914	Geikie J	1874 glacial–interglacial cycles	1781–1840	Poisson	Motion through planetary system
1890	Howorth	Against antisymmetry between hemispheres	1876	Wiener	Insolation, elliptic integrals
1858–1943	de Geer	Dated post-glacial	1822–1920	Stockwell	Astronomical parameters
1840–1913	Ball	Claimed to refine Croll			Neptune included
1855–1931	Culverwell	Small variations but obliquity missing	1924	King	Numerical values of elliptic integrals
1857–1936	de Marchi	Atmospheric transmission			
1859–1927	Arrhenius	CO ₂			
1797–1875	Lyell	Astronomical theory exaggerated			
1896	Hargreaves	Obliquity annual insolation			
1901	Ekholm	Extreme obliquity on insolation no precession			
1849–1946	Spitaler	Astronomical values for glaciation			
1881–1949	Hopfner	Missed discontinuity insolation high latitudes			
1904	Pilgrim	Effect of 3 astronomical parameters on insolation			

affected. . . the obliquity of the ecliptic being confined within too narrow limits for its variation to have any sensible influence.”

Within the next decades, largely because of the discovery of the repetitive aspect of global glaciation (for example, in the Vosges, in Wales, and in the American records), glacial geology became strongly tied to astronomy (Table 2 and for a detailed list of the papers from the nineteenth century to 1980, see Berger 1988). An astronomer in Paris, Urbain Le Verrier (1811–1877), famed for having discovered the planet Neptune, calculated the planetary orbital changes of the Earth over the last 10⁵ years (Le Verrier 1855), although he did not seem to be interested in the astronomical theory of paleoclimates (Lequeux 2009). In parallel, L.W. Meech (1856) published the first detailed determination of the instantaneous, daily and seasonal amount of energy received by any latitude of

the Earth from the Sun. This calculation was based on the elliptic integrals introduced in 1825–1828 by the French mathematician André-Marie Legendre (1752–1833). Meech further analyzed the influence of Le Verrier’s secular values of eccentricity (mainly the extreme values) on the Sun’s annual intensity and calculated it for 10,000 years BP. After discussing it in relation to the Northern and Southern hemispheres, he concluded (page 30): “this wide fluctuation of winter and summer intensities, in relation to the two hemispheres, scarcely affected the aggregate annual intensities.” Taking into account the impact of the maximum variation of obliquity given by the French astronomer Pierre-Simon Laplace (Marquis de 1749–1827), he finally concluded (page 41): “that Great geological Changes must be referred to other causes than the secular inequalities of the Earth’s orbit and might result from the motion of the whole

Planetary System in Space,” a conclusion for which he referred to the work of the French astronomer and physicist Siméon-Denis Poisson (1781–1840) (Poisson 1835). Twenty years later, Chr. Wiener (1877) published a very similar calculation, but which included the total irradiation received over different parts of the year.

It was also at that time that the Scottish scientist James Croll (1821–1890) initiated a series of important works that would continue to bear much fruit into modern times (for details, see Imbrie and Imbrie 1979; Fleming 2005). Croll’s theory (Croll 1875) depends upon the inequality in the length of the seasons, but unlike Adhémar he considered it at the time of a great eccentricity of the Earth’s orbit. Three major astronomical factors were recognized in his model: precession, orbital eccentricity, and axial tilt. The importance of Croll is that he approached the glaciation problem from the synergistic standpoint of the combined effects of these three major astronomical factors on seasonal insolation during perihelion and aphelion. Moreover, a specific characteristic of his model lies essentially in his hypothesis that the critical season for the initiation of a glacial is the Northern Hemisphere winter. He argued that a decrease in the amount of sunlight received during the winter favors the accumulation of snow, and that any small initial increase in the size of the area covered by snow would be amplified by the snowfields themselves (positive feedback). After having determined which astronomical factors control the amount of sunlight received during winter, he concluded that the precession of the equinoxes must play a decisive role (Croll 1864). But his main contribution was to show that changes in the shape of the orbit which were unknown to Adhémar determine how effective the precessional wobble is in changing the intensity of the seasons (Croll 1867a). Croll’s first theory predicts therefore that one hemisphere or the other will experience an ice age whenever two conditions occur simultaneously: a markedly elongated orbit and a winter solstice that occurs when the Earth is far from the Sun. This would produce a climate so severe that the snow falling during the long cold winter would be heavy enough to persist through the short hot summer and thus develop ice sheets. According to Croll’s calculations based on the planetary orbital changes of the Earth determined by Urbain Le Verrier in 1855 for the last 10^5 years, these conditions were reached

240,000 years ago and ended 80,000 years ago (We know now that the cold conditions ended much later, about 12,000 years ago, the Last Glacial Maximum having culminated 20,000 years ago (CLIMAP 1976)). Later, Croll hypothesized that an ice age would be more likely to occur during periods when the axis is closer to vertical, for then the Polar Regions receive a smaller amount of heat (Croll 1867b). However, Croll did not have accurate data on the variations of obliquity which will become available only a few years later with Stockwell (1873) and much later with the Milankovitch complete formulation of the astronomical theory. In the mean time, Croll received the support of the English naturalist Charles Robert Darwin (1809–1882) who wrote in his book “On the Origin of Species” (Darwin 1872): “Mr Croll in a series of admirable memoirs, has attempted to show that a glacial condition of climate is the result of various physical causes, brought into operation by an increase in the eccentricity of the Earth’s orbit. . . and its influence on the oceanic currents” (it is surprising that reference to climate and Croll disappeared in the 1900 popular impression of the “Origin of Species”). The Scottish geologist Archibald Geikie (1835–1924) and his brother James Geikie (1839–1914) showed convincingly that several glacial phases follow one after the other separated by interglacial periods with a moderate climate as warm or warmer than present (Geikie 1874). The German geographers, Albrecht Penck (1858–1945) and Eduard Brückner (1862–1927) also came with their multiple glaciations in the Alps (Günz, Mindel, Riss, and Würm; Penck and Brückner 1909) whereas, at about the same time, the American geologist Thomas Chouder Chamberlain (1843–1928) presented the classification of the American glaciations (Nebraskan, Kansan, Illinoian, and Wisconsinian; Chamberlin 1882).

But, as time went on, many geologists in Europe and America became more and more dissatisfied with Croll’s theory, finding it at variance with new evidence about the last ice age. His calculations lead indeed to great climatic changes opposite in the two hemispheres (e.g., Howorth 1890), whereas geological investigations were showing that the glacial periods are practically synchronous in the two hemispheres. Moreover, the duration of post-glacial time estimated by the Swedish geologist Gerald de Geer (1858–1943) was much smaller than the 80,000 years necessary in the framework of Croll’s theory.

The theory of glacial periods was then taken up by the Irish astronomer Sir Robert Stawell Ball (1840–1913) who claimed to refine the Croll’s theory and calculations (Ball 1891). Actually, he calculated only the quantity of heat received by a whole hemisphere in winter and summer, using the ratio between the two to argument about glaciations (this ratio is independent of eccentricity, Berger and Yin 2012). Not only these calculations were already made by Chr. Wiener (1877) but they also refer only to one hemisphere as a whole preventing application to one latitude in particular. Similar critics of Ball’s “astronomical theory” were drawn by the Irish scientist Edward P. Culverwell (1894) who used Meech’s results to calculate the heat received by the latitudes 40–80° for winter at aphelion (i.e., at the height of the ice age). These calculations allowed him to show that for a winter longer than now, the present-day latitude of 54° has the same solar climate as latitude 50° during the supposed ice age, with a conclusion that an ice age could not be produced with such a small insolation difference. It must be stressed however that Culverwell did not take the variation of obliquity into account which explains the low amplitude of his insolation variations.

Facing all these discussions, it is not surprising that scientists turned to other theories. For example, Sir Charles Lyell (1872) considered that the astronomical theory was exaggerated and turned toward the rearrangement of land and sea to show that this might produce extremes of heat and cold in global climates. Other propositions to explain the glaciations were also made in relationship with the greenhouse theory which was starting to be scientifically elaborated. Such working hypothesis was advanced by Tyndall (1861, already cited) and later by Chamberlin (1899) who assumed that “the changes in atmospheric carbon dioxide result from the weathering of rocks and through the agency of organisms.” Based on his investigation of the effect of the atmospheric composition on climate, Luigi de Marchi (1857–1937) concluded (de Marchi 1895) that neither the astronomical nor the geological theories can lead to a plausible explanation of the ice age. His analysis of the dependence of the air temperature upon the ratio of the radiant energy received to that lost by the Earth, as well as the distribution of land and sea water, convinced him that “a slight change in the transmission of the atmosphere for solar rays and heat would suffice to produce

an ice age in the middle and high latitudes” and that “The diminution of the air’s transparency ought chiefly to be attributed to a greater quantity of aqueous vapor in the air, which would cause not only a direct cooling but also copious precipitation of water and snow on the continents. The origin of this greater quantity of water vapor is not easy to explain” (Arrhenius 1896, p. 274). He was however not prepared to link such changes in the atmospheric transmission to changes in the concentrations of the other greenhouse gases. It is the Swedish chemist Svante Arrhenius (1859–1927) who considered that the ice ages were caused by falls in the atmospheric content of carbon dioxide, amplified by an increase of the snow-covered areas and the oceanic currents (Arrhenius 1896). Citing both de Marchi (1895, p. 166) and Arrhenius (1896, p. 274):

“From the point of view of climatology and meteorology, in the present state of sciences the hypothesis of Croll seems to be wholly untenable as well as in its principles and his consequences. . . . It becomes more and more impossible to reconcile the chronology demanded by Croll’s hypothesis with the facts of observations.” By supplementing the notion of the carbon cycle developed by Arrhenius, Thomas Chamberlin (1843–1928) suggested in 1899 that the rhythmic action of the carbon cycle could partly explain the glaciations cycle. It became therefore clear that the astronomical theory of the glacial period was unable to explain the new geological facts and that improvements were definitely necessary.

Such a revival started with attempts to improve the astronomical calculations. Hargreaves (1896) estimated the impact of obliquity on the insolation of different latitudes but only for the annual average. He was not interested in the variability induced by the seasonal cycle. Analyzing the impact of extreme values of obliquity on insolation, Nils Ekholm (1901) missed the extreme values of insolation itself as he did not account for the influence of precession and eccentricity. The Austrian astronomer Rudolf Ferdinand Spitaler (1849–1946) tried in 1907 to calculate which values of the three astronomical parameters are the most favorable for glacial formation and growth. Unfortunately his work was based on the calculation made in 1907 by the Austrian geophysicist Friedrich Hopfner (1881–1949) who failed to take into account the discontinuity of insolation in the Polar Regions (Hopfner, 1907). Based on John Nelson Stockwell

(1822–1920) work (1873), the German mathematician Ludwig Pilgrim (known mostly as a pioneer in colorimetry) calculated in 1904 the combined effect of the eccentricity of the orbit, the obliquity, and the precession of the equinox and tabulated the variations in the solar radiation for about 1 million years prior to 1850, but the values of the planetary masses used by Stockwell were not necessarily the most recent ones (see Milankovitch below). Over the last decade of the nineteenth century and the beginning of the twentieth century, there were therefore many calculations made and hypotheses offered concerning the astronomical theory of paleoclimates. However, these studies were dealing only with part of the problem, like discussing the annual mean but not resolving the seasonal behavior, or suffering from a lack of precision in particular in the long-term variations of the astronomical parameters, and/or being incomplete namely in using only one of the three astronomical parameters. But principally, no real attempt to model the response of the climate system to the astronomical forcing could be found. This was about the situation when, at the beginning of the twentieth century, Milutin Milankovitch became interested in the astronomical theory of paleoclimates or, in his own words, by the “mathematical climate of the Earth.”

The Milankovitch Era

It was during the first decades of the twentieth century that Rudolf Spitaler (1921) rejected Croll’s theory that the conjunction of a long, cold winter and a short, hot summer provides the most favorable conditions for glaciations. He adopted the opposite view, as already put forward by Joseph John Murphy (1869), that a long, cool summer and a short, mild winter are the most favorable. Under these conditions, the cool summer prevents the winter snow from melting and allows, with time, its accumulation to build ice sheets. In a landmark paper published half a century before Spitaler, Murphy pointed out not only his agreement but also his disagreement with Croll as to the cause of the glacial climate. He argued that “a glacial period occurs when the eccentricity of the Earth’s orbit is at its maximum and only one hemisphere is glaciated at the same time” but contrary to Croll, he believed that “the glaciated hemisphere is that of which the summer occurs at aphelion.” In addition, Murphy (1876) used

the more recent calculation by J.N. Stockwell (1873) taking into account the disturbance of the planet Neptune, the existence of which was not known when Urbain Le Verrier’s computations were made and used later by Croll. The diminution of heat during the summer half-year resulting from this new hypothesis was later recognized by the Austrian climatologist Eduard Brückner (1862–1927), the German Russian-born climatologist Wladimir Peter Köppen (1846–1940), and the German geophysicist Alfred Wegener (1880–1930) as the decisive factor in glaciations (Brückner et al. 1925). The hypothesis put forward by Murphy in the middle of the nineteenth century was going to appear, one century later, as being one of the most brilliant proposals made for explaining the generation of the ice sheets (Table 3).

However, this idea of a cool Northern Hemisphere summer became popular mainly because it was also adopted in the early part of the twentieth century by the Serbian engineer, astronomer and geophysicist Milutin Milankovitch (1879–1958). Milankovitch was actually the first to complete a full astronomical theory of Pleistocene ice ages, using the available astronomical elements to compute the subsequent changes in the insolation and climate. Milankovitch’s main contribution was to explore the solar irradiance at different latitudes and seasons in great mathematical detail and to relate these in turn to the planetary energy balance as determined by the albedo and by the reradiation in the infrared according to Stefan’s law. The basis at the heart of Milankovitch’s argument is that “under those astronomical conditions in which the heat budget around the summer solstice falls below average, so will summer melt, with uncompensated glacial advance being the result.” This theory requires therefore that the summer in northern high latitudes must be cold enough to prevent the winter snow from melting. This leads to a positive value in the annual budget of snow and ice which initiates a positive feedback cooling over the Earth through a further extension of the snow cover and a subsequent increase of the surface albedo. On the assumption of a perfectly transparent atmosphere and of the northern high latitudes being the most sensitive to insolation changes, that hypothesis requires a minimum of Northern Hemisphere summer insolation at high latitudes. It is therefore not surprising that the most used product of the Milankovitch theory is his curve that shows how the intensity of summer sunlight

Table 3 Milankovitch era

Milankovitch era			1879–1958	Milankovitch life
1921	Spitaler	Suggested idea of Murphy	1904	Ph.D
1869	Murphy	NH summer at aphelion	1912	Mathematical theory of climate
1876	Murphy	Insolation based on Stockwell	1920	Monograph in French
1925	Penck et al.	Adopted Murphy	1923	New calendar
			1928	Popular book
			1924	Koppen-Wegener Milankovich curves in their book
			1930	Handbook Klimatologie
			1931	Handbook Geophysik
			1931	Milankovitch Calculated astr parameters based on Le Verrier
			1938	Snow line
			1941	Kanon
			1950	Memoirs
			1953	INQUA regrettable experience
			1957	Last paper
			1957	Fempl Extend Milankovitch to high polar latitudes
			1995	Milankovitch V. Biography of Milutin

varied over the past 600,000 years at 65°N. It is on such curves that he identified certain low points with four European ice ages (nonperiodic and without hemispheric alternation) reconstructed 15 years earlier by Albrecht Penck and Eduard Brückner (1909).

One of the ideas originally introduced by Milankovitch was the concept of caloric season. These seasons are exactly half a year long, the caloric summer half-year comprising all the days receiving more irradiation than any of the winter half-year. This avoids taking into account the variations of the length of these seasons as is the case for the astronomical ones (Berger and Yin 2012). Although this does not solve the difficulty of taking insolation into account because the beginning and end of these seasons vary in time, it remains a very interesting concept in natural sciences where the environment has no calendar.

A brief survey of Milankovitch's life might help now to better understand the personality of this great scientist and to follow more easily the development of his work which culminated in his 1941 "Kanon der Erdbestrahlung."

Milankovitch's Life

Milutin Milankovitch was born in Dalj (Austria-Hungary, today Croatia) in 1879 and died in Beograd (Capital of Serbia) in 1958. He was a contemporary of the Alfred Wegener (1880–1930), with whom

he became acquainted through Wladimir Köppen (1846–1940), Wegener's father-in-law (Schwarzbach 1985).

The father of Milankovitch died when Milutin was only 7 years old. His uncle, Vasilije Muacevic then took care of him and continued to support him throughout his life (in gratitude, Milankovitch gave his name Vasilije to his only son and dedicated his work to him). Milankovitch graduated in 1896 from the Realka High School in Osijek where his Professor of Mathematics Vladimir Varicak had a great influence on his vocation for science. He then left for the University of Vienna where he was strongly inspired by his Professor of mechanics, Johann Brick. He graduated in civil engineering in 1902. After 1 year of military service in the Habsburg Monarchy, Milankovitch returned to Vienna in 1903 and earned his Ph.D. in 1904 with a thesis on "Beitrag zur Theorie der Druckkurven." At the beginning of 1905, he started to work in the construction company of Adolf Baron Pittel Betonbau-Unternehmung in Vienna where he gained a high reputation among the engineers for the quality of his theoretical work and his practical innovation in building of dams, bridges, and factory halls.

In 1909, he was invited by the Philosophical Faculty of Belgrade University where he became a Professor at the Department of Applied Mathematics teaching rational and celestial mechanics and theoretical physics, which he continued for the next 46 years

until 1955. It is during the first decade of the twentieth century that he decided to concentrate on fundamental research. During his time in Belgrade, Milankovitch remained in close contact with numerous scientists and institutions, but also with engineer Petar Putnick with whom he was going to build bridges of reinforced concrete for the Railway Company.

As early as 1912, his interest turned to solar climates with a first work on “Contribution to the mathematical theory of climate” (Milankovitch 1912). This is also the time when ice ages became one of his major research interests. In 1914, he married Christine Topuzovic in Belgrade and they went to Dalj, his native village, for their honeymoon. Unfortunately, because of the war between Serbia and Austria-Hungary, he was arrested as a Serbian citizen and put in prison in Osijek. Benefiting from the help of Professor Emmanuel Czuber, he was liberated but had to exile in Budapest. During the 4 years that he had to spend in Budapest, he had access to the Library of the Hungarian Academy of Sciences owing to its Director, Kolomon von Celia, another lover of mathematics. This gave him the opportunity to work on the mathematical theory of climate change on Mars, which laid the foundations of modeling the climate of the Earth and of the other planets (Milankovitch 1914, 1916). He returned to Belgrade with his family in March 1919 and was promoted to full Professor at the University of Belgrade.

His main contribution to science dates from this time with his first monograph, written in French and published in 1920 in the Publications of the Yugoslavian Academy of Sciences and Arts of Zagreb by Gauthier Villars in Paris: “Théorie Mathématique des Phénomènes Thermiques produits par la Radiation Solaire.” It is the need to clarify and critically analyze all the calculations available at that time which led him to write such a bible for the astronomical theory and insolation. It is amazing to see that most of the fundamental concepts of the astronomical theory developed by Milankovitch are already present in great detail in this monograph. In the first part, he formulates ways to compute the instantaneous and daily insolation (incoming solar radiation) and the irradiation received over a season and for each hemisphere. In addition to these formulas already available in L.W. Meech (1856), he introduced those for calculating the irradiation for any interval of the year. Very surprisingly he did it only through series expansion

without using a much better mathematical tool, the elliptic integrals, introduced by L.W. Meech in 1855 and developed extensively by Chr. Wiener in 1876. But a large part of the monograph is devoted to the impact of the atmosphere on insolation and climate including the problem of the albedo-temperature feedback for which he introduced the idea of snowline. His development of one of the very first climate models (if not the first) based on physical principles is probably the most original contribution of Milankovitch to science, but unfortunately the least cited. In the second part, tables with numerical values are given for the interval from 500,000 years BP to the present. These were based on Stockwell for the orbital elements and Pilgrim for the numerical values of the three astronomical elements. From these numerical values, he counted the number of cycles over 500,000 years to identify the average period of climatic precession: 20,700 years which was already estimated theoretically by Adhémar about one century before, of obliquity: 40,040 years and of eccentricity: 91,800 years. No attempt was made, however, to find an analytical expression which lead to the list and origin of all the spectral components characterizing the long-term variations of these astronomical parameters (this became available much later in Berger 1978a). From these numerical values he also produced tables and figures for insolation from 130,000 years BP to the present, including his “equivalent latitudes,” i.e., the latitudes which presently receive, at the summer solstice, the same amount of energy as 70°N in the past. Finally, one section is devoted to the secular motion of the poles and one to the climate of the Planets. Significant to the scrupulous honesty of Milankovitch is a 13-page list of references on which he based his work.

It is also in 1920 that he was elected a member of the Serbian Academy of Sciences and Arts. A few years later, he was invited to participate in the ecumenical congress of the Eastern Orthodox Church held in Constantinople (Istanbul today) on May 1, 1923. On this occasion, he calculated a new calendar which appeared to be the most accurate at that time (Milankovitch 1923). It was accepted by the congress, but only partially implemented in practice. His fundamental research on incoming solar radiation did not prevent him to continue to work as a civil engineer and to start writing popular books, like “Through the Distant Worlds and Times,” a collection of letters written

to a young (virtual?) friend and published in 1928 (Milankovitch 1928).

Captivated by the Milankovitch monograph, Wladimir Köppen offered to collaborate with him on the study of past climates. This was a key step for the recognition of Milankovitch's work. His insolation curves became much better known after Wladimir Köppen and Alfred Wegener introduced them for the equivalent latitudes 55, 60, and 65°N, and the caloric summer insolation at 65°N and 65°S, in their work "Die Klimate der geologischen Vorzeit" (Climate of the Geological Past) published in 1924. In 1927, he was invited to contribute to two important publications. One was the "Handbuch der Klimatologie" for which he wrote the introduction: "Mathematical science of climate and the astronomical theory of climatic variations" published in 1930 in German (Milankovitch 1930). In this chapter, we find, as in his 1920 monograph, his calculations of the daily insolation and of the energy received from the Sun over the hemispheres and the whole Earth for all latitudes and for different seasons, and a chapter on modeling the influence of the atmosphere on surface air temperature and climate. It is also in this publication that a chapter is devoted to the climate of the past 600,000 years with his famous curve of the 65°N equivalent latitude comparing his calculation based on Pilgrim and Stockwell used in his 1920 monograph to those obtained when using Le Verrier and Miskovitch (1931). The second in which he was asked to contribute was the "Bontraeger Handbuch der Geophysik" published in 1931. There, his chapter: "Position and Motion of the Earth in the Universe" shows his skill and great passion for the theory of planetary motion which is at the heart of his astronomical theory of paleoclimates (Milankovitch 1931). In the following years, Milankovitch concentrated on the impact of snow on the summer insolation. His results (Milankovitch 1938a) were very helpful to geologists because they allowed calculating the long-term variations of the snow line over the last 600,000 years.

In 1939, pulling together his earlier papers in a single work, he decided to write his "Kanon der Erdbestrahlung und seine Anwendung auf das Eiszeitenproblem" published in 1941 by the Königlich Serbische Akademie (Milankovitch 1941). The last page on the Kanon was printed on 2 April 1941, but the bombing of Belgrade on 6 April destroyed

16 pages of the book. The only copy left and kept by Milankovitch allowed finally the whole book to be rebounded a few weeks after the German air raid and the first sample of copies of the Kanon to reappear in the autumn of 1941. The German edition was translated into English in 1969: "Canon of Insolation and the Ice Age Problem" by Israel Program for Scientific Translation and published for the Department of Commerce and the National Science Foundation, and republished in 1998 by the Zavod za udzbenike i nastavna sredstva in Belgrade with an additional 35-page biography of Milankovitch by Nikola K. Pantic.

This book, being more complete than his 1920 monograph, is a real compendium on the astronomical theory. It is divided into six parts. Parts One and Two, devoted to the planetary motion around the Sun and the rotation of the Earth, provide all the necessary information to compute the numerical values of the eccentricity, obliquity, and climatic precession. Part Four deals with the terrestrial insolation and its secular changes and permits the computation of the daily insolation, seasonal irradiation and the caloric season insolation, but also their long-term variations. In paragraph 86 (of the 1969 English translation), Milutin Milankovitch stresses again the influence of obliquity on insolation, as was done by his predecessors, but with many more details: "The variations of the quantities of radiation at an increase of obliquity by 1°, already published in 1914, were of fundamental importance because they showed for the first time the influence of the variations of obliquity upon insolation in full detail....an increase of obliquity slightly reduces the annual irradiation of the equatorial zones while those of the polar zones are notably increased. . . boundary lies at 43°33'. . .it reduces the geographical contrast. The summer radiation is reduced with an increase of obliquity only up to 11°23', otherwise it is increased. The winter radiation is reduced at all latitudes." For the irradiation over a season (paragraph 85), we find: "Wiener in his treatise. . . His results agree exactly with mine, though his method of computation is different. The same is also true of the results obtained by Lambert, Meech, Angot and Hargreaves." As in his preceding papers, he did not attempt to use the elliptic integrals, although their numerical calculation was available (King 1924). This might have helped him to resolve the problem raised by the convergence of his series expansion for the insolation at high latitudes about which he wrote

(end paragraph 76): “For the higher latitudes (*above* 55°), for which a greater number of coefficients would be necessary, we would have to set up a greater number of equations...”) It is Fempl (1957, 1958), Milankovitch’s assistant and colleague, who has started using the elliptic integrals for computing the long-term variations of insolation up to the latitudes of 80° and 85°. It is also in this chapter of his book that Milankovitch came back with the average and extreme periodicities of the astronomical elements that he deduced from their numerical values calculated either from Pilgrim-Stockwell (Table VIII) or from Le Verrier-Miskovitch (Table IX): “The secular variations of precession has a rather irregular behaviour...with an average interval of 21,000 years (16,200–25,800 years). The average period of the oscillations of eccentricity amounts to 92,000 years (77,000–103,000 years). The average between two consecutive maxima of obliquity was on the whole about 40,000 years (38,000–45,000 years).” We find however no indication about the split of the 21,000-year precession period into 19,000 and 23,000 years (as calculated by Berger 1978a) and found also in the geological records (Hays et al. 1976). This split is playing a fundamental role in the explanation of the 100,000-year cycle found in geological record, as this period is often assumed to originate from a nonlinear response of the climate system to these two precessional periods (Wigley 1976; Berger 1989). The same is true for the Berger (1978a) 400,000-year cycle which is a key period in the search for analogs of our interglacial and its future (Berger and Loutre 1996, 2002). The 72 pages of Part Five are devoted to his mathematical climate research, exploring the influence of insolation on the Earth’s temperature and atmosphere. Part Six deals extensively (117 pages) with the Ice Age, its mechanism, structure, and chronology. In Part Two, Milankovitch develops also the secular motion of the poles, another subject which fascinated him.

During World War II, Milankovitch decided to write his memoirs, not because “he considered himself as an important scientist, but because nobody knew him and his contributions better than him.” This comprehensive autobiography of about thousand pages, “Memories, experiences and knowledge,” written in Serbo-Croatian was published by the Serbian Academy of Sciences and Arts (Milankovitch 1950, 1952, 1957, 1979) but never translated. This is one of the

reasons which encouraged Vasko Milankovitch, Milutin’s son, to write the history of his father’s life (Milankovitch 1995). The most important human and scientific features of Milutin Milankovitch’s life are described in a lively and lovely way. This book will remain the most important contribution to Milankovitch’s biography. To my knowledge, there are mainly four out in Serbian: Berger and Andjelic (1988) in French, Pantic (1998) in English, Petrovic (2002) in both English and Serbian, and Petrovic (2011) in Russian. However, there are many short notes about Milankovitch’s life and the astronomical theory; some are excellent summaries, others do not necessarily provide an objective view of Milankovitch’s contributions to science.

Following World War II, Yugoslavia became a federal state relatively held behind the Iron Curtain. Milankovitch became increasingly disappointed mainly because of his difficulty to continue working in his field, the German troops having, during their retreat, destroyed the library of the Institute of Mathematics patiently created by Milankovitch over decades. It is the time he completed his book on the history of astronomy (Milankovitch 1948), a textbook still used presently at the Faculty of Astronomy in Belgrade. In 1947, his son Vasko and his daughter-in-law Vera left the communist country to finally settle in Australia. Milankovitch “tried to bridge the enormous gap which separated them, looking to their future and offering advice...” In January 1953, he wrote to Vasko: “One consolation is that my Astronomical Theory of Climatic Changes is appearing more and more in the scientific literature around the World. My scientific authority has given me, even here, a unique independent position, so no one bothers me and I live in peace” (Milankovitch 1995). Unfortunately, his experience at the I.N.Q.U.A. conference in Rome in September 1953, the last meeting he attended, was very unfortunate and most regrettable: he was forced by the president of the session, Richard Flint, to leave the floor after delivering only half of his paper (Jovanovic et al. 2004), although he was doing his best by delivering his lecture in French, not his native language (Milankovitch 1954, 1956). This often mentioned incident is based mainly on Milankovitch’s own recollection and feelings, but it was also reported to me by the Belgian climatologist Étienne Bernard who was present. I would like to see whether there is another independent account, either from Flint’s

papers or memoirs, if such exist, or from any other attendee of the Congress. Milankovitch might have overreacted, although this is purely hypothetical. His last publication was on the Astronomical theory published by the Serbian Academy of Science in 1957.

Milutin Milankovitch died in Belgrade on 12th December 1958. He was initially buried in the Topuzovic family grave in Belgrade, but later in the Milankovitch family grave in Dalj.

The Milankovitch Debate

If we consider the Milankovitch insolation curve, however, we are left in no doubt that Milankovitch's success was partial, because the Quaternary has had many more glacial periods than was claimed during the first part of the twentieth century (Kukla 1975a). In fact, until roughly 1970 the Milankovitch theory was largely disputed because the discussions were based on fragmentary geological sedimentary records and on inaccurate time scales, and because the climate was considered too resilient to react to "such small changes" in his summer half-year caloric insolation (Simpson 1940). Moreover, the accuracy of the long-term variations of the three astronomical parameters and of the related insolation (namely in polar latitudes) had also to be evaluated.

The first criteria used to test the astronomical theory was the visual or statistical relationship between minima and maxima of geological and insolation curves, the Milankovitch summer radiation curve for 65°N being used more frequently because of the more extensive nature of Pleistocene glaciation in the Northern Hemisphere.

These qualitative coincidences of the principal maxima and minima of both curves would, however, have remained somewhat illusory until the ambiguities stemming from a priori assumptions about sensitive latitudes and response mechanisms were resolved. As an attempt to solve this problem, many insolation values for different seasons and latitudes or combination of them (Broecker and van Donk 1970; Kukla 1972, 1975b; Kukla and Kukla 1972; Kukla et al. 1981) were used up to the late 1970s. For a more extensive review of the publications of this epoch and the following ones, the reader should refer to Berger (1988).

In the meantime, climatologists (Shaw and Donn 1968; Budyko 1969; Sellers 1970; Saltzman and

Vernekar 1971) started to approach the problem theoretically, but found that the climatic response to orbital change was too small to account for the succession of Pleistocene ice ages. However, if these early numerical experiments are viewed narrowly as a test of the astronomical theory, they are open to question because the models used much too simple parameterizations of important physical processes.

The Milankovitch Renaissance

In the late 1960s, judicious use of radiometric dating and other techniques gradually clarified the details of the time scale, better instrumental methods came on the scene for using oxygen isotope as an indicator of ice volume and ocean temperature (Shackleton and Opdyke 1973) but also salinity (Duplessy 1970; Duplessy et al. 1991), ecological methods of core interpretation were perfected (Imbrie and Kipp 1971), global climates in the past were reconstructed (CLIMAP Project Members 1976), and atmospheric general circulation models and climate models became available (Alyea 1972). In 1969, Hays et al. showed that 8 distinct carbonate cycles are present in the Brunhes series of their equatorial Pacific core with periodicities of about 75,000 years in the upper Brunhes to over 100,000 years in the lower Brunhes. This progressive transition from the 40-ka world characterizing the lower Pleistocene (Ruddiman et al. 1986) to the 100-ka of the upper Pleistocene was confirmed by an evolutive spectral analysis made by Pestiaux and Berger (1984). Owing to the improvements of the 1970s, Hays et al. (1976) showed, for the first time, that quasi-periods of 100,000, 41,000, 23,000, and 19,000 years are significantly present in proxy records of the past climate. Independently, Berger (1973, 1976, 1978a) had already found these periods in the long-term variations of eccentricity, obliquity and climatic precession that he calculated using a new more accurate solution of the planetary system. This definitely confirmed the astronomical origin of the periodicities found in geological records. The existence, in particular, of a double precessional peak both in the geological record and in the astronomical solution has been, according to John Imbrie himself, one of the first most delicate and impressive tests of the Milankovitch theory and critical for its validation.

These results were at the origin of a revival of the astronomical theory of paleoclimates. New researches were going to be initiated in the four main branches of any astronomical theory, namely: (1) the computation of the astronomical elements, (2) the computation of the appropriate insolation parameters, (3) the development of suitable climate models, and (4) the analysis of geological data in both the time and frequency domains in order to investigate the physical mechanisms which are responsible for the long-term climatic variations and to calibrate and validate the climate models. An extensive list of the main contributions to this revival published up to 1980 is given in Berger (1988).

The large amount of papers related to the astronomical theory over the last 30 years show updates of the Milankovitch calculations and theory, but also new proposals of how astronomical elements of the Earth's orbit and axis of rotation might impact climate (Shackleton et al. 1990; Berger et al. 1995). The list here below does not include modeling the response of the climate system to astronomical forcing (for a review see, e.g., Kutzbach 1985; Berger 1995; Stocker and Marchal 2001; Claussen et al. 2002; Sirocko et al. 2007; PMIP-Paleoclimate Modeling Intercomparison Programme) but focuses only on research dealing with the astronomical parameters and the related solar irradiation which were at the basis of Milankovitch's work. The purpose is not to produce an extensive review of what has been done since Milankovitch's last publication (this would be out of the scope of this introductory survey), but rather to give a feeling of how fertile the work of Milankovitch was.

Milankovitch Follow-Up

About the Astronomical Solutions

New analytical astronomical solutions for the Quaternary appeared at the end of Milankovitch's life with Brouwer and Van Woerkom (1950) and later with Sharaf and Budnikova (1967), Anolik et al. (1969), Bretagnon (1974), Berger (1976, 1977, 1978a), Berger and Loutre (1991), Laskar (1988) and Laskar et al. (2004).

Milankovitch concentrated on how to obtain the best numerical values for the long-term variations of the three astronomical parameters and the insolation. His primary aim was to produce curves for climate or

proxies (like his 65°N equivalent latitude) that, as shown in Penck, Brückner, Köppen, and Wegener's books, he correlated with the first geological record covering the last million years. Apparently, probably because of the limited number of data and techniques available at that time, he did not draw attention to the spectral characteristics of the astronomical parameters. He could have done it from a complete analytical solution of the system of equations which governs the motions of the Moon and the planets. Such analytical solution, calculated by Berger in the early 1970s, generated the numerical values of precession, obliquity and eccentricity expressed in trigonometric form as quasi-periodic functions of time:

$$e \sin \tilde{\omega} = \sum P_i \sin(\alpha_i t + \eta_i),$$

$$\varepsilon = \varepsilon^* + \sum A_i \cos(\gamma_i t + \zeta_i)$$

$$e = e^* + \sum E_i \cos(\lambda_i t + \phi_i)$$

where the amplitudes P_i , A_i , E_i , frequencies α_i , γ_i , λ_i and phases η_i , ζ_i , ϕ_i were calculated in the 1970s by Berger (1978a) and later by Berger and Loutre (1991) using the development of the orbital elements by respectively Bretagnon (1974) and Laskar (1988) and the analytical expansions of obliquity and precession by Anolik et al. (1969). Such expressions for $e \sin \tilde{\omega}$, ε and e can be used over 1–3 million years (Berger and Loutre 1992), but for more remote times numerical solutions are necessary (see below, Laskar et al. 2004).

These formulae show that ε and e vary quasi-periodically only around the constant values ε^* (23.32°) and e^* (0.0287). This implies that, estimating the magnitude of the terms the insolation formulae where ε and e occur, they may be considered as a constant to a first approximation. Moreover, in the insolation formulas, the amplitude of $\sin \tilde{\omega}$ is modulated by eccentricity in the term $e \sin \tilde{\omega}$. The envelope of $e \sin \tilde{\omega}$ is therefore given exactly by e , allowing the frequencies of e to be expressed as combinations of the frequencies of $\tilde{\omega}$; for example: $\lambda_1 = \alpha_2 - \alpha_1$, $\lambda_2 = \alpha_3 - \alpha_1$, $\lambda_3 = \alpha_3 - \alpha_2$, $\lambda_4 = \alpha_4 - \alpha_1$, $\lambda_5 = \alpha_4 - \alpha_2$, and $\lambda_6 = \alpha_3 - \alpha_4$ (Berger 1978a; Berger and Loutre 1990). This leads to the conclusion that the periods characterizing the expansion of e are nonlinear combinations of the precessional periods (and vice versa) and, in particular that the eccentricity periods close to 100,000 years

originate from periods close to 23,000 and 19,000 years in precession. This also shows that the frequencies of a given parameter are not all independent of each other. For example, $\lambda_3 = \lambda_2 - \lambda_1$, a relationship which can also be deduced directly from the frequencies of the fundamental orbital elements when creating the series expansion of the eccentricity. Similar relationships between the periods of eccentricity, obliquity and precession are available in Berger and Loutre (1990).

The full spectral characteristics of the astronomical elements and of insolation date back only from the 1970s. Emiliani (1955), like Milankovitch (1920) 35 years earlier, estimated the mean periods of the astronomical parameters by counting the number of peaks from the Milankovitch curves which gave him about 92,000, 40,000, and 21,000 years for e , ε , and $e \sin \tilde{\omega}$, respectively. These were confirmed in 1973 when Berger had completed his calculation of the long-term variations of precession, obliquity and eccentricity. Besides its high accuracy, the Berger calculation provided indeed, for the first time, a full list as well as the origin of the periods characterizing the theoretical expansion of e (with periods of 413,000, 95,000, 123,000, 99,000, 131,000, and 2,305,000 years in decreasing order of amplitude of the terms), of ε (with periods of 41,000, 53,600, and 29,700 years) and of $e \sin \tilde{\omega}$ (with periods of 23,700, 22,400, 18,900, and 19,200 years) (see also Berger 1978a, and Berger and Loutre 1991). Among these periods, those of 413,000, 2,305,000, 54,000, 23,000, and 19,000 years were new, their existence having never been even suspected before.

In their Science paper, Hays et al. (1976) used a spectral analysis technique which they applied on the numerical values of the astronomical parameters calculated by Brouwer and Van Woerkom (1950) and Vernekar (1972) and found also 125,000 and 96,000 years for e ; 41,000 years for ε ; and 23,000 and 19,000 years for precession.

Because of new techniques available (like the wavelet transforms), the complex structure of the long-term variations of the astronomical parameters became possible (Berger et al. 1998). For the eccentricity, it can be shown that the 100,000 years period is not stable in time, being remarkably shorter near the present. Actually, the most important theoretical period of eccentricity, 400,000 years, is weak before 1 Ma BP, and becomes particularly strong over the

next 400,000 years, with the strength of the components in the 100,000 years band changing in the opposite way. It is worth pointing out that this weakening of the 100,000 years period started about 900,000 years ago when this same period began to appear very strongly in paleoclimatic records. This implies that the 100,000 years period found in paleoclimatic records is definitely not linearly related to eccentricity. We are now approaching a minimum of e at the 400,000 years time scale: at 27,000 years AP (after present), the Earth's orbit will be circular. Actually, transitions between successive strong 400,000-year cycles (as it is the case now) are characterized by very small eccentricity and short eccentricity cycles with a low amplitude of variation. At the 400,000-year time scale, the amplitude and frequency modulations of precession are inversely related: when the amplitude is small, the period is short. The reverse is observed at the 100,000-year time scale where a large amplitude is accompanied by a short period and vice versa. For obliquity, the main period is pretty stable, but there is an amplitude modulation with time duration of about 1,300,000 years (Mélise et al. 2001). At that time scale, a large amplitude corresponds to a short period, the reverse being observed at the 170,000-year time scale. The spectra of both the amplitude and frequency modulations of obliquity display significant power at 171,000 and 97,000 years (Mélise et al. 2001). Although this last period might look close to the so-called 100,000 years eccentricity period, these periods are not related.

Because of the great interest devoted to the 100,000-year cycle (Crucifix 2011), the most important period in ice volume and CO₂ record, it was interesting to look for the presence of the 100,000-year cycle in the astronomical data first (Berger et al. 2005a). In addition to the already mentioned 100,000-year cycles in the eccentricity and amplitude modulation of obliquity, this cycle can also be found in the rate of change of eccentricity where it becomes stronger than the 400,000-year cycle, contrary to what happens in the eccentricity. It is also present in the inclination of the Earth's orbit on the invariable plane (plane perpendicular to the total angular momentum of the planetary system), but its origin prevents it from being associated with the 100,000-year cycle present in the geological record.

Geological record are now available with a high accuracy over tens of millions of years (e.g., Lourens

et al. 2001), allowing to calibrate the astronomical solutions by Laskar (1990, 1999) and Laskar et al. (2004) who was the first to calculate them over such long time scales (a possibility foreseen by Deprit et al. (1984) at the Milankovitch symposium (Berger et al. 1984)).

Because of the huge ice sheets present during the Pleistocene glaciations, their influence over the spectral characteristics of the astronomical elements was estimated by Dehant et al. (1990). For the much earlier geological periods (e.g., Hinnov and Goldhammer 1991), a similar sensitivity of the astronomical frequencies was performed to the changes in the Earth's rotation rate, the distance from the Earth to the Moon and the dynamical ellipticity of the Earth (Berger et al. 1989, 1992; Peltier and Jiang 1994), showing a shortening of all of them back in time.

For more recent times, the variations of the astronomical parameters at the decadal to millennial time scales became available owing to the work of Bretagnon (1982) and its application to the astronomical theory by Loutre et al. (1992) and Bertrand et al. (2002).

About Insolation

In addition to the critical high northern latitudes proposed by Milankovitch, other latitudes were suggested, as for example the tropics (Bernard 1962) or the equatorial latitudes (McIntyre and Molfino 1996; Berger and Loutre 1997), as well as seasons other than Northern Hemisphere summer, as for example fall and winter (Kukla 1975b).

In addition to the caloric insolation of Milankovitch (up-dated by Vernekar 1972 and Berger 1978b), the seasonal and latitudinal distribution (Berger 1979) of the daily solar irradiance (Berger 1978a) began to be used to force climate models (Kutzbach 1981; Berger et al. 1990; Gallée et al. 1991, 1992; Ganopolski and Calov 2012). This led to a consideration of precession as a main driving factor of the climate system as it is for the daily irradiance everywhere on Earth (except close to the polar night). Such behavior is fundamentally different from the behavior of the Milankovitch caloric insulations where precession and obliquity controls respectively the low and high latitudes (Berger and Pestiaux 1984). This is the reason why, more recently, the total energy received during the

astronomical seasons, which depends exclusively upon obliquity (Berger et al. 2010), is tentatively used to explain climatic changes of the lower Pleistocene and the glacial–interglacial cycles of the last 900,000 years. Huybers and Wunsch (2005) argue that the 41,000-year cycle has always been dominant and the 100,000-year cycle is created by averaging groups of two and three obliquity cycles (80,000 and 120,000 years). This theory is consistent with the multistate model by Paillard (1990) and the model by Ditlevsen (2008), leading to the 100,000-year cycle being a nonlinear response to the 41,000-year obliquity cycle, but remains controversial.

Taking back the idea of Milankovitch about the important role played by the albedo of the Earth's surface, analysis of such impact on the spectral characteristics of solar energy absorbed at the surface of the Earth (Blatter et al. 1984; Tricot and Berger 1988) showed that the gradient of insolation between the tropics and the polar regions has a spectrum which depends upon the kind of insolation used; the 40,000-year periodicity dominates in the extraterrestrial insolation whereas in the absorbed insolation by the surface, a 23,000-year signal is also present. This difference is due to attenuation by the atmosphere and the surface albedo, which reduces insolation variations in the high polar latitudes more strongly than in the tropics.

Much can be said about the astronomical signals found in the paleoclimatic record and about modeling the response of the climate system to the astronomical forcing (e.g. Berger et al. 2005b), but that would be beyond the scope of this short introduction to the history of the astronomical theories over the last 200 years.

Conclusions

The purpose of this short note was to describe the scientific environment in which Milankovitch lived and developed his astronomical theory of paleoclimates. It was also a good opportunity to give credits to those scientists who introduced the key concepts of the astronomical theory of paleoclimates. These early scientists are often forgotten in the references list of papers where some authors are crediting Milankovitch for most of the ideas which in fact have been discussed much before his time or after. Milankovitch would probably have objected to this oversight as he was

known for his meticulous referencing on which he based his research and his integrity. For example, in his conference at the Charles University on 11 November 1937, he thanked not less than “34 eminent scientists for their fundamental contributions to geology and climate on which he could base his own work,” Milankovitch 1938b).

The most striking and original feature of the way Milankovitch conducted his research lies in his deductive approach. Contrary to most of his predecessors who were concentrating their efforts on specific problems, he started with the development of a general astronomical theory of insolation and climate applicable to the Earth and planets like Venus and Mars in order to understand better the ice ages.

The most important contributions of Milankovitch are:

1. Writing such a compendium where all chapters related to the astronomical theory are clearly written with all the details necessary for an in-depth understanding—masterfully written lecture notes.
2. Introducing a new insolation parameter, the caloric season insolation. Although it does not completely solve the problem of using the irradiation over a given interval of the year (the beginning and end are changing with time), it has the advantage to have a fixed length accumulating the energy requested by many natural living species.
3. Introducing the concept of physical models based on the principles of physics to try approaching the real climate much better than by using only the energy available at “the top of the atmosphere.” Milankovitch actually wrote many more papers on modeling the impact of atmosphere and of the surface of the Earth on the insolation and climate than on insolation itself. He must definitely be considered as the “father” of climate modeling. Unfortunately very few people acknowledge his important contribution to this research field. For example, using only the daily insolation “at the top of the atmosphere” presents a real danger, namely because the latitudinal distribution of this parameter, the magnitude of which is much larger at the summer poles than at the equator, leads to a latitudinal gradient of insolation which has a sign opposite to the sign of the latitudinal gradient of temperature, usually cited to control the strength of the general circulation of the atmosphere, a key point for climate.

Contrary to what is often claimed, Milankovitch, as he recognized himself, cannot be credited for:

1. The calculation of eccentricity, obliquity and precession, referring to Stockwel-Pilgrim and to Le Verrier-Milankovitch respectively in his 1920 monograph and his 1941 Canon.
2. The calculation of daily insolation and the irradiation received during the astronomical seasons, which were already published decades before by Meech and Wiener. However, Milankovitch has introduced a clear analysis of the impact of obliquity variation on insolation and the calculation of the energy available for a given time interval of the year.
3. The very fundamental hypothesis that the occurrence of the Northern Hemisphere summer at the aphelion is the cause of glaciations. This is probably the greatest mistake done in the present-day literature because this is exactly what people refer to as the “Milankovitch theory of paleoclimates.” This theory must definitely be attributed to Murphy who introduced the idea four decades before Milankovitch took it back.
4. Some periods characterizing the long-term variations of the astronomical parameters. Not only Milankovitch did not seem to be much interested by these periods, but the precessional period of 21,000 years was well known since Adhémar at least and the periods of about 400,000, 54,000, 30,000, 23,000 and 19,000 years as well as of 2,305,000 and 1,300,000 years appeared for the first time with Berger’s work in the early 1970s.

Before ending this short note, I would like to stress again that my above remarks have been clearly underlined by Milankovitch himself, rendering unto Caesar that which is Caesar’s, and does not minimize his fundamental contribution to the scientific understanding of long-term climatic variations. Finally, let us point out that this great scientist is also one of the very few, even now, who lectured and published not only in his native language, but also in German, French, and Russian.

Acknowledgements A. Berger benefits from a European Research Council Advanced Grant N°227348, EMIS of the programme SP2-Ideas. Thanks are due to Vladimir Jankovic for his advices as a historian of sciences, to Fedor Mesinger and Jim Hays for their editorial help and to Tobias Krüger and Aleksandar Petrovic for their comments.

References

- Adhémar JA (1842) *Révolution des mers, Déluges périodiques*. Première édition: Carilian-Goeury et V. Dalmont, Paris. Seconde édition: Lacroix-Comon, Hachette et Cie, Dalmont et Dunod, Paris, 359 p
- Agassiz L (1838) Upon glaciers, moraines, and erratic blocks. Address delivered at the opening of the Helvetic History Society at Neuchâtel, 24 July 1937 by its President L. Agassiz. *Edinb New Philos J* 24(48):364–383
- Agassiz L (1840) *Études sur les Glaciers*. Jent and Gassmann, Neuchâtel, 346 p
- Alyea FN (1972) Numerical simulation of an ice-age paleoclimate. *Atmosphere Science Papers* 193, Colorado State University, Fort Collins, CO
- Anolik MV, Krasinky GA, Pius LJ (1969) Trigonometrical theory of secular perturbations of major planets (in Russian). *Trudy Inst Teor Astr Leningr* 14:1–48
- Arrhenius S (1896) On the influence of carbonic acid in the air upon the temperature of the ground. *Lond Edinb Dublin Philos Mag J Sci* 41(251):237–276
- Ball R (1891) *The cause of an ice age*. D. Appleton, New York, 180 p
- Bard E (2004) Greenhouse effect and ice ages: historical perspective. *CR Geosci* 336:603–638
- Benhardi AR (1832) Über das Vorkommen der Geschiebe in den Süd-Baltischen Ländern, besonders in der Mark Brandenburg. *Jahrbuch für Mineralogie, Geognosie, Geologie und Petrefaktenkunde* vol III, pp 257–267, 419
- Berger A (1973) *Théorie Astronomique des Paléoclimats*. Dissertation doctorale, Université catholique de Louvain, Belgium, 2 volumes
- Berger A (1976) Obliquity and general precession for the last 5 000 000 years. *Astron Astrophys* 51:127–135
- Berger A (1977) Long-term variations of the Earth's orbital elements. *Celestial Mech* 15:53–74
- Berger A (1978a) Long-term variations of daily insolation and Quaternary climatic changes. *J Atmos Sci* 35(12):2362–2367
- Berger A (1978b) Long-term variations of caloric insolation resulting from the Earth's orbital elements. *Quat Res* 9:139–167
- Berger A (1979) Insolation signatures of Quaternary climatic changes. *Il Nuovo Cimento* 2C(1):63–87
- Berger A (1988) Milankovitch theory and climate. *Rev Geophys* 26(4):624–657
- Berger A (1989) Pleistocene climatic variability at astronomical frequencies. *Quat Int* 2:1–14
- Berger A (1995) Modelling the response of the climate system to astronomical forcing. In: Henderson-Sellers A (ed) *Future climate of the world. A modelling perspective*. Elsevier, Amsterdam, pp 21–69
- Berger A, Andjelic PT (1988) Milutin Milankovitch, père de la théorie astronomique des paléoclimats. *Histoire et Mesure* III-3:385–402
- Berger A, Loutre MF (1990) Origine des fréquences des éléments astronomiques intervenant dans le calcul de l'insolation. *Bulletin de la Classe des Sciences de l'Académie royale de Belgique* 6ème série I:1–3, 45–106
- Berger A, Loutre MF (1991) Insolation values for the climate of the last 10 million years. *Quat Sci Rev* 10(4):297–317
- Berger A, Loutre MF (1992) Astronomical solutions for paleoclimate studies over the last 3 million years. *Earth Planet Sci Lett* 111(2/4):369–382
- Berger A, Loutre MF (1994) Precession, eccentricity, obliquity, insolation and paleoclimates. In: Duplessy JC, Spyridakis MT (eds) *Long-term climatic variations: data and modeling*, vol I22, NATO ASI series. Springer, Berlin, pp 107–151
- Berger A, Loutre MF (1996) Modelling the climate response to astronomical and CO2 forcings. *CR Acad Sci Paris* 323 (1):1–16, série IIa
- Berger A, Loutre MF (1997) Intertropical latitudes and precessional and half precessional cycles. *Science* 278:1476–1478
- Berger A, Loutre MF (2002) An exceptionally long interglacial ahead? *Science* 297:1287–1288
- Berger A, Pestiaux P (1984) Accuracy and stability of the Quaternary terrestrial insolation. In: Berger A, Imbrie J, Hays J, Kukla G, Saltzman B (eds) *Milankovitch and climate*. Reidel, Dordrecht, pp 83–112
- Berger A, Yin QZ (2012) Astronomical theory and orbital forcing. In: Matthews JA (ed) *The Sage handbook of environmental change*, Vol 1, Section III Causes, mechanisms and dynamics of environmental change. Sage, London
- Berger A, Imbrie J, Hays J, Kukla G, Saltzman B (eds) (1984) *Milankovitch and climate. Understanding the response to orbital forcing*, vol 126, NATO ASI series C. Reidel, Dordrecht, 895 pp
- Berger A, Loutre MF, Dehant V (1989) Influence of the changing lunar orbit on the astronomical frequencies of pre-Quaternary insolation patterns. *Paleoceanography* 4(5):555–564
- Berger A, Gallée H, Fichefet T, Marsiat I, Tricot C (1990) Testing the astronomical theory with a coupled climate-ice sheet model. *Global Planet Change* 3(1/2):125–141
- Berger A, Loutre MF, Laskar J (1992) Stability of the astronomical frequencies over the Earth's History for paleoclimates studies. *Science* 255:560–566
- Berger A, Loutre MF, Mélice JL (1998) Instability of the Astronomical Periods from 1.5 Myr BP to 0.5 Myr AP. *Palaeoclim Data Model* 2(4):239–280
- Berger A, Mélice JL, Loutre MF (2005a) On the origin of the 100-kyr cycles in the astronomical forcing. *Paleoceanography* 20:PA4019
- Berger A, Ercegovac M, Mesinger F (eds) (2005b) *Paleoclimate and the Earth climate system*. In: *Milankovitch Anniversary Symposium*. Serbian Academy of Sciences and Arts Scientific Meetings, vol. CX, Department of Mathematics, Physics and Geosciences, Book 4, Belgrade, 190 pp
- Berger A, Loutre MF, Yin QZ (2010) Total irradiation during any time interval of the year using elliptic integrals. *Quat Sci Rev* 29:1968–1982
- Berger WH, Bickert T, Wefer G, Yasuda, MK (1995) Brunhes-Matuyama boundary: 790 k.y.date consistent with ODP Leg 130 oxygen isotope records based on fit to Milankovitch template. *Geophys Res Lett* 22(12):1525–1528
- Bernard EA (1962) *Théorie astronomique des pluviaux et interpluviaux du Quaternaire africain*. Acad. Roy. Sc. Outre-Mer, Brussels, Classe Sci. Tech., Mémoire in 8e, nouvelles séries, vol 12, issue1, 232 p
- Bertrand C, Loutre MF, Berger A (2002) High frequency variations of the Earth's orbital parameters and climate change. *Geophys Res Lett* 29(18):40. doi:10.1029/2002GL015622

- Blatter H, Funk M, Ohmura A (1984) Atlas of Solar Climate. Zürcher Geographische Schriften, Heft 10, ETH, Zurich
- Bretagnon P (1974) Termes à longues périodes dans le système solaire. *Astron Astrophys* 30:141–154
- Bretagnon P (1982) Théorie du mouvement de l'ensemble des planètes. Solution VSOP82. *Astron Astrophys* 114:278–288
- Broecker WS, van Donk J (1970) Insolation changes, ice volume and the O¹⁸ record in deep-sea cores. *Rev Geophys* 8(1): 169–198
- Brouwer D, Van Woerkom AJJ (1950) Secular variations of the orbital elements of principal planets. *Astronomical papers prepared for American Ephemeris and Nautical Almanac, US Naval Observatory*, vol 13, issue 2, pp 81–107
- Brückner E, Köppen W, Wegener A (1925) Über die Klimate der geologischen Vorzeit. *Zeitschrift für Gletscherkunde* 14, pp 149–169
- Budyko MI (1969) Effect of solar radiation variations on the climate of Earth. *Tellus* 21(5):611–620
- Chamberlin TC (1882) Preliminary paper on the terminal moraine of the second glacial epoch. U.S. Geological Survey, Annual Report III, pp 291–402
- Chamberlin TG (1899) An attempt to frame a working hypothesis of the cause of glacial epochs on an atmospheric basis. *J Geol* 7:545–561, 607–685, 751–787
- Claussen M, Mysak LA, Weaver AJ, Crucifix M, Fichefet T, Loutre M-F, Weber SL, Alcamo J, Alexeev VA, Berger A, Calov R, Ganopolski A, Goosse H, Lohman G, Lunkeit F, Mokhov II, Petoukhov V, Stone P, Wang Z (2002) Earth system models of intermediate complexity: closing the gap in the spectrum of climate system models. *Clim Dyn* 18:579–586
- CLIMAP Project Members (1976) The surface of the Ice-Age Earth. *Science* 191:1131–1136
- Croll J (1864) On the physical cause of the change of climate during geological epochs. *Philos Mag* 28(187):121–137
- Croll J (1867a) On the eccentricity of the Earth's orbit, and its physical relations to the glacial epoch. *Philos Mag* 33(221): 119–131
- Croll J (1867b) On the change in the obliquity of the ecliptic, its influence on the climate of the polar regions and on the level of the sea. *Philos Mag* 33:426–445
- Croll J (1875) Climate and time in their geological relations. Appleton, New York
- Crucifix M (2011) Glacial-interglacial cycles. In: Singh VP, Singh P, Haritashya UK (eds) Springer Encyclopaedia of snow, ice and glaciers. Springer Dordrecht NL, pp 359–365
- Culverwell EP (1894) A criticism of the astronomical theory of the ice age. *Nature* 51:33–35
- Darwin C (1872) On the origin of species by means of natural selection. D. Appleton, New York, pp 342–350, 1st edition, 1859, John Murray, London
- de Charpentier J (1836) Account of one of the most important results of the investigations of M. Venetz regarding the present and earlier condition of the glaciers of the Canton du Valais. *Edinb New Philos J* 21:210–222
- de Charpentier J (1841) Essai sur les glaciers et sur le terrain erratique du basin du Rhône. M. Dubroux, Lausanne, 363 p
- de Marchi L (1895) La causa dell'era glaciale. *Premiato dal R. Istituto Lombardo*, Pavia
- Dehant V, Loutre MF, Berger A (1990) Potential impact of the Northern Hemisphere Quaternary ice sheets on the frequencies of the astroclimatic orbital parameters. *J Geophys Res* 95(D6):7563–7572
- Deprit A, Bretagnon P, Berger A (1984) Orbital elements and insolation. In: Berger A, Imbrie J, Hays J, Kukla G, Saltzman B (eds) Milankovitch and climate. D. Reidel, Dordrecht, pp 823–826
- Ditlevsen P (2008) The bifurcation structure and noise-assisted transitions in the Pleistocene glacial cycles. *Paleoceanography* 24:PA3204. doi:10.1029/2008PA001673, 11 pp
- Duplessy JC (1970) Note préliminaire sur les variations de la composition isotopique de l'Océan Indien à la relation O¹⁸-salinité. *C R Académie des Sciences de Paris* 271(D): 1075–1078
- Duplessy JC, Labeyrie L, Juillet-Leclerc A, Maitre F, Sarnthein M (1991) Surface salinity reconstruction in the North Atlantic Ocean during the last glacial maximum. *Oceanol Acta* 14(4):311–324
- Ebelmen JJ (1845) Sur les produits de la décomposition des espèces minérales de la famille des silicates. *Ann Mines* 7:3–66
- Ekhholm N (1901) On the variations of the climate of the geological and historical past and their causes. *Q J R Meteorol Soc* 27:1–61
- Emiliani CRW (1955) Pleistocene temperatures. *J Geol* 63(6): 538–578
- Esmark J (1824) Bidrag til vor Jordklodes Historie. *Magazin for Naturvidenskaberne* 2(1):28–49
- Esmark J (1827) Remarks tending to explain the geological history of the Earth. *Edinb New Philos J* 2:107–121
- Evans EP (1887) The authorship of the glacial theory: Karl Schimper. Notes and Comments, *North American Review* (1815–1900), vol 0145, issue 368, July
- Fempl S (1957) Über die Insolation der Polarzonen unsere Erde. *Bulletin de l'Académie Serbe des Sciences*, vol XX, Classe des Sciences Mathématiques et Naturelles, issue 3, pp 41–45
- Fempl S (1958) Variations séculaire d'insolation de la Terre au cours des cent millénaires futurs, vol II. *Académie Serbe des Sciences*, Belgrade, issue 10–20, pp 45–59
- Fleming JR (1998) Historical perspectives on climate change. Oxford University Press, New York, 194 pp
- Fleming JR (2005) James Croll in context: the encounter between climate dynamics and geology in the second half of the nineteenth century. In: Berger A, Ercegovac M, Mesinger F (eds) Paleoclimate and the Earth climate system. Serbian Academy of Sciences, Belgrade, pp 13–20
- Gallée H, van Ypersele JP, Fichefet T, Marsiat I, Tricot C, Berger A (1991) Simulation of the last glacial cycle by a coupled sectorially averaged climate-ice sheet model. I. The climate model. *J Geophys Res* 96(D7):13139–13161
- Gallée H, van Ypersele JP, Fichefet T, Marsiat I, Tricot C, Berger A (1992) Simulation of the last glacial cycle by a coupled sectorially averaged climate-ice sheet model. II. Response to insolation and CO₂ variations. *J Geophys Res* 97(D14):15713–15740
- Ganopolski A, Calov R (2012) Simulation of glacial cycles with an Earth system model. In: Berger A, Mesinger F, Sijacki D (eds) Climate change: inferences from paleoclimate and regional aspects. Springer, Vienna
- Geikie J (1874) The great ice age and its relation to the antiquity of man, 1st edn. W. Isbister, London, 575 p, 2d edn, E. Stanford, London (1877)

- Hargreaves R (1896) Distribution of solar radiation on the surface of the Earth and its dependence on astronomical elements. *Trans Camb Philos Soc* 16:58–94
- Hays JD, Saito TN, Opdyke ND, Burckle LH (1969) Pliocene-Pleistocene sediments of the equatorial Pacific: their paleomagnetic, biostratigraphic and climatic record. *Geol Soc Am Bull* 80:1481–1514
- Hays JD, Imbrie J, Shackleton NJ (1976) Variations in the earth's orbit: pacemaker of the ice ages. *Sciences* 194:1121–1132
- Herschel JW (1832) On the astronomical causes which may influence geological phenomena. *Trans Geol Soc Lond* 3:293–300, 2d Series
- Hinnov LA, Goldhammer RK (1991) Spectral analysis of the Middle Triassic Latemar Limestone. *J Sediment Petrol* 61(7):1173–1193
- Hopfnfer F (1907) Untersuchung über die Bestrahlung der Erde durch die Sonne. *Wiener Sitzungsberichte*, vol CXVI Abt II a
- Howarth HH (1890) A criticism of Dr Croll's theory of alternate glacial and warm periods in each hemisphere and of interglacial climates. *Mem Proc Manch Lit Philos Soc 4th series III*:65–11
- Huybers P, Wunsch C (2005) Obliquity pacing of the late Pleistocene glacial terminations. *Nature* 434(7032):491–494
- Imbrie J, Imbrie KP (1979) Ice ages, solving the mystery. Enslow, Berkeley Heights
- Imbrie J, Kipp NG (1971) New micropaleontological method for quantitative paleoclimatology: application to a Late Pleistocene Caribbean core. In: Turekian KK (ed) *Late Cenozoic glacial ages*. Yale University Press, New Haven, pp 71–181
- Jovanovic M, Markovic S, Gaudery T (2004) Milutin Milankovitch and INQUA. In: *Paleoclimate and the Earth system*, Milutin Milankovitch Anniversary symposium, abstracts, Serbian Academy of Sciences, Belgrade, pp 177–181
- King LV (1924) On the direct numerical calculation of elliptic functions and integrals. Cambridge University Press, Cambridge, 43 p and VIII
- Köppen W, Wegener A (1924) *Die Klimate der geologischen Vorzeit*. Verlag von Gebrüder Bornträger, Berlin, 256 p
- Krüger T (2008) *Die Entdeckung der Eiszeiten: Internationale Rezeption und Konsequenzen für das Verständnis der Klimageschichte*. Schwabe, Basel, 619 p
- Kukla G (1972) Insolation and glacial. *Boreas* 1(1):63–96
- Kukla GJ (1975a) Loess stratigraphy of Central Europe. In: Butzer KW, Isaac GLL (eds) *After the Australopithecines*. Mouton, The Hague, pp 99–188
- Kukla G (1975b) Missing link between Milankovitch and climate. *Nature* 253:600–603
- Kukla G, Kukla HJ (1972) Insolation regime of interglacials. *Quat Res* 2(3):412–424
- Kukla G, Berger A, Lotti R (1981) Orbital signature of interglacials. *Nature* 290(5804):295–300
- Kutzbach JE (1981) Monsoon climate of the early Holocene: climate experiment with the Earth's orbital parameters 9000 years ago. *Science* 214(2):59–61
- Kutzbach JE (1985) Modeling of paleoclimates. *Advances in Geophysics* 28A:159–196
- Laskar J (1988) Secular evolution of the solar system over 10 million years. *Astron Astrophys* 198:341–362
- Laskar J (1990) The chaotic motion of the solar system. A numerical estimate of the size of the chaotic zones. *Icarus* 88:266–291
- Laskar J (1999) The limits of Earth orbital calculations for geological time scale use. In: Shackleton NJ, McCave IN, Weedon GP (eds) *Astronomical (Milankovitch) calibrations of the geological time scale*. Philosophical Transactions of the Royal Society, London, Series A, vol 357, pp 1735–1759
- Laskar J, Robutel P, Joutel F, Gastineau M, Correia ACM, Levrard B (2004) A long-term numerical solution for the insolation quantities of the Earth. *Astron Astrophys* 428:261–285
- Le Verrier UJJ (1855) *Recherches astronomiques*. Annales Observatoire Impérial de Paris II
- Lequeux J (2009) *Le Verrier, Savant magnifique et détesté*. EDP Sciences/Observatoire de Paris, Les Ulis/Paris, 401 p
- Lourens LJ, Wehausen R, Brumsack HJ (2001) Geological constraints on tidal dissipation and dynamical ellipticity of the Earth over the past three million years. *Nature* 409(6823):1029–1033
- Loutre MF, Berger A, Bretagnon P, Blanc PL (1992) Astronomical frequencies for climate research at the decadal to century time scale. *Clim Dyn* 7(4):181–194
- Lyell C (1830) *Principles of geology*, 1st edn. J. Murry, London, 3 vol 1830 (511 p), 1832 (330 p), 1833 (507 p)
- Lyell C (1872) *Principles of geology*, 11th edn. J. Murry, London, 2 vol, 671 p and 652 p
- McIntyre A, Molino B (1996) Forcing of Atlantic Equatorial and subpolar millennial cycles by precession. *Science* 274:1867–1870
- Meech LW (1856) On the relative intensity of the heat and light of the Sun upon different latitudes of the Earth. *Smithsonian Contribution to Knowledge*, vol IX, Washington, DC, 64 p (accepted for publication 1855)
- Mélice JL, Coron A, Berger A (2001) Amplitude and frequency modulations of the Earth's obliquity for the Last Million Years. *J Clim* 14(6):1043–1054
- Milankovitch M (1912) *Prilog teoriji matematske klime*. Report of the Royal Serbian Academy, LXXXVII first class 36, printed by the Kingdom of Serbia, Belgrade, pp 136–160
- Milankovitch M (1914) Ueber die Verringerung der Wärmeabgabe durch die Marsatmosphäre. *Annalen der Physik*. Vierte Folge, vol 44
- Milankovitch M (1916) *Ispitavanja klime planete Marsa*. Jugoslavenska akademija znanosti i umjetnosti, Zagreb, pp 64–96. doi:64
- Milankovitch M (1920) *Théorie Mathématique des Phénomènes Thermiques Produits par la Radiation Solaire*. Académie Yougoslave des Sciences et des Arts de Zagreb. Gauthier Villars, Paris
- Milankovitch M (1923) *Reforma julijanskog kalendara (Reform of the Julian Calendar)*. Posebna izdanja, Srpska kraljevska akademija nauka i umetnosti, vol 47. Odeljenje prirodnomatematičkih nauka, vol 11. 52 p
- Milankovitch M (1928) *Kroz vasionu i vekove, pisma jednog astronoma (Through distant worlds and times, letters of an astronomer)*. (Durch ferne Welten und Zeiten. Leipzig, 1936 (1st edn), 1941 (2ed edn))
- Milankovitch M (1930) *Mathematische Klimalehre und Astronomische Theorie der Klimaschwankungen*. In: Köppen W,

- Geiger R (eds) *Handbuch der Klimatologie*, vol I. Borntraeger, Berlin, Part A, 176 p
- Milankovitch M (1931) *Stellung und Bewegung der Erde in Weltall*. *Handbuch der Geophysik*, Band I, Abschnitt II, Verlag von Gebrüder Borntraeger in Berlin W35, pp 69–138
- Milankovitch M (1938a) *Neue Ergebnisse der astronomische Theorie der Klimaschwankungen*. *Bulletin de l'Académie des Sciences Mathématiques et Naturelles*, A. Sciences Mathématiques et Physiques, issue 4, Académie Royale Serbe, Belgrade, 41 p
- Milankovitch M (1938b) *Un chapitre de l'histoire de la Terre dans la lumière des sciences mathématiques*. *Revue Mathématique de l'Union Balkanique* II(1):53–64
- Milankovitch M (1941) *Kanon der Erdbastrahlung und seine Anwendung auf des Eiszeitenproblem*. Special Publication 132, Section of Mathematical and Natural Sciences, vol 33, p 633. Belgrade, Royal Serbian Academy of Sciences ('Canon of Insolation and the Ice-Age Problem', translated from German by the Israel Program for Scientific Translations and published for the U.S. Department of Commerce and the National Science Foundation, Washington DC, 1969. Reprinted by Zavod za udzbenike i nastavna sredstva in cooperation with Muzej nauke i tehnike Srpske akademije nauka i umetnosti, Beograd, 1998)
- Milankovitch M (1948) *History of the astronomical science, from the beginning until 1727*. *Naucna knjiga*, Beograd, In Serbian
- Milankovitch M (1950, 1952, 1957, 1979) *Memories, experiences and knowledge*. Vol 1 (1879–1909), vol 2 (1909–1949), vol 3 (after 1949). Serbian Academy of Sciences, Section of Mathematical and Natural Sciences, issue 50, 6 and 16. In Serbo-Croatian also vol 1–3, Zavod za udzbeniken Belgrade, 2009, pp 1–977 (in Serbian)
- Milankovitch M (1954) *Über den Anteil der exakten Wissenschaften an der Erforschung der geologische Vorzeit*. Publication de l'Institut Mathématique, Académie Serbe des Sciences VI:1–11
- Milankovitch M (1956) *La part des sciences exactes dans les recherches des âges géologiques*. In: *Actes du IVème Congrès International du Quaternaire II*, Rome, pp 858–862
- Milankovitch M (1957) *Astronomische Theorie der Klimaschwankungen: ihr Werdegang und Widerhall*. *Serbische Akademie der Wissenschaften, Monographie*, vol CCLXXX, Mathematisches Institut, issue 3, Belgrade, 58 p
- Milankovitch V (1995) *Milutin Milankovic 1879–1958*, from his autobiography with comments by his son, Vasko, and a preface by André Berger. European Geophysical Society, Katlenburg-Lindau, p 181 p
- Miskovitch VV (1931) *Variations séculaires des elements astronomiques de l'orbite terrestre*. *Glas Srp. kraljevske akad.*, vol 143, Première Classe, issue 70, Belgrade
- Murphy JJ (1869) *On the nature and cause of the glacial climate*. *Q J Geol Soc* 25:350–356
- Murphy JJ (1876) *The glacial climate and the polar ice-cap*. *Q J Geol Soc Lond* 32:400–406
- Paillard D (1990) *The timing of Pleistocene glaciations from a simple multiple – state climate model*. *Nature* 391(6665): 378–381
- Pantic N (1998) *Milutin Milankovitch and his Canon of Insolation*. In: *Canon of insolation and the ice age problem*. *Zavod za udzbenike i nastavna sredstva*, Beograd, pp 13–48
- Peltier WR, Jiang X (1994) *The precession constant of the Earth: variations through the ice age*. *Geophys Res Lett* 21(21):2299–2302
- Penck A, Brückner E (1909) *Die Alpen in Eiszeitalter*. Tauchnitz, Leipzig, 1042 p
- Pestiaux P, Berger A (1984) *An optimal approach to the spectral characteristics of deep-sea climatic records*. In: Berger A, Imbrie J, Hays J, Kukla G, Saltzman B (eds) *Milankovitch and climate, part I*, vol 126, Nato ASI series C. D. Reidel Publishing Company, Dordrecht, pp 417–445
- Petrovic A (2002) *Insolation and climate*. Serbian Society of History of Science, Belgrade, 34 p
- Petrovic A (2011) *Kanon lednikovog periode*. Russian Academy of Sciences, St Petersburg
- Pilgrim L (1904) *Versuch einer rechnerischen Behandlung der Eiszeitalters*. *Jahresshefte des Vereins für Vaterl. Naturkunde in Württemberg*, vol 60
- Poisson SD (1835) *Théorie mathématique de la chaleur*. Bachelier Imprimeur-Libraire, Paris
- Ruddiman WF, McIntyre A (1979) *Warmth of the sbpolar North Atlantic ocean during Northern Hemisphere ice sheet growth*. *Science* 204(4389):173–175
- Ruddiman WF, Raymo M, McIntyre A (1986) *Matuyama 41,000-year cycles: North Atlantic Ocean and northern hemisphere ice sheets*. *Earth Planet Sci Lett* 180:117–129
- Saltzman B, Vernekar AD (1971) *Note on the effect of Earth orbital radiation variations on climate*. *J Geophys Res* 76 (18):4195–4198
- Schellnhuber HJ, Crutzen P, Clark WC, Claussen M, Held H (2004) *Earth system analysis for sustainability*. Dalhem Workshop Report, Massachusetts Institute of Technology and Freie Universität Berlin, 463 p. ISBN:0-262-19513-5
- Schimper KF (1837a) *Über die Eiszeit*. *Actes Soc. Helv. Natur*, Neuchâtel, pp 38–51
- Schimper KF (1837b) *Auszug aus dem Briefe des Hern Dr Schimper Ueber die Eiszeit an Pr Agassiz, President der Gesellschaft*. *Actes de la Société Helvétique des Sciences Naturelles*, 21, 50
- Schwarzbach M (1985) *Alfred Wegener and the Drift of the Continents*. Belin, Paris, 144 p
- Sellers WD (1970) *The effect of changes in the Earth's obliquity on the distribution of mean annual sea-level temperatures*. *J Appl Meteorol* 9:960–961
- Shackleton NJ, Opdyke ND (1973) *Oxygen isotope and paleomagnetic stratigraphy of equatorial Pacific core V28-238: oxygen isotope temperatures and ice volumes on a 105 and 106 year scale*. *Quat Res* 3:39–55
- Shackleton NJ, Berger A, Peltier WR (1990) *An alternative astronomical calibration of the lower Pleistocene timescale based on ODP site 677*. *Trans of the Royal Soc of Edinburgh: Earth Sciences* 81:251–261
- Sharaf SG, Budnikova NA (1967) *Secular variations of elements of the Earth's orbit which influence the climate of the geological past*. *Tr Inst Teor Astron* 11:231–261
- Shaw DM, Donn WL (1968) *Milankovitch radiation variations: a quantitative evaluation*. *Science* 162(3859):1270–1272
- Simpson GC (1940) *Possible causes of change in climate and their limitations*. *Proc Linn Soc (Lond)* 152:190–219
- Sirocko F, Claussen M, Sanchez Goni MF, Litt J (eds) (2007) *The climate of past interglacials*. *Developments in Quaternary science*, vol 7. Elsevier, Amsterdam, 621 p

- Spitaler R (1907) Die jährlichen und periodischen Aenderungen der Wärmeverteilung auf der Erdoberfläche und die Eizeiten. Gerland's Beiträge zur Geophysik, vol VIII
- Spitaler R (1921) Das Klima des Eiszeitalters. Selbstverlag, Prag (lithographed)
- Stocker Th, Marchal O (2001) Recent progress in paleoclimates modelling: climate models of reduced complexity. Pages News 9(1):4–7
- Stockwell JN (1873) Memoir on the secular variations of the elements of the eight principal planets. Smiths Contr. Knowledge, Washington, vol 18, issue 3, 199 p (accepted for publication in 1870)
- Tricot C, Berger A (1988) Sensitivity of present-day climate to astronomical forcing. In: Wanner H, Siegenthaler U (eds) Long and short-term variability of climate, Earth sciences series. Springer, Berlin, pp 132–152
- Tyndall J (1861) On the absorption and radiation of heat by gases and vapour and on the physical connection of radiation, absorption and conduction. Philos Mag 22:167–194, 273–285
- Tyndall J, Huxley TH (1857) On the structure and motions of glaciers. Philos Trans R Soc Lond 147:327–346
- Tzedakis PC, Raynaud D, McManus JF, Berger A, Brovkin V, Kiefer T (2009) Interglacial diversity. Nat Geosci 2(11):751–755
- Vernekar AD (1972) Long-period global variations of incoming solar radiation. Meteorol Monogr 12(34):130
- von Hann J (1903) Handbook of climatology. McMillan, London, 437 p
- Wiener Chr (1877) Ueber die Stärke der Bestrahlung der Erde durch die Sonne in ihren verschiedenen Breiten und Jahreszeiten. Zeitschrift f Mathematik u Physik XXII:6, 341–368
- Wigley TML (1976) Spectral analysis: astronomical theory of climatic change. Nature 264:629–631
- Yin QZ, Berger A (2010) Insolation and CO₂ contribution to the interglacial climate before and after the Mid-Brunhes Event. Nat Geosci 3(4):243–246

Canon of Eccentricity: How Milanković Built a General Mathematical Theory of Insolation

Aleksandar Petrović

Abstract

Milutin Milanković is considered to be the founder of the modern astronomical theory of climate change. In 1912, in an article entitled “On the Mathematical Theory of Climate,” he began to mathematically demonstrate the interrelation of celestial mechanics and the Earth sciences. At the intersection of a number of scientific fields, including spherical astronomy, celestial mechanics, and mathematical physics, he developed climatology as an integrated cosmic science that could be applied to specific problems of the Earth sciences, including the problem of the Pleistocene ice ages. Milanković’s achievement was facilitated by his position as Chair of Applied Mathematics at the University of Belgrade where a nonspecialized, holistic culture of education was prevalent. The ultimate educational aim of the University, “acquiring unity among the sciences,” was in dissonance with a specialization-driven scientific culture of that time, but without that cultural eccentricity the problems that Milanković solved would probably not even have been posed.

Milutin Milanković (1879–1958), professor of Applied Mathematics at Belgrade University, considering seasonal and latitudinal distribution of the Earth’s insolation, caused by changes of the Earth’s orbital geometry, formulated a theory of climate that can be verified mathematically and tested geologically. In six papers published from 1912 to 1914, he introduced differential and integral calculus into climatology, formulated a precise, numerical climatological model with the capacity for reconstruction of the past and prospecting of the future, and established the astronomical theory of climate as a generalized mathematical theory of insolation.

In this way, he enabled consistent transition from celestial mechanics to the Earth sciences and transformation of the descriptive sciences into exact ones. “It remains, however, that the basis of all sciences involved in any theory of paleoclimates can be found in the Milanković’s Canon. Critically read, it will remain for ever a milestone in climate science.” (Berger and Mesinger 2000)

Overcoming the descriptive approach of climatology of his time, Milanković calculated the temperatures of the upper layers of the Earth’s atmosphere as well as temperatures at the surfaces of Mercury, Venus, Mars, and the moon—results that were mainly supported by later observations. He began working in the extraterrestrial field in 1913 in his paper *On the Application of the Mathematical Theory of Heat Condition to the Problems of Cosmic Physics*, and as early as 1914, he had already

A. Petrović (✉)
University of Belgrade, Belgrade, Serbia
e-mail: petralist@gmail.com

calculated the basic climatological data for Mars (Milanković 1913). His calculations concerning Mercury, Venus, Mars, and the Moon were published in 1920 as a part of his book *Mathematical Theory of Heat Phenomena Produced by the Solar Radiation* (Milankovic 1920). Such advanced research set up a basis for cosmic climatology, enabled mathematical interpretation of long quasiperiodic climate changes, and became an organon for the understanding of the Earth's Pleistocene ice ages which is one of the main scientific challenges today. Our aim is to point out that his unscrambling of the glacial dynamics riddle was initialized through the “eccentricity-driven” scientific culture of university education in the Kingdom of Serbia in the early decades of the twentieth century.

The riddle of the Earth's paleoglacial dynamics was first noticed by the philosophers of the Enlightenment, Hume and Montesquieu, as well as Goethe (Fleming 1998; Engelhardt 1999). But the strongest impact on contemporary science was made by the Swiss naturalist Louis Agassiz, who at a conference of the Swiss Society of Natural Sciences in 1837 delivered his famous *Neuchatel lecture*. He pointed at “erratic boulders” of granite resting upon the limestone of the Jurassic mountains—huge stones which were detected at geologically inappropriate sites. The phenomenon of “erratic boulders” had puzzled geology because the steady-state theory of the Earth was attacked implicitly and a new horizon on the Earth as a perpetual motion structure was opened. Alexander von Humboldt promptly advised Agassiz to leave this research and to return to his fossil fishes' exploration. Fortunately, Agassiz rejected the suggestion of one of the leading European scientific connoisseurs and in 1840 published *Études sur les glaciers*, where he proclaimed that Alpine glaciers had been far more extensive in the past and that at a geologically recent period “great sheets of ice, resembling those now existing in Greenland, once covered all the countries in which unstratified gravel (boulder drift) is found” (Agassiz 1840). British geologist Charles Lyell at first abandoned, but later supported him with the “uniformitarian” view that all features of the Earth's surface are produced by physical, chemical, and biological processes through long periods of geological time.

For a long time this idea was strongly opposed by geologists, but when they accepted it—laboring hard to refine the actual ice age causes and history—new ideas appeared which quickly pulled down obsolete

geological weltanschauung. It was found that there had been not just one ice age but several large glaciations separated by warm periods. All these efforts prepared a decisive point in the history of the modern Earth sciences, when a decrepit old picture was definitively left behind. It occurred in 1912 when *The Origin of the Continents*, a seminal article written by the meteorologist and astronomer Alfred Wegener, was published. In this paper, Wegener additionally advanced new geological dynamics of “erratic boulders” by his notions of “drifting continents” and “wandering poles” (Wegener 1912). His theory was immediately subjected to scientific and public dispute because it was, like before Agassiz', an implicit critique of the prejudices of the Earth sciences at the beginning of the twentieth century. Wegener presented the new theory on January 6, 1912, at the meeting of the Geological Association in Frankfurt, and, as with Agassiz', it was completely rejected. However, he was determined to publicize it because he felt that “it is, perhaps, revolutionary” and that he should proceed without heeding the disbelief of the mainstream geology. “If such a series of astonishing simplifications follows, if it is shown that rhyme and reason will not come to Earth history, why should we hesitate to cast the old view overboard?” (Wegener 1911).

Old views were overturned and the Earth became an aggregate of different motions which demanded an adequate explanation. But “static,” descriptive geology was not able to offer it—the old picture was dethroned and a new one was not born. This hiatus is one of the reasons why Wegener's theory was repudiated. Geology lacked a plausible interpretation of the forces that kept the continents moving and did not have even a slightest picture of the internal Earth dynamics.

In the very same year, the paper *On the Mathematical Theory of Climate* appeared. It was Milanković' first contribution to the mathematical theory of climate which laid a foundation for a mathematical explanation of the Earth's secular thermodynamics and an exact understanding of the atmospheric processes. It came out at the moment when the Earth sciences were not able to relate causally the intermittent appearance of glacial epochs with any specific natural mechanism. Along with Wegener's *The Origin of Continents*, this paper gave a new perspective to the Earth's dynamics. It was a new chapter of the Earth sciences, building the bridge between descriptive and exact sciences, because Milanković mathematically linked climate dynamics to the orbital geometry.

This idea of a correlation between long-term changes in climate and the solar-astronomical cycles was not new. It goes back to a hypothesis put forth in 1830 by Sir John Herschel, who thought that the change of eccentricity might have a determining effect on climate history. In his paper *On the Astronomical Causes which may influence Geological Phenomena* he proposed “a theorem, of which any one may easily satisfy himself by no very abstruse geometrical reasoning, that, the eccentricity of the orbit varying, the total quantity of heat received by the Earth from the sun in one revolution is inversely proportional to the minor axis of the orbit” (Herschel 1830). But this idea came too early, before Agassiz delivered the lecture which implicitly raised the question of the ice ages. Herschel himself was persuaded soon that the signal of eccentricity is too weak to initiate differences in the Earth’s warming. Moreover, his authoritative abandonment of his idea for a long time dissuaded other scientists to proceed this way.

Astronomical theory did not attract scientific attention until 1842 when it was taken up and elaborated by the French mathematician Joseph Adhémar. According to his words, he had thought about astronomical theory 20 years before, “considering precession of equinoxes probably the ground of a series of revolutions which convulsed surface of the Earth” (Adhémar 1842). But when he learned about Herschel’s assertion that astronomical causes are not enough to generate climatic changes, “it seemed to me that Herschel was right, and without further research I abandoned everything that I was working on before. I changed my mind and I left my project for the time to come.” However, when he found in *Comptes rendus* of the Paris Academy of Science a contribution which induced him to read Agassiz’ *Études*, he immediately realized that his unfinished theory could explain Agassiz’ evidences and that it gave enough arguments that Herschel was wrong.

In the book *Revolutions of the Sea*, Adhémar allowed that changes in Earth’s orbital parameters led to the ice ages. He hypothesized that the precession of the equinoxes provokes an ice age and postulated a periodic, catastrophic global deluge triggered by the collapse of the polar ice cap, causing a dramatic shift in the Earth’s center of gravity. He considered the duration of daylight and darkness in each hemisphere, the imbalance of received solar radiation, a key factor in explaining ice ages, but soon it was realized that whatever quantity of solar radiation is lost in one

season is balanced in the next, and each hemisphere receives equal amounts of heat.

The astronomical theory of climate change continued to receive attention and emerged in a recognizably modern form between 1864 and 1890 with the work of the Scottish natural philosopher, autodidact, and independent scholar James Croll (1821–1890). As an open-minded scholar, Croll recognized the complexity of glacial dynamics and pointed out the necessary coherence of astronomy and geology (Croll 1864). Essentially, he was continuing Herschel’s pondering on eccentricity, trying to better expound on the relationship of celestial mechanics and climate dynamics to the geological record (Croll 1865). As Milanković said in his *Canon of Insolation*: “Croll correctly recognized the influence of the eccentricity of the Earth’s orbit upon the duration of the astronomical seasons”¹ (Milanković 1941).

Croll’s theory caused an immediate stir among astronomers and geologists, notably John Herschel and Charles Lyell, leading to its appreciation as a probable *causa vera* of multiple glaciations. However, because of uncertainties in the astronomical elements, in the location and timing of ice ages, in feedback mechanisms, and in the paleostratigraphic record, Croll was not able to conceptualize the synergetic action of all three orbital cycles and to give results in accordance with proxy data. Moreover, Croll considered seasonal insolation of a hemisphere as a whole, and believed that cold winters are the trigger of the ice ages (Croll 1875). Contrary to that, Milanković showed that the key lies in the latitudinal distribution of insolation, that the most important are climatic events at higher latitudes, and that ice ages are triggered by cold summers, the last point as stressed in his memoirs with admiration by Milanković a suggestion of Wladimir Köppen. According to Milanković’ theory, changes in obliquity play the

¹ In addition to the cycle of eccentricity and the precession of the equinoxes, Croll afterward also added to his considerations the change of the tilt of the Earth’s axis, although he could not calculate its real effect. He proposed that the “true cosmical cause” of climate change “must be sought for in relations of our Earth to the Sun,” that “geological and cosmical phenomena are physically related by a bond of causation,” and that changes in the Earth’s orbital elements, combined with physical feedbacks, were “sufficiently great to account for every extreme of climatic change evidenced by geology.”

Fig. 1 Milanković in late twenties of the previous century when he was developing his theory most intensively



major role, which are not given much significance in Croll's work (Croll 1867; Fig. 1).

None of the aforementioned early efforts were successful in linking celestial mechanics to the geological record, so that they remained unproven. Thus, geologists and climatologists neglected not only the best among them—Croll's theory—they abandoned any possibility of an astronomical theory of climate. Albrecht Penck, a German geographer and geologist who as it was believed determined the phases of glaciations in the Alps (later found inaccurate), considered Croll's theory useless, holding that the climate changes might be caused by periodic changes of the intensity of solar insolation, and not by the dynamics of the Earth's motion. Moreover, one of the leading Alpine geologists of his time, Gustav Steinmann, thought that all the theories that explain glaciations from an alternating unfavorable effect on the two hemispheres by astronomical processes could be abandoned. The Austrian climatologist Julius Hann, confused by the results of different astronomic theories, also thought them useless and

viewed the secular variations of orbital geometry as too weak to cause changes of climate. As a result, the astronomical theories fell into disrepute and were largely disregarded for at least three decades following Croll's death.

Milanković' historic merit is that he turned himself toward the astronomical theory when it was entirely abandoned, having almost every geologist against it. He realized that the first reason for the decline of astronomical theory was his predecessors' insufficient knowledge of celestial mechanics, neglecting certain elements of the Earth's movement, their inadequate mathematical skill, and subsequent descriptive approach. The second reason, Milanković' principal objection to the geology of the early twentieth century, was a lack of interdisciplinary approach and a consequent weakness to perceive the holistic nature of the climate change problem (Petrović 2009).

Milanković was aware that in the early twentieth century, the geosciences, with a few exceptions, were overspecialized and overloaded with empiricism, so

that its practitioners lacked the ability to attain an appropriate degree of interdisciplinarity. The problem of proving the existence and timing of the ice ages was left to geographers and geologists who had incomplete knowledge of the laws of celestial mechanics and were not able to apply the mathematical sciences. Among them, Albrecht Penck was the leading opponent of Milanković' theory. However, he had poor knowledge of mathematics which Milanković considered the main reason for his opposition:

Penck was an excellent observer, a pure empiric, but not a theorist. His world, limited to the Earth's surface, had only two dimensions. He couldn't peek deeply into the cosmos by his spiritual sight. . . Our natural sciences have branched so wide, that there is no man who could encompass them all. The times when this was possible have long passed, and because of that Penck couldn't be a scientist like Alexander von Humboldt, a geographer and cosmologist, was a century ago. (Milanković 1952–1979)

Even so, Penck in 1938 finally accepted the accuracy of Milanković' calculations and was the first who named them “the true canon.” He called the Milanković' tables “a true canon of the earth's insolation secular changes during the past 600,000 years. It reflects not only the validity of hypothesis, but also the accuracy of numbers themselves which give us exceptionally important material” (Penck 1938). But generally, although many Earth scientists of the nineteenth and the beginning of the twentieth century speculated on the causes of ice ages, the problem lacked an attempt that could yield a proper solution. Inherited paradigmatic determinations led scientific efforts into divided approaches and they failed to recognize complex scientific problems like ice ages, which required nonstereotypical, subtle connections among seemingly disparate phenomena.

Because of that, the real breakthroughs in the science of the climate were made exclusively by unconventional, “eccentric” thinkers. First of them was a self-taught climatologist, James Croll, who approached the problem from the perspective of natural philosophy and a general theory of the unity of nature. The second was a physicist and astronomer Alfred Wegener who established a new picture of a dynamic Earth in contrast to the then prevailing notions of the permanence of continents and oceans. A civil engineer Milutin Milanković, the third of them, addressed independently the question of climate changes while holding the Chair of Applied Mathematics at Belgrade University, where the “achievement of unity

among sciences” was the widely agreed upon basic university approach; a program which was in complete dissonance with the prevailing scientific culture of that time, with a strong affinity for much narrower fields of studies. The organization of teaching and research at Belgrade University did not promote specialization; rather, it sought to address problems at the intersections of different sciences.

Milanković felt confident that the mystery of the ice ages had not been resolved yet because its solution demanded coupling of three disciplines. He wrote in his *Memoirs*:

“The reason for that lays in the fact that, in order to get to the bottom of the problem, one has to solve a set of rather complicated component problems which really belong to different sciences that are sharply separated from one another. . . Therefore, the question was not answered, and it was left amid a triangle between spherical astronomy, celestial mechanics and theoretical physics. The chair at Belgrade University offered to me included all the three sciences which were separated at other universities. Therefore I was able to address that cosmic problem, see his importance, and start with its unraveling” (Milanković 1952–1979).

This methodological approach, substantially different from other universities', forced him to set appropriate, firm ground for understanding the core of the climate problem.

“That coincidence, which enabled me to adhere to the given problem, was not a pure accident, although it looked like that. Exactly because I was involved in all the mentioned sciences, it was possible for me to sniff out that problem and assess its importance” (Milanković 1952–1979).

Milanković was aware that narrow scientific experience and separated astronomical and geological knowledge makes the comprehension of the climate impossible. It was a blind way which ultimately would be replaced by a new, open methodology—the triangle which couples sciences to frame Proteus like climate dynamics. Therefore Milanković' climatology was one among the most powerful and productive interdisciplinary efforts at the beginning of the twentieth century. Although he was not involved in geological research, his theory strongly demanded of geology to take celestial mechanics into consideration. It was an utterly eccentric demand which went against the mainstream academic culture, but without it the problem of the astronomical cycles' impacts on climate would not have been mathematically properly posed and solved.

Although Milanković and almost all important Serbian scientists of the nineteenth century (both in the natural and mathematical sciences) were educated at the most prominent European universities, they were dissatisfied with intensive diversification of the scientific disciplines. There was an ambiguous relationship in which they accepted the details of contemporary scientific knowledge, but not its direction toward specialization. It seems that they had an instinctive resistance toward specialism, because the Serbian culture was influenced by strong centrifugal forces which tried to fracture it into smaller and smaller parts with a variety of different names.

That culture was determined by the works of the most prominent professors of Belgrade University at the beginning of the twentieth century, namely, his predecessor in the Chair, mathematician Kosta Stojanović, and his colleague, acclaimed mathematician Mihailo Petrović Alas, who worked to create a genuine mathematical picture of the world as a basis for their scientific research. In doing so, their work encompassed mechanics, physics, chemistry, biochemistry, and electrodynamics, as well as descriptive sciences such as geology, economics, sociology, and medicine. The fundamental idea of this phenomenology was that one can affirm, by an adequate mathematical apparatus, the correspondence of facts and link apparently unconnected phenomena belonging to different levels of natural events. They believed that, “apart from numbers, dimensions, and orders, modern mathematics should capture other general details in the world of facts that are independent from the concrete nature of their bearers” (Petrović 1933). Their essential concern was the insight that different names were given to the same phenomena in different domains of human perception. Because of that, the quantity of our presumptions is overly large and unwieldy. They attempted to make it theoretically as small as possible, trying to find as many analogies between phenomena as possible and observing the identity of mathematical relations which describe different phenomena. That identity is comprehensive and includes a certain number of equations (differential or explicit) by which these relations are expressed, including the analytical form of elements and the parameters of the phenomena, their differentials or some other combinations, as well as constants in these equations. This identity allowed quantitative descriptions of phenomena (no matter how much they differ) to be the same analytical problem involving

integration, discussion, and interpretation of the same equations. Their main idea persuasively exposed in Mihailo Petrović’ *Elements of Mathematical Phenomenology* was the following:

“Mathematical analogies. . . are an appropriate auxiliary means for the materialization of analytical problems. Materialization here means finding, for a given analytical form, a real phenomenon on which the same mathematical relations could be applied, so that by following materialized process, the analytical solution could be obtained. In this materialization the kind of relation or the kind of particular detail that is hidden in the equations of the analytical problem and which is difficult to highlight by purely analytical means, becomes obvious in the definite phenomenon which the problem materializes” (Petrović 1911).²

This specific theoretical and cultural milieu encouraged Milanković to think about the analogy between the celestial and Earth sciences. His attempts were facilitated and enhanced through an intensive and continual dialogue at the Belgrade University Mathematicians’ Club which brought together a rather numerous group of university professors. The Club was founded in 1926 by Anton Bilimovich, a Russian mathematician who came to Belgrade in 1921 during the exodus of Russian intellectuals and scientists after the October Revolution. Until the beginning of 1922, there came the then Kingdom of Yugoslavia 88 university professors, many of them from the field of mathematics and natural sciences, which made the Club a populated place where different bold ideas and hypotheses were considered. Members of the Club left a significant number of papers on celestial mechanics, geophysics, and other topics related to Milanković’ work which share a close theoretical background (Petrovic and Kolchinsky 2010).

As a result, Milanković was able to demonstrate persuasively that the astronomical theory had not fallen into disrepute because of its actual failure, but because of the poor scientific methodology of his predecessors and the lack of reliable knowledge of the facts involved. Determined to promote it, he built an interdisciplinary mathematical apparatus for the analysis of insolation (*incoming solar radiation*) received by a planet, including the distribution and effects of heat in its atmosphere, thus enabling calculation of the resulting impacts on its

² For more about computational realization of the mathematical principle of analogy, see Petrović (2005).

climate. His research program combined astronomy and celestial mechanics, atmospheric and Earth sciences. But unlike his predecessors, Milanković was not primarily solving the specific problem of the Earth's ice ages. He considered that such a specific terrestrial problem should be elucidated as part of a general cosmic problem. Until his cooperation with Wladimir Köppen and

Alfred Wegener in 1923, he never considered extensively the specific problem of the ice ages, which he afterward tried to solve as one of the consequences of his theory in the frame of the general mathematical climatology of the planets of the solar system (Fig. 2).

Milanković looked at the question of climate changes as a cosmic problem with the Sun at its center.

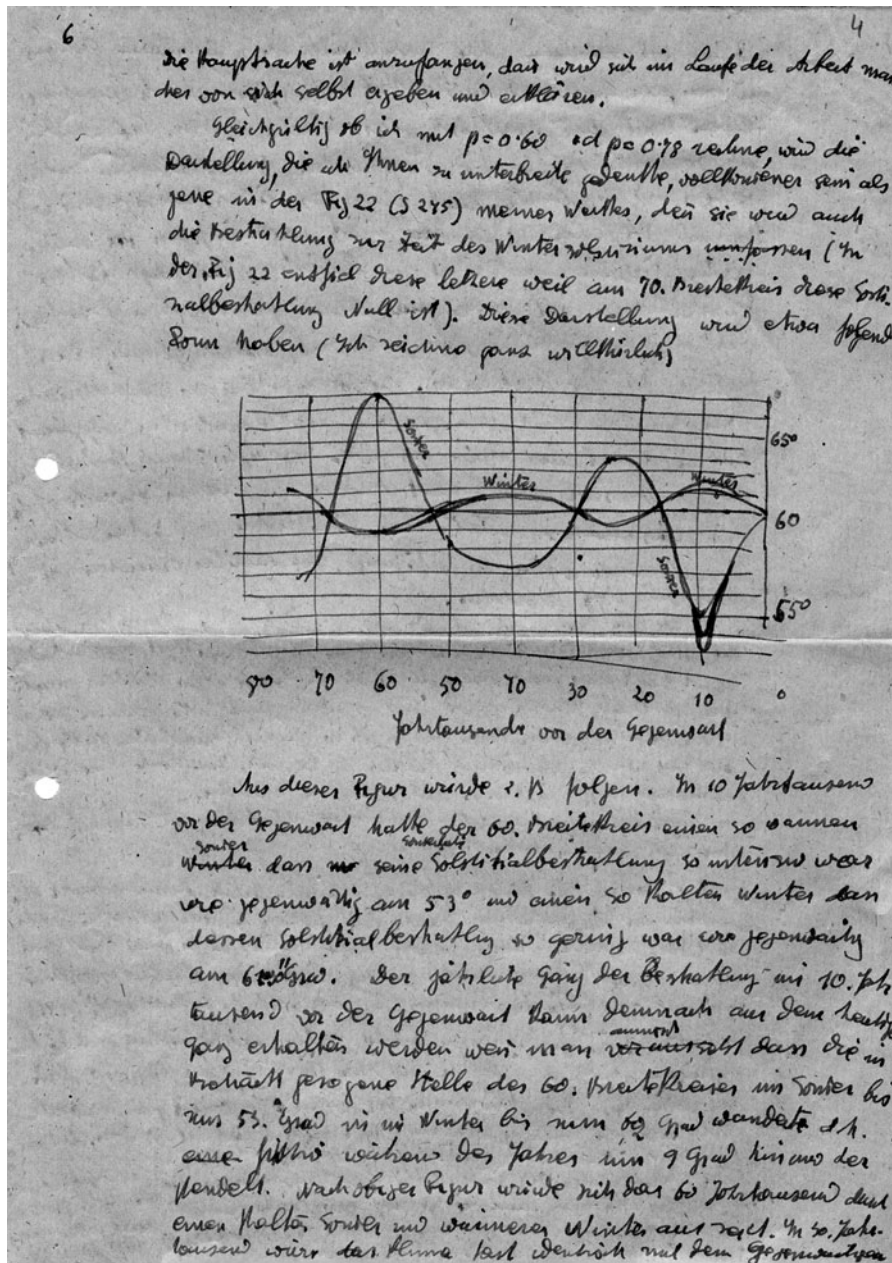


Fig. 2 One page of Milanković' letter from Sept. 29, 1922 to Wladimir Köppen and his son-in-law Alfred Wegener in which Milanković for the first time sketched his Curve of Insolation

Fig. 3 James Hays, leader of the CLIMAP project, delivering his lecture on Milanković' theory during the symposium "Paleoclimate and the Earth Climate System" (Belgrade, September 2004)



While Croll had proposed that the “true cosmical cause” of climate change “must be sought for in relations of our Earth to the Sun” and had sought this relationship, Milanković’s aim was the creation of a general mathematical climatology valid for all the planets of the Sun’s family, applicable to the past as well as to the future, to their surfaces, as well as to their upper atmospheric layers. In his own words, he set out to describe and calculate “the effects of the sun rays on their journey through a planet’s atmosphere and on its surface” and offered to the scientific world the first comprehensive theory of thermal phenomena caused by insolation (Petrovic and Markovic 2010; Fig. 3).

Similar to that, the cultural eccentricity of Milanković’ science, standing almost alone against the prevailing scientific consensus of his time, made a fundamental impact on the modern understanding of the solar system’s thermodynamics, including that of the Earth’s secular pace of the ice ages and interglacials. His starting point in between the celestial and the Earth sciences appeared uncertain and obsolete to Penck and many other geoscientists; also his task, long before the existence and implementation of modern computers in the Earth sciences, seemed not only scientifically difficult, but practically impossible, because every computation had to be done manually.³ Nevertheless,

Milanković was convinced of the feasibility of his project. Its success was possible due to the synergy with the heterodox scientific efforts of Croll and Wegener and the culturally unique, relatively autonomous, and discrete scientific environment of Belgrade University where, at the same chair, diverse scientific disciplines were hosted. Although all of these for the time eccentric theories had initially a small impact on contemporary science, they eventually energized scientific knowledge and enforced an efficient reversal in the perception of the problem. In this way, what may have seemed to be a weakness was transformed into a strength, and a relatively small initial influence of eccentricity-driven understanding spun climate science to be fully insolated. Therefore, Milanković theory, as the link between the celestial and the Earth sciences, can be used not only to calibrate the paleoclimatological timescale, as was done in the 1970s, primarily by the contribution of the CLIMAP project, but perhaps more importantly to obtain a broad vision of an integrated cosmic science that can be applied to the specific problems in climatology—including the problems of the past ice ages of the Earth and the various impacts on other planets as well.

References

- Adhémar J (1842) Révolutions de la Mer – formation géologique des couches supérieures du globe. Carilian-Goery et Dalmont, Paris, p 21
- Agassiz L (1840) Études sur les glaciers. Aux frais de l’auteur, Neuchâtel
- Berger A, Mesinger F (2000) Canon of insolation. Bull Am Meteorol Soc 81:1615

³ Vilhelm Bjerknes also had to face this computational challenge in his attempt to formulate a “true physics of the atmosphere.” See V. Bjerknes, (Jan. 1914) *Meteorology as an Exact Science*, Monthly Weather Review.

- Croll J (1864) On the physical cause of the change of climate during geological epochs. *Philos Mag* 28:121–137
- Croll J (Feb. 14, 1865) Letter to Herschel, J. In: Irons JC (1896) *Autobiographical sketch of James Croll with memoir of his life and work*. London, p 123
- Croll J (1867) On the change in the obliquity of the ecliptic, its influence on the climate of the polar regions and on the level of the sea. *Philos Mag* 33:426–445
- Croll J (1875) *Climate and time in their geological relations*. Dady, Isbister & Co, London
- Engelhardt W (1999) Goethe's discovery of the ice age. *Ecl Geol Helv* 92:123–128
- Fleming JR (1998) *Historical perspectives of climate change*. Oxford University Press, New York, NY
- Herschel J (1830) On the astronomical causes which may influence geological phenomena. *Trans Geol Soc Lond* III:293–300, Paper was first read before the Geological Society, 15 Dec 1830
- Миланковић М (1912) О математичкој теорији климе (On the mathematical theory of climate), (in Serbian). *Глас СКА LXXXVII*:136–160
- Milanković M (1913) О primjeni matematičke teorije sprovođenja toplote na probleme kosmičke fizike (On the application of the mathematical theory of heat condition to the problems of cosmic physics), (in Serbian). *Rad JAZU* 22:109–131
- Milankovic M (1920) *Théorie Mathématique des Phénomènes Thermiques Produits par la Radiation Solaire*. Gauthier-Villars et Cie, Paris, p XVI + 338
- Milankovic M (1941) *Kanon der Erdbestrahlung und seine Anwendung auf das Eiszeitenproblem*. Königliche Serbien, Akademie, Belgrade, p XX + 633 (Special publication, vol 132: Section of Mathematics and Natural Sciences)
- Миланковић М (1952–1979) Успомене, доживљаји и сазнања (Memoirs, experiences and knowledge), vol 1–3. Serbian Academy of Science and Arts, Belgrade. Last critical edition (2009) (in Serbian). In: Petrović A (ed) *Memoirs, experiences and knowledge*. Agency for Textbooks, Belgrade, pp 1–977
- Penck A (1938) *Die Strahlungstheorie und die geologische Zeitrechnung*. *Zeitschrift der Gesellschaft für Erdkunde*: 321–350
- Petrović M (1911) *Elementi matematičke fenomenologije* (The elements of mathematical phenomenology, Serbian Royal Academy, Belgrade), (in Serbian). Srpska kraljevska akademija, Beograd
- Petrović M (1933) *Fenomenološko preslikavanje* (Phenomenology of correspondence), (in Serbian). Serbian Royal Academy of Science, Belgrade, p 9
- Petrović A (2005) Development of the first hydraulic analog computer. *Arch Int Hist Sci (Paris)* 54(153):97–112
- Petrović A (2009) *Cycles and records – Opus solis of Milutin Milankovic*, (in Serbian). Serbian Academy of Sciences and Arts, Belgrade, pp 1–350
- Petrović A, Kolchinsky E (eds) (2010) *A Distant Accord: Russian-Serbian links in the fields of science, humanities and education: the 19th – the first half of the 20th century*, Institute for the History of Science of the Russian Academy of Science, Center for Scientific Research of the Serbian Academy of Science and Arts and University of Kragujevac, St. Petersburg, Kragujevac
- Petrovic A, Marković S (2010) *Annus mirabilis and the end of the geocentric causality: why celebrate the 130th anniversary of Milutin Milanković*. *Quat Int* 214:114–118
- Wegener A (6 December 1911) Letter to Köppen. V Deutsches Museum München, Manuscript Department, 1968 – 596/17, N 1/36
- Wegener A (1912) *Die Entstehung der Kontinente*. Dr. A. Petermanns Mitteilungen aus Justus Perthes' Geographischer Anstalt, vol 58, pp 185–195, 253–256, 305–309

Exaggerated Milankovitch-Like Eccentricity Cycles and Extreme Exoplanet Climate Variation

David S. Spiegel, Sean N. Raymond, Courtney D. Dressing, Caleb A. Scharf, and Jonathan L. Mitchell

Abstract

Although our solar system features predominantly circular orbits, the exoplanets discovered so far indicate that this is the exception rather than the rule. This could have crucial consequences for exoplanet climates, both because eccentric terrestrial exoplanets could have extreme seasonal variations, and because giant planets on eccentric orbits could excite Milankovitch-like variations of a potentially habitable terrestrial planet's eccentricity, on timescales of thousands-to-millions of years. A particularly interesting implication concerns the fact that the Earth is thought to have gone through at least one globally frozen, "snowball" state in the last billion years that it presumably exited after several million years of buildup of greenhouse gases when the ice cover shut off the carbonate–silicate cycle. Water-rich extrasolar terrestrial planets with the capacity to host life might be at risk of falling into similar snowball states. Here, we show that if a terrestrial planet has a giant companion on a sufficiently eccentric orbit, it can undergo Milankovitch-like oscillations of eccentricity of great enough magnitude to melt out of a snowball state.

Even very mild astronomical forcings can have dramatic influence on the Earth's climate. Although the orbital eccentricity varies between ~ 0 and only ~ 0.06 , and the axial tilt, or obliquity, between $\sim 22.1^\circ$ and 24.5° , these slight quasiperiodic changes are sufficient to help drive the Earth into ice ages at regular intervals. Milankovitch articulated this possibility in his astronomical theory of climate change. Specifically, Milankovitch posited a causal connection between three astronomical cycles (precession— $23 \sim \text{kyr}$ period, and variation of both obliquity and

eccentricity— 41-kyr and 100-kyr periods, respectively) and the onset of glaciation/deglaciation. Though much remains to be discovered about these cycles, often in the literature referred to as "Milankovitch cycles," they are now generally acknowledged to have been the dominant factor governing the climate changes of the last several million years (Berger 1975, 1976, 1978; Hays et al. 1976; Berger et al. 2005).

The nonzero (but, at just 0.05 , nearly zero) eccentricity of Jupiter's orbit is the primary driver of the Earth's eccentricity Milankovitch cycle. Were Jupiter's eccentricity greater, it would drive larger amplitude variations of the Earth's eccentricity. This same mechanism might be operating in other solar systems. Among the more than 460 currently known extrasolar planets, there are many that have masses comparable to Jupiter's and that

D.S. Spiegel (✉)
Astrophysics, School of Natural Sciences,
Institute for Advanced Study, Einstein Dr., Princeton, NJ 08540
e-mail: dave@ias.edu

are on highly eccentric orbits; $\sim 20\%$ of the known exoplanets have eccentricities greater than 0.4, including such extreme values as 0.93 and 0.97 (HD 20782b; HD 80606). Furthermore, tantalizing evidence suggests that lower mass terrestrial planets might be even more numerous than the giant planets that are easier to detect. Therefore, it seems highly likely that many terrestrial planets in our galaxy experience exaggerated versions of the Earth's eccentricity Milankovitch cycle.

These kinds of cycles could have dramatic influence on life that requires liquid water. Since the seminal work of Milankovitch several decades ago, a variety of theoretical investigations have examined the possible climatic habitability of terrestrial exoplanets. Kasting et al. (1993) emphasized that the habitability of an exoplanet depends on the properties of the host star. Several authors have considered how a planet's climatic habitability depends on the properties of the planet, as well. In particular, two recent papers have focused on the climatic effect of orbital eccentricity. Williams and Pollard (2003) used a general circulation climate model to address the question of how the Earth's climate would be affected by a more eccentric orbit. Dressing et al. (2010) used an energy balance climate model to explore the combined influences of

eccentricity and obliquity on the climates of terrestrial exoplanets with generic surface geography (see also Williams and Kasting 1997 and Spiegel et al. 2008, 2009a for further description of the model). A more eccentric orbit both accentuates the difference between stellar irradiation at periastron and at apoastron, and increases the annually averaged irradiation. Thus, periodic oscillations of eccentricity will cause concomitant oscillations of both the degree of seasonal extremes and of the total amount of starlight incident on the planet in each annual cycle. Since these oscillations depend on gravitational perturbations from other companion objects, the present paper can be thought of as examining how a terrestrial planet's climatic habitability depends not just on its star, not just on its own intrinsic properties, but also on the properties of the planetary system in which it resides.

There is evidence that, at some point in the last billion years, Earth went through a "Snowball Earth" state in which it was fully (or almost fully) covered with snow and ice. The high albedo of ice gives rise to a positive feedback loop in which decreasing surface temperatures lead to greater ice cover and therefore to further net cooling. As a result, the existence of a low-temperature equilibrium climate might be a generic

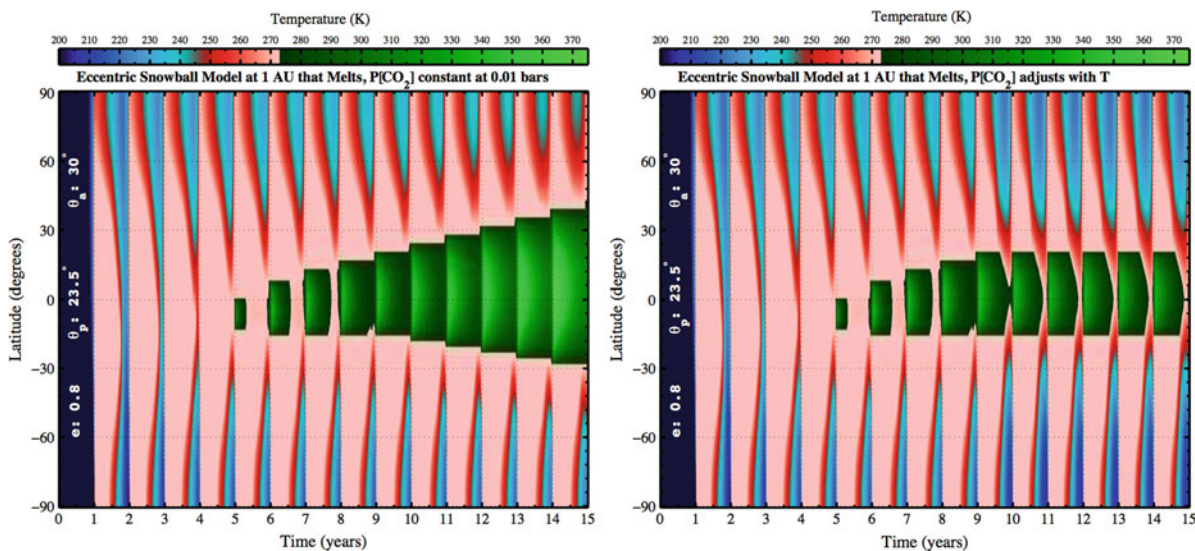


Fig. 1 Temperature evolution maps for cold-start models at 1 AU. Both models have orbital eccentricity of 0.8 along with Earth-like 23.5° polar obliquity and 1-bar surface pressure. Temperature is initialized to 100 K and quickly rises to near 273 K. The melting of the ice cover is handled in accordance with the prescription of Spiegel et al. (2010). *Left*: CO_2 partial pressure is held constant at 0.01 bars. In this model, once the

equatorial region melts, the region of surface that has melted ice cover grows steadily until the entire planet has melted, and temperatures eventually grow to more than 400 K over much of the planet (not shown). *Right*: CO_2 partial pressure varies with temperature, in a crude simulation of a "chemical thermostat." In this model, the climate reaches a stable state with equatorial melt regions and polar ice cover

feature of water-rich terrestrial planets, and such planets might have a tendency to enter snowball states. The ice-albedo feedback makes it quite difficult for a planet to recover from such a state. In temperate conditions, the Earth's carbonate–silicate weathering cycle acts as a “chemical thermostat” that tends to prevent surface temperatures from straying too far

from the freezing point of water. A snowball state would interrupt this cycle. The standard explanation of how the Earth might have exited its snowball state is that this interruption of the weathering cycle would have allowed carbon dioxide to build up to concentrations approaching ~ 1 bar over a million to 10-million years, at which point the greenhouse effect

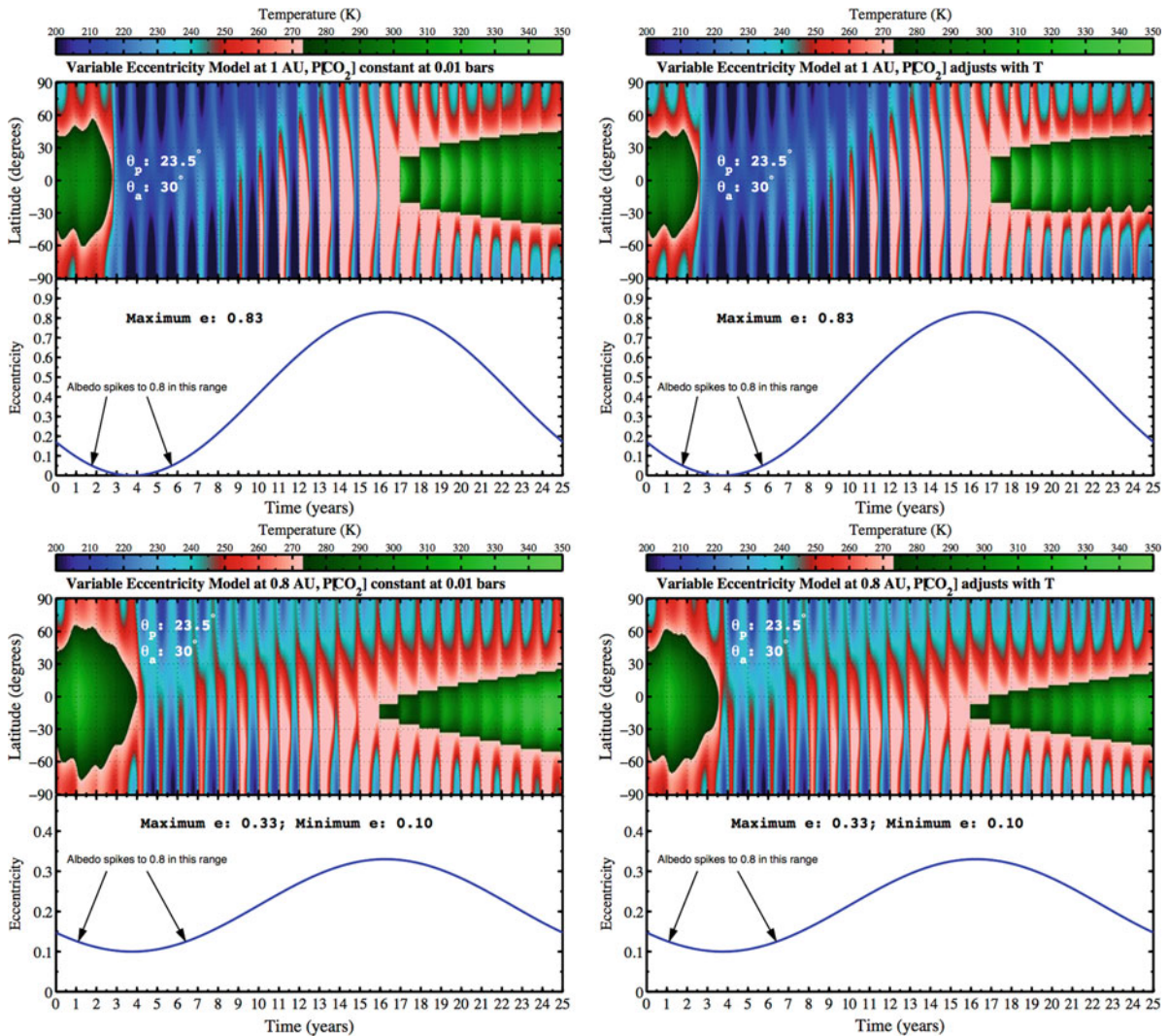


Fig. 2 Compressed Milankovitch-like evolution of eccentricity and temperature at 1 AU and at 0.8 AU. Planets are initialized with warm equator and cold poles, similar to present-day Earth. In the top row (1 AU), the model planets are the same as in Fig. 1, except the eccentricity varies sinusoidally between 0 and 0.83 with a 25-year period, to simulate a time acceleration (by a factor of $\sim 10^2$ to $\sim 10^4$) of a Milankovitch-like cycle. When the eccentricity falls below 0.05, the planet's albedo spikes to 0.8, simulating a catastrophic event that

plunges the planet into a snowball state, with the latent heat prescription of Spiegel et al. (2010). In the bottom row (0.8 AU), the eccentricity varies between 0.1 and 0.33, also with a 25-year period. *Left*: CO_2 partial pressure is held fixed at 0.01 bars. As in the left panel of Fig. 1, these planets do not establish a temperate equilibrium. *Right*: CO_2 partial pressure varies with temperature. Here, temperature increases are muted by reduced greenhouse effect once the ice cover has melted somewhere

would have been sufficient to melt the ice cover and restore temperate conditions.

However, an exoplanet in a snowball state that is undergoing a large excitation of its eccentricity might be able to melt out of its globally frozen state in significantly less time, depending on the magnitude of the eccentricity variations and on other properties of the planet. Exploring this possibility is the primary focus of Spiegel et al. (2010), in which, using an energy balance climate model, we searched for orbital configurations that would lead to an ice-covered planet melting out of the snowball state. In brief, we found that orbital configurations that are not unlikely could cause a snowball-Earth-analog to melt out by dint of increased eccentricity.

Figure 1 shows the temperature evolution of two cold-start planet models, one of which (on the right) has a crude approximation of a carbonate–silicate cycle incorporated in the infrared cooling term and the other (on the left) does not. Both model planets have orbital semimajor axis 1 AU and are initialized to very cold temperatures. The high orbital eccentricity of these models (0.8) causes them to intercept more stellar irradiation over the annual cycle than would a model on a circular orbit. They therefore heat rapidly and, with a crude accounting of the latent heat of melting/freezing water (see Spiegel et al. 2010), are eventually able to melt through the ice layer. Figure 2 shows two different compressed Milankovitch-like cycles. In each, a cycle that might take 10,000–

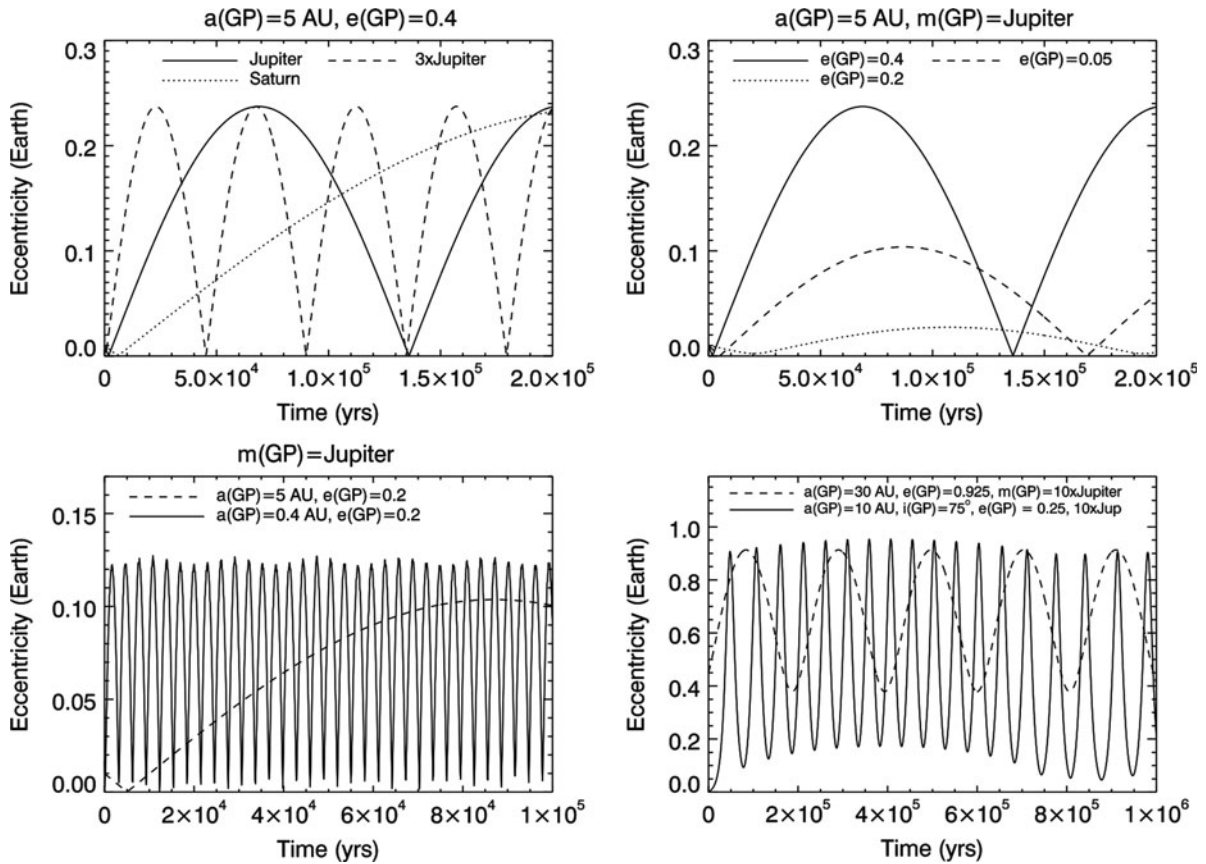


Fig. 3 Eccentricity evolution of an Earth-mass planet at 1 AU under the influence of a range of giant planet masses and orbits, labeled by the giant planet (GP) semimajor axes a , eccentricities e , and masses M . *Top left*: Effect of changing the giant planet mass between Saturn’s mass and $3\times$ Jupiter’s mass for the case of $a_{\text{GP}} = 5$ AU, $e_{\text{GP}} = 0.4$. *Top right*: Effect of changing the giant planet eccentricity between 0.05 and 0.4 for the case of $a_{\text{GP}} = 5$

AU, $M_{\text{GP}} = M_{\text{Jup}}$. *Bottom left*: Two cases with similar eccentricity amplitudes but very different planetary system architectures, although both with $M_{\text{GP}} = M_{\text{Jup}}$: $a_{\text{GP}} = 0.5$ AU, $e_{\text{GP}} = 0.1$ (solid line) and $a_{\text{GP}} = 5$ AU, $e_{\text{GP}} = 0.4$ (dashed line). *Bottom right*: An extreme case, with $a_{\text{GP}} = 30$ AU, $e_{\text{GP}} = 0.925$, and $M_{\text{GP}} = 10 M_{\text{Jup}}$ (dashed line) and with $a = 10$ AU, $e_{\text{GP}} = 0.25$, and $M_{\text{GP}} = 10 M_{\text{Jup}}$, and $i_{\text{G}} = 75^\circ$ (solid line)

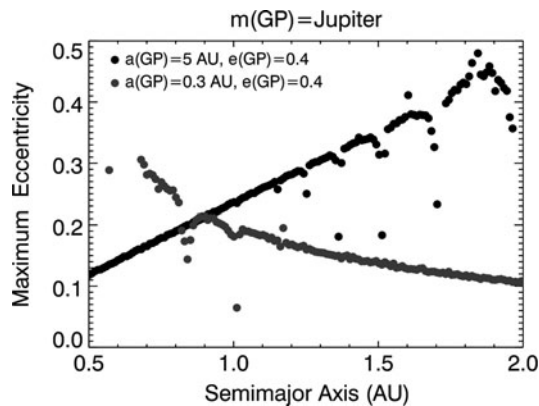


Fig. 4 The maximum eccentricity reached by a disk of massless test particles over a million-year integration of two systems containing a single Jupiter-mass giant planet in different configurations: $a_{\text{GP}} = 5$ AU, $e_{\text{GP}} = 0.4$ (black dots), and $a_{\text{GP}} = 0.4$ AU, $e_{\text{GP}} = 0.2$ (gray dots)

400,000 years is compressed to 25 years for computational feasibility and visualization purposes. In one (the top row), the planet is at semimajor axis 1 AU and has eccentricity varying sinusoidally between 0 and 0.83. In the other (bottom row), the planet is at semimajor axis 0.8 AU and has eccentricity varying between 0.1 and 0.33. In each case, after several years, a “catastrophic event” dramatically increases the albedo for several years, so as to plunge the model planet into a snowball state. The increasing eccentricity, then, eventually leads the planet to melt out of the snowball state. Finally, Figs. 3 and 4 exemplify the magnitudes and frequencies of Milankovitch-like eccentricity oscillations that can result from gravitational interactions between an eccentric giant planet and a terrestrial planet. The lower-right panel of Fig. 3 displays several extreme eccentricity cycles that are possible with Kozai interactions, with eccentricity oscillating to above 0.9 and back to near 0. Though these kinds of oscillations might be rare, they are not impossible. Entirely prosaic planetary system architectures can lead to less dramatic, but still highly important, variations of a terrestrial planet’s eccentricity.

In the coming years, as new observatories such as the James Webb Space Telescope come online,

exploring the atmospheres and atmospheric dynamics of exoplanets will become an increasingly tractable research problem. Already, planets of the hot Jupiter class have been amenable to investigation with the *Spitzer* Space Telescope, *Kepler*, and various ground-based observatories (Harrington et al. 2006; Knutson et al. 2007; Spiegel et al. 2009b; Showman et al. 2009). It might even be possible to probe the atmospheric composition of even extremely distant exoplanets, in the Galactic bulge (Spiegel et al. 2005). Discerning the spectral signatures of habitability and of life will be the next frontier (Kaltenegger et al. 2010). As the field of exoplanets matures, it will be important to keep in mind that the long-term climatic habitability of a planet might depend not just on the intrinsic properties of the host star and of the planet itself, but also on the detailed architecture of the planetary system in which the planet resides.

References

- Berger A (1975) *Ciel et Terre* 91:261
 Berger AL (1976) *Astron Astrophys* 51:127
 Berger AL (1978) *J Atmos Sci* 35:2362
 Berger A, Mélice JL, Loutre MF (2005) *Paleoceanography* 20:A264019+
 Dressing CD, Spiegel DS, Scharf CA, Menou K, Raymond SN (2010) *ApJ*, 721, 1295–1307
 Harrington J, Hansen BM, Luszcz SH, Seager S, Deming D, Menou K, Cho JYK, Richardson LJ (2006) *Science* 314:623
 Hays JD, Imbrie J, Shackleton NJ (1976) *Science* 194:1121
 Kaltenegger L et al (2010) *Astrobiology* 10:89
 Kasting JF, Whitmire DP, Reynolds RT (1993) *Icarus* 101:108
 Knutson HA, Charbonneau D, Allen LE, Fortney JJ, Agol E, Cowan NB, Showman A, Cooper CS, Megeath ST (2007) *Astrophys J* 447:183
 Showman AP, Fortney JJ, Lian Y, Marley M, Freedman RS, Knutson HA, Charbonneau D (2009) *Astrophys J* 699:564
 Spiegel DS, Zamojski M, Gersch A, Donovan J, Haiman Z (2005) *Astrophys J* 628:478
 Spiegel DS, Menou K, Scharf CA (2008) *Astrophys J* 681:1609
 Spiegel DS, Silverio K, Burrows A (2009a) *Astrophys J* 699:1487
 Spiegel DS, Menou K, Scharf CA (2009b) *Astrophys J* 691:596
 Spiegel DS, Raymond SN, Dressing CD, Scharf CA, Mitchell JL (2010) *ApJ*, 721, 1308–1318
 Williams DM, Kasting JF (1997) *Icarus* 129:254
 Williams DM, Pollard D (2003) *J Astrobiol* 2:1

Part III

**Ecohydrology, Water Resources and Climate
Change**

Aquatic Vegetation in River Floodplains: Climate Change Effects, River Restoration and Ecohydrology Aspects

Georg A. Janauer

Abstract

Climate change is one of the most severe threats to the environment in this century. Its possible effects on the aquatic vegetation in river and floodplain habitats are described by relation to carbon dioxide, temperature, precipitation and water discharge, as well as species migration and alien aquatic plants. Potential conflicts between river restoration and habitat conservation are briefly explained. Sensible solutions need approaches that include ecohydrology principles and mediate between diverging stakeholder interests.

Introduction

Aquatic macrophyte vegetation is an important biotic component in rivers, lakes and floodplain waters, and it is part of land/water ecotones (Naiman et al. 1988; Janauer 2003; Zalewski et al. 2008). Ecotones can be determined in different scales, from transients between vegetation types to the borders of individual ecotone patches and to river floodplains intersecting terrestrial areas. In relation to their size, they provide different types of ecosystem services and to a different extent (MEA 2005; Zalewski et al. 2008, p.308). These ecosystem services are ecosystem functions (Keddy 2002, p.57, Regulation/Carrier/Production/Information functions) that serve human needs of many kinds, but are vulnerable with regard to climate change effects (Exler et al. 2009).

Ecosystem services can be seen as low-cost tools for, e.g. controlling hydrological properties on catchment or floodplain level, nutrient retention or as food source (Table 1). On the other hand, hydrological effects can be used to control macrophytes. Species composition and especially the type of dominant growth form are subject to water flow impact and in return define available ecosystem services (Fig. 1).

Knowledge about aquatic macrophyte-dominated floodplains is available for several geographic regions, but the adoption of ecosystem services in the sense of ecohydrological planning is scarce. The difficulties mainly arise from different goals of stakeholders when proposing ecohydrological strategies, i.e. sustaining wetland areas as a flood retention tool and biodiversity focus in regions with high or increasing population density (Wagner et al. 2009).

Ecohydrological strategies and planning (Janauer 2002; Zsuffa et al. 2002) face one essential obstacle: how to inter-relate processes and models developed for environmental drivers, like climate and hydrology, with the biological elements—in this study, the focus is directed to the vegetation of riparian wetlands, ranging from elements which can be detected by

G.A. Janauer (✉)
Department of Limnology and Hydrobotany, University of
Vienna, Althanstrasse 14, 1090 Vienna, Austria
e-mail: georg.janauer@univie.ac.at

low-resolution remote sensing down to habitat types and, e.g. individual, especially protected, species.

Today, river floodplains and their water bodies, like side channels, oxbows, sloughs, etc., are the refuges for aquatic plants, as their native habitats have fallen victim to changing and intensifying land use in the cultural landscape of Europe. Few floodplain waters are still directly influenced by the water levels in the main river channel, as many are located today outside dams, protecting the agricultural areas and settlement and urban areas.

Climatic changes are predicted for this century which may influence terrestrial but also aquatic environments to some, possibly great, extent (Fig. 2).

Aquatic environments, especially running waters, may not be influenced to such a great extent by rising temperatures, but certainly, increase or decrease of precipitation will modify run-off conditions by amount and seasonality. This may change the basic character of some types of running waters and their

Table 1 Ecosystem services, which are based on the existence of wetlands (Keddy 2002)

- Groundwater recharge/discharge
- Flood flow alteration/flood reduction
- Sediment stabilisation/retention (incl. toxicants)
- Nutrient removal/transformation
- Carbon transformation
- Wildlife diversity/abundance/breeding/migration/wintering
- Aquatic diversity/abundance
- Uniqueness/heritage
- Recreation

floodplains. In the Danube River basin, the existing gradients between high- and low-elevation areas and the western and eastern parts will be enhanced in any case. The examples for possible climate change effects on the aquatic vegetation are presented for the Danube River basin in this context.

The Aquatic Vegetation in the Danube River

Two studies reflect the present status of the aquatic macrophyte vegetation in the Danube River main channel and in the floodplain waters. The main channel was last studied in selected reaches during the Joint Danube Survey 2, organised by the International Commission for the Protection of the Danube River (Janauer et al. 2008). Additional information is drawn from the database of the full river length study Danube Macrophyte Survey, carried out during 1998 (Pilot Study, Janauer et al. 2003) and between 2000 and 2004 (MIDCC project, Janauer et al. 2005).

Climate Change Effects and the Aquatic Vegetation

Atmospheric CO₂ Concentration

Concentrations of CO₂ and O₂ in water bodies are in equilibrium with the concentration in the atmosphere, when considering longer time periods. Quicker

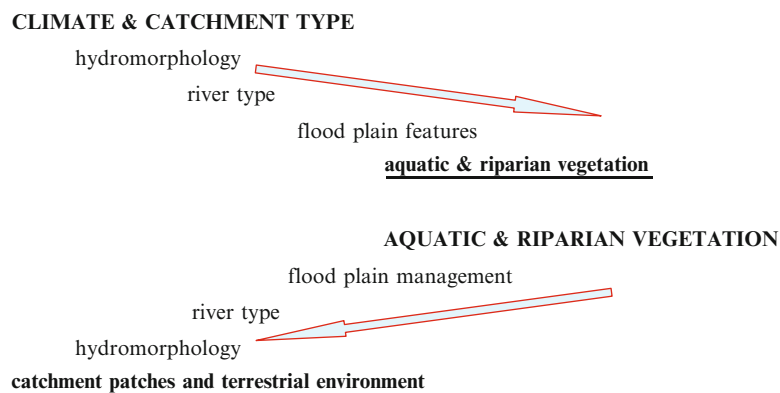


Fig. 1 The employment of ecohydrological strategies focus at reversing, in part, the cascade driven by climate and physical environment into directions where vegetation elements and

floodplain management lead to determining discharge pattern and river impact on the adjacent terrestrial environment

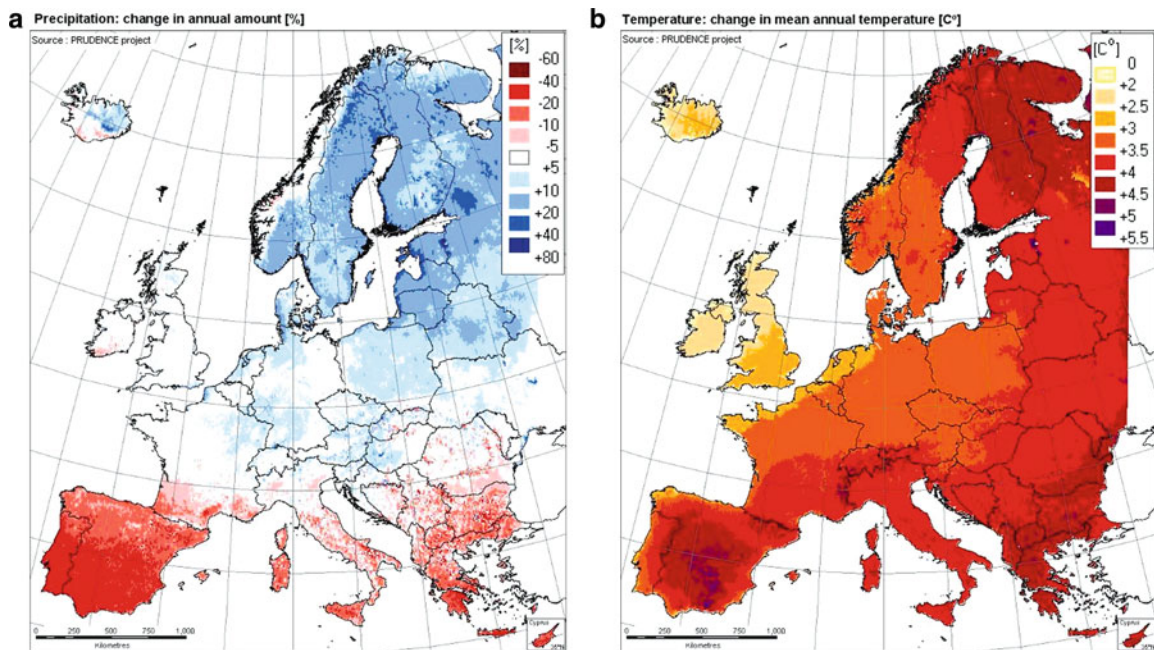


Fig. 2 Predicted changes until 2100 in temperature (*left*; annual, %) and precipitation (*right*; annual, %). Danube River basin marked by *elliptical line*. Modified after PRUDENCE project (<http://prudence.dmi.dk/>)

equilibration occurs in turbulent water, but biotic processes (photosynthesis, respiration) modify the gas regime especially in still or slow-flowing water (Wetzel 2001; Schönborn 2003). Should CO₂ concentrations increase above the present level especially those growth types of aquatic plants, which raise their leaves to the water surface or even above, as well as all reed species, may gain the highest advantages of that situation. Access to the atmospheric carbon pool offers to all aquatic species capable of such a strategy a competitive benefit, with the chance to outgrow especially the submersed vegetation, which will benefit from higher CO₂ concentrations in water, too, but to a much lesser extent. As reeds play a prime role in the littoral succession, all processes converting water bodies into semi-terrestrial and terrestrial environments will be stimulated.

Temperature

Aquatic environments provide habitats with more constrained seasonal amplitudes of temperature than terrestrial systems. The development of many aquatic organisms, e.g. the succession of larval stages of invertebrates, is determined by the ambient

temperature regime (Humpesch 1982). Moreover, a shift in this regional regime uncouples their development from the food requirement of other organisms higher up in the food chain. Aquatic plants are somewhat more tolerant to temperature changes, but rising temperature induces seasonal shifts in germination period, which will influence the pattern of competition: there is little knowledge how the different strategies of vegetative propagation (stolons, turions, winter buds, hibernating full size plants, etc.) and seed banks will react (Jensch and Poschold 2008; Saatkamp et al. 2009).

Higher temperatures are expected to have their strongest influence on aquatic macrophytes especially in still waters, where the competitive power of plant species adapted or tolerant of these conditions will increase. Among the emergent plants living on riverbanks and in the supra-littoral of still waters, species with a C₄ metabolism of photosynthesis get a higher chance of invading habitats of native reed and bank species. With increasing temperature, the growth periods of plants will be influenced and, especially in sheltered habitats species which so far could not finish their reproductive cycle, may have a chance to propagate successfully, enhancing their invasive potential.

Precipitation and Discharge

Climate change models (Fig. 2) predict increased precipitation in the mountain regions of the Danube basin, with a direct effect on discharge. More frequent flood events and a higher frequency of spates will increase erosive powers in the streams and rivers but not in all regions to the same extent (Toffol et al. 2008). Submersed as well as bank species will thus be threatened by enhanced physical eradication due to higher water flow velocities. Also the negative effects of deeper and possibly longer immersion, but seasonally distributed to periods less synchronised with plant development cycles are a direct threat to the aquatic vegetation.

In the lowland regions of the Danube basin, models predict up to severe decreases in precipitation, which will result in essential losses in water depth during summer periods especially in floodplain waters. Such effects can already be seen, e.g. in some oxbows of the Tisza River (Janauer, Mandoki, Zsuffa, unpublished), where water level lowering supports a progressive expansion of highly competitive water nut (*Trapa natans*). Less run-off will also affect water flow velocities, which will enhance the competitive power of aquatic species which tend to form dense biomass on the water surface, especially floating leaf types (water lilies, water nut) and free-floating species (duckweeds, water fern), capable of exterminating the submersed vegetation and its associated aquatic fauna.

Some less direct effects accompany enhanced run-off: heavy precipitation, possibly more frequent in the future, and shifting from snow to rain in the cold season increase surface erosion and lead to nutrient enrichment in streams and rivers and in their adjacent floodplain waters. This can lead to enhanced growth of aquatic vegetation: if the nutrient-storing capacity of macrophyte species fails to accumulate this additional load, a real threat of enhanced eutrophication, extreme phytoplankton development ('algal blooms', Dokulil and Janauer 2000) and deterioration of water quality exists.

In regions with less-developed wastewater and sewage treatment, similar effects of increased run-off and flood frequency are expected: examples from the Brahmaputra catchment clearly indicate strong pollution effects resulting from flooding of septic pits in regions lacking modern sewage treatment systems

(personal communication, Brahmatwin Project, Lhasa Workshop, 2008). However, some authors have shown evidence that socio-economic decisions shaping future development of landscapes are considered a stronger driver for sustaining protected areas and conservation of biodiversity than climate change impact (Richards et al. 2008).

Species Migration and Alien Species

Plant species establish their area of occurrence where favourable environmental conditions are present. Following climate change impact, these areas will shift inevitably. For species native to and/or established already in some parts of the Danube River corridor—which consists mainly of what is left of the floodplain after river regulation and the construction of flood retention levees—this can trigger regional migration, e.g. species occurring in the lower and middle Danube River, and adapted to higher temperatures, migrate up the river corridor into habitats which have then transformed into suitable ecological niches. Despite the fact of being 'native' to the Danube River corridor, such species may turn 'invasive', either in their present habitats or in habitats they reach due to climate change-induced migration.

The other type of invasion is linked to aquatic macrophyte and true riverbank-based species, which are alien to the Danube River corridor. Table 2 provides an overview on these alien species recorded so far in Germany's large river systems, which are a good example for the situation in all Western European countries. A few species (Table 2) are already established in the Danube but so far with no detrimental effect on the whole aquatic plant community. Yet, the connection of the Danube and Rhine basins by the Rhine–Main–Danube–Canal will eventually lead to other non-native species crossing the natural geological barrier between Western and Central–Eastern Europe.

Alien species (EU 2009; IDB 2009) belonging to the group of submersed plants may shift the dominance pattern but need not bear the threat of exterminating all other species, as present examples from channels and lakes in the Danube Delta are indicating, where extremely dense aquatic vegetation was recorded (Sarbu 2003). Danger of extermination of native species will be related to all kinds of plants

that tend to cover the water surface completely with dense and thick canopies (Fig. 3), depriving all submersed plant species of light and—in case of developing anaerobic conditions below these mats—of the necessary access to oxygen for the aquatic

fauna, as French examples have shown (Gassmann et al. 2002).

Distribution lines for aquatic species are the natural river corridors as well as man-made canals and other water bodies. In the Danube basin, there is evidence that *Salvinia* has a tendency for proceeding up-river, as two short—however man-induced—outbreaks in Vienna have shown. Journeying down the Danube was *Elodea nuttallii* in the last decades, which finally reached the Delta area (Sarbu 2003), and *Callitriche obtusangula*, known from Germany in the 1980s, proceeded from W to E along the Austrian Danube in the next decade (Englmaier, personal communication). Species of foreign origin are usually propagated by man, as too abundant aquatic plant biomass from aquaria and ‘bio-swimming pools’ (e.g. *Pistia*, *Vallisneria*, *Salvinia*) ends up in rivers and still waters, not to forget commercial navigation as a carrier of propagules. This process is already an increasing current threat, especially for still and slow-flowing water bodies, where canopy-building species find perfect conditions for mass development. Therefore, many negative effects are expected for aquatic ecosystems and biodiversity on international and national scale, on fish ecology and sports fishery, with regard to sedimentation rates in still waters (due to decaying plant biomass) and enhanced water loss by transpiring reed-like species, but also on leisure and recreation activities. Great concern is devoted to alien species invasion and migration of native species in the context of the European Water Framework Directive and the Reference Conditions, which provide the benchmark for assessing the ecological status of water bodies (EU WFD GD 24 2009).

Table 2 Alien aquatic species with relevance to the Danube basin

<i>Azolla filiculoides</i>	(1980)
<i>A. mexicana</i> c.f.	(?)
<i>Crassula helmsii</i>	(1988)
<i>Egeria densa</i>	(1914)
<i>Eichhornia crassipes</i>	(?)
<i>Elodea canadensis</i>	(?)
<i>E. nuttallii</i>	(1953)
<i>Hydrocotyle ranunculoides</i>	(2004)
<i>Hydrilla verticillata</i>	(1907)
<i>Hygrophila polysperma</i>	(2005)
<i>Lagarosiphon major</i>	(1970)
<i>Lemna aequinoctialis</i>	(1980)
<i>L. minuta</i>	(1990)
<i>L. turionifera</i>	(1965)
<i>Myriophyllum aquaticum</i>	(1988)
<i>M. heterophyllum</i>	(1960)
<i>Pistia stratiotes</i>	(?)
<i>Sagittaria latifolia</i>	(1952)
<i>S. subulata</i>	(1980)
<i>Salvinia</i> sp.	(?)
<i>Shinnersia rivularis</i>	(1992)
<i>Vallisneria spiralis</i>	(1900)

Dates in brackets: first occurrence in Germany (Adapted after van de Weyer, <http://www.aquatischeneophyten.de/>). Alien species present in the Danube basin today are indicated by bold italics

Unknown date of introduction indicated by (?)



Fig. 3 Csatloi oxbow, Tisza River (Hungary). Infestation of water nut (*Trapa natans*) in 2004 (left) and 2006 (right). Copyright: Georg A. Janauer © 2006

River Restoration Strategies and Ecohydrology

In the nineteenth and first of the twentieth century, rivers have been regulated throughout the world and in the Danube basin as well. Flood protection levees separating former floodplain areas and flood retention space, river straightening that resulted in cutting off meanders and river bends and triggered enhanced bed erosion and water level lowering in the adjacent floodplain, integration of constructions for flow regulation to the benefit of navigation, and the construction of hydroelectric power plants which interrupted the river continuum transformed natural rivers into the man-made environments we can see today. River restoration today aims at merging flood protection and environmental restoration. In this process, protected parts of the floodplain are re-activated for retention purposes, and the river course is directed back into its former main and secondary channels, where feasible. The European Water Framework Directive supports these aims as it requests all water bodies to reach good ecological status by 2015, or latest 2027. However, floodplain waters like oxbows and smaller side channels have developed into individual habitats since regulation often more than 100 years ago. They converted from active river channel in last refuges for aquatic vegetation and associated fauna, as the former floodplain outside the levees was restructured into agricultural, urban or industrial areas. The European Habitats Directive (CD 1992), together with the Birds Directive and the Natura 2000 networks, focuses on such relict, and rare habitats and their biotic contents, which necessarily leads to a conflict of interest regarding the above-mentioned restoration strategies. The same is true when considering the implementation of basic ecohydrological strategies, which call for increasing the active floodplain areas: as a result, many refuge habitats will be exterminated when separated floodplain waters like oxbow systems will get flushed with the river taking back its old course.

Conclusion

Upon deeper consideration, there are no fundamental obstacles against the implementation of ecohydrological principles (see Fig. 1), like enlarging areas with appropriate vegetation for flood retention and saving water bodies with aquatic

plants for nutrient and sediment retention. Even climate change impacts may be mediated by ecohydrological strategies as an integrated part of water management. But as examples have shown, e.g. in the Assam Brahmaputra reach, this depends on the attitude and the prioritisation of goals by stakeholders and decision-makers—and on area planning that reaches beyond the local perimeter. As long as food production, development of settlements and other economic aspects are seen separate from the need of protecting biological diversity, and from the benefits provided by ecosystem services, no ecologically sustainable solutions can be reached in river restoration and river basins management. Recent EU documents do not rank climate change effects prior to direct social and economic impacts on aquatic environments in the near future. This should provide decision-makers and engineers with enough time to consider ecohydrological solutions, based on ecosystem services, for establishing Integrated Water Resource Management wherever possible in Europe's cultivated landscapes.

Acknowledgements The author thankfully acknowledges UNESCO's support for participation in the Milutin Milankovitch Anniversary Symposium 2009.

References

- CD (1992) Council Directive 92/43/EEC of 21 May 1992 on the conservation of natural habitats and of wild fauna and flora. <http://eur-lex.europas.eu/LexUriServ/LexUriServ.do?uri=CELEX:31992L0043:EN:NOT;20100214>
- de Toffol S, Engelhard C, Rauch W (2008) Influence of climate change on the water resources in an alpine region. *Water Sci Technol* 58:839–846
- Dokulil MT, Janauer GA (2000) Alternative stable states of macrophytes versus phytoplankton in two interconnected impoundments of the New Danube (Vienne, Austria). *Arch Hydrobiol* 135:75–83
- EU (2009) Invasive alien species. European Commission/Environment. Publication Office, Brussels, 4pp
- EU WFD GD 24 (2009) River basin management in a changing climate. Guidance document 24. Technical report – 2009-040. European Commission/Environment, Brussels, 141pp
- Exler N, Wagner I, Janauer GA (2009) Biodiversity and remote sensing in relation to diverging scales in the BRAHMATWINN project. In: Hartmann M, Weipert J (eds) Biodiversität & Naturlandschaft im Himalaya, vol III. pp 25–30

- Gassmann A, Cock M, Shaw R (2002) The potential for biological control of exotic *Ludwigia* species and other alien aquatic weeds in France and in Europe. In: Dutartre A, Montel MH (eds) Proceedings of the 11th EWRS symposium, Moliets et Maa (France). CEMAGREF, Bordeaux, pp 359–362
- Humpesch U (1982) Effect of fluctuating temperature on the duration of embryonic development in two *Ecdyonurus* spp. and *Rhithrogena cf. hybrida* (Ephemeroptera) from Austrian Streams. *Oecologia* 55:285–288
- IDB (2009) Invasive alien species. Secretariat of the Convention on Biological Diversity, Montreal, 45pp
- Janauer GA (2002) Establishing ecohydrology in the real world: the Lobau Biosphere Reserve and the integrated water scheme in Vienna. *Ecohydrol Hydrobiol* 2:119–126
- Janauer GA (2003) Makrophyten der Augewässer. In: Janauer GA, Hary N (eds) Ökotonie Donau – March. Austrian MAB-Programme – AAS Series 29. Universitätsverlag Wagner, Innsbruck, pp 156–200
- Janauer GA, Hale P, Sweeting R (2003) Macrophyte inventory of the river Danube: a pilot study. *Arch Hydrobiol* 147:205–216
- Janauer GA, Link FG, Kohler A (2005) Wasserpflanzen und Habitate an der Donau: Streiflichter aus dem internationalen Donau-Studienprojekt, Beiträge der Akademie für Natur- und Umweltschutz Baden-Württemberg. Wissenschaftliche Verlagsgesellschaft mbH, Stuttgart, pp 110–125
- Janauer GA, Schmidt B, Greiter A (2008) Macrophytes. In: Liska I, Wagner F, Slobodnik J (eds) Joint Danube Survey 2 – Final scientific report. International Commission for the Protection of the Danube River, Vienna, Austria, pp 54–60
- Jensch D, Poschlod P (2008) Germination ecology of two closely related taxa in the genus *Oenanthe*: fine tuning for the habitat? *Aquat Bot* 89:345–351
- Keddy PA (2002) Wetland ecology. Principles and conservation. Cambridge University Press, Cambridge, 614pp
- MEA – Millennium Ecosystem Assessment (2005) Ecosystems and human well-being: wetlands and water. General synthesis report. World Resources Institute, Washington, DC, 155pp. <http://www.millenniumassessment.org/documents/document.356.aspx.pdf>
- Naiman RJ, Decamps H, Pastor J, Johnston CA (1988) The potential importance of boundaries to fluvial ecosystems. *J N Am Benthol Soc* 7:289–306
- Richards JA, Mokrech M, Berry BM, Nicholls RJ (2008) Regional assessment of climate change impacts on coastal and fluvial ecosystems and the scope for adaptation. *Clim Chang* 90:141–167
- Saatkamp A, Affre L, Dutoit T, Poschlod P (2009) The seed bank longevity index revisited: limited reliability evident from a burial experiment and database analyses. *Ann Bot* 104:715–724
- Sarbu A (2003) Inventory of aquatic plants in the Danube Delta: a pilot study in Romania. *Arch Hydrobiol* 147:205–216
- Schönborn W (2003) Lehrbuch der Limnologie. Schweizerbart, Stuttgart, 588pp
- Wagner I, Exler N, Janauer GA (2009) Natural environment assessment and vegetation indicators for IWRM scenarios in the Upper Brahmaputra River Basin. *Geophys Res Abstr* 11, EGU 2009-9919
- Wetzel RG (2001) Limnology. Lake and River Ecosystems. Academic, San Diego, 1006pp
- Zalewski M, Harper DM, Demars B, Jolankai G, Crosa G, Janauer GA, Pacini N (2008) Linking biological and physical processes at the river basin scale: the origins, scientific background and scope of ecohydrology. In: Harper DM, Zalewski M, Pacini N (eds) Ecohydrology: processes, models and case studies. CABI, Wallingford, UK, pp 1–17
- Zsuffa IJ, Patake B, Jolankai G (2002) Hydro-ecological revitalisation of the Gemenc floodplain in Hungary. *Ecohydrol Hydrobiol* 2:127–134

Canadian Regional Climate Model as a Tool for Assessing Hydrological Impacts of Climate Change at the Watershed Scale

Biljana Music, Daniel Caya, Anne Frigon, André Musy, René Roy, and David Rodenhuis

Abstract

Recent impact studies indicate that water resources in many regions of the world can be strongly affected by climate change. Different approaches and techniques have been developed to assess the hydrological impacts at different scales. The first part of this chapter is an overview of the techniques designed to evaluate global warming effects on runoff, which can be considered as a measure of water availability. The advantages and shortcomings of these techniques are briefly discussed. The second part focuses on direct use of climate-model runoff for hydrological impact studies. Uncertainties associated with this approach are discussed, and some of them are assessed by comparing hydrological balance components for several watersheds in western North America simulated by the Canadian GCM and the Canadian RCM.

Introduction

Numerical modeling is a commonly accepted approach for assessing climate change impacts on hydrological regimes at various scales. The following modeling tools/techniques are normally used: Global Climate Models (GCMs), Regional Climate Models (RCMs), statistical downscaling techniques, and hydrological models (HM). Global Climate Models simulate future climate under assumed greenhouse gas emission scenarios. As these models have a coarse spatial resolution, application of downscaling techniques is

required to provide information at regional/local scale. Downscaling of GCM large-scale variables involves application of RCMs and/or statistical downscaling techniques. An overview of various methods used to assess hydrological impacts of climate change at the watershed scale is given in section “Methods for Evaluation of a Watershed Hydrological Response to Global Climate Change.” Some advantages and shortcomings of these approaches are also discussed.

The second part of this study explores the opportunity of directly using climate-model runoff for hydrological impact studies. Water budget components simulated by the Canadian Global Climate Model (CGCM, Flato and Boer 2001; Scinocca et al. 2008) and the Canadian Regional Climate Model (CRCM, Caya and Laprise 1999; Plummer et al. 2006; Music and Caya 2007) for several watersheds in western North America (Columbia, Fraser, Upper Peace, and Campbell) are investigated. These watersheds covered by the CRCM and CGCM computational grids are

B. Music (✉)

Ouranos, Consortium sur la climatologie régionale et l'adaptation aux changements climatiques, Montréal, QC, Canada

Centre ESCER, Université du Québec à Montréal, Montréal, QC, Canada

e-mail: music.biljana@ouranos.ca

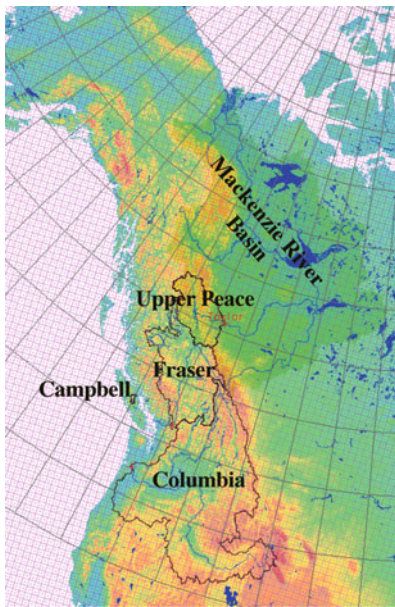


Fig. 1 Western North America with the Columbia, Fraser, Upper Peace, and Campbell watersheds outlined

presented in Fig. 1. Columbia and Fraser outlines are taken from US Geological Survey, while Upper Peace and Campbell watersheds are defined by BC Hydro.

Information about expected hydrological impacts of climate change at the watershed scale is of great interest and should help decision makers to better manage available water resources in the region. The Columbia River is the largest river in the Pacific Northwest with a drainage area of about 670,000 km², and is one of the most economically important rivers in the region. The Fraser River Basin is an unregulated river and drains a region of approximately 230,000 km². The Upper Peace River (Peace above Taylor) is important for hydroelectricity production with major power generation facilities located at W. A.C. Bennett Dam near Taylor. This watershed is a part of the Mackenzie River Basin and drains an area of about 100,000 km². The Campbell River is located on the Vancouver Island with a drainage area of approximately 1,050 km² with power generation facilities at Strathcona. In contrast to other watersheds considered, this is a very small drainage that will challenge the ability of the relatively coarse grid of the climate models. It is expected that the uncertainty involved in climate modeling becomes greater when moving from larger to smaller scale. The chaotic and nonlinear nature of the climate system processes

induces an irreducible uncertainty usually referred to as “internal variability”. Another important source of uncertainty is related to climate models’ imperfections: different models use different parameterization schemes, which involve many approximations of the actual physical processes. This uncertainty could be reduced by improving the reliability of our models. The choice of the computational grid and an appropriate numerical method to resolve model equations also contributes to the model’s structural uncertainty. The use of regional climate models involves an additional structural uncertainty associated with the nesting of the RCM domain in the driving GCM. Some of these uncertainty issues are addressed in sections “Investigation of a Watershed Hydrology as Simulated by the Canadian GCM and RCM and Related Uncertainty: Experimental Design” and “Simulated and Observed Annual Means of Hydro-meteorological Variables: Upper Peace Watershed” through comparison of water budget components over the Upper Peace watershed derived from several CGCM and CRCM simulations. An evaluation against available observations for the recent past (1961–1990) is also included in the analysis. Section “Hydrological Change Signal at a Watershed Scale: Upper Peace, Fraser, Campbell, and Columbia Watersheds” presents hydrological impacts of climate change as projected by an ensemble of simulations generated by a recent version of the CRCM (CRCM 4.2.3; Music and Caya 2007; de Elia and Côté 2010). Section “Summary and Conclusions” summarizes the results of this study.

Methods for Evaluation of a Watershed Hydrological Response to Global Climate Change

Various methods have been developed in the past few decades to assess the impacts of climate change on watershed hydrology. A schematic representation of these methods is shown in Fig. 2.

- (a) Direct use of GCMs’ hydrological outputs: this method is typically applied to assess future hydrological regime of the world’s largest river basins. For example, Arora (2001) investigated the potential effects of global warming on the hydrology of 23 macroscale watersheds using direct output from the Canadian GCM. The main advantage of this approach is conservation of water and energy that

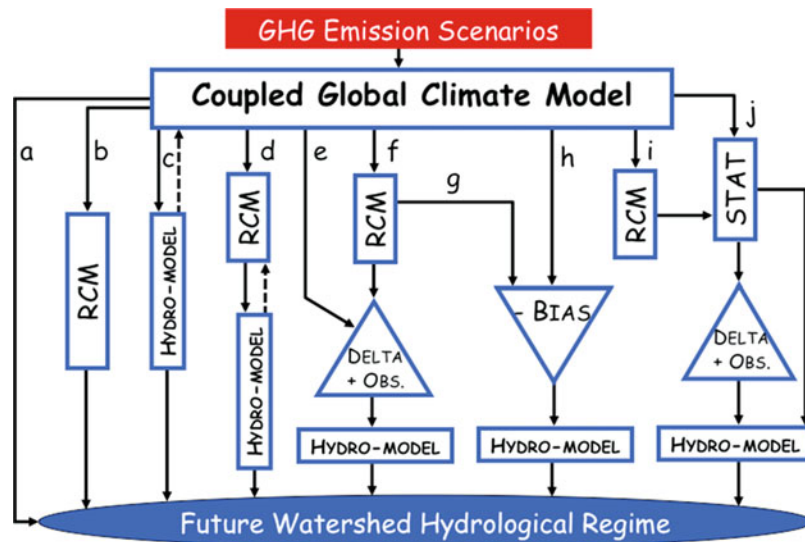


Fig. 2 Schematic representation of the methods used to assess watershed hydrological response to global climate change

allows an internal consistency of simulated hydrological cycle components. An important limitation is that coarse GCM's horizontal resolution limits model's ability to reproduce climate at the regional scale, especially in the regions with complex land-surface characteristics. This generally results in important systematic biases in water-related variables.

- (b) Direct use of RCMs' hydrological outputs: nesting an RCM within a GCM increases the spatial resolution of climate projections in a physically based way, while still maintaining the advantage of conservation in the water and energy budgets. RCM's finer horizontal resolution, typically of the order of tens of kilometers or less, is expected to improve reliability of simulated hydrological variables.
- (c) One-/two-way coupling of GCMs with hydrological models (HMs): terrestrial branch of the hydrological cycle is generally better described in HMs than in GCMs. Two-way coupling is possible between the so-called macroscale land-surface hydrological models (MLS-HMs) and GCMs, because MLS-HMs (as climate models) deal not only with water balance, but also with energy balance processes at the land surface. The energy and water budget equations are linked through the evapotranspiration term (Xu et al. 2005).
- (d) One-/two-way coupling of RCMs and HMs: this coupling is facilitated by the fact that the

difference in horizontal resolutions between these models is not as large as in the case of GCM-HM coupling.

- (e-h) Transferring GCM/RCM climate change signal to a hydrological model with perturbation (delta) and bias-correction methods: this technique is widely used in the hydrological science community. In the perturbation method, the change in climate variables derived from climate simulations is applied to observed time series; the resulting perturbed time series is then used as input to a hydrological model. One of the major disadvantages of this approach is that the extremes resulting from this approach are simply the extremes from present climate observations that have either been enhanced or dampened according to the delta factors. Recently, a more direct approach of transferring climate change signal from climate to hydrological models has been developed, referred to as bias-correction method. To correct the systematic biases in climate model outputs, some kind of scaling is applied to those outputs before transferring them to hydrological models. Although these techniques also have limitations, they are more consistent with the climate models compared to the perturbation approach (Graham et al. 2007).
- (i, j) Statistical downscaling of GCM/RCM outputs for use in hydrological models: GCM's

simulated present and future climates are first downscaled either by applying statistical downscaling technique or using a RCM, whose outputs are then statistically downscaled into local/regional-scale variables. These variables may be then used to drive a hydrological model or to derive climate perturbations, allowing application of the perturbation (δ) method. The major difference between statistical and dynamical downscaling is that the statistical approach does not attempt to simulate physical processes governing the climate system, but rather relies on cross-scale relationships between the large-scale atmospheric variables (*predictors*) and regional/local climate variables (*predictands*). The major theoretical weakness of statistical downscaling is that the cross-scale relationships derived for the present climate are considered to be also valid under altered climate conditions.

Investigation of a Watershed Hydrology as Simulated by the Canadian GCM and RCM and Related Uncertainty: Experimental Design

An appropriate experimental protocol was designed to answer the following questions:

1. What are the influences of natural variability and model structure/physical parameterizations on simulated hydrological regime by the CGCM?
2. What is the influence of driving CGCM's internal variability on a dynamically downscaled hydrological cycle?
3. What is the sensitivity of the water budget components to different physical parameterizations used in the CRCM?
4. What are CGCM's and CRCM's abilities to simulate the watershed hydrology?

Table 1 describes the simulations used to address the first question. The simulations named *AA*, *BB*, *CC*, *DD*, and *EE* were generated with the same version of the Canadian GCM (CGCM3) but differing in their initial conditions to allow the assessment of natural (or internal GCM) variability. Analysis is carried out over the period 1961–1990. The simulation *FF* is generated with CGCM2, which differs from CGCM3

Table 1 List of simulations used to assess natural variability as expressed in the CGCM as well as effects of the CGCM structure on simulated hydrological cycle

Experiment 1	Model version #member	GHG emission scenario	Analyzed period
AA	CGCM3#1	A2	1961–1990
BB	CGCM3#2	A2	1961–1990
CC	CGCM3#3	A2	1961–1990
DD	CGCM3#4	A2	1961–1990
EE	CGCM3#5	A2	1961–1990
FF	CGCM2#3	A2	1961–1990

in resolution but also in its physical parameterizations. Therefore, by comparing *FF* with the first five simulations, an idea of the structural uncertainty, which is related to the model design, can be obtained. Note that the CGCM2 uses spectral dynamics and resolution of T32 with ten vertical atmospheric levels (T32L10), while CGCM3 simulations were generated at a resolution T47L32. The parameterization package of CGCM3 version includes several important changes compared to CGCM2 (see Scinocca et al. 2008).

The second question is addressed by analyzing simulations listed in Table 2. Dynamical downscaling of five CGCM3 simulations, differing only in initial conditions, is performed by the CRCM using a 45-km horizontal mesh on a polar-stereographic projection (true at 60°N) with 29 vertical levels over the North American domain (AMNO; 200 × 192 grid points). Thirty-year means (1961–1990) of downscaled near-surface temperature and water budget components were calculated and compared to the corresponding value derived from CGCM3 simulations.

In order to assess the sensitivity of water budget components to different physical parameterizations being used in climate models, three additional CRCM simulations, generated with three CRCM versions, were analyzed (Table 3). Differences in the physical parameterizations of these three CRCM versions are described by Music and Caya (2007, 2009). Note that regional model in this experiment was nested within the same GCM simulation (CGCM2#3).

The question 4 is addressed by comparing simulated recent past (1961–1990) near-surface temperatures and water budget components with available observations. Gridded analyses of precipitation and near-surface temperature were taken from the Climatic Research Unit (CRU; Mitchell and Jones 2005) and the Center

Table 2 List of simulations used to assess effects of CGCM's internal variability on CRCM water budget components

Experiment 2	Model and version	Driving data	Analyzed periods
A	CRCM Ver. 4.2.3	CGCM3#1	1961–1990; 2041–2070
B	CRCM Ver. 4.2.3	CGCM3#2	1961–1990; 2041–2070
C	CRCM Ver. 4.2.3	CGCM3#3	1961–1990; 2041–2070
D	CRCM Ver. 4.2.3	CGCM3#4	1961–1990; 2041–2070
E	CRCM Ver. 4.2.3	CGCM3#5	1961–1990; 2041–2070

Table 3 List of simulations used to assess sensitivity of the CRCM hydrological cycle to different physical parameterizations

Experiment 3	Model and version	Driving data	Analyzed periods
F	CRCM Ver. 4.2.3	CGCM2#3	1961–1990
G	CRCM Ver. 3.7.1	CGCM2#3	1961–1990
H	CRCM Ver. 3.6.3	CGCM2#3	1961–1990

for Climate Research (CCR; Willmott and Matsuura 2001). For precipitation, two additional gridded datasets were used: the Global Precipitation Climatology Project (GPCP; Adler et al. 2003) and the Canadian gridded precipitation dataset (CAN; Louie et al. 2002). It is believed that gridded datasets are more preferable for model evaluation than data from an irregularly distributed station network. Also, bringing together datasets from different research centers allows for an evaluation of uncertainty in the observations. The research centers use different techniques to interpolate observed in situ precipitation (temperature) onto a selected grid. Also, the surface stations are not necessarily the same; some centers (e.g., GPCP) merge information coming from surface gauge with data from satellite measurements.

For runoff validation, streamflow observations at Taylor (Peace River) from the Canadian Hydrological Service are used (HYDAT; CD-ROM-version 99–2.00), as well as the unregulated (naturalized) flow dataset provided by BC HYDRO. The observed flow is divided by drainage area for comparison with the simulated runoff. Data of vertically integrated moisture flux convergence have been obtained from two atmospheric reanalysis: NCEP/NCAR (Kalnay et al. 1996) and ERA-40 (Uppala et al. 2005). Simulated snow water equivalent is validated against the Brown et al. (2003) dataset, which is based on observed and estimated snow depths from a simple snow model.

Simulated and Observed Annual Means of Hydro-meteorological Variables: Upper Peace Watershed

The first part of this section shows (1) the analysis of natural variability in the climate system as estimated by CGCM3 and (2) the sensitivity to structural changes in the model. Analysis is performed for six variables (near-surface temperature, T ; precipitation, P ; evapotranspiration, E ; moisture flux convergence, C ; snow water equivalent; SWE; and runoff, R) spatially and temporally averaged over the Upper Peace and over the 30-year period. Figure 3 shows that sensitivity of 30-year annual means to internal GCM variability is relatively small (see the differences in the purple bars). Maximum differences between values simulated by different CGCM3 members are 0.09 mm/day (3%) for P , 0.4°C for T , 0.09 mm/day (4%) for R and C , 9 mm (6%) for SWE, and 0.01 mm/day (2%) for E . On the other hand, simulated climate may be quite different when changes in model structure are introduced. Comparing FF (CGCM2 simulation; pink bar) to the AA , BB , CC , DD , and EE (CGCM3 simulations; purple bars), a large difference in simulated temperature (of about 5°C) can be noticed. Warmer temperature in CGCM2 simulation is consistent with smaller SWE (–120 mm or –84%) and higher evapotranspiration (1.13 mm or 200%). Precipitation in FF is higher by 1.43 mm/day (51%) than the CGCM3 ensemble mean. Runoff and moisture flux convergence were not available as CGCM2's prognostic variables, but can be estimated as a difference between simulated precipitation and evapotranspiration. The latter are higher by 0.30 mm/day (13%) than the CGCM3 runoff. In summary, the above results indicate that uncertainty induced by the chaotic nature of the climate system is much smaller than structural uncertainty related to the model design.

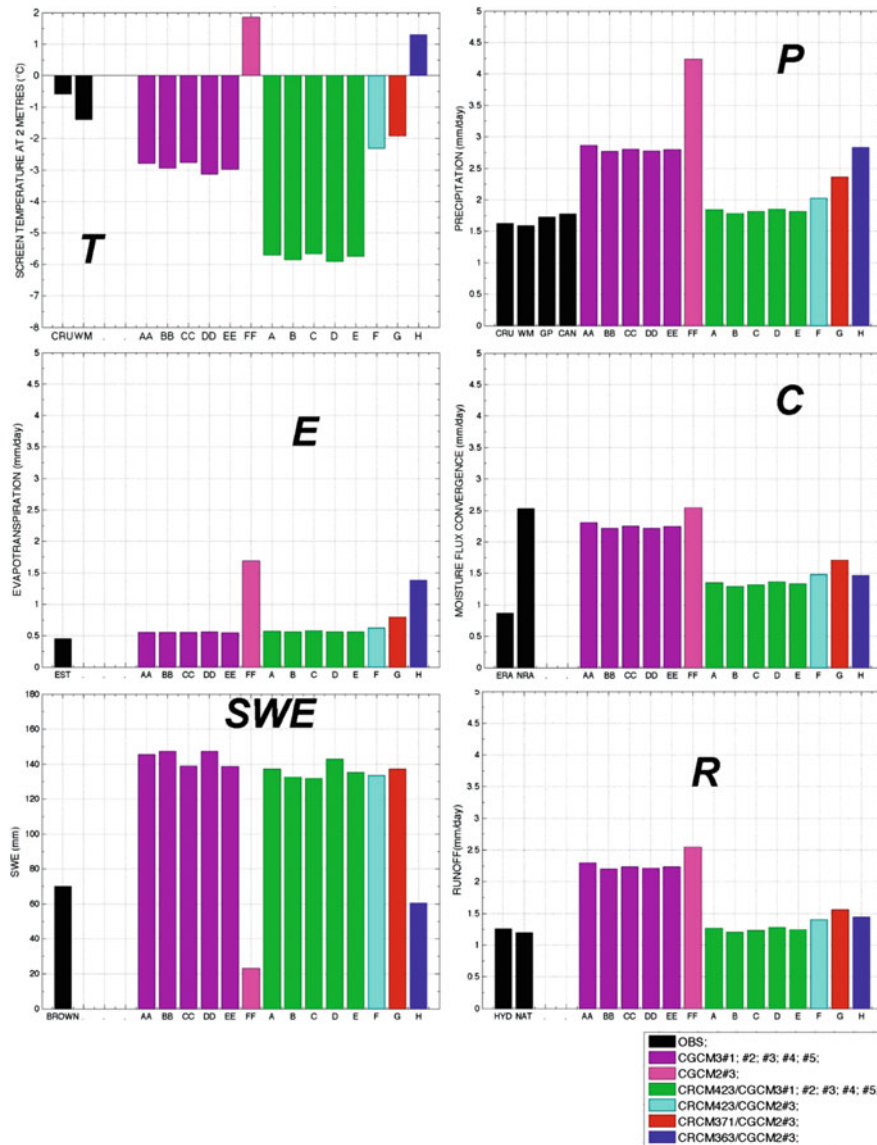


Fig. 3 Observed (black) and simulated hydro-meteorological variables averaged over the Upper Peace watershed and over the period 1961–1990

Combination of models for climate impact studies, which differ in their structure, in their parameterizations, and in the processes they include or neglect, as well as interpretation of their results is a big challenge. One of the factors that should be considered when building a model ensemble for climate projections is models’ performance. When a model has large biases, the confidence in its projections is lower. However, observational datasets used for model validation are not free from errors. In order to obtain an estimate of the observational error, which is inherent to each observed variable, data from different

sources are used (see section “Investigation of a Watershed Hydrology as Simulated by the Canadian GCM and RCM and Related Uncertainty: Experimental Design”). The maximum difference between annual mean precipitations derived from different observational datasets is 0.18 mm/day (10%), while for runoff, it is 0.06 mm/day (5%). For temperature, this difference is about 0.8°C. The largest discrepancy is found for moisture flux convergence: value derived from NCEP/NCAR reanalysis is larger than that of ERA-40 by 1.66 mm/day (66%). Note that ERA-40 convergence agrees better with observed runoff: water

mass conservation over a multi-year period requires that moisture flux convergence over the basin balances runoff, as well as the difference between precipitation and evapotranspiration (see Music and Caya 2007). Note also that an estimate of the evapotranspiration as difference between ensemble means of observed precipitation and runoff is used as a surrogate for the true evapotranspiration. In general, Fig. 3 shows that the CGCM3 has smaller biases compared to the observations and hence better performances than CGCM2. However, important biases still remain in the CGCM3: T is colder than the observed mean of about 2°C; P , SWE , and R are larger than observed by 1.12 mm/day (67%), 73 mm (105%), and 1.01 mm/day (82%), respectively.

Comparing the CRCM simulations listed in Table 2 with the CGCM3 simulations (see Table 1) gives an idea of the influence of driving model's internal variability on downscaled temperature and water budget components. In general, variations between values derived from the CRCM simulations (green bars in Fig. 3) are a bit smaller than those between the CGCM3 members (purple bars). When compared to observations, the CRCM results are within the observational error range for that watershed. Simulated SWE remains almost two times larger than observations, while evapotranspiration in both models is close to those estimated from observations. On the other hand, cold bias in near-surface temperature increased to almost 5°C with the CRCM.

The last three bars in Fig. 3 show sensitivity of simulated climate to different physical parameterizations being used in the regional model. As expected, the CRCM's sensitivity to the changes in parameterizations is rather larger than sensitivity to the driving model's initial conditions. It is interesting to mention that the use of more sophisticated parameterizations does not necessarily result in an improvement in all simulated variables.

Hydrological Change Signal at a Watershed Scale: Upper Peace, Fraser, Campbell and Columbia Watersheds

Projections of future hydrological regimes presented below are based on simulations generated with the CRCM4.2.3. As these RCM simulations are driven within CGCM members differing in their initial

conditions (see Table 2), the obtained projections should give an estimate of the uncertainty arising from the natural variability of the climate system.

Figure 4 shows a map of the investigated watersheds with projected changes in near-surface temperature to 2050s (A2 emission scenario) and associated uncertainty. The bar graphs are used to indicate projections for each CRCM simulation, while numbers above each watershed denote interval of projected change as $[\Delta T \pm \text{uncertainty}]$: ΔT is the ensemble mean (from five CRCM simulations) of projected changes in T (difference between the future (2041–2070) and present (1961–1990) temperature), and “uncertainty” is defined as the maximal deviation from this ensemble mean. For investigated watersheds, projected warming ranges from 2.4°C (Fraser) to 2.7°C (Campbell), while uncertainty related to the chaotic nature of climate varies from 0.2 to 0.3°C.

Figure 5 shows projected changes in water budget components. The bar graphs are presented to make a point about the balance of precipitation, evapotranspiration, and runoff changes, i.e., to indicate what portion of precipitation change goes to runoff and what goes to evapotranspiration changes. As can be seen, the changes in climate result in an intensification of the water cycle over all basins. Over the Upper Peace, Fraser, and Campbell, a larger portion of precipitation increase goes to runoff rather than to evapotranspiration increase, while over Columbia, this partitioning is reversed. Numbers over the watersheds have the same meaning as for the temperature map, but projected changes and associated uncertainty in precipitation, runoff, and SWE are given in percentages. The biggest relative increases in precipitation and runoff are projected for Upper Peace ($17 \pm 5\%$ and $18 \pm 8\%$, respectively), followed by Fraser (16 ± 3 and 17 ± 4 , respectively). For Campbell and Columbia these changes are about 10% smaller. Concerning SWE , the ensemble mean of projected change is negative for all watersheds with the greatest impact toward the south.

Summary and Conclusions

The analysis presented in the above sections contributes to the challenging task of evaluating the uncertainties associated with the direct use of climate models to assess hydrological regime and its change at a watershed scale. The uncertainty arising from the natural

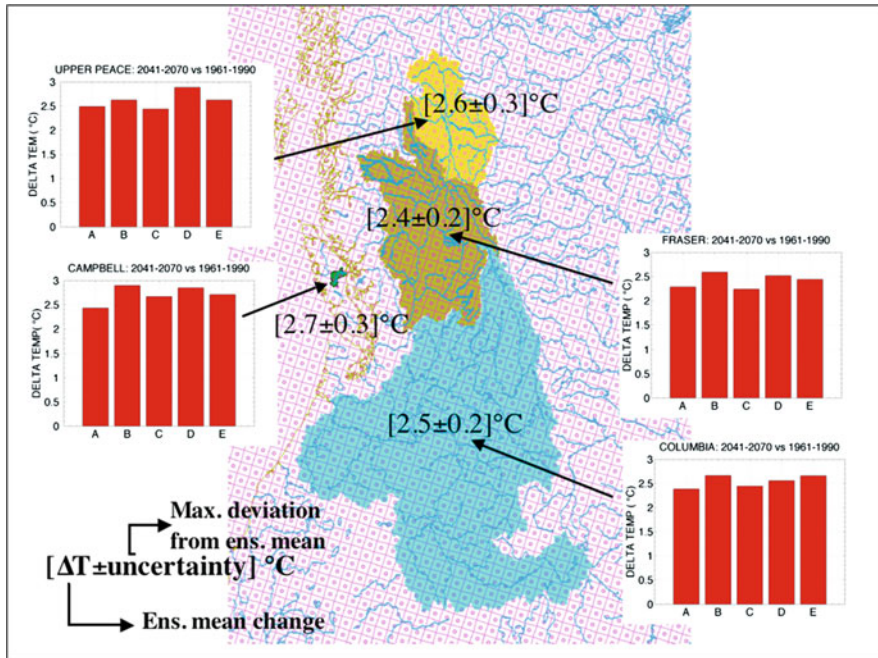


Fig. 4 CRCM projected changes and associated uncertainties in near-surface temperature from 1961–1990 to 2041–2070 over the Upper Peace, Fraser, Campbell, and Columbia watersheds, under the A2 scenario

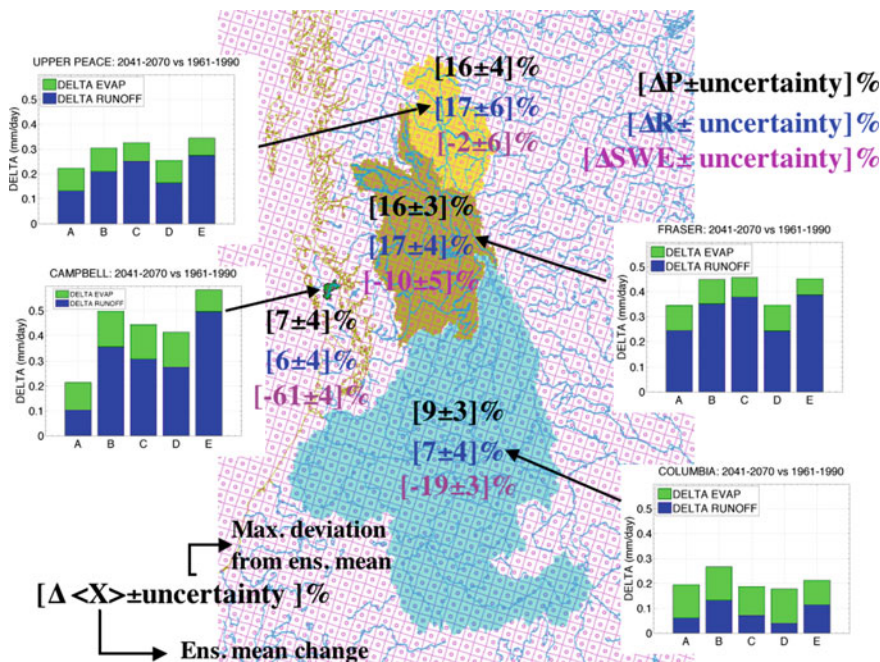


Fig. 5 Same as Fig. 4 but for water budget components

variability of the climate system has been evaluated using the CRCM to dynamically downscale several CGCM3 simulations differing only in initial conditions.

Some issues related to the sensitivity of simulated hydrological regime to model structure/physical parameterizations have also been investigated.

The CRCM hydrological variables averaged spatially (over a watershed) and temporally (over a 30-year period) appear to be less sensitive to the change in CGCM initial conditions than to the model physical parameterizations and driving global model. However, when climate change signals at the watershed scale for these variables were estimated (as a difference between 30-year mean of a future and current time period), the uncertainty associated with the natural variability was shown to be non-negligible. Some preliminary results of our recent study performed over a set of Quebec watersheds (Music et al. 2010) show that effects of natural variability on estimated change of a watershed hydrological regime may become as important as uncertainties related to the choice of physical parameterizations, simulation domain, and choice of driving global model. Similar conclusions can be drawn from the studies of De-Elia and Côté (2010) and Frigon et al. (2010), where the sensitivity of climate change signal to a modification in the CRCM configuration (driving data interval, CRCM initial conditions, driving GCM, nesting technique, etc.) was shown to be enhanced or reduced compared to the sensitivity of 30-year means.

Acknowledgments The authors would like to thank the Ouranos Climate Simulation team for generating and supplying outputs from the numerous CRCM climate change simulations and the Canadian Center for Climate Modelling and Analysis (CCCma) for kindly providing access to CGCM archives. A special thanks goes to Mourad Labassi for maintaining the Ouranos computing facilities and for technical support. A big thanks to Sanela Music for her language editing service. This research is financially supported by the Ouranos Consortium, BC Hydro, and the British Columbia Ministry of Environment and we gratefully acknowledge their support.

References

- Adler RF et al (2003) The version-2 Global Precipitation Climatology Project (GPCP) monthly precipitation analysis (1979–present). *J Hydrometeorol* 4:1147–1167
- Arora VK (2001) Assessment of simulated water balance for continental-scale river basins in an AMIP II simulation. *J Geophys Res* 106:14827–14842
- Brown RD, Brasnett B, Robinson D (2003) Gridded North American monthly snow depth and snow water equivalent for GCM evaluation. *Atmos Ocean* 41:1–14
- Caya D, Laprise R (1999) A semi-implicit semi-Lagrangian regional climate model: the Canadian RCM. *Mon Weather Rev* 127:341–362
- de Elia R, Côté H (2010) Climate and climate change sensitivity to model configuration in the Canadian RCM over North America. *Meteorol Z* 19:1–15
- Flato GM, Boer GJ (2001) Warming asymmetry in climate change simulations. *Geophys Res Lett* 28:195–198
- Frigon A, Music B, Slivitzky M (2010) Sensitivity of runoff and projected changes in runoff over Quebec to the update interval of lateral boundary conditions in the Canadian RCM. *Meteorol Z* 19:225–236. doi:10.1127/0941-2948/2010/0453
- Graham LP, Hagemann S, Jaun S, Beniston M (2007) On interpreting hydrological change from regional climate models. *Clim Change* 81:97–122
- HYDAT (1999) Canadian hydrological data available on CD-ROM (version 99–2.00), National Water Data Archive, Environment Canada. Available through Environment Canada at http://www.wsc.ec.gc.ca/products/hydat/main_e.cfm?cname=hydat_e.cfm
- Kalnay E et al (1996) The NCEP/NCAR 40-Year Reanalysis Project. *Bull Am Meteorol Soc* 77:437–471
- Louie PYT, Hogg WD, MacKay MD, Zhang Z, Hopkinson RF (2002) The water balance climatology of the Mackenzie Basin with reference to the 1994/95 water year. *Atmos Ocean* 40:159–180
- Mitchell TD, Jones PD (2005) An improved method of constructing a database of monthly climate observations and associated high-resolution grids. *Int J Climatol* 25:693–712
- Music B, Caya D (2007) Evaluation of the hydrological cycle over the Mississippi River Basin as simulated by the Canadian Regional Climate Model (CRCM). *J Hydrometeorol* 8:969–988
- Music B, Caya D (2009) Investigation of the sensitivity of the water cycle components simulated by the Canadian Regional Climate Model (CRCM) to the land surface parameterization, the lateral boundary data and the internal variability. *J Hydrometeorol* 10:3–21
- Music B, Frigon A, Slivitzky M, Caya D, Roy R, Labassi M (2010) Défis et opportunités de l'utilisation directe de l'écoulement simulé par les modèles régionaux de climat (MRC) dans les études d'impact hydrologique. 4e Symposium scientifique d'OURANOS, Québec, QC, Canada, 17–18 Novembre 2010
- Plummer D et al (2006) Climate and climate change over North America as simulated by the Canadian Regional Climate Model. *J Clim* 19:3112–3132
- Scinocca JF, McFarlane NA, Lazare M, Li J, Plummer D (2008) The CCCma third generation AGCM and its extension into the middle atmosphere. *Atmos Chem Phys Discuss* 8:7883–7930
- Uppala SM et al (2005) The ERA-40 re-analysis. *Quart J R Meteorol Soc* 131:2961–3012
- Willmott CJ, Matsuura K (2001) Terrestrial air temperature and precipitation: monthly and annual time series (1950–1999), Version 1.0.2. Center for Climatic Research, University of Delaware. Available online at http://climate.geog.udel.edu/climate/html_pages/download.html
- Xu C-Y, Widén E, Halldin S (2005) Modelling hydrological consequences of climate change – progress and challenges. *Adv Atmos Sci* 22:789–797

Analysis of the Changes of the Streamflows in Serbia Due to Climate Changes

Dejan Dimkić and Jovan Despotović

Abstract

The effect of climate change on river flow trends in Serbia is analyzed. To reduce the impact of human activity on results, eight hydrological stations where human impact is negligible, or only minor, were selected. The chapter focuses on average annual river discharges and temperatures and total annual precipitation. The aim of the research is to document the observed trends of streamflow and air temperature, and assess and forecast average relationships between the changes in the streamflow and increases in air temperature in Serbia. Of the eight analyzed watersheds, the results obtained for the Pek and Resava rivers are highlighted to illustrate the range of departures of an individual watershed in our eight watersheds ensemble statistics.

The results indicate that the long-term average downward river discharge trend in Serbia is approximately -30% per 100 years. Another conclusion is that all the selected stations exhibit an inversely proportional correlation between the annual temperatures and average annual river discharges. On the average, a 1°C increase in average annual temperatures roughly corresponds to a $25\text{--}30\%$ reduction in average annual discharges of relatively small rivers in Serbia.

Introduction

A number of global and regional climate and hydrology models have been developed to assess air temperature, precipitation regime, and runoff changes for a number of future IPCC scenarios (IPCC 2007). The research done for that purpose showed that a general increase in air temperature and a decrease in streamflow are to be expected in Serbia, as a part of

Southeast Europe. Trends which we have identified and analyzed so far include air temperature and streamflow data for over a dozen rivers in Serbia, and also show a decrease of streamflows with time.

The present case study emphasizes the data for the Pek and Resava rivers and is extracted from a more comprehensive study of small rivers in Serbia. The aim of the research is to assess and forecast average relationships of an increase in air temperature vs. changes in the streamflows of rivers in Serbia, including observed trends for air temperature and streamflow.

Section “Some Global Change Conclusions of the Available Literature” of this chapter reports on main conclusions regarding changes in temperature,

D. Dimkić (✉)
Institute for Water Resources “Jaroslav Černi”, Jaroslav Černi
Str. 80, 11226 Pinosava, Belgrade, Serbia
e-mail: dejan.dimkic@jcerni.co.rs

precipitation, and runoff as we found available in cited literature, and sections “Records of Streamflows and Trends in Serbia” and “Average Dependence of the Streamflow and Precipitation on Temperature” reports on the results of our research. In section “Conclusions,” the main conclusions are given.

Some Global Change Conclusions of the Available Literature

General

Based on the literature cited below, some of the general and most important conclusions for the topic of this chapter are as follows:

- In many regions of the world, trends are apparent in the increase or in the decrease of discharge. The direction of the changes is generally in accordance with the forecasts based on International Panel for Climate Change (IPCC) scenarios, but the magnitudes of these changes may differ. In some regions, the direction of change is uncertain (Arnell and Liu 2001; Arnell 2003; Fowler et al. 2007; Ma et al. 2008).
- Many studies show that hydrologic changes should be regarded as complex processes with many factors at play, where climate change often represents the most significant parameter, but certainly not the only one (Arnell and Liu 2001; Juckem et al. 2008; Novotny and Stefan 2007).
- In many regions, maximum discharge is shifted from spring to winter. With climate change frequent and more severe floods should be expected, even if there is a trend of reduction in average discharge (Arnell and Liu 2001; Arnell et al. 2003; Steele-Dunne et al. 2008).
- Due to higher water temperature, water quality should worsen, but higher discharge can compensate for this in many regions (Arnell and Liu 2001; Thodsen 2007).
- As a result of population growth and agricultural developments, an increase in the demand for water should be expected, although, in a very few countries, the demand might stagnate or even decline (Arnell and Liu 2001; Fujihara et al. 2008).
- The effect of climate change on water resources depends on the development of water management

as well as on the ability to adjust to the expected changes (Arnell and Liu 2001; Fujihara et al. 2008).

- Water systems with poor or inadequate management will be most impacted by the effects of climate change. Integrated water resources management helps adapting to changes (Arnell and Liu 2001).
- Practically all studies also address the uncertainties in hydrologic and climate predictions.

Observed and Predicted Hydrologic Changes

- Most hydrologic studies confirm that hydrologic changes occur in accordance with the GCM forecasts done for the IPCC (2007) according to the A1B scenario.
- These observed and predicted hydrologic changes indicate:
 - Small increase in the amount of rainfall and small increase in runoff in tropical regions
 - Greater or smaller amount of rainfall and significantly reduced runoff in subtropical regions
 - More rainfall and significantly more runoff in higher latitudes and Arctic regions

Temperature Trends and Predictions for Southeast Europe

IPCC (2007) projections indicate that the temperature will rise in Europe and Mediterranean, thus also in Serbia. During the twentieth century, there has already been a change in global temperature of 0.74°C, with land temperature being around 1.0°C and sea surface temperature around 0.6°C greater. Trend analysis for upcoming decades, in Southeast (SE) Europe, gives an increase of 0.1–0.2°C per decade. Projections for the end of the twenty-first century are of an increase of 1–5°C, depending on which emission scenario is selected. The most probable scenario might be the one with an increase of 2.0–3.0°C in the 100-year period (IPCC 2007). This can be compared with the past temperature change of approximately 1.2°C in 100 years, as illustrated by the Belgrade temperature plot for the past 120 years, 1988–2007, shown in Fig. 1.

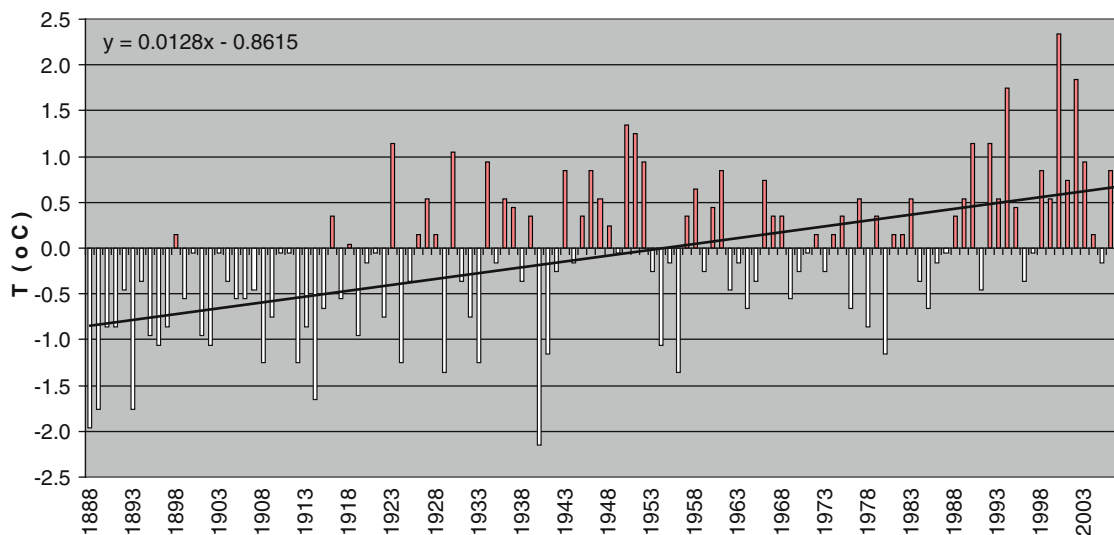


Fig. 1 Average yearly temperature in Belgrade from 1888 to 2007, relative to the average of the 1961–1990 period. Linear least squares fit is shown by the *black line*

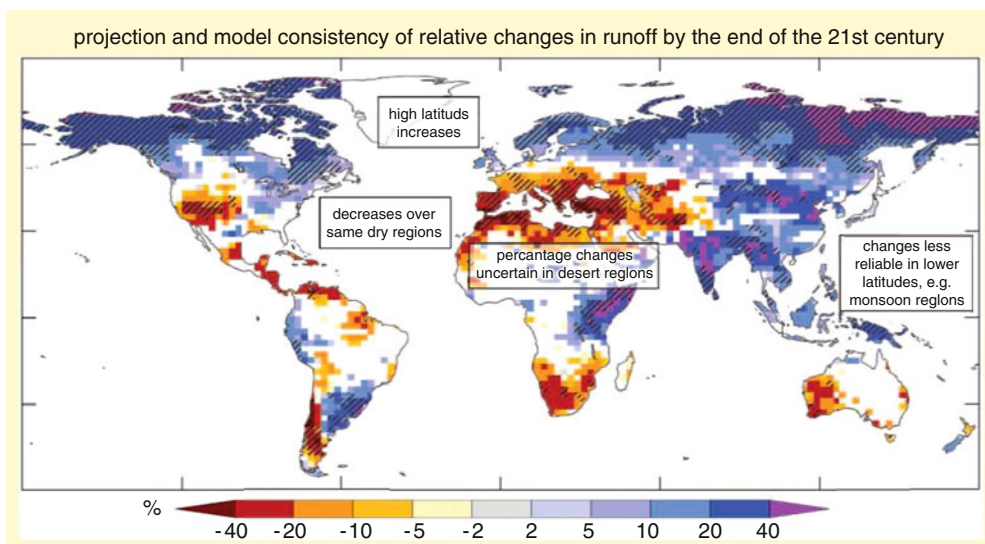


Fig. 2 Change in annual runoff (in percentage) projected for the end of the twenty-first century, relative to 1980–1999. Values represent the median of 12 climate models using the SRES A1B scenario (IPCC 2007)

Discharge Trends and Predictions for Southeast Europe

Figure 2 shows the global change in runoff at the end of the twenty-first century according to the IPCC’s SRES (Special Report on Emissions Scenarios) A1B

scenario of the Fourth Synthesis Report of IPCC, of November 2007. Most of the authors were focused on the A1B scenario, and also on the SRES A2 scenario, which is somewhat less favorable for the south-east Europe. For Serbia, Fig. 2 shows a decrease in runoff by 25–30% in 100 years (IPCC 2007).

Records of Streamflows and Trends in Serbia

General

Climate or hydrologic process component, such as temperature, precipitation, or streamflow:

1. May or may not have trend (i.e., trend equals 0)
2. May or may not have periodicity
3. Always has a stochastic component

As *trend* we shall normally consider the value of the coefficient a of the least squares fit of the yearly average discharge values y_i to the linear function $y = ax + b$, x denoting the year, a , b being constants, and the subscript i running from the initial to the last year of the discharge series considered. We shall refer to the function $y = ax + b$ as the *trend line* and denote the coefficient a also as $\Delta_{\text{year}}Q_{\text{trl}}$, with Q_{trl} being discharge along the trend line. But at times, as frequently done, we shall express trend also in percent

change per 100 years. This chapter analyzes trends and to some degree stochastic components, but not periodicities.

For a number of watersheds, we shall discuss the average annual streamflows and temperatures and total annual precipitation. Our goal is to provide an assessment of:

- The average change in streamflow in Serbia's watersheds (section "Records of Streamflows and Trends in Serbia")
- The average dependency of the streamflow change on the temperature change (section "Average Dependence of the Streamflow and Precipitation on Temperature")

Our analysis is limited to rivers whose entire watershed is within Serbia and whose area is between 200 and 1,000 km². A large number of watersheds were analyzed. In Figs. 3 and 4, the average annual streamflows of the rivers Pek and Resava are shown, respectively, for the past 50 years. Once more, as in similar plots to follow, the linear least squares fit lines

Fig. 3 Average annual streamflow, the Pek River (at Kučevo), 1954–2006

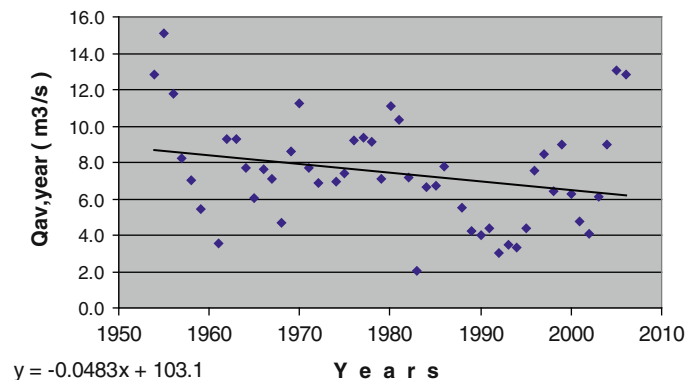
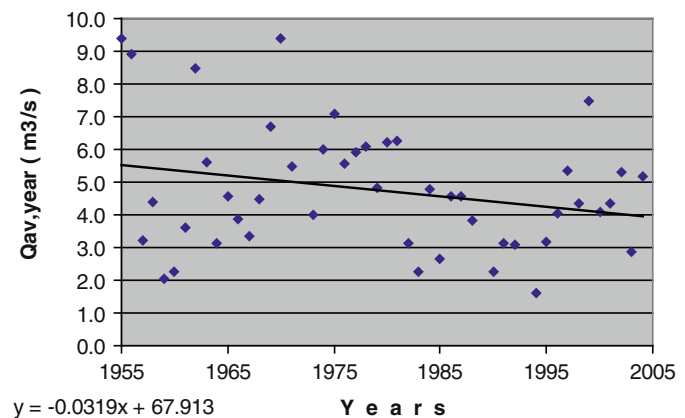


Fig. 4 Average annual streamflow, the Resava River (at Svilajnac), 1955–2004



are displayed. The linear fit equations are displayed as well, as they will be in most other plots to be shown.

Average Trend of Streamflows in Serbia

Table 1 shows past trends obtained for the eight analyzed watersheds, all with catchment areas not greater than 1,000 km². In the table, $Q_{av,year}$ denotes the average discharge over all years of the period considered. It is seen that all streamflows included exhibit a downward trend and that the average trend is markedly negative: more than -50% in 100 years, for Pek and

Resava about -65% in 100 years. Based on further research involving a larger number of Serbia's rivers, with different lengths, beginnings and ends of the data series, as will be discussed below, the average downward trend of the Table 1 of -58% in 100 years is twice greater than what we find to be the likely average long-term trend ($\approx -30\%$ to -35% per 100 years).

The longest hydrologic data series available in Serbia, for the Danube river at Bezdan and for the Sava River at Sremska Mitrovica, are summarized in Fig. 5.

Table 2 shows that for different lengths, beginnings and ends of the data series, including periods of at least

Table 1 Streamflow trends and average discharges obtained for the eight analyzed watersheds

River →	Veliki Rzav	Skrapež	Kolubara	Jadar	Bjelica	Jasenica	Resava	Pek	Average
Monitoring site →	Roge	Požega	Valjevo	Zavlaka	Guča	Smederevska Palanka	Svilajnac	Kučevo	
Rain gauge station →	Skržuti	Kosjerić	Počuta	Osečina	Vučkovica	Topola	Veliki Popović	Vlaole	
Monitoring period →	1964–2006	1953–2000	1951–2005	1960–2006	1961–2006	1961–2005	1955–2004	1954–2006	
Streamflow $Q_{av,year}$ (m ³ /s)	6.157	5.011	3.835	3.040	2.724	1.815	4.741	7.414	4.34
$\Delta_{year}Q_{Tn}$ (m ³ /s/year)	-0.0008	-0.0276	-0.0114	-0.0242	-0.0334	-0.0084	-0.0319	-0.0483	-0.023
Trends in % per 100 years	-1.3	-55.1	-29.7	-79.6	-122.6	-46.3	-67.3	-65.1	-58

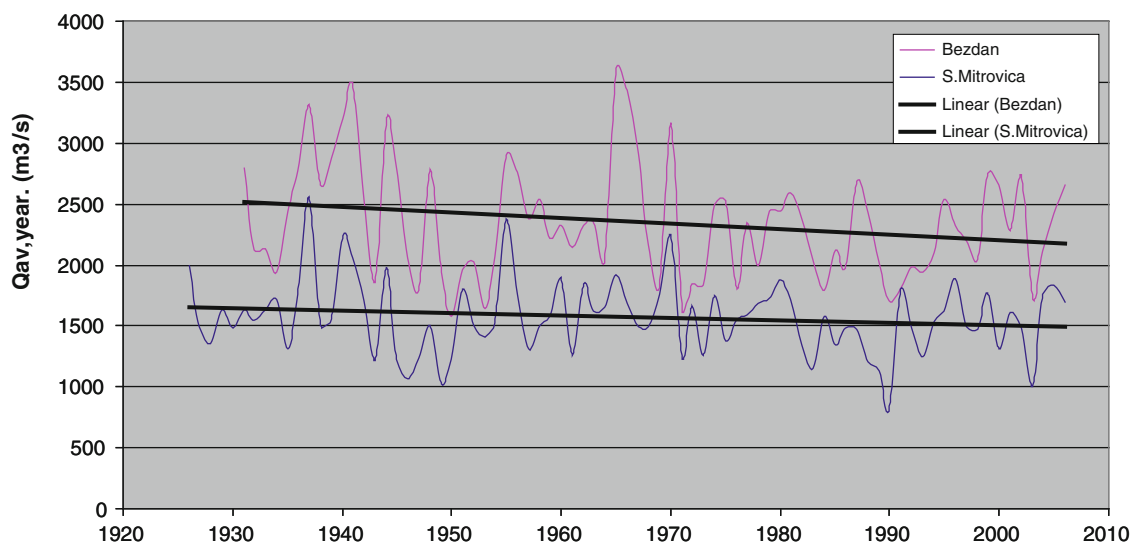


Fig. 5 Average annual discharges of the Danube river (Bezdan, 1931–2006) and the Sava river (Sremska Mitrovica, 1926–2006)

Table 2 Trends and average discharges obtained for the Sava and Danube rivers for various periods

Monitoring period →	1926– 2006	1936– 2006	1946– 2006	1956– 2006	1966– 2006	1926– 2001	1931– 2001	1941– 2001	1951– 2001	1961– 2001
Sava $Q_{av,year}$ (m ³ /s)	1570	1569	1535	1548	1527	1572	1570	1541	1564	1540
$\Delta_{year}Q_{tri}$ (m ³ /s/year)	-2.0	-2.8	-0.25	-3.0	-2.4	-2.4	-2.8	-1.3	-4.9	-5.1
Trends in % per 100 years	-13.0	-18.1	-1.7	-19.7	-15.9	-15.3	-17.8	-8.6	-31.4	-33.1
Danube $Q_{av,year}$ (m ³ /s)		2,352	2,267	2,305	2,265		2,349	2,304	2,285	2,285
$\Delta_{year}Q_{tri}$ (m ³ /s/year)		-6.0	0.39	-4.8	-2.4		-5.5	-3.9	-3.1	-6.9
Trends in % per 100 years		-25.5	1.7	-21.0	-10.7		-23.5	-17.1	-13.4	-30.2

Table 3 Trends and average discharges of eight watersheds and of the Sava and Danube rivers for various periods

River →	Pek	V. Rzav	Skrpež	Resava	Kolubara	Jadar	Bjelica	Jasenica	Average
Monitoring site →	Kučevo	Roge	Požega	Svilajnac	Valjevo	Osečina	Guča	Smederevska Palanka	
Monitoring period →	1954–2006	1964–2006	1953–2000	1955–2004	1951–2005	1960–2006	1961–2006	1961–2005	
$Q_{av,year}$ (m ³ /s)	7.414	6.157	5.011	4.741	3.835	3.04	2.724	1.815	4.342
$\Delta_{year}Q_{tri}$ (m ³ /s/year)	-0.0483	-0.0008	-0.0276	-0.0319	-0.0114	-0.0242	-0.0334	-0.0084	-
Trends in % per 100 years	-65.1	-1.3	-55.1	-67.3	-29.7	-79.6	-122.6	-46.3	-58.4
Sava at S. Mitrovica $Q_{av,year}$ (m ³ /s)	1,563	1,539	1,560	1,556	1,561	1,549	1,542	1,538	1,551
$\Delta_{year}Q_{tri}$ (m ³ /s/year)	-4.3	-3.7	-5.5	-6.3	-4.2	-4.0	-3.3	-4.0	-4.4
Trends in % per 100 years	-27.7	-24.0	-35.5	-40.2	-26.8	-25.8	-21.3	-25.8	-28.4
Danube at Bezdán $Q_{av,year}$ (m ³ /s)	2,312	2,291	2,297	2,308	2,282	2,291	2,290	2,282	2,294
$\Delta_{year}Q_{tri}$ (m ³ /s/year)	-5.0	-5.4	-5.2	-7.7	-2.7	-4.1	-4.3	-5.7	-5.0
Trends in % per 100 years	-21.7	-23.7	-22.8	-33.4	-12.0	-17.9	-18.7	-24.9	-21.9

40 years, these trends are between 0 and -30% per 100 years. Longer data series exhibit a tendency toward $\approx -15\%$ per 100 years.

This chapter does not address the issue of which portion of this reduction may be attributable to climate change and which to increased human demand. Instead, it compares the assessed trends of the Sava and the Danube ($\approx -15\%$ per 100 years) to the trends obtained for time periods such as those presented for our eight studied watersheds (Table 3).

It is apparent that the recorded trends of the Sava and the Danube, during the time periods shown in Table 3, are greater than the assessed probable trends

for the past 70–80 years about 1.5–2.0 times. This relationship, when applied to the eight studied watersheds, suggests that the probable streamflow reduction trend in watersheds up to 1,000 km² is about 30–35% per 100 years.

This result was checked against a number of small and medium-size rivers in Serbia. The results obtained indicate that an average of -30% per 100 years can roughly be considered a reference level for assessment of the current streamflow decline trends in Serbia, with regard to watersheds whose surface area is not greater than 1,000 km² and which are located at an average altitude above sea level of about 300–700 m.

As expected, there is a general reduction in the negative trend, in percentage, with increasing river or watershed size.

Average Dependence of the Streamflow and Precipitation on Temperature

The Methodology Used

While in the previous section we have looked into the discharge trends of a number of rivers in Serbia and have seen evidence of the general flow reduction, it is not possible from this information alone to deduce to what degree if any this reduction is caused by the general warming occurring in the later parts of the periods considered. Given the generally expected increase in temperature associated with the climate change in progress, we are suggesting that some indication to that effect can be obtained by considering the relationship between the yearly discharges of various rivers and average temperatures in these years in the areas of the watersheds considered.

In Figs. 3 and 4, and in Table 3, similar periods but not quite the same were analyzed for various rivers. We should note that our choices of these periods resulted from the requirement to have temperature, streamflow, and precipitation data covering all of the periods to be analyzed. For the periods, we thus arrived at and for each of the rivers, values of the following parameters were calculated:

- Average annual streamflow at a given monitoring site, relative to the average for the entire period available, Q_{rel}
- Annual precipitation sum recorded at a rain gauge station close to the monitoring site, once again relative to the average annual sum for the entire period available, P_{rel}
- Difference, ΔT_{av} , between the average annual temperature at the same station and the average temperature at that station for the entire period available

To arrive at the relationships desired, data were grouped into categories according to deviations of the average annual temperatures from period means, at intervals of 0.5°C . Average values were then calculated for each category of the temperature deviation, and of the annual discharge and precipitation relative to their period means, respectively. These data were

then used to construct graphs of the relationships of the values obtained, displaying also the linear fit to the composite data shown and the associated coefficient of determination R^2 , R being the correlation coefficient.

Results

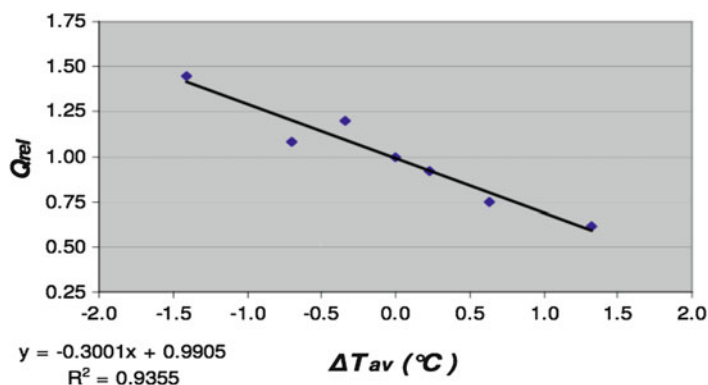
Even though each of the eight studied watersheds of Table 1 exhibits specific features, in our examination of the dependence of their relative streamflow on temperature deviation there was no dramatic difference. Each of them displayed a general decrease in average streamflow with increased temperature and vice versa. In addition, each of these watersheds comes from a relatively small area of Serbia, and as pointed out earlier are all watersheds of not very different areas and average altitudes above the sea level. We thus felt justified in merging the data obtained in each of the temperature deviation categories. This diminishes the impact of odd years, in particular for categories with temperature deviations greater than a degree, with not many data points. We consider the rivers Pek and Resava separately, along with the merged data for all eight watersheds. Our results of thus obtained average dependence of the annual streamflow and precipitation on temperature are shown in Table 4 and in graphical form in Figs. 6–11.

Table 5 shows the slopes of the linear fit lines of the average streamflow and annual precipitation as functions of the temperature deviation. The table also shows to what extent a variation in the average annual temperature of $\pm 1^{\circ}\text{C}$ affects the average deviation of the change in the average annual streamflow or annual precipitation, in percent, according to the statistics reported here.

The values obtained can be summarized as follows. A deviation of the average annual temperature by $\pm 1^{\circ}\text{C}$ has an inversely proportional effect on the average variation in the annual precipitation levels by almost 5–10% and on variation in the average annual streamflow by 20–30%. The results obtained differ from watershed to watershed, but in most cases this variation is not greater than 50%. Thus, the average change in the annual precipitation to be expected according to the results presented would range from 0 to 15%, and the variation in average annual streamflow from 10 to 40%.

Table 4 Average values of the relative streamflow and precipitation on temperature deviation

	Temperature deviation category (°C)	Relative streamflow (average)	Relative precipitation (average)	Relative temperature (average)	Number of data points (years)
Pek	$\Delta T_{av} < -1.0^{\circ}\text{C}$	1.44	1.10	-1.41	4
	$-1.0 < \Delta T_{av} < -0.5$	1.08	1.02	-0.70	5
	$-0.5 < \Delta T_{av} < 0.0$	1.20	1.06	-0.34	12
	All data for river Pek	1.00	1.00	0.00	50
	$0.0 < \Delta T_{av} < 0.5$	0.92	0.98	0.23	18
	$0.5 < \Delta T_{av} < 1.0$	0.75	0.96	0.64	8
	$1.0^{\circ}\text{C} < \Delta T_{av}$	0.61	0.84	1.33	3
Resava	$\Delta T_{av} < -1.0^{\circ}\text{C}$	1.23	1.08	-1.05	4
	$-1.0 < \Delta T_{av} < -0.5$	0.99	0.91	-0.71	6
	$-0.5 < \Delta T_{av} < 0.0$	1.13	1.03	-0.28	12
	All data for river Resava	1.00	1.00	0.00	47
	$0.0 < \Delta T_{av} < 0.5$	1.03	1.03	0.19	14
	$0.5 < \Delta T_{av} < 1.0$	0.73	0.97	0.65	8
	$1.0^{\circ}\text{C} < \Delta T_{av}$	0.77	0.90	1.31	3
All eight water-sheds	$\Delta T_{av} < -1.0^{\circ}\text{C}$	1.37	1.09	-1.19	20
	$-1.0 < \Delta T_{av} < -0.5$	1.03	1.01	-0.69	49
	$-0.5 < \Delta T_{av} < 0.0$	1.10	1.01	-0.24	123
	All data for eight watersheds	1.00	1.00	0.00	377
	$0.0 < \Delta T_{av} < 0.5$	0.97	1.01	0.22	115
	$0.5 < \Delta T_{av} < 1.0$	0.77	0.95	0.68	49
	$1.0^{\circ}\text{C} < \Delta T_{av}$	0.70	0.88	1.38	21

Fig. 6 Average annual streamflow as a function of temperature deviation (river Pek, monitoring site Kučevo, 1954–2006)

In all of the eight watersheds, there were only 2 years during which the average annual temperature at a station or stations used for the watershed differed from the period average by more than $\pm 1.5^{\circ}\text{C}$:

- 1976: station Žagubica (-1.86°C)
- 2000: station Zlatibor ($+1.84^{\circ}\text{C}$), station Valjevo ($+1.74^{\circ}\text{C}$), and station Smederevska Palanka ($+1.86^{\circ}\text{C}$)

There was no year on record during which the average annual temperature differed by more than $\pm 2^{\circ}\text{C}$ from the watershed period average. It is, therefore, not possible to speak reliably about any projections in the event of a greater change in the average annual temperature. It appears however, based on research conducted to date but without tangible evidence, that changes significantly higher or

Fig. 7 Average annual precipitation, relative to the period average, as a function of temperature deviation (river Pek, monitoring site Kučevo, 1954–2006)

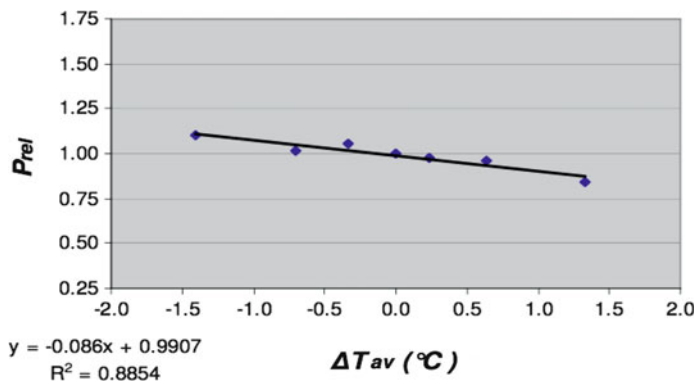


Fig. 8 Average annual streamflow as a function of temperature deviation (river Resava, monitoring site Svilajnac, 1955–2004)

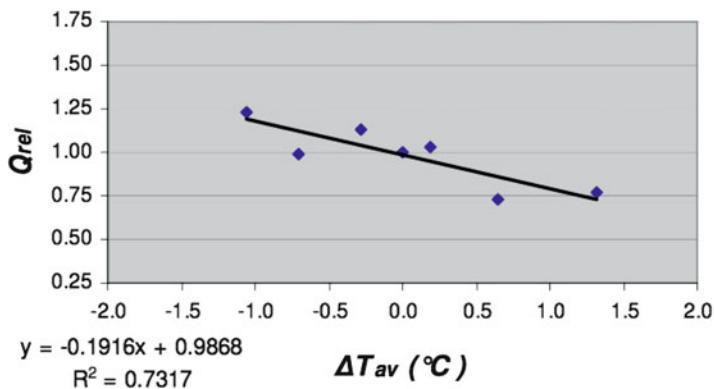
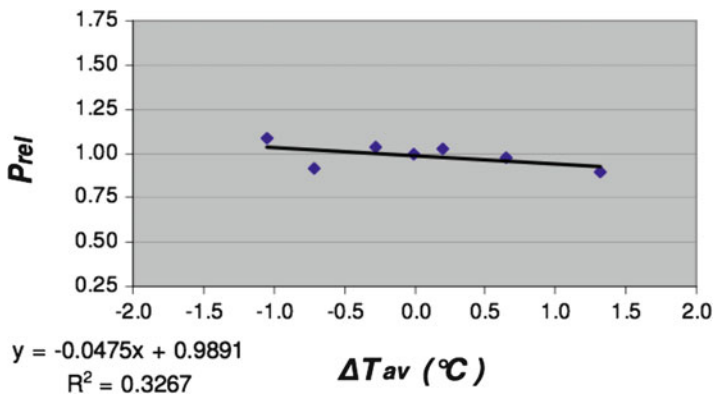


Fig. 9 Average annual precipitation, relative to the period average, as a function of temperature deviation (river Resava, monitoring site Svilajnac, 1955–2004)



significantly lower than those we have above for deviations of up to $\pm 1^\circ\text{C}$ are unlikely. The only projection one can be confident about is that any increase in the average annual temperature above the discussed $\pm 1^\circ\text{C}$ will result in an additional average deviation of the average annual streamflow and annual

precipitation. Not wishing to “gamble with forecasts,” but to clarify the issue discussed, the authors believe that in the case of Serbia and subject to the constraints pointed out, any deviation of the average annual temperature of $\pm 2^\circ\text{C}$ will result in an average deviation of the *change* in the average annual streamflow on the

Fig. 10 Average annual streamflow as a function of temperature deviation (all eight watersheds)

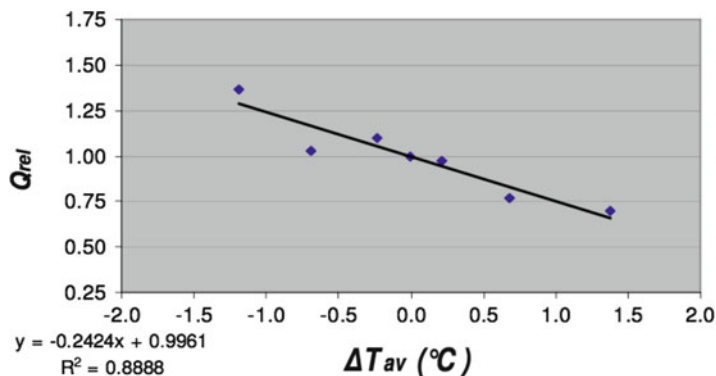


Fig. 11 Average annual precipitation, relative to the period average, as a function of temperature deviation (all eight watersheds)

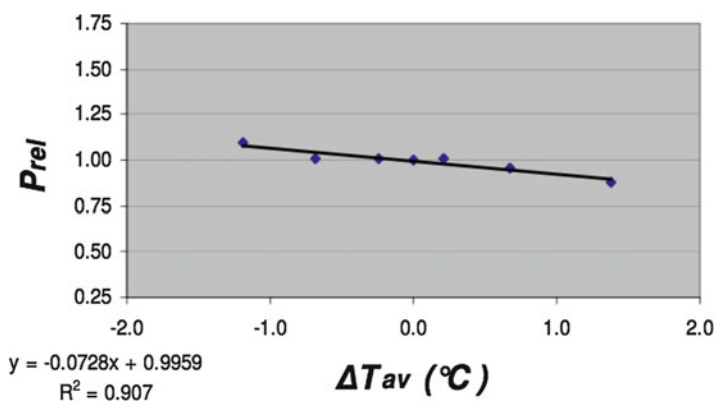


Table 5 Average changes associated with a deviation of the average annual temperature by $\pm 1^\circ\text{C}$

	River and monitoring site	Average $Q_{av,year}$ (%)	Average annual precipitation (%)
1.	Veliki Rzav at Roge	11	6
2.	Skrpež at Požega	23	11
3.	Kolubara at Valjevo	24	6
4.	Jadar at Zavlaka	27	13
5.	Bjelica at Guča	22	- ^a
6.	Jasenica at Smederevska Palanka	36	8
7.	Resava at Svilajnac	19	5
8.	Pek at Kučevo	30	9
	Total	24	7

^aNo realistic fit line could be established because in this watershed there was only 1 year in which temperature differed by more than $+1^\circ\text{C}$ (higher-than-average precipitation recorded, 1.10 = relative value)

order of about 50% or in the annual precipitation level by about 15%. Any such change, and particularly any greater change in the average annual temperature, will

lead to dramatic changes in the water balance which must be addressed very seriously in the water management planning.

Conclusions

Regarding present hydrologic trends in Serbia investigated so far, the most important conclusions we feel are as follows.

1. It is observed that an increase in the air temperature is associated with a decrease in discharge. As to the timescale, the average trend of a decrease in the average flow was seen to amount to 58% per 100 years for our eight analyzed catchments, based on samples of 45–50 years. It is suggested above that this trend is about twice greater than the actual likely average trend in Serbian rivers of –30% per 100 years. Average decrease in discharge for the catchments studied is 24% for an increase in air temperature of 1°C. Since long-term air temperature trend in Serbia is at present almost +1.0°C per 100 years, this would be the projection in place if it were to be based on the temperature trend at present. These results are generally in line with the obtained IPCC evaluation of general hydrologic trends using GCM models (Fig. 2).
2. Based on previous comments and observed correlations, under the assumption that there will be no dramatic increase or decrease in the global warming compared to what is typically projected by the IPCC's GCM models to take place by the end of the century, with a temperature increase over Serbia of 2.0–2.5°C, one could expect on average about twice less streamflow in Serbian rivers, at least with catchments of up to 1,000-km² area than is in place at present.

One should be reminded that the above results are given in terms of averages, while the flow trends for specific catchments can be significantly different, both up and down, due to differences in human activities.

References

- Arnell NW (2003) Effects of IPCC SRES emissions scenarios on river runoff: a global perspective. *Hydrol Earth Syst Sci* 7:619–641
- Arnell N, Liu C (coordinating lead authors) (2001) Hydrology and water resources, Chapter 4. In: Mc Carthy JJ, Canziani OF, Leary NA, Dokken DJ, White KS (eds) *Climate change 2001: impacts, adaptation and vulnerability*. Contribution of Working Group II to the third assessment report of the Intergovernmental Panel on climate change. Cambridge University Press, Cambridge, UK
- Arnell NW, Hudson DA, Jones RG (2003) Climate change scenarios from a regional climate model: estimating change in runoff in southern Africa. *J Geophys Res–Atmospheres* 108(D16):4519
- Fowler HJ, Kilsby CG, Stunell J (2007) Modelling the impacts of projected future climate change on water resources in north-west England. *Hydrol Earth Syst Sci* 11:1115–1126
- Fujihara Y, Tanaka K, Watanabe T, Nagano T, Kojiri T (2008) Assessing the impacts of climate change on the water resources of the Seyhan River Basin in Turkey: use of dynamically downscaled data for hydrologic simulations. *J Hydrol* 353:33–48
- IPCC (2007) *Climate change 2007: synthesis report*. Contribution of Working Groups I, II and III to the fourth assessment report of the Intergovernmental Panel on climate change. Core Writing Team, Pachauri RK, Reisinger A (eds) IPCC, Geneva, Switzerland, 104pp. Available online at http://www.ipcc.ch/publications_and_data/publications_ipcc_fourth_assessment_report_synthesis_report.htm
- Juckem PF, Hunt RJ, Anderson MP, Robertson DM (2008) Effects of climate and land management change on stream flow in the driftless area of Wisconsin. *J Hydrol* 355:123–130
- Ma Z, Kang S, Zhang L, Tong L, Su X (2008) Analysis of impacts of climate variability and human activity on stream flow for a river basin in arid region of northwest China. *J Hydrol* 352:239–249
- Novotny EV, Stefan HG (2007) Stream flow in Minnesota: indicator of climate change. *J Hydrol* 334:319–333
- Steele-Dunne S, Lynch P, McGrath R, Semmler T, Wang S, Hanafin J, Nolan P (2008) The impacts of climate change on hydrology in Ireland. *J Hydrol* 356:28–45
- Thodsen H (2007) The influence of climate change on stream flow in Danish rivers. *J Hydrol* 333:226–238

Part IV

Regional Climate Modeling

Considerations of Domain Size and Large-Scale Driving for Nested Regional Climate Models: Impact on Internal Variability and Ability at Developing Small-Scale Details

René Laprise, Dragana Kornic, Maja Rapačić, Leo Šeparović, Martin Leduc, Oumarou Nikiema, Alejandro Di Luca, Emilia Diaconescu, Adelina Alexandru, Philippe Lucas-Picher, Ramón de Elía, Daniel Caya, and Sébastien Biner

Abstract

The premise of dynamical downscaling is that a high-resolution, nested Regional Climate Model (RCM), driven by large-scale atmospheric fields at its lateral boundary, generates fine scales that are dynamically consistent with the large scales. An RCM is hence expected to act as a kind of magnifying glass that will reveal details that could not be resolved on a coarse mesh. The small scales represent the main potential added value of a high-resolution RCM.

Several issues remain with respect to nested RCMs: are the large scales perfectly replicated, degraded or improved by an RCM? For a given set of lateral boundary conditions, is the course of an RCM simulation uniquely defined? Is lateral-boundary driving sufficient to control RCM simulations? What domain size and location should be used for a given application? Almost 20 years after the inception of RCMs, and despite recognition that RCMs' results are sensitive to the choice of domain and driving technique, these questions have still not been fully answered.

A series of methodical investigations spread over the course of several years have been performed to address these issues in an unambiguous manner, following a strict experimental protocol: the Big-Brother Experiment. The results to date point to the advantage of using rather large domains that permit the full spin-up of small scales, acknowledging however that such configuration permits the intermittent occurrence of divergence in phase space and large internal variability in RCM simulations. Alternative driving techniques to the traditional imposition of lateral boundary conditions, which allow forcing the large scales throughout the domain, appear to offer definite advantages.

R. Laprise (✉)

Centre pour l'Étude et la Simulation du Climat à l'Échelle Régionale (ESCER), UQAM, 201, Avenue du Président-Kennedy, C.P. 8888, Succ. Centre-ville, Montréal, QC, Canada H3C 3P8

Canadian Network for Regional Climate Modelling and Diagnostics (CRCMD), Montréal, QC, Canada

Université du Québec à Montréal (UQAM), Montréal, QC, Canada

e-mail: laprise.rene@gmail.com

Introduction

Coupled Global Climate Models (GCM) constitute the most sophisticated tools to investigate the processes responsible for the maintenance of the dynamical equilibrium of the climate system and to make projections of anticipated climate changes associated with anthropogenic effects such as emissions of greenhouse gases and

aerosols and changes in land-surface use. However due to the high computational cost of climate simulations, the length of simulations spanning centuries to millennia, the need for ensemble simulations to obtain statistical significance of the results, and the fact that models' computing cost is proportional to Δx^{-n} , with $3 \leq n \leq 4$, operational GCMs typically employ rather coarse meshes. This results in substantial numerical truncation and limits the physical processes that can be explicitly resolved; hence, GCMs have to rely heavily on parameterisation for subgrid-scale processes such as moist convection and clouds.

Limited-area, nested, Regional Climate Models (RCM) constitute a pragmatic approach to reduce computing cost of high-resolution climate modelling. In this approach, high resolution is only applied over a subset of the globe, and low-resolution GCMs' simulations are used to define the lateral (and often ocean surface) boundary conditions of RCM. In fact RCMs are not only used for downscaling climate-change projections (e.g. Jones et al. 1997; Laprise et al. 1998, 2003; Plummer et al. 2006; Déqué et al. 2006, to cite just a few), but also to study past climate variability (e.g. Weisse et al. 2009), to downscale seasonal predictions (e.g. Fennessy and Shukla 2000; Cocke and LaRow 2000; Díez et al. 2005; Herceg et al. 2006), and for process studies (e.g. Wyser et al. 2008).

“Dynamical downscaling” (von Storch et al. 1993) is based on the concept that fine scales are generated during simulations with a high-resolution RCM that is initialised and driven by low-resolution GCM data, and the ensuing fine scales are dynamically consistent with the large-scale flow. RCMs are hence thought as a kind of “magnifying glass” that reveals fine scales that are latent but are not permitted by coarse-mesh GCM simulations. The increased resolution has the benefit of reducing numerical truncation, of explicitly resolving dynamical interactions for wider range of spatial scales, and hence of relying less strongly on parameterisation of the ensemble effects of subgrid scales, and last but not least, the increased resolution permits the simulation of fine-scale details that constitute the main potential added value of RCM.

This chapter summarises several studies realised by ESCER Centre scientists, relating to the potential and limitations of regional climate modelling, spread across various publications as well as some recent results that have not yet been published. This chapter is organised as follows. The next section discusses the

concept of dynamical downscaling of climate simulations. Section “RCM Validation Issue: Big-Brother Experiment” discusses the validation issue of high-resolution nested models for climate application. Section “Internal Variability” discusses the presence of internal variability, defined as inter-member differences that develop in nested simulations under identical model configuration and lateral boundary forcing. Section “Development of Fine Scales” shows the development of fine scales in simulations that are initialised and driven by large-scale flow. Section “Impact of Imperfect Lateral Boundary Conditions” analyses the impact of imperfect LBC. Section “Nesting Technique: Driving Through LBC Versus Large-Scale Spectral Nudging” compares two nesting techniques: the conventional driving through LBC and large-scale spectral nudging. Finally section “Discussion and Conclusions” summarises the main conclusions.

Dynamical Downscaling and Potential Added Value

To illustrate the process of dynamical downscaling, let us look at an example of generation of small scales generated during the course of a high-resolution RCM simulation driven by a coarse-resolution GCM. Figure 1a displays an instantaneous field of 900-hPa specific humidity over eastern North America, on a winter day in a GCM simulation at T32 spectral resolution, corresponding roughly to a 600-km mesh. Figure 1b displays the same field on which is superimposed the corresponding field simulated by a 45-km RCM driven by the GCM. The increased level of details in the RCM simulation compared to its driving GCM is outstanding.

The presence of fine-scale details in RCM simulations constitutes a necessary condition for adding value to the coarser resolution driving data. A method to sort out atmospheric variables according to different scales can be very handy to identify and quantify the added value. One possibility is to estimate the potential added value by evaluating different climate statistics of a simulated dataset in several temporal and/or spatial scales (e.g. Errico 1985; Denis et al. 2002a; Feser 2006; Feser and von Storch 2006; Feser et al. 2009; Bresson and Laprise 2009).

It can be expected that extremes in the frequency distribution of climate variables will be particularly

sensitive to the resolved scales. To test this hypothesis, Di Luca et al. (2010) used a simulation of the Canadian RCM (CRCM; Caya and Laprise 1999; Laprise et al. 1998, 2003; Plummer et al. 2006) performed on a 45-km mesh for the period 1981–2000, using the archived three-hourly accumulated precipitation as reference. This data is then methodically aggregated onto coarser meshes (ranging from 0.5° to 4°) and for longer period (from 3 h to 192 h) in order to estimate the impact of changing resolution on precipitation extremes. Figure 2 shows the 99th percentile of precipitation for a region centred on 45.0° and 100.0° West (near the Dakotas, USA). It is clearly seen that coarser spatial resolution results in a decrease of precipitation extreme by about a factor of two, with important differences between seasons: fine spatial scales appear to be more important in summer than in winter. In both seasons, there is a clear link between fine spatial and short time scales: fine spatial scales lose their importance when precipitation is accumulated on time scales exceeding about 48 h.

RCM Validation Issue: Big-Brother Experiment

Even though fine-scale features are present in RCM simulations and may superficially seem realistic, it does not mean that their climate statistics, such as

time average and variability or extremes, are free of errors. The verification of high-resolution climate simulations is complicated by data availability. High-resolution limited-area objective analyses from atmospheric data assimilation are only starting to be available over some regions of the world. But given the paucity of regions with dense upper-air network and the limitations in assimilating surface observations (e.g. Annamalai et al. 1999), the regional analyses reflect to a large extent the assimilation model and hardly constitute an absolute reference for RCM-simulated climate verification.

RCMs like any numerical model are not perfect and the assessment of the quality of simulated fine scales is a central issue in regional climate modelling. Several RCMs' errors are common with GCMs, such as the numerical approximations, the impact of finite resolution, the parameterisation of subgrid-scale physical effects and the prescription of geophysical fields. There are on the other hand errors that are specific to nested RCMs, such as the limited-area computational domain, the nesting technique, the resolution jump between a RCM and its driving data, the update frequency of the lateral boundary conditions (LBC) and the imperfections in LBC data. It is hence of interest to use a validation approach that allows focussing on errors that are specific to RCMs. The Big-Brother Experimental (BBE) protocol was designed for this goal (Denis et al. 2002b).

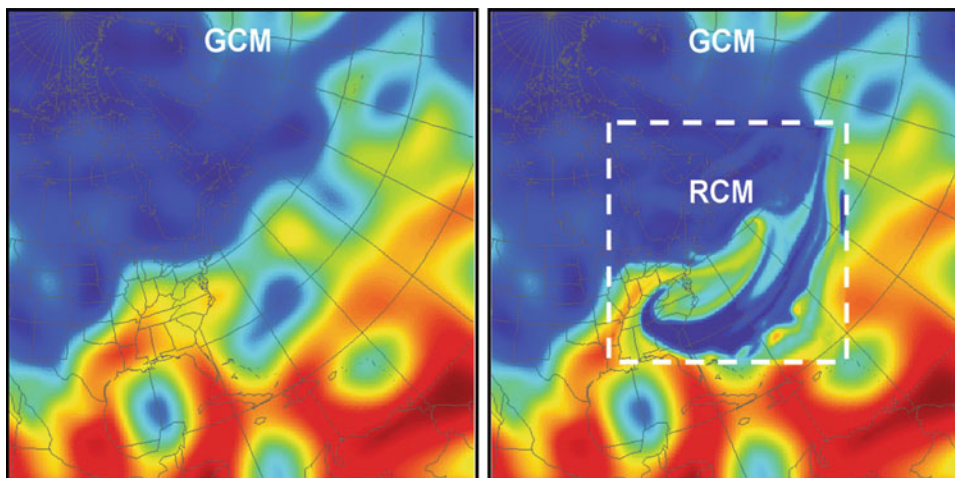


Fig. 1 Instantaneous field of 900-hPa specific humidity over eastern North America and western North Atlantic, on a winter day in a T32 CGCM simulation (*left panel*). *Right panel* displays the same field on which is superimposed the

corresponding CRCM-simulated field (taken from Denis et al. (2003) © 2003 Clim Dyn)

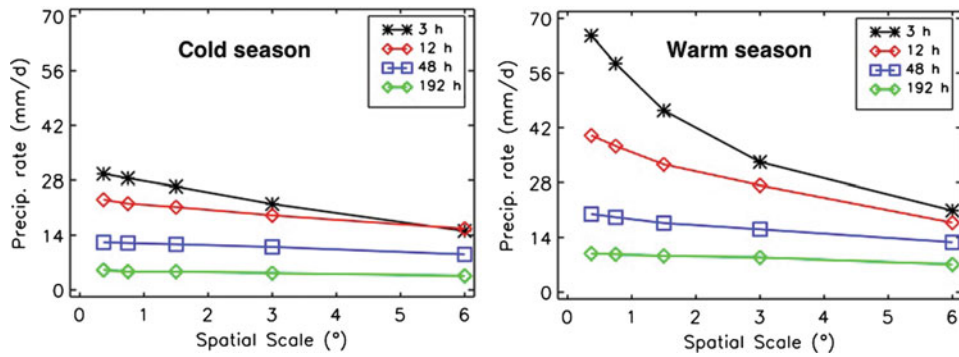


Fig. 2 Precipitation 99th percentile for a region centred on 45.0° and 100.0° West (near the Dakotas, USA) in a 45-km CRCM simulation for 1981–2000, and the corresponding data

aggregated onto coarser meshes and for longer periods (adapted from Di Luca et al. 2011)

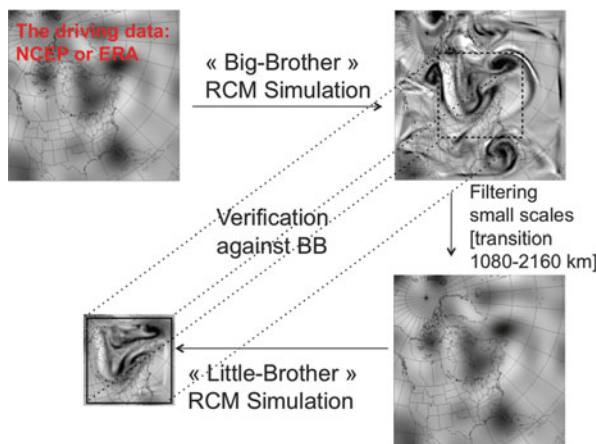


Fig. 3 The various steps involved in the Big-Brother experiment (adapted from Kornic 2010)

The BBE is an application of the general “perfect prognosis” approach. Figure 3 shows the steps involved in the BBE. First a reference simulation is performed with a high-resolution RCM on a very large domain (ideally a global domain); this is called the Big-Brother (BB) simulation. The BB simulation is then filtered to remove fine scales that are not resolved by operational coarse-mesh GCMs: the resulting field is called the filtered BB (FBB). Next the FBB data is used to drive RCM simulations over smaller domains: these are called the Little Brothers (LB). By verifying the LB simulations against the BB reference simulation over a common subset of the domain, the differences can be unambiguously attributed to the limited domain, the nesting technique or the resolution of the driving data. This BBE has since been used for several studies at the

ESCCER Centre (Denis et al. 2003; de Elía et al. 2002; de Elía and Laprise 2003; Antic et al. 2005; Dimitrijevic and Laprise 2005; Diaconescu et al. 2007; Leduc and Laprise 2009; Leduc et al. 2011; Rapačić et al. 2011; Kornic 2010) and elsewhere (e.g. Nutter et al. 2004; Herceg et al. 2006).

We note in passing that the name Big Brother was not inspired by the fictional character in George Orwell’s novel, but rather by the mentoring organisation “Big Brothers Big Sisters of America” whose mission is to help children reach their potential through professionally supported, one-to-one relationships with mentors that have a measurable impact on youth. In an analogous sense, in the BBE, the BB simulation provides guidance to, although not a perfect control upon, the LB simulation.

Internal Variability

Underlying the concept of dynamical downscaling is the premise that large-scale fields imposed as lateral boundary conditions (LBC) of a nested limited-area RCM will constrain its simulations. The fine scales that are generated by a high-resolution RCM when driven by low-resolution data are expected to be dynamically consistent with the large-scale flow imposed as LBC (e.g. Miyakoda and Rosati 1977; Anthes et al. 1982). A corollary of the above is that the fine scales that so develop are assumed to be uniquely determined. RCM are hence thought of as a kind of “magnifying glass” that reveals fine scales that are latent but are not permitted by coarse-mesh

GCM simulations. Implicit in the above statement is that the RCM solution is unique for a given model configuration (domain, resolution, numerics, parameterisation) and set of LBC. It is well documented however that RCM simulations are subject to internal variability, i.e. the details of RCM simulations do differ when initialised with even slightly different initial conditions (e.g. Ji and Vernekar 1997; Jones et al. 1995 and 1997; Weisse et al. 2000; Giorgi and Bi 2000; Rinke and Dethloff 2000; Christensen et al. 2001; de Elía et al. 2002; Caya and Biner 2004; Rinke et al. 2004; Wu et al. 2005; Alexandru et al. 2007, 2009; Vanvyve et al. 2007, Lucas-Picher et al. 2008a,b, Šeparović et al. 2008; Feser and von Storch 2008; Zahn et al. 2008; Rockel et al. 2008), but the implications do not seem to have been fully grasped by a large part of the RCM community. The presence of IV in RCM simulations contributes to making more difficult testing the statistical significance of simulation differences resulting from changes in forcing (e.g. Weisse et al. 2000, Weisse and Feser 2003; Feser 2006; de Elía et al. 2007).

Figure 4 illustrates the phenomenon of internal variability (IV), by showing the 500-hPa geopotential

height at some instant in five simulations of CRCM that used identical configuration of the model and LBC, but were initialised 24-h apart. At that particular moment, there is a large closed circulation within the regional domain and the simulations are rather distinct; a few days before and later, however, the simulations were much more similar.

IV in RCM simulations will here be defined as the variance σ_{IV}^2 between ensemble members of LB simulations performed with identical configuration and LBC:

$$\sigma_{IV}^2 = \frac{1}{M-1} \sum_{m=1}^M (X_m - \bar{X}^M)^2, \quad (1)$$

where M is the number of members in the ensemble and

$$\bar{X}^M = \frac{1}{M} \sum_{m=1}^M X_m \quad (2)$$

is the ensemble mean, which is the part that can be considered as common to all the members in the

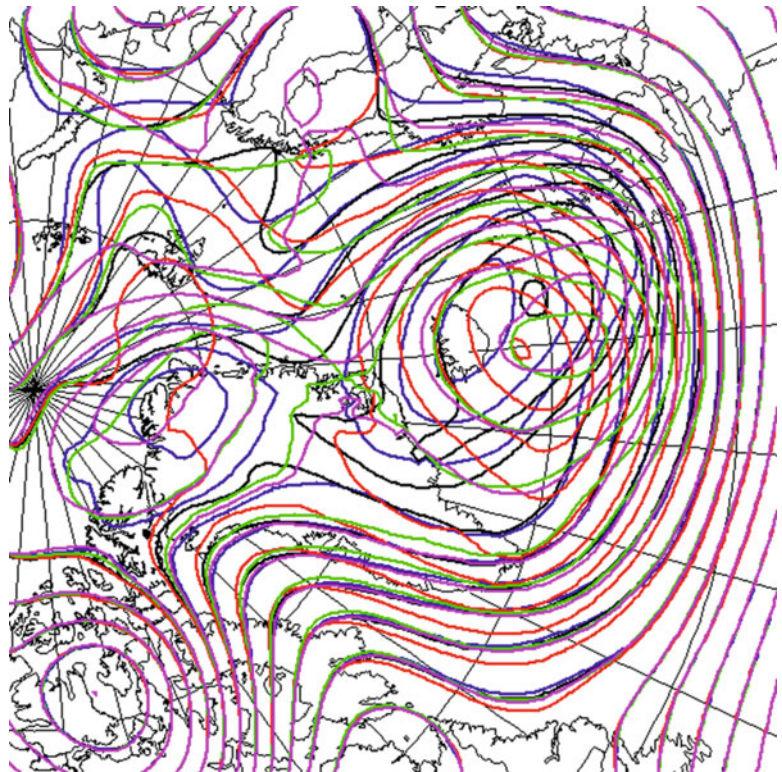


Fig. 4 Instantaneous fields of 500-hPa geopotential height in an ensemble of 45-km CRCM simulations. The five-member simulations used identical configuration of CRCM and the same lateral boundary conditions, but were initialised 24-h apart (adapted from Rapačić et al. 2011)

ensemble. For this reason, the ensemble mean and the departure thereof may also be termed the reproducible and irreproducible components of an ensemble of RCM simulations (Šeparović et al. 2008).

Two ensembles of 20 LB members were performed with a 45-km version of CRCM on small and large domains with 106 by 106 and 190 by 190 grid points, respectively (Rapaić et al. 2011). All members were driven by LBC from a BB simulation performed on a 250 by 250 grid-point domain for the 3-month period August to October 1999. The individual LB members were started 24-h apart, and the statistics will be presented for the 2-month period September to October 1999 over a 74 by 74 grid-point verification domain (Fig. 5). Figure 6 shows the time evolution of the IV for temperature at 925, 850, 700 and 500 hPa, for the small- and large-domain LB simulations. The IV variance has been averaged over the verification domain, and normalised by the BB transient-eddy variance σ_{TEBB}^2 defined as

$$\sigma_{TEBB}^2 = \frac{1}{T} \sum_{t=1}^T \left(X_{tBB} - \overline{X_{BB}}^T \right)^2, \quad (3)$$

where T is the number of time samples and

$$\overline{X}^T = \frac{1}{T} \sum_{t=1}^T X_t \quad (4)$$

is the time average. Furthermore, the statistics have been calculated separately for the large- and small-scale component of the spectrum, using a length scale of 1,400 km for separation. Figure 6 shows that IV is weaker for the large scales than for the small scales, because of the control exerted by LBC on the large scales. Figure 6 also shows that IV is much stronger on large domains due to the weaker control exerted by distant LBC. In fact, the small-scale IV on large domain frequently reaches normalised values of unity, indicating that these scales behave almost freely in the various members of the ensemble. Figure 7 shows the

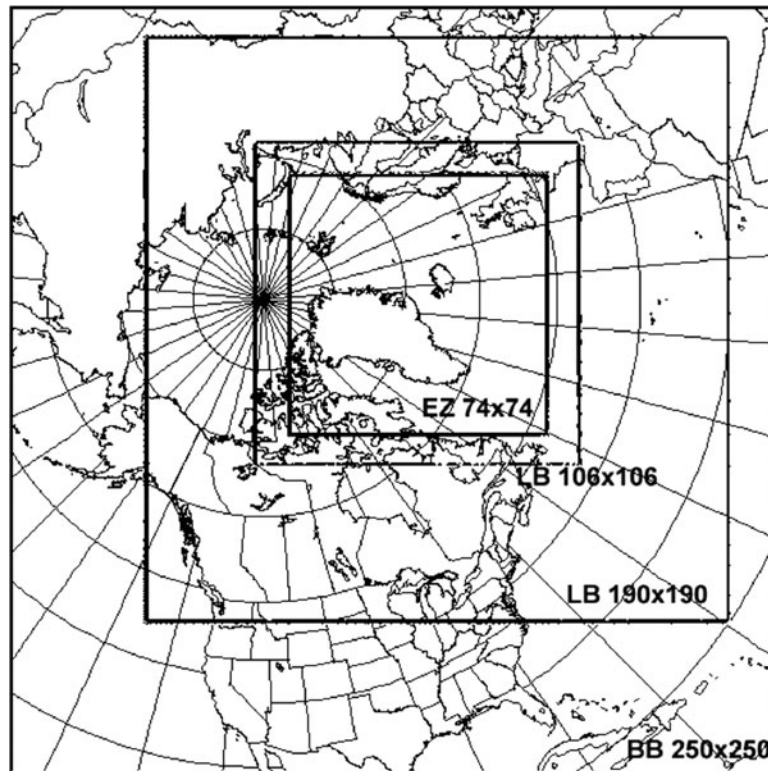


Fig. 5 The 250 by 250 grid-point domain of the BB simulation used to drive the two ensembles of LB simulations: a small 106 by 106 grid-point domain and a large 190 by 190 grid-point

domain. The verification domain comprises 74 by 74 grid points (taken from Rapaić et al. (2011) © 2011 Clim Dyn)

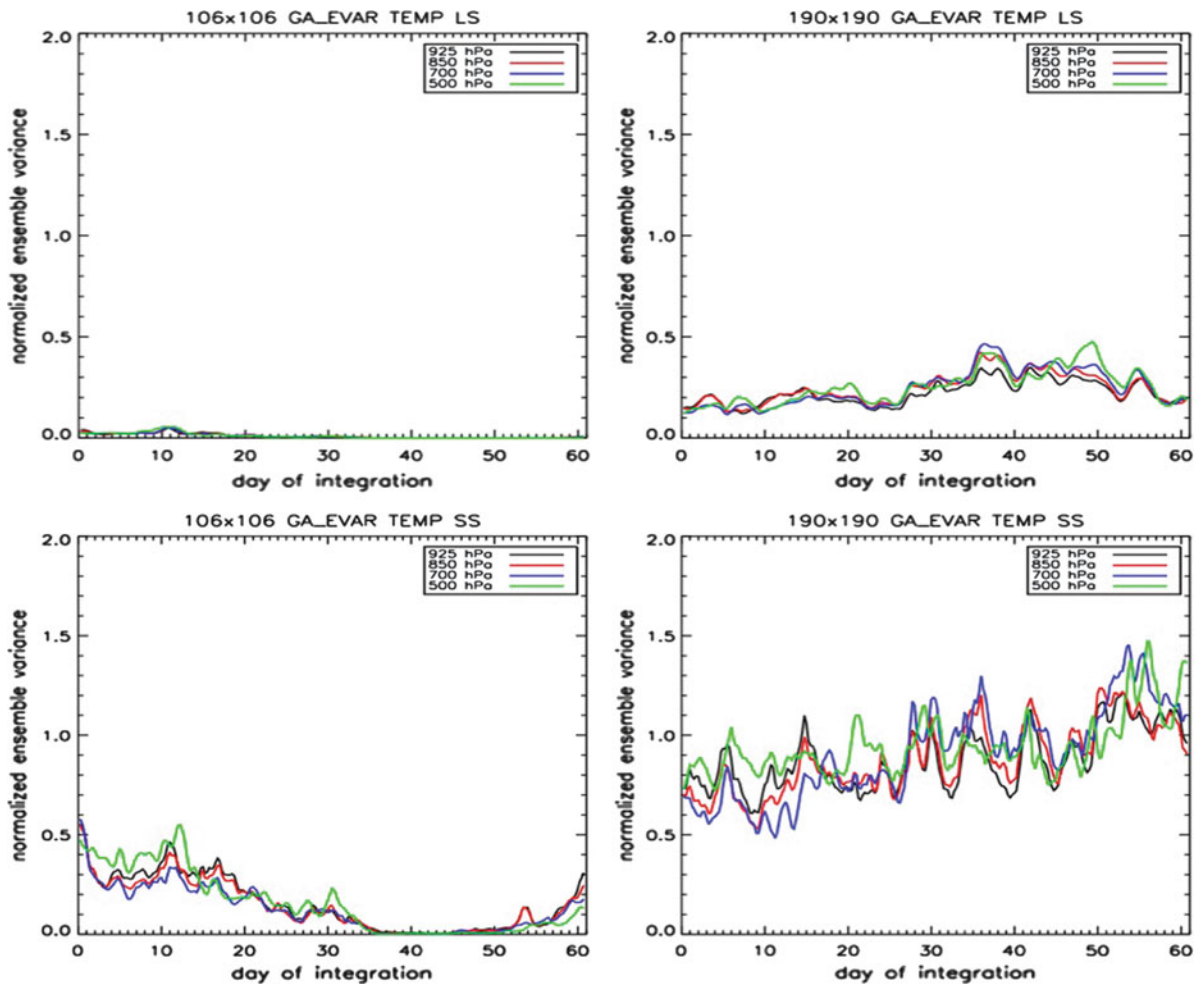


Fig. 6 Time evolution of temperature IV in LB simulations over small (*left column*) and large domains (*right column*), for the large (*upper row*) and small scales (*lower row*), using a separation length scale of 1,400 km. The IV variances are

averaged over the verification domain and normalised by the BB transient-eddy variance (adapted from Rapačić et al. (2011) © 2011 Clim Dyn)

corresponding time evolution of the normalised IV variance for precipitation. We note that precipitation IV is much stronger than for temperature, and on large domains IV is strong even for large scales. This is probably due to the fact that precipitation results from a series of complex interactions between the dynamics and thermodynamics, and it is not a variable that is driven by the LBC. Above all, we note the episodic, intermittent character of IV.

Figure 8 shows the spatial distribution of the normalised time-averaged small-scale IV for the variables of 500- and 925-hPa kinetic energy (KE) and precipitation, on the small and large LB domains. This figure serves to show that the location of

maximum IV depends on the variables and, for a given variable, on the level. We have often noted in other simulations that the maximum IV tends to occur on the downstream side of the domain, with respect to the dominant flow. But for these simulations, the presence of high topography appears to affect greatly the location of IV.

Šeparović et al. (2008) in their experiments with a different configuration of CRCM, without the BBE framework and on different domains, calculated the climatological spectrum of simulated precipitation. Figure 9 shows the fraction of precipitation contained in its reproducible (ensemble-mean) and irreproducible (IV) components; we can note the clear

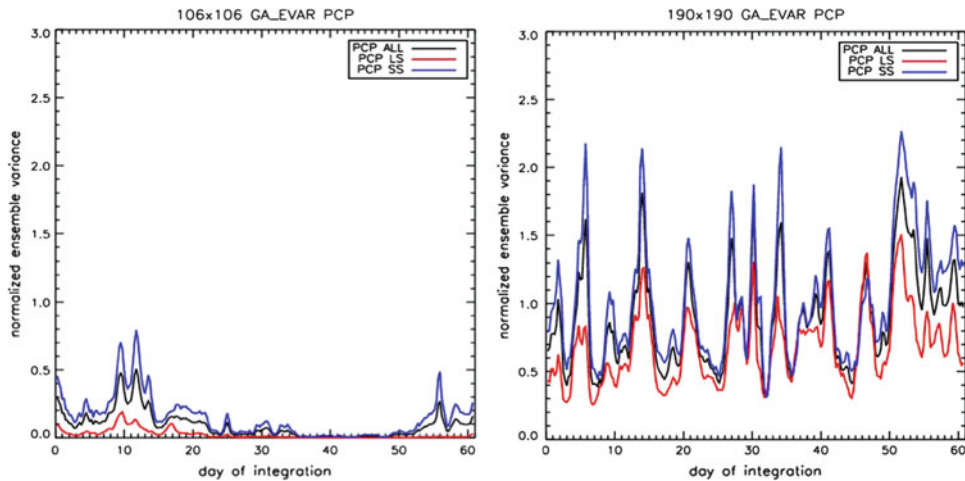


Fig. 7 Time evolution of precipitation IV in LB simulations over small (*left column*) and large domains (*right column*), for all scales as well as for the large and small scales, using a separation length scale of 1,400 km. The IV variances are

averaged over the verification domain and normalised by the BB transient-eddy variance (adapted from Rapaic et al. (2011) © 2011 Clim Dyn)

dominance of reproducible component in the longer scales and of IV in the shortest scales.

Although the presence of IV in nested RCM simulation is increasingly acknowledged, the physical reasons for its development are still elusive. de Elía et al. (2002) have hinted to the nonlinear transfers operating in nested RCM which limit the deterministic predictability skill in RCM simulations despite the control exerted by LBC upon the larger scales; a similar argument might explain the development of IV for those scales that are poorly controlled by the LBC. Lucas-Picher et al. (2008b) noted that the magnitude of IV correlated well with the residence time of air parcels within the regional domain; hence large domains and episodes of recirculation flow tend to lead to large IV, whereas small domains and weather regimes characterised by strong flow through the domain lead to weak IV. Recently Nikiema and Laprise (2011) developed a diagnostic budget equation for the time evolution and space distribution of inter-member variance in ensemble simulations, to characterise the importance of individual contribution of various diabatic and non-linear terms in the generation of IV for the variables of vorticity and potential temperature; their study reveals that the dominant terms responsible for the growth of IV are either the covariance term involving the potential temperature fluctuations and diabatic heating fluctuations, or the covariance of inter-member fluctuations acting upon ensemble-mean gradients. In another

ongoing study Diaconescu, Zadra and Laprise (personal communication) are attempting to relate the growth of IV with hydrodynamic instabilities that develop differently in members of an ensemble of simulations, through the use of singular vector analysis at various moments in the course of RCM simulations.

All indications point to the fact that IV is a rather episodic phenomenon and the occurrence of IV is related to the large-scale weather regime and model domain size, and it is not specific to a particular model. As noted in our middle-latitude experiments, large domains and weak flow regimes resulting in long parcel-residence time lead to enhanced IV. Further investigations are required to extend these results to polar, tropical and subtropical regions.

With large IV “Differences ‘RCM versus observations’ are not necessarily reflecting model errors” (von Storch 2005); model tuning experiments and process studies employing short experiments may be quite vulnerable to misinterpretation of differences arising between simulations performed with different formulations or forcings. It is worth noting that the trace of IV remains even in the time-averaged climate statistics of long climate simulations (e.g. de Elía et al. 2007). The presence of IV in RCM simulations contributes to making more difficult testing the statistical significance of simulation differences resulting from changes in forcing (e.g. Weisse et al. 2000; Feser 2006).

Fig. 8 Time-averaged small-scale IV for kinetic energy at 500 hPa (*top row*) and 925 hPa (*middle row*) and for precipitation (*lower row*), in LB simulations over small (*left column*) and large (*right column*) domains. The LB IV is normalised by the BB transient-eddy variance (adapted from Rapačić et al. (2011) © 2011 Clim Dyn)

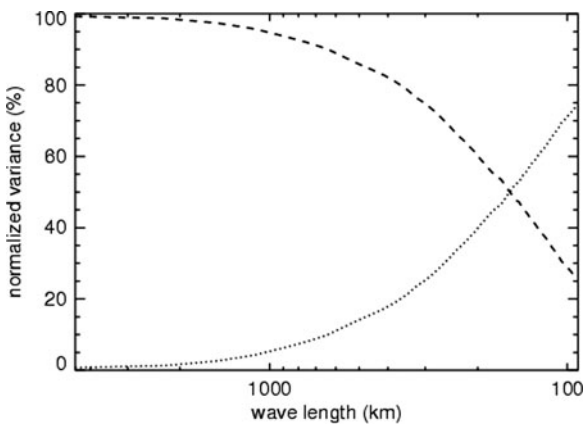
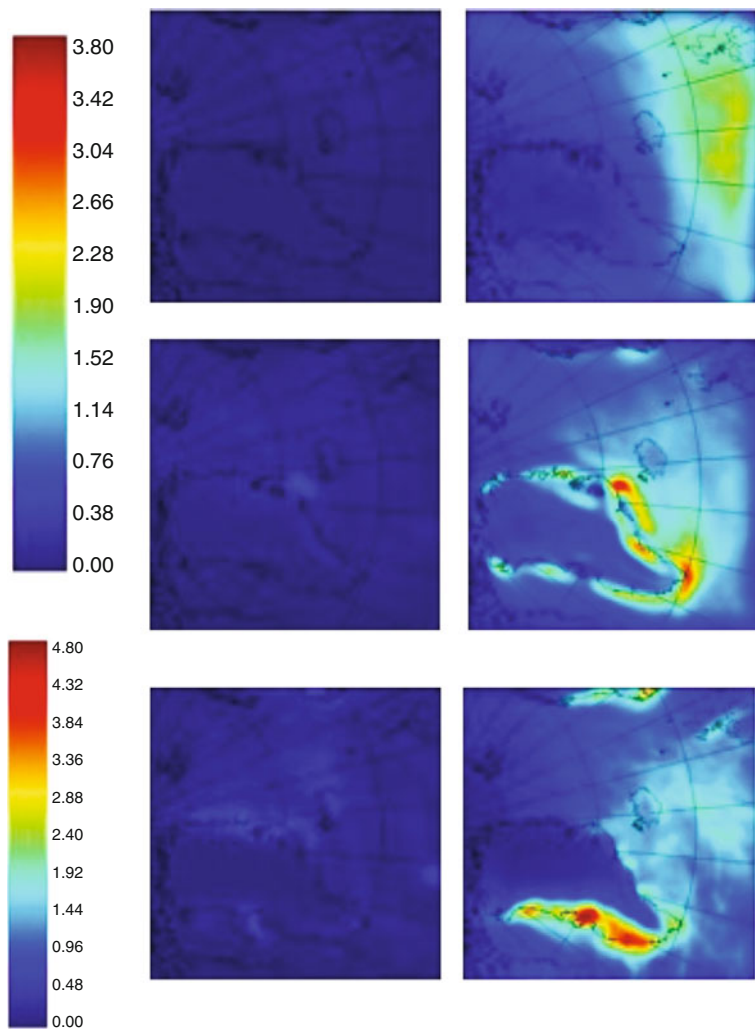


Fig. 9 Fraction of variance of precipitation at various length scales, that is contained in the reproducible (ensemble-mean; *dashed line*) and irreproducible (internal variability; *dotted line*) components (adapted from the study of Šeparović et al. 2008)

Development of Fine Scales

As mentioned earlier, the paradigm of dynamical downscaling is that a nested, high-resolution RCM will generate fine scales that are dynamically consistent with the large-scale fields used to drive it; these fine scales constitute the main potential added value of an RCM.

Figure 10 shows Taylor diagrams of small-scale transient-eddy component of the fields of 500- and 925-hPa KE and precipitation, 850-hPa temperature and precipitation, as simulated in the two 20-member ensembles of LB simulations performed over small and large domains shown in Fig. 5. On each panel, the green dots and black triangles represent the results of the individual members for the large and small

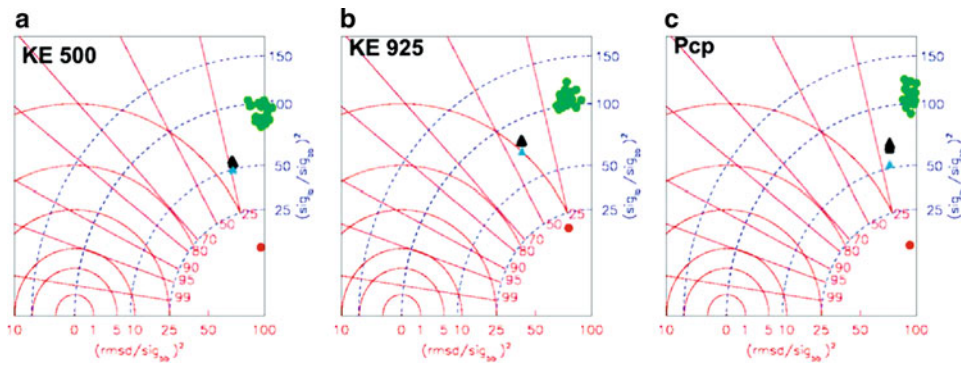


Fig. 10 Taylor diagrams of small-scale transient-eddy component of the fields of 500- and 925-hPa KE and precipitation, as simulated in the two 20-member ensembles of LB simulations performed over small (*black triangles*) and large (*green dots*)

domains shown in Fig. 5. On each panel, the *turquoise triangle* and *red dot* represent the results of the statistics of the ensemble-mean over the small and large domains, respectively (adapted from Rapačić et al. (2011) © 2011 Clim Dyn)

domains, respectively, while the red dot and turquoise triangle represent the corresponding ensemble-mean statistics. One can see that the small-scale variance ratio is quite good for the large domain, while they are variance deficient in the small-domain simulations. This reflects the earlier discussed issue of spatial spin-up; small scales are absent in the LBC data that drive the RCM, and these take time to develop while they are transported by the mean flow. This is particularly true at higher altitude where the flow is stronger, and for fields such as precipitation that result from a series of complex physical interactions (Leduc and Laprise 2009; Leduc et al. 2010). Lucas-Picher et al. (2008b) have documented that the flushing rate by the flow through the domain is an important factor in determining the domain size required for achieving the full development of fine scales.

We note the larger dispersion of the members in the ensemble of simulations over the larger domain, reflecting the stronger IV. The ensemble-average fields are all variance defective, especially over the larger domain, due to the destructive interference between patterns subject to large IV, which acts to partly cancel fine-scale amplitudes in the ensemble mean.

Although LB small scales are seen to reach realistic amplitudes over larger domains, we note that their time correlation with the BB reference is vanishingly small. This means that small-scale features appear statistically with the right amplitude (and at the right location on average, not shown), but not necessarily at the right time compared to the BB reference. This reflects the limited deterministic predictability skill discussed by Anthes et al. (1989) in forecast experiments, and by de Elía et al. (2002) in their idealised

prediction experiments. This lack of time correlation may not be very important for climate downscaling applications where the interest lies in the climate statistics; but it is an issue for case studies and even for downscaling seasonal prediction, because time correlation errors can have an impact regarding inter-annual variability.

Impact of Imperfect Lateral Boundary Conditions

The opinions of the RCM community are rather divided on the treatment of the large scales (LS) in RCM simulations: whether they are simply reproduced, improved or degraded.

According to a strict, and somewhat naïve, interpretation of dynamical downscaling, the LS of the driving fields are to be simply reproduced, unaffected, within the RCM domain. We have alluded however to the fact that the traditional treatment of LBC with sponge layers does not ensure a perfect control of the LS, particularly over large domains or for weather regimes characterised by weak flows, resulting in long residence time within the regional domain.

On the other hand, it has been argued that RCM can actually improve the LS when these contain errors, such as when driving fields come from coarse-mesh GCM simulations. Mesinger et al. (2002) have reported improvements of LS during the first three and a half days of numerical weather prediction forecasts with a high-resolution RCM over a very large regional domain (of the order of 10,000 km). The improvement may be the result of the reduced

numerical truncation and explicit treatment of some mesoscale processes.

There is however some evidence that LS may be degraded in nested RCM simulations. For example, Fig. 8a of de Elía et al. (2002) showed some loss in the amplitude of LS. The reasons may be related to the limited domain being too small to handle the LS adequately and may also reflect remaining problems with the nesting technique.

In order to investigate the treatment of LS by a nested RCM and the impact of imperfect LBC, Diaconescu et al. (2007) have designed an idealised experimental framework called the “Imperfect Big-Brother Experiment” (IBBE). In the IBBE as in the BBE, a large-domain simulation called the “Perfect Big Brother” (PBB) is done to serve as reference for the LB simulations that will be performed over smaller domains. However in the IBBE, the LB simulations are not driven by the filtered BB, but by a so-called “Imperfect Big-Brother” (IBB) simulation in which controlled errors have been introduced; this can be achieved by employing a different domain size and coarser resolution typical of GCM, as shown in the flowchart on Fig. 11.

Figure 12 shows the LS errors of LB simulations over a 100 by 100 grid-point domain over eastern North America, as a function of corresponding error

in their driving IBB, using the PBB as reference. The error is here defined as the departure from 100% of the spatial correlation coefficient of the patterns of time mean (stationary) and transient-eddy variance, for the fields of precipitation, mean sea level pressure and 850-hPa temperature. It can be seen that by-and-large the LB error scales linearly with that of the driving IBB, except for precipitation in which case it is systematically larger; we recall that precipitation is not a field that is driven at the lateral boundary and that it results from a complex series of physical interactions.

Hence in this specific experiment, for a modest domain size and for this error metrics, the LS errors are simply reproduced, unaffected, by the RCM. Further experimentation is required to verify how general is this conclusion.

Nesting Technique: Driving Through LBC Versus Large-Scale Spectral Nudging

Nested models need to be driven by the prescription of time-dependent LBC for the atmospheric prognostic variables all around the perimeter of their limited-area domain. It is well established though that such boundary-value problem is mathematically ill posed for hyperbolic (wave) equations (e.g. Olinger and

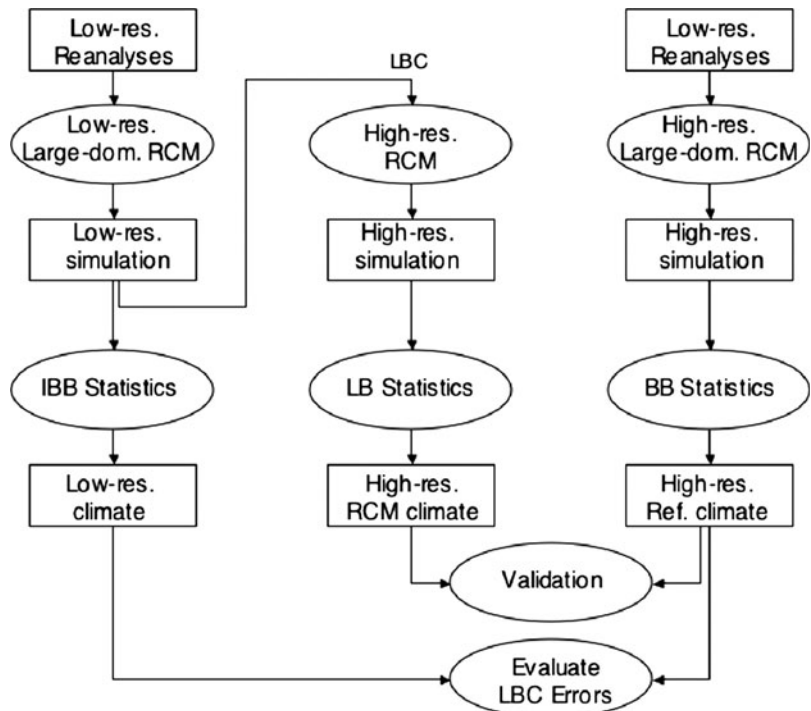


Fig. 11 The “Imperfect Big-Brother Experiment” (IBBE): The Perfect Big Brother (PBB) simulation (*right column*) is used as reference to verify the Little-Brother (LB) simulations (*middle column*) that are driven by the Imperfect Big-Brother (IBB) simulation (*left column*) (reproduced from Laprise et al. (2008) © 2008 Meteorol Atmos Phys)

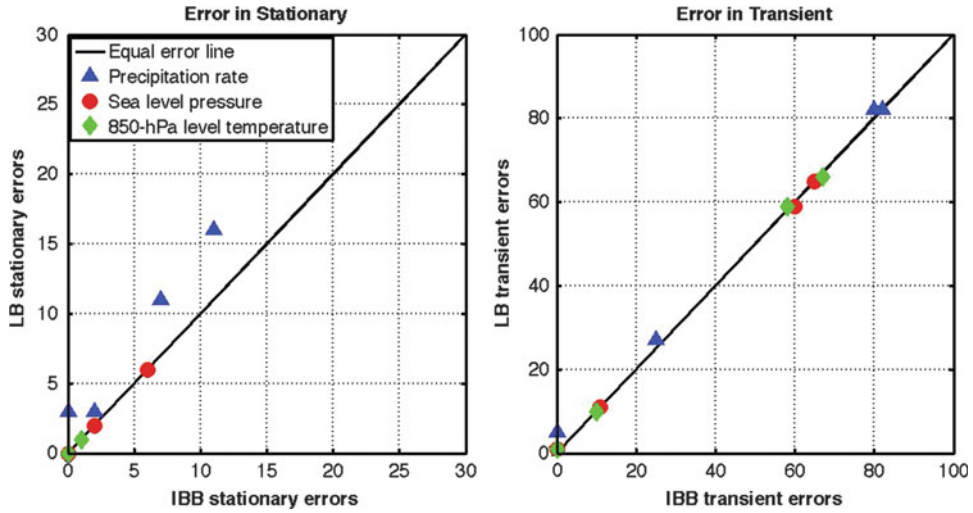


Fig. 12 Large-scale errors of LB simulations over a domain of 100 by 100 grid points over eastern North America, as a function of corresponding error in their driving IBB, using the PBB as reference. The error is here defined as the departure from 100%

Sundström 1978; Staniforth 1997). To address this problem, Davies (1976) proposed the application of an *ad hoc* relaxation in sponge layers adjacent to the lateral boundary:

$$\begin{aligned} \Psi_{\text{RCM}}^{\text{Driven}}(X, Y, p, t) = & \Psi_{\text{RCM}}(X, Y, p, t) \\ & + (-1)^n \beta_{(\Psi, n)}(X, Y) \nabla^{2n} \\ & \{ \Psi_0(X, Y, p, t) - \Psi_{\text{RCM}}(X, Y, p, t) \}, \end{aligned} \quad (5)$$

where Ψ_{RCM} is the RCM-simulated variable, Ψ_0 is the corresponding driving field, interpolated on the RCM grid, and β is the relaxation coefficient, function of the distance from the boundary and possibly of the variable. The case $n = 0$ corresponds to a Newtonian relaxation, and $n \geq 1$ to (hyper-) diffusion. Modified in this way, the field equations adopt a parabolic (diffusion) character and constitute a well-posed problem under the application of the LBC around the perimeter. Robert and Yakimiw (1986) and Yakimiw and Robert (1990) have shown that such an approach constitutes an acceptable pragmatic solution to the LBC problem for numerical weather prediction, and this is the most commonly used procedure for driving nested RCMs. In CRCM we normally use $n = 0$ only, with β varying smoothly from unity at the lateral boundary to zero over a 10 grid-point wide sponge zone, and the sponge is only applied to the horizontal wind components, while boundary conditions for other

of the spatial correlation coefficient of the patterns of time mean (stationary) and transient-eddy variance, for the fields of precipitation, mean sea level pressure and 850-hPa temperature (adapted from the study of Diaconescu et al. 2007)

variables are only imposed on the outer boundary grid points.

It is well known from RCM modellers however that non-physical solutions do occasionally develop in the artificial viscous sponge layers. As mentioned in preceding sections, the control exerted by LBC varies with domain size and weather regime. Some loss in the amplitude of the largest scales is often noted (e.g. Fig. 8a of de Elía et al. 2002). Several remaining issues with nested models, some of which relate to the LBC treatment, have been discussed by Warner et al. (1997), McGregor (1997), Laprise et al. (2002), Wang et al. (2004), Laprise (2007), and in the proceedings edited by Barring and Laprise (2005).

Spectral RCMs usually apply spectral nudging (SN) of the large scales in the interior of their regional domain (e.g. Tatsumi 1986; Segami et al. 1989; Kuo and Williams 1992, 1998; Cocke and LaRow 2000; Juang and Hong 2001). SN has also been applied in some grid-point RCMs as an alternative to the traditional driving at the LBC (e.g. von Storch et al. 2000; Biner et al. 2000; Riette and Caya 2002; Miguez-Macho et al. 2004; Castro et al. 2005). With SN, the driving condition is modified as follows:

$$\begin{aligned} \Psi_{\text{RCM}}^{\text{Nudged}}(X, Y, p, t) = & \Psi_{\text{RCM}}(X, Y, p, t) \\ & + \alpha_{(\Psi, p, k)} \Im \{ \Psi_0(X, Y, p, t) \\ & - \Psi_{\text{RCM}}(X, Y, p, t) \}, \end{aligned} \quad (6)$$

where \mathfrak{S} is a low-pass filter and α is the SN strength that defines the fraction of RCM field that is replaced by the large-scale component of the driving data at each time step; α is often a function of the variable, level in the vertical and spatial length scale \mathbf{k} . In CRCM, a Discrete Cosine Transform (DCT; Denis et al. 2002a) is used to separate length scales, with a cut-off length scale generally corresponding to about one-third of the domain size, SN is usually only applied to horizontal winds and α is chosen to increase from zero in the low levels to its maximum value (0.05) at the top of the model.

Introducing SN changes the nature of the mathematical problem from one of boundary value to a kind of “poor-man” data assimilation (von Storch et al. 2000; Kanamaru and Kanamitsu 2007; Thatcher and McGregor 2009). Experience has shown that the application of SN greatly reduces the development of intermittent divergence in phase space (IDPS; von Storch 2005) as well as the occurrence of unphysical flow behaviour in the lateral viscous zone. Ensuring the coherence of large scales of RCM with driving data has also the advantage of facilitating the identification of the significance of added value in RCM simulations (e.g. Feser 2006) and of reducing IV.

Figure 13 shows two vertical profiles of SN strength that will be tested next. In one case, the SN coefficient is constant in the vertical with a strength corresponding to replacing 5% of the large scales every time step (SN 5%); in the other case, the SN coefficient increases from zero at the surface to the

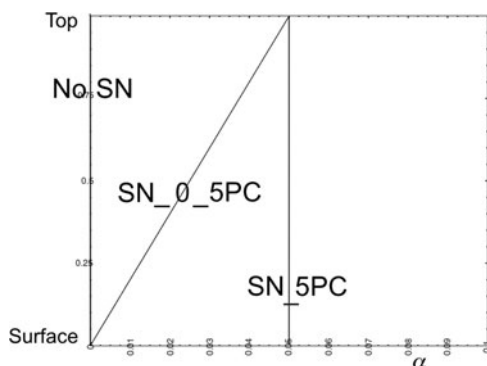


Fig. 13 Vertical profiles of SN strength: constant with a strength corresponding to replacing 5% of the large scales every time step (SN 5%), increasing from zero at the surface to the same maximum value at the top of the CRCM (SN 0–5%), and without SN (No SN)

same maximum value at the top of the CRCM (SN 0–5%). An experiment without SN is also made for comparison (No SN). Figure 14 shows the BB domain comprising 250 by 250 grid points, and the five LB domains that were tested, although only three will be reported here: LB1 with 196 by 196 grid points, LB2 with 160 by 160 grid points and LB4 with 120 by 120 grid points. The BB simulation was performed for January and February 1990, and the LB simulation will be compared to the BB simulation for February over a central verification domain labelled QC that comprises 86 by 86 grid points. Figure 15 shows Taylor diagrams for the small-scale transient eddies for four fields (mean sea level pressure, 700-hPa KE and relative humidity, and precipitation), over three domain sizes (LB1, LB2 and LB4) and three SN strengths (No SN, SN 0–5% and SN 5%). Small scales are here defined on the basis of a DCT with a gradual cut-off, retaining all variance for scales longer than 2,160 km and removing all variance for scales shorter than 1,080 km. Figure 15 shows that, as noted before, large domains are required for the full development of small scales. We note that SN improves the time coherence of small-scale eddies despite the fact that driving fields only contain large scales.

Next we illustrate the fact that SN reduces IV. Figure 16 shows the results obtained with two ten-member ensembles of simulations, driven by ERA40 reanalyses (without the BBE framework), for 1 year (from 1 December 1992 to 30 November 1993), on a 120 by 120 grid-point domain over North America (slightly shifted westward from that shown on Fig. 14). One simulation was performed without SN (labelled NA), and the other used a linear profile of SN strength above 500 hPa (labelled NASN). The curves labelled “spread” correspond to the square root of IV variance and “bias” to the root-mean square deviation of the CRCM simulations from the ERA driving reanalyses, for the 500-hPa geopotential. We note that, although SN was only applied to the largest scales and above the 500-hPa level, the application of SN decreases the difference with the driving fields and the occurrence of intermittent divergence in phase space. We note on Fig. 16 that SN also reduces the amplitude of IV.

In summary, SN constitutes a practical way of forcing, or imposing, the LS throughout the regional domain at all times. Alexandru et al. (2009) have discussed some of the possible side effects of SN.

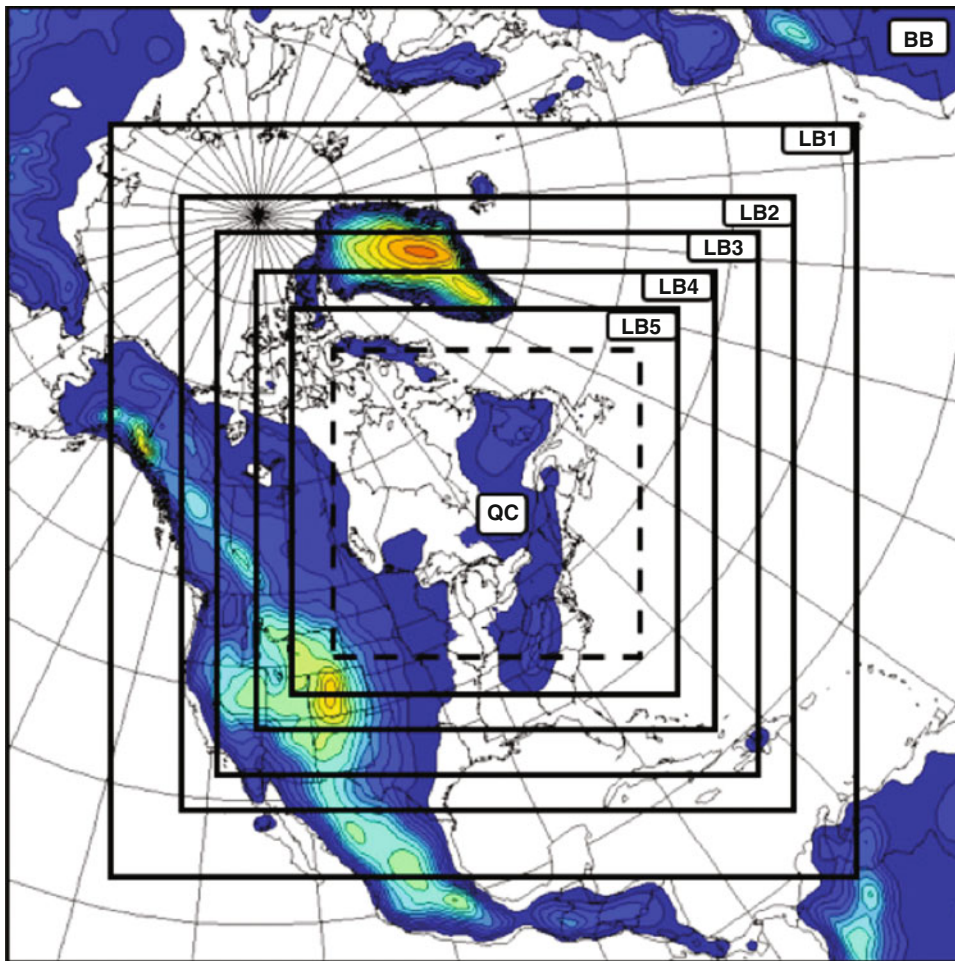


Fig. 14 Domains of BB and various LB simulations (LB 1–5), and verification domain (QC) (taken from Kornic (2010) © 2010 Clim Dyn)

Discussion and Conclusions

This chapter summarised the current understanding of its authors relating to the potential and limitations of regional climate modelling, developed through several investigations of the ESCER Centre scientists as well as from other results published in the literature on the subject.

First and above all, dynamical downscaling with RCMs does work, as evidenced by the development of fine scales in high-resolution RCM simulations that are initialised and driven by low-resolution data. These fine scales constitute the main potential added value of an RCM. The full development of the fine scales requires the use of fairly large regional

domains, of the order of 200 by 200 grid points for a resolution jump of an order of magnitude between the driving data and the RCM mesh and for domains located in middle latitudes. Large domains on the other hand result in weak control by LBC, intermittent divergence in phase space, episodic unphysical behaviour in the artificial lateral viscous zones and large internal variability between members in ensemble simulations performed under identical configurations and LBC forcing.

The presence of intermittent internal variability in RCM simulations has received insufficient attention by practitioners of dynamical downscaling. Internal variability has been shown to be function of the flow regime, season, location and size of the domain, and to differ for different variables. With large internal

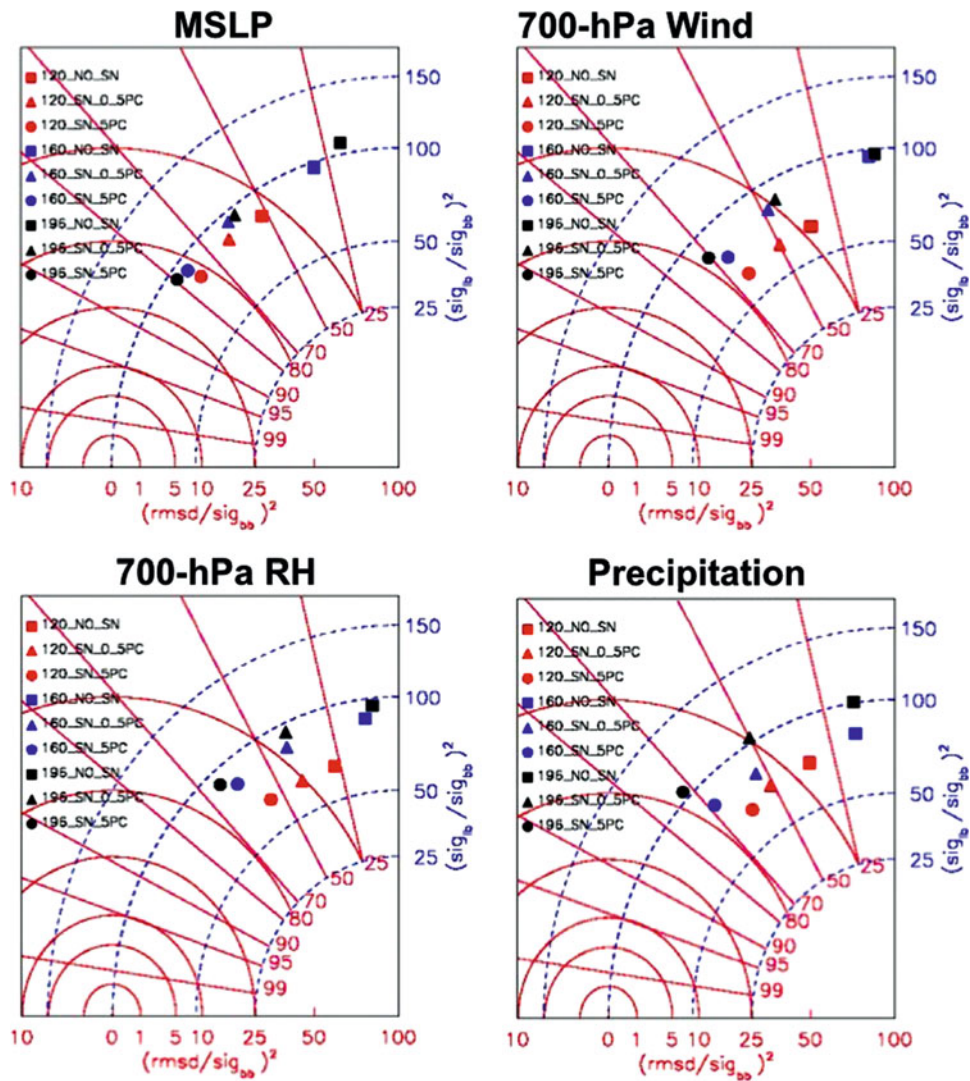


Fig. 15 Taylor diagrams for the small-scale transient eddies of the fields of mean sea level pressure, 700-hPa KE and relative humidity, and precipitation, for LB simulations carried over

three domain sizes and with three SN strengths (adapted from Kornic (2010) © 2010 Clim Dyn)

variability, short experiments performed in the context of process studies are most vulnerable to misinterpretation of differences between simulations performed with different forcings; in such case RCM ensembles may be necessary for proper interpretation of differences. It is worth noting the climate statistics of long climate simulations are also subject to IV, as noted for example by de Elía et al. (2007). On large domains internal variability can reach substantial amplitudes, making harder the statistical significance

tests of differences in simulations, even for time-averaged statistics in long simulations.

In our limited study of the impact of large-scale errors in driving the LBC of RCM, we obtained that large-scale errors are mainly reproduced by RCM, although this conclusion may be the result of the modest domain size employed for this study.

Large-scale spectral nudging can be an effective means of maintaining control by driving fields, independently of domain size. Large-scale nudging is also

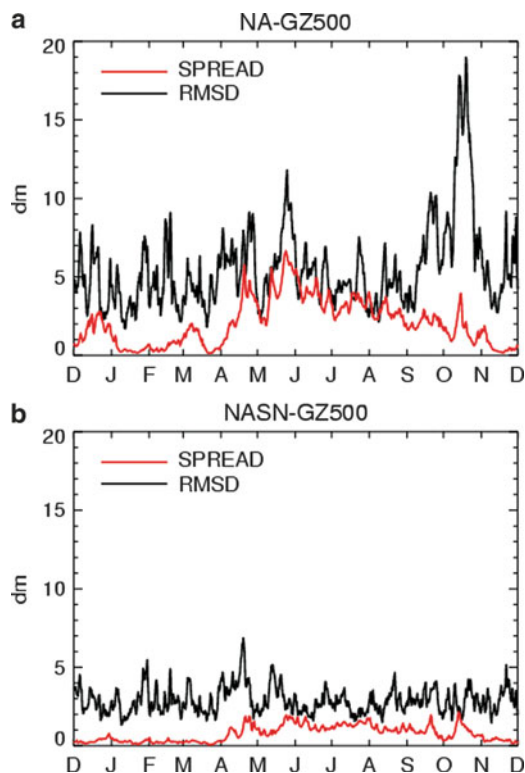


Fig. 16 Time evolution of the square-root of IV variance (curves labelled “spread”) and root-mean square deviation of the CRCM simulations from the ERA40 driving reanalyses (curves labelled “bias”), in two 10-member ensembles of 1-year simulations: one simulation was without SN (NA) and the other (NASN) used a linear profile of SN strength above the 500-hPa level (from the study of Šeparović et al. 2008)

very effective in decreasing internal variability in RCM simulations, although the potential side effects of SN (e.g. Alexandru et al. 2009) deserve further investigation.

Acknowledgements The authors benefited greatly from constructive comments made by Dr Hans von Storch on an earlier paper (Laprise et al. 2008) that discussed related issues. This research was achieved as part of the scientific research programmes of the Canadian Regional Climate Modelling and Diagnostics Network (CRCMD; <http://www.mrcc.uqam.ca/>)—funded by the Canadian Foundation for Climate and Atmospheric Sciences (CFCAS; <http://www.cfcas.org/>) and the Ouranos Consortium on Regional Climatology and Adaptation to Climate Change (<http://www.ouranos.ca/>), as well as the Canadian Climate Variability Network (CLIVAR)—funded by CFCAS and the Natural Sciences and Engineering Research Council of Canada (NSERC; <http://www.nserc-crsng.gc.ca/>). The authors thank Georges Huard, Mourad Labassi, Abderrahim Khaled and Nadjet Labassi for maintaining an efficient and user-friendly local computing facility.

References

- Alexandru A, de Elía R, Laprise R (2007) Internal variability in regional climate downscaling at the seasonal time scale. *Mon Weather Rev* 135(9):3221–3238
- Alexandru A, de Elía R, Laprise R, Šeparović L, Biner S (2009) Influence of large-scale nudging on ensemble simulations with a regional climate model. *Mon Weather Rev* 137(5): 1668–1688
- Annamalai H, Slingo JM, Sperber KR, Hodges K (1999) The mean evolution and variability of the Asian summer monsoon: comparison of ECMWF and NCEP-NCAR reanalyses. *Mon Weather Rev* 127(6):1157–1186
- Anthes RA, Kuo Y-H, Benjamin SG, Li Y-F (1982) The evolution of the mesoscale environment of severe local storms: preliminary modeling results. *Mon Weather Rev* 110:1187–1213
- Anthes RA, Kuo Y-H, Hsie E-Y, Low-Nam S, Bettge TW (1989) Estimation of skill and uncertainty in regional numerical models. *Quart J R Meteorol Soc* 115:763–806
- Antic S, Laprise R, Denis B, de Elía R (2005) Testing the downscaling ability of a one-way nested regional climate model in regions of complex topography. *Clim Dyn* 23:473–493
- Barring L, Laprise R (eds) (2005) High-resolution climate modelling: assessment, added value and applications. Extended abstracts of a WMO/WCRP-sponsored regional-scale climate modelling Workshop, 29 Mar–2 Apr 2004, Lund, Sweden. Lund University electronic reports in physical geography, 132pp. (<http://www.nateko.lu.se/ELibrary/Lerpg5/Lerpg5Article.pdf>)
- Biner S, Caya D, Laprise R, Spacek L (2000) Nesting of RCMs by imposing large scales. In: Research activities in atmospheric and oceanic modelling, WMO/TD – No. 987, Report No. 30, 7.3–7.4
- Bresson R, Laprise R (2009) Scale-decomposed atmospheric water budget over North America as simulated by the Canadian regional climate model for current and future climates. *Clim Dyn* 1–20. doi:10.1007/s00382-009-0695-4
- Castro CL, Pielke RA Sr, Leoncini G (2005) Dynamical downscaling: an assessment of value added using a regional climate model. *J Geophys Res (Atmospheres)* 110:05108. doi:10.1029/2004JD004721
- Caya D, Biner S (2004) Internal variability of RCM simulations over an annual cycle. *Clim Dyn* 22(1):33–46
- Caya D, Laprise R (1999) A semi-Lagrangian semi-implicit regional climate model: the Canadian RCM. *Mon Weather Rev* 127(3):341–362
- Christensen OB, Gaertner MA, Prego JA, Polcher J (2001) Internal variability of regional climate models. *Clim Dyn* 17:875–887
- Cocke S, LaRow TE (2000) Seasonal predictions using a regional spectral model embedded within a coupled ocean-atmosphere model. *Mon Weather Rev* 128:689–708
- Davies HC (1976) A lateral boundary formulation for multi-level prediction models. *Quart J R Meteorol Soc* 102: 405–418
- de Elía R, Laprise R (2003) Distribution-oriented verification of limited-area models forecast in a perfect-model framework. *Mon Weather Rev* 131:2492–2509

- de Elía R, Laprise R, Denis B (2002) Forecasting skill limits of nested, limited-area models: a perfect-model approach. *Mon Weather Rev* 130:2006–2023
- de Elía R, Plummer D, Caya D, Frigon A, Côté H, Giguère M, Paquin D, Biner S, Harvey R (2007) Evaluation of uncertainties in the CRCM-simulated North American climate. *Clim Dyn*. doi:10.1007/s00382-007-0288-z
- Denis B, Côté J, Laprise R (2002a) Spectral decomposition of two-dimensional atmospheric fields on limited-area domains using discrete cosine transforms (DFT). *Mon Weather Rev* 130(7):1812–1829
- Denis B, Laprise R, Caya D, Côté J (2002b) Downscaling ability of one-way-nested regional climate models: the Big-Brother experiment. *Clim Dyn* 18:627–646
- Denis B, Laprise R, Caya D (2003) Sensitivity of a regional climate model to the spatial resolution and temporal updating frequency of the lateral boundary conditions. *Clim Dyn* 20:107–126
- Déqué M, Rowell DP, Lüthi D, Giorgi F, Christensen JH, Rockel B, Jacob D, Kjellström E, de Castro M, van den Hurk B (2006) An intercomparison of regional climate simulations for Europe: assessing uncertainties in model projections. *Clim Chang* 81(1):53–70. doi:10.1007/s10584-006-9228-x
- Di Luca A, de Elía R, Laprise R (2011) Potential for added value in precipitation simulated by high-resolution nested Regional Climate Models and observations. *Clim Dyn* doi: 10.1007/s00382-011-1068-3
- Diaconescu EP, Laprise R, Sushama L (2007) The impact of lateral boundary data errors on the simulated climate of a nested regional climate model. *Clim Dyn* 28(4):333–350
- Díez E, Primo C, García-Moya JA, Gutiérrez JM, Orfila B (2005) Statistical and dynamical downscaling of precipitation over Spain from DEMETER seasonal forecasts. *Tellus* 57A:409–423
- Dimitrijevic M, Laprise R (2005) Validation of the nesting technique in an RCM and sensitivity tests to the resolution of the lateral boundary conditions during summer. *Clim Dyn* 25:555–580
- Errico RM (1985) Spectra computed from a limited area grid. *Mon Weather Rev* 113:1554–1562
- Fennessy MJ, Shukla J (2000) Seasonal prediction over North America with a regional model nested in a global model. *J Clim* 13:2605–2627
- Feser F (2006) Enhanced detectability of added value in limited area model results separated into different spatial scales. *Mon Weather Rev* 134(8):2180–2190
- Feser F, von Storch H (2006) A spatial two-dimensional discrete filter for limited area model evaluation purposes. *Mon Weather Rev* 133(6):1774–1786
- Feser F, von Storch H (2008) A dynamical downscaling case study for typhoons in SE Asia using a regional climate model. *Mon Weather Rev* 136:1806–1815
- Feser F, von Storch H, Winterfeldt J, Zahn M (2009) Added value of limited area model results, 2pp. In: 2nd international Lund RCM conference “21st Century Challenges in Regional-scale Climate Modelling”, 4–8 May 2009, Lund, Sweden, pp 43–44. (http://www.baltex-research.eu/RCM2009/Material/RCM2009_Proceedings_print.pdf)
- Giorgi F, Bi X (2000) A study of internal variability of a regional climate model. *J Geophys Res* 105:29503–29521
- Herceg D, Sobel AH, Sun L, Zebiak SE (2006) The big brother experiment and seasonal predictability in the NCEP regional spectral model. *Clim Dyn* 26(4):1–14. doi:10.1007/s00382-006-0130-z. <http://dx.doi.org/10.1007/s00382-006-0130-z>
- Ji YM, Vernekar AD (1997) Simulation of the Asian summer monsoons of 1987 and 1988 with a regional model nested in a global GCM. *J Clim* 10:1965–1979
- Jones RG, Murphy JM, Noguer M (1995) Simulation of climate change over Europe using a nested regional-climate model. I: assessment of control climate, including sensitivity to location of lateral boundaries. *Quart J R Meteorol Soc* 121:1413–1449
- Jones RG, Murphy JM, Noguer M, Keen AB (1997) Simulation of climate change over Europe using a nested regional climate model. II: comparison of driving and regional model responses to a doubling of carbon dioxide. *Quart J R Meteorol Soc* 123:265–292
- Juang H-MH, Hong S-Y (2001) Sensitivity of the NCEP regional spectral model to domain size and nesting strategy. *Mon Weather Rev* 129:2904–2922
- Kanamitsu H, Kanamitsu M (2007) Scale-selective bias correction in a downscaling of global analysis using a regional model. *Mon Weather Rev* 135:334–350
- Kornic D (2010) Sensibilité des simulations du modèle régional du climat à la taille du domaine et à la technique de pilotage. M.Sc. Dissertation in Atmospheric Sciences. Department of Earth and Atmospheric Sciences, UQAM
- Kuo H-C, Williams RT (1992) Boundary effects in regional spectral models. *Mon Weather Rev* 120:2986–2992
- Kuo H-C, Williams RT (1998) Scale-dependent accuracy in regional spectral models. *Mon Weather Rev* 126:2640–2647
- Laprise R (2007) Regional climate modelling. *J Comput Phys* 227:3641–3666, Special issue on “Predicting weather, climate and extreme events”
- Laprise R, Caya D, Giguère M, Bergeron G, Côté H, Blanchet J-P, Boer GJ, McFarlane NA (1998) Climate and climate change in Western Canada as simulated by the Canadian regional climate model. *Atmos Ocean XXXVI*(2):119–167
- Laprise R, Jones R, Kirtman B, von Storch H, Wergen W (2002) Atmospheric regional climate models (RCMs): a multiple purpose tool? In: Report of the “Joint WGNE/WGCM ad hoc Panel on Regional Climate Modelling”, 19pp. (available from the corresponding author)
- Laprise R, Caya D, Frigon A, Paquin D (2003) Current and perturbed climate as simulated by the second-generation Canadian Regional Climate Model (CRCM-II) over north-western North America. *Clim Dyn* 21:405–421
- Laprise R, de Elía R, Caya D, Biner S, Lucas-Picher Ph, Diaconescu EP, Leduc M, Alexandru A, Šeparović L (2008) Challenging some tenets of regional climate modelling. *Meteorol Atmos Phys* 100:3–22. doi:10.1007/s00703-008-0292-9, Special Issue on Regional Climate Studies
- Leduc M, Laprise R (2009) Regional climate model sensitivity to domain size. *Clim Dyn* 32(6):833–854. doi:10.1007/s00382-008-0400-z
- Leduc M, Laprise R, Moretti-Poisson M, Morin J-Ph (2011) Sensitivity to domain size of Regional Climate Model simulations in middle latitudes for summer. *Clim Dyn* 37(1-2), 343–356. doi:10.1007/s00382-011-1008-2
- Lucas-Picher Ph, Caya D, de Elía R, Laprise R (2008a) Investigation of regional climate models’ internal variability with

- a ten-member ensemble of ten-year simulations over a large domain. *Clim Dyn* 31:927–940. doi:[10.1007/s00382-008-0384-8](https://doi.org/10.1007/s00382-008-0384-8)
- Lucas-Picher Ph, Caya D, Biner S, Laprise R (2008b) Quantification of the lateral boundary forcing in a regional climate model using an ageing tracer. *Mon Weather Rev* 136:4980–4996. doi:[10.1175/2008MWR2448.1](https://doi.org/10.1175/2008MWR2448.1)
- McGregor JL (1997) Regional climate modelling. *Meteorol Atmos Phys* 63:105–117
- Mesinger F, Brill K, Chuang H, DiMego G, Rogers E (2002) Limited area predictability: can upscaling also take place? In: *Research activities in atmospheric and oceanic modelling, Report No. 32, WMO/TD – No. 1105, 5.30–5.31*
- Miguez-Macho G, Stenchikov GL, Robock A (2004) Spectral nudging to eliminate the effects of domain position and geometry in regional climate model simulations. *J Geophys Res* 109(D13):D13104. doi:[10.1029/2003JD004495](https://doi.org/10.1029/2003JD004495)
- Miyakoda K, Rosati A (1977) One-way nested grid models: the interface conditions and the numerical accuracy. *Mon Weather Rev* 105:1092–1107
- Nikiéma O, Laprise R (2011) Diagnostic budget study of the internal variability in ensemble simulations of the Canadian Regional Climate Model. *Clim Dyn* 36(11), 2313–2337, doi:[10.1007/s00382-010-0834-y](https://doi.org/10.1007/s00382-010-0834-y)
- Nutter P, Stensrud D, Xue M (2004) Effects of coarsely resolved and temporally interpolated lateral boundary conditions on the dispersion of limited-area ensemble forecasts. *Mon Weather Rev* 132(10):2358–2377
- Oliger J, Sundström A (1978) Theoretical and practical aspects of some initial boundary value problems in fluid dynamics. *SIAM J Appl Math* 35:419–446
- Plummer DA, Caya D, Frigon A, Côté H, Giguère M, Paquin D, Biner S (2006) Climate and climate change over north America as simulated by the Canadian RCM. *J Clim* 19:3112–3132
- Rapačić M, Leduc M, Laprise R (2011) Evaluation of internal variability and estimation of the downscaling ability of the Canadian RCM for different domain sizes over the North Atlantic region using the Big-Brother Experimental approach. *Clim Dyn* 36(9–10), 1979–2001, doi:[10.1007/s00382-010-0845-8](https://doi.org/10.1007/s00382-010-0845-8)
- Riette S, Caya D (2002) Sensitivity of short simulations to the various parameters in the new CRCM spectral nudging. In: Ritchie (eds) *Research activities in atmospheric and oceanic modelling, WMO/TD – No 1105, Report No. 32, 7.39–7.40*
- Rinke A, Dethloff K (2000) On the sensitivity of a regional Arctic climate model to initial and boundary conditions. *Clim Res* 14(2):101–113
- Rinke A, Marbaix P, Dethloff K (2004) Internal variability in Arctic regional climate simulations: case study for the SHEBA year. *Clim Res* 27:197–209
- Robert A, Yakimiw E (1986) Identification and elimination of an inflow boundary computational solution in limited area model integration. *Atmos Ocean* 24:369–385
- Rockel B, Castro CL, Pielke RA Sr, von Storch H, Leoncini G (2008) Dynamical downscaling: assessment of model system dependent retained and added variability for two different regional climate models. *J Geophys Res Atmospheres* 113: D21107. doi:[10.1029/2007JD009461](https://doi.org/10.1029/2007JD009461)
- Segami A, Kurihara K, Nakamura H, Ueno M, Takano I, Tatsumi Y (1989) Operational mesoscale weather prediction with Japan spectral model. *J Meteorol Soc Jpn* 67:907–923
- Šeparović L, de Elía R, Laprise R (2008) Reproducible and irreproducible components in ensemble simulations of a regional climate model. *Clim Dyn* 136(12):4942–4961. doi:[10.1175/2008MWR2393.1](https://doi.org/10.1175/2008MWR2393.1)
- Staniforth A (1997) Regional modeling: a theoretical discussion. *Meteorol Atmos Phys* 63:15–29
- Tatsumi Y (1986) A spectral limited-area model with time dependent lateral boundary conditions and its application to a multi-level primitive equation model. *J Meteor Soc Jpn* 64:637–663
- Thatcher M, McGregor JL (2009) Using a scale-selective filter for dynamical downscaling with the conformal cubic atmospheric model. *Mon Weather Rev* 137:1742–1752
- Vanvyve E, Hall N, Messenger C, Leroux S, van Ypersele J-P (2007) Internal variability in a regional model over West Africa. *Clim Dyn* 30(2–3):191–202. doi:[10.1007/s00382-007-0281-6](https://doi.org/10.1007/s00382-007-0281-6)
- von Storch H (2005) Conceptual basis and applications of regional climate modeling, pp 26–27. In: Barring L, Laprise R (eds) *Extended abstracts “High-resolution climate modelling: Assessment, added value and applications”*. WMO/WCRP-sponsored regional-scale climate modelling Workshop, 29 Mar–2 Apr 2004, Lund, Sweden. Lund University electronic reports in physical geography, 132pp. (<http://www.nateko.lu.se/ELibrary/Lerpg/5/Lerpg5Article.pdf>)
- von Storch H, Zorita E, Cubasch U (1993) Downscaling of global climate change estimates to regional scales: an application to Iberian rainfall in wintertime. *J Clim* 6:1161–1171
- von Storch H, Langenberg H, Feser F (2000) A spectral nudging technique for dynamical downscaling purposes. *Mon Weather Rev* 128:3664–3673
- Wang Y, Leung LR, McGregor JL, Lee D-K, Wang W-C, Ding Y, Kimura F (2004) Regional climate modelling: progress, challenges, and prospects. *J Meteorol Soc Jpn* 82(6): 1599–1628
- Warner TT, Peterson RA, Treadon RE (1997) A tutorial on lateral conditions as a basic and potentially serious limitation to regional numerical weather prediction. *Bull Am Meteorol Soc* 78(11):2599–2617
- Weisse R, Feser F (2003) Evaluation of a method to reduce uncertainty in wind hindcasts performed with regional atmosphere models. *Coast Eng* 48(4):211–225
- Weisse R, Heyen H, von Storch H (2000) Sensitivity of a regional atmospheric model to a sea state-dependent roughness and the need for ensemble calculations. *Mon Weather Rev* 128(10):3631–3642
- Weisse R, von Storch H, Callies U, Chrastansky A, Feser F, Grabemann I, Guenther H, Pluess A, Stoye T, Tellkamp J, Winterfeldt J, Woth K (2009) Regional meteorological-marine reanalyses and climate change projections: results for Northern Europe and potentials for coastal and offshore applications. *Bull Am Meteorol Soc* 90:849–860
- Wu W, Lynch AH, Rivers A (2005) Estimating the uncertainty in a regional climate model related to initial and lateral boundary conditions. *J Clim* 18(7):917–933
- Wyser K, Jones CG, Du P, Girard E, Willén U, Cassano J, Christensen JH, Curry JA, Dethloff K, Haugen J-E, Jacob

- D, Køltzow M, Laprise R, Lynch A, Pfeifer S, Rinke A, Serreze M, Shaw MJ, Tjernström M, Zagar M (2008) An evaluation of Arctic cloud and radiation processes during the SHEBA year: simulation results from 8 Arctic regional climate models. *Clim Dyn* 30(2–3):203–223. doi:[10.1007/s00382-007-0286-1](https://doi.org/10.1007/s00382-007-0286-1)
- Yakimiw E, Robert A (1990) Validation experiments for a nested grid-point regional forecast model. *Atmos Ocean* 28:466–472
- Zahn M, von Storch H, Bakan S (2008) Climate mode simulation of North Atlantic Polar Lows in a limited area model. *Tellus A* 60:620–631. doi:[10.1111/j.1600-0870.2008.00330.x](https://doi.org/10.1111/j.1600-0870.2008.00330.x)

Value Added in Regional Climate Modeling: Should One Aim to Improve on the Large Scales as Well?

Fedor Mesinger, Katarina Veljovic, Michael J. Fennessy,
and Eric L. Altshuler

Abstract

Expectations various regional climate modelers have expressed as to the impact on large scales are recalled. While some authors do mention the possibility of improvement also at large scales (e.g., Giorgi, *J Phys IV France* 139:101–118, 2006), the majority clearly accepts the view of “downscaling” as an effort in which the driver global model large scales are hoped to be preserved as much as possible and only small scales improved compared to those of the driver model. Many authors find it even desirable to use the so-called “large-scale nudging” in order to help achieve this objective. Mesinger et al. (Limited area predictability: can “upscaling” also take place? Research activities in atmospheric and oceanic modeling, WMO, Geneva, CAS/JSC WGNE Rep. No. 32, 5.30-5.31, 2002; see also Mesinger, *The Eta model: design, history, performance, what lessons have we learned?* In: Symposium on the 50th anniversary of operational numerical weather prediction, University of Maryland, College Park, MD, 14–17 June 2004, Preprints CD-ROM, 20pp, 2004) have however argued that various NWP results of the Eta model at NCEP strongly suggest that improvements in the large scales of the global driver model have been taking place more often than not. In addition, there was a four-month nine-member ensemble result of Fennessy and Altshuler in the early 2000s, published recently (Veljovic et al. *Meteorol Z* 19:237–246, 2010), in which an RCM achieved a dramatic improvement over its driver AGCM in hindcasting the precipitation difference over the central United States between the “flood year” of 1993 and the “drought year” of 1988; which we do not believe could have been possible without a significant improvement in the large scales. If this indeed is so and could be generalized, then large-scale nudging would not only be unnecessary but may also be harmful to the result. It could however be that this holds for some models while not for others. In that case, why so is a question of obvious importance. Given however that claims have even been made that improvements in large scales in regional climate modeling may be impossible for *any* models, hard evidence of specific large-scale improvements achieved are desirable. The preceding and additional points are discussed as well as more detail

F. Mesinger (✉)
Serbian Academy of Sciences and Arts, Belgrade, Serbia
e-mail: fedor@essic.umd.edu

given, summarizing the results of perhaps the first comprehensive direct tests of the issue (Veljovic et al. *Meteorol Z* 19:237–246, 2010). Additional results are shown regarding the impact of the choice of the lateral boundary conditions (LBC) scheme, pointing to the advantage of the Eta (Mesinger, *Contrib Atmos Phys* 50:200–210, 1977) over the conventional and costlier relaxation scheme. As to the large scales question posed, the results summarized show that driving the Eta by ECMWF 32-day ensemble members the driver model large scales tended to be improved more often than not, giving support for our tenet that improving large scales as well in RCM efforts is possible. We furthermore argue that pursuing this objective should be beneficial for the improvement in smaller scales as well.

Introduction

The dominant mode of regional climate modeling consists of running a one-way nested regional climate model (RCM) driven by lateral boundary conditions provided by a global climate model (GCM). The prevailing philosophy is that the RCM is not supposed to change the larger scales of the driver GCM but should add regional detail in view to its higher resolution, enabling, e.g., more detailed topography and surface boundary condition. A number of review papers are available in which these and related points are discussed in more detail (e.g., McGregor 1997; Giorgi 2006; Laprise et al. 2008).

The issue we are addressing of the RCM impact on larger scales is obviously closely related to the domain size used. Thus, in line with the prevailing philosophy pointed out above, Jones et al. (1995) conclude “that the RCM domain should be sufficiently small that the synoptic circulation does not depart far from that of the driving GCM” (quotation from McGregor 1997). Giorgi (2006) on the other hand does point out a possibility of “a partial improvement of the simulation also at the large scale,” referring for more detail to Giorgi et al. (1998). But if the intention is to improve also on the larger scales, clearly a larger domain is needed so that larger scales can be accommodated, contrary to the prescription of Jones et al. (1995). The larger the domain however, the more opportunity there is for the chaotic nature of the atmospheric dynamics to have an impact on the result (e.g., Vannitsem and Chomé 2005). As a result, with a larger domain, RCM generated small scales will not be uniquely defined for a given set of lateral boundary conditions (LBCs); instead, there will be noticeable “internal

variability” in the terminology used by Laprise et al. (2008). What we wish to stress here is that an ability to achieve even a small but systematic improvement in the large scales, may well be expected to be associated with a significant improvement in the small scales.

Can this be done? It has been repeatedly argued by the first of the authors (e.g., Mesinger et al. 2002) that in the regional weather forecasting at NCEP using the Eta model strong indications were seen that the Eta model benefited from its very large domain, and that this can only be explained by its improving on the large scales compared to those of the driver global model. Following in the footsteps of this experience, also in the regional climate use of the Eta large domains tended to be used (e.g., Mitchell et al. 2001; Altshuler et al. 2002; Katsafados et al. 2005; Chou et al. 2005; 2011, and references therein). Of these various regional climate results possibly the most convincing in terms of our current interest is that of Fennessy and Altshuler, now included in Veljovic et al. (2010; V2010 further on). This is a nine ensemble members experiment discussed previously in Mitchell et al. (2001) at the time when only three members were available.

The nine-member result is shown in Fig. 1. In the figure, the observed June–August mean 1993 minus 1988 CMAP precipitation difference (Xie and Arkin 1996) is shown in the middle panel. Recall that 1993 was a year with considerable flooding in the upper Mississippi–lower Missouri area (e.g., Junker et al. 1999), while 1988 was a year with a prominent drought over the central US region. The nine-member 1993 minus 1988 ensemble mean precipitation differences for the COLA AGCM and the nested Eta

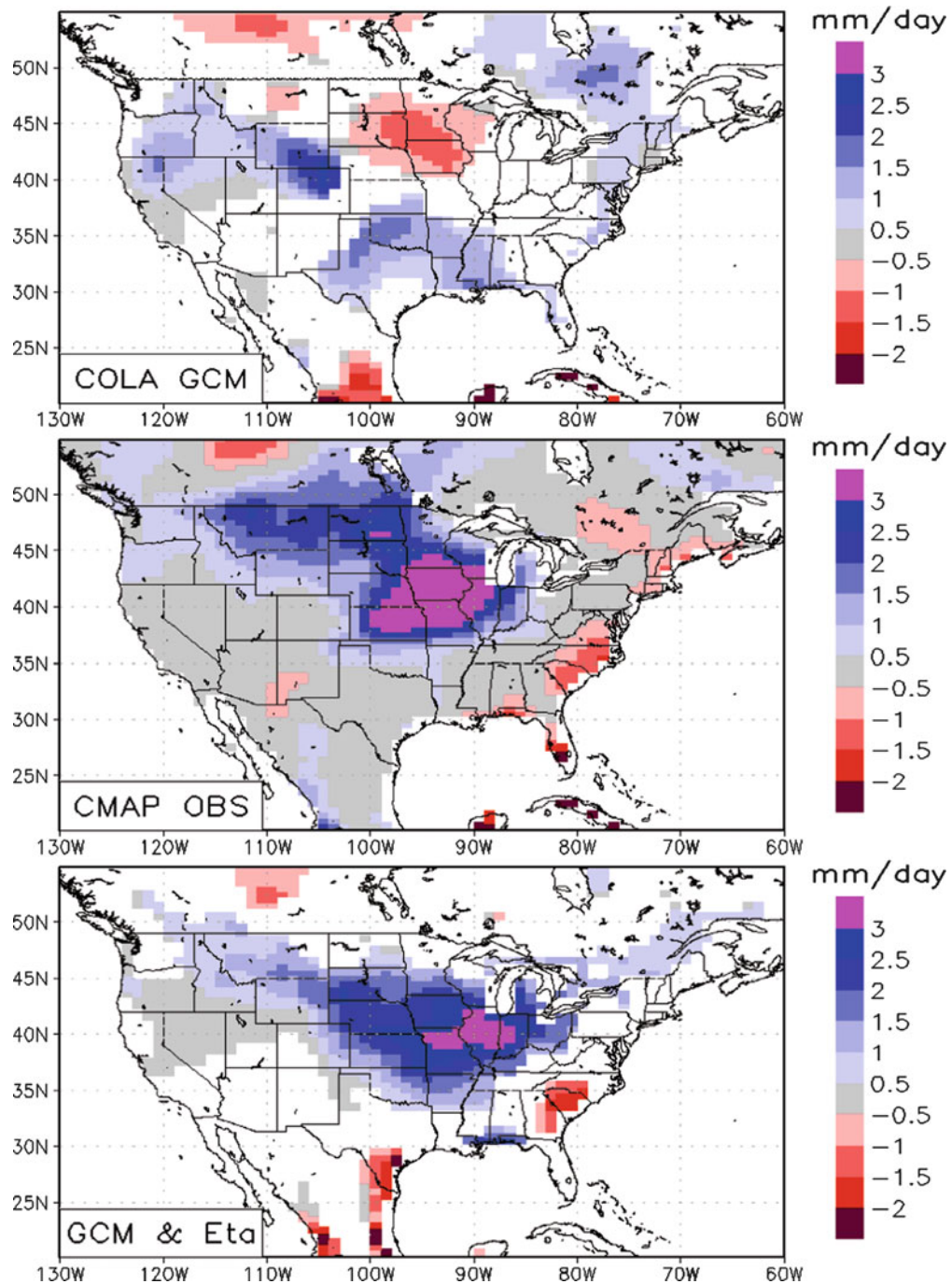


Fig. 1 June–July–August mean 1993 minus 1988 precipitation difference for (*top*) COLA AGCM 9-member ensemble, (*middle*) CMAP observations, (*bottom*) nested Eta model 9-member ensemble. Only differences significant at the 95% level are shaded (From Veljovic et al. 2010 © by Gebrüder Borntraeger 2010)

model are shown in the upper and the lower panel of the figure, respectively. Only differences significant at the 95% level are shaded.

The COLA AGCM used for the two ensemble results shown was the so-called V1.4, run at R40 horizontal resolution with a 1.8° latitude by 2.8° longitude

Gaussian grid on which the physical calculations were done. There were 18 unevenly spaced sigma levels in the vertical. The land surface model was the simplified version of the Simple Biosphere Model. The convection parameterization was the relaxed Arakawa–Schubert. Reference Fennessy and Shukla (2000) contains more model details and references. The nine different model initial conditions were initialized 12 h apart in late May of 1988 and 1993 from NCEP analyses. The Eta model was one-way nested from AGCM output that was every 12-h linearly interpolated in time. Again, referring to the Fennessy and Shukla (2000) would cover most of these and other details, save there it was only three members for 1988 and three members for 1993. There was no spin-up period in either case. The soil wetness used to initialize the AGCM was derived from operational ECMWF analysis–forecast cycle soil moisture. The Eta soil wetness was also observationally based, but from NCEP reanalysis soil wetness. Both models utilize the same time-varying observed weekly SST (Reynolds and Smith 1994). Otherwise, the AGCM receives no additional input after initialization, and the nested Eta model receives only the lateral boundary conditions from the AGCM.

Prominent in the observations is a broad 1 mm day^{-1} positive precipitation difference that spans much of the central United States and reaches over 4 mm day^{-1} over the upper Mississippi basin. The AGCM does not predict this signal at all, but rather has weaker positive differences both westward and southward of the observed positive difference. The nested model does a far better job of predicting the broad 1 mm day^{-1} difference, though it extends it a bit too far southward and eastward. The nested model also properly places the center of the large difference over the corn belt with a maxima of over 3 mm day^{-1} , which is somewhat less than observed, but a drastic improvement over the AGCM simulation.

We find this result hardly obtainable without an improvement in the large scales. While persistent heavy rains of 1993 were presumably a result of predominantly convective activities over the central United States, to set up convection favoring situations requires a realistic interaction between the moisture supplying low-level jet from the Gulf and the jet stream dominated upper-level flow over the Rockies. This had to be inadequately handled by the GCM to generate a result in such disagreement with the observations as that of the upper panel of Fig. 1.

While this argument might be convincing it is only an argument and not a numerically supported result. An improvement in the largest scales within the RCM, this time MM5, can also be claimed for the wintertime simulation shown in Gustafson and Leung's (2007) Fig. 4, compared to those of the driver GCM in their Fig. 5; and, in addition to Giorgi et al. (1998), most likely for some of the other simulations also. But for an objective support of a claim of an added value in the largest scales of an RCM clearly direct tests are required. Following V2010, we shall here summarize the design and the results of their direct numerical tests in our sections "Experiment Design" and "Results," respectively. Prior to that in the next section we shall recall some of the reasoning various authors offered in their belief in the need to artificially support RCMs in their generation of large scales, discuss experiment designs used to that end, and offer our own arguments as to what we see as downsides of some of these experiment designs and why in principle we consider artificial interventions in RCM's large scales undesirable.

The Pros and Cons of Large-Scale (Spectral) Nudging

As hinted above the intention to improve not only on the small scales but on the large ones as well is not widespread within the RCM community. Thus, Lo et al. (2008) quote Giorgi (2006) as stating that "The RCM is not intended to modify/correct the large-scale circulation of the AOGCM but is intended to add regional detail in response to regional scale forcing (e.g., topography, coastlines, and land use/land cover) as it interacts with the larger scale atmospheric circulations." As to the possibility of a beneficial impact of RCM on large scales if one were desired, many authors have claimed in a way just the opposite, that large-scale nudging is needed in order to prevent the RCM's large scales from deteriorating compared to those of the driver global fields (e.g., references in Laprise et al. 2008; and quite a few contributions to the discussion posted at <http://cires.colorado.edu/science/groups/pielke/links/Downscale/>).

So how can views that different coexist? As expressed in the present corresponding author's contributions to the above discussion, the design of most of the experiments could be the a major, as follows. Not looking for improvement in large scales of the driver

global fields, in most experiments the authors have used reanalysis-derived LBCs and have been checking how close their RCMs were able to approach the large scales of the reanalysis fields. In some of the studies, the authors have performed a limited domain spectral analysis of the RCM result and the driver fields, which permitted a comparison of, for example, fractional change in spectral power per wavenumber of one of those vs. the other (e.g., Castro et al. 2005; Rockel et al. 2008). In yet others they have looked at the differences between the chosen driver and RCM fields (e.g., Miguez-Macho et al. 2004, 2005). In all of these, and many others, “spectral nudging” was performed in one way or another of RCM larger scales toward those of the global driver fields, in order to reduce the large-scale differences considered.

There is a downside of these types of experiments with verification performed against global driver fields as follows. The purpose of the RCMs is to obtain descriptions over the chosen domain of the actual atmospheric fields such as those predicted in seasonal or decadal forecasts, or longer term climate change projections, *better* than those of the driver GCM. Whether and if so to what degree this is achieved can be tested only if the RCM is driven by the LBCs generated by a GCM, and the verification is performed against real data, or analyses of real data. This of course cannot be done for longer term climate change projections but can be done in hindcast mode for shorter term RCM runs for which we have information on what actually happened, such as in the experiment illustrated in Fig. 1 of the preceding section.

To emphasize this point, we can consider a thought experiment in which we have a perfect RCM, performing as the real atmosphere, and being aware of the actual topography and land surface forcings. We now assume to be driving this perfect RCM with the reanalysis LBCs which although sampled from the real atmosphere are sampled with an error; compared to the real atmosphere they are only approximate. While in a run long enough our perfect RCM will forget its initial condition, it will not forget the approximate LBCs that are constantly fed to it. To quote Ed Lorenz—from a posting on Eugenia Kalnay office’s door at the University of Maryland at College Park—“Chaos: when the initial condition determines the future but approximate initial condition does not approximately

determine the future.” Approximate LBCs will inflict the same kind of behavior on our perfect RCM, the more so the bigger its domain is. Thus, our perfect RCM will fail the test of emulating the reanalysis “truth,” because its “future” will unavoidably be different from the one that was used to sample the LBCs it is driven by. But being perfect, and being aware of the actual topography and land surface forcings neither of which the reanalysis data is, it stands to reason that, in most cases, it should have performed better.

Another concern posted in the discussion referred to addresses the spectral analysis over the RCM’s limited domain typically used for identification of large scales in the experiments done. Perhaps most readers will agree that in extratropics, the position and/or shape of the upper tropospheric jet stream gives the best identification of large scales from the physical point of view. But suppose an RCM produces a jet stream which is somewhat more accurate than that of the global driving reanalysis, being in a slightly better position here and there. Although the jet stream may be the largest scale feature that we want to know about the RCM impact on, the difference in the RCM skill resulting from this improved jet stream position compared to that of the driver fields will likely show primarily as the difference in smaller scales. Thus, it could well be that a direct verification of the skill in placing the largest scale features is a more revealing way to go, and this has therefore been the approach favored in the experiments to be summarized in the following two sections.

Experiment Design

The majority of experiments addressing RCM value-added issues was done using global reanalysis, global analysis, or “Big Brother” (BB, Laprise et al. 2000) driven RCMs, so that by design verifying the possibility of RCM’s improving on the large scales was not possible. Namely, with the fields providing the LBCs being the same as those used for verification, no fields are available compared to which an ability to improve on large scales could be looked for. Somewhat of an exception to this is the use of the “Imperfect Big Brother” design (IBB, Diaconescu et al. 2007), in which just as in the BB design running

an RCM over a large domain synthetic high-resolution data are produced to be used for verification of the RCM nested inside this domain and also, sampled at lower resolution, for the provision of its LBCs; but in contrast to the BB design these LBCs are supplied with errors generated so as to mimic assumed GCM errors RCMs have to absorb in their standard use.

There should be advantages in experimenting with the actual GCM or global forecast and LBC errors, and this is the approach taken in the experiments of V2010 to be summarized here. Experiments were run in which the Eta RCM was driven by ECMWF 32-day ensemble forecast members. The driver ECMWF ensemble at the time used was run out to 15 days at T399 (~50 km)/62 level resolution, and with a reduced horizontal resolution of T255 (~80 km) afterward. It consisted of a control and 50 members. Verification performed was against ECMWF analyses, with the main goal to compare the large-scale skill of the Eta RCM against the skill of its driver ensemble members.

The Eta model used was a version upgraded in a number of ways compared to that used by COLA to achieve the result shown in Fig. 1, and also compared to the latest NCEP operational version. One of those upgrades is the nonhydrostatic option adopted from the WRF-NMM, but in view of the Eta resolution used, on the order of 30 km, the model was run in its hydrostatic mode. Upgrades that were used included the “sloping steps” discretization of the eta coordinate (Mesinger and Jovic 2004) and the piecewise linear/finite volume vertical advection of dynamic variables, using the scheme of Mesinger and Jovic (2002). Given however that verification of results was focused on winds in the upper troposphere, we find it not likely that these upgrades as well as the others made (<http://etamodel.cptec.inpe.br/download.shtml>) had a significant impact on the verification results.

The verification chosen for the intended direct test of the large-scale skill was that of the position accuracy of the strongest forecast winds at the jet stream level, taken as 250 mb. Thus, this is a verification of the type that is customary in precipitation verification. Bias-adjusted equitable threat scores were calculated (Mesinger 2008) and bias scores for wind speeds greater than chosen wind speed thresholds. The motivation for the bias adjustment of the equitable threat scores is the desire to arrive at a measure which would assess the accuracy of the *placement* of the variable verified. Namely, the standard equitable threat score

(ETS) is sensitive to bias, so that, just as with a variety of other verification measures, a better number can be obtained by “hedging,” under- or overforecasting the variable considered (Hamill 1999; Mesinger 2008; Brill 2009; Brill and Mesinger 2009). Bias adjustment is designed to arrive at the ETS value appropriate to unit bias, and thus have the position accuracy remain the only forecast feature affecting the verification value.

For greater confidence, the traditional root-mean-square (rms) difference between the forecast and analyzed 250 mb winds was calculated as well. While this more conventional verification measure is not as focused as the adjusted ETS, it should still mostly reflect the accuracy of stronger wind speeds, as they will of course tend to make the major contribution to a squared difference of the two fields. For both verification measures, biases of the two fields were calculated as well.

While the rms wind difference is an accuracy measure of an obvious physical meaning, an advantage of the adjusted ETS should be noted, in that it shows skill above random, the random skill being equal to the adjusted ETS value of zero. Deducing existence of a positive skill from the rms wind difference is of course not straightforward.

For an illustration of the domain used, and wind speeds over this domain at a specific time, in Fig. 2 ECMWF wind speed analysis is shown over the Eta domain used, at the final time of the 32-day experiments, 0000 UTC 2 February 2009. In its upper panel, wind arrows are plotted at every 9th grid point of the Eta. In its lower panel, wind speed contours are shown at 10 ms^{-1} intervals, labeled in ms^{-1} . Several possibilities were considered as to what value of wind speed to choose for the definition of the location of the jet stream. The value of 45 ms^{-1} was eventually chosen. At the initial time of the experiment, 0000 UTC 1 January 2009, wind speeds of over of 45 ms^{-1} covered about 10% of the domain; this coverage was subsequently generally rising to almost 25% during 18–21 January, dropping then quickly to about 15% and somewhat more until the end of the 32-day period.

The Eta ensemble members were run driven by the control and the first 25 members of the ECMWF ensemble; thus, 26 forecasts were available. They were run at 31 km/45 layer resolution, on the domain just shown, of 108×64 degrees of the model’s

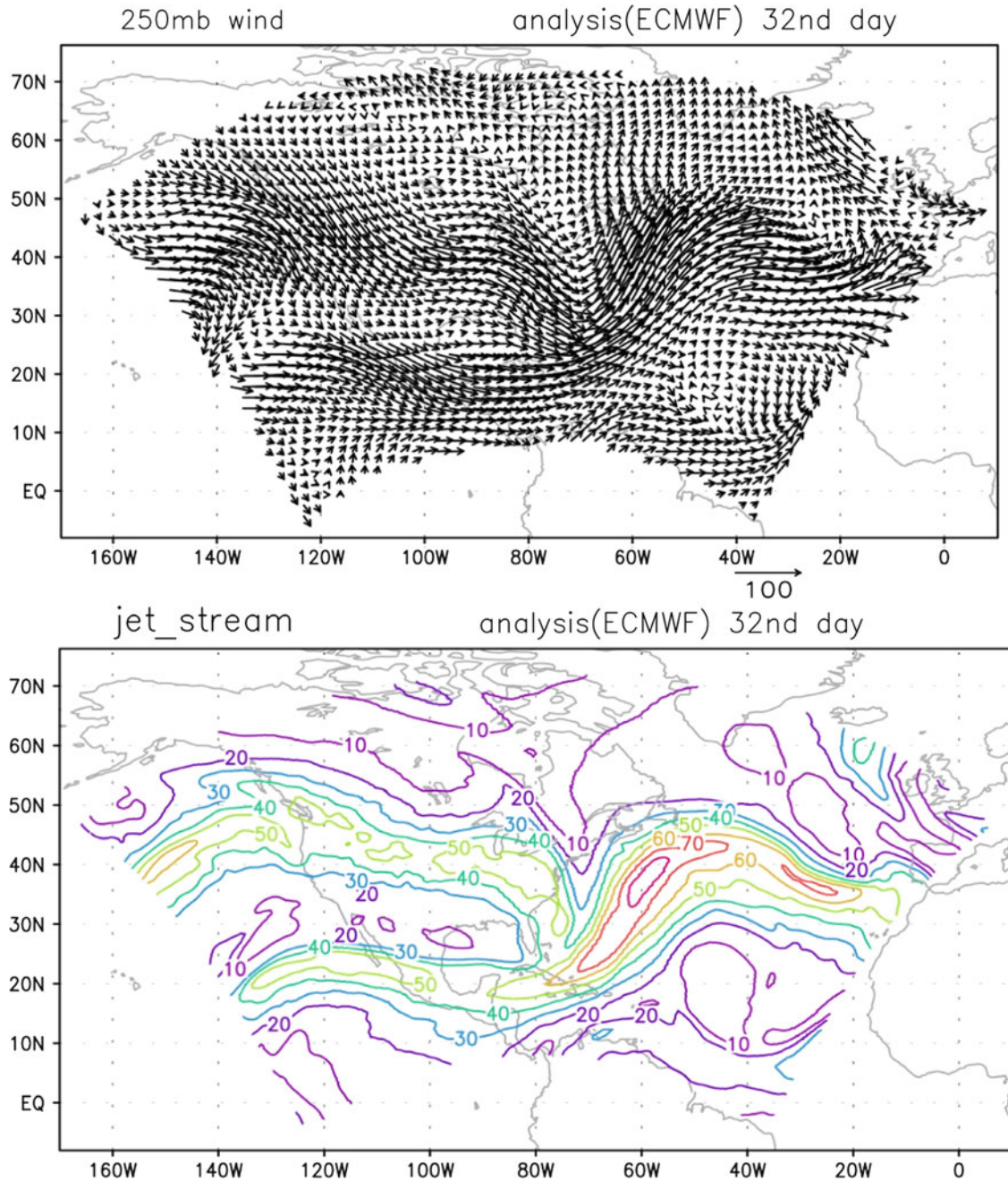


Fig. 2 ECMWF T799 250 hPa wind speed analysis valid at 0000 UTC 2 February 2009, within the domain used for the Eta forecasts made. In the *upper panel*, wind *arrows* are shown at every ninth grid point of the Eta. In the *lower panel*, wind speed *contours* are shown labeled in ms^{-1} , at 10 ms^{-1} contour intervals (From Veljovic et al. 2010 © by Gebrüder Borntraeger 2010)

rotated longitude \times latitude, or $12,000 \times 7,111 \text{ km}$. The domain boundary was hereby defined as running on top of the model's boundary points; in other words, only half of the boundary points cell area was counted

as belonging to the model domain. Note that, inadvertently, in V2010 the north-south domain extent was erroneously given as somewhat greater. Calculated on the model's spherical Earth, this is a domain of

$80.9657 \times 10^6 \text{ km}^2$ area. It resulted from the domain size chosen at 271×321 points, with the I,J indexing as shown in Fig. 16 of Mesinger et al. (1988), and h to v grid point distances of 0.2 degrees. This is a domain slightly smaller than that of the latest NCEP operational Eta, but still considerably greater, by a factor of at least 2 and maybe even 4, than the domains typically used in RCM experiments. It included 86,831 height grid points, and one less wind point, with 429 of these height points being boundary points.

Results

In Fig. 3, upper panel, bias-adjusted ETS scores are shown, ETSa, for the 26 members of the Eta ensemble (blue), along with those of their 26 driver ECMWF ensemble forecasts (red). Note that scores for multiple forecasts as shown here in Fig. 3 are obtained by adding the forecast, F , correctly forecast (“hits”, H), and observed (O) values of all the forecasts for a given lead time; averaging of individual scores would not be appropriate as it is generally understood in precipitation verification (e.g., Hamill and Juras 2006). Bias, area forecast over the area observed, is shown in the lower panel.

In the upper panel of the figure, we can see that after the initial 10-day period of the integration the ETSa of the Eta ensemble for the chosen 45 ms^{-1} category is most of the time slightly better than that of its driver forecasts. One should recall that the ETS score is not credited for random skill so that in contrast to some of the individual forecasts (scores shown in V2010) in the overall ensemble scores both models do exhibit some large-scale skill throughout the 32-day integration period. Not much difference is seen between the two models during the first 12 days of the integration in the bias of their maintaining the area of over 45 ms^{-1} as analyzed, lower panel, but they do fall behind the analysis during the time of the very intense analyzed jet stream around days 18–21, recovering later on.

A similar picture is obtained inspecting the traditional rms difference in 250 mb winds between the Eta ensemble members and the ECMWF analyses, vs. the same difference for the ECMWF ensemble members, shown in the upper panel of Fig. 4. A small advantage of the Eta ensemble is seen throughout days 12–28 of the experiment, with the rms difference values being

just about identical the last 4 days. The advantage of the Eta might be even slightly more visible than in the upper panel of Fig. 3, given that the blue line showing the Eta rms score is slightly below the ECMWF global ensemble red line almost continuously during the period of more than 15 days. The Eta and the ECMWF ensemble forecasts show the same general trend in terms of their biases, Fig. 4, lower panel.

Discussion and Conclusions

While the advantage of the Eta over its driver ECMWF ensemble members seen in Figs. 3 and 4 following the initial about 10 days or so of the flushing out of the initial condition is slight, it may still be found as rather surprising. It is not only that at quite a few places statements were made that a nested RCM cannot retain the value of the large scale, or similar, and therefore needs help via large scale nudging. Recall that, for example, addressing the domain size, we can read about “ineffectiveness of the nesting for controlling the large scales” (Denis et al. 2002); and that to avoid dependence of the results on domain position, nudging of the large scales “is necessary for all downscaling studies. . .with domain sizes of a few thousand kilometers and larger” (Miguez-Macho et al. 2004); or that, for a particular case and for driving with a global reanalysis “dynamical downscaling with RAMS in RCM mode does not retain value of the large scale which exists in the larger global reanalysis,” and that this conclusion “is expected to be true for other RCMs as well” (Castro et al. 2005; see also Rockel et al. 2008). The point to note is that in all these cases, and many others, investigators looked at the driver large scales as those to stay close to as much as possible. Given that existence of the LBC errors is undisputable and that atmosphere exhibits a chaotic behavior, this obviously cannot be achieved to perfection; or even near perfection. As pointed out earlier, the greater the domain the larger the difference will necessarily be; and large-scale nudging is then a convenient tool that, used with some care, will reduce the difference.

In contrast, what was looked for in the V2010 experimental setup is whether the nested model can *improve* on the driver global large scales, *in spite* of absorbing its LBC errors. In verification against analysis data, the nested model then has its LBC errors as a

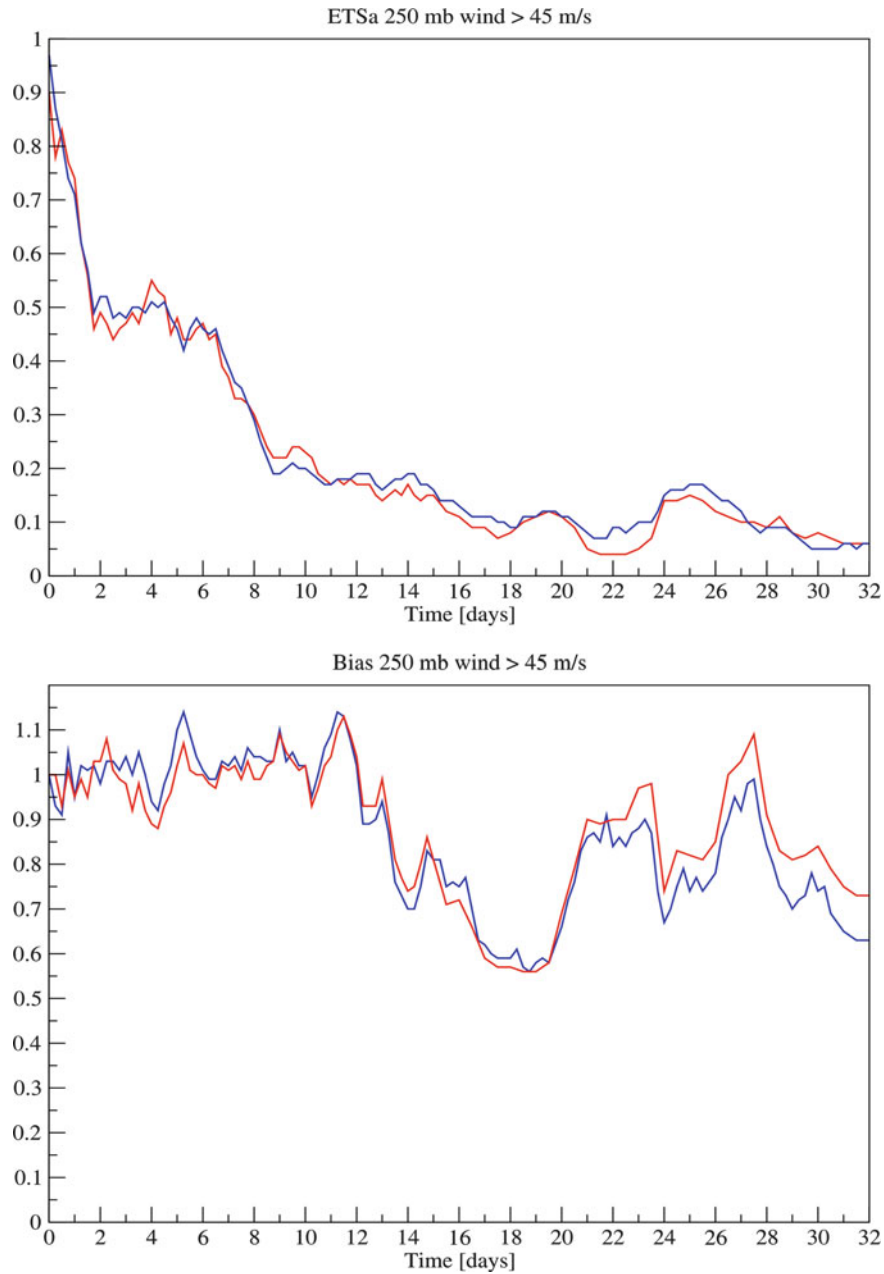


Fig. 3 Bias-adjusted ETS score, *upper panel*, and bias, *lower panel*, of 250 hPa wind speed $\geq 45 \text{ ms}^{-1}$, of the ECMWF global ensemble (control plus 25 members, *red lines*) used for the initial condition and for the LBCs of the 32-day Eta forecasts whose scores are shown in *blue*; verified against ECMWF T799 analyses, as a function of forecast time (days). Initial time is 0000 UTC 1 January 2009

handicap compared to its driver ensemble forecasts. It is the ability demonstrated in the plots of Figs. 3 and 4 of the RCM used to verify better than its driver global forecast more often than not in spite of this handicap that we felt might be found surprising. This because of the fairly popular support for nudging, e.g., the

references above, with additional ones in Laprise et al. (2008, 2012). In cases when an RCM is forecasting the large scales better than its driver model, even to a very modest degree, nudging not only would be unnecessary but should also be detrimental.

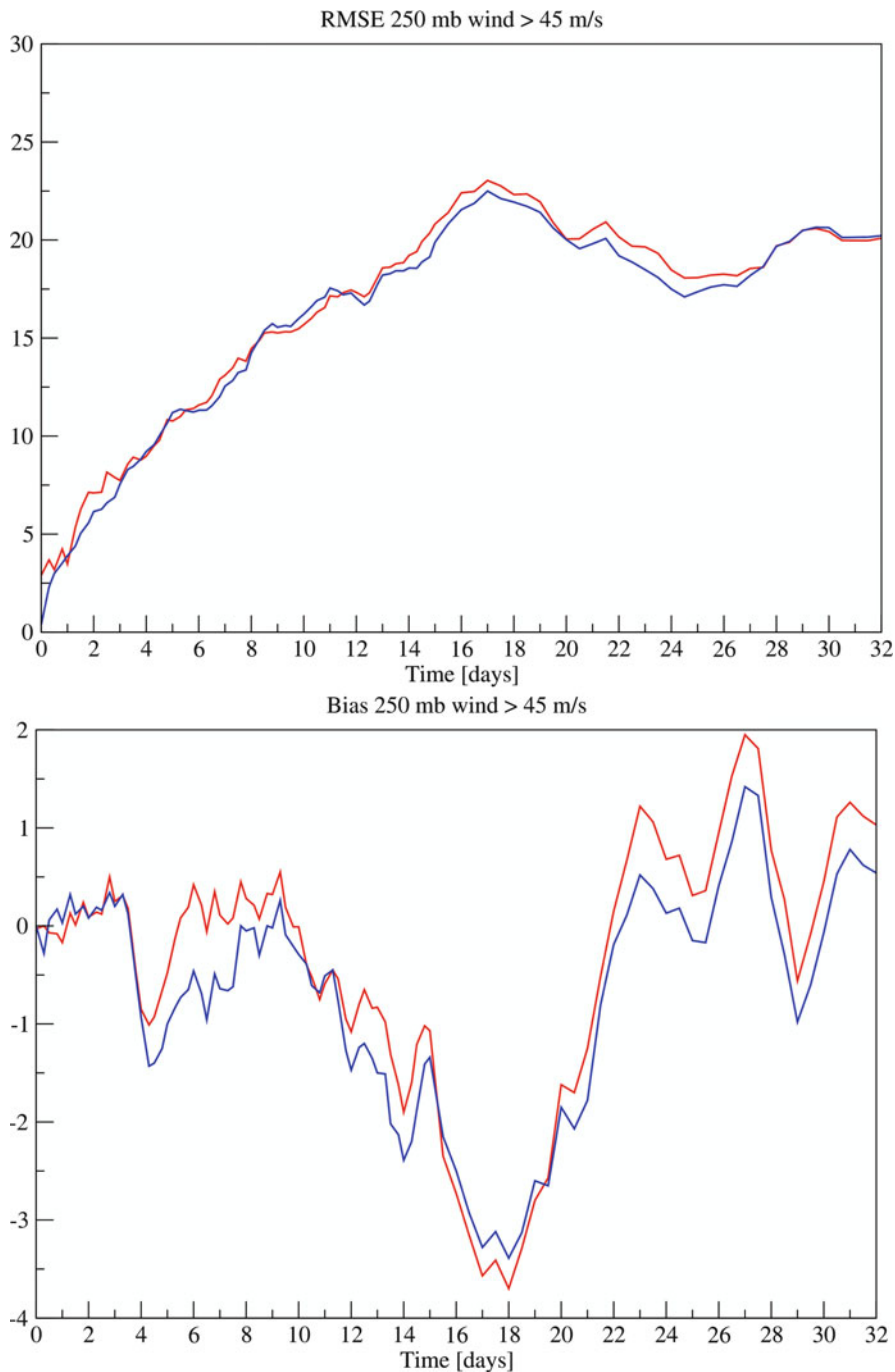


Fig. 4 Same as Fig. 3 except for the verification measures used, RMS forecast minus analysis difference (*upper panel*) and standard bias (*lower panel*) of the 250 hPa wind

Given that we are advocating a conclusion or view that differs from that put forth by some of the other investigators, a question of obvious interest is could it be that a feature or better features of the V2010

experiment and/or model design are responsible for the difference in views arrived at. What might be the first to come to mind is the resolution of the nested model used; yet higher resolution is a standard feature

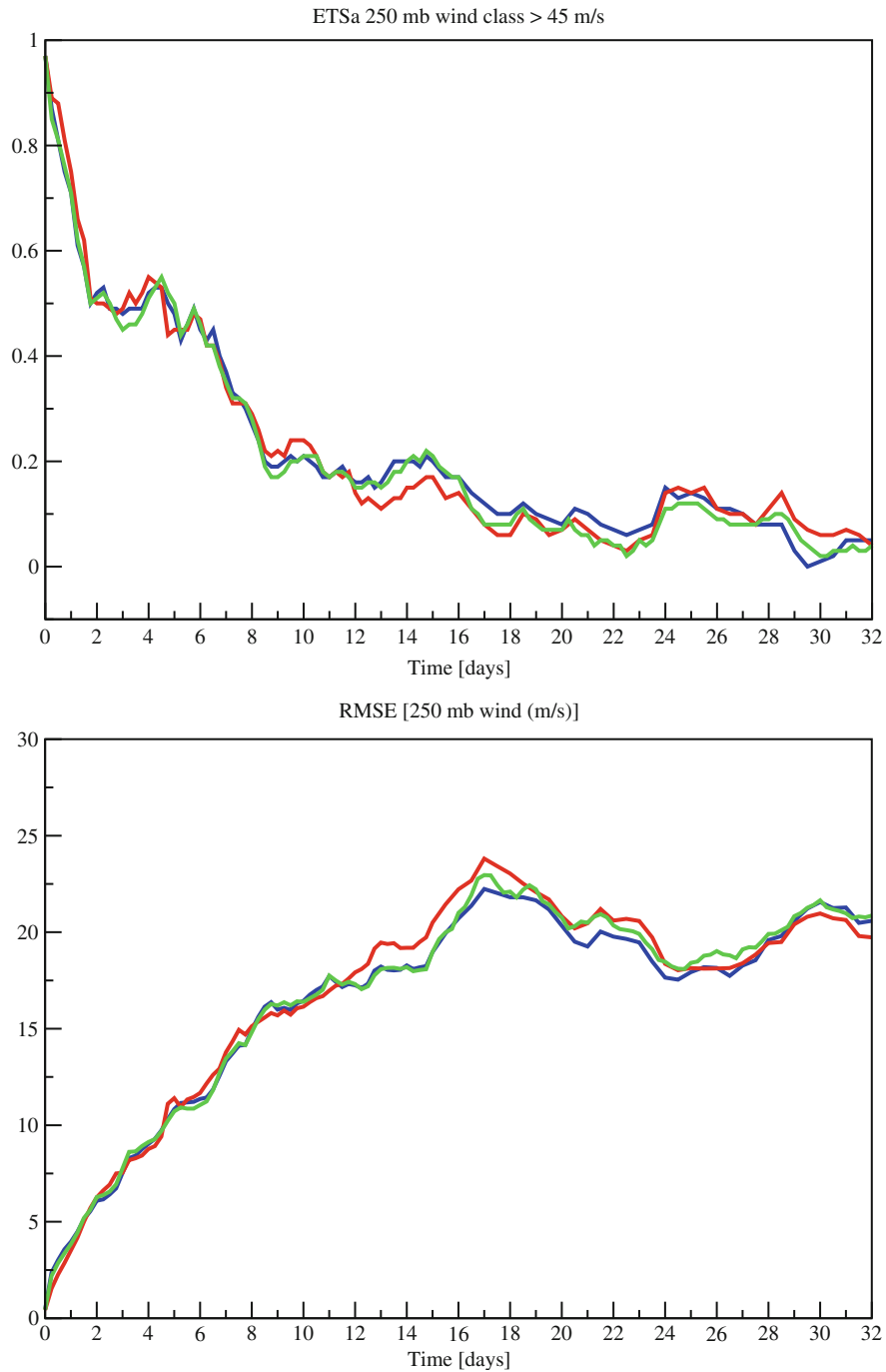


Fig. 5 Bias-adjusted ETS score of 250 hPa wind speed $\geq 45 \text{ ms}^{-1}$, *upper panel*, and 250 hPa RMS forecast minus analysis wind difference, *lower panel*, of the driver ECMWF global ensemble (control plus the first five members), *red lines*; of the Eta forecasts using the Eta LBC scheme, *blue lines*; and of the Eta forecasts using the Davies relaxation LBC scheme, *green lines*. See text for additional information

of the RCM experiments. We feel that the difference in resolution, ~31 km of the Eta, versus ~50 km the first 15 days and ~80 km further on of the ECMWF ensemble, while certainly making a positive contribution to the results is not exceptional and certainly not that great as to enable by itself the Eta to overcome its LBC handicap and generate the results shown.

One other feature that V2010 looked into is the LBC scheme of the Eta, different from the usual Davies (1976) relaxation scheme used in possibly all other RCM models. In the Eta scheme (Mesinger 1977), prognostic variables are prescribed at the inflow boundary, while at the outflow boundary the tangential velocity is extrapolated from inside of the model domain. This in fact is one of the options recommended by Sundström (1973). In the Eta, in addition, four-point averaging along the row next to the boundary is done in order to couple the gravity waves of the two C-subgrids of the model's E-grid. Semi-Lagrangian advection three rows further inside the model domain seems to successfully eliminate problems due to spurious reflections at the model boundary. While not strictly a part of the LBC scheme, use of a C-subgrids gravity-wave coupling scheme of Mesinger (1974) should be mentioned, given that an early experiment of Mesinger and Janjic (1974) demonstrated that noise could still be generated by lateral boundary forcing unless schemes are used inside the model domain that control the tendency for separation of the C-subgrids gravity waves when not using the C-grid.

This LBC scheme being mathematically more appropriate than the overspecification of the relaxation scheme [note the puzzlement expressed by McDonald (2003) at the situation totally dominating meteorological literature in the area], V2010 ran the first three of their forecasts also using the relaxation scheme, and compared the results against those of the Eta scheme. The verification plots of these three forecasts using the bias-adjusted ETS and bias have been displayed in V2010: the forecasts using the Eta scheme verified slightly better more often than did the relaxation scheme forecasts, but the difference overall was not great. Plots of the more standard RMS difference and bias, not shown in V2010, gave a similar result.

For more confidence, three more ensemble members were run subsequently using the relaxation scheme, to arrive to a total of six forecasts, control and the first five ensemble members, run using each of the two LBC schemes. Verifications of the six forecasts, using each of our two principal verification measures, along with

the verification of the six driver ECMWF forecasts, are shown in Fig. 5. In the figure, red lines show the values of the ECMWF driver ensemble members; blue lines those of the Eta forecasts using the Eta LBC scheme, and green lines those of the Eta forecasts using the relaxation scheme. Bias-adjusted ETS scores, upper panel, following only an intermittent and small advantage of one or the other Eta ensemble until the day 16, show a consistent advantage of the Eta LBC ensemble over the relaxation one for a period longer than 10 days all the way until the day 27.5 time, followed by a 3-day period of the advantage of the relaxation ensemble, and ending with a 1.5 day advantage once again of the Eta LBC ensemble. RMS forecast minus analysis difference plots, lower panel, once again display a consistent advantage of the Eta LBC ensemble over the relaxation one for an extended period during the second half of the experiment, with hardly any time to be noticed throughout the experiment of the advantage of the relaxation ensemble.

As a summary these LBC experiments strongly suggest that the use of the relaxation scheme, with its additional resource requirements, should not be necessary provided care is taken to control noise generation at the boundary due to the gravity wave separation when using grids other than the C-grid, and the reflection at the boundary.

While the LBC experiments shown thus do point to a positive contribution of the Eta LBC scheme to the Eta-favorable results shown, the LBC impact is certainly not as decisive as seems needed to answer the overall question posed, in particular in view of the COLA ensemble result shown in our Introduction. Mitchell et al. (2001) asking about the same question but at the time when only three COLA ensemble members were available as a tentative explanation offered that "a nested continental model whose complex physics package has evolved over one to two decades with an emphasis on performance over land may indeed have some advantage over its parent GCM for seasonal-range predictions (1–6 months lead) of continental anomalies during the weak circulation regime of summer." In contrast, we have here in section "Results" summarized results for winter, when a model dynamics feature such as the treatment of the strong jet stream impinging upon and crossing Rocky Mountains looks like a better candidate for the advantage of the Eta than the physics package performance over land. Thus, it seems to us that the treatment of topography, consistent with earlier Eta

NWP results and the use of the eta coordinate (as reviewed, e.g., in Mesinger 2004), is a strong candidate for a major contribution to the favorable RCM results summarized.

Note in this connection also another cool season result favoring the Eta against two sigma system models in verifications of the NCEP Short-Range Ensemble Forecast System (SREF) done by Charles and Colle (2009). For the six-month cool season 2006–2007 in verifications of the cyclone central pressure and cyclone displacement of four SREF subgroups of members, over the region of about the central United States and southern Canada east of the Rockies, the two non-Eta subgroups were found to be “the poorest performing subgroups for most hours.”

But back to the general RCM issues, we certainly do not wish to claim that the Eta is unique in its apparent ability to generate large scales most of the time better than its driver forecasts; recall our references to Giorgi et al. (1998) and Gustafson and Leung (2007). We in fact see no reason why an RCM should *not* be able to do so, in principle; and see experiments in the manner of V2010 as highly desirable model tests. Granted, there are LBC errors, but we believe they are identifiable, and can be reduced, the Eta scheme included. In the Eta scheme, other schemes too, an effort to eliminate space interpolations at the boundary should be an obvious refinement, so that the inflow into the nested model domain can be made equal to the outflow from the driver model.

Objections could be raised that aiming for improvements including those in the large scales, a large domain such as that of V2010 is required, with questionable rewards. One should note though that large domain requires only relatively modest additional resources compared to higher resolution which RCM effort implies already. For example, had one run the V2010 experiments using a domain half the size actually used—which would be more like domains typically used in RCM experiments—with the intention of using the resources saved to increase the horizontal resolution, this would have enabled an increase in resolution by 1/8, from 31 to about 27 km. This of course with no changes in the model physics setup. This increase in resolution seems to us not likely to offer rewards which might compensate for the benefits of the larger domain lost in doing so.

This might sound strange given that by definition the purpose of RCM work is achieving improvements

at regional scales, which clearly does not include large scales. Recall however our suggestion made earlier that even minor improvements in large scales should be expected to lead to increased and significant improvements in small scales compared to what would be achieved if large scales were left unchanged.

Acknowledgement We have benefitted from several comments of Professor René Laprise on the original version of our manuscript, one of those leading us to notice an error we had in V2010 in specifying the north-south size of the domain used.

References

- Altshuler E, Fennessy M, Shukla J, Juang H, Rogers E, Mitchell K, Kanamitsu M (2002) Seasonal simulations over North America with a GCM and three regional models. COLA Tech Rpt 115, 66pp. Available from COLA, 4041 Powder Mill Road, Suite 302, Calverton, MD 20705
- Brill KF (2009) A general analytic method for assessing sensitivity to bias of performance measures for dichotomous forecasts. *Weather Forecast* 24:307–318
- Brill KF, Mesinger F (2009) Applying a general analytic method for assessing bias sensitivity to bias adjusted threat and equitable threat scores. *Weather Forecast* 24:1748–1754
- Castro CL, Pielke RA Sr, Leoncini G (2005) Dynamical downscaling: assessment of value retained and added using the Regional Atmospheric Modeling System (RAMS). *J Geophys Res* 110:D05108. doi:10.1029/2004JD004721
- Charles ME, Colle BA (2009) Verification of extratropical cyclones within the NCEP operational models. Part II: the short-range ensemble forecast system. *Weather Forecast* 24:1191–1214
- Chou SC, Bustamante JF, Gomes JL (2005) Evaluation of seasonal precipitation forecasts over South America using Eta model. *Nonlinear Proc Geophys* 12:537–555
- Chou SC, Marengo JA, Lyra AA, Sueiro G, Pesquero JF, Alves LM, Kay G, Betts R, Chagas DJ, Gomes JL, Bustamante JF, Tavares P (2011) Downscaling of South America present climate driven by 4-member HadCM3 runs. *Clim Dyn* 38:635–653. doi:10.1007/s00382-011-1002-8
- Davies HC (1976) A lateral boundary formulation for multi-level prediction models. *Quart J R Meteorol Soc* 102:405–418
- Denis B, Laprise R, Caya D, Côté J (2002) Downscaling ability of one-way nested regional climate models: the Big-Brother Experiment. *Clim Dyn* 18:627–646
- Diaconescu EP, Laprise R, Sushama L (2007) The impact of lateral boundary data errors on the simulated climate of a nested regional climate model. *Clim Dyn* 28:333–350
- Fennessy MJ, Shukla J (2000) Seasonal prediction over North America with a regional model nested in a global model. *J Clim* 13:2605–2627
- Giorgi F (2006) Regional climate modeling: status and perspectives. *J Phys IV France* 139:101–118. doi: 10.1051/jp4:2006139008. Available online at <http://jp4.journaldephysique.org/>

- Giorgi F, Mearns LO, Shields C, McDaniel L (1998) Regional nested model simulations of present day and 2XCO₂ climate over the Central Plains of the U.S. *Clim Change* 40:457–493
- Gustafson WI Jr, Leung LR (2007) Regional downscaling for air quality assessment. *Bull Am Meteorol Soc* 88:1215–1227
- Hamill TM (1999) Hypothesis tests for evaluating numerical precipitation forecasts. *Weather Forecast* 14:155–167
- Hamill TM, Juras J (2006) Measuring forecast skill: is it real skill or is it the varying climatology? *Quart J R Meteorol Soc* 132:2905–2923
- Jones RG, Murphy JM, Noguer M (1995) Simulation of climate change over Europe using a nested regional climate model. I: assessment of control climate, including sensitivity to location of lateral boundaries. *Quart J R Meteorol Soc* 121:1413–1449
- Junker NW, Schneider RS, Fauver SL (1999) A study of heavy rainfall events during the great Midwest flood of 1993. *Weather Forecast* 14:701–712
- Katsafados P, Papadopoulos A, Kallos G (2005) Regional atmospheric response to tropical Pacific SST perturbations. *Geophys Res Lett* 32:L04806. doi:10.1029/2004GL021828
- Laprise R, Varma MR, Denis B, Caya D, Zawadzki I (2000) Predictability of a nested limited-area model. *Mon Weather Rev* 128:4149–4154
- Laprise R, de Elía R, Caya D, Biner S, Lucas-Picher P, Diaconescu E, Leduc M, Alexandru A, Separovic L (2008) Challenging some tenets of regional climate modelling. *Meteorol Atmos Phys* 100:3–22
- Laprise R, Kornic D, Rapaic M, Šeparović L, Leduc M, Nikiema O, Di Luca A, Diaconescu E, Alexandru A, Lucas-Picher P, de Elía R, Caya D, Biner S (2012) Considerations of domain size and large-scale driving for nested regional climate models: impact on internal variability and ability at developing small-scale details. In: Berger A, Mesinger F, Sijacki Dj (eds) *Climate change: inferences from paleoclimate and regional aspects*. Springer, Heidelberg
- Lo JC-F, Yang Z-L, Pielke RA Sr (2008) Assessment of three dynamical climate downscaling methods using the Weather Research and Forecasting (WRF) model. *J Geophys Res* 113:D09112. doi:10.1029/2007JD009216
- McDonald A (2003) Transparent boundary conditions for the shallow-water equations: testing in a nested environment. *Mon Weather Rev* 131(4):698–705
- McGregor JL (1997) Regional climate modelling. *Meteorol Atmos Phys* 63:105–117
- Mesinger F (1974) An economical explicit scheme which inherently prevents the false two-grid-interval wave in the forecast fields. Proceedings of the symposium on difference and spectral methods for atmosphere and ocean dynamics problems, Academy of Sciences, Novosibirsk, 17–22 Sept 1973, part II, pp 18–34
- Mesinger F (1977) Forward-backward scheme, and its use in a limited area model. *Contrib Atmos Phys* 50:200–210
- Mesinger F (2004) The Eta model: design, history, performance, what lessons have we learned? In: Symposium on the 50th anniversary of operational numerical weather prediction, University of Maryland, College Park, MD, 14–17 June 2004, Preprints CD-ROM, 20pp. Available from NCEP, 5200 Auth Road, Room 101, Camp Springs, MD 20746-4304; ppt at <http://www.ncep.noaa.gov/nwp50/Presentations/>
- Mesinger F (2008) Bias adjusted precipitation threat scores. *Adv Geosci* 16:137–143. Available online at <http://www.adv-geosci.net/16/index.html>
- Mesinger F and Janjić ZI (1974) Noise due to time-dependent boundary conditions in limited area models. The GARP Programme on Numerical Experimentation, Rep 4, WMO, Geneva, pp 31–32
- Mesinger F, Jovic D (2002) The Eta slope adjustment: contender for an optimal steepening in a piecewise-linear advection scheme? Comparison tests. NCEP Office Note 439, 29pp. Available online at <http://www.emc.ncep.noaa.gov/officenotes>
- Mesinger F, Jovic D (2004) Vertical coordinate, QPF, and resolution. The 2004 workshop on the solution of partial differential equations on the sphere, Frontier Res. Center for Global Change (FRGC), Yokohama, Japan, 20–23 July 2004. CD-ROM, vol 2. Available online at <http://www.jamstec.go.jp/frgc/eng/workshop/pde2004/agenda.html>
- Mesinger F, Janjić ZI, Ničković S, Gavrilov D, Deaven DG (1988) The step-mountain coordinate: model description and performance for cases of Alpine lee cyclogenesis and for a case of an Appalachian redevelopment. *Mon Weather Rev* 116:1493–1518
- Mesinger F, Brill K, Chuang H-Y, DiMego G, Rogers E (2002) Limited area predictability: can “upscaling” also take place? Research activities in atmospheric and oceanic modelling, WMO, Geneva, CAS/JSC WGNE Rep. No. 32, 5.30-5.31
- Miguez-Macho G, Stenchikov GL, Robock A (2004) Spectral nudging to eliminate the effects of domain position and geometry in regional climate model simulations. *J Geophys Res* 109:D13104. doi:10.1029/2003JD004495
- Miguez-Macho G, Stenchikov GL, Robock A (2005) Regional climate simulations over North America: interaction of local processes with improved large-scale flow. *J Clim* 18:1227–1246
- Mitchell K, Fennessy MJ, Rogers E, Shukla J, Black T, Kinter J, Mesinger F, Janjić Z, Altshuler E (2001) Simulation of North American summertime climate with the NCEP Eta Model nested in the COLA GCM. *GEWEX News* 11(1): 3–6. Available online at http://www.gewex.org/gewex_nwsltr.html
- Reynolds RW, Smith TM (1994) Improved global sea surface temperature analyses using optimum interpolation. *J Clim* 7:929–948
- Rockel B, Castro CL, Pielke RA Sr, von Storch H, Leoncini G (2008) Dynamical downscaling: assessment of model system dependent retained and added variability for two different regional climate models. *J Geophys Res* 113:D21107. doi:10.1029/2007JD009461
- Sundström A (1973) Theoretical and practical problems in formulating boundary conditions for a limited area model. Rep. DM-9, Institute of Meteorology, University of Stockholm. Available from Department of Meteorology, Stockholm University, 106 91 Stockholm, Sweden
- Vannitsem S, Chomé F (2005) One-way nested regional climate simulations and domain size. *J Clim* 18:229–233
- Veljovic K, Rajkovic B, Fennessy MJ, Altshuler EL, Mesinger F (2010) Regional climate modeling: should one attempt improving on the large scales? Lateral boundary condition scheme: any impact? *Meteorol Z* 19:237–246. doi:10.1127/0941-2948/2010/0460
- Xie P, Arkin P (1996) Analysis of global monthly precipitation using gauge observations, satellite estimates, and numerical model predictions. *J Clim* 9:840–858

Eta Model Simulations and AMSR Images to Study an Event of Polynya at Terra Nova Bay, Antarctica

Sandra Morelli and Flavio Parmiggiani

Abstract

In the Terra Nova Bay (TNB) region, near-surface winds are persistently strong, in particular during the winter season and blow offshore with a high degree of directional constancy. This region is also known as a preferential zone of coastal polynyas. Polynyas are recurring areas of open water/thin ice surrounded by an ice-covered sea. Coastal polynyas form along ice-bound coasts; they are believed to be due to strong and persistent offshore winds and/or ocean currents which drive the sea ice away. As the ice is removed from the region of origin, open water is exposed and refrozen and the new ice is pushed away, so that coastal polynyas provide a source of new ice production. As the ice forms, much of the salt content in the freezing water is rejected, forming dense salty water, which tends to sink, eventually contributing to the deep ocean circulation. The horizontal surface temperature differences among the land ice, water, and sea ice are strong because the open water is close to the freezing point (-1.8°C for typical salt water). The energy exchange between the ocean and the atmosphere in the Antarctic marginal sea-ice zone is strongly influenced by the extent of sea-ice cover. While the sea ice acts as insulation, a direct contact between water and air is established in areas of open water, and intense energy exchanges occur due to the large difference of temperature between the water and the air above it. As a result, the polynya areas have an important impact on polar meteorology/climate.

In Antarctica, atmospheric numerical models which provide good results at mid-latitudes are put to test because the observations are scarce, the initial and boundary conditions are sometimes inadequate, and complex terrain, sea ice, and polynyas are present. In the present contribution, numerical simulation of a real event of a coastal polynya at TNB is shown, using a recent version of the Eta model. The horizontal resolution used is approximately 20 km, with 50 layers in the vertical, and the model atmosphere top at 25 hPa. Initial and boundary conditions are obtained from ECMWF analyses. An event which occurred from 12 to 18 July 2006 was selected by inspection of the sequence of daily

S. Morelli (✉)
Department of Physics, University of Modena and Reggio E,
via Campi 213/A, 41100 Modena, Italy
e-mail: sandra.morelli@unimore.it

AMSR-derived sea-ice concentration (SIC) maps. Evaluation of the area with sea-ice concentration values below a predetermined threshold provided information on the temporal development of the polynya, which reached its maximum extent of about 4,000 km² on 16 July. Thus, an open water polynya of realistic size was included within the initial conditions of the simulation, done for the period 15–17 July. The Eta model reproduced the evolution of upper and mid-atmospheric states in what we find a good agreement with AVHRR observations. The evolution of the simulated 10 m winds is well correlated with the observed extent of the polynya. In order to identify the effect of the presence of the open water area on the structure of the atmospheric boundary layer and atmospheric circulation, an additional simulation was performed without the presence of the polynya. Comparison of these two numerical simulations shows that the polynya acted to increase the air speed above it and had induced intense heat fluxes, warming the air. This polynya modification impacted the atmosphere over a rather long distance and up to a height of several hundred meters.

Introduction

The Antarctic topography is characterized by quite gentle terrain slopes in the interior of the continent, while much steeper slopes are generally found near the coast. In the Terra Nova Bay (TNB) region (Fig. 1), three glaciers, Priestley, Reeves, and David glaciers, slope toward the coast. These topographic features, in particular the Reeves and David glaciers, are important for the wind regime. The near-surface winds converge into the glaciers, blowing downward and offshore over the western Ross Sea with high directional constancy and with intensity that may be sufficient to advect sea ice far from the coastal zone. A seaward wind component exceeding 10 m s⁻¹ appears sufficient to maintain a polynya in coastal areas (Pease 1987; Gallée 1997). Pease (1987) pointed out that based on one-dimensional numerical experiments, an important factor for the expansion of a sea-ice-free area is also the air temperature: for a given wind speed warmer air should produce a wider polynya. At the same time, an area of open water close to the freezing point (temperature of approximately -1.8°C) is a source of heat for the polar air. Thus, mutual interactions and feedback mechanisms between atmosphere, polynyas, and ocean occur. In this chapter, aspects of the interactions between atmosphere and open water polynya are examined. During the polar cold season, observed data of wind and air temperature are unavailable over the polynyas and the numerical

models become indispensable tools. However, even though the models used might perform well in the mid-latitudes, the complexity of the Antarctic environment, including processes not fully understood, and facing the lack of data, requires verifying their performances as much as possible.

For real data case studies, satellite images can be used to produce detailed sea-ice mapping in the polynya zone. Because of the frequent cloud cover of polar regions, sea-ice concentration (SIC) maps can only be provided by images from active (SAR) and passive (AMSR-E) microwave sensors. Archived SAR images over TNB are only available, on average, in numbers of 2–3 per month. As a polynya event may last only a few days, the use of passive microwave observations becomes a compulsory choice.

Here a recent version of the Eta model is used for the simulation of an actual event of TNB polynya and to study the impact of a warm area of realistic size on the atmosphere. AMSR-derived SIC maps have been used to select the case study and to obtain the extent of the TNB polynya included in the initial conditions.

AMSR-Derived SIC Maps

Sea-ice concentration maps derived from AMSR-E data are produced daily by the Institute of Environmental Physics (IEP) of the University of Bremen, with a pixel size equal to the original one, for both

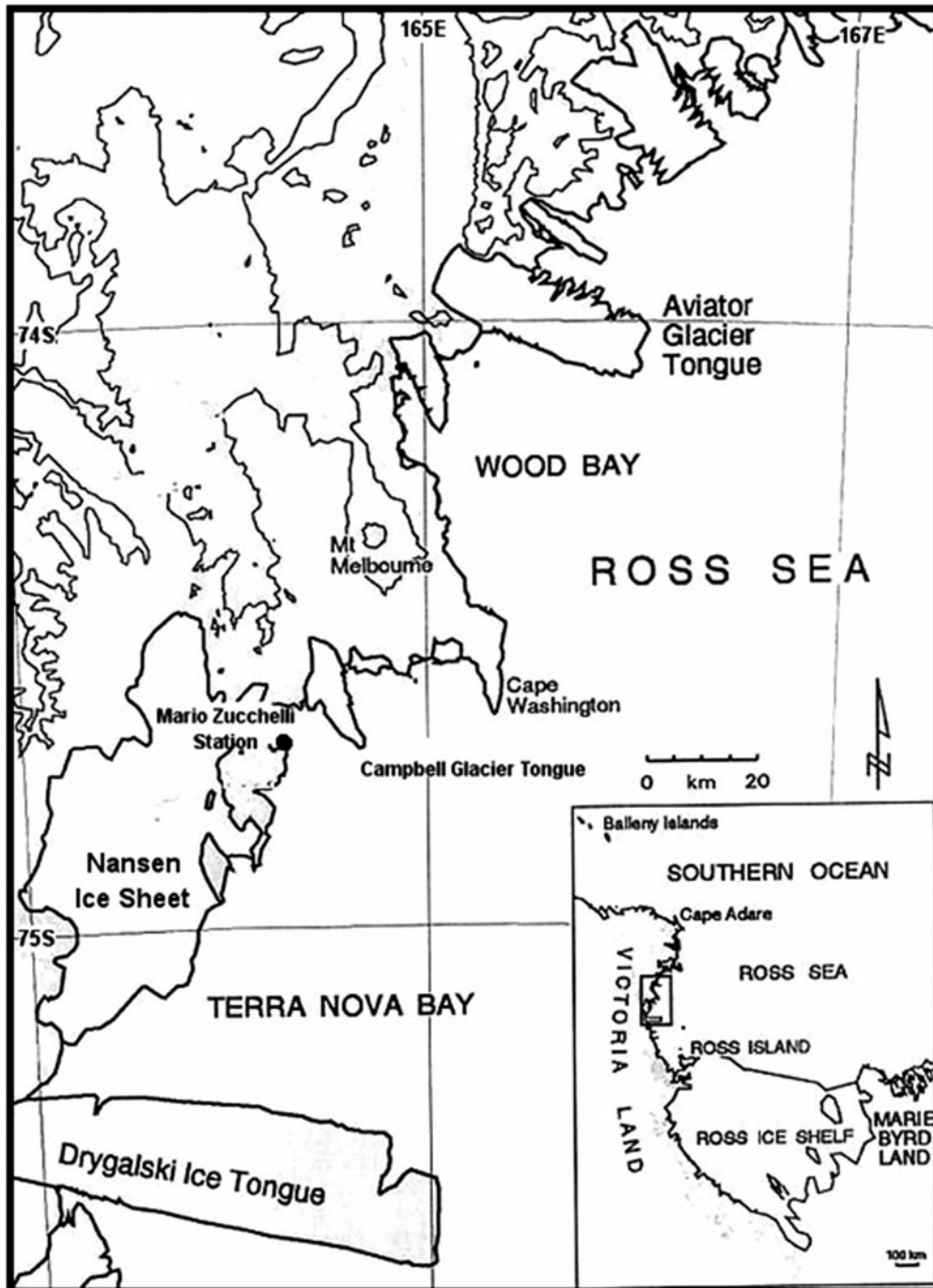


Fig. 1 Map of Terra Nova Bay (from Parmiggiani 2006)

polar regions. With a pixel size of 6.25 km, the AMSR-E, mounted on board of NASA Aqua satellite, is the most advanced passive microwave sensor currently operational. These maps are made available

through the Institute web site only hours after the satellite pass over polar regions.

After downloading the data file in HDF format, any subset covering specific areas of interest can be

extracted. Image subsets covering the area of TNB, approximately from 74.5 to 76.0°S and from 163 to 167°E, were extracted from the Antarctic SIC data set. These image subsets, 20 × 20 pixel size, i.e., 125 × 125 km, which almost exactly circumscribes the TNB polynya, are used for the computation of the polynya area. Figure 2 shows an image subset of TNB during the polynya event of July 2006.

On the basis of previous studies (Markus and Burns 1995; Parmiggiani 2006; Hauser et al. 2002), a SIC pixel will be considered as “open water” when its value goes below 70%; polynya area can then be measured by simply counting the number of “open water” pixels and multiplying by the area of one pixel (39.0625 km²).

The analysis of the sequence of image subsets from SIC maps for July 2006 revealed a significant polynya event at TNB (Fig. 2). The computation of the daily extents of the polynya shows that the open water area quickly increased from 15 to 16 July, reaching its maximum on 16 July, while it was still small from 12 to 14 July compared to the subsequent 3 days (Fig. 3).

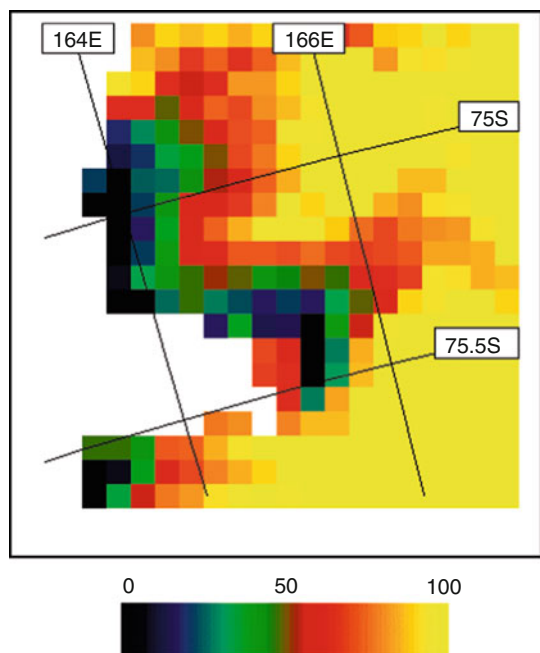


Fig. 2 AMSR-derived SIC map for 16 July 2006. The iced land and the permanent sea ice are not colored. The *color bar* is in percent

Eta Model Simulations Design

The Eta model is a well-known atmospheric model described, e.g., by Mesinger et al. (1988), Mesinger and Loboeki (1991), Janjic (1994). The code and setup information are available at the Brazilian Center for Weather Prediction and Climate Studies (CPTEC) Eta web site. General information about the Eta model and some more of the references are given in Table 1.

A number of upgrades and changes to the Eta model compared to the workstation version of the National Centers for Environmental Prediction (NCEP Workstation Eta) were made in recent years (Mesinger et al. 2006, Mesinger et al. 2012; Pyle et al. 2008). Our simulations were performed using this upgraded version of the model, including a sloping discretization of the eta coordinate, a piecewise linear scheme for the vertical advection of temperature and wind, standard four-point averaging for the wind interpolation to mass grid points needed to obtain surface exchange coefficients, and 10 m wind diagnosed at the velocity grid points. We have in addition amended the preprocessing codes so as to use the European Centre for Medium Range Weather Forecasts (ECMWF) analyses for initialization and boundary conditions, to include the polynya in the sea-ice cover, and to take into account some of the peculiarities of the Antarctic domain. Several 72-h simulations were performed for the 3-day periods 12–14 and 15–17 July 2006. Here results of two simulations covering the period 15–17 July 2006 will be shown. The first of those was performed with the Ross Sea completely ice covered (no polynya run), the second one with the TNB polynya included (polynya run). Currently, the Eta model distinguishes open water grid points and thick sea ice grid points by a mask which is established as initial condition and remains fixed in the simulations. As we are dealing with a winter event, it is likely that the polynya was not entirely an area of open water but rather it consisted of open water and thin sea-ice (Hauser et al. 2002), which formed a warm area. On 15 and 16 July with clear sky, AVHRR images show the region of TNB in channel 4 (11.5 μm) with a well developed warm area, surrounded by much colder pack ice. Unfortunately, the AVHRR images do not contain the visible channels but only the thermal ones, because, in the days of the event, the most of the integration domain is under polar night condition and, in

Fig. 3 Development of the polynya extent from 1 July to 20 July 2006, as evaluated by AMSR-derived SIC maps

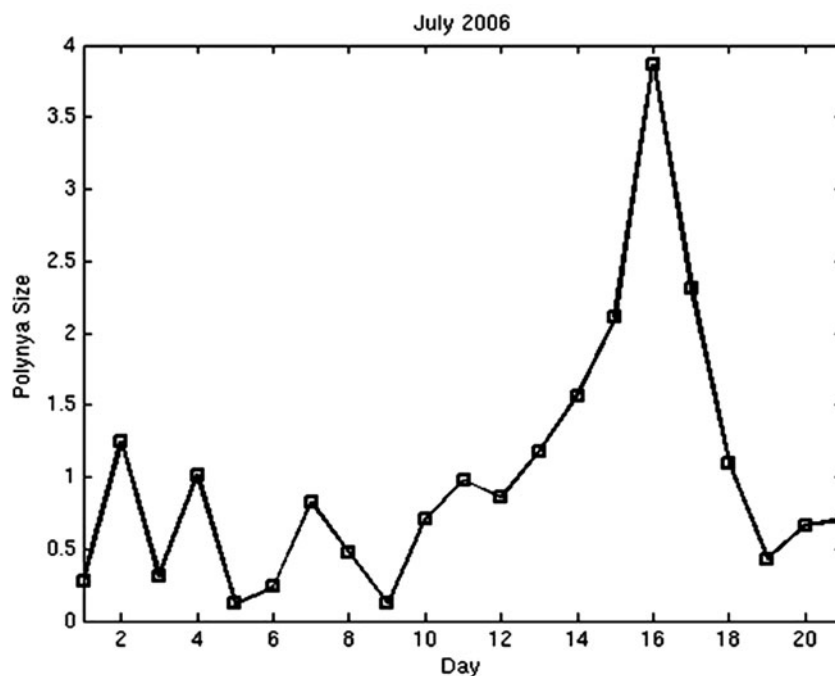


Table 1 The Eta model

Eta model	Grid point model, semi-staggered Arakawa E grid, rotated spherical coordinate system, vertical η coordinate (quasi-horizontal coordinate surfaces) (Mesinger et al. 1988)
Type	Hydrostatic or nonhydrostatic
Topography	Mountain height from Digital Elevation Model (DEM) data set at 30" horizontal resolution, use of the "effective roughness" length approach (Georgelin et al. 1994)
Parameterizations, turbulent fluxes	Surface layer: Paulson (1970) over the land and sea-ice grid points, Loboeki (1993) (derived from the Mellor Yamada level 2 formulation) over the water grid points Roughness length from Charnock (1955) relation for sea grid points Roughness length for heat and water vapor different from that for momentum (Zilitinkevich 1995) elsewhere PBL: revised Mellor–Yamada level 2.5 scheme (Janjic 1996)
Soil model	Soil model with 4 layers (Chen et al. 1996; Koren et al. 1999)
Sea ice	Fixed thickness at 3 m Thermal conductivity = $2.2 \text{ W m}^{-1} \text{ K}^{-1}$ Heat capacity = $1.724 \cdot 10^6 \text{ J m}^{-3} \text{ K}^{-1}$
Radiation	Geophysical Fluid Dynamics Laboratory radiation scheme
Convection and clouds	Betts–Miller–Janjic convection scheme (Janjic 1994), a large-scale cloud microphysics scheme (Ferrier et al. 2002)

particular, the Sun is below the horizon at TNB. In this chapter, an open water polynya (SST = -1.8°C) with size comparable to the polynya extent as evaluated by AMSR-derived SIC maps is included in the initial conditions of the simulations. Figure 4 shows the integration domain, while Table 2 summarizes the two simulations.

Results

Thermal infrared radiometer (AVHRR) images show that a sequence of cyclones moved southeastward over the Ross Sea from 12 to 17 July. The presence of these cyclones and their path are also evident in the

Fig. 4 The simulation domain (*red square*), having 161×161 grid points

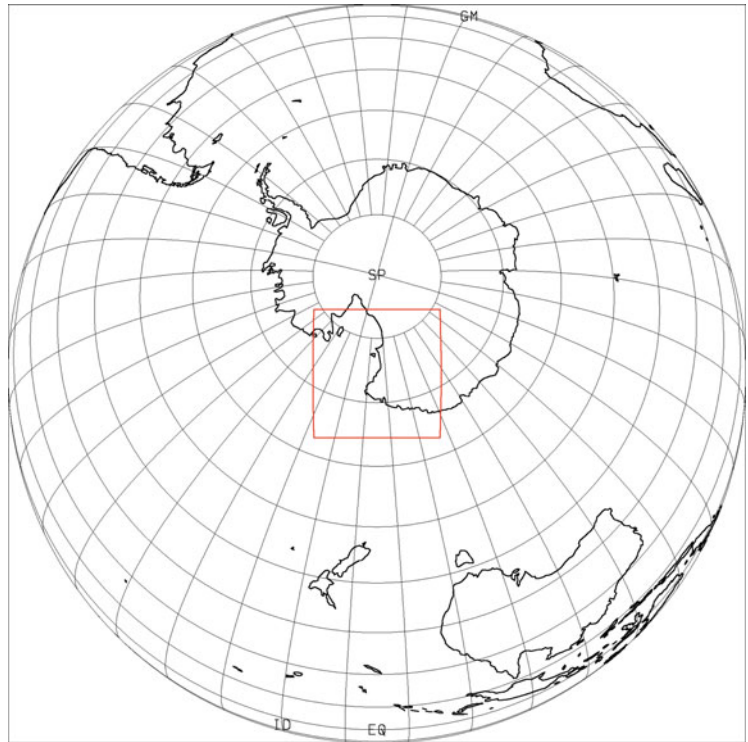


Table 2 Design of the simulations

Name (referred as)	Run 1 (no polynya run)	Run 2 (polynya run)
Initial and boundary conditions	ECMWF data (res. $0.5625^\circ \times 0.5625^\circ$, 12 isobaric levels in the vertical), updated every 6 h SST = -1.8°C	Same as run 1
Period	0000 GMT 15 July 2006 0000 GMT 18 July 2006, output every 1 h	Same as run 1
Type	Hydrostatic run	Same as run 1
Integration domain (defined by points)	Horizontal: (143.1°E, 62.6°S), (165.0°E, 64.5°S), (186.8°E, 62.6°S), (226.8°E, 78.8°S), (165.0°E, 84.5°S), (103.2°E, 78.8°S) Vertical, top: 25 hPa	Same as run 1
Vertical and horizontal resolution	Vertical: 50 layers (higher resolution near the bottom of the domain) Horizontal: about 20 km (approximate distance between two mass points on the semistaggered Arakawa E grid)	Same as run 1
Presence of polynya	No	Yes

geopotential height fields simulated for the same period; in particular, maps of the 850 hPa geopotential seem to present a good numerical representation of these structures. As an example, a comparison between satellite observations and our numerical results is shown in Fig. 5. In its left panel, AVHRR image of the study area is shown, while in its right panel, an 850 hPa geopotential field of the model run is

displayed. Because AVHRR image is valid at 0436 GMT 16 July, the simulated field of 850 hPa geopotential height that we chose to show is that valid at 0500 GMT 16 July.

The position of the cyclone simulated along the northern coast of the continent is seen to agree well with that indicated in the AVHRR image of Fig. 5. During subsequent hours, both AVHRR images and

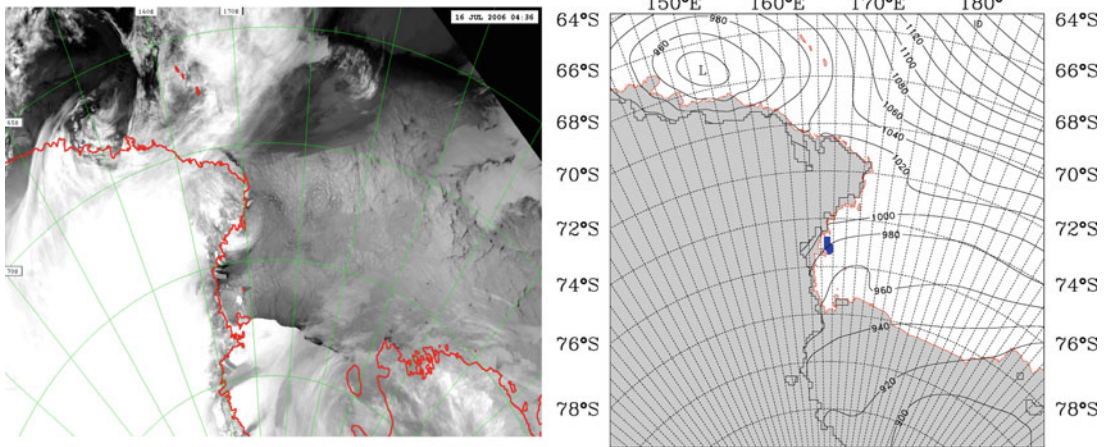


Fig. 5 AVHRR channel 4 image of East Antarctica at 0436 GMT 16 July (left side panel). The 850 hPa geopotential height at 0500 GMT 16 July from run 1 (no polynya run). Isolines are plotted at 20-gpm intervals (right side panel)

maps of geopotential heights show the structure to slowly move toward southeast.

In addition to the lows referred to just above, during the days considered, subsynoptic troughs were simulated over the southwestern Ross Sea, illustrating a persistent mesoscale cyclonic activity in this area at the time. The southwestern corner of the Ross Sea is known as a very active area for mesoscale cyclogenesis.

In both of our 3-day periods (from 12 to 14 July and from 15 to 17 July), a more prominent synoptic system, moving from the northwest, and a southerly low were converging over the Ross Sea and subsequently moved eastward. Thus, the surface pressure system registered by Automatic Weather Stations (AWS) over the western Ross Ice Shelf around Ross Island (Fig. 1) displays two episodes of low values separated by relatively high values on 14 July. This influenced the winds in Terra Nova Bay region. Over the Nansen Ice Sheet (Fig. 1), two automatic stations were active: Manuela AWS (latitude: 74.946°S, longitude: 163.687°E, altitude: 78 m) at Inexpressible Island and Eneide AWS (latitude: 74.70°S, longitude: 164.10°E, altitude: 92 m) near the Italian “Mario Zucchelli” base. The data are available at the Antarctic Meteorological Research Center, University of Wisconsin-Madison (<http://amrc.ssec.wisc.edu/index.html/>) and at the Italian Antarctic Research Program (PNRA) Meteo-climatological Observatory (<http://www.climantartide.it/>) web sites, respectively. Data of Manuela and Eneide AWS of 15–17 July show an intense near-surface wind that

developed over the area with direction toward the Ross Sea. In that same period, an intense wind, channeled by the Reeves and David glaciers, with offshore direction was simulated. Our simulated 10 m wind speeds during that time reached their maxima approximately at 2100 UTC 15 July, irrespective of the presence of the polynya in the simulation. Comparison between the run 1 (no polynya run) and run 2 (polynya run) illustrates the impact of the open water on horizontal wind speeds and temperature. The polynya can be seen to have led to increased both the low-level wind speeds and temperatures over the area. For a look at the wind speed impact, in Fig. 6, wind speed at 10 m is shown for run 1 (no polynya run) and for run 2 (polynya run), respectively, at 0500 GMT 16 July. The wind intensity is generally stronger in the run 2 over the area of the polynya. For example, near the grid point 165°E, 75°S, the wind speed increased from about 8 m s^{-1} to about 16 m s^{-1} with the presence of the polynya compared to the run without it. Differences in wind intensity of more than 1 m s^{-1} were simulated over the Ross Sea up to the height of about 1,000 m.

As for temperature, comparison of the simulations with and without the polynya shows a significant heating of the air over the Ross Sea when the presence of the polynya is taken into account. For an illustration, in Fig. 7, vertical cross sections of temperature along the approximate direction of the main flow over the sea-ice-free area are displayed, valid at the same time as the plots of Fig. 6. The black lines of Fig. 6 denote the

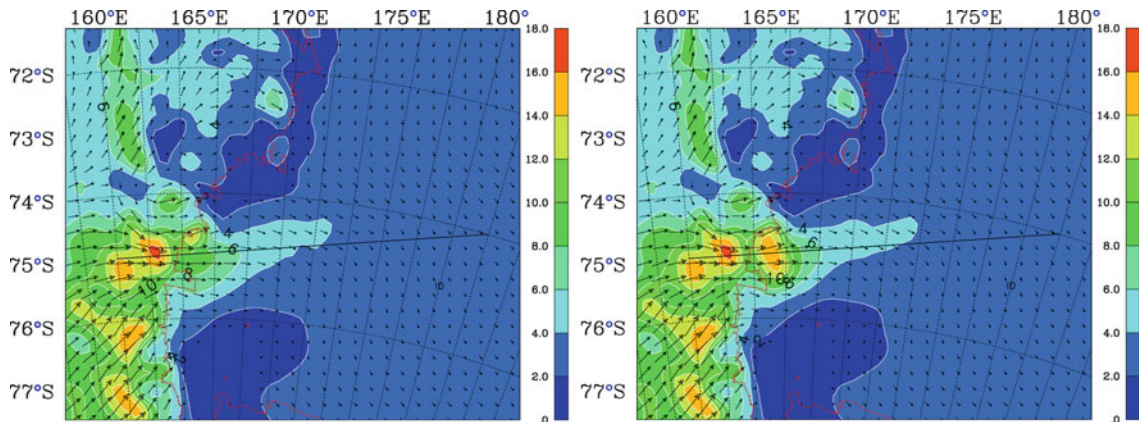


Fig. 6 Wind maps at 10 m valid at 0500 UTC 16 July for run 1 (*left panel*) and run 2 (*right panel*). Isolines at 2 m s^{-1} . The *black line* indicates the position of the vertical cross sections in Fig. 7

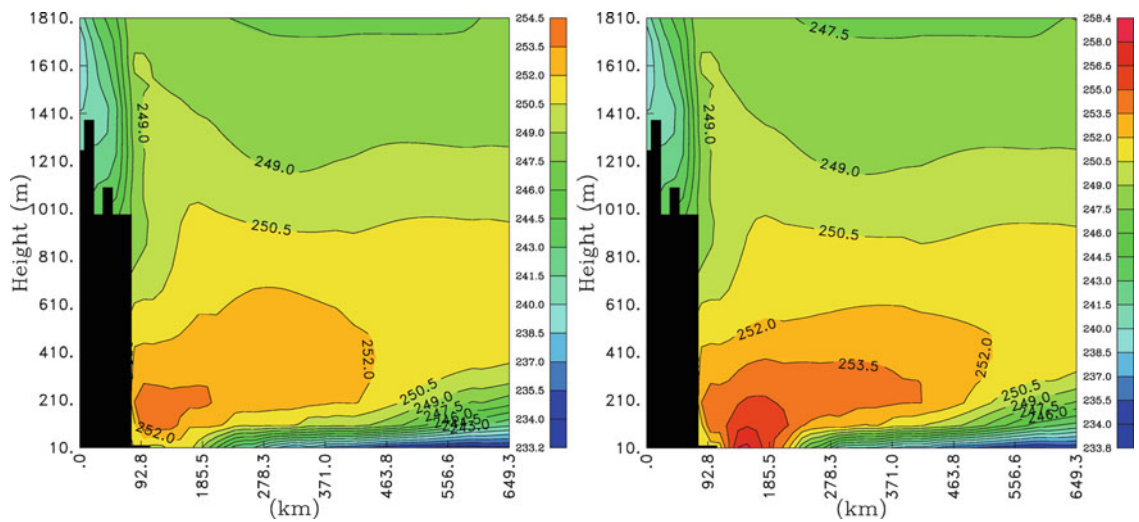


Fig. 7 Vertical temperature cross sections valid at 0500 UTC 16 July for the run 1 (*left panel*) and for run 2 (*right panel*). Contours at intervals of 1.5 K

position of the cross sections shown. The temperatures in the left panel of Fig. 7 are those obtained in run 1 (no polynya), while temperatures in the right panel are those of run 2 (polynya). The panels illustrate a significant heating of the air above the polynya and an advection of the heated air downstream.

As a result, the geopotential heights of the isobaric surfaces obtained in run 2 (polynya) are of course also different from those obtained in run 1 (no polynya). When the polynya is taken into account, the geopotential height of the 900 hPa isobaric surface increases in a fairly wide area, as shown by the plot of the differences

in the geopotential between the run 2 and run 1 (Fig. 8, left panel). Positive values extend from the eastern side of the polynya up to a longitude of more than 190°E . Small differences in the geopotential height between the two runs are found up to 750 hPa. For more detail over the TNB region, the area inside the black line of the left panel of Fig. 8 is shown magnified in the right panel of the figure. The raising 900 hPa geopotential height is seen advected downwind of the polynya.

The polynya heating impacts also the sea level pressure values, as evidenced by the sea level pressure maps of Fig. 9. It shows the sea level pressure

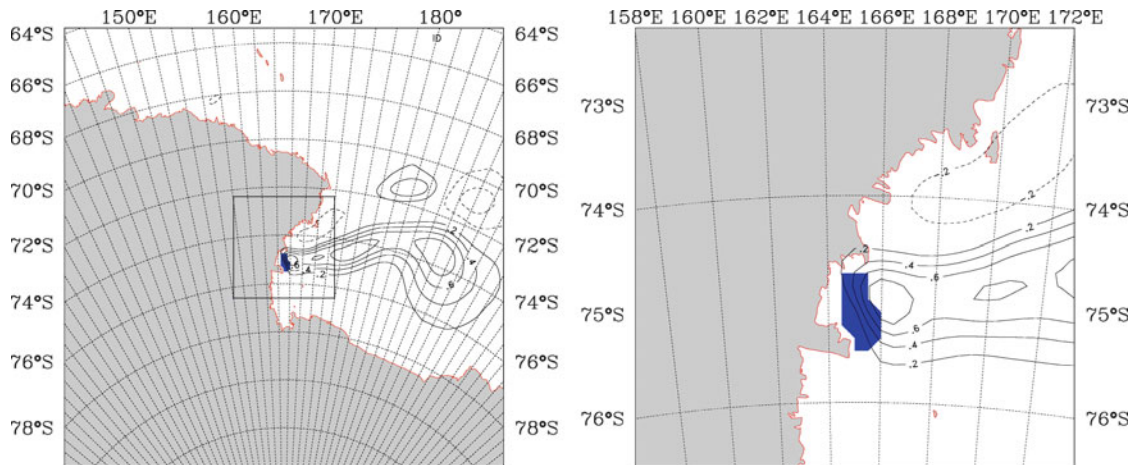


Fig. 8 Difference in the geopotential height of 900 hPa surface between the run with polynya and the run without polynya, at 0500 GMT 16 July. Contour interval is 0.2 gpm

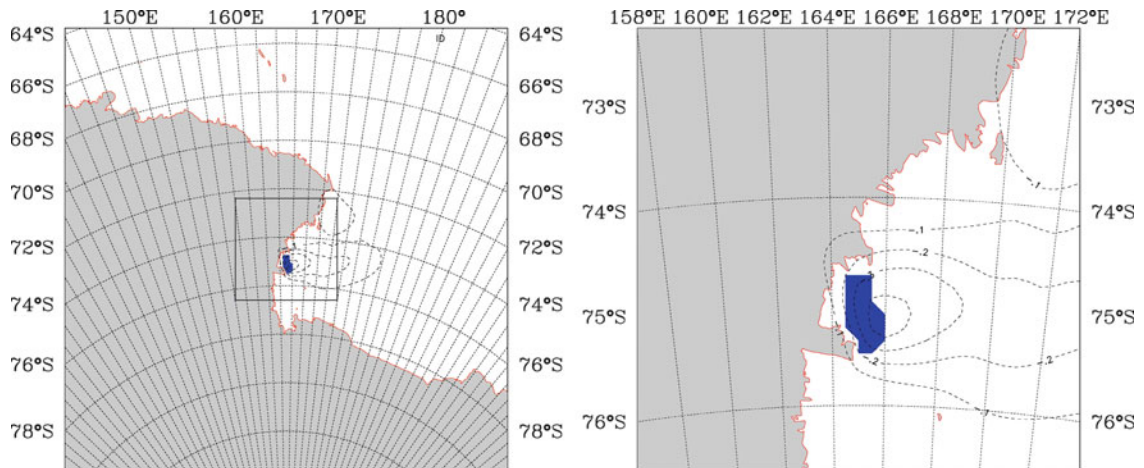


Fig. 9 Difference in the sea pressure between the run with polynya and the run without polynya, at 0500 UTC 16 July. Contour interval is 0.1 hPa

differences between runs 2 and 1, once more with all of the model region in the left and the blown-up section in its right panel. Lower pressure values of the run 2 are seen over the entire TNB area, in particular at the eastern side of the polynya.

Thus, our simulations show that, due to the presence of a relatively warm sea-ice-free area, a zone of lower near-surface pressure develops downwind of the polynya. This structure, embedded in the complex pressure field, modifies horizontal pressure gradients so as to

change the near-surface wind intensity. Results from our Eta model runs show that the included polynya modifies the atmosphere up to a height of several hundred meters and for a considerable distance from its location.

Conclusions

Polynyas are recurring areas of open waters/thin ice surrounded by ice-covered sea in polar regions. Because the open water is close to the freezing point (-1.8°C for typical salt water), they are warm

compared to the surrounding sea ice and the air above. Here we have discussed aspects of the atmospheric response to a realistic-size area of open water. We simulated an event of polynya that was observed at Terra Nova Bay (TNB), Antarctica. This was done via numerical simulations using the Eta model. AMSR-E satellite images, which are not affected by cloud cover, were used to observe and evaluate the extent of the polynya on a daily basis. AVHRR images were used to follow the associated cloud and synoptic dynamics.

We have run a recent version of the Eta model that includes a sloping steps eta discretization, a piecewise linear scheme for the vertical advection of temperature and wind, standard four-point averaging for the wind interpolation to mass grid points needed to calculate exchange coefficients, and 10-m wind diagnosed at the velocity grid points. Several changes were also introduced in the original preprocessing code in order to use analyses of the European Centre for Medium Range Weather Forecasts (ECMWF) for providing the initial and boundary conditions. In addition, modifications were necessary to include the polynya in the sea-ice cover and to take into account some of the peculiarities of the Antarctic domain. The comparison of the simulated geopotential height fields and the AVHRR satellite images showed that this setup performed well. We have made other tests of the performance of the Eta model that we found successful and plan to discuss in a paper in preparation.

Results of our numerical simulations demonstrate that the impact of the polynya on the atmosphere is significant, in particular on the air temperature and on the low-level wind speeds. A relatively warm air was polynya-generated, moving downstream and flowing over the sea ice, producing an area of lower near-surface pressure. Pressure gradients were changed as a result, modifying near-surface winds. Low-level wind speeds over the polynya area were significantly higher with the polynya present than without it. The impact of the polynya presence was found at a considerable distance from the TNB area and at elevations of up to several hundred meters. The change of the baric field is not the only process which may act on the wind (Dare and Atkinson 2000, Morelli 2011),

downward mixing of higher momentum air is another factor.

Acknowledgments Sandra Morelli is grateful to Prof. Mesinger for his valuable suggestions and for making available the “sloping steps” version of the Eta Model and other routines. The authors are grateful to:

- The Institute of Environmental Physics of the University of Bremen for providing AMSR-E imagery (http://www.iup.uni-bremen.de:8084/amsredata/asi_daygrid_swath/l1a/s6250/)
- The Arctic and Antarctic Research Center, Scripps Institution of Oceanography at the University of California, San Diego, for providing AVHRR imagery
- The European Centre for Medium Range Weather Forecasts (ECMWF) for providing analysis data

We are also thankful to the Serbian Academy of Sciences and Arts for the excellent organization of the symposium and for the kindness of the staff involved.

This study was supported by PNRA, the Italian National Program for Antarctic Research, under the Projects: “Meteo-climatological Observatories in Antarctica,” “Turbulent fluxes at the surface in katabatic wind events on the Nansen Ice Sheet in Terra Nova Bay area,” and “The Terra Nova Bay polynya: its integral and innovative study by using in situ observations, remote sensing, numerical and laboratory experiments.”

References

- Charnock H (1955) Wind stress on a water surface. *Quart J R Meteorol Soc* 81:639–640
- Chen F, Mitchell K, Schaake J, Xue Y, Pan H, Koren V, Duan QY, Ek M, Betts A (1996) Modeling of the land surface evaporation by four schemes and comparison with FIFE observations. *J Geophys Res* 101(D3):7251–7268
- Dare RA., Atkinson BW, 2000: Atmospheric response to spatial variations in concentration and size of polynyas in the southern ocean sea-ice zone. *Boundary-Layer Meteorol.*, 94, 65–88.
- Ferrier BS, Jin Y, Lin Y, Black T, Rogers E, DiMego G (2002) Implementation of a new grid-scale cloud and precipitation scheme in the NCEP Eta Model. In: 19th conference on weather analysis and forecasting/15th conference on numerical weather prediction, San Antonio, TX, American Meteorological Society, pp 280–283
- Gallée H (1997) Air-sea interactions over Terra Nova Bay during winter: simulation with a coupled atmosphere-polynya model. *J Geophys Res* 102(D12):13835–13849
- Georgelin M, Richard E, Petitdidier M, Druilhet A (1994) Impact of subgrid-scale orography parameterization on the simulation of orographic flows. *Mon Weather Rev* 122:1509–1522
- Hauser A, Lythe M, Wendler G (2002) Sea-ice conditions in the Ross Sea during Spring 1996 as observed on SAR and AVHRR Imagery. *Atmosphere-Ocean* 40(3):281–292
- Janjic ZI (1994) The step mountain coordinate model: further developments of the convection, viscous sublayer and turbulence closure schemes. *Mon Weather Rev* 122:927–945

- Janjic ZI (1996) The Mellor Yamada level 2.5 turbulence closure scheme in the NCEP Eta Model. In: Atmospheric and oceanic modelling, WMO, Geneva, CAS/WGNE, pp 4.14–4.15
- Koren V, Schaake J, Mitchell K, Duan QY, Chen F, Baker JM (1999) A parameterization of snowpack and frozen ground intended for NCEP weather and climate models. *J Geophys Res* 104(D16):19569–19584
- Lobocki L (1993) A procedure for the derivation of surface-layer bulk relationship from simplified second-order closure models. *J Appl Meteorol* 32:126–138
- Markus T, Burns A (1995) A method to estimate subpixel-scale coastal polynyas with satellite passive microwave data. *J Geophys Res* 100:4473–4487
- Mesinger F, Lobocki L (1991) Sensitivity to the parameterization of surface fluxes in NMC's eta model. In: 9th conference on numerical weather prediction, Denver, CO, American Meteorological Society, pp 213–216
- Mesinger F, Janjic ZI, Nickovic S, Gavrilo D, Deaven DG (1988) The step-mountain coordinate: model description and performance for cases of Alpine lee cyclogenesis and for a case of an Appalachian redevelopment. *Mon Weather Rev* 116:1493–1518
- Mesinger F, Jovic D, Chou SC, Gomes JL, Bustamante JF (2006) Wind forecast around the Andes using the sloping discretization of the Eta coordinate. CDROM: Proceedings of 8 ICSHMO, Foz do Iguacu, Brazil, 24–28 April 2006, 1837–1848. <http://mtc-m15.sid.inpe.br/col/sid.inpe.br/mtc-m15@80/2006/07.06.14.48/doc/wind%20forecast.chou.pdf>
- Mesinger F, Chou SC, Gomes JL, Jovic D, Bastos P, Bustamante JF, Lazic L, Lyra AA, Morelli S, Ristic I, Veljovic K (2012) An upgraded version of the Eta model. *Meteorol Atmos Phys* (in press) DOI 10.1007/s00703-012-0182-z
- Morelli S (2011) A modeling study of an Antarctica polynya event. *Meteorol Atmos Phys* 114:67–81 DOI 10.1007/s00703-011-0157-5.
- Parmiggiani F (2006) Fluctuations of Terra Nova Bay polynya as observed by active (ASAR) and passive (AMSR-E) microwave radiometers. *Int J Rem Sens* 27:2459–2467
- Paulson CA (1970) The mathematical representation of wind speed and temperature profiles in the unstable atmospheric surface layer. *J Appl Meteorol* 9:857–861
- Pease CH (1987) The size of wind-driven coastal polynyas. *J Geophys Res* 92:7049–7059
- Pyle ME, Djurdjevic V, Mesinger F (2008) A guide to the Eta model. In: Workshop on design and use of regional weather prediction models. The Abdus Salam International Centre for Theoretical Physics, Trieste, Italy, 29 Sept–7 Oct 2008
- Zilitinkevich SS (1995) Non-local turbulent transport: pollution dispersion aspects of coherent structure of convective flows. In: Power H, Moussiopoulos N, Brebbia CA (eds) Air pollution III – Vol 1. Air pollution theory and simulation. Computational Mechanics, Boston, pp 53–60

Some Indicators of the Present and Future Climate of Serbia According to the SRES-A1B Scenario

Aleksandra Kržič, Ivana Tošić, Borivoj Rajković,
and Vladimir Djurdjević

Abstract

According to the last IPCC report, there are several indications that the area of Southeastern Europe might experience large climate changes due to the increase of the concentration of greenhouse gases. These include results of several regional climate studies. In order to objectively study the climate change, precipitation and temperature indices can be used. Climate indices can be calculated either from the local observations of temperature and precipitation or from climate simulations. In this study, we use the results of dynamical downscaling of global simulations obtained by the atmosphere–ocean global circulation model SINTEX-G (AOGCM SX-G/INGV) using a regional climate model, the EBU-POM. The EBU-POM is the combination of the Eta/NCEP as the atmospheric component and Princeton Ocean Model (POM) as the ocean component. Global simulations were done for the very long period 1771–2100, while downscaling was done for the 1961–1990 and 2071–2100 periods according to the SRES-A1B scenario.

Climate indices of two groups are considered. The first group is related to temperature: frost days, growing season length, maximum number of consecutive frost days, and number of tropical days. The second group is related to precipitation: number of days with precipitation ≥ 10 mm/day, maximum number of consecutive dry days, and simple daily intensity index. The analyses of these climate indices are done for all seasons. Results are presented separately for northern (plains) and southern (mountainous) regions of Serbia.

According to the SRES-A1B scenario, the results from the regional model show an overall increase in the surface air temperature of about 2°C and decrease in precipitation of about 6 mm (~10%) per year over Serbia. The results indicate that number of tropical days will increase, while total number of frost days and heavy rain days will decrease in the future. The results also indicate shorter duration of frost periods and longer duration of dry and vegetation periods over the Serbian region.

Introduction

The latest IPCC report (Meehl et al. 2007) as well as several regional climate studies (Bartholy and Pongrácz 2007; Khon et al. 2007) provide numerous

A. Kržič (✉)
Southeast European Virtual Climate Change Center, RHMSS,
Kneza Viseslava 66, 11000 Belgrade, Serbia
e-mail: aleksandra.krzic@hidmet.gov.rs

indications that the area of Southeastern Europe might experience large climate changes as a result of the increase of the greenhouse gases (GHG). Impacts of climate change are felt more strongly through changes in the extremes than in the means. One of the first global studies on extreme temperature and precipitation was done by Frich et al. (2002). This work has been updated by Alexander et al. (2006). The analysis of climatic changes over a region for the present climate was done by Klein Tank and Können (2003), Moberg et al. (2006), and Kiktev et al. (2003) for observed data. The development of climate models enabled simulation of present and future climate under the IPCC emission scenarios. Déqué (2007) used the Météo-France atmospheric model to simulate present climate (1961–1990) and a possible future climate (2071–2100) through two ensembles of three 30-year numerical experiments. He found that the maximum number of consecutive dry days per summer over Corsica will likely be more than 50 days. Also, he pointed out that number of winter days with precipitation above 10 mm will increase in the northern half of France. Goubanova and Li (2007) analyzed potential future changes of the extreme temperature and precipitation around the Mediterranean region for two future periods, 2030–2059 and 2070–2099, with respect to the control period 1970–1999, under the A2 emission scenario. According to their study, the Mediterranean basin will experience a warmer climate with less total precipitation but more intense precipitation events. Oikonomou et al. (2008), in their study, attempted to estimate future potential changes in duration of extreme dry and wet spells and rainfall intensity in Eastern Mediterranean, for the period 2070–2100, as derived from the results of the regional model HadRM3. They found a general tendency towards drier Eastern Mediterranean, with reduced rainfall intensity. The main objective of the study of Tolika et al. (2008) was the estimation of the future changes of the extreme temperature and precipitation conditions over Greece.

In this study, the Serbian region was considered. Serbia is located in the western Balkan, covering roughly the window from 42 to 46°N and 19 to 23°E. This study will present the evolution of some of the severe climate indices calculated for the end of the twentieth and twenty-first centuries for the Serbian region, according to the A1B scenario.

Methods

Global ocean–atmosphere coupled models are certainly the best tool that we have to make climate change projections. Due to their coarse spatial resolution, however, they can be hardly used in impact-oriented studies for which a downscaling procedure is necessary. A widely used approach to do it is to use a high-resolution limited-area model nested into a global model. This approach allows implementation of detailed physical parameterizations in regional climate models and their higher resolution to achieve a better simulation of local weather and climate events.

The Global Model

The global modeling data employed in this work are time series obtained from climate simulations carried out with the SINTEX-G (SX-G) coupled atmosphere–ocean general circulation model (AOGCM), which is a descendent of the SINTEX and SINTEX-F models (Gualdi et al. 2003a, b; Guilyardi et al. 2003). The ocean model component is the so-called reference version 8.2 of the Ocean Parallelize (OPA) with the ORCA2 configuration (Madec et al. 1998). For more details about the ocean model and its performance, readers are referred also to the web site <http://www.lodyc.jussieu.fr/opa/>. The evolution of the sea ice is described by LIM (Louvain-la-Neuve sea ice model). The atmospheric model component is the latest version of ECHAM-4. The horizontal resolution used was T106, corresponding to a Gaussian grid of about $1.125^\circ \times 1.125^\circ$. A hybrid sigma-pressure vertical coordinate was used with 19 vertical levels. A detailed discussion of the model physics and performances can be found in Roeckner et al. (1996).

The Regional Model

The EBU-POM is a two-way coupled regional climate model, with Eta/NCEP limited-area model as its atmospheric part and Princeton Ocean Model as its ocean part. Both models have been extensively evaluated. The atmospheric component is a limited-area forecast

model defined on the E-grid and with eta vertical coordinates (Mesinger et al. 1988). The original radiation scheme (GFDL radiation scheme of Fels and Schwarzkopf (1975)) was replaced by the scheme of the Goddard Climate and Radiation Branch as done earlier by Pérez et al. (2006), which enabled changes of GHG concentrations during experiment. Surface turbulent fluxes, important for atmosphere–ocean interaction, are calculated by model physics package (Janjić 1990). The center of the atmospheric model is at 16°E, 42.5°N. In the vertical direction, the model was used with 32 layers, with the bottom layer depth of 20 m and the top at 10 hPa. In our runs, concentrations of the greenhouse gases were prescribed following the A1B scenario, which means changing of the CO₂ amount from the present value to roughly 2 × CO₂. The ocean component is the Princeton Ocean Model (POM), a three-dimensional, primitive equation, numerical model, developed by Blumberg and Mellor (1987). A comprehensive description of POM can be found in Mellor (2003).

An important part of every coupled model is the method of exchange of data between its two components. Due to very different geometries of the two components of the model, special care was taken in

design of this coupling module (Djordjevic and Rajkovic 2008). Exchanges of atmosphere fluxes and sea surface temperature (SST) between the two components are done interactively, during integration, using specially designed coupler software. In every physical time step of the atmospheric model (360 s), surface fluxes, needed for the ocean forcing, are transferred to the ocean model grid, and after that, the SST is transferred back onto the atmosphere model grid, serving as the new lower boundary condition.

In this study, the EBU-POM domain used (Fig. 1) covers a Mediterranean/South European region. The atmospheric model horizontal resolution was 0.25°, and the ocean model horizontal resolution was 0.2°.

Data

The simulated climate of the Mediterranean/South European region and the main features of its variability are evaluated comparing the model results with observational data sets. Specifically, we use data from the NCEP reanalysis and the observed precipitation and air surface temperature from the Climate Research Unit (CRU) data set (Jones et al.

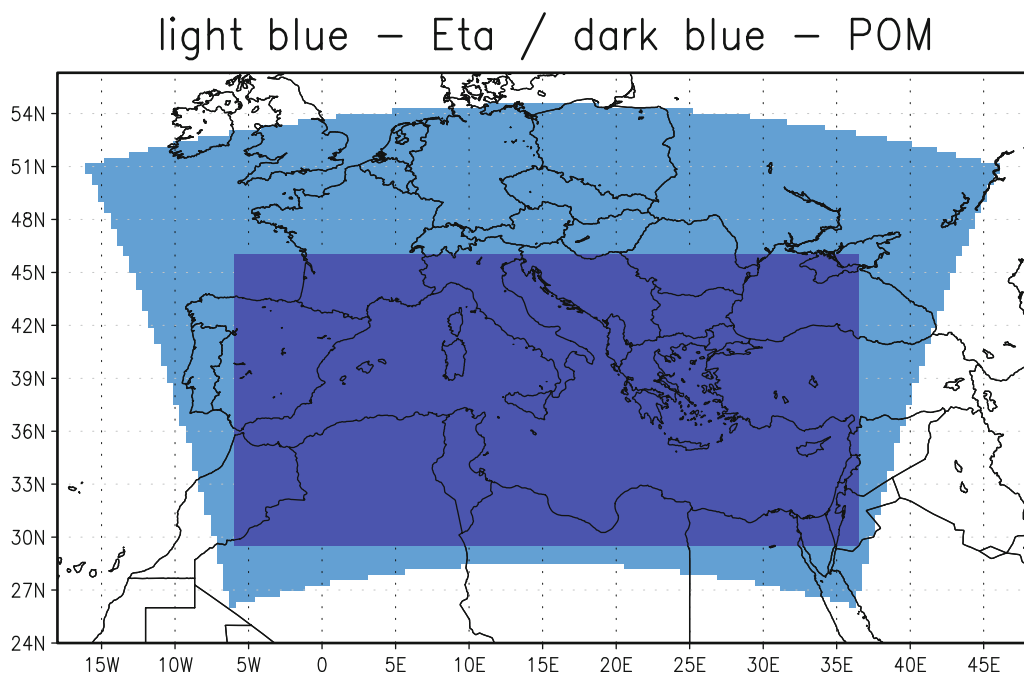


Fig. 1 Domain of the EBU-POM coupled regional climate model

2006). The daily precipitation and temperature time series from 17 meteorological stations (Table 1) evenly distributed throughout the study region, for the period 1961–1990, were employed for the calculation of the indices for the Serbian region. All the data series were complete and without any missing values. Technical and quality controls of these measurements were made by the National Meteorological Service of Serbia.

Table 1 List of the stations used with their latitudes, longitudes, and altitudes

Stations	Latitude	Longitude	Altitude (m)
Palic	46°06'	19°46'	102
Kikinda	45°51'	20°28'	81
Sombor	45°47'	19°05'	88
Novi Sad	45°20'	19°51'	84
Veliko Gradiste	44°45'	21°31'	82
Loznica	44°33'	19°14'	121
Smederevska Palanka	44°22'	20°57'	122
Negotin	44°14'	22°33'	42
Kragujevac	44°02'	20°56'	185
Cuprija	43°56'	21°23'	123
Zajecar	43°53'	22°17'	144
Pozega	43°50'	20°02'	310
Zlatibor	43°44'	19°43'	1,028
Nis	43°20'	21°54'	201
Kursumlija	43°08'	21°18'	414
Dimitrovgrad	43°01'	22°45'	450
Vranje	42°29'	21°54'	432

In order to better describe the spatial features of the estimated changes, the region was divided into two subregions that we named North Serbia (NS) and South Serbia (SS), respectively. Our motivation for this was that mountains dominate in the south and lowlands characterize the north (north of the rivers Sava and Danube).

Indices

In order to study the climate change, precipitation and temperature indices can be used (Bartholy and Pongrácz 2007). The indices are recommended by the joint Working Group on Climate Change Detection of the World Meteorological Organization-Commission for Climatology (WMO-CCL) and the research program on Climate Variability and Predictability (CLIVAR), as well as by the European research project STARDEX (Peterson et al. 2001).

In our study, we used the indices presented in Table 2. These indices were selected in order to examine and simulate the changes of the severe weather and climate conditions over Serbia under the SRES-A1B scenario. The indices are calculated for the present period 1961–1990 and for the future period 2071–2100 for all seasons, and for both station and grid point values averaged over the two subregions of the country. Also, the seasonal differences between future averages and corresponding present values of indices are calculated, as well as the difference between the indices based on simulated and observed data.

Table 2 Extreme temperature and precipitation indices

Indicators	Definition	Units
Based on temperature		
Td—total number of tropical days	Days with absolute maximum temperature above 30°C	Days
Fd—total number of frost days	Days with absolute minimum temperature below 0°C	Days
CFD—maximum number of consecutive frost days	Maximum number of consecutive days with absolute minimum temperature below 0°C	Days
GSL—growing season length	Number of days between the first occurrence of at least 6 consecutive days with daily mean temperature above 5°C and the first occurrence after 1 July of at least 6 consecutive days with daily mean temperature below 5°C	Days
Based on precipitation		
R10—heavy precipitation days	Number of days with precipitation ≥ 10 mm/day	Days
CDD—maximum number of consecutive dry days	Maximum number of consecutive days with daily precipitation less than 1 mm	Days
SDII—simple daily intensity index	Period total/no. of days with precipitation ≥ 1 mm	mm/day

Results

Simulation

The first step in establishing the quality of a climate model is the comparison of its simulations with observed climatology. Evaluation of the EBU-POM for the Mediterranean/South European region was done using the CRU data (Djurdjevic and Rajkovic 2010). In Figs. 2 and 3, seasonal means over the period 1961–1990 for the winter season, December–January–February (DJF), and summer season, June–July–August (JJA) from the EBU-POM and CRU data set of the 2 m temperature and precipitation are presented, respectively. Annual bias for temperature is 0.64, mean absolute error (MAE)

is 1.63, and root mean square error (RMSE) is 1.87. There is a general agreement between the EBU-POM and CRU DJF 2 m temperature except in the northeast part where the EBU-POM has larger temperature (Fig. 2). Over Balkans, agreement is relatively good having in mind the differences in the horizontal resolutions. The summer results show clearly the excessive warming in the eastern part of the domain. Positions of the extreme precipitation over Alps and on the Eastern Adriatic coast are captured, but the values are larger in the EBU-POM simulations than the observed in DJF (Fig. 3). For the summer season, we get reduction of the precipitation through the integration region, which is consistent with the higher 2 m temperatures earlier documented.

We next present an analysis of the EBU-POM values for the Serbian region. Model results are

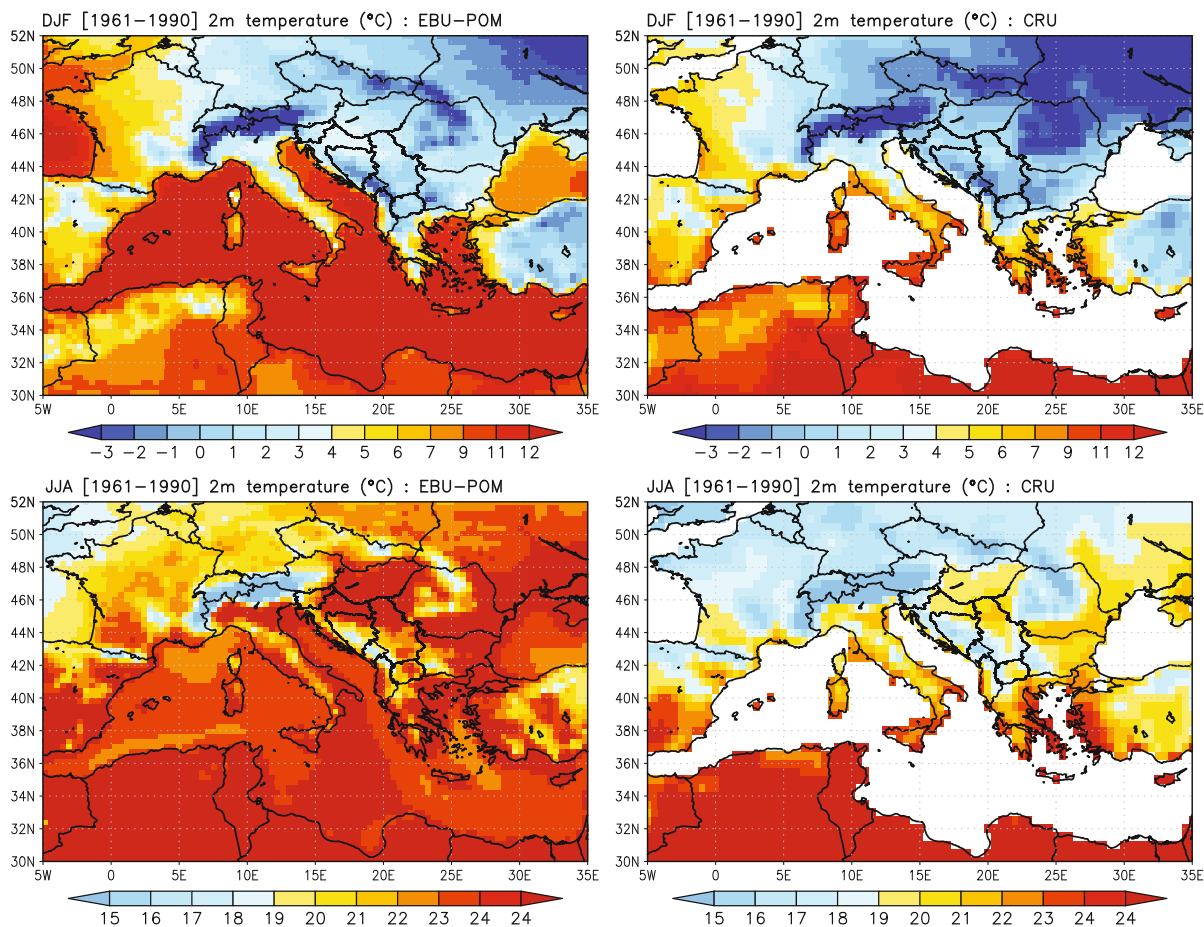


Fig. 2 Seasonal means of air surface temperature (°C) for DJF (*upper panels*) and for JJA (*lower panels*) season from the EBU-POM (*left*) and CRU data set (*right*) (Djurdjevic and Rajkovic 2010)

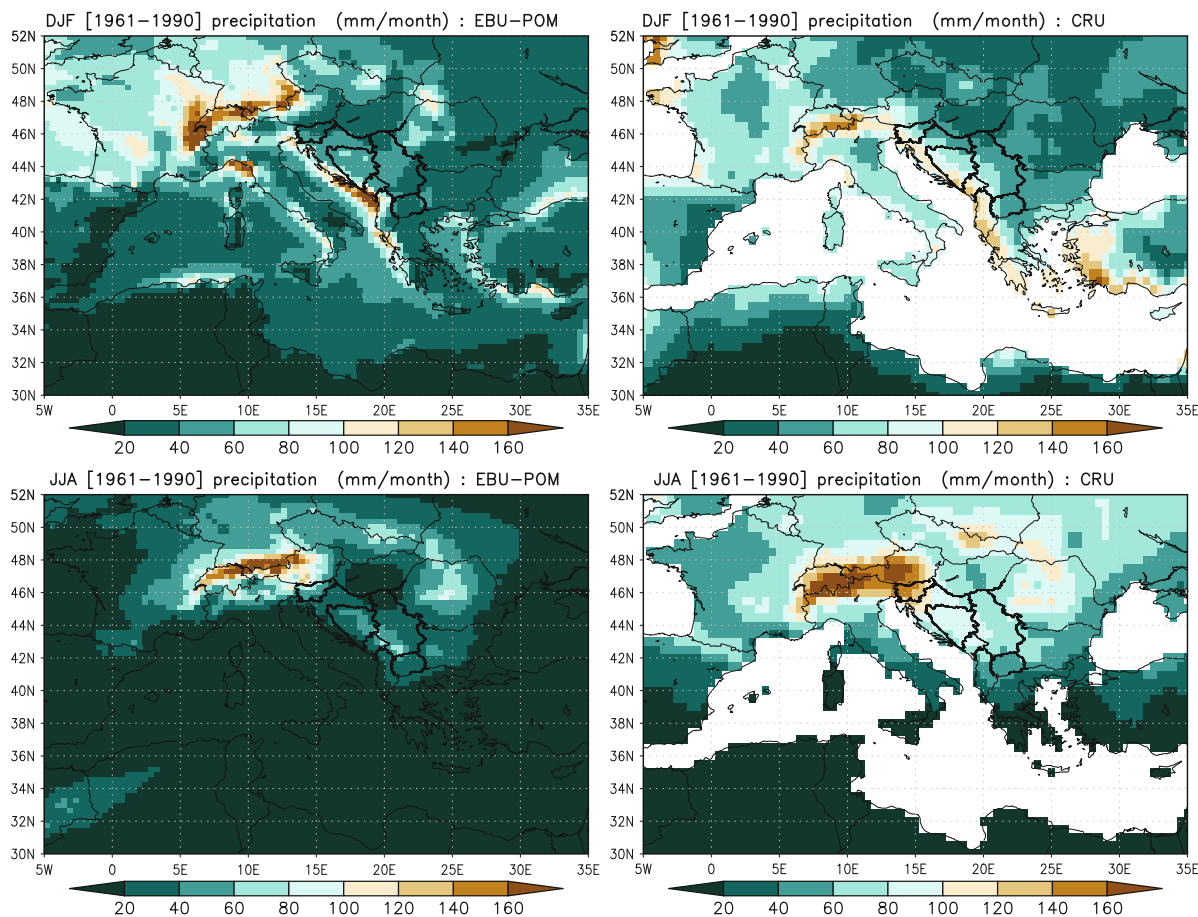


Fig. 3 Same as in Fig. 2 but for accumulated precipitation (mm/month) (Djordjevic and Rajkovic 2010)

compared against the observed data at 17 stations. Spatial distribution of the mean seasonal 2 m temperature and precipitation over Serbia during the period 1961–1990 is shown in Figs. 4 and 5, respectively. The largest differences in temperatures between the model and the observations are seen to occur in summer, particularly in the north, while the smallest differences are seen in autumn. The precipitation during winter is in a very good agreement with observations. In other seasons, the model gives smaller amounts of precipitation than what is observed.

Climate Indices

The Reference Period (1961–1990)

Relative differences (in percent of the observed values, only for Td in 1/10 of percent) of the indices between the EBU-POM results and observations are

presented in Fig. 6 for the NS and SS subregions and for the reference period 1961–1990. It can be noted that the model overestimates the total number of tropical days (Td) in NS; overestimation is more than 150%. In SS, this overestimation is not so pronounced. For autumn in SS, the model even underestimates Td by 50%. Differences between NS and SS are also evident.

The model underestimates the number of frost days (Fd) in both regions and all frost-affected seasons. It can be observed that there are more frost days in SS than in the north, especially in winter. The model well presents consecutive frost days (CFD) for spring and autumn for South Serbia. There is an underestimation in CFD, with less than 65% in the north and during winter in SS.

Precipitation greater or equal to 10 mm (R10) is underestimated for both subregions. Simulated values are more than 80% smaller than observed during

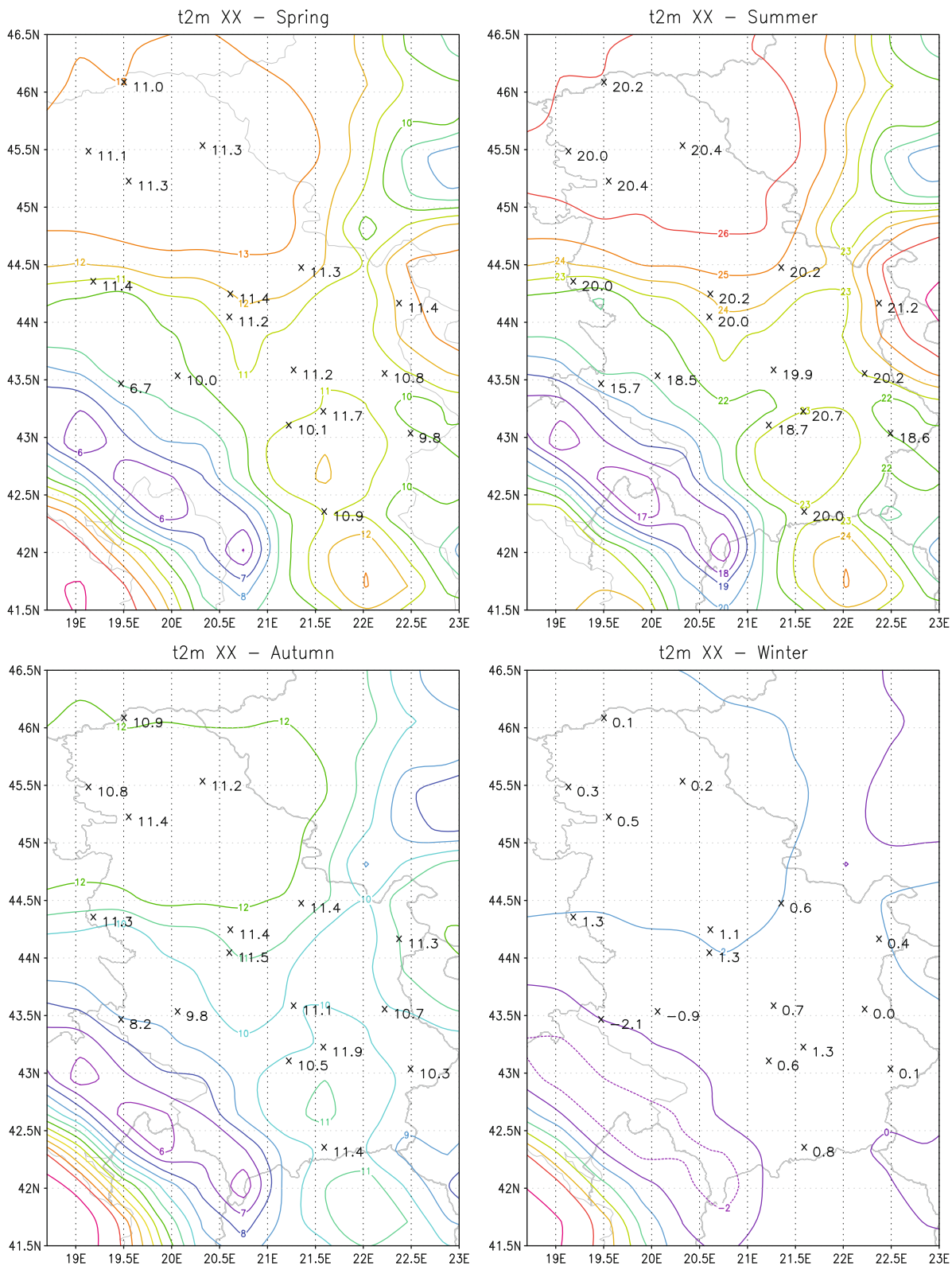


Fig. 4 Spatial distribution of the mean seasonal temperature (°C) over Serbia (1961–1990). Isolines present the model values. Numbers show the observations

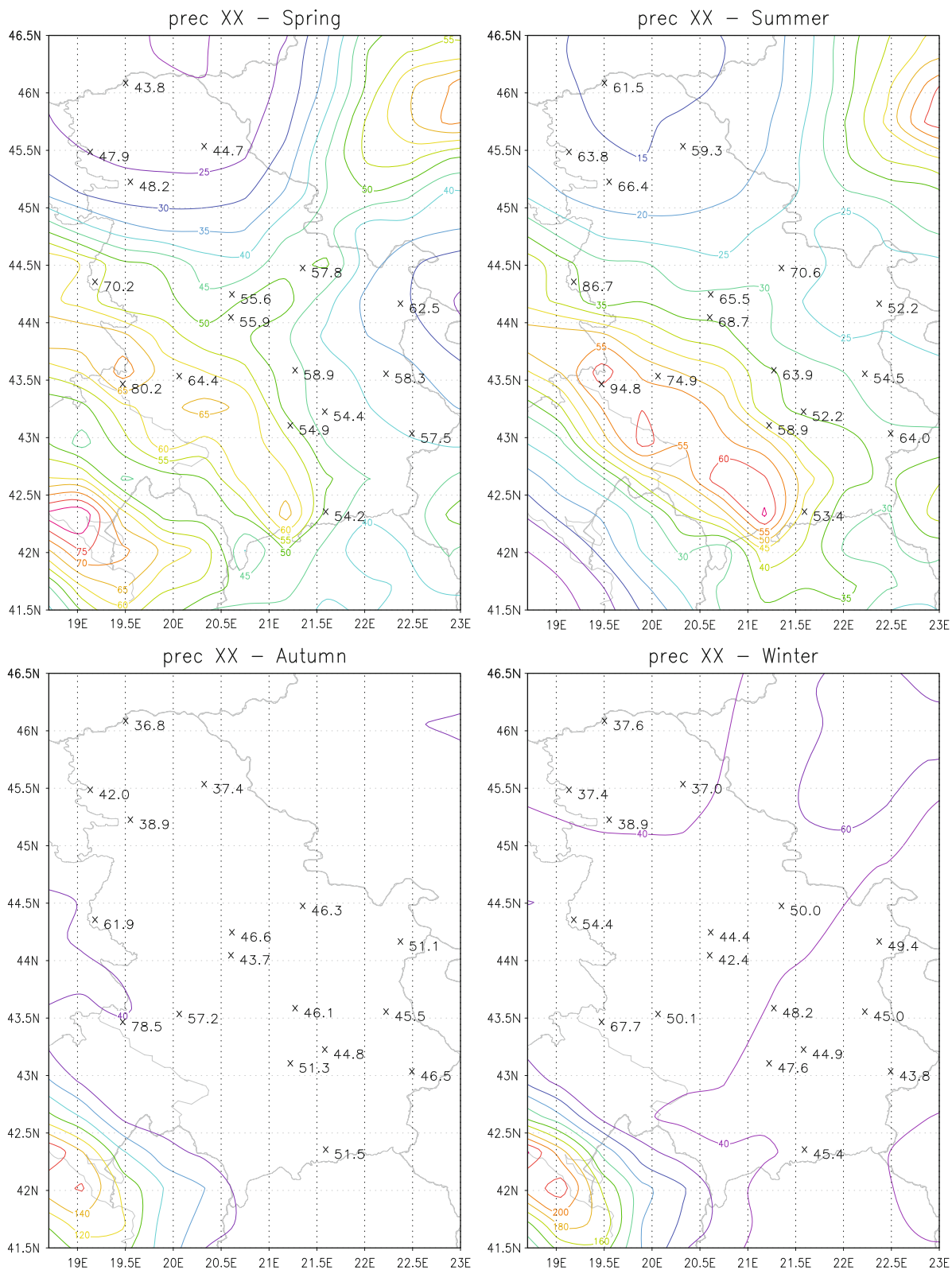


Fig. 5 Spatial distribution of the mean seasonal precipitation (mm/season) over Serbia (1961–1990). Isolines present the model values. Numbers show the observations

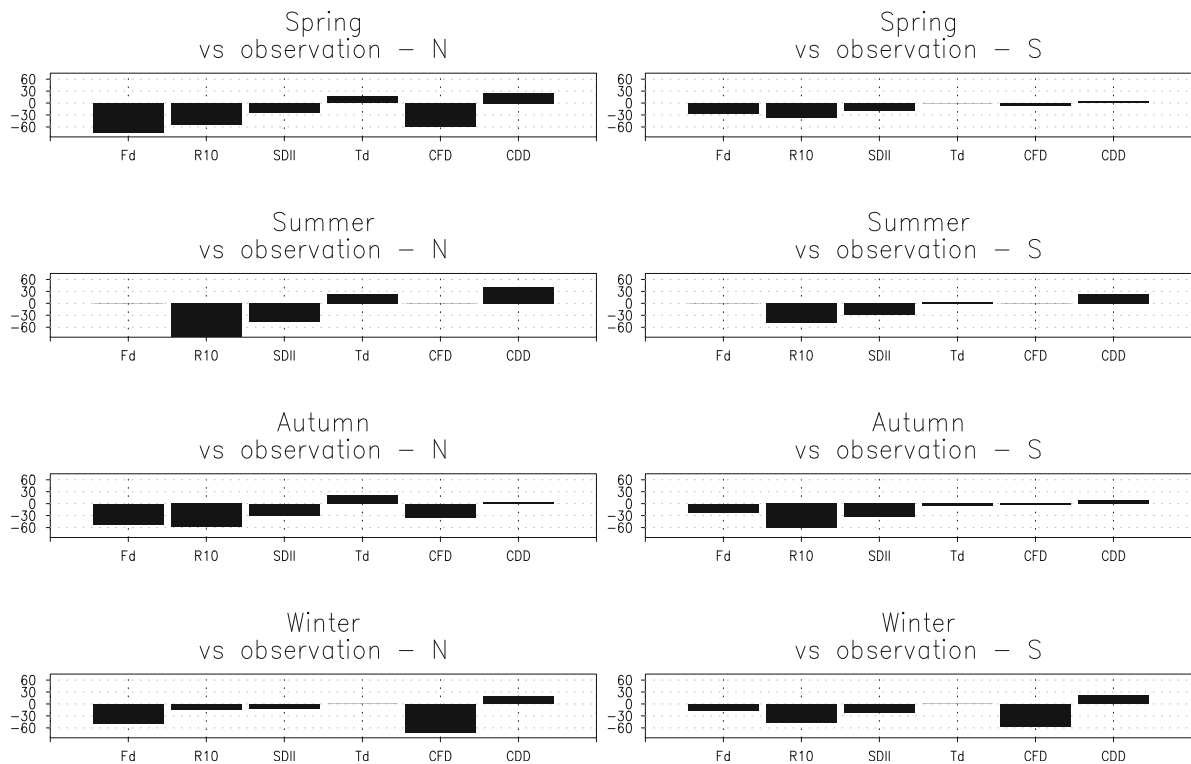


Fig. 6 Differences of the indices (percent of observed values, except for Td, which is shown in 1/10 of percent) between the EBU-POM results and observations for the 1961–1990 period

summer in NS. Better agreement between model results of heavy rains and observations is obtained for SS than for NS.

The model is seen to have performed well in simulating simple daily intensity index (SDII) for spring in SS and for winter in both subregions. In other cases, the simulation resulted in less rain on wet days than observed. Distinction of SDII between model and observations is the largest during the summer period in NS and during autumn in SS (~30%).

It can be noted that the model has performed well in simulating CDD. There is an overestimation during summer in NS, which is in agreement with comments already made about R10, SDII, and Td. Autumn is the season with the longest dry periods according to both the model and observations (not shown).

The growing season length (GSL) is very well simulated (Fig. 7, left). Better agreement is achieved for the SS than for the NS. In SS, the difference between the modeled and the observed data is less than 5%, while in NS, the difference is 30% only at

the beginning of the growing season. The model shows an earlier beginning for both subregions of Serbia than observed and a longer duration of the vegetation period for the NS while it shows a shorter GSL for the SS.

The Future Period (2071–2100)

Relative differences of the indices between the EBU-POM results for the period 2071–2100 and the reference period are presented in Fig. 8 for the NS and SS subregions. An increase in the Td is projected, but it is not so pronounced in the north during summer and in the south during spring. Warming is intensive during spring in NS and during autumn in SS.

A smaller number of CFD is projected for all seasons. A pronounced decrease is expected in Fd. A decrease of Fd and CFD of more than 60% is observed in NS during spring, and South Serbia is projected to have more frost days than the north, as in the reference period. According to the results of Bartholy et al. (2008), the largest warming is expected

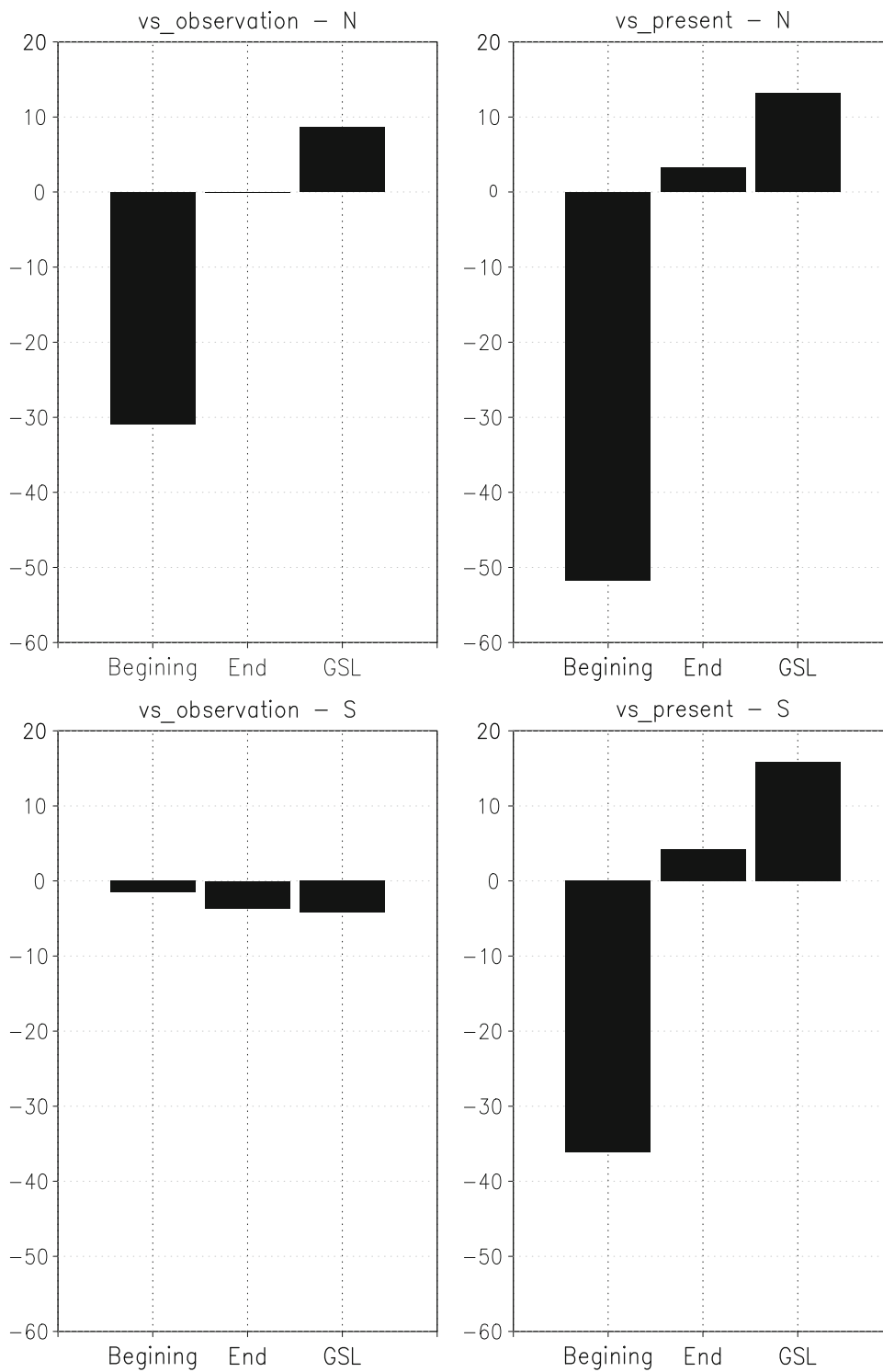


Fig. 7 Differences of the GSL (%) between the EBU-POM results and observations for the 1961–1990 period (*left*) and between the time period 2071–2100 and the reference period 1961–1990 (*right*)

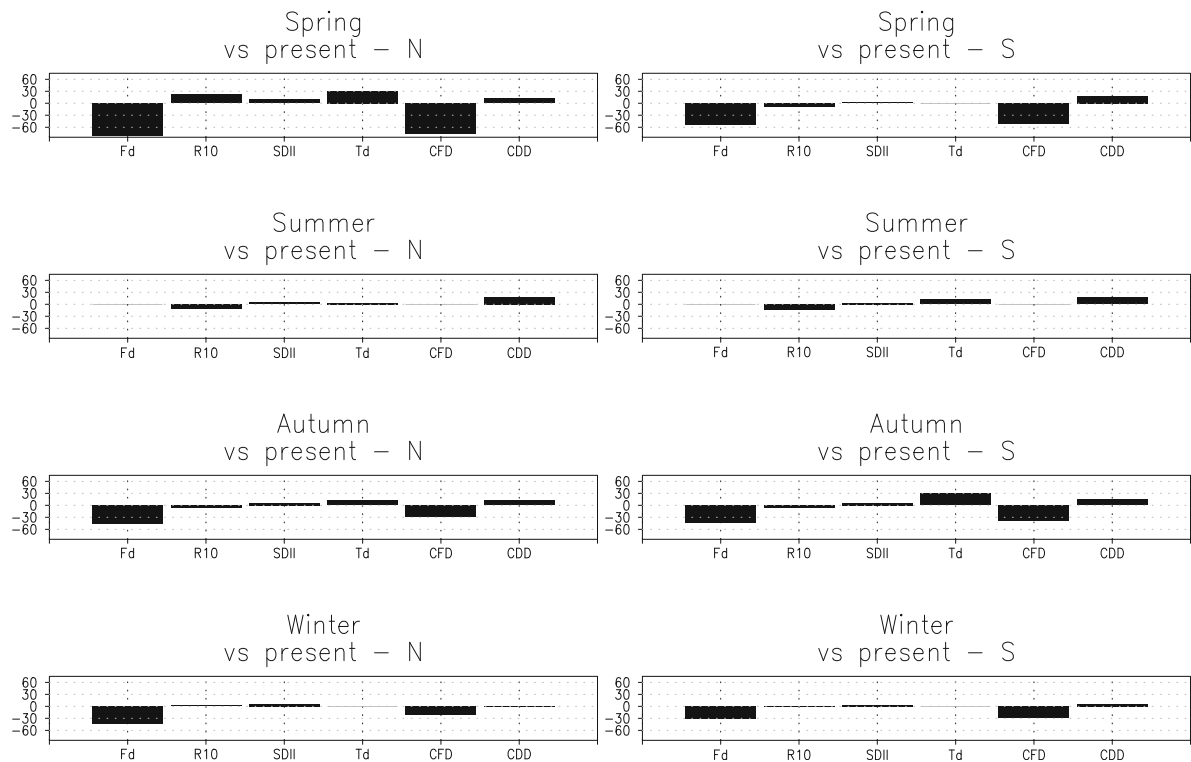


Fig. 8 Differences of the indices (%) between the time period (2071–2100) and the reference period (1961–1990)

in summer over the Carpathian Basin (partly the northern part of Serbia). They found that negative temperature extremes will decrease, while warm extremes will tend to increase significantly.

According to the EBU-POM results, the duration of dry periods will become longer than in the reference years and will be somewhat longer in the south than in the north. The projections indicate a tendency of CDD to increase in the period 2071–2100 during autumn and winter (not shown). Chauvin and Denvil (2007) found longer dry events in summer, while our results show longer duration of dry periods for all seasons. Analysis of Oikonomou et al. (2008) showed a general tendency towards longer dry spells and accordingly shorter wet spells for all seasons, except autumn when the opposite behavior is predicted. Tolika et al. (2008) pointed out that the duration of the maximum dry spells will increase both on an annual and seasonal basis over the Greek region.

Also, there is a projected growth in R10 (up to 30%) during spring in the north. In other seasons and

in the south, a small decrease is obtained, less than 15% (Fig. 8).

In all seasons and for both subregions of Serbia, a small increase of SDII is shown (Fig. 8). The increase is most pronounced in autumn. But even with this increase, it does not reach the observed values of the reference period (Fig. 6).

According to the model projections (Fig. 7, right), vegetation period will start earlier and the end will come later, with this tendency more pronounced in the south. Thus, the vegetation period will be extended, as expected. Frich et al. (2002) already showed a lengthening of the thermal growing season (GSL) throughout major parts of the Northern Hemisphere mid-latitudes during the second half of the twentieth century.

Conclusions

In this chapter, we analyzed potential future changes of the climate indices at the regional scale as observed and simulated by the regional EBU-POM model. As an illustration of the use of

these indices, four temperature- and three precipitation-related indices were presented. Although there are some differences in the reproduction of the present climate, the model is quite close to observations, except for the summer when it is warm. Probably, this is due to the selected soil and vegetation types. With regard to model-simulated climate indices for the reference period, we found that:

- The model overestimates the total number of tropical days and underestimates the number of frost days.
- South Serbia is obtained to be colder than North Serbia (smaller number of tropical days and larger number of frost days), which is consistent with the observed data.
- The model does well in presenting consecutive frost days for South Serbia during spring and autumn, and consecutive dry days.
- The number of heavy rain days and simple daily intensity index are underestimated.
- The best agreement between the model and the observations is for the beginning, the end, and the duration of vegetation period for South Serbia and for the end for the North Serbia.

The results from the regional model for the end of the twenty-first century, according to the SRES-A1B scenario, show an overall increase in the surface air temperature of about 2°C and decrease in precipitation of about 6 mm (~10%) per year over Serbia. The largest warming of 3.6°C and decrease of precipitation up to 12 mm per season is projected for summer. The results of the EBU-POM model indicate that the number of tropical days will increase, while the total number of frost days and heavy rain days (except in the north during spring) will decrease. Consequently, shorter duration of frost periods and longer duration of dry and vegetation periods are expected.

The results presented for temperature- and precipitation-related indices in this chapter are in general agreement with results of previous studies.

References

- Alexander LV, Zhang X, Peterson TC, Caesar J, Gleason B, Klein Tank A, Haylock M, Collins D, Trewin B, Rahimzadeh F, Tagipour A, Ambenje P, Rupa Kumar K, Revadekar J, Griffiths G, Vincent L, Stephenson D, Burn J, Aguilar E, Brunet M, Taylor M, New M, Zhai P, Rusticucci M, Vazquez-Aguirre JL (2006) Global observed changes in daily climate extremes of temperature and precipitation. *J Geophys Res* 111:D05109. doi:10.1029/2005JD006290
- Bartholy J, Pongrácz R (2007) Regional analysis of extreme temperature and precipitation indices for the Carpathian Basin from 1946 to 2001. *Global Planet Change* 57:83–95
- Bartholy J, Pongrácz R, Gelyó G, Szabó P (2008) Analysis of expected climate change in the Carpathian Basin using the PRUDENCE results. *Időjárás* 112:249–264
- Blumberg A, Mellor G (1987) A description of a three-dimensional coastal ocean circulation model. In: Heaps N (ed) *Three-dimensional coastal ocean models*. American Geophysical Union, Washington, DC, pp 1–16
- Chauvin F, Denvil S (2007) Changes in severe indices as simulated by two French coupled global climate models. *Global Planet Change* 57:96–117
- Déqué M (2007) Frequency of precipitation and temperature extremes over France in an anthropogenic scenario: model results and statistical correction according to observed values. *Global Planet Change* 57:16–26
- Djurđević V, Rajković B (2008) Verification of a coupled atmosphere-ocean model using satellite observations over the Adriatic Sea. *Ann Geophys* 26:1935–1954
- Djurđević V, Rajković B (2010) Development of the EBU-POM coupled regional climate model and results from climate change experiments. In: Mihailović DT, Lalić B (eds) *Advances in environmental modeling and measurements*. Nova, New York, pp 23–32
- Fels SB, Schwarzkopf MD (1975) The simplified exchange approximation: a new method for radiative transfer calculations. *J Atmos Sci* 32:1475–1488
- Frich P, Alexander LV, Della-Marta P, Gleason B, Haylock M, Klein Tank AMG, Peterson T (2002) Observed coherent changes in climatic extremes during the second half of the twentieth century. *Clim Res* 19:193–212
- Goubanova K, Li L (2007) Extremes in temperature and precipitation around the Mediterranean basin in an ensemble of future climate scenario simulations. *Global Planet Change* 57:27–42
- Gualdi S, Navarra A, Guilyardi E, Delecluse P (2003a) Assessment of the Tropical Indo-Pacific Climate in the SINTEX CGCM. *Ann Geophys* 46:1–26
- Gualdi S, Guilyardi E, Navarra A, Masina S (2003b) The Inter-annual Variability in the Tropical Indian Ocean as Simulated by a CGCM. *Clim Dyn* 20:567–582
- Guilyardi E, Delecluse P, Gualdi S, Navarra A (2003) Mechanisms for ENSO phase change in a coupled GCM. *J Clim* 16:1141–1158
- Janjić ZI (1990) Physical package for step-mountain, Eta coordinate model. *Mon Weather Rev* 118:1429–1443
- Jones PD, Parker DE, Osborn TJ, Briffa KR (2006) Global and hemispheric temperature anomalies – land and marine instrumental records. In: *Trends: a compendium of data on global change*. Carbon Dioxide Information Analysis Center, Oak Ridge National Laboratory, U.S. Department of Energy, Oak Ridge, TN. doi:10.3334/CDIAC/cli.002
- Khon CV, Mokhov II, Roeckner E, Semenov AV (2007) Regional changes of precipitation characteristics in Northern Eurasia from simulations with global climate model. *Global Planet Change* 57:118–123

- Kiktev D, Sexton D, Alexander L, Folland K (2003) Comparison of modeled and observed trends in indices of daily climate extremes. *J Clim* 16:3560–3571
- Klein Tank AMG, Können GP (2003) Trends indices of daily temperature and precipitation extremes in Europe, 1946–99. *J Clim* 16:3665–3680
- Madec G, Delecluse P, Imbard M, Levy C (1998) OPA 8.1 Ocean General Circulation Model reference manual. Technical Report, LODYC/IPSL, Note 11, Paris, France, 91 pp
- Meehl GA et al (2007) Global climate projections. In: Solomon S et al (eds) *Climate Change 2007: the physical science basis*. Cambridge University Press, Cambridge, pp 747–845
- Mellor GL (2003) Users guide for a three-dimensional, primitive equation, numerical ocean model. Program in Atmospheric and Oceanic Sciences, Princeton University, Princeton, 53 pp
- Mesinger F, Janjić ZI, Ničković S, Gavrilov D, Deaven D (1988) The step mountain coordinate: model description and performance for cases of Alpine lee cyclogenesis and for a case of an Appalachian redevelopment. *Mon Weather Rev* 116:1493–1518
- Moberg A, Jones P, Lister D, Walther A, Brunet A et al (2006) Indices for daily temperature and precipitation extremes in Europe analyzed for the period 1901–2000. *J Geophys Res* 111:D22106
- Oikonomou Ch, Flocas HA, Hatzaki M, Asimakopoulos DN, Giannakopoulos C (2008) Future changes in the occurrence of extreme precipitation events in eastern Mediterranean. *Global NEST J* 10:255–262
- Pérez C, Nickovic S, Pejanovic G, Baldasano JM, Özsoy E (2006) Interactive dust-radiation modeling: a step to improve weather forecasts. *J Geophys Res* 111:D16206. doi:[10.1029/2005JD006717](https://doi.org/10.1029/2005JD006717)
- Peterson T, Folland C, Gruza G, Hogg W, Mokssit A, Plummer N (2001) Report on the activities of the working group on climate change detection and related rapporteurs 1998–2001. WMO Rep. WCDMP 47, WMO – TD 1071, Geneva, 143 pp
- Roeckner E, Arpe K, Bengtsson L, Christoph M, Claussen M, Dümenil L, Esch M, Giorgetta M, Schlese U, Schulzweida U (1996) The atmospheric general circulation model ECHAM-4: model description and simulation of present-day climate. Max-Planck-Institute for Meteorology, Report No. 218, 90 pp
- Tolika K, Anagnostopoulou C, Maheras P, Vafiadis M (2008) Simulation of future changes in extreme rainfall and temperature conditions over the Greek area: a comparison of two statistical downscaling approaches. *Global Planet Change* 63:132–151

Index

A

A1B scenario, 228–230, 238
Adh mar, J., 110–113, 117, 124
Adjoint compiler, 94, 103
Adjoint method, 94, 95, 98, 99, 101–103
Adjoint model, 94, 95
Aerosol indirect effect, 30
Aerosols, 6–8, 25, 27–31, 36, 42
Air temperature, 167, 177
Albedo, 22, 24, 26–28, 30–34, 36, 37, 39, 42, 43
Alien, 152–153
All fast-feedback, 28, 30, 31, 36
Alpine Valleys, 108
Amplifying feedbacks (carbon), 22, 25, 26, 44
AMSR-E image, 216, 224
Annual mean, 83–86
Antarctica, 110
Aphelion, 109, 112–116, 124
Assessment, 22, 25, 27, 35, 36, 39, 41
Astronomical forcing, 58, 62
Astronomical parameters, 108, 112, 114, 115, 117, 120–122, 124
Astronomical precession, 110
Astronomical theory, 107–124
Astronomical theory of climate change, 133
Atmospheric CO₂, 22, 24, 28, 38
Atmospheric CO₂ concentration, 96, 98, 99, 103
Automatic differentiation, 94, 103
Automatic weather station (AWS), 221
AVHRR image, 218–220, 224

B

Background term, 102, 103
Bayesian approach, 94, 103
Boreal summer, 62, 63
Boreal winter, 62, 63
Boundary forcing (vs. feedback), 27, 28, 30, 31, 34

C

Calculation, 28, 29, 33, 36
Calibration, 94
Caloric season, 116, 118
Carbonate-silicate cycle, 143, 144

Carbon cycle, 7, 8

Carbon cycle (source & sink), 22, 24

Carbon dioxide (CO₂), 4, 5, 7, 8, 10, 12, 13, 16, 22, 24–30, 33, 34, 36, 38, 40, 42–44, 110, 114, 142, 143, 150–151

Catastrophic floods, 108, 109

Cenozoic, 22–25, 34

Chamonix, 108

Chaos, 205

Charney climate, 28–31

Climate, 51

change, 3–16, 21–44, 149–154, 167–177

feedback, 22, 25, 27, 30–33, 39, 43, 54

forcing, definition, 30

indices, 228, 232–238

model, 93, 95, 102, 103

modeling, 117, 120, 121, 123, 124

oscillations, 22, 26–27, 34

sensitivity, 22, 25–31, 33–35, 42, 43

Climatic habitability, 142, 145

Climatic precession, 108, 112, 117, 118, 120

Clouds, 7

CO₂ equivalent, 60–62

Comet, 109

Conference of the Parties, 15th (COP15), 5, 6, 12–13

Control variable, 95, 98–100, 103

Conveyor belt, 110

Cooling effect, 41–42

Copenhagen, 4–13, 15

Copenhagen Diagnosis, The, 4, 7–13, 15

Correlation, 173, 177

Cosmic problem, 137

Cost function, 94–99, 101

Croll, J., 112–115

D

Dangerous level, 21, 22, 35–36

Data assimilation, 103

Deep ocean, 22, 23, 28, 29, 31–33, 37, 38, 43

Definitions, 28, 33–35

Deglacial forcings, 81–82

Diluvian glaciers, 110

Dome C, 28, 29, 31, 32, 36

Double precessional peak, 120

Dynamical downscaling, 182–183

E

Earth's energy budget, 22–23
 Earth system, 33–35, 49
 Earth system models, 50
 Eccentricity, 58–60, 108, 111–115, 117–122, 124, 141–145
 Ecohydrology, 149–154
 Ecosystem services, 149, 150
 Einstein, 16
 Elliptic integrals, 112, 117–119
 e-mails, of prominent climate scientists, 13
 Emissions, 4, 7–13
 Energy balance-climate model, 95, 96, 98, 101, 103
 Energy balance model, 95, 96, 103, 142, 144
 Eolian dust, 54
 Equilibrium climate sensitivity, 102, 103
 Equilibrium global surface temperature (ΔT_{eq}), 25
 Equivalent latitudes, 117, 118, 121
 Erratic boulders, 108–110
 Esmark, 109, 110
 Eta model, 202–204, 206, 215–224
 Exoplanets, 141–145

F

Factor separation, 62
 Fast-feedbacks, 25, 27–28, 30, 31, 33, 34, 36, 42, 43
 Feedback, 113, 115
 Fine scales, 189–190
 Flip, 26, 36, 37
 Flooding, 110
 Floodplain, 149–154
 Forcing, 21–36, 39, 40, 42–44. *See also* Sensitivity
 Forecast skill scores, 206, 208
 Forward method, 94
 Forward model, 94
 Fossil fuel, 4, 7, 9, 10, 16
 Fourth Assessment Report of IPCC (AR4), 3–15

G

Galileo, 15
 Glacial cycles, 50
 Glacial-interglacial cycles, 57, 107, 112, 123
 Glacials, 57, 58, 60, 107–109, 111–115, 120, 123
 Glacial to interglacial, 31, 42
 Glaciers, 108–110
 GLAMAP 2000, 96, 102, 103
 Global climate models (GCM), 181
 Global deluge, 133
 Global, predicted, 28
 Global warming, 7, 8, 12–14, 22, 24, 31, 35–37, 39.
 See also Climate, change
 Greenhouse effect, 7, 16, 110
 Greenhouse gas, 57, 58, 62
 Greenhouse theory, 114
 Greenland, 4, 7, 10, 11
 Gulf Stream, 110, 111
 Günz, 113

H

Hockey stick, 14
 Hot Jupiter, 145
 Hydrological impacts, 157–165

I

Ice ages, 14, 16, 108–110, 113–120, 124
 Iceberg cooling effect, 41–42
 Iceberg discharge, 44
 Ice caps, 109, 110
 Ice core, 27, 31, 33, 35–37, 43
 Ice sheet, 4, 7, 10, 11, 51, 107, 108, 111, 113, 115, 123
 mass loss, 41
 models, 31, 36
 Ice volume, 120, 122
 Ice vs. ocean core, 36
 Illinoian, 113
 Impact of interannual variability, 86–88
 Imperfect Big-Brother (IBB), 191
 Imperfect Big-Brother Experiment (IBBE), 191
 Insolation, 58–63, 107, 108, 111–124
 Insolation pattern, 59–61, 63
 Interglacial periods, 35–39, 43
 Interglacials, 57–63, 107, 108, 111–113, 119, 123
 Intergovernmental Panel on Climate Change
 (IPCC), 3–11, 13–15
 Internal variability, 158, 161, 184–189
 International Scientific Congress in Copenhagen, 5–8
 IPCC, 22, 27, 30, 35, 39–42
 Irradiance, 115, 123
 Irradiation, 111–113, 116–118, 124

J

James Webb Space Telescope, 145
 Jupiter, 141, 144, 145

K

400-ka cycle, 59, 60
 Kansan, 113
 Keeling curve, 5
 Köppen, 115, 116, 118, 121
 Kozai interactions, 145

L

Large scales (LS), 181–196, 201–213
 Last glacial maximum (LGM), 80, 96, 97, 99, 102,
 103, 111
 Lateral boundary conditions (LBC), 190–194, 202, 204
 Lead Authors, 4, 5
 Length of the seasons, 111–113
 Loess, 65–76
 Longitude of perihelion, 58–60
 Long-term trend, 177
 LOVECLIM, 57, 80

M

Macrophyte, 149–152
 MARGO, 96, 102
 Mathematical analogies, 136
 Mathematical climate, 115, 119
 Mathematicians' Club, 136
 Meech, 112, 114, 117, 118, 124
 Memoirs, 113, 116, 119, 120
 Mid-Brunhes event (MBE), 57–63
 Migration, 150, 152–153
 Milankovitch first contribution, 132
 Milankovitch historic merit, 134
 Milankovitch, M., 93, 107, 108, 111, 113, 115–124, 131
 Milankovitch theory, 50
 Mindel, 113
 MIS-1, 58–61
 MIS-5, 60, 61
 MIS-7, 58, 59, 61
 MIS-9, 60, 61, 63
 MIS-11, 60, 61
 MIS-13, 57–61, 63
 MIS-15, 58, 61
 MIS-17, 58, 60, 61, 63
 MIS-19, 58, 61
 MIS-21, 60, 61
 Model-data misfit, 94
 Mont Blanc, 108
 Moraines, 108, 109
 Murphy, J.J., 115, 116, 124

N

Natural vs. human-made, 21, 22, 42
 Nebraskan, 113
 Negative feedbacks
 carbon, 44
 thermal & freshwater, 41
 Nested regional climate models, 181–196

O

Obliquity, 58–60, 108, 112–115, 118–124
 Ocean core, 22, 35–38, 43
 Optimal solution, 101, 102
 Optimization, 97–98, 101, 102
 Optimized solution, 103
 Orbital tuning, 68, 71
 $\delta^{18}\text{O}$ record, 61, 63
 Outgassing and burial, 24
 Overfitting, 103
 Oxygen isotope, 120

P

Paleoclimate, 65, 107–124
 data, 21, 27, 30, 35, 39
 reconstructions, 53
 state, 21–44
 Paleo-sea surface temperature data, 95
 Parameter estimation, 94, 103
 Parametric error, 101

Perceptions, public, 3–16
 Perfect Big Brother (PBB), 191
 Perihelion, 58–60, 108, 112, 113
 Periods, 108–111, 113–115, 117, 119–124
 Phase shift, 58
 Phasing relationship, 58
 Phenomenology, 136
 Physical parameterizations, 160, 161, 165
 Pleistocene, 115, 120, 123
 Polynya definition, 222
 Polynya impact
 on geopotential height, 222
 on sea level pressure, 222
 on temperature, 221, 224
 on wind, 221, 224
 Post-MBE, 57, 58, 60–63
 Potential added value, 182–183
 Precession, 58–60, 63
 Precipitation, 4, 7, 8, 167, 168, 170, 173–177
 Predictions, climate, 10, 16
 Pre-MBE, 57, 59–63
 Projections, 4, 7, 8
 Proxy data, 96

Q

Quaternary, 108–110, 120

R

Radiative forcing, 7, 51
 Regional climate model (RCM), 182, 201–213
 domain size, 202
 value added, 205
 Regional model, 228–229, 238
 Restoration, 149–154
 Rise estimates for 21st century, 39–41
 Riss, 113
 Ross Sea, 216, 218, 219, 221
 Runoff, 157, 161, 163

S

Science, climate, 3–16
 Sea ice, 4, 7, 10, 11, 16
 Sea-ice concentration (SIC), 216–219
 Sea level, 4, 7, 8, 11, 12, 16, 22, 28–33, 36–42, 44
 Seasonal insolation, 113
 Seasons, 107, 108, 110–118, 120, 123, 124
 Sensitivity, 22, 25–31, 33–36, 42, 43
 Serbian culture, 136
 Simulation Antarctic, 215–224
 Simulations, 57, 59, 62, 63
 Skeptics, climate, 15–16
 Slow feedback, 26, 30, 33, 34, 42–44. *See also* Slow surface
 Slow surface, 26, 33, 34
 Snowball state, 143–145
 Solar constant, 111
 Solar energy, 123
 SPECMAP, 58
 Spectral characteristics, 121–123

Spectral nudging (SN), 192
State estimation, 94, 103
Streamflow, 167–177
Structural error, 101–103
Structural uncertainty, 158, 160, 161
Subtropics, 7
Summer, 108, 110–118, 120, 123, 124
Sun, 6, 16
Surface air temperature, 83–88
Surface forcing, 24, 28, 30–34, 38

T

Temperature, 4, 6–8, 10–12, 14, 16, 21–29, 31–39, 41–44, 150–152
Temperature change, 22, 24, 25, 27, 28, 31, 34–39, 41–43
Terra Nova Bay region (TNB), 216, 218, 221–223
Terrestrial planet, 142, 143, 145
Time scale, 65–76
Trend, 167–173, 177
Troposphere, 6
True canon, 135

U

Underfitting, 103
United Nations Framework Convention on Climate Change (UNFCCC), 5
University of Belgrade, 135

V

Values, 30, 31, 33, 36

W

Wandering poles, 132
Water framework directive, 153, 154
Watershed, 170–174, 176
Water vapor, 7
Wegener, 115, 116, 118, 121
Winter, 108, 110–116, 118, 123
Wisconsinian, 113
Working Group I (WGI) of IPCC, 4, 5, 11, 15
Würm, 113